SEISMIC PERFORMANCE EVALUATION OF RESIDENTIAL RC TEMPLATE BUILDINGS USING NON-LINEAR ANALYSES PROCEDURES

A THESIS SUBMITTED TO
THE FACULTY OF ARCHITECTURE AND ENGINEERING
OF
EPOKA UNIVERSITY

BY

MARSED LETI

IN PARTIAL FULFILLMENT OF THE REQUIREMENTS
FOR
THE DEGREE OF DOCTOR OF PHILOSOPHY
IN
CIVIL ENGINEERING

JUNE, 2022

Approval of the thesis:

SEISMIC PERFORMANCE EVALUATION OF RESIDENTIAL RC TEMPLATE BUILDINGS USING NON-LINEAR ANALYSES PROCEDURES

submitted by **Marsed Leti** in partial fulfillment of the requirements for the degree of **Doctor of Philosophy in Department of Civil Engineering, Epoka University** by,

Prof. Dr. Sokol Devishi _____
Dean, Faculty of Architecture and Engineering

Assist. Prof. Dr. Erjon Luga _____
Head of Department, **Civil Engineering, EPOKA University**

Prof. Dr. Hüseyin Bilgin _____
Supervisor, **Civil Engineering, EPOKA University**

Examining Committee Members:

Prof. Dr. …….. _____
……. Dept., …….. University

Prof. Dr. ……. _____
……. Dept., …….. University

Assoc. Prof. Dr. ,,,,,,,,,,,,,,,,,, _____
……. Dept., …….. University

Assoc. Prof. Dr. ……. _____
……. Dept., …….. University

Assist. Prof. Dr. …….. _____
……. Dept., …….. University

Date: 04.07.2022

I hereby declare that all information in this document has been obtained and presented in accordance with academic rules and ethical conduct. I also declare that, as required by these rules and conduct, I have fully cited and referenced all material and results that are not original to this work.

Name, Last name: **Marsed Leti**

Signature:

ABSTRACT

SEISMIC PERFORMANCE EVALUATION OF RESIDENTIAL RC TEMPLATE BUILDINGS USING NON-LINEAR ANALYSES PROCEDURES

Leti, Marsed

Ph.D., Department of Civil Engineering

Supervisor: Prof. Dr. Hüseyin Bilgin

Recent damaging tremors in Balkans have shown insufficient earthquake performance of reinforced concrete (RC) buildings intended for residential purposes. In Albania, typified designs developed by the governmental authorities during socialist era are used for many of the buildings intended for residential and governmental services including administrative centers, health clinics, hospitals, schools as a common practice to save on architectural fees and confirm quality control. Therefore, such template designed buildings must be dealt with firstly.

This thesis assesses seismic performance of residential buildings with the chosen template designs in Albania considering inelastic response of RC sections. Five residential buildings with template designs were chosen to represent an important percentage of residential buildings in mid-size cities located in high seismic districts of Albania. Selection of template designed buildings and material properties were based on site investigation on residential buildings in several cities of the region. Pushover curves of studied buildings were constructed by nonlinear static and incremental dynamic analyses conducted in two orthogonal directions. The nonlinear dynamic characteristics

were represented by equivalent single-degree-of-freedom (ESDOF) systems and their earthquake deformation demands were estimated under selected ground motions represented by near and far fault recordings. Seismic performance evaluation was carried out in accordance with modern seismic guidelines following the capacity spectrum method. Reasons of building damages during the November 26, 2019 earthquakes are examined using the results of performance assessment of studied buildings. The effects of material quality and detailing effect on earthquake performance of residential RC buildings were investigated. The detailed examination of capacity curves and performance evaluation identified deficiencies and possible solutions for template designs. Earthquake capacity evaluation was deployed in accordance with capacity spectrum method.

Evaluation of the capacity curves for the investigated typologies points out that concrete quality and detailing has remarkable effects in both displacement and lateral load bearing capacity of buildings.

Unsatisfactory performance of residential buildings makes the development of the effective and affordable retrofitting techniques essential. The rehabilitation techniques are broken into two different categories: the local methods, which improve the response of individual structural elements and the global ones, which operate on the whole structure. Since in Albania the poor material and construction quality is common problem, the most suitable technique is the use of additional shear walls to increase lateral load capacity and decrease deformation demands. As a result, existing weaknesses in frame elements would be less pronounced and poor construction quality in buildings could be somewhat compensated. Finally, conclusions are provided, and future research needs on the topic are outlined.

Keywords: Earthquake Capacity, Pushover Analysis, Incremental Dynamic Analysis, Time history Analyses, Performance Based Seismic Evaluation, Template Designs.

ABSTRAKT

VLERËSIMI I PERFORMANCËS SIZMIKE TË NDËRTESAVE TË BANIMIT DUKE PËRDORUR PROCEDURAT E ANALIZAVE JOLINEARE

Leti, Marsed

Doktoraturë, Departamenti i Inxhinierisë së Ndërtimit

Udhëheqësi: Prof. Dr. Hüseyin Bilgin

Lëkundjet e fundit të forta në Ballkan kanë treguar performancë të pamjaftueshme të ndërtesave betonarme të destinuara për qëllime banimi ndaj tërmeteve. Në Shqipëri, dizajne të tipizuara që u zhvilluan nga autoritetet qeveritare gjatë kohës së komunizmit, përdoren për shumë nga ndërtesat e destinuara për shërbime rezidenciale dhe qeveritare, duke përfshirë qendrat administrative, klinikat shëndetësore, spitale dhe shkolla, si një praktikë e zakonshme për të kursyer tarifat arkitekturore dhe për të konfirmuar kontrollin e cilësisë. Prandaj, dizajnet e këtyre ndërtesave duhet të trajtohen së pari.

Kjo tezë vlerëson performancën sizmike të ndërtesave të banimit me modelet e zgjedhura në Shqipëri duke marrë parasysh sjelljen joelastike të seksioneve betonarme. Pesë ndërtesa banimi me dizajn shabllon u zgjodhën për të përfaqësuar një përqindje të rëndësishme të ndërtesave të banimit në qytetet me përmasa mesatare të vendosura në rrethe me sizmicitet të lartë në Shqipëri. Përzgjedhja e ndërtesave të dizajnuara me shabllon dhe karakteristikat e materiale u bazuan në investigimet e bëra ne terren në ndërtesave të banimit në disa qytete të rajonit. Kurbat e kapacitetit të ndërtesave të studiuara janë ndërtuar duke përdorur analiza jolineare statike dhe analizen e njohur si

“Incremental Dynamic Analyses” të kryera në dy drejtimet e godines. Karakteristikat dinamike inelastike u përfaqësuan nga sisteme ekuivalente me një shkallë lirie dinamike (ESDOF) dhe kapiciteti i tyre për zhvendosje sizmike u vlersua nga lëvizjet nëntokësore të zgjedhura, me epiqendër të thellë dhe të cekët. Vlerësimi i performancës sizmike u krye në përputhje me standartet moderne sizmike duke ndjekur metodën e spektrit të kapacitetit. Shkaqet e dëmtimeve të ndërtesave gjatë tërmetit të 26 Nëntorit 2019 shqyrtohen duke përdorur rezultatet e vlerësimit të performancës së ndërtesave të studiuara. Efektet e cilësisë së materialit dhe perforcimit në performancën e tërmeteve të ndërtesave të banimit betonarme, u shqyrtuan. Ekzaminimi i detajuar i kurbave të kapacitetit dhe vlerësimi i performancës identifikuan mangësi dhe zgjidhje të mundshme për dizajnet shabllon të selektura. Vlerësimi i kapacitetit sizmik u vendos në përputhje me metodën e spektrit të kapacitetit.

Vlerësimi i kurbave të kapacitetit për tipologjitë e studiuara vë në dukje se cilësia dhe perforcimi i betonit ka efekte të jashtëzakonshme si në zhvendosjen ashtu edhe në kapacitetin mbajtës të ngarkesës anësore të ndërtesave.

Performanca e pamjaftueshme e ndërtesave të banimit e bën të domosdoshme zhvillimin e teknikave efektive dhe të përballueshme të rikonstruksionit. Teknikat e rikonstruksionit ndahen në dy kategori të ndryshme: metodat lokale, të cilat përmirësojnë sjelljen e elementëve strukturorë individualë dhe ato globale, të cilat veprojnë në të gjithë strukturën. Meqenëse në Shqipëri materiali i dobët dhe cilësia e ndërtimit janë problem i zakonshëm, teknika më e përshtatshme është përdorimi i mureve prerëse shtesë për të rritur kapacitetin e ngarkesës anësore dhe për të ulur zhvendosjet. Si rezultat, dobësitë ekzistuese në elementë do të ishin më pak të theksuara dhe cilësia e dobët e ndërtimit mund të kompensohej disi. Së fundi, jepen konkluzionet dhe përshkruhen nevojat e ardhshme kërkimore mbi këtë temë.

Fjalët kyçe: Kapaciteti i tërmetit, Analiza Pushover, Incremental Dynamic Analysis, Analizat Time History, Vlerësimi sizmik i bazuar në performancë, Dijane Shabllon.

Dedicated to my family

ACKNOWLEDGEMENTS (optional)

I would like to express my special thanks to my supervisor Prof. Dr. …….. for his continuous guidance, encouragement, motivation and support during all the stages of my thesis. I sincerely appreciate the time and effort he has spent to improve my experience during my graduate years.

I am also deeply thankful to……..

My sincere acknowledgements go to my thesis progress committee members, ……., for their comments and suggestions throughout the entire thesis.

I deeply thank to …….

I am especially grateful to ……

I would like to thank to …….

TABLE OF CONTENTS

LIST OF TABLES

TABLES

LIST OF FIGURES

FIGURES

LIST OF ABBREVIATIONS

KTP	Kushti Teknik i Projektimit (Technical Code of Design)
PDT	Performance Based Design
NW	North-West
NE	North-East
RC	Reinforced Concrete
URM	Unreinforced Masonry
AQTN	Arkivi Qendror Teknik i Ndertimit (Central Technical Archive of Construction)
IO	Immediate Occupancy
LS	Life Safety
CP	Collapse Prevention
GI	Global Instability
PP	Performance Point
ESDOF	Equally single-degree-of-freedom systems
IDA	Incremental Dynamic Analysis
Mw	Magnitude
GTM	Greenwich Mean Time
I	Intensity
CET	Central European Time
DOF	degree of freedom
PGV	peak ground velocity
PGA	peak ground acceleration
PGD	peak ground displacement
DCM	decision of the Council of Ministers
S_k	seismic force (KTP)
Q_k	loads which initiate the inertia forces (KTP)
K_c	seismic coefficient (KTP)
η_k	coefficient which is affected by the mode shape of the building (KTP)

B	dynamic coefficient (KTP)
DL	Dead Load
LL	Live Load
S_a	Spectral Acceleration
k_E	the seismic coefficient (KTP)
k_r	importance coefficient of the building type (KTP)
Ψ	the structural behavior coefficient (KTP)
CSM	Capacity Spectrum Method
ATC	APPLIED TECHNOLOGY COUNCIL
EC-8	Eurocode
PBEE	Performance Based Earthquake Engineering
FEMA	The Federal Emergency Management Agency
V_i	the base shear value
W	the weight of the structure
Δ_{roof}	roof displacement
α_1	the modal mass coefficient of first natural mode of structure
PF_1	the modal mass participation factor for the first natural mode of structure
$\Phi_{1,roof}$	roof level amplitude in the first mode
K	the damping modification factor
Ø	Diameter of steel bars
%	Percentage
$S_{a,d(T1)}$	value taken from the design response spectrum of the first mode period
$m_{eff,1}$	the estimation of the modal mass in that mode
i	the degrees of freedom
m_i	mass concentrated in the degree of freedom i
F_i	the later load applied to the degree of freedom i
δ_i	the displacement of the degree of freedom i gained from the elastic analysis of the structure
ω_n	natural frequencey
Φ_n	Mode shape vector
ζ	damping ratio
IM	Intensity measure

DM	Damage measure
λ	lambda, scale factor
Θ_{max}	roof displacement ratio
$_{v}$	Poisson's ratio
γ_c	Partial factor
f_{cd}	Design value of compressive strength
E_{cd}	Design value of modulus of elasticity
E_{cm}	Young's Modulus
f_{ctm}	Mean value of axial tensile strength
$f_{ctk(5\%)}$	Characteristic axial tensile strength
f_{cm}	Mean value of cylinder compressive strength (28 days)
f_{ck}	Compressive cylinder strength
$f_{c,cube}$	Cubic strength
GUI	Graphical User Interface
MDOF	multi-degree-of-freedom
SPO	Static Pushover
DPO	Dynamic Pushover

CHAPTER 1

INTRODUCTION

1.1 General

Albania is located in the peninsula of Balkan which is part of Alpine-Mediterranean seismic belt in the middle of the Eurasian and African plates. The seismicity of Balkan region is defined as the highest in Europe (Aliaj et. al., 2010). Therefore, Albania is part of an active seismic region which has been struct by several devastating earthquakes.

After every devastating earthquake that occurred in our country, where a significant part of its lands is exposed to earthquake risk, the determination of the earthquake resistance of the existing building stocks and their reinforcement needs have always been on the agenda of the country. In a country like Albania, a large part of which is under serious earthquake risk, minimizing the losses that may occur as a result of this natural event is an important issue for the country. Determining the safety levels of the buildings that contain a significant part of the population is one of the most important and foremost stages of the preparations to be made against earthquake disasters.

Although it is not possible to predict when and how large an earthquake will occur, it is possible to minimize the loss of life and property in the event of an earthquake by using today's technology. Earthquake regulations, prepared in the light of scientific studies and experiences gained from past earthquakes, are mainly to serve this purpose. Basically, in these regulations, which target the level of life safety, building-type structures are

classified according to their purpose and importance and prescribe rules in the calculation of the forces that are based on the design.

The 1989 Loma Prieta (Mw = 7.1) and 1994 Northridge (Mw = 6.7) earthquakes occurred in the most densely populated areas of the Americas. Although the loss of life in earthquakes remained at low levels, economic losses of billions of dollars occurred. Similarly, after the devastating earthquakes that took place in our country and some other parts of the world in the last two decades, various rules have been tried to be imposed on the construction of buildings, and the need to limit the damages caused by these earthquakes has been a motivation tool in the studies in the field of structural engineering, and great progress has been made in this field. The adequacy of existing earthquake resistant building design methods has been questioned. Based on this need, various projects have been initiated and developed for the evaluation of existing structures and for new structures to be built. These include SEAOC (1995), ATC-40 (1996), FEMA 273-274 (1997), FEMA 356-357 (2000), FEMA 440 (2005). With the results of all these studies, a new method called Performance Based Design (PDT) has been developed among structural engineers. In this method, especially in the design for the evaluation and strengthening of existing structures, the main objective is to find the current capacity of the structure using simplified non-linear static analysis methods and to estimate the damage situation that will occur in a possible earthquake.

Unlike force-based methods, this method has alternative performance targets for different groups of structures. After strengthening, besides whether the building has reached the targeted performance level; not only the displacements in the whole structure, but also the deformations of each structural element can be obtained. This can provide practitioners with more economical and more effective reinforcement options.

Recently, on November 26, 2019, a 6.4 righter magnitude earthquake struck the central western part of Albania. Its epicenter was located off-shore NW of Durrës, about 7 km

North of the city and 30 km West from the capital city of Tirana. The most affected cities nearby the epicenter, in Tirana, Laç, Fushë-Krujë, Vorë, Kamës etc. The damage caused by the earthquake has lost the lives of 51 peoples and injured more than 3,000. The material cost is reflected on more than 14,000 damaged buildings. After the earthquake, the EPOKA reconnaissance team conducted several site investigations on most of the affected regions of Durrës earthquake. The most effected buildings are reported the ones designed according to premodern codes. The reinforced concrete (RC) buildings built during the communism era in Albania following template designs by the Ministry of Public Works to save architectural fee, experienced heavy damages. Buildings falling into this category were constructed during the development of our country in 1982 where the workmanship was not at the desired level whereas the adequate seismic design code didn't even exist. The main deficiencies observed in site were the poor material quality and inadequate shear reinforcement.

The design of these building typologies must have been done using the 2nd version of the Albanian design code. The timeline starts on 1963 when the first building standard was developed (KTP-63). Furthermore, in 1978 the second version (KTP-78) was released, mostly based on the previous standard and some Russian experiences. The last update of the code was done on 1989 (KTP-N2-89) also including the seismic design calculation considerations. KTP-N2-89 is the last update which is still enforce nowadays.

For this study, there are selected five different building templates designed with premodern building codes in Albania, four of which fall into the category of 1982 designs whereas the fifth one is part of a more recent construction (2005) which was found heavily damaged during the site investigations.

1.2 Objective of the study

An important part of the residential buildings in our country have been built using template designed projects. When there are changes in the regulation, the projects of this type are rearranged according to the requirements of the renewed regulation by keeping the

architecture unchanged. After the 1989 earthquake regulation, these types of projects were revised according to the new regulations and their earthquake safety was tried to be ensured. However, in our country's building stock, there are many types of housing structures built before this date, which are of great importance (Leti and Bilgin, 2022; Bilgin et. al., 2021).

The main target of this study is to evaluate the seismic performance of the selected buildings taking into account the concrete compressive strengths and stirrups spacings that maybe encountered in practice by considering the nonlinear methods. Therefore, the blueprints of the selected buildings are ensured from the Central Technical Archive of Construction (AQTN). The detailing of reinforcement and materials properties are checked and compared from the data gathered visually during the site inspection of the reconnaissance team. Furthermore, from one of the template buildings which was destroyed during the November 26 earthquake, there were taken samples from concrete and steel and tested in laboratory. In the performance evaluation, the dimensions on the plans of the buildings with template projects were taken into account and analytical models were prepared. The results confirm undoubtedly the conclusions derived from the site inspections. In addition, the performance assessment is conducted by three different methods: based on capacity spectrum method, based on the demand exceedance ratio from time history analyses and performance assessment based on the Incremental Dynamic Analysis. The mathematical model of the buildings selected is done in the environment of Zeus-NL software whereas the demand values from time history analysis are calculated using NONLIN V8. The interpretation of results is done based on the modern and old seismic codes as well as the target-performance level defined for the residential reinforced concrete template buildings considered in this study. In line with the results obtained from the above analyses, the parameters to be considered in the modeling of reinforced concrete residential buildings and solutions for eliminating the deficiencies are presented.

Here, with the work to be done on a certain number of projects, it will be possible to have information on many buildings that they will represent. It is thought that the findings

obtained in this study will be useful in studies to make the examined structures meet the performance levels predicted in modern regulations.

1.3 Scope and methodology

The building templates are selected from 5 to 7 story height, to represent the commonly encountered reinforced concrete building stock constructed per pre-modern code requirements. From the site investigations the main deficiencies observed were the poor material quality and inadequate reinforcement of shear links in beams and columns. Based on the blueprint detailing, the concrete type belongs to M200, equivalent to C16/20, and the average stirrups spacings 100mm. These values totally contradict the outcomes derived in the end of the investigations of the same template buildings done during the November 26, 2019 earthquake. On the other hand, two samples of concrete and three samples of steel bars were tested in compression and tension respectively. Based on the findings of these tests, compressive strength of the concrete samples was found to be about half of the design requirements read from the blueprint details whereas the steel specimens show that they are acceptable according to the design calculations. Therefore, the influence of the material quality and transverse reinforcement is one of the main key points of this thesis.

Each of the structures is analytically modelled in Zeus-NL considering different types of concrete (C16, C14, C12 and C10) and stirrups spacings (S100, S150, S200 and S250 mm). The performance assessment is done based on three main procedures. The first procedure considered is the demand calculation based on the capacity spectrum method according to ATC-40 using the response spectra defined from EuroCode8 and KTP-N2-89. The capacity of the structures is derived from the static pushover analysis (SPO) applied using an inverted triangular lateral load pattern. Furthermore, the performance levels are defined based on FEMA 356 guidelines as immediate occupancy (IO), Life Safety (LS) and collapse prevention (CP). The second assessment method is based on the

time history analyses conducted in the environments of NONLIN software using a suite of 68 far- and 78 near-field records. The structural models are represented as equally single-degree-of-freedom systems (ESDOF). The influence of near field versus distant field records is another goal of this study. Finally, a new and promising method known as Incremental Dynamic Analysis (IDA) is utilized in ZeusNL software using a set of 18 earthquake records without directivity influence. The dynamic pushover curves are plotted from the values generated together with immediate occupancy (IO), collapse prevention (CP) and global instability (GI). The representation of IDA curves is done in different ways: as simple IDA curves, to check the influence of each of the records individually, summarized into 16%, 50% and 84% fractiles (percentiles) and compared with static capacity curves, to check the correlations among two different analyses. Furthermore, the performance of buildings selected is done based on the collapse prevention performance level for an intensity measure of 0.36g based on the probabilistic hazard seismic map prepared for Albania for a return period of 475 years.

In the end, outcomes are presented graphically for better understanding while the interpretation of seismic performance assessment is done based on the target performance levels.

1.4 Brief description of the content

The main content of this thesis is structured in eight chapters.

Chapter 1 provides the objectives, problem statements and a brief methodology of the study.

Chapter 2 describes mainly the seismic history of the Albania based on the previous earthquakes happened since year 1851.

Chapter 3 explains the damage assessment of Albanian earthquake of November 26, 2019, during the site investigations done by the reconnaissance team. The failure types on

especially reinforced concrete buildings are clearly described in the content of this chapter.

Chapter 4 focus on the earthquake design codes and performance based seismic designs. In this chapter, a detailed description of the Albanian codes and regulation is provided according to the development timeline. Furthermore, the principles of Performance-Based assessment are explained.

Chapter 5 presents the details of each of the template designs selected for the seismic performance assessment in this study. Moreover, the far- and near-field lists of ground motion records used for time history analysis and list of records used for Incremental Dynamic Analysis are provided in the end of this chapter.

Chapter 6 explains the analytical modelling and evaluation by providing a full interpretation of the methods of analyses used for performance evaluation, description of the material characteristics, ZeusNL software and the modelling methodology of the case studies.

Chapter 7 provides the results for each of the analyses and buildings considered for this research study. In addition, it deals with the interpretation of results based on the methods mentioned in the previous section.

Chapter 8 summarizes the interpretations of the performance assessment conducted in the previous chapter by providing necessary conclusions and recommendations for future work.

CHAPTER 2

LITERATURE REVIEW

2.1 Seismicity of Albania

The seismicity of a specific region is defined as a function of earthquake size in seismic magnitude, intensity, and frequency of their occurrence. According to earthquake classification based in the magnitude by (Hagiwara, 1964; Lee and Stewart, 1981) the Albanian region is categorized from an intensity of seismic microactivity of 1<M<3, from small earthquakes 3<M<5, from medium size earthquakes 5<M<7 and very seldom and strong earthquakes M>7 (Aliaj et. al., 2010). A summary of major earthquakes happened in Albania after 90's and its causalities are presented in **Table 1.**

Table 1: Major tremors in Albania (Bilgin et. al., 2022; Aliaj et. al., 2010)

Date	**Impacted region**	**Magnitude (M_w)**	**Depth (km)**	**Consequences**	
				Dead	**Injured**
26-Nov-	Durres	6.4	20.0	51	Over 3000
21-Sep-	Durres	5.6	10.0	-	108
9-Jan-1988	Tirana	5.4	24.0	-	-
16-Dec-	Fier	5.6	21.9	1	12
15-Apr-	Shkoder;	6.9	10.0	136	Over 1000
30-Nov-	Diber	6.6	20.0	12	174
18-Mar-	Fier	6.0	-	5	77
26-May-	Korçe	6.4	-	7	127
1-Sep-1959	Fier	6.2	20.0	2	-
27-Aug-	Shkoder	5.5		1	27

27-Aug-	Diber	6.0	33.0	43	110
21-Nov-	Vlore	6.0	35.0	30	100
26-Nov-	Tepelena	6.4	-	36	102
22-Dec-	Leskovik;	6.1	-	-	-
6-Jan-1905	Shkoder	6.6	-	200	500

The first seismic zone intensity map for Albania was prepared in 1952 from the Science institution and the ministry.

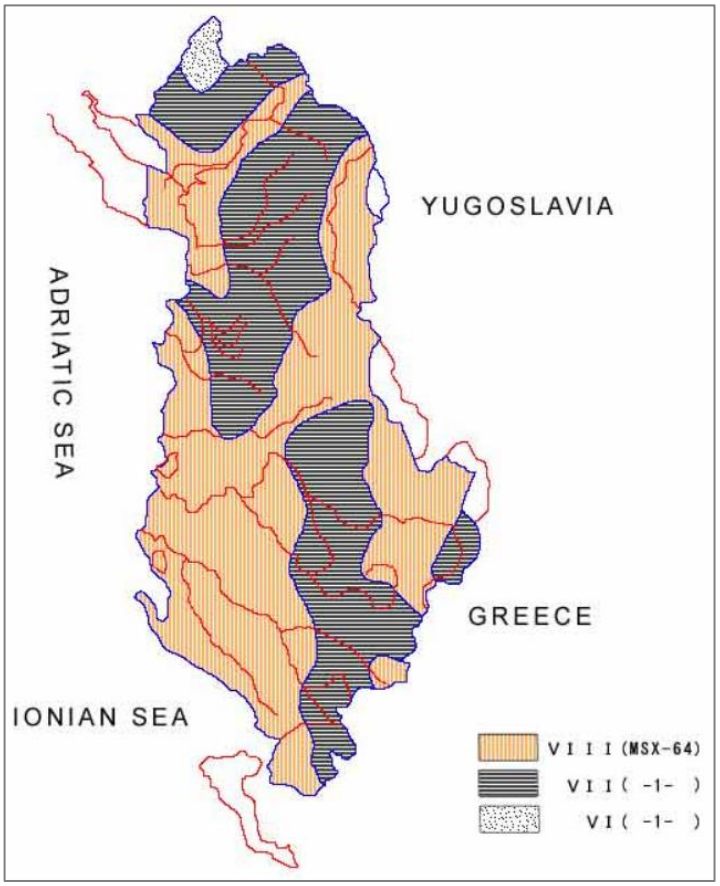

Figure 1: Albanian Seismic Intensity Zone Map (KTP-2-78, 1978).

Later, the seismic intensity map has been updated multiple times for a period 27 years until its last version (1979) as shown in **Figure 1**. The 79's version of this map, even though quite old, is still the law map for the seismic estimations nowadays. Albanian

former code regulations, KTP-63 and KTP-78 are based on the seismic intensity map of 1979.

2.1.1 Historical seismicity

Albanian seismicity has been defined by different authors (Mihajlovic, 1927; Moreli, 1942; Mihajlovic, 1951; Shebalin et. al., 1974; Makropoulos and Burton, 1985; Sulstrarova and Koçiaj, 1975; Papazachos and Papazachos, 1989; Shebalin et. al., 1998; Guidoboni et. al., 1994; Soloviev et. al., 2001).

Historical data show that from the III-II century BC until 1990, Albania was hit by a large number of earthquakes with high intensity. 89 earthquakes with intensity above VIII "ballë" were reported where 15 of them had intensity above IX according to MSK-64 scale.

An interesting fact is that 57 of these earthquakes that extend for a period of 2000 years, date back to the XIX century. This can be explained by the fact that some of them are not well evidenced in early history (Aliaj, 2000).

There are data that the city of Durrës (Dyrrahum) has been constantly affected by strong earthquakes with consequences in material as well as in people. From further studies in the city of Durrës, it results that the archaeological letters were found deep into the ground by several meters. This justifies the fact of the numerous damages that occurred in the city of Durrës (Koçiu and Kapllani, 1995; Koçiu and Kapllani, 1995).

Another old and well-known city, Apollonia, turns out to have been hit by a large number of earthquakes with economic as well as human consequences. Additionally, the city of Ohër was destroyed in 526 A.C. by numerous earthquakes which was later rebuild by the emperor Justinian (Reicherter et. al., 2008).

In advance, it is provided a list of earthquakes and its consequences happened to Albanian territorial and surrounding regions. The description is done based on the collection of

earthquakes histories of “SIZMICITETI, SIZMOTEKTONIKA DHE VLERËSIMI I RREZIKUT SIZMIK NË SHQIPËRI” book (Aliaj et. al., 2010).

2.1.2 The earthquake of October 12, 1851

In the morning of October 12, 1851 (7 o'clock), the bay of Vlora was hit by a strong earthquake, destroying a good part of the buildings, and leaving the rest damaged. According to the information at that time, the number of victims reached up to 2000. Other sources say that the sea level rose by 66 cm as a result of a tsunami that followed the earthquake (Soloviev et. al., 2001), thus causing major floods.

Figure 2: The coast of Vlora damaged by the earthquake of October 12, 1851. Image taken from the collection of Jan Kozak, KZ628, The Earthquake Engineering Online Archive NISEE e-Library (NISE, 2022)

Four hours before the earthquake of October 12, 1851, a slight foreshock was felt in the city of Vlora. The main shock was followed by many other aftershocks. The earthquake was felt strongly in Italy in cities such as: Taranto, Bari, Barleta, Canosa and Cerignola.

According to ***Aliaj et. al.***, the maximum intensity of this earthquake must have been 9 "ballë" and the epicenter at 40.5° North, 19.5° East. Figure 2 demonstrates consequences of the Vlora offshore after October 12, 1851 earthquake.

2.1.3 The earthquake of October 17, 1851

On October 17, 1851, an 8.1 magnitude earthquake shook the region of Berat. The city fort had been destroyed and 400 soldiers buried under its ruins. There were observed cracks in the ground and springs of sand and water mixed with some form of sulfur dust, making it difficult to breathe. A massive landslide has also been observed. Based on the ruins of the city fort, the estimated magnitude of the earthquake would be 9.0 "ballë".

2.1.4 The earthquakes of the 1855

During July and August 1855, a series of earthquakes hit the Shkodra region very hard. The strongest shocks occurred on July 3, 1855, which destroyed the villages of Bushat, Juban, Kosmac and VauDejes. In addition to Shkodra, serious damages were observed in Karme, Dushan, Toplane and Bruc where in many cases cracks were observed in the earth surface. The greatest intensity is marked as 8 "*ballë*". After the main shock, during July and August, were noted more ground shakings: July 7, 1855 of intensity 7 *"ballë";* July 16, 1855 of intensity 8 *"ballë"; August 11, 1855* of intensity 7 *"ballë"; August 14, 1855* of intensity 8 *"ballë".*

2.1.5 The earthquake of October 10, 1865

On October 10, 1865, a strong earthquake hit the southern region of Albania damaging the villages of Izvor and Rabije located in city of Tepelene, Osmanzeze and Velcan located in the city of Berat and Klos in Fier. The intensity of October 10, 1865 earthqauke was 8

"ballë" and the epicenter 40.5°N, 19.9°E. During this earthquake there were noted great damages in buildings and people. 14 deaths were identified in the village of Rabije and 13 in the village of Klos. On the other hand, large ground cracks have been observed in Izvor of Tepelena and Skerkaj forming a width of 10-15 m along several kilometers.

2.1.6 The earthquake of June 14, 1893

In June 1893, the region of Himara was hit by a devastating earthquake with the highest intensity, 9 "ballë" and epicenter in the villages of Kudhes and Corraj (40.1° N, 19.8° E). The village of Kudhes was totally destroyed. Moreover, there were observed landslides up to the village of Fushe-Bardhe in Gjirokaster. Other damages occurred also in the city of Vlora and a church build on rock in Saranda. The earthquake left a great panic among the people who will experience another earthquake later in 1966. The June 14, 1893, earthquake was felt also in Puglia followed by a tsunami.

2.1.7 The earthquakes of the 1905 year (Shkodra earthquakes)

During 1905 the region of Shkodra was hit by a large series of earthquakes which caused a lot of injuries in buildings as well as people. Several aftershocks occurred over a period of 1 year, bringing other damages to the city of Shkodra, its surrounding villages and causing panic among the people. These ground shakings were also felt in the neighbor regions of Albania.

The biggest shock started at 4:42:43 AM in the morning of June 1, 1905, with an intensity of 9 "ballë", magnitude M_s = 6.6 and epicenter at 42.02° N, 19.5° E. This earthquake continued 10-12 seconds and caused severe damages in Shkodra, to surrounding villages and in people. According to the records of that time, 1500 houses were destroyed, and the remaining ones were severely damaged. Furthermore, 200 dead and 500 injured people were reported.

In the region of Bahcallëk (Shkodra) all houses were completely destroyed. The walls of the Shkodra castle were damaged and some of them fell partially, causing consequences

in the houses below it. Also, the bridge over the river Drin was damaged but it didn't fall. The river also had an immediate rise in water level after the earthquake. The water of Kiri and Drini rivers caused floods in the surrounding areas. In the areas between Berdica and Bahcallëk, there were observed large cracks in the earth surface which released the underground water to surface. In the village of Berdicë none of the houses was left without being completely destroyed. The same fate befell the village of Trush, located next to Berdicë. According to witnesses, the houses moved up and then went down being destroyed by the earthquake waves. The highest intensity affected Bahcallëk but also the center of Shkodra, which had major damages in buildings. All the churches were severely damaged, and their domes were cracked in the middle. Ships sailing in the Adriatic Sea between the Buna River and Tivar (Montenegro) feel the earthquake too. Ships sailing on the Buna River were endangered by earthquake waves and rocks falling from the hills adjacent to the river.

The aftershocks of the June 3, 1905, earthquake caused severe damages in the cities of Lezha, Ulcinj, Tivar, Podgorica and Tuz. They continued more than one year (until July 1906) and were felt strongly in Hungary, Bulgaria, Greece, and Italy.

2.1.8 The earthquake of February 18, 1911

On February 18, 1911 a strong earthquake struck the region of Ohri lake destroying many houses nearby, in the city of Pogradec and villages such as Starove, Tushemisht and Zagrocan. One part of the buildings collapsed while others which resisted the earthquake were heavily damaged increasing thus the number of dead people. In addition, three mosques were destroyed. The level of Ohrid lake arose by half a meter. The earthquake started at 23:35 (GTM) and was recorded in many seismological stations of Europe. Its magnitude was M_s=6.7 and epicenter located in the southern part of Ohri Lake in the 42.52°N, 20.45°E coordinates. The February 18, 1911 earthquake was followed by many aftershocks until year 1912 which also destroyed the village of Hudenisht.

2.1.9 The earthquake of December 22, 1919

During the midnight of December 22, 1919 (23:40 GTM) an Ms=6.1 earthquake struck the city of Leskovik (Albania) and Konice (Greece). Many buildings were heavily damaged in Leskuvik while in Greece the villages of Isboros, Plavoli, Belthonsi and Kapazitko were destroyed. After the earthquake there were reported many cracks in walls, falling chimneys and landslide in Leskovik. The intensity of this earthquake was estimated to be 8 *"ballë"* which was followed by several aftershocks.

2.1.10 The earthquake of November 26, 1920

On November 26, 1920 a M_s=6.4 earthquake hit the city of Tepelenë, causing a devastating damages in the city and villages of Bënça, Turan, Dhemblan, Memaliaj, Kashisht, Salari, Dragot, Luzat etc. Marked as one of the strongest earthquakes which destroyed the city of Tepelenë, it caused 36 deaths and 102 injuries. The only building remained un-collapsed in the city, was a timber construction building. The bridge of Bënça was partially damaged, most of the walls of the old castle were destroyed and Bënça area was ruined completely. It is reported that about 2500 houses were destroyed by the earthquake, leaving about 15000 people homeless. Among several aftershocks, the strongest one happened three days later, on November 29, 1920.

2.1.11 The earthquakes of Durrës of 1926

In December 1926, the city of Durrës was hit continuously by different earthquake shocks. First shock started on December 16 at 17:64 which will be followed by another earthquake in the morning of December 17 of the same year. After 10 minutes, at 06:31 the strongest shock with magnitude M_s=5.8, hit the region of Durrës and Shijak which caused a lot of damages in the buildings. This earthquake was felt also in Galatina, Otranto, Alessano, Lecce, Masafi, Taranto, Galipoli located in Italy and Dubrovnik, Ulcinj, Trepce, Izvor in Yugoslavia. Nonetheless, the main shock had didn't happen yet. At 11:39:50 of December 1926, the strongest shock with magnitude M_s=6.2 and epicenter in Durrës (41.3N 19.5E),

caused a lot of serious damages in the region of Kavaja, Shijak and the surrounding villages. In Durrës and Kavaja many buildings were seriously damaged. All minarets of the mosques were cut off. Even the newly built constructions had significant damages. This shock was felt also in cities of Tirana, Shkodra, Berat, Lushnje, Elbasan as well as in the surrounding countries: Italy in Puglie, Greece in Korfuz and Janine. The number of victims was relatively small, which can be explained by the fact that there were foreshocks before the main one and people were expecting another earthquake.

2.1.12 The earthquake of August 27, 1942

The city of Peshkopi and nearby villages were be hit by the earthquake of August 27, 1942. The earthquake started at 06:14 GTM and had a magnitude M_s= 6.0. Although it lasted only 4 seconds, there were observed serious damages in buildings and people. It is reported that 80% of the houses in these areas were collapsed. The number of buildings remained uninhabitable reached to 220. The Maqellar mosque was also damaged, and its minaret collapsed immediately during the earthquake. There were great losses in people as well. According to information at the time, the number of death people reached to 44 and 119 were injured.

Other damages were also registered in Skopje, Macedonia. Earth was cracked around 15-20 cm in the areas of Vojnik and Tren where their length corresponds to 200 m and 400 m respectively. The maximum intensity of this earthquake must have been 8-9 "ballë" located at (41.65N 20.45E). The earthquake of August 17, 1942 was followed by several aftershocks.

2.1.13 The earthquake of September 1, 1959

On September 1, 1959 at 11:37 (GTM) an earthquake with magnitude M_s = 6.2 stroke the villages near Ura e Kuçit located in Lushnjë, and cities of Lushnjë, Fier, Rrogozhinë, Peqin, Kuçovë, Berat etc. The consequences were massive. All houses built in the region

of Karbunara, located in Lushnjë, were damaged, many of which were built carefully and in a professional way. In the area of Karbunara e vogël 32 houses were collapsed, 44 heavily damaged and around 15 of them had minor damages. In Karbunara e madhe many houses were affected seriously by the earthquake, out of which 26 collapsed, 17 heavily and 23 slightly damaged. In Lushnja city, 693 houses were damaged, 51 collapsed, 407 heavily damaged and the rest slightly damaged. Among many buildings damaged, the school of Lushnja and the building of the committee was collapsed. Furthermore, it is reported heavily damage of the mosque dome. Besides the damages counted in buildings, the earth also cracked for hundreds of meters in a width of 20-25 cm. Underground water came to the ground surface mixed with sand.

Many foreshocks took place before the September 1, 1959 earthquake such as the one of August, 17 (M_s=5.8) which didn't cause too many consequences in the city of Lushnjë. After the September 1, 1959 earthquake, many aftershocks followed the main shock with magnitude less than M_s=5.5.

2.1.14 The earthquake of May 26, 1960

The earthquake of May 26, 1960 occurred early morning at 05:10 (GTM) in the region of Korça. The main shock had a magnitude of Ms=6.4, intensity I=8-9 ballë and caused many serious damages in the city of Korça and villages nearby. Villages such as Lavdari, Vithkuq and Voskopojë were heavily damaged. The earthquake also killed 7 people while 127 others were injured. The number of damaged buildings in Korca reached in 1479, of which 103 were damaged so severely that they had to be built from the beginning. Another 878 were seriously damaged, 470 had moderate damages and the rest slightly damages. The electricity network and water supply were also damaged. From numerous damages, the number of uninhabitable buildings reached 25%. The main shock also caused damages in the cities of Pogradec, Erseke, Permet and Konica in Greece. The May 26, 1960 earthquake was also followed by many aftershocks in the upcoming days.

2.1.15 The earthquake of March 18, 1962

On March 18, 1962, the city of Fier and the surrounding villages were damaged by an earthquake with magnitude Ms = 6.0 and intensity I = 8 "Ballë". The earthquake started at 15:30 (GMT) and its epicenter was near city of Fier and Rëra village at coordinated 40.4°N, 19.36°E.

More consequences occurred in other cities such as Vlora, Tepelena, Berat and Lushnje. In Fier, the earthquake caused 5 deaths and 77 others were injured. Also, there are reported several damages in material properties. 2700 houses were severely damaged, from which about 1000 of them remain uninhabitable. The water supply and the electricity network in Fier were also damaged together with 66 houses that collapsed from which 12 of them were completely demolished, nothing was left of them. Subsequently 121 houses were severely damaged and another 194 suffered minor damages. The village of Rërë was followed by cracks up to 100 meters long and up to 40 cm wide. Underground water was released in the surface mixed with sand.

There were severe damages in the surrounding regions about Vlora and Fier where 71 houses collapsed and 73 others heavily damaged. Furthermore, villages such as Molisht, Paftal, Kutalli, Krast, Buzi and Sinanaj experienced serious damages from the main shock. The March 18, 1962 earthquake had an intensity at least 8 “ballë”.

2.1.16 The earthquake of November 30, 1967

In the morning of November 30, 1967 (at 07:23 GTM), a strong earthquake with magnitude M_s = 6.6 damaged heavily the region of Dibra, Librazhd and western part of Macedonia (Sulstarova and Koçiaj, 1980; Sulstarov et. al., 2000). In the area of Dibër and Librazhd, 177 villages were seriously affected, 12 people died and 174 injured. Moreover, 6336 buildings were damaged from which 534 collapsed, 1623 had serious damages and 4179 moderate damages. More damages occurred in the region of Elbasan, Tirana,

Rrëshen, Burrel and Pogradec. Human and material losses were reported in Macedonia as well.

An interesting fact is that the earthquake caused a long crack in the surface of the ground with a width 30-50 cm passing through qafa e Përvadhës until Prodan, in Zabun. This distance is relatively 1 km long and the cracking pattern follows the shape of a zigzag but keeping the direction of North-East 40°. Also, a house was cut in half from the ground movement and the crack formed. The earthquake of November 30, 1967 seems to have released a massive energy in this area. The number of aftershocks exceeds 1200, with the largest one occurred on December 2, 1967 at 12:44 with a magnitude of M_s=5.3, intensity I=7-8 ballë and epicenter: 41.25°N, 20.35°E between region of Lunik and Përvallë.

2.1.17 The earthquake of April 15, 1979

On April 15, 1979, at 16:19 a very strong earthquake hit the Balkan region with epicenter in Adriatic Sea, near Petrovac, Montenegro. Known also as "Montenegro Earthquake", this has been one of the strongest shocks in the peninsula of Balkan during the 20th century. The magnitude of the earthquake is estimated as M_s=6.9 (Karnik, 1983). The consequences were great in both people and materials. Around 35 deaths and 382 injured people are reported whereas more than 100.000 left homeless especially in the region between Shkodër and Lezhë. The number of collapsed buildings reached to 17.122 including houses and cultural centers. This earthquake occurred after many foreshocks which started two weeks before the main shock. Aftershocks continued regularly for the following nine months. The greatest aftershock happened on May 24, 1979 with magnitude M_s=6.3.

The April 15, 1979 earthquake was followed by different physical and geological phenomena. In Shkodër and Lezhë there were observed many cracks in the ground surface, falling rocks, liquifying phenomena etc (Shehu and Dhima, 1983; Dibra, 1983).

2.1.18 The earthquake of January 9, 1988

On January 9, 1988 at 01:02 (GMT) an earthquake with magnitude M_s=5.4 hit the city of Tirana and its surrounding villages with relatively low consequences. The epicenter of this earthquake is located 10 km to southwestern part of Tirana city with a maximum intensity of VII ballë (MSK-64). Most destructed villages were Petrela and Arbana. Different authors have also highlighted the fact that the acceleration instrument recorded a horizontal component which is high and unusual: 404.8 cm/s^2. This can be explained by the fact that the instrument was almost breaking when it recorded the earthquake (Sulstarova et. al., 1989; Kociaj and Pitarka, 1990).

2.1.19 The earthquake of September 21, 2019

On Saturday of November 21, 2019, the northwestern part of Albania was hit by an earthquake with a shallow depth and moment magnitude, M_w = 5.6 (Bilgin and Hysenlliu, 2020). The main shock took place at 15:15 CET with epicenter close to the city of Durrës, as shown in Figure 3. The city of Durrës, the capital city of Albania, Tirana, and the areas between them were strongly shaken and there was panic among people. Dozens of people are reported by local medias to have been injured by being thrown from the balconies to escape the earthquake. Although close to the city of Durrës, the damages were counted especially in materials and there were no casualties in people (Freddi et. al. 2021).

The main shock was followed by several aftershocks where the strongest among them occurred a few minutes later with magnitude M_w = 5.1 of the Richter scale. The tremors of the September 21st earthquake were also felt in other areas such as Gjirokastër, Fier, Shkodër and Dibër.

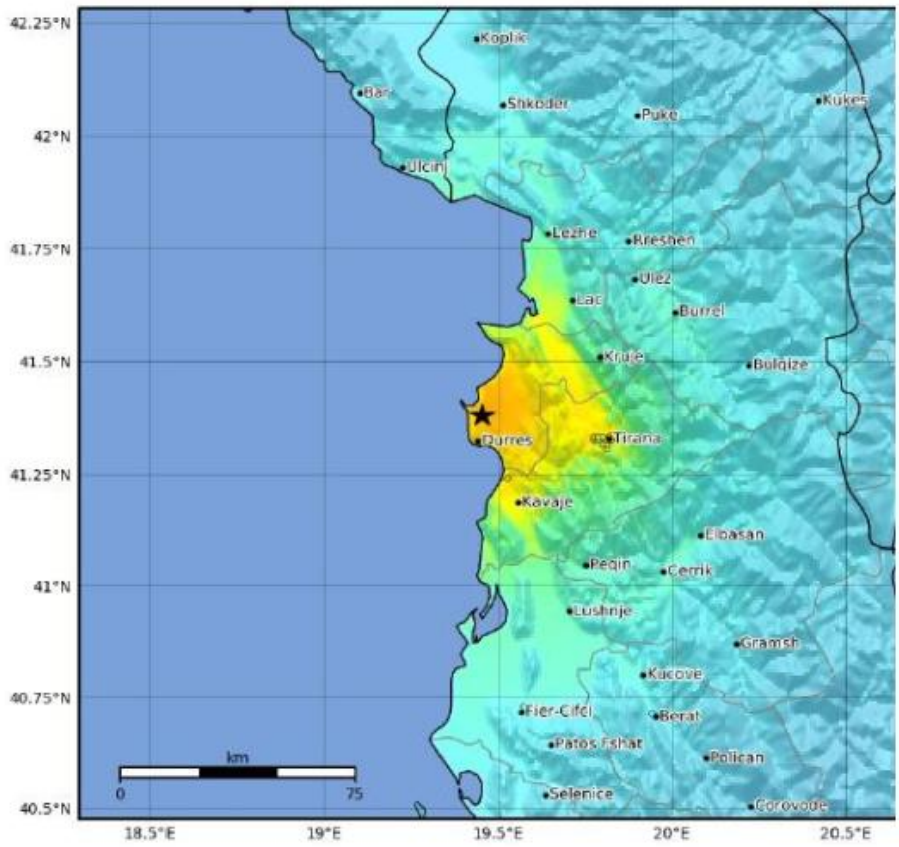

Figure 3: Epicentral locations for the September 21, 2019 Albanian earthquake (USGS, 2018).

2.1.20 The earthquake of November 26, 2019

The morning of November 26, 2019 would mark a tragic event in the history of Albania, leaving many consequences both in materials and human. At 04:54 CET, the central western part of Albania was hit by an earthquake with a 6.4 magnitude of Richter scale. The epicenter of this earthquake was located offshore of northwest city of Durrës. From the capital of Albania, Tirana, the epicenter was 7 km north and 30 km west as shown in the Figure 4. According to the information on the focal plane provided by various seismological institutes of Albania, the earthquake was activated from the northwest-southeast reverse fault.

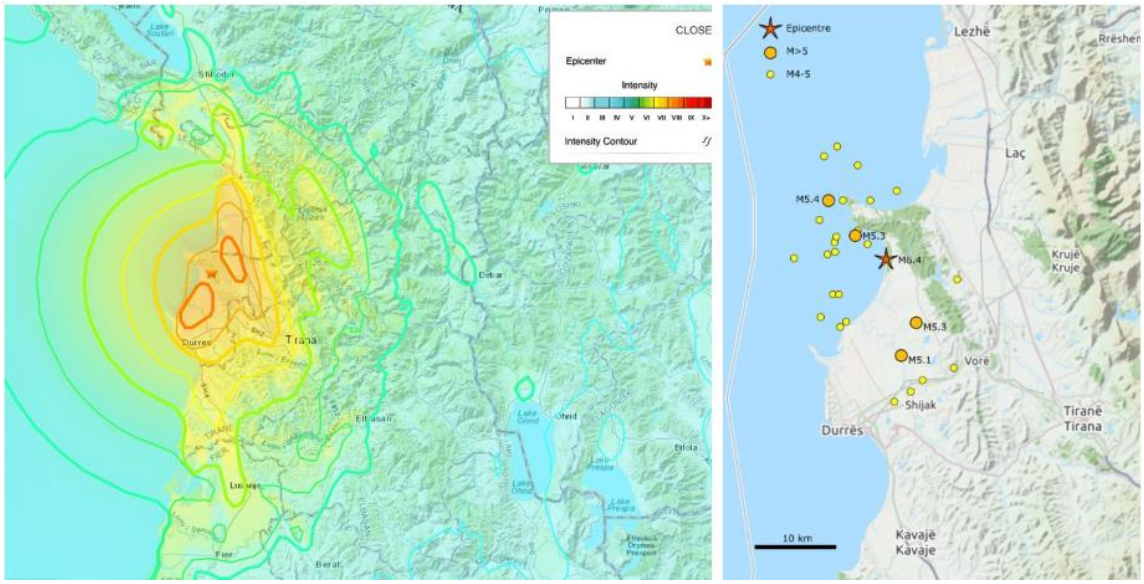

Figure 4: Location of epicenter and aftershocks in the first twenty days of the 26 November Earthquake

Besides city of Durrës and Tirana, the surrounding areas were affected seriously by the earthquake too. Regions such as Thumanë, Fushë-Krujë, Kamëz, Bubq etc. experienced the strong ground shakings of this earthquake.

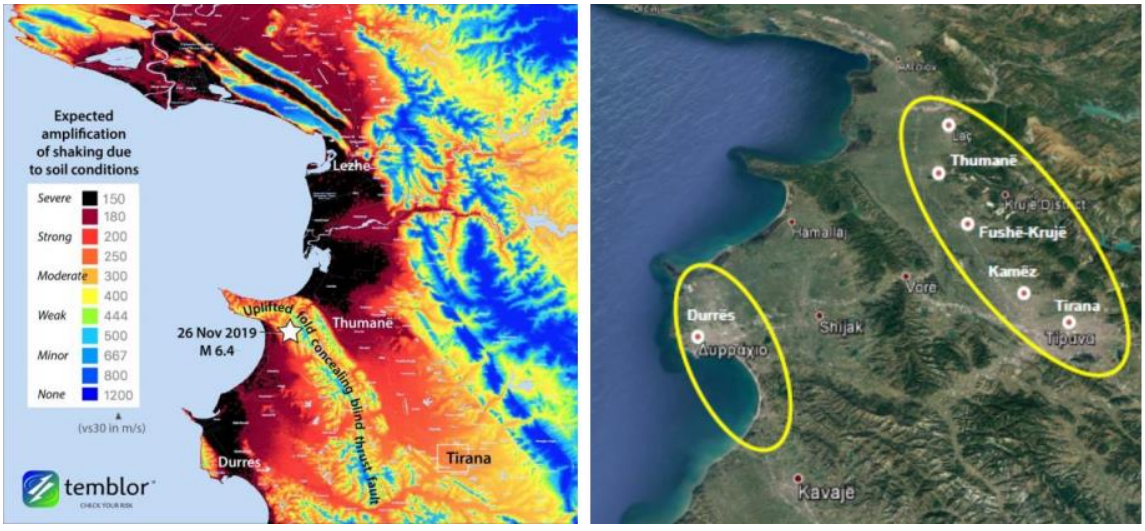

Figure 5: Earthquake-affected area during the November 26, 2019 Durres Earthquake.

As shown in Figure 5, two ellipses are formed around the most damaged zones. The main axis of these ellipses is oriented massively in northwest-southeast direction, which corresponds with the strike of seismogenic fault plane provided by the seismological institutes.

The Intensity Shake map (Mercalli) for the November 26, 2019 earthquake shown in Figure 6 demonstrates the peak ground acceleration distribution in terms of gravity acceleration percentage (INVG, 2019).

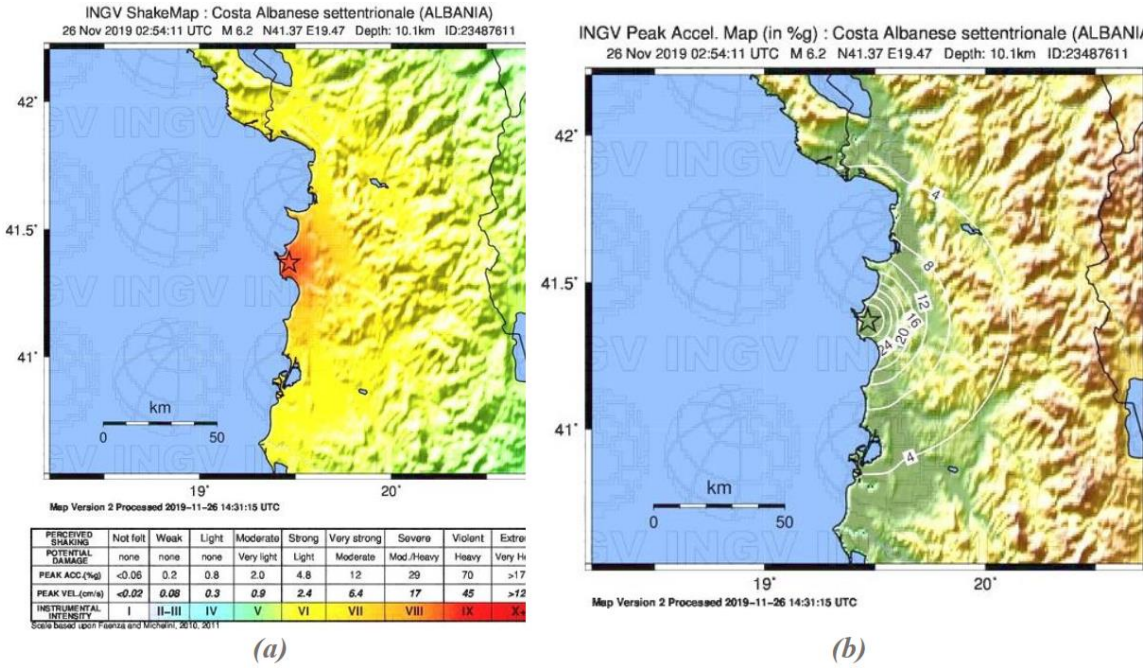

Figure 6: Intensity Shake map of the 26 November Albania Earthquake (INGV, 2019),

The Mercalli intensity scale depends on the effects observed by the viewers from a certain earthquake.

The combination of strong ground shakings with soft soil of Durrës bay and surroundings, has amplified the level of damages even more. Masonry buildings were mostly the target of this earthquake. On the other hand, old, reinforced concrete (RC) frame buildings suffered lots of damages too. Usually in this category includes the early constructed RC

buildings designed with old code provision dating to 1990. During this time, reinforced concrete buildings were constructed using hollow clay tile infills. Due to the rapid development of the country, seems the local government were not able to monitor the construction which brought weak structures with insufficient lateral-force systems. During November 26, 2019 earthquake, the comparison with recently constructed buildings and old ones is easily differentiated.

Figure 7: People observing rescues on Nov. 26 Albania earthquake – asked to remain quiet and stationary so that rescuers can listen for the victims

This can be explained by the fact that code regulation of that time, did not account for such seismic hazards during the design process. **Figure 7** shows some of the consequences during November 26 while working on rescuing people lives under building ruins.

2.1.21 Seismo-active faults in the region

Active faults represent the weakness of a zone which opens periodically and generates earthquake. Therefore, the proper identification of the active fault plays a crucial role in the seismotectonic analysis. According to previous studies, the epicenter of earthquakes in Albania is located in the active faults (Aliaj, 1988). Albanian active faults are mapped based on geological, geomorphological, and geophysical investigations. As one of the most seismic countries in Europe, Albanian earthquake occur along three seismic belts:

- The Ionian-Adriatic coastal belt, northwest to southeast extending along the eastern boundary of the Adriatic microplate,

- The Drini seismic belt (Peshkopi-Korça) inland, extending along north to south,
- Transverse belt of Elbasan-Dibër earthquakes, extending from southwest to northeast (Sulstarova et. al., 1980; Aliaj, 2003).

In the Albanian orogen there are observed two transverse and three longitudinal active fault zones as shown below:

- The Ionian-Adriatic thrust fault zone, northwest to north northwest trending,
- Shkodër-Mat-Librazhd graben fault zone, northwest trending,
- Peshkopi-Korçë graben fault zone, north-south trending,
- Shkodër-Tropojë normal fault zone, northeast trending,
- Elbasan-Dibër normal fault zone, northeast trending (Aliaj, 2000).

In addition, three longitudinal and three transverse seismoactive zones are defined in Albania based on seismotectonic synthesis (Aliaj, 1988) as shown below:

- ✓ Ionian-Adriatic longitudinal seismoactive zone,
- ✓ Shkodër-Mat-Librazhd longitudinal seismoactive zone,
- ✓ Drini longitudinal seismoactive zone,
- ✓ Shkodra-Peja transverse seismoactive zone,
- ✓ Lushnje-Elbasan-Dibër transverse seismoactive zone,
- ✓ Vlorë-Tepelenë transverse seismoactive zone

2.2 Seismic Hazard of Albania

Seismic data collection is important for a country that is constantly hit by earthquakes. In Albania, data collection has been a problem for many years. However, over the past decades, sufficient data has been collected, cataloged, and mapped. These data provide necessary information on the positioning of epicenters which are used to identify the active faults (Sulstarova et. al., 1980; Muço, 1995; Muço, 1998; Peci et. al., 2002). Furthermore, first studies were initiated as regards to the evaluation of Albanian seismic hazards. The first one is conducted in 1971 titled as "Map of seismic zonation of PR of Albania in scale 1:2,500,000". Moreover, a methodology was introduced by experts of Seismological European Commission which is use for the Albanian map and included in the European map (Sulstarova et. al., 1971). Later in 1972, a newly study "Seismic Map of PR of Albania in scale 1: 2,500,000" was considered as the basis of construction in the country. Furthermore, in 1979 the "Seismic Zonation of PSR of Albania" (Sulstarova et. al., 1980)and its representative map was approved by the Council of Ministers and used as the design of ant-seismic constructions in Albania. According to this map, the Albanian territory is divided into three main zones with intensity VIII, VII and VI degrees of MSK-64 scale considering average soil condition. Later in 1990, maps on the probability of return period of seismic intensity were produced (Kociu, 2000).

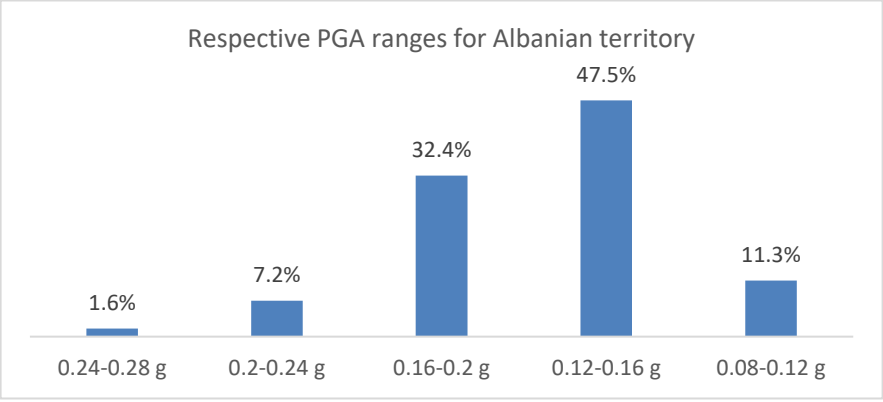

Figure 8: PGA values for different territory percentage in Albania.

Another study developed in the framework of NATO project, conducted the analysis of the seismic hazard using probabilistic approach for the country (Muço et. al., 2002; Kiratzi and Muco, 2004). The hazard calculation in this study was developed using the module OHAZ (Lapajne et. al., 1997; Poljak et. al., 2000). Figure 8 represents the range of PGA values for its respective percentage area in Albanian territory. The highest PGA values are concentrated in the Montenegro-Albanian border, in Vlora and Tepelena region and in the southwestern part of Albania (Muço et. al., 2002; Kiratzi and Muco, 2004).

2.3.1 Deterministic hazard maps

Albania has adopted the deterministic procedure developed by (Costa et. al., 1993) for the seismic zonation. Deterministic method is based on computation of synthetic seismograms generated by the modal summation technique (Panza et. al., 1996; Panza and Suhadolc, 1987; Florsch et. al., 1991; Panza et. al., 2001). The Albanian region was divided into 0.2° by 0.2° cells and for each of the cells is assigned the biggest magnitude of seismic event happened. Using the application on the centered smoothing window (Panza et. al., 1999) the maximum magnitude is calculated for each of the subdivision in association to other cells. This process is done in this way for source dimensions, catalogue incompleteness and finding the location of errors in epicentral coordinates. All seismograms are computed for a hypocentral depth of 10 km and 1 Hz cut-off frequency. In compliance with Eurocode EC8, the deterministic results are extended for higher frequencies using design response spectra and soil type A of Albanian structural models. In addition, the Design Ground Acceleration (DGA) can be determined using EC8 parameters and soil type A (Panza et. al., 1999). The design ground acceleration for Albania is in the range of 68-311 cm/sec^2. The largest DGA value (over 300 cm/sec^2) belongs to a zone in the southern part of Albania at the Greece border. The second zone covers around 80% of the country (Albania) with a DGA between 150 and 300 cm/sec^2. The third zone with a DGA from 80 to 150 cm/sec^2 covers the Albanian territory in the direction from north to south. The fourth zone covers the northernmost part of Albanian territory and has a DGA between 40 to 80 cm/sec^2.

2.3.2 Probabilistic hazard maps

In Albania is used the probabilistic seismic hazard analysis (PSHA) method for the seismic hazard calculation. This method determines the number of events per unit time, also known as frequency, with which a seismic hazard can take place (MsGuire, 2004). This probabilistic approach of seismic hazard analysis was initially proposed by Cornell (Cornell, 1968) and it can be achieved using two steps. The first step focuses on the identification of the seismic source zones whereas the second step aims to compute the calculation of the seismic effect of these sources on the surface. The elements of the modern probabilistic hazard evaluation can be grouped into four main categories as given below (McGUIRE et. al., 1993):

1. Earthquake catalogues: This category deals with the collections of information on the seismic catalogues and instruments used before 1900.
2. Characterization of the earthquake source zone: This step focuses on the identification of the seismic source zones and their seismic parameters.
3. Strong seismic ground motion: Aims the selection of the attenuation relationships to estimate the intensity of ground motion.
4. Computation of seismic hazard: Determines the annual frequency of exceedance of the ground motion intensity parameter, peak ground acceleration (PGA), velocity (PGV) or spectral acceleration (SA) for the probability analysis.

The seismic hazard evaluation for Albania was done through four basic steps as given below (Aliaj et. al., 2010):

- Earthquake catalogue
- Characterization of seismic source zones and their parameters seismic parameters
- The used Seismotectonic Model

- Seismicity Parameters.

In Albania and surrounding areas, there are defined nine seismic source zones as given below (Aliaj et. al., 2010):

- Lezhë-Ulcinj zone (LU), M_{max} = 7.2
- Peri-Adriatic Lowland zone (PL), M_{max} = 7.0
- Ionian Coast zone (IC), M_{max} = 7.0
- Ohrid-Korçë zone (KO), M_{max} = 6.9
- Elbasan-Dibër-Tetov zone (EDT), M_{max} = 6.8
- Kukës-Peshkopi zone (KP), M_{max} = 6.5
- Shkodër-Tropojë zone (ST), M_{max} = 6.5
- Pejë-Prizren zone (PP), M_{max} = 6.8
- Skopje zone (SK), M_{max} = 6.5

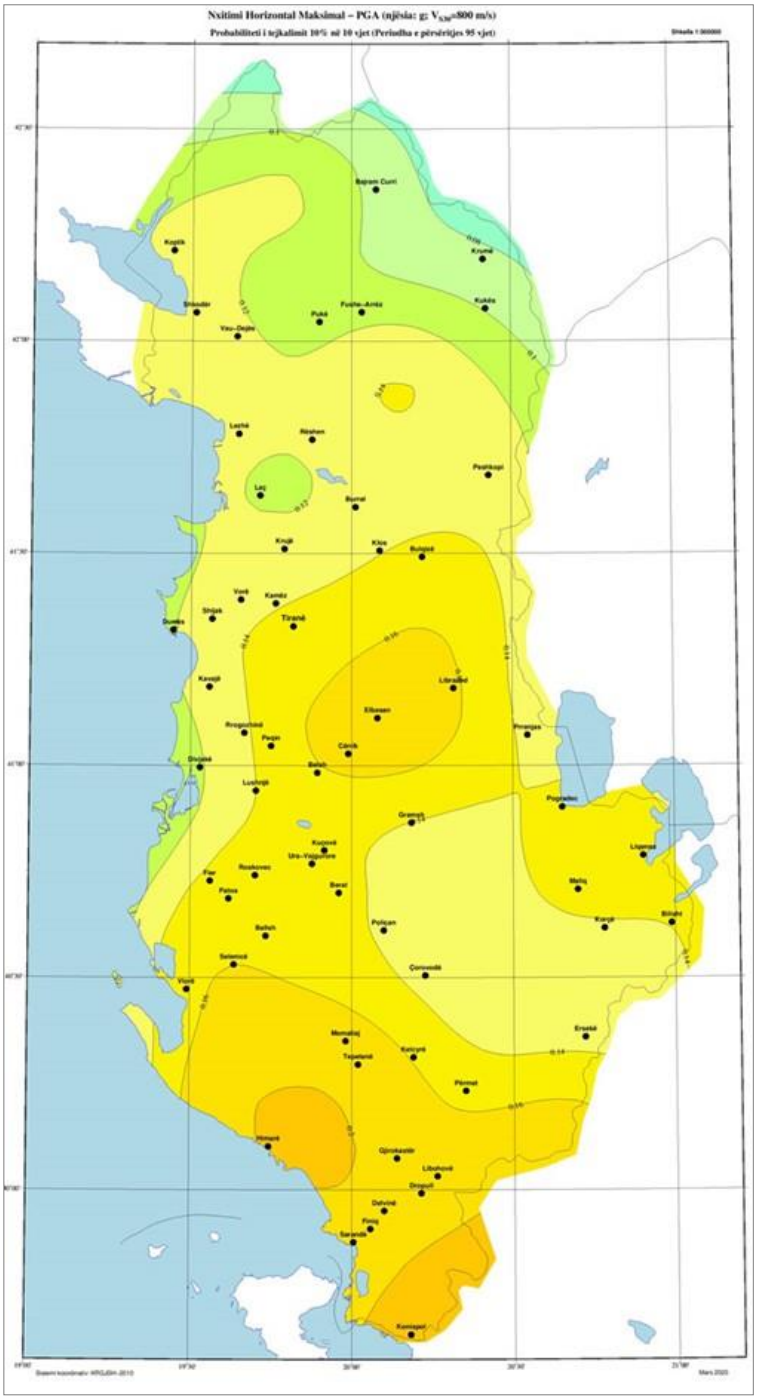

Figure 9: Probabilistic seismic hazard map for horizontal PGA, with the return period of 95 years, for hard rock conditions ($V_{s30} \geq 800$ m/sec) (NATO, 2010).

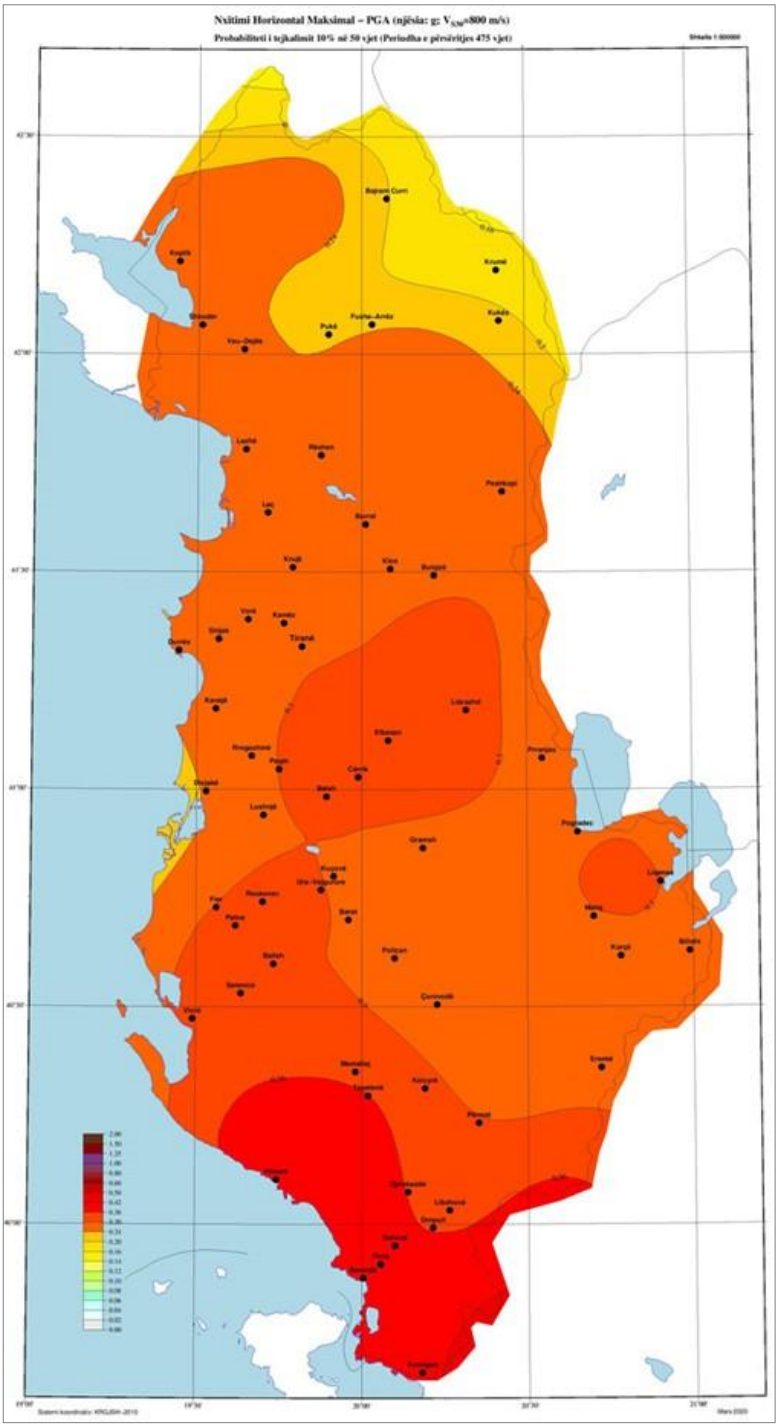

Figure 10: Probabilistic seismic hazard map for horizontal PGA, with the return period of 475 years, for hard rock conditions ($V_{s30} \geq 800$ m/sec) (NATO, 2010).

As the Albanian building code KTP-89 (KTP-2-78, 1978) uses intensity values, calculations for the seismic map of Albania are based on the same parameters. However, recent code regulations and updated ones such as Eurocode EC8 (Eurocode8, 2004) base their calculations in peak ground acceleration (PGA). The probabilistic seismic hazard maps are prepared for different return periods of the horizontal PGA. Based on the Nato SfP project (NATO, 2010), probabilistic seismic hazard maps for horizontal PGA with a return period of 95 and 475 years are prepared as shown in Figure 9 and Figure 10 respectively.

Guidelines give suggestions for the required building performance considering different return periods. For example, for a return period of 95 years, reinforced concrete (RC) buildings should perform in Life Safety (LS) limit state.

In addition, for an earthquake with PGA withing the extends of return period of 475 years, the RC buildings should satisfy Collapse Prevention (CP) limit state.

2.3 Geotechnical characteristics of Albanian territory

Aliaj has prepared a study in which the Albanian geotechnical map is developed in a scale of 1:200,000 (Aliaj, 2000). He divides the geotechnical map into three main zones based on the natural slope stability as shown in Figure 11. The first zone belongs to stable terrains. This zone covers around 56.6% of Albanian territory and is composed of strong effusive magmatic, limestones, dolomites, breccias and conglomeration of carbonate and siliceous cementation, metamorphic rocks, and schists. The second zone belongs to relatively stable zone. It is composed of conglomeratic, effusive-sedimentary, schistose, epavoric rocks and sand schists. This zone covers an area of 33.6% of Albania. The thirst and last zone belong to unstable terrains composed of different types of schists, molasses and sand-conglomerates which occupies 9.8% of Albanian territory.

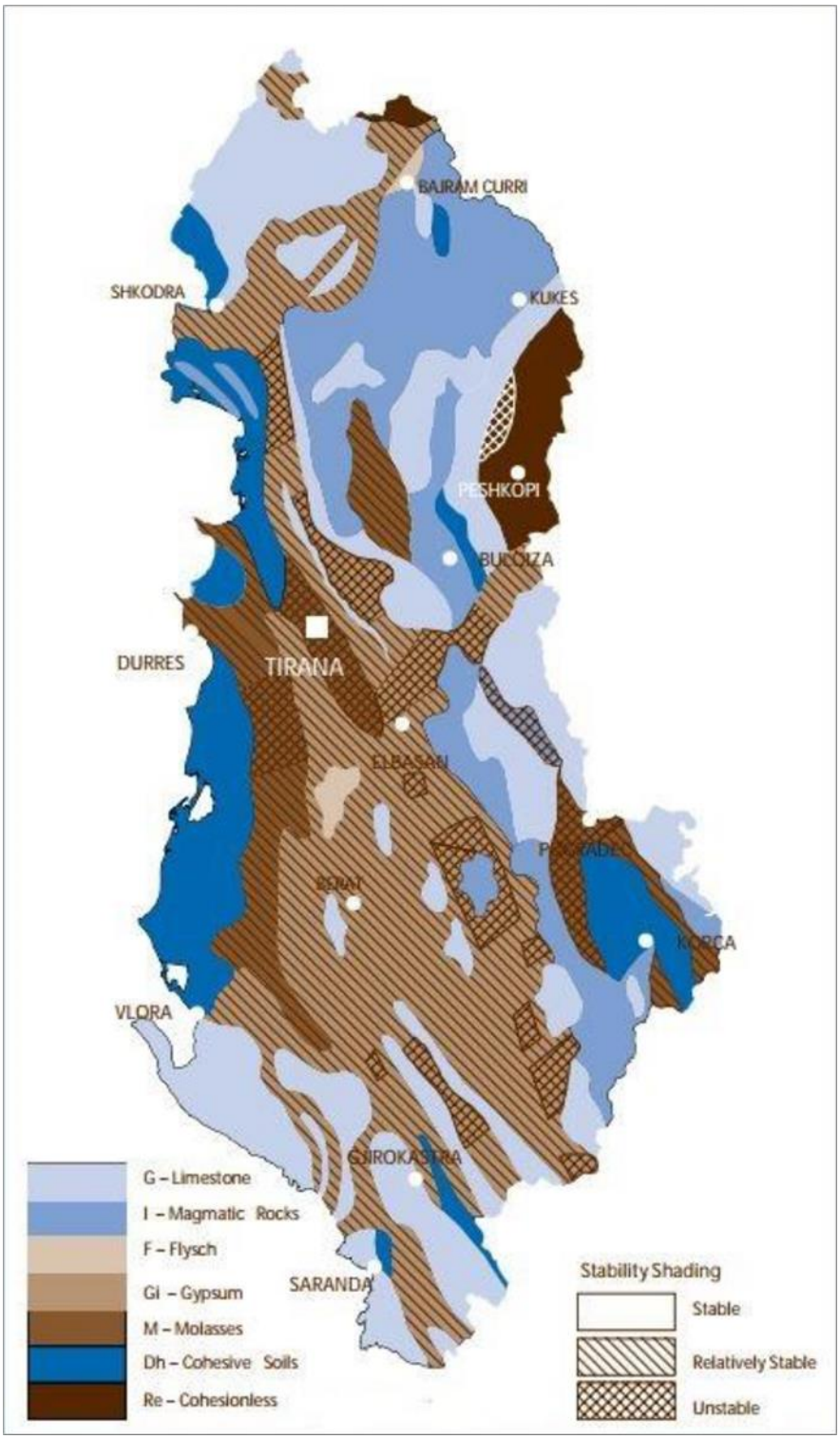

Figure 11: Geotechnical map of Albania (Aliaj, 2000)

CHAPTER 3

DAMAGE ASSESSMENT OF ALBANIAN EARTHQUAKE OF NOVEMBER 26, 2019

3.1 General

The principal function of building structures is to protect their occupants from potentially harmful environmental conditions, particularly rare but potentially destructive natural hazards. The collapse of buildings during earthquakes is a social failure to recognize and must be prevented by providing our community with a satisfactory level of earthquake resilience. This can be achieved by the realization of many steps including the acknowledgement of the seismic risk and the necessity for the preparedness for such disastrous, execution of comprehensive seismic-resistant codes for the design and construction of new buildings, identification of the hazards posed by the buildings constructed prior to the enactment of modern seismic codes providing an acceptable level of protection, and formulation of a financially liable seismic retrofitting policy that will be in line with social expectations.

Unfortunately, many of these steps were not taken in Albania prior to the November 26, 2019 Adriatic earthquake. The latest KTP-N2-89 (1989) Albanian building code, and its earlier version KTP-78 (1978) to some extent, embody the knowledge on how to design effective seismic-resistant buildings. Unfortunately, many existing buildings were not constructed in accordance with these codes, and one may think that the amount of structural damage and number of victims would have been significantly decreased had

execution been more efficient. Nevertheless, this would not have affected the thousands of buildings built prior to the enactment of efficient earthquake-resistant design rules, which would have remained seismically vulnerable.

3.2 Response of Reinforced Concrete Structures

The predominant structural system used for buildings in Albania consist of URM masonry structure until 1990s and RC frames with unreinforced masonry infills after 1990s. This structural form has been used for all building heights and occupancy. Dual systems are also used in relatively new buildings. Industrial buildings are either pre-cast/conventional RC or rarely steel framed structures. A typical RC frame building in Albania consist of a regular symmetric floor plan with rectangular of square columns and connecting beams. The exterior enclosure as well as interior partition walls are formed by non-load bearing unreinforced hollow clay tiles. These partition walls contributed substantially to the lateral stiffness of the building during the earthquake and, in many cases, controlled the lateral deformation and resisted seismically induced forces. In particular, this is true for low-to-mid-rise older buildings where the ratio of wall to floor area was relatively high, and buildings constructed on firm soil. Once the infills fails, the lateral stiffness and strength must be provided by the frames alone, which then experience significant nonlinearity in the critical locations. At this point, the capacity of the RC columns, beams, and the connections to withstand deformation demands depend on how well the earthquake design and detailing requirements were followed, both in design and construction. The observed damaged patterns to the RC buildings from this earthquake are mentioned in this section.

The region that earthquake was felt mostly was the region of Durrës and its surrounding cities. Many buildings were completely collapsed, and tens of deaths were reported. On the other hand, the rest of the affected buildings from the November 26, 2019 earthquake suffered heavy damages. Most of these buildings were evacuated due to the failure of structural elements. Therefore, the investigation of these buildings plays an important role in the study of Albanian building stock especially due to hazardous earthquakes.

Such factors as: poor concrete quality, steel corrosion, inadequate reinforcement detailing in structural elements, steel corrosion due to insufficient concrete cover were a few of the deficiencies that led to heavy damages in the buildings hit by 6.4 Mw earthquake in Albania.

Figure 12: Heavily damaged high story Reinforced Concrete building

Figure 13: Building collapsed completely

In this chapter, the failure patterns observed during the investigation of reinforced concrete building in the effected cities are categorized as shown below:

- Short column

- Insufficient reinforcement in columns and beams
- Poor concrete quality and corrosion
- Inadequate gaps between adjacent buildings
- Corner damages
- In-plane/out of plane effect

3.2.1 Short column

Short column mechanism usually develops as a reason of continuous openings located at the top or bottom of infill walls between columns as demonstrated in Figure 14. During an earthquake, the horizontal movements are converted to lateral forces in the building which are carried by columns and shear walls. In an earthquake, both tall and short column of the same cross-sectional area move horizontally with the same amount. A shorter column is stiffer than a tall column, therefore it attracts more force. By stiffness it is understood the ability of a structural element to resist deformations. Therefore, as the stiffness increases the force required to deform the element will increase too. If a short column is not properly designed to resist large forces, it can undergo major damages during an earthquake.

Figure 14: Formation of short column due to band window

(a) *(b)*

Figure 15: Typical shear failure of short columns in Reinforced Concrete buildings

Due to the openings in the infill walls of these buildings, the short column mechanism is formed resulting in accumulation of large shear forces. Usually, the damage in these short columns is in the form of X-shaped cracking as shown in the **Figure 15**a and **Figure 15**b.

Figure 16: Short column formation and in plane failure of partition walls

Figure 17: Short column formation and corrosion in reinforcement

In another reinforced concrete building, it was observed corrosion of reinforcement that connects upper beams found above the region of short columns. During earthquakes, shear

force increases especially at the column-beam connections. Therefore, special attention should be paid to the detailing of the reinforcement and its maintenance.

Damage on columns varied as a function of the column geometry and detailing. Examples in above Figures demonstrate the shear failure in short captive columns “trapped” between partial height infills or band windows.

3.2.2 Insufficient reinforcement in columns and beams

Based on most of the observations during the November 26, 2019 earthquake, a number of detailing flaws were observed in damaged buildings (**Figure 18**). This included the use of 90^{o} hooks, insufficient splice lengths, lack of anchorage of column and beam reinforcements, poor concrete quality, less than full height masonry infill walls, and the combination of many above. These deficiencies were often combined by geometric irregularities such as column-to-beam connections that induced torsion in short perpendicular stubby beams. As belongs to the design principles, the plastic hinges are the regions of the building that should not be damaged. Plastic hinges involve the joints or connects of beams and columns mostly in the reinforced concrete structures.

Figure 18: Inadequate detailing caused buckling of longitudinal reinforcement in plastic hinge regions (spacing of transverse reinforcement is indicated by thumb and index fingers as shown in the left)

A properly designed building requires to reach sufficient ductile behavior of elements. Most of the observations demonstrate insufficient reinforcement in the elements of the damaged buildings as shown in **Figure 18**.

Figure 19: Buckled rebars on a reinforced concrete column base

Reinforced concrete buildings suffered heavy damages and buckling of rebars occurred as shown in (**Figure 18** - **Figure 22**). It was observed that stirrup detailing was insufficient. Similar effects are also seen massively in the damaged buildings investigated during the November 26, 2019 earthquake. **Figure 22** a,b,c shows the inadequate application of stirrups in the structural elements. Some cases the stirrups space goes over 25 cm from each other. On the other hand, due to insufficient concrete cover and lack of maintenance, rebars were corroded completely.

Figure 20: Reinforced concrete column with no stirrups

Figure 21: Insufficient stirrups, bar buckled

Figure 22: Corroded rebars and lack of stirrups

3.2.3 Soft Story

Several residential and commercial buildings were constructed with soft stories at first floor level. These floors are mostly used as commercial areas and stores and enclosed with glass windows and sometimes with masonry infill at the back side. Masonry infill walls start immediately above the first floor. During an earthquake, building with soft stories are subjected to very high deformation demands and this puts the whole burden of energy dissipation on the 1st floor elements. A commercial building having open street façade collapsed towards that weaker direction as a result of the torsional eccentricity in its plan (**Figure 23**).

Concrete quality plays a significant role on the structural performance against earthquakes. In Albania there are many cases where handmade concrete is used, especially in the old buildings. On the other hand, workmanship service was not at the desired level resulting thus in a very low material quality. As seen in **Figure 24** the homogenic mixing was not achieved properly therefore the compressive strength of the concrete is not at the required level.

Figure 23: Reinforced concrete industrial building collapsed completely

Moreover, the concrete looks to be not bounded properly with reinforcement as indicated (**Figure 24** and **Figure 25**) with deep cracks and corroded stirrups. Besides the low quality of the concrete, the vibration process must have been not controlled accordingly. In addition, if it is observed carefully, it is seen that a piece of wood is found inside the concrete columns. All these factors conclude in a poor-quality material of the building as well as low workmanship.

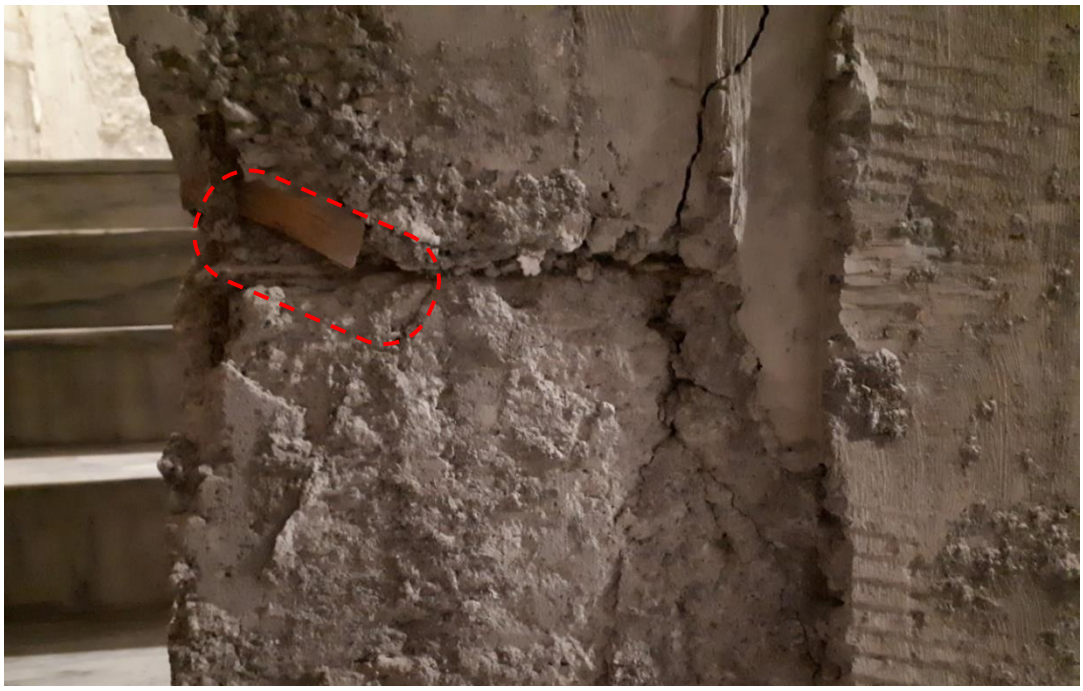

Figure 24: Poor quality of concrete, part of formwork found inside the concrete

Figure 25: Corroded rebars and damaged column

Figure 26: Column failure, corroded rebars, poor concrete

Figure 27: Damaged corner column, corroded bars

- **Inadequate gaps between adjacent buildings**

Other damages were observed in many nearby buildings due to hammering effect. It can be said that the main reason for this is the lack of minimal joint space. The building seen in **Figure 28** can be considered as one of the typical examples of the hammering/pounding effect damage seen during the investigations.

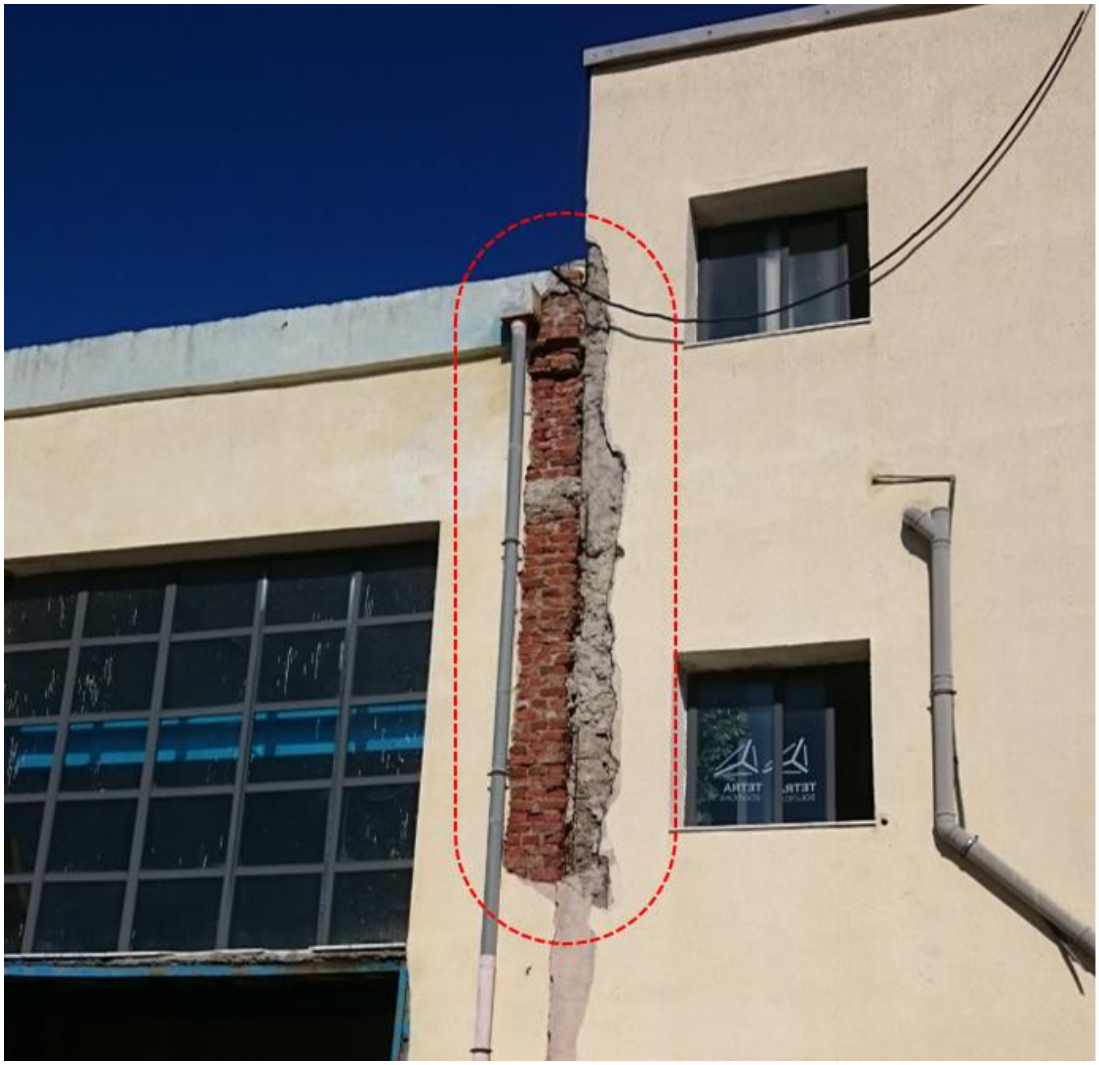

Figure 28: Pounding failure due to lack of dilatation joints

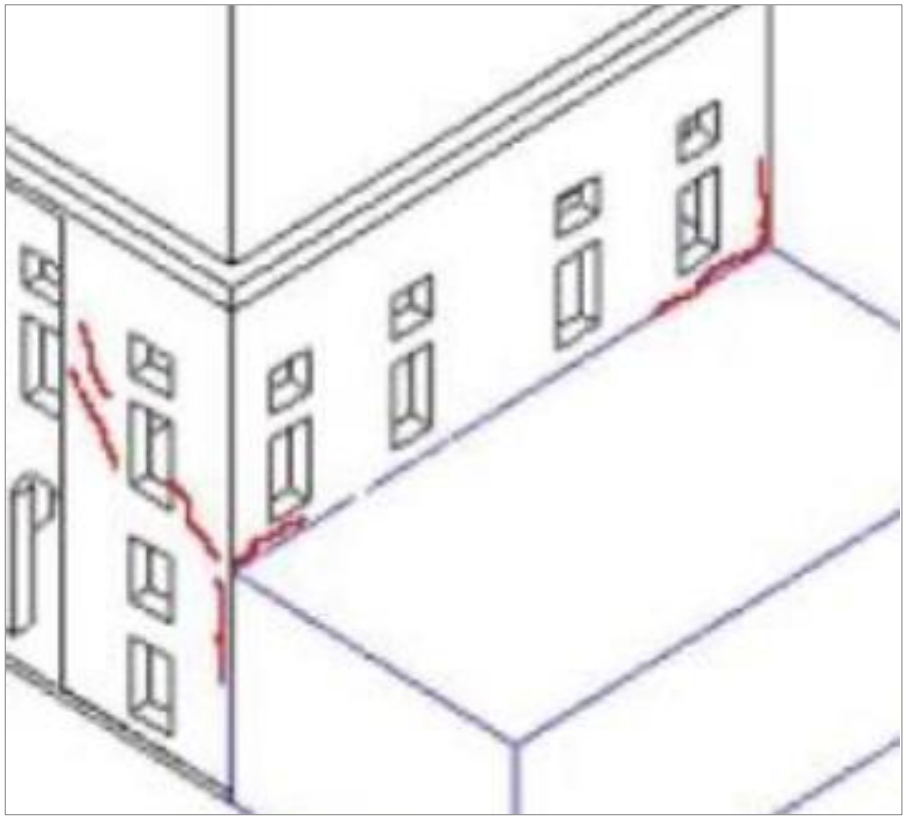

Figure 29: Schematic representation of pounding damage

Insufficient wrapping in the building, poor concrete quality, lack of strength and rigidity, detailing and workmanship defects caused a significant increase in damage.

3.2.4 Corner damages

Another damage pattern has been observed at the corners of reinforced concrete buildings during November earthquake. As shown in the figure below, the corner of the wall is heavily damaged. From the observations, seems that the overhanging beam has failed to withstand cantilever loads during the earthquake.

Figure 30: Heavy overhang and failure at the corner

There may be different factors affecting in this failure such as: increased weight, long cantilever arm, weak floors, degrading the material quality and insufficient cross-section of beams and columns. It is significant to emphasize that this failure may increase more, and major damages are expected in cases where the vertical acceleration of the earthquake is large.

3.2.5 In-plane/out of plane effect

In-plane and out-of-plane damages of masonry infill wall are widely observed in the buildings damaged during November 26 earthquake. Especially for low and mid-rise buildings it is expected that the infill walls of the ground story in the reinforced concrete frames will fail earlier. This happens as the fact that infill walls found in the ground story, obtain higher in-plane demands during an earthquake. As the in-plane demand reduces at the upper floor, the out-plane forces increase due to acceleration increases. Studies in the past have shown that this phenomenon can be prevented by increasing the capacity of in-plane walls and increasing the ductility of the out-plane nonstructural elements. At the same time, it is suggested to apply the bed-joint reinforcements and wire meshing so the infill walls will be properly connected to reinforced concrete elements. Figures below show the in-plane and out-plane damages of the investigated buildings.

Figure 31: In-plane failure of partition walls

Figure 32: Out of plane failure and heavily damaged partition walls

Figure 33: Out of plane failure of partition walls

Figure 34: Out of plane failure of partition walls

Figure 35: Heavily damaged high-rise RC building

3.3 Response of Masonry Structures

Damage to other buildings constructed by different materials was also observed throughout the affected area. For example, many URM buildings and industrial facilities were severely damaged or collapsed as a result of failures induced by several reasons including poor quality of construction, old construction age, interventions made by people, poor workmanship, the design code of the time – if ever was applied- lack of maintenance and inadequate repair after previous damaging seismic events. Damage to unreinforced masonry buildings was also very common. Buildings suffered severe shear failure of its corner wall, as a result of bi-axial seismic action. The number of such buildings was, however, small in proportion to the overall building inventory.

Unreinforced masonry structures (URM) with load-bearing masonry walls and buildings with RC framing system and infill baked clay and/or concrete walls, compose a major part of the construction in the Albanian building stock. Most of these buildings have been constructed based on the Albanian Technical Codes (KTP).

Figure 36: Heavily damaged walls on a masonry building

The URM structures with the load-bearing masonry walls suffered the most by the Durrës Earthquake due to reasons comprising old construction age, poor quality of construction, poor workmanship, interventions made by people, the design code of the time – if ever was applied- lack of maintenance and inadequate repair after previous damaging seismic events. This type experienced not only non-structural damage but also structural damage comprising partial or total collapse of the load-bearing masonry walls.

3.3.1 In-plane failure of URM

The in-plane failure pattern is observed generally in the masonry building which are affected due to shear cracks caused by shear forces developed in a wall during an earthquake. This failure mechanics develops mainly in the walls of URM buildings as well as at the connections. As the shear force increases during an earthquake, the shear stress develops inside the walls which leads to cracking. This failure is commonly observed near the openings as shown in **Figure 37**.

Figure 37: Spandrel crack above the openings (URM building)

Figure 38: Spall of mortar, shear and bending cracks

Figure 39: Shear cracks on the front façade of a masonry building

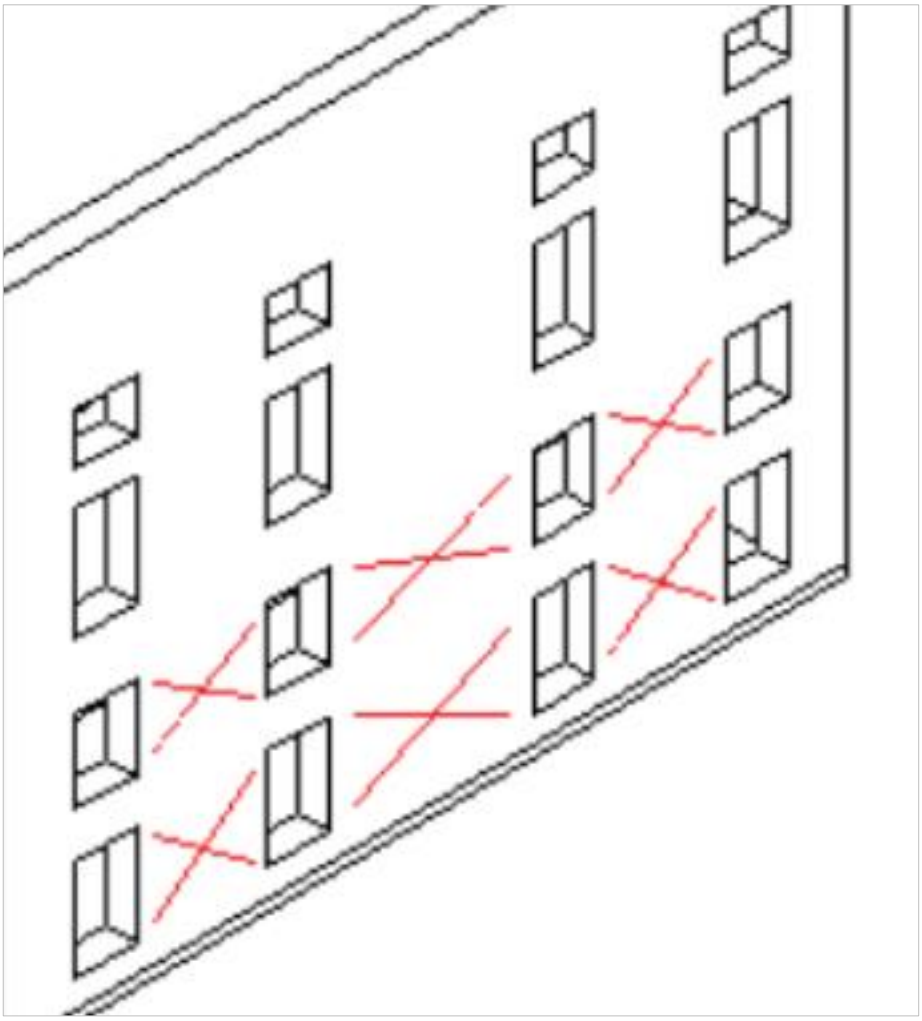

Figure 40: Schematic representation of diagonal shear cracking of piers

3.3.2 Out-plane failure of URM

Out of plane failure happens due to the increase if perpendicular forces towards the building walls. Generally, this pattern is observed when connection between walls and slabs is poor or as a lack of bond beams. Therefore, during an earthquake, these loads may lead to separation of walls from other structural elements. During the recent earthquake in our country, similar results were investigated as shown also in **Figure 41**.

Figure 41: Out of plane failure of masonry walls

3.3.3 Corner failure

Poor connection between walls or walls and roof, the lack of bond beams leads usually to the failure of corners of masonry buildings.

Figure 42: Example of residential URM buildings with cement mortar and RC floor and roof diaphragms: Formation of heavy shear cracks on the corners

Figure 43: Observed example of return wall separation

During an earthquake, as the force demand in these connections' increases, then due to lack of proper connection, poor material properties and insufficient detailing, the damage is inevitable. Some patterns of this failure are shown from the images below during the observations done after November 26 earthquake.

3.3.4 Disintegration of stone masonry

A major part of masonry walls is composed of stone walls. The large thickness of these walls is achieved by using more than one stone along the thickness of the wall. A large thickness of walls is preferred due to its good thermal insulation characteristics. However, instead of cement mortar in general mud mortar is used. Therefore, the adherence between stones is insufficient to withstand shear forces. During November 26, 2019 earthquake, the deficiencies of these walls were clearly seen from the damage patterns as shown in the figures below. The layers lost the bonding ability resulting in disintegration of stone masonry walls.

Figure 44: Disintegration in stone masonry building

Figure 45: Pier damage on a stone masonry building

3.3.5 Pier damage

The masonry piers after November 26, 2019 earthquake seems to be heavily damaged. In most of the buildings partial destruction were observed while in some others total failure of piers was observed. Poor workmanship, usage of mud mortar instead of cement mortar,

poor material quality used, insufficient detailing, were some of the reasons leed these elements to undergo deep cracks until the complete failure.

Figure 46: Heavily damaged pier of masonry building

Moreover, it is seen that a major part of the shear failure of piers in masonry buildings were attributed to the short column effect.

Figure 47: Damage due to short column and lack of maintenance

Figure 48: Shear crack on piers of a masonry school building

This failure mechanism is observed especially in building containing openings above the wall and between two piers. In this way, the accumulation of shear forces during the earthquake will be in this region. Hence these elements are not designed to undergo extensive forces and will go failure. Figures shown below are good examples of the pier damage during the Durrës earthquake.

3.3.6 Poor material quality and insufficient detailing

Different failure patterns are shown in this study for the buildings damaged during November 26, 2019 earthquake. Some of these buildings undergo slight damages with some minor cracks. In another group of buildings have been experienced severe damages in structural and nonstructural elements. Most of these deficiencies are related with poor material quality used to construct these masonry buildings. On the other hand, the workmanship was of an unprofessional degree which significantly reduced the building performance. Moreover, insufficient detailing of elements, plays a crucial role against the seismic forces during an earthquake. Such inadequacies were observed constantly while studying the condition of the damaged buildings after the earthquake. Figures below show some examples of poor material properties and insufficient detailing.

Figure 49: Poor material quality of a school damaged during November 26 earthquake

Figure 50: Damaged masonry buildings, a) spall of concrete cover of concrete from diagonal shear cracking, b) failure of the roof on adobe building, c)moderate damaged stair connection

Figure 51: Very low quality of the material used in masonry building, support failure due to improper detailing

3.4 Collapse of Durrës castle

From 111 monuments inspected by National Institute of Cultural Heritage, 23 monuments were classified as highly effected and at critical risk. Among these monuments are the castle of Durrës, castle of Kruja and the castle of Preza located in Vorë municipality.

Figure 52: Heavy damages in the fortified walls of Durrës Castle

The castle of Durrës was built during 491-518 years by Byzantine Emperor Anastasius hence turning in one of the most fortified cities on the region and broader. Later on, 1273 a hazardous earthquake destroyed the ancient walls of the Durrës castle which had to be

repaired again. Many earthquakes hit our country from that period, however the castle was strong enough to maintain its sustainability. After 750 years from its last damage, on November 26, the antient castle suffered severe damages during the earthquake due to lack of maintenance and aging. In the figures below are shown most of the partial collapse of Durrës castle tower exposing the wall cross-section and internal construction.

Figure 53: Massive destruction of the outer walls of the antient castle

Figure 54: Cultural Monument classified at high risk

3.5 Conclusion and Suggestions

Earthquakes have been considered as the Act-of-God for centuries. However, this is now recognized to be in-defensible all over the world considering the huge information that exists on how to construct earthquake-resistant design of buildings. The ignorance of the seismic threat that existed in Albania and that results in the poor implementation of existing seismic codes caused serious damage during this earthquake. The most important

lesson learned from this Adriatic earthquake is that seismic resistance is not inherent to structures that are capable of resisting gravity loads. To ensure earthquake survival and control the structural damage, lateral loads should be explicitly considered together with the ductile detailing. In this perspective, several non-ductile structures likely to suffer extensive damage in future earthquakes and become potential for enormous losses of lives and properties.

Generally, the structural performance of the buildings was not satisfactory. The main structural materials are URM composed of rubble stone, brick, and hollow clay tile. Masonry units suffered the worst damage. Several modern, non-ductile concrete frame buildings have collapsed. In RC structures, many structural deficiencies such as non-ductile detailing and poor concrete quality were commonly observed.

Several damage patterns have been recognized and presented in this report from the damages of RC and URM buildings.

In the settlements under similar earthquake risk, the necessary precautions must be taken into consideration. In an anticipated earthquake, the potential for damage of masonry buildings is high. For these kinds of buildings, a new retrofitting methodology must be proposed, which will not influence the functionality and will not disturb normal usage by the inhabitants.

To summarize, thousands of existing structures designed and constructed in accordance with earlier or no seismic codes at all, are present in seismically active areas of our country. These buildings must be properly retrofitted as soon as possible in order to prevent future loss of lives. The November 26, 2019 earthquake which happened in Durrës, is an indisputable fact of the "concept of earthquake resistant building design".

CHAPTER 4

EARTHQUAKE DESIGN CODES AND PERFORMANCE BASED SEISMIC DESIGN

4.1 General

Albania has been constantly hit by moderate to strong earthquakes since early times and continuing in the same trend nowadays. A timeline showing some of the strongest earthquake happening in our country, including also the recent earthquake of November 26, 2019, are presented in **Figure 55**. Simultaneously, the history of Albanian seismic design codes is presented. The evolution of these codes starts with the first one in 1952 until the last update in 1982. During this period, the Albanian building code is updated four times and the last one is still in use.

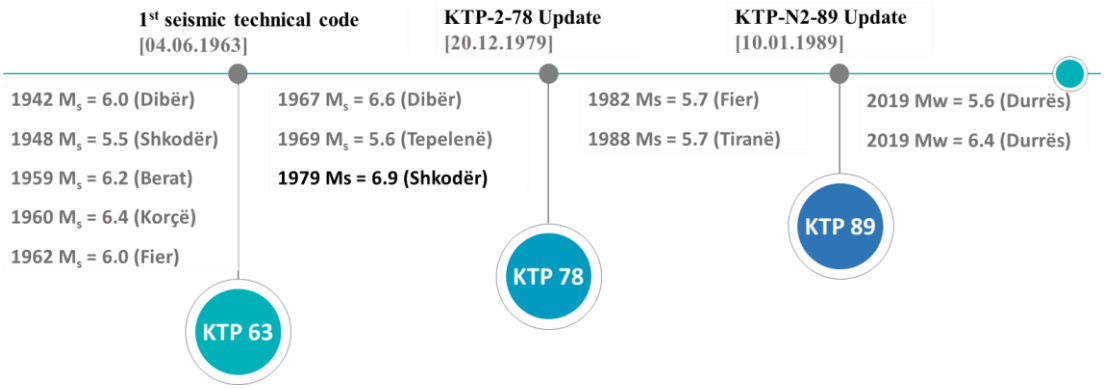

Figure 55: Timeline of seismic design codes in Albania and their evolution and updates (Baballëku and Myftaraga, 2020).

The information shown in the figure may be limited as some of the previous documentations are lost. Regardless of the missing documentations, researchers believe that there have been literatures especially from Italy in this scope such as the Italian Seismic Code (*"Norme tecniche di edilizia asismica per i paesi colpiti da terremoti"*) (Italian Seismic Code).

The first seismic map of Albania was developed in 1942 by Carlo Morelli in his material called "Carta sismica dell'Albania" as shown in **Figure 56**.

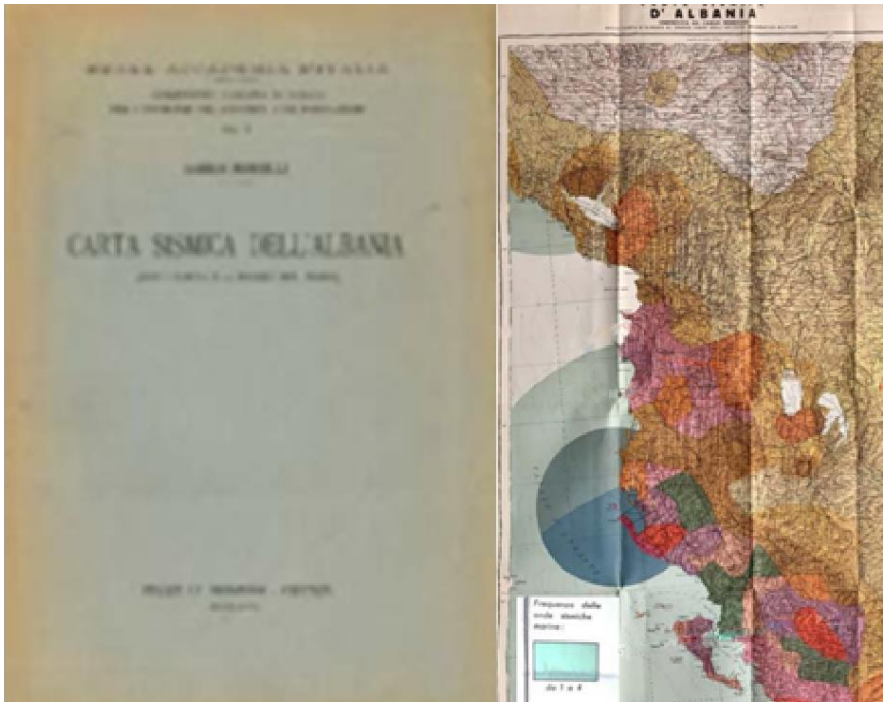

Figure 56: First seismic map of Albania published in "Carta sismica dell'Albania" in 1942

4.2 Seismic design code of 1952 (KTP-52)

The first Albanian seismic design code was introduced in 1952. The seismic code was approved on December 27th of the same year by the decision of the Council of Ministers (DCM) No. 817 and titled "Technical provisions for Seismic design of constructions" (KT-52, 1952) as shown in **Figure 57**.

Figure 57: Seismic design code of 1952 (KT-52, 1952)

The seismic intensity was expressed in terms of expected earthquake damages and accelerations. Albanian country is divided into regions with intensity 6,7 and 8. However, the KT-52 standard does not give any guidance for intensity scale 9.

Furthermore, the calculations of seismic forces are based in the formula given below:

$$S_1 = K_1 * P_1 \qquad \textbf{Equation 1}$$

Where S_1 is the seismic force to be calculated, P_1 represents the weight of the structure including dead loads (DL) and live loads (LL), and K_1 defines the seismic coefficient based on the seismic intensity of that zone. KT-52 provisions include few recommendations as regard to the load combinations of seismic forces on structure in association with other possible external forces. Furthermore, less information is also provided for the seismic load calculation of retaining walls. In KT-52 there are mentioned some rules on the expansion joints which must not be smaller than 2 cm and should applied along the height of the entire building.

4.3 Seismic design code of 1963 (KTP-63)

After the first seismic code (KT-52), on 1963 the second version was updated by the government based on the DCM No. 206. The new update was titled “Technical design code for reinforced concrete buildings – based on theory of rupture” (KTP-63, 1963).

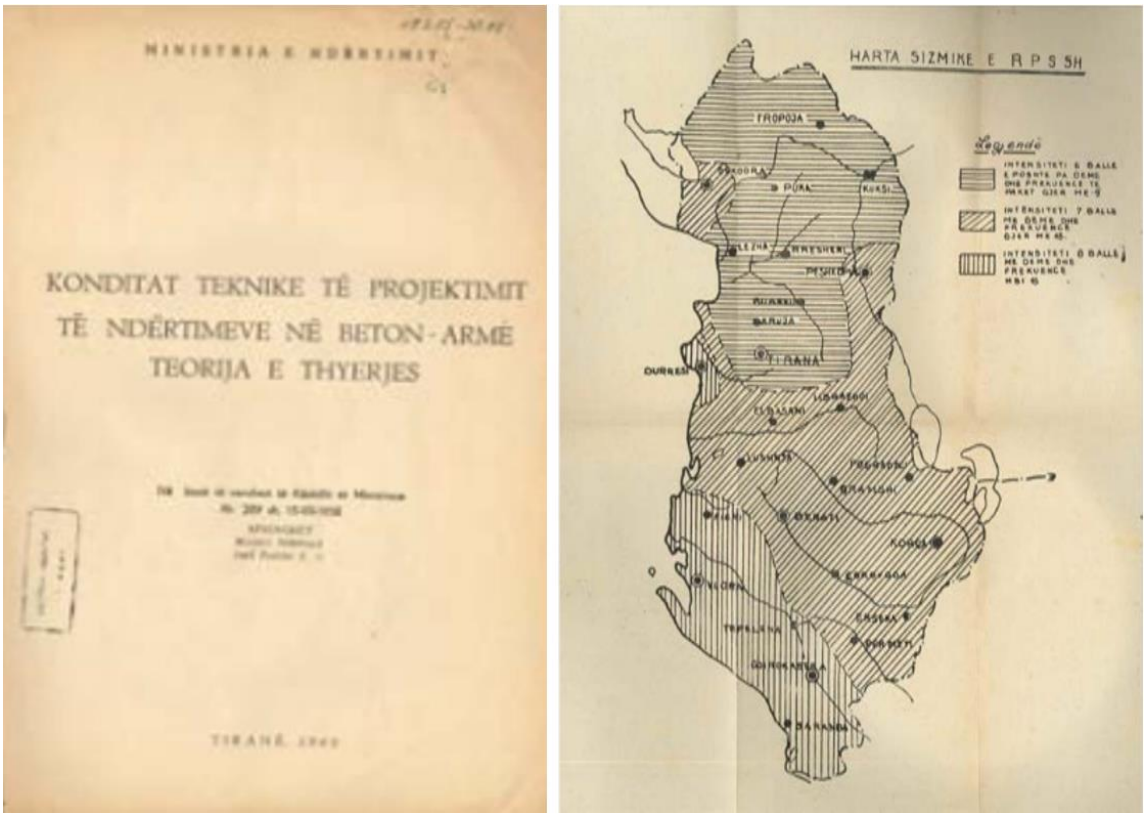

Figure 58**:** Seismic design code of 1963 (KTP-63) and seismic intensity map

As shown in **Figure** 58, the KTP-63 introduces the seismic intensity map which divides Albanian territory in regions with three intensity zones such as: 6,7 and 8. In addition, to each of the municipalities is assigned a seismic intensity. The intensity may be increased with one scale by the Technical Council of the Construction Works Ministry in case of higher importance structures.

According to this guideline, the distribution of the structural members has to be in a way, so the stiffness and mass are uniformly distributed. Also, the geometrical shape of the plan must be configured carefully so the symmetry is maintained in both directions whereas the center of gravity of the entire building must be close to the center of rigidity.

Furthermore, the plastic hinges must be predicted in the case of reinforced concrete building design to increase the resistance of the structure against seismic forces. In addition, the formula for seismic force calculation was updated as shown below:

$$S_k = K_c * \beta * \eta_k * Q_k \qquad \textbf{Equation 2}$$

Where S_k stands for the seismic force, Q_k considers the loads which initiate the inertia forces such as: self-weight, dead load, live load, snow load etc., K_c includes the seismic coefficient, η_k considers the coefficient which is affected by the mode shape of the building and β defines the dynamic coefficient which depends on the period of the structure.

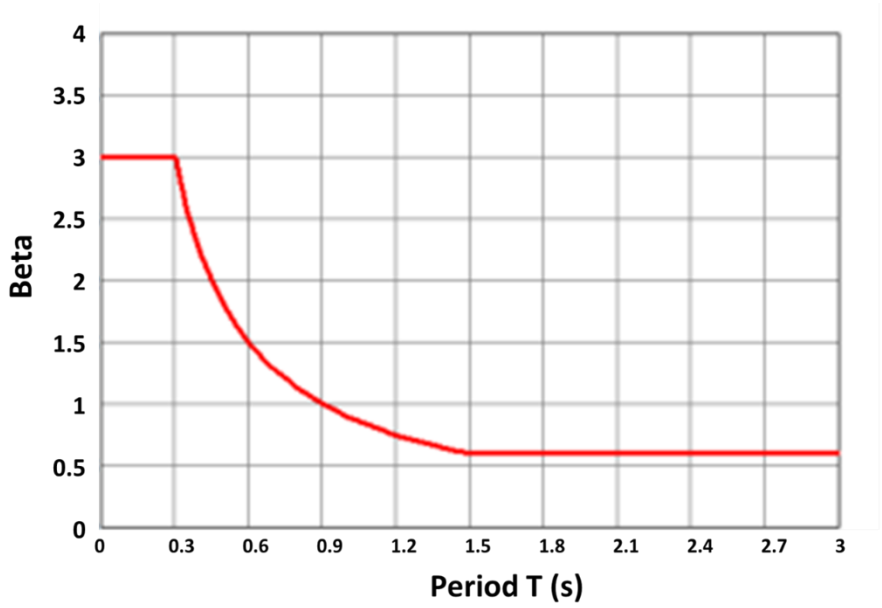

Figure 59: β -coefficients for a period up to 3 seconds (T = 3s)

Therefore, this coefficient is considered by the ratio of 0.9/T where T is the period of the structure. For the calculation of β coefficient, KTP-63 suggest considering the chart given in **Figure 59**.

KTP-63 suggests that for reinforced concrete buildings, the first and fundamental mode of vibration should be considered in calculations. Nevertheless, for structures with higher period such as chimneys, towers etc., the vibrations modes to be taken into account may go until the 3rd one.

As regards to the load combinations, the seismic design code does not consider the wind forces. Live loads are multiplied by 0.8 whereas the forces coming from furniture are not taken into account. Load calculations are based especially in the seismic forces and self-weight of the structure.

4.4 Seismic design code 1978 (KTP-2-78)

The next version of the Albanian seismic design (KTP-2-78, 1978) was released in 1978 as an update of KTP-63 as shown in **Figure 60**. Generally, this guideline was adopting design codes from Russian technical codes but there were almost no changes compared with its previous version, KTP-63 (Baballëku and Myftaraga, 2020). Hence, the load combinations remain the same, the live load factor is used 0.8 and seismic joint recommendations are repeated from the KTP-63. Nevertheless, while designing for seismic actions, following principles must be fulfilled:

- adequate resistance distribution,
- adequate distribution of the structural mass and stiffness,
- designing for the most favorable mechanism during plastic deformations,
- designing for stability even after the partial collapse of the structure.

Figure 60: Seismic design code of 1978 (KTP-2-78)

Nonetheless, the updated version would need to be improved in 1981 and republished again in 1982 after the severe damages caused by the earthquake of April 15, 1979. The new version was released from the decision of council of ministers (DCM No. 371) considering the seismic intensity from the new improved map, the ground types and importance of construction works. The ground types are categorized into three main types. Buildings are also categorized into three categories based on their type and importance. As belongs to the seismic design criteria, the only parameter changing in the new version of KTP-2-78 was the formula of seismic load calculations which considers the live load with coefficient 1.5 as given below:

$$S_k = K_c * \beta * \eta_k * 1.5 * Q_k \qquad \textbf{Equation 3}$$

4.5 Seismic design code 1989 (KTP-N2-89)

The last Albanian seismic design code was released in 1989 titled "Technical design code for seismic resistance" (KTP-2-78, 1978) as shown in **Figure 61**. The KTP-N.2-89 represents a massive upgrade from the previous versions of design codes. The detailing of reinforced concrete elements considering seismic effects is included in the material. In addition, the seismic microzonation maps prepared from 1984 until 1991 are included in the code. Intensity was assessed based on the microzonation map and importance class. On the other hand, the intensity of sites without any micro zonation defined, are taken from the overall seismic map, ground type and important class of construction works.

Furthermore, KTP-N.2-89 describes in detail the structural uniformity by considering different terms such as geometrical shape of the building, description of the structural members, construction materials as well as plastic hinge mechanisms.

The design method in KTP-N.2-89 is based on the spectral analysis using a well-defined design response spectrum. Furthermore, a simplified analysis is considered using the fundamental period and 1st mode shape by the empirical formula given below:

$$\mathbf{S_a = k_E * k_r * \psi * \beta * g} \qquad \textbf{Equation 4}$$

Where the S_a is the spectral acceleration of the horizontal seismic component, k_E is the seismic coefficient and it's values are shown in **Table 2**, k_r is the importance coefficient of the building type as given in

Table 4, ψ is the structural behavior coefficient under seismic loading and its values are shown in **Table 3**, β is the dynamic coefficient which takes values based on the calculations of the structural period as shown in **Figure 62**, g is the acceleration of earth gravity.

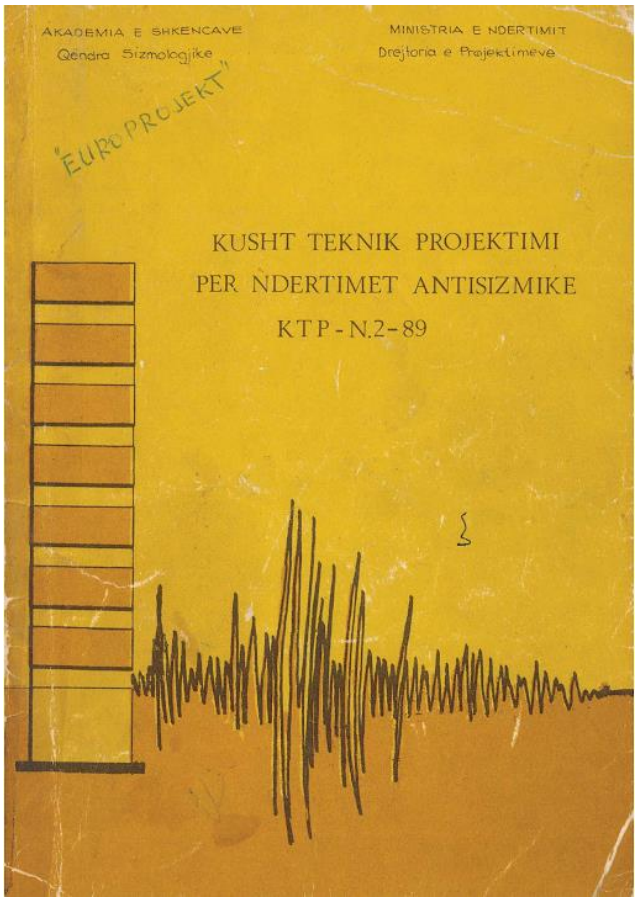

Figure 61: Seismic design code of 1989 (KTP-N.2-89)

From 1990 there has been no update in the Albanian design code and KTP-N2-89 is still in use nowadays. However, the adoption of Eurocodes has been introduced in an Albanian material initially in 2012.

Table 2: Values of the seismic coefficient k_E given in KTP-N.2-89

Soil Category	Seismic Intensity (MSK-64)		
	VII	VIII	IX
I	0.08	0.16	0.27
II	0.11	0.22	0.36
III	0.14	0.26	0.42

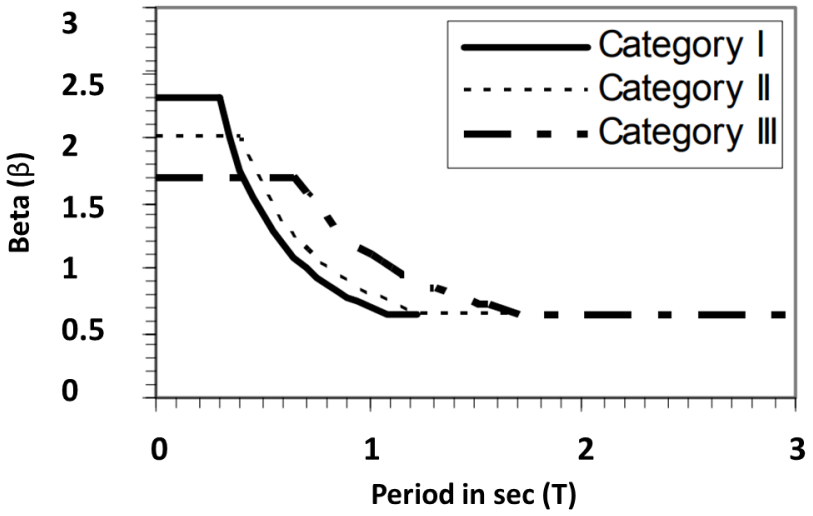

Figure 62: Values of dynamic coefficient $\beta_{(T)}$ given in KTP-N.2-89 (Kuka, 2004)

Table 3: Values of structural coefficient (ψ) given in KTP-N.2-89

Nr	**Type of structural system**	**Structural coefficient ψ**
1	Steel framed	0.20
2	RC structures with brick masonry infilling walls not participating in seismic force resistance	
	$\frac{h}{b} \leq 15$	0.25
	$\frac{h}{b} \leq 25$	0.38
	$15 < \frac{h}{b} < 15$	By interpolation

where:

h- column height.
b - the dimension of the cross section of column, parallel to the direction of seismic force.

3	RC framed structures with brick masonry infilling walls participating in seismic force resistance	0.30
4	Frame-shear wall structures	0.28
5	Cast-in-place or prefabricated large panel RC structures.	0.30
6	Brick masonry structures without reinforced columns.	0.45
7	Brick masonry structures with reinforced columns.	0.38
8	Tall structures such as chimneys, mats, towers, and others	
	a) steel	0.30
	b) reinforced concrete	0.40
	c) brick masonry	0.45
9	Silos, bunkers, tanks and other similar structures:	
	a) steel	0.20
	b) reinforced concrete	0.25
10	Bridges and other types of transportation structures	
	a) with reinforce concrete understructure	0.20
	b) with partially or completely concrete understructure	0.28

11	Retaining walls:	
	a) reinforced concrete	0.25
	b) concrete and stone	0.28
12	Underground structures	0.25
13	Hydrotechnical structures:	
	▪ earth fill dams and rock fill dams	0.25
	▪ concrete and reinforce concrete	0.35
14	Other types of hydrotechnical structures:	0.35

Table 4: Values of importance coefficient (k_r) given in KTP-N.2-89

Category	**Description of building and structures**	**Importance coefficient k_r**
I	Buildings and Structures of Extraordinary Importance	
	a) Buildings and structures where small damage may cause catastrophic damage like: poisoning of the population, fire explosions, explosions, etc.	4.00
	b) Buildings and structures of a very big economic or strategic importance.	1.75
	c) Buildings and structures where the interruption of the technological process is not allowed.	1.50

II	Buildings and Structures of Special Importance	
	a) Buildings and structures which have a special importance for post earthquake recovery, like: telecommunication network, fire stations, big hospitals, big flour factories etc.	1.50
	b) Buildings and structures whose damage may cause big causalities, like: schools, nursery schools, kindergarten, cinema, stadiums, hotels, and other objects like these where there are big concentration of peoples.	1.30
	c) Buildings and structures whose damage may cause serious losses for the economy.	1.20
	d) Buildings and structures of special cultural and monumental value.	1.20
III	Buildings and Structures of Ordinary Importance Buildings and structures that are not included in other categories, like: residential buildings, different institutions, like: museums, libraries, hotels, schools, cinemas, etc., different factories and plants, big warehouses, engineering structures like: retaining walls, water towers and others.	1.00
IV	Buildings and Structures of Secondary Importance Buildings and structures whose damage does not cause big losses of human life or intenuption of technological process.	0.50
V	Temporary Buildings and Structures	No calculation is needed

	Buildings and structures whose collapse do not risk the people's life.

4.6 Basic principles of Performance-Based assessment

There are different nonlinear analyses procedures used to determine the performance points for reinforced concrete structures. The well-known methods used in today's literature are Capacity Spectrum Method (CSM) detailed in ATC-40 (ATC-40, 1996) and the displacement coefficient method (Eurocode8, 2004; FEMA-273, 1997). Furthermore, the Performance Based Earthquake Engineering (PBEE) was developed as a new and fast-growing concept. The main target of PBEE is to design the building so it satisfies the performance objectives during the severe earthquake shakings following various analysis procedures. Recently a new method was developed in compliance with the PBEE requirements known as Incremental Dynamic Analysis (IDA) (Vamvatsikos and Cornell, 2002). IDA is known as a suitable repetitive nonlinear dynamic analysis procedure which uses a suite of ground motion records to conduct the massive analysis and finally generate IDA curves. Furthermore, IDA curves are summarized into 16%, 50% and 84% fractiles (Fragiadakis and Vamvatsikos, 2011). In addition, limit states are defined for the 50% fractile (IDA median) which can be used to evaluate the structural performance of selected buildings.

In this study, the Capacity Spectrum Method (CSM) and Incremental Dynamic Analysis evaluation procedures are used to conduct the seismic performance assessment of the selected template reinforced concrete buildings.

4.6.1 Damage Limit States in Capacity Curve

In recent codes such as FEMA 356, Eurocode 8 etc., there are presented three main boundaries as regards to the structural behavior from initial stage until collapse. These boundaries are known in different guidelines as limit states.

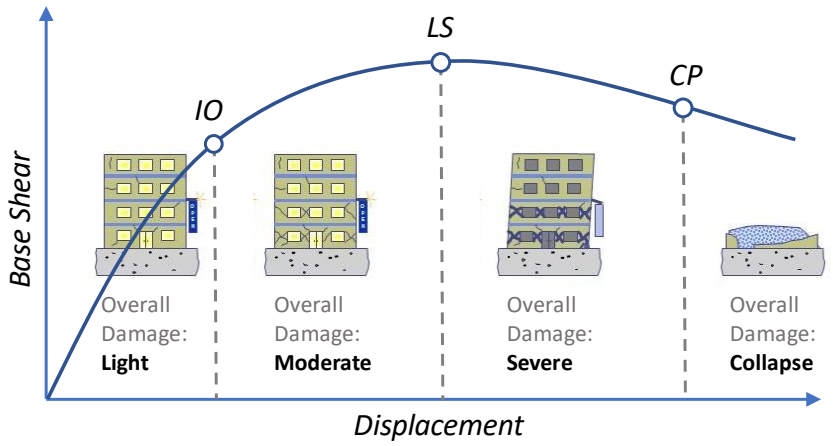

Figure 63: Immediate Occupancy, Life Safety, Collapse Prevention limit states

FEMA 356, Eurocode 8 etc., suggest that structural performance should be assessed using Immediate Occupancy (IO), Life Safety (LS) and Collapse Prevention (CP) limit states. In the IO level, building remains safe to be occupied. The damages are minor and usually this boundary defines the uppermost point of elastic region in the pushover curve as shown in **Figure 63**.

The second limit state, LS, must be designed to achieve a structural stability and reserve more capacity after the external forces is removed. The hazardous nonstructural damage is controlled in this level. Whereas the CP limit state must be considered so the building remains uncollapsed but at critical level. Major damages can be subjected to this boundary. After the collapse prevention limit state, the building is supposed to be collapsed totally.

4.6.2 Building Earthquake Performance Levels

The damage control for building performance levels is well defined in FEMA 356 guidelines for all structure types. In particular for reinforced concrete frames, the guideline approves certain rules for vertical elements as given in **Table 5**.

Table 5: Structural Performance Levels and Damages for vertical and horizontal elements (FEMA 356)

Element	Type	Immediate Occupancy (IO)	Life Safety (LS)	Collapse Prevention (CP)
Concrete Frames	Primary	Minor hairline cracking. Limited yielding possible at a few locations. No crushing (strains below 0.003).	Extensive damage to beams. Spalling of cover and shear cracking (<1/8" width) for ductile columns. Minor spalling in nonductile columns. Joint cracks <1/8" wide.	Extensive cracking and hinge formation in ductile elements. Limited cracking and/or splice failure in some nonductile columns. Severe damage in short columns.
	Secondary	Minor spalling in a few places in ductile columns and beams. Flexural cracking in beams and columns. Shear cracking in joints <1/16" width.	Extensive cracking and hinge formation in ductile elements. Limited cracking and/or splice failure in some nonductile columns. Severe damage in short columns.	Extensive spalling in columns (limited shortening) and beams. Severe joint damage. Some reinforcing buckled.
	Drift	4% transient or permanent	2% transient; 1% permanent	1% transient; negligible permanent
Concrete Diaphragms		Distributed hairline cracking. Some minor cracks of larger size (<1/8" width).	Extensive cracking (<1/4" width). Local crushing and spalling.	Extensive crushing and observable offset across many cracks.

The building performance levels for the selected templates in this study will be determined directly in the pushover curve. The software selected to conduct the analysis (Zeus NL) does not provide an automated way for determining the plastic hinge formations in the structural elements. Therefore, a direct assignment of performance levels in pushover curve will be done.

The immediate occupancy (IO) level is defined at the end of the elastic curve of pushover. Furthermore, the limit states have been defined as the middle point from IO to CP based on different studies and research. Whereas for the CP limit states a useful guideline will be followed based on previous studies (Rejec and Fajfar, 2014). Authors have presented a simple and practical procedure to define the CP point directly in the capacity curve. They suggest considering a 20% drop of the maximum base shear force for the collapse prevention region as shown in the graph below:

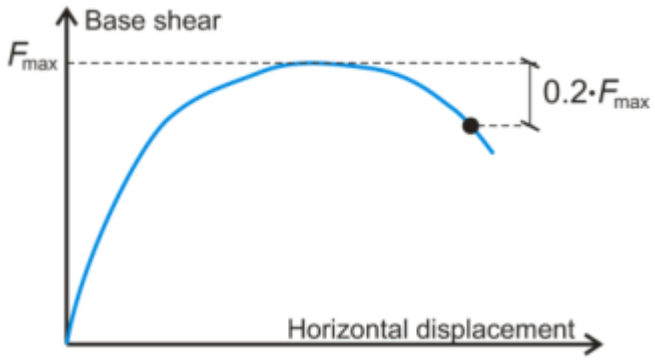

Figure 64: Defining of collapse prevention (CP) limit state at structural level (Rejec and Fajfar, 2014).

4.6.3 Earthquake ground motion

Seismic resistant design of buildings must have in priority the safety of lives and avoidance of structural collapse. The most widespread approach to achieve this goal is to design the structures with a large ductility capacity so it is able to resist earthquake shakings and withstand the large inelastic deformations, hence decreasing the probability to collapse. On the other hand, the earthquake occurrence frequency is a part of seismic design guidelines which must be considered according to the target performance level (Tsompanakis, 2014). There are three main earthquake levels for which a return period is specified during the design stage or performance assessment.

- **Serviceability earthquake** refers the earthquakes whose return period is 72 years and probability of exceedance 50% in 50 years.
- **Design earthquake** has a return period of 475 years with the probability of exceedance of 10% in 50 years
- **Maximum/Ultimate earthquake** is an earthquake whose return period happens in 2475 years and has a probability of exceedance 2% in 50 years (FEMA-750, 2009).

4.6.4 Performance targets

The performance-based design defines different levels of the structural damages during a seismic action. The prediction of the structural performance due to earthquake loadings is defined as performance target. Different levels for the performance design and seismic actions are given in **Figure 65** (FEMA-356, 2000).

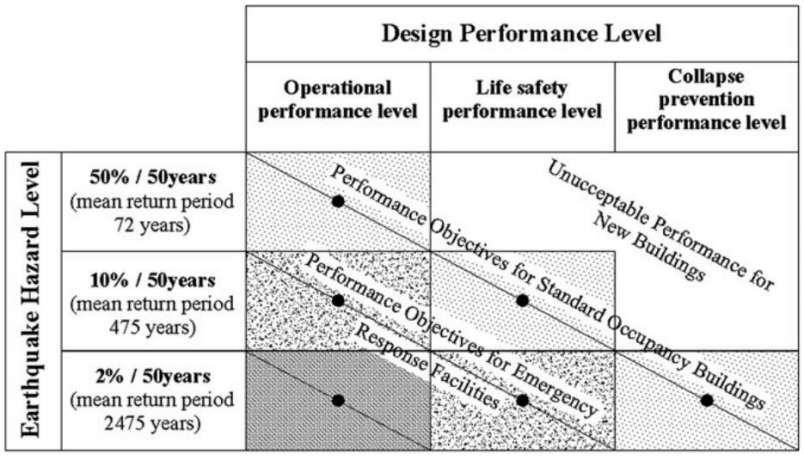

Figure 65: Different performance levels at several seismic intensity targets

4.6.5 Determination of the seismic capacity and demand

The seismic capacity and demand are calculated based on the ATC-40 guideline (ATC-40, 1996). To generate the capacity curves for each of the template buildings selected in

this study, static nonlinear (Pushover) analysis is utilized. The data gathered from the software is plotted initially in a 2D graph representing the base shear in vertical axis and global drift in the horizontal axis as shown in **Figure 66**.

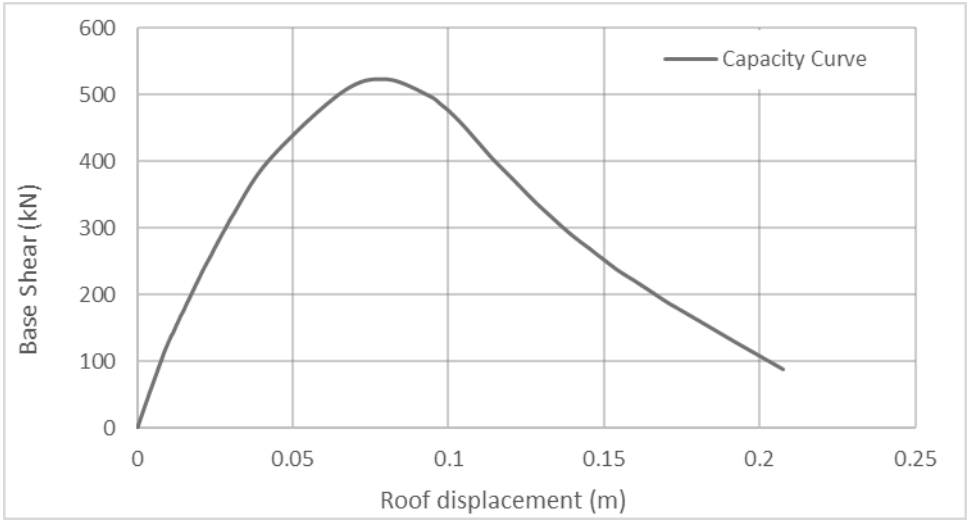

Figure 66: An example capacity curve

In order to develop the capacity spectrum from the pushover curve, it is necessary to perform calculations and convert each of the base shear vs roof displacement points to first mode spectral acceleration. Hence, all V_i, Δ_{roof} points of the capacity curve must be calculated as S_{ai}, S_{di} using the equations given in the ATC-40 standard:

$$S_{ai} = \frac{\frac{V_i}{W}}{\alpha_1} \qquad \textbf{Equation 5}$$

$$S_{di} = \frac{\frac{\Delta_{roof}}{W}}{PF_1 * \Phi_{1,roof}} \qquad \textbf{Equation 6}$$

Where: V_i is the base shear value at any point of the capacity curve, W is the weight of the structure, Δ_{roof} is the roof displacement at any point in the capacity curve, α_1 is the modal mass coefficient of first natural mode of structure, PF_1 is the modal mass participation

factor for the first natural mode of structure, and $\Phi_{1,\text{roof}}$ is the roof level amplitude in the first mode.

To calculate the modal mass coefficient and participation factors, ATC-40 suggests to use the following equations:

$$PF_1 = \frac{\sum_{i=1}^{N}(w_i\,\Phi_i)/g}{\sum_{i=1}^{N}(w_i\,{\Phi_i}^2)/g} \qquad \textbf{Equation 6}$$

$$\alpha_1 = \frac{[\sum_{i=1}^{N}(w_i\,\Phi_i)/g]^2}{[\sum_{i=1}^{N} w_i/g][\sum_{i=1}^{N}(w_i\,{\Phi_i}^2)/g]} \qquad \textbf{Equation 7}$$

In addition, the bilinearization calculations are performed for each of the pushover curve. The bilinearization is necessary to effectively evaluate the damping as well as the reduction of the spectral demand. Development of the bilinear lines requires the determination of point a_{pi} and d_{pi}. This is also known in ATC-40 as "trial performance point" used to develop a reduced scale of the response spectrum demand.

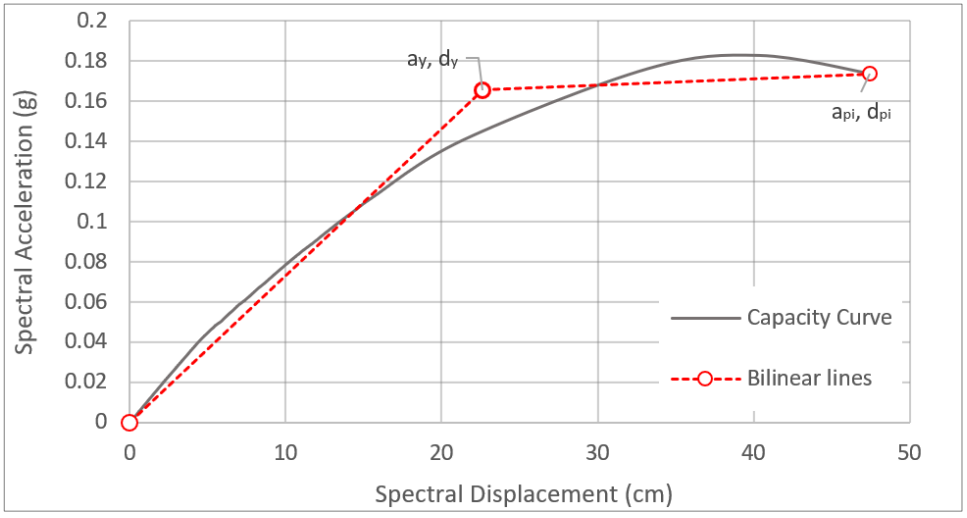

Figure 67: An example of conversion from pushover curve to seismic capacity curve together with bilinearization

Developing bilinearization in a pushover curve requires a balance of areas below and above the graph with respect to bilinear lines as shown in **Figure 67**.

On the other hand, the seismic demand is based on the response spectrum ADRS format. The conversion from the standard format to ADRS format is done using the equation as shown below:

$$S_{di} = \frac{T_i^{\,2}}{4\pi^2} S_{ai}\, g$$

Equation 8: Conversion to ADRS format as Sai, Svi

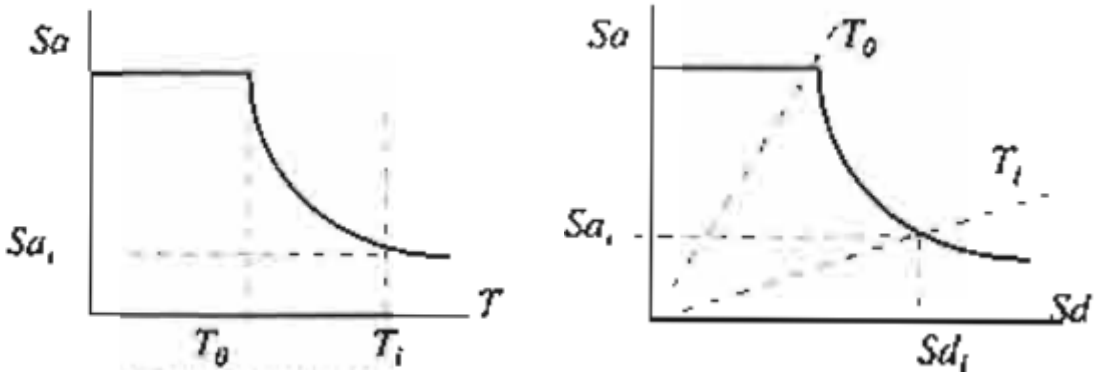

Standard Format (S_a vs T) ADRS Format (S_a vs S_d)

Figure 68: An example of conversion from Standard format to ADRS format (ATC-40, 1996)

4.6.6 Modal displacement demand and determination of performance point

ATC-40 provides three procedures for the modal displacement demand known as Procedure A, Procedure B and Procedure C. For this study it is used procedure A as it provides a better yet simple way to develop the calculations. Moreover, since all modal displacement demand will be automated, this procedure is suggested as the most suitable for programming (ATC-40, 1996).

Once the bilinearization for each of the pushover curve is done, then two values must be specified, a_y,d_y and a_{pi},d_{pi}. The first value represents the end point of the first bilinear line

while a_{pi},d_{pi} represents the far end of the bilinear lines as shown in **Figure 67**. These two points are always depending on the equally displacement approximation using the elastic region of the curve. After properly locating in graph both points the equivalent viscous damping (5% damped) must be calculated using the formula as below:

$$\beta_{eff} = \frac{63.7\ \kappa\ (a_y\ d_{pi} - \ d_y\ a_{pi})}{a_{pi}\ d_{pi}} + 5 \qquad \textbf{Equation 9}$$

Where κ is the damping modification factor and is taken as 0.33 for stryctural behavior type C which represents poor hysteretic behavior (ATC-40, 1996).

Furthermore, the numerical derivation for spectral reduction factor is performed using the formula as shown below:

$$SR_A = \frac{3.21 - \ 0.68\ ln\ (\beta_{eff})}{2.12} + 5 \qquad \textbf{Equation 10}$$

After the spectral reduction factor is calculated then values from the elastic response spectrum (5% damped) must be reduced using the formula: 2.5*CA*SR_A, where CA is taken as 0.4 building behavior type A, B and C (ATC-40, 1996).

The last stage requires to extend the equally displacement linear segment from bilinear lines and find the intersection with reduced response spectrum. Then from this point another perpendicular line must be drown towards capacity curve. The intersection points must be then compared with intersection between response spectrum reduced and seismic capacity curve (a_{pi_new}, d_{pi_new}) as shown in **Figure 69**.

The distance between a_{pi}, d_{pi} point and a_{pi_new}, d_{pi_new} point must satisfy the condition provided in ATC-40: 0.95 d_{pi} $\leq d_{pi\_new} \leq$ 1.05 d_{pi}.

Satisfying this condition means the determination of the performance point is done properly. Unless it is satisfied, then the new point (a_{pi_new}, d_{pi_new}) becomes (a_{pi}, d_{pi}) and

whole procedure repeats again. This may require multiple calculations and often is considered as time consuming process when applied for many case studies. Therefore, am automation procedure is prepared in the environment of Python V.3.3 (Van Rossum and Drake, 1995) to accelerate the entire process.

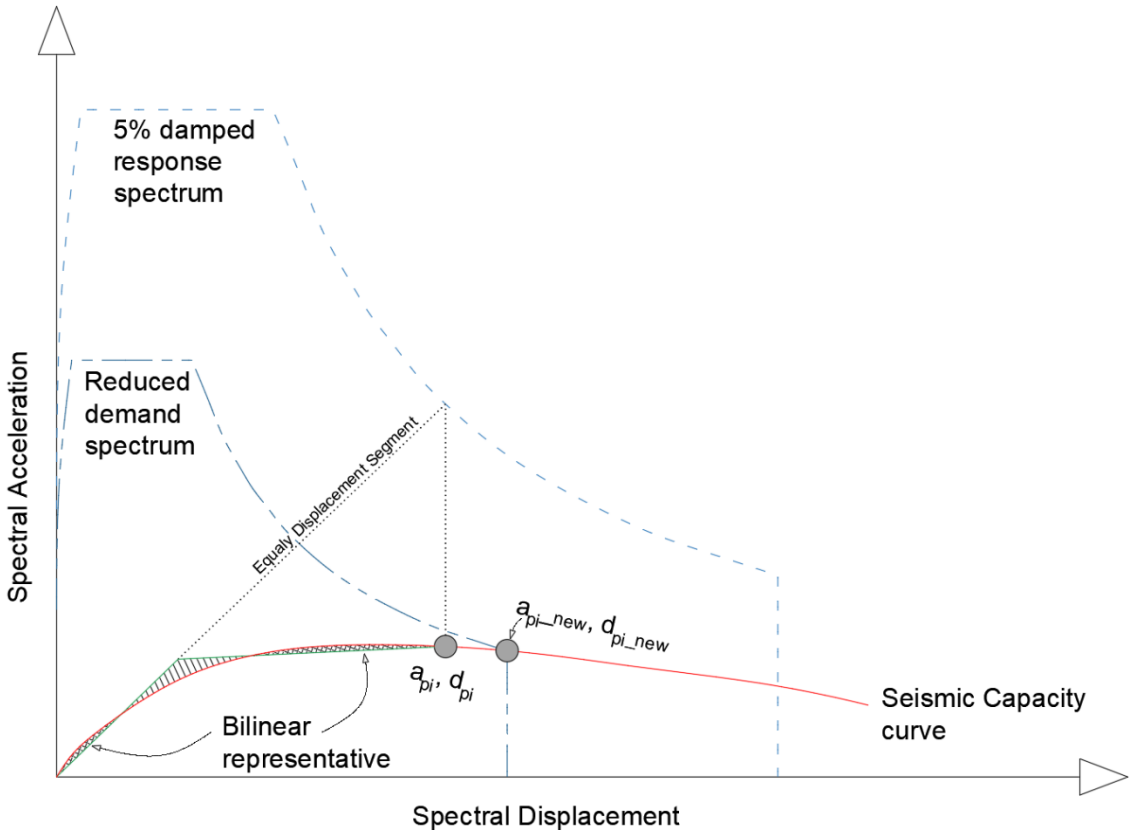

Figure 69: Computing performance point [Procedure A (ATC-40, 1996)]

4.6.7 Determination of building seismic safety

Performance assessment of the selected template reinforced concrete buildings are done to ensure life safety level is not exceeded. The performance point (PP) from the demand spectrum and capacity curve are compared for life safety (LS) limit state and building performance level is determined.

CHAPTER 5

DESCRIPTION OF THE SELECTED TEMPLATE DESIGNS WITH PERFORMANCE EVALUATION AND EARTHQUAKE RECORDS USED IN ANALYSES

5.1 General

Buildings used in this study are selected to represent the reinforced concrete (RC) building blocks which are in a poor seismic condition and continuously threatened by earthquakes. Therefore, the focus goes especially to the oldest RC residential buildings in Albania that are designed with old building codes, dating to the communism period which had a fast development in construction sector. Hence, 4/5 buildings included in this study are part of the template building category. A template building was designed to save time and reduce the cost of the architectural stage during the communism era. These designed templates were used throughout Albanian region and were built multiple times in different cities maintaining the same structural configuration. Hence, by studying even a limited amount of template buildings, it is possible to cover a wide range of old buildings in the country.

The 5th and the last building included in this thesis belongs to a recent construction which was heavily damaged during the November 26, 2019 earthquake in Albania. This building will be considered as a template too for the fact that the same plan is used for two identical buildings close to each other. Even though a recent construction, its main structural elements suffered from the recent Albanian earthquakes leaving it as inhabitable.

In this chapter it is presented a detailed description for each of the building templates used in this study. The plan layout, elevation view, material and section properties, reinforcement detailing etc. are provided according to respective blueprints.

The blueprints are ensured from "ARKIVI QËNDROR TEKNIK I NDËRTIMIT" (AQTN) located in Tirana, Albania. AQTN refers to the Central Technical Archive of Construction and was established by DCM NO.377 dated 26.07.1993 based on the law of the People's Assembly No.7726, dated 29.06.1993 "On the National Archival Fund and Archives". The archive started collecting construction documents since 1911 until 1990 enriching its database. Currently, AQTN claims to possess around 45 000 files which are then distributed to stakeholders against a specific payment.

Additionally, to the description of the building templates, a dataset of earthquakes used in this research thesis is provided with sufficient information. To achieve the target of this study, several nonlinear static and dynamic analysis are performed. Hence, a reach list of earthquakes is selected in line with code regulations and proposed research in literature for the seismic performance assessment of considered template buildings.

5.1.1 A Template

The identification of this building in its project is given as 82/1 but for the scope of this study will be named as "A Template". The "A Template" building was designed as reinforced concrete (RC) building during the communism period. This template is a moment resisting frame building in both transverse and longitudinal directions with masonry infills. The blueprint of "A Template" dates on 1982 and is part of the first RC buildings in Albania. The planimetry of the case study building is given in **Figure 70**. As shown, the plan is composed of three frames and five bays having no special structural irregularities. The dimensions of the footprints are 17.3 m by 10.0 m, making a total plan area of 173 m^2. In longer direction, building has a symmetrical structural configuration with respect to vertical axis, composed of five bays each 3.4 m wide whereas in its shorter direction, building has three frames distanced by 5.4 m and 4.2 m from each other.

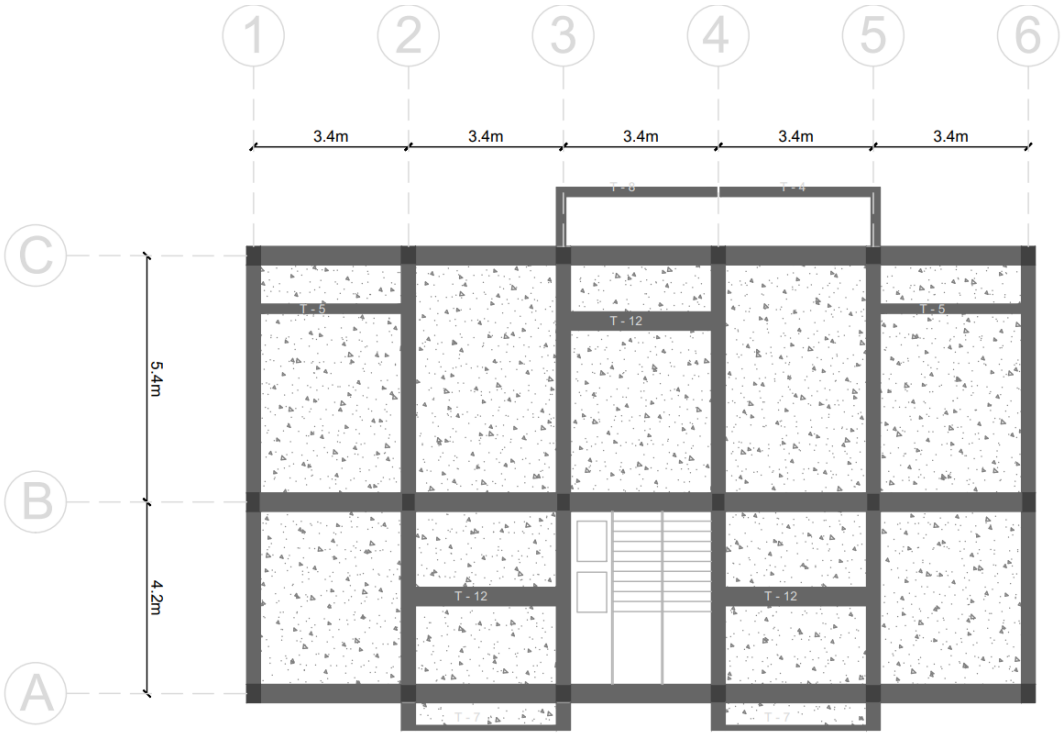

Figure 70: The plan view of the A Template (82/1) building

According to blueprint detailing, the building is 14.42 m height, composed of five stories. The first four stories are regular ones with a height of 2.8 m each while the last one 3.22 m including the parapet at the roof top as shown in **Figure 71**. The building has no shear-walls in any of its directions. Its outer walls are composed of lightweight ceramic bricks, composed of clay material and with inner holes to reduce the weight of the building resulting in no load bearing capacity. Main structural elements of "A Template" are beams and columns. These elements are of RC and in the blueprint, there are no indications of any size reduction in upper stories. The size of the columns remains the same for each of them allocated in the structure. The dimensions of the columns and beams are 30 x 40 cm accordingly.

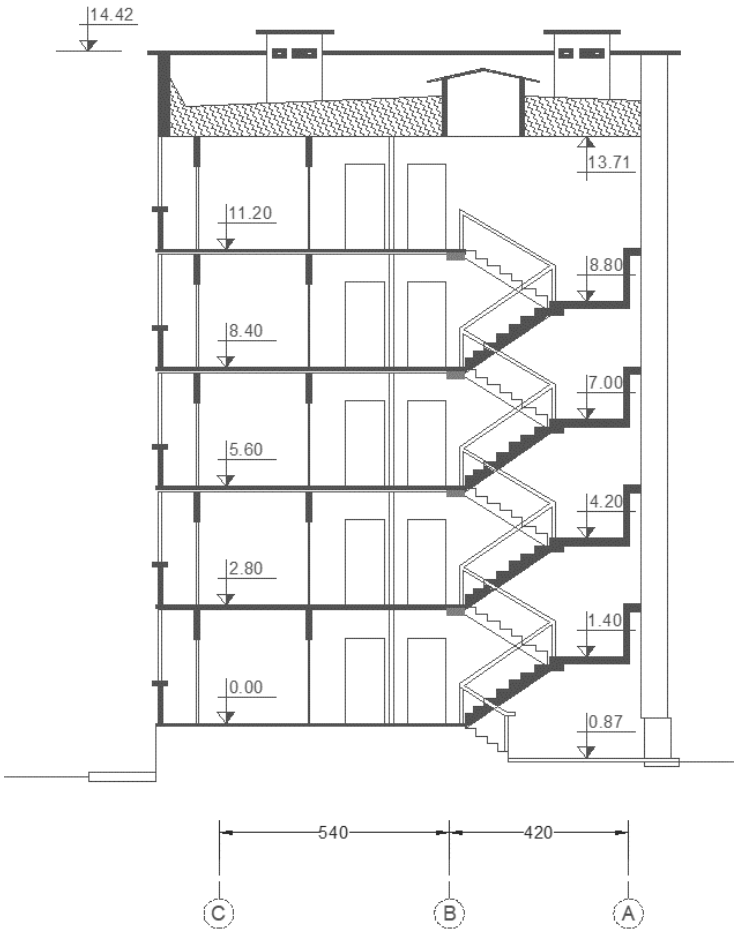

Figure 71: The elevation view of the A Template (82/1) and B Template (82/2) buildings

Typical longitudinal reinforcement for beams and columns is demonstrated in **Figure 72**. The symbol 'Ø' is used to determine the diameter in mm of the steel bars and is placed after the number of rebars. As shown in **Figure 72**, both columns and beams have low amount of reinforcement. The area ratio of the rebars with cross-sectional one, is low for this template building. Expressed in percentage, the ratio is generally 1.05% for columns and 0.77% for beams.

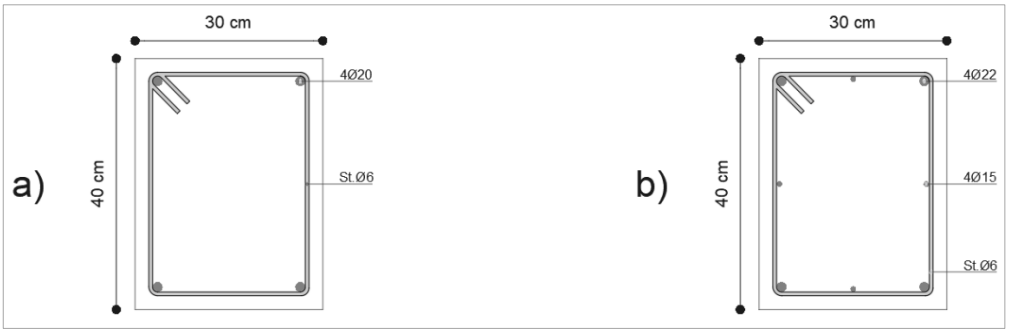

Figure 72: Representative column (a-left) and beam (b-right) reinforcement details for A Template (82/1), B Template (82/2) and C Template (82/2.1) buildings

Standard transverse reinforcement given in the design for columns and beams is Ø6 mm. Their spacing is given for beams and columns as 100 mm and 150 mm respectively in the footprints for this template building. The concrete class and the steel grade are defined in blueprint too. Referring to this template design, the concrete class used is M-200. Letter "M" has been integrated in the pattern of concrete material during the Union of Soviet Socialist Republics (USSR) in the construction industry. This letter is used to describe the compressive strength of concrete in cubic test. A summary of letter "M" type concrete with its respective compressive strength in MPa is provided in **Table 6**. Referring to the table below, the type of concrete used for this template building corresponds to C16/20.

Table 6: The respective MPa values for old concrete grade used in this study

No.	Concrete Grade	Concrete Strength in MPa (N/mm^2)
1	M-100	10
2	M-150	15
3	M-200	20
4	M-250	25
5	M-300	30
6	M-350	35
7	M-400	40
8	M-450	45

9	M-550	50
10	M-600	55

The footprint characterizes the steel material as 2100 Kg/cm^2 (Ç3) used in the project as the reinforcement of the structural elements. A detailed summary of project values for the concrete and steel materials are provided in **Table 7** and **Table 8** respectively.

Table 7: Properties of concrete material

Properties of Concrete	**C16/20**
Cubic strength	fck = 16 MPa (fc,cube)
Compressive cylinder strength	fck = 20 MPa
Mean value of cylinder compressive strength (28 days)	fcm = 28 MPa
Characteristic axial tensile strength	fctk(95%) = 2.9 MPa
Characteristic axial tensile strength	fctk(5%) = 1.5 MPa
Mean value of axial tensile strength	fctm = 2.2 MPa
Young's Modulus	Ecm = 30 GPa
Design value of modulus of elasticity	Ecd = 25 GPa
Design value of compressive strength	fcd =α ∗ fck⁄γc = 11.3 MPa
Partial factor	γc = 1.5 and α = 0.85
Poisson's ratio	ν = 0.20

Table 8: Properties of steel material

Properties of Steel Material	**"Ç-3"**
Tensile strength	fck = 250 MPa
Yield strength	fyk = 320 MPa
Young's Modulus	Es = 210 GPa
Partial factor	γs = 1.15
Design yield (shear)	fywd = 180 MPa
Design yield (strength)	fyd = 215 MPa
Poisson's ratio	ν = 0.30

5.1.2 B Template

The second building considered is of type 82/2 and named in this study as “B Template”. Similar to “A Template”, it was designed in 1982 as a reinforced concrete residential building and is comprised of moment resisting frames in both directions. The planimetry area is 207 m^2 with dimensions 10 m and 20.7 m. In its short direction it is composed of three frames while in the longer direction it has six bays. Compared to “A Template” it has one more bay while the spaces between them remain exactly the same, each of 3.4 m as shown in **Figure 73**. This template shows no plan irregularities in its structural configuration and is symmetrical with respect to the vertical axis.

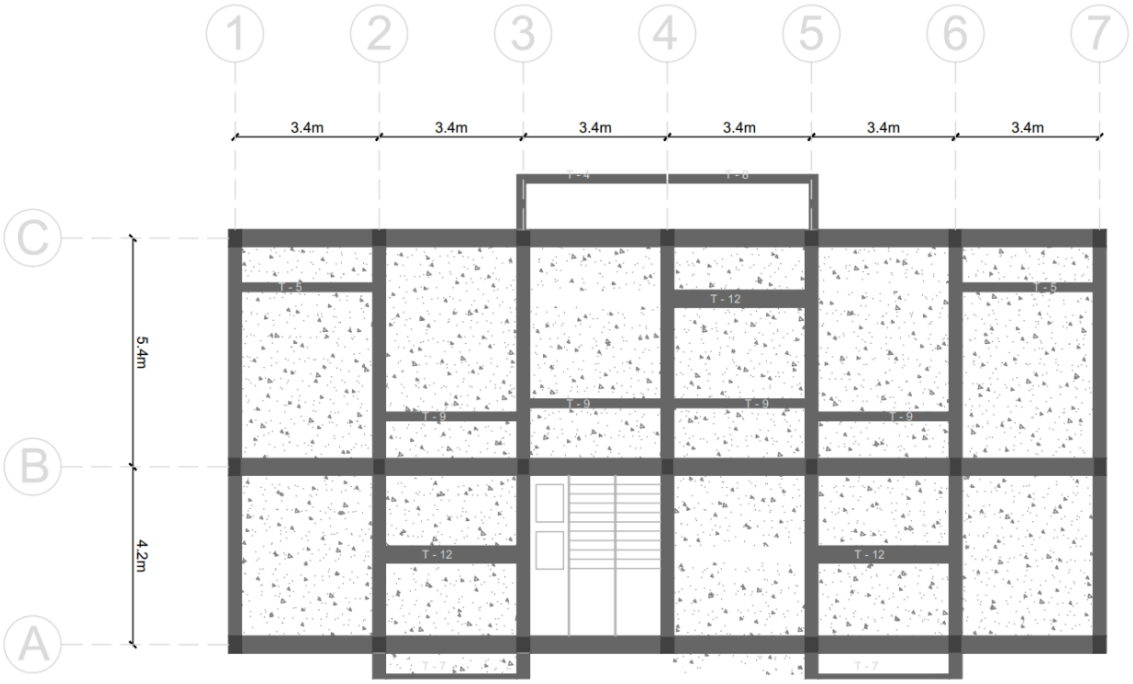

Figure 73: The plan view of the B Template (82/2) and C Template (82/2.1) building

As belongs to the elevation profile, “B Template” shares the same properties with “A Template”, a maximum height of 14.42 m, composed of five stories, each 2.8 m tall except the last one which is 3.22 m, as shown in **Figure 71**. The main structural elements such as columns and beams as well as their reinforcement detailing, remain also the same with

"A Template" as shown in **Figure 72**. The concrete type used belongs to M-200 grade which is equivalent to C16/20 whereas steel is of 2100 Kg/cm^2 (Ç3). All other material properties remain the same as shown in **Table 7** and **Table 8**. The stirrups spacings used in beams is 100 mm and in columns ranges from 200 to 250 mm. The transverse reinforcement is composed of Ø6 mm rebars. "B Template" has no shear walls in any of its directions. Its structural walls are made of lightweight clay bricks with holes to reduce the total weight of the building. Since there are no shear walls in any of its directions, the lateral load bearing system will be weak which leads to the formation of plastic hinges in columns. This phenomenon will significantly affect the overall response of the buildings, causing loss of lateral stiffness in an individual floor level. Additionally, the reinforcement used for beams and columns is weak and its ratio to cross-sectional area remain very low, 1.05% and 0.77% for columns and beams respectively.

5.1.3 C Template

Third building considered in this thesis is of type 82/2.1 and named as "C Template". It falls in the same group of design year as previous two templates, 1982. This building uses the same planimetry as "B Template" shown in **Figure 73**. It is composed of six bays, each 3.4 m wide and three frames distanced from each other by 5.4 m and 4.2 m. The plan configuration remains symmetrical with respect to vertical axis and the structure shows no particular irregularities in plan or elevation.

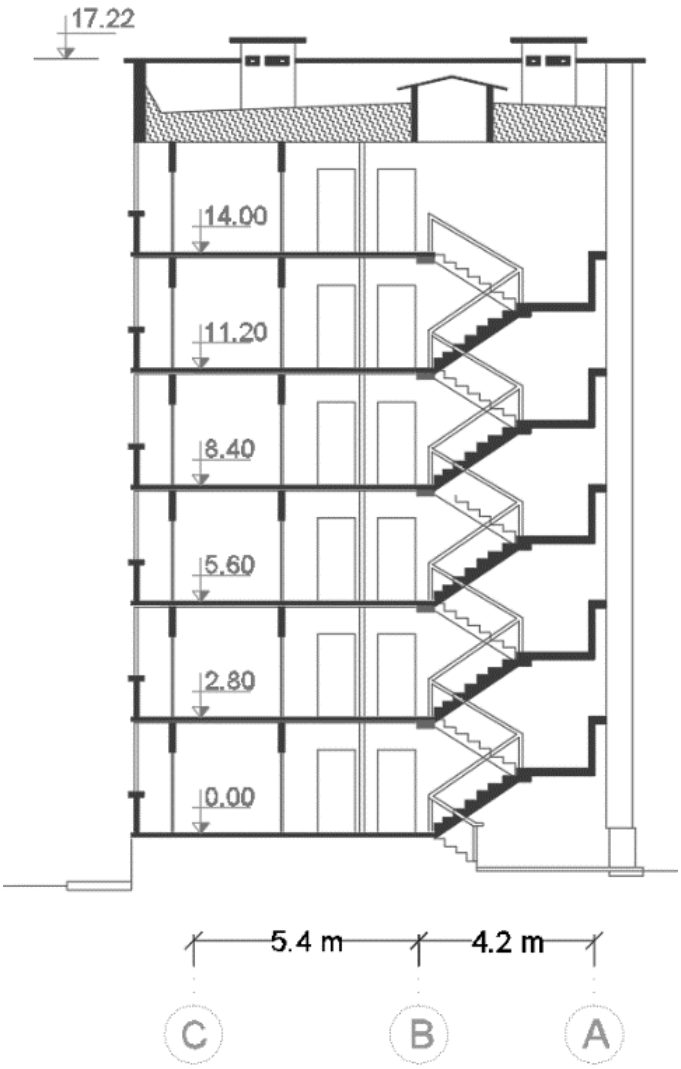

Figure 74: The elevation view of the C Template (82/2.1) building

According to blueprint detailing, the building is 17.22 m tall, composed of six stories. First five stories of this template building are regular and have a height of 2.8 m. Top story differs from other five as it is higher and has a height of 3.22 m including the parapet. "C Template" is constructed as a residential building throughout Albanian region during the communism period. The structural model is composed of columns, beams and hollow clay brick walls but there are no shear walls in any of its directions. According to the footprint, the column and beam size if of 40*30 cm as shown in **Figure 72**.

The material used for concrete belongs to the brand M-200 which corresponds to C16/20 as demonstrated in **Table 6** whereas for the longitudinal reinforcement it is used steel 2100 Kg/cm^2 (Ç3). Material characteristics are shown in **Table 7** and **Table 8** for concrete and steel reinforcement respectively. Additionally, the blueprint provides information regarding transverse reinforcement spacings for beams and columns. The steel bars used in this template building are Ø6 mm and spaced by 100 mm and 250 mm for beams and columns respectively.

5.1.4 D Template

"D Template" is the fourth building selected for the performance assessment in this study. It was designed as reinforced concrete residential building in 1982.

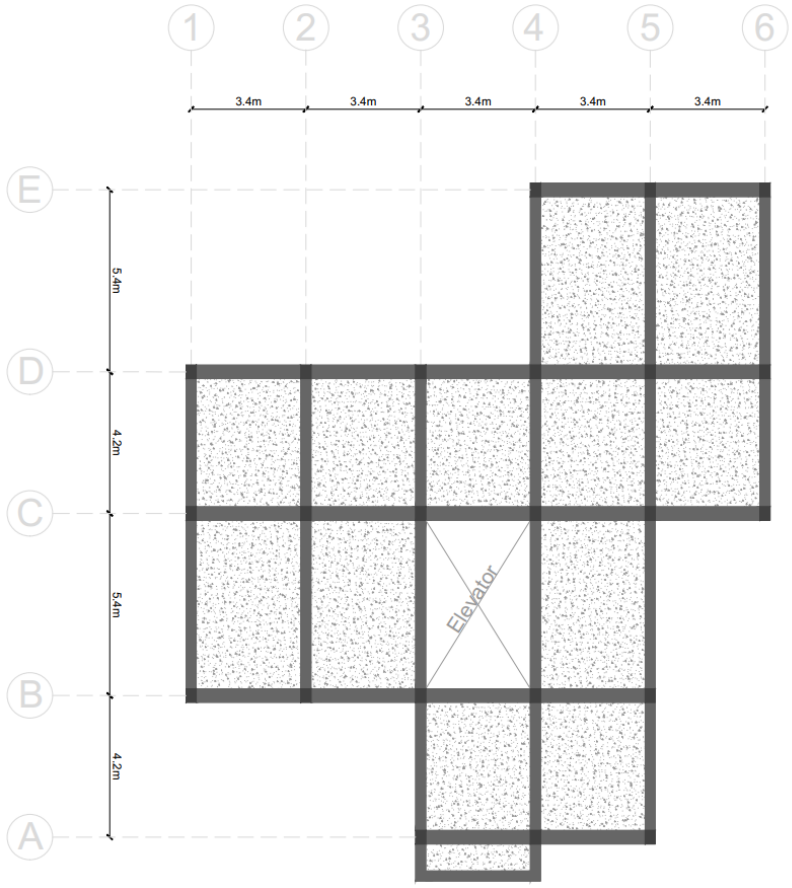

Figure 75: The plan view of the D Template (82/3) building

The footprint of this building categorizes it as type 82/3 which was built as moment resisting frame. “D Template” is composed of five bays in transverse direction and five frames in the longitudinal one. The plan configuration is an irregular one as shown in **Figure 75**. Its dimensions are 17.3 m in the horizontal direction and 19.6 m in the vertical one. Due to the plan irregularities, this type of template building is expected to attract more torsional forces during an earthquake. In the elevation view, “D Template” shows no irregularities. The overall height of the building reaches to 17.67 m and is composed of six stories. First five stories have a regular height of 2.8 m whereas the last one reaches to 3.8 m considering the parapet on the roof top. An elevation view and plan details are shown in **Figure 76**.

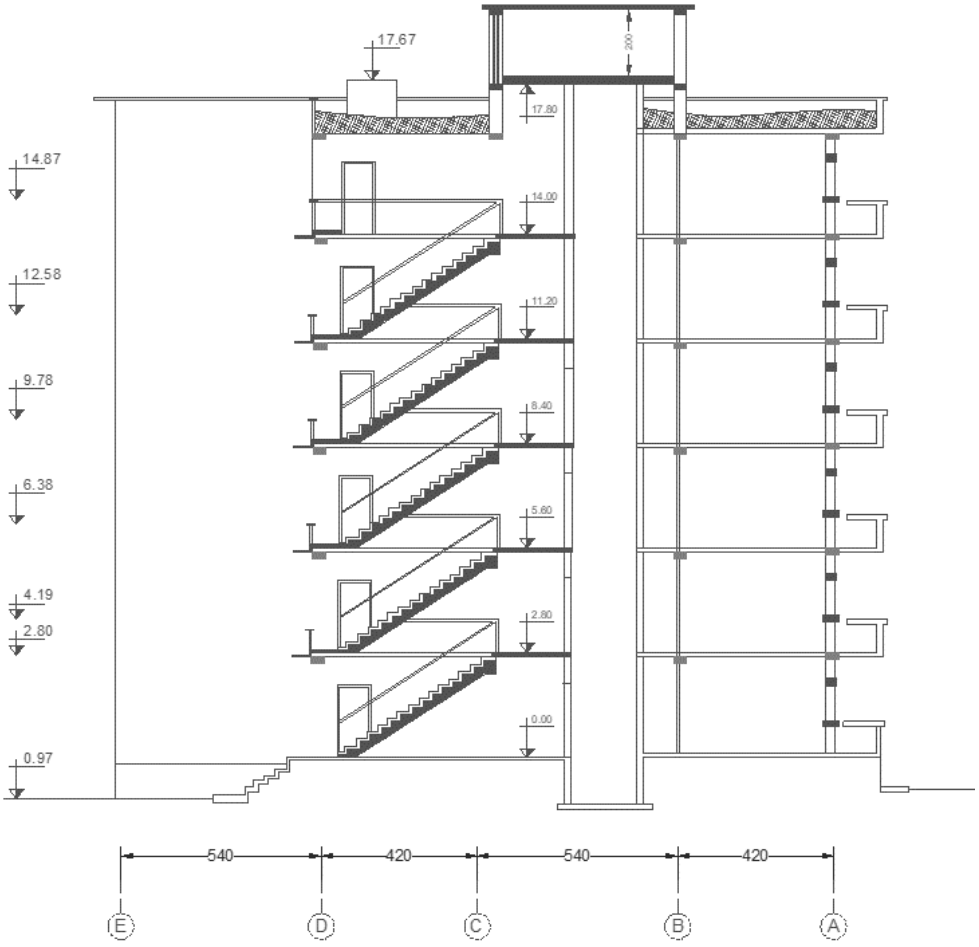

Figure 76: The elevation view of the D Template (82/3) building

Because its design dates to 1982, there are no shear walls planned nor constructed in any of its directions. Beams and columns have same cross-sectional size throughout the building. Column dimensions are of 40*30 cm and beams 40*20 cm as shown in **Figure 77**. The concrete material used for structural elements belongs to the M-200 (C16/20) type as specified in the template blueprint. On the other hand, the steel used for the reinforcement belongs to 2100 Kg/cm^2 (Ç3). The longitudinal reinforcement of beams and columns are designed using 8 bars of 11 mm diameter (Ø11) and 6 bars of 14 mm diameter (Ø14) respectively. In addition, the transverse reinforcement is composed of 6 mm diameter (Ø6) for both beams and columns. The stirrups spacing provided in the plan details, is of 250 mm in beams and 150 mm in columns.

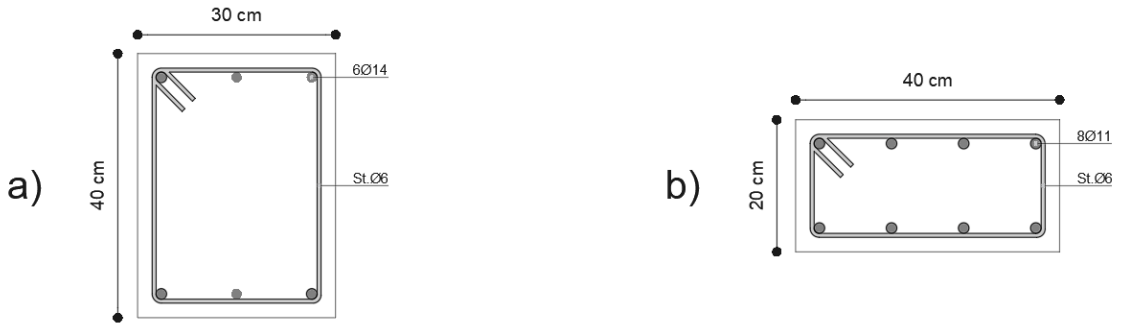

Figure 77: Typical column (left) and beam (right) reinforcement details for D Template (82/3) building

The insufficient amount of reinforcement used for this template building follows the same trend of the previous ones as they date back to the same construction year. An overall ratio of the reinforcement with the cross-sectional area of beams and columns expressed in percentage is 0.45% and 1.27% respectively. **Figure 77** demonstrates the cross-section and reinforcement details of beams and columns used in "D Template" building.

5.1.5 E Template

"E Template" is the last case study building used in this thesis. It was designed and built during 2005 years as residential reinforced concrete building in Durrës, near Iliria beach

as shown in **Figure 78**. Compared with previous templates, this structure is newer and represents a more updated version of Albanian construction. The location of E Template represents one of the cities which has been strongly hit during the recent earthquakes in Albania. As a matter of fact, during November 26, 2019 earthquake, “E Template” suffered serious damages in its structural elements. Therefore, it represents an example of relatively new construction with poor seismic performance.

Figure 78: Location of E Template buildings at Iliria beach in Durrës, close to November 26, 2019 epicenter

According to the plan layout, “E Template” is symmetrical with respect to horizontal and vertical directions. The plan dimensions are 20.7 m by 18.7 m resulting in a total area of nearly 387 m^2. In its longitudinal direction is composed of four bays and in the transverse direction of four frames. Middle bays have a distance of 4 m from each other and the corner ones 5 m whereas the space between frames is uniformly 5 m. The planimetry details of E Template are demonstrated in **Figure 79**.

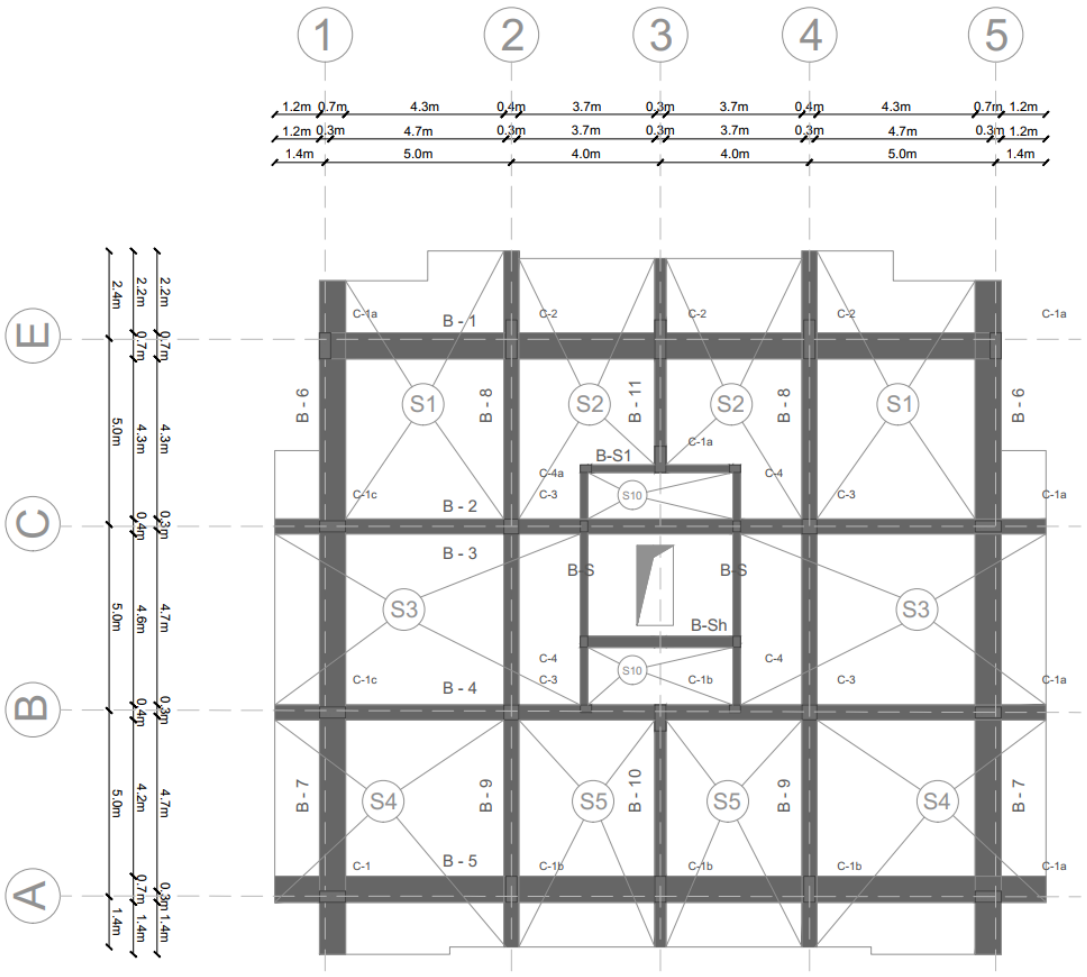

Figure 79: The plan view of the E Template (Durrës) building

As shown in the plan, there are different types of columns and beams used in the structure. Typical columns dimensions are of 70 cm by 30 cm. The beam dimensions are 50 cm by 25 cm. Even though the design belongs to 2005 the structure has no shear walls in any of its directions. This also can be interpreted with the fact that all energy during the earthquake has been obtained by columns which has been heavily damages as shown in **Figure 80**.

Figure 80: Damages of the E Template building during November 26, 2019 earthquake

The material characteristics are defined in the footprint of the buildings as well. For the concrete it is used M-250 which corresponds to C20/25 as shown in **Table 6**. Whereas for the longitudinal and stirrups reinforcement, steel 3200 Kg/cm^2 is applied.

Figure 81 - **Figure 84** show columns and beam reinforcement used in the E Template building. As demonstrated, there are four main types of columns labeled as “C-1b”, “C-1c”, “C2” and “C4” allocated in the building layout as shown in **Figure 79**. From the project footprint it can be observed that the cross-section of columns and their reinforcement changes as the building height increases. Hence, in **Figure 81** it can be seen how longitudinal bars of columns type “C-1b” reduce in number from fourth story to the fifth, from fifth to sixth and from sixth to seventh. As the number of stories increases, the reinforcement decreases and also cross-sectional area reduces, as shown in **Figure 81**-d.

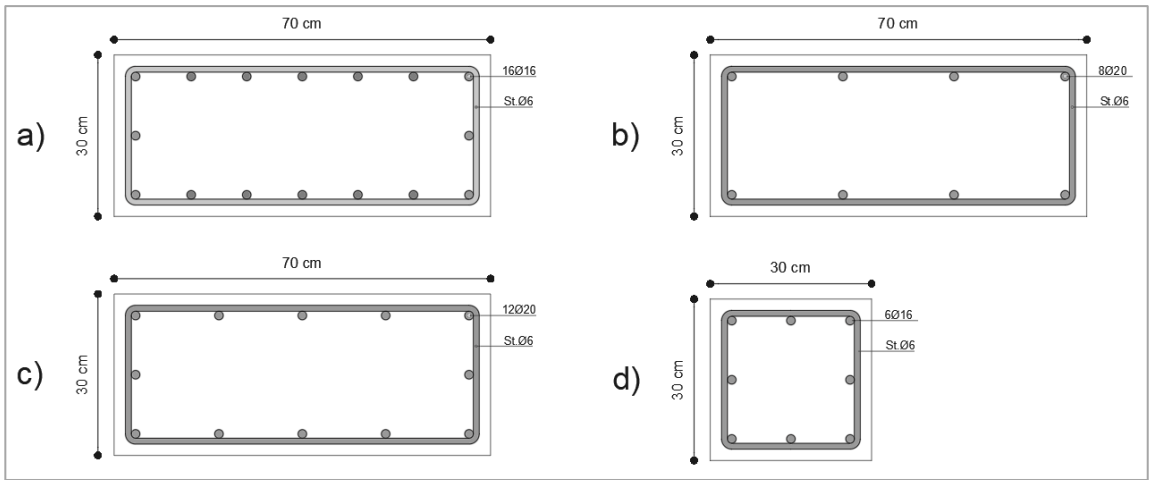

Figure 81: Column type "C – 1b" reinforcement details, a) used in floor 1-4, b) used in floor 5, c) used in floor 6 and d) used in floor 7 of E Template (Durrës) building

The second type of columns used belongs to "C – 1c" and allocated in the corner frames of the plan, **Figure 79**.

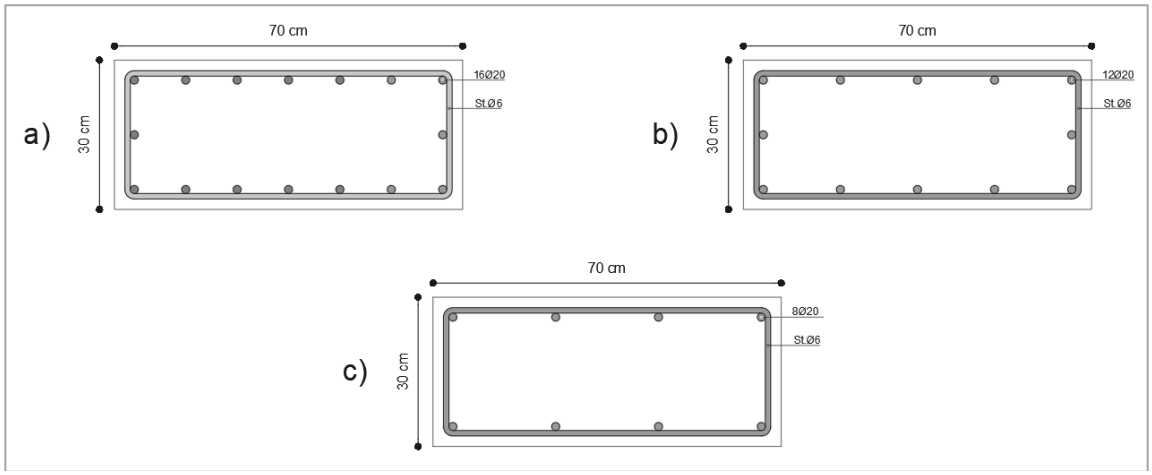

Figure 82: Column type "C – 1c" reinforcement details, a) used in floor 1-5, b) used in floor 6 and c) used in floor 7 of E Template (Durrës) building

The cross-sectional area does not decrease over floors, but the number of longitudinal bars reduces significantly from the fifth floor to the upper ones by half. Their dimensions

remain constant, 70 cm by 30 cm and longitudinal bars have a common diameter of 20 mm. Whereas the transverse reinforcement used belongs to 6 mm diameter.

Column type "C - 2" is the longest used in this building, 100 cm by 30 cm, as illustrated in **Figure 83**. These columns are positioned in the front of the building and withstand forces from the cantilever balconies of about 2.3 m long. Their reinforcement drops from 4th floor to 5th and 6th one especially in the number of bars, whereas the bar diameter remains the same of 20 mm. From the 6th to 7th story, number of bars reduces again, and their diameter drops to 16 mm diameter. The cross-sectional are of the columns get lower as well as shown in **Figure 83**-d.

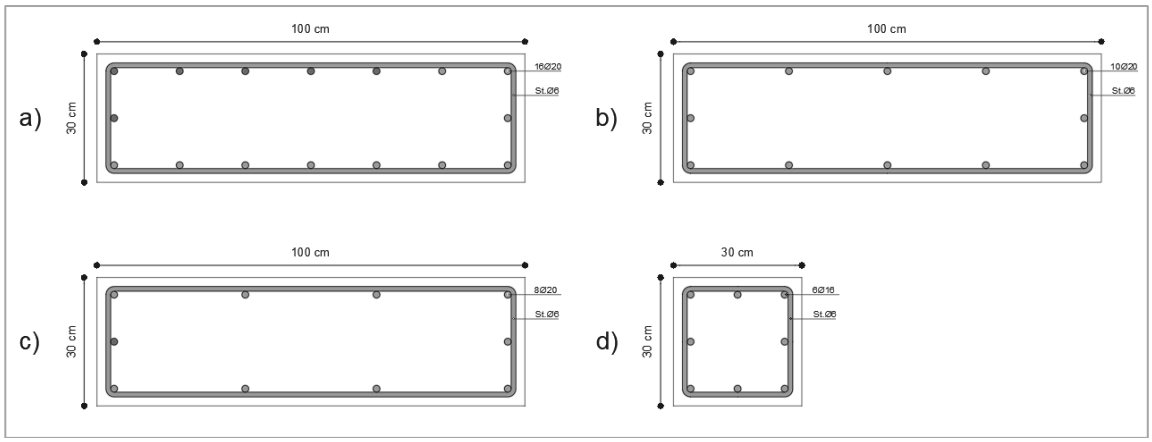

Figure 83: Column type "C – 2" reinforcement details, a) used in floor 1-4, b) used in floor 5, c) used in floor 6 and d) used in floor 7 of E Template (Durrës) building

The last type of columns considered for the modelling stage is of type "C – 4" with dimensions 40 cm by 20 cm. Its reinforcement is composed of 6 longitudinal bars of 16 mm diameter in the transverse direction, there are used stirrups of Ø6 **Figure 84**-left. The beams cross-section is unified throughout the E Template building and has dimensions 50 cm by 25 cm as shown in **Figure 84**-right. Its longitudinal reinforcement is composed of 8 bars at the top and 8 bars at bottom of 20 mm diameter. Whereas stirrups used for beam elements are of 6 mm diameter.

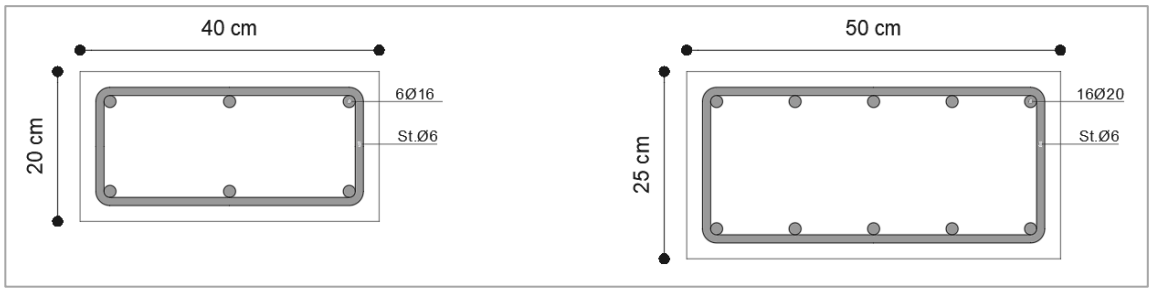

Figure 84: Column type "C - 4" (left) and beam (right) reinforcement details of E Template (Durrës) building

The typical percentage of the reinforcement and concrete ratio expressed in percentage for columns and beams is 1.47% and 4.02% respectively.

E Template is the tallest building considered in this study, composed of seven stories which reaches an overall height of 22.32 m at the roof top. Unlike 1982 template buildings which have regular floors except the top one, this template uses the first floor as shopping services and the rest as residential stories. As seen from the elevation view in **Figure 85**, first story is almost 4 m height whereas the other ones are regular stories each of 3.06 m. Furthermore, it is shown that at below ground level, there is used a distance of 2.32 m as a under parking area for the residents of the apartment. This is a typical structural configuration followed recently in any reinforced concrete residential construction in Albania.

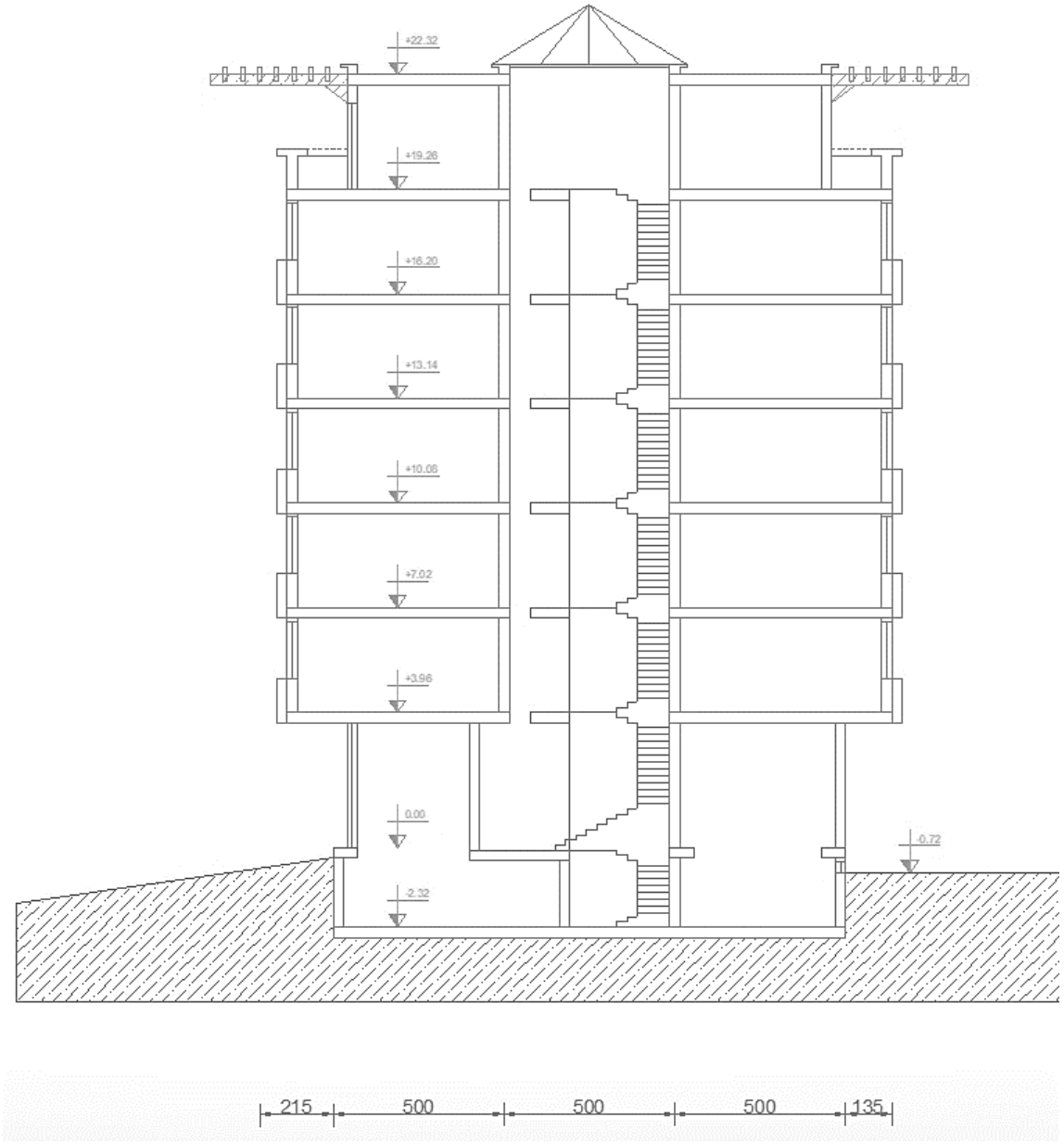

Figure 85: The elevation view of the E Template (Durrës) building

5.2 Earthquake ground motion records used in the nonlinear dynamic analysis

The nonlinear dynamic analysis requires a set of ground motion records in order to conduct a calculation of structural demand under seismic loadings. The proper selection

of the earthquake records has a great significance due to the reason that same earthquake features may overestimate or underestimate the structural response. For instance, many researchers have studied the effect of near field and far field earthquake records. As a matter of fact, some researchers (Kalkan and Kunnath, 2007) have found that the influence of near field records is much higher compares to far field record in terms of the absolute and relative energy input to building system. Therefore, to comparatively investigate the effects of far-field and near-field records as well as investigate the structural assessment of selected template reinforced concrete buildings, this study uses a dataset of 146 records among which 78 are of near fault and 68 of far-fault ground motions recorded on dense to firm soil conditions. This dataset of earthquake records is used under the environments of NONLIN V8.0 (Charney and Barngrover, 2004) computer software for the time history analysis. In advance, there is provided the list of Far-fault records associated with the main attributes respectively as shown in **Table 9**.

Table 9: The dataset of FAR-Fault ground motion records used for the dynamic nonlinear analysis

Nr	Earthquake	Record and component	Year	M_w	Site	d(km)	PGD (cm)	PGV (cm/s)	PGA (g)
1	San Fernando	LA HOLLYWOOD STOR LOT (90)	1971	6.6	C	62.2	12.42	18.93	0.21
2	San Fernando	LA HOLLYWOOD STOR LOT (180)	1971	6.6	C	62.2	6.32	14.87	0.17
3	Friuli, Italy	TOLMEZZO (0)	1976	6.5	C	37.7	4.11	22.03	0.35
4	Friuli, Italy	TOLMEZZO (270)	1976	6.5	C	37.7	5.09	30.80	0.32
5	Imperial Valley	DELTA (262)	1979	6.9	D	43.6	11.99	26.00	0.24
6	Imperial Valley	DELTA (352)	1979	6.9	D	43.6	19.03	33.02	0.35

7	Imperial Valley	EL CENTRO ARRAY #11 (140)	1979	5.2	D	30.3	16.08	34.44	0.36
8	Imperial Valley	EL CENTRO ARRAY #11 (230)	1979	5.2	D	30.3	18.63	42.14	0.38
9	Superstition Hills	EL CENTRO IMP CO CENTER (0)	1987	6.5	B	18.5	17.53	46.36	0.36
10	Superstition Hills	EL CENTRO IMP CO CENTER (90)	1987	6.5	B	18.5	20.10	40.87	0.26
11	Superstition Hills	POE (270)	1987	6.5	B	14.7	8.82	35.80	0.45
12	Superstition Hills	POE (360)	1987	6.5	B	14.7	11.28	32.80	0.30
13	Loma Prieta	CAPITOLA (0)	1989	7.1			9.13	35.01	0.53
14	Loma Prieta	CAPITOLA (90)	1989	7.1			5.49	29.21	0.44
15	Loma Prieta	GILROY ARRAY #3 (0)	1989	7.1	D	14.4	8.26	35.69	0.56
16	Loma Prieta	GILROY ARRAY #3 (90)	1989	7.1	D	14.4	19.33	44.67	0.37
17	Cape Mendocino	RIO DELL OVERPASS FF (360)	1992	7.0	D	18.5	19.55	42.00	0.55
18	Cape Mendocino	RIO DELL OVERPASS FF (270)	1992	7.0	D	18.5	7.02	10.54	0.20
19	Landers	COOLWATER (LN)	1992	7.3	C	69.2	13.71	25.64	0.28
20	Landers	COOLWATER (TR)	1992	7.3	C	69.2	13.81	42.34	0.42
21	Landers	YERMO FIRE STATION (270)	1992	7.3	D	23.6	43.85	51.44	0.25
22	Landers	YERMO FIRE STATION (360)	1992	7.3	D	23.6	24.63	29.71	0.15
23	Northridge	BEVERLY HILLS - 12520 MULH (35)	1994	6.7			8.57	40.86	0.62

24	Northridge	BEVERLY HILLS - 12520 MULH (125)	1994	6.7			4.83	30.19	0.44
25	Northridge	BEVERLY HILLS - 14145 MULH (9)	1994	6.7	C	19.6	13.15	58.94	0.42
26	Northridge	BEVERLY HILLS - 14145 MULH (279)	1994	6.7	C	19.6	11.07	62.78	0.52
27	Northridge	CANYON COUNTRY - W LOST CANYON (0)	1994	6.7	D	13.0	11.71	43.03	0.41
28	Northridge	CANYON COUNTRY - W LOST CANYON (270)	1994	6.7	D	13.0	12.54	45.38	0.48
29	Kobe	NISHI-AKASHI (0)	1995	6.9	D	22.5	9.53	37.29	0.51
30	Kobe	NISHI-AKASHI (90)	1995	6.9	D	22.5	11.26	36.67	0.50
31	Kobe	SHIN-OSAKA (0)	1995	6.9	D	19.2	8.55	37.86	0.24
32	Kobe	SHIN-OSAKA (90)	1995	6.9	D	19.2	7.64	27.94	0.21
33	Kocaeli	ARCELIK (0)	1999	7.4	C	17.0	13.65	17.69	0.22
34	Kocaeli	ARCELIK (90)	1999	7.4	C	17.0	35.58	39.55	0.15
35	Kocaeli	DUZCE (180)	1999	7.4	D	17.1	44.13	58.88	0.31
36	Kocaeli	DUZCE (270)	1999	7.4	D	17.1	17.62	46.39	0.36
37	Chi-Chi	CHY101 (E)	1999	7.6	D	11.1	45.30	70.64	0.35
38	Chi-Chi	CHY101 (N)	1999	7.6	D	11.1	68.76	115.00	0.44
39	Chi-Chi	TCU045 (E)	1999	7.6	C	26.0	50.68	36.70	0.47
40	Chi-Chi	TCU045 (N)	1999	7.6	C	26.0	14.35	39.09	0.51
41	Duzce	BOLU (0)	1999	7.1	D	12.0	23.07	56.49	0.73
42	Duzce	BOLU (90)	1999	7.1	D	12.0	13.56	62.12	0.82
43	Iran_Manjil	LONGITUDINAL COMP	1990	7.4	-	74.0	14.92	43.26	0.52
44	Iran_Manjil	TRANSVERSE COMP	1990	7.4	-	74.0	20.83	55.55	0.50

45	Hector Mine	HEC (0)	1999	7.1	-	22.0	22.54	28.58	0.27
46	Hector Mine	HEC (90)	1999	7.1	-	22.0	13.96	41.75	0.34

In addition, **Table 10** represents the list of Near-Fault earthquakes with relevant sufficient details.

Table 10: The dataset of NEAR-Fault ground motion records used for the dynamic nonlinear analysis

Nr	**Earthquake**	**Record and component**	**Year**	**M_w**	**Site**	**d(km)**	**PGD (cm)**	**PGV (cm/s)**	**PGA (g)**
1	Imperial Valley	CHIHUAHUA (12)	1979	6.5		-	9.13	24.85	0.27
2	Imperial Valley	CHIHUAHUA (282)	1979	6.5		-	12.91	30.12	0.254
3	Imperial Valley	EL CENTRO ARRAY #6 (140)	1979	6.5	D	1	27.57	64.83	0.41
4	Imperial Valley	EL CENTRO ARRAY #6 (230)	1979	6.5	D	1	65.82	109.8	0.439
5	Imperial Valley	EL CENTRO ARRAY #7 (140)	1979	6.5	D	0.6	24.65	47.6	0.338
6	Imperial Valley	EL CENTRO ARRAY #7 (230)	1979	6.5	D	0.6	44.71	109.24	0.463
7	Imperial Valley	BONDS CORNER (140)	1979	6.5	D	2.5	0.34	3.61	0.084
8	Imperial Valley	BONDS CORNER (230)	1979	6.5	D	2.5	1.42	8.18	0.1
9	Irpinia Eq / Italy	STURNO (0)	1980	6.9	C	10.8	11.58	36.39	0.251
10	Irpinia Eq / Italy	STURNO (270)	1980	6.9	C	10.8	32.02	51.82	0.358
11	Nahanni, Canada	SITE 1 (10)	1985	6.8	B	6	9.64	46.05	0.978
12	Nahanni, Canada	SITE 1 (280)	1985	6.8	B	6	14.52	46.13	1.096

13	Nahanni, Canada	SITE 2 (240)	1985	6.8	B	6	7.54	29.26	0.489
14	Nahanni, Canada	SITE 2 (330)	1985	6.8	B	6	6.57	33.13	0.323
15	Superstition Hills	PTS (225)	1987	6.6	D	0.7	52.83	112	0.455
16	Superstition Hills	PTS (315)	1987	6.6	D	0.7	15.25	43.9	0.377
17	Loma Prieta	BRAN (0)	1989	6.9			11.69	55.74	0.481
18	Loma Prieta	BRAN (90)	1989	6.9			11.86	41.91	0.526
19	Loma Prieta	CORRALITOS (0)	1989	5.1	D	5.1	10.82	55.16	0.644
20	Loma Prieta	CORRALITOS (90)	1989	5.1	D	5.1	11.29	45.5	0.479
21	Loma Prieta	SARATOGA ALOHA AVE (0)	1989	6.9	C	4.1	16.24	51.15	0.512
22	Loma Prieta	SARATOGA ALOHA AVE (90)	1989	6.9	C	4.1	27.61	42.61	0.324
23	Erzican / Turkey	ERZICAN EAST-WEST COMP ()	1992	6.7	D	4.4	21.92	64.3	0.496
24	Erzican / Turkey	ERZICAN - NORTH-SOUTH COMP ()	1992	6.7	D	4.4	27.66	83.95	0.515
25	Cape Mendocino	CAPE MENDOCINO (0)	1992	7.1	B	9.5	39.74	125.57	1.497
26	Cape Mendocino	CAPE MENDOCINO (90)	1992	7.1	B	9.5	12.18	41.33	1.039
27	Cape Mendocino	PETROLIA (0)	1992	7.1	B	9.5	21.97	48.32	0.59
28	Cape Mendocino	PETROLIA (90)	1992	7.1	B	9.5	29.01	90.08	0.662
29	Landers	LUCERNE (260)	1992	7.3	B	2	217.12	146.03	0.727
30	Landers	LUCERNE (345)	1992	7.3	B	2	52.78	32.94	0.789

31	Northridge Earthquake	CA:LA;SEPULVEDA VA (BLD 40 GND; 270)	1994	6.7	D	9.5	13.39	78.1	0.749
32	Northridge Earthquake	CA:LA;SEPULVEDA VA (BLD 40 GND; 360)	1994	6.7	D	9.5	17.39	76.15	0.934
33	Northridge Earthquake	NORTHRIDGE - SATICOY (90)	1994	6.7	D	13.3	8.44	28.96	0.368
34	Northridge Earthquake	NORTHRIDGE - SATICOY (180)	1994	6.7	D	13.3	22.07	61.46	0.477
35	Northridge Earthquake	RINALDI RECEIVING STA (228)	1994	6.7	D	8.6	29.62	160.33	0.825
36	Northridge Earthquake	RINALDI RECEIVING STA (318)	1994	6.7	D	8.6	26.96	74.54	0.487
37	Northridge Earthquake	SYLMAR - HOSPITAL (90)	1994	6.7	D	6.4	16.82	78.37	0.604
38	Northridge Earthquake	SYLMAR - HOSPITAL (360)	1994	6.7	D	6.4	31.96	130.4	0.843
39	Kocaeli / Turkey	IZMIT (90)	1999	7.4	B	4.3	17.13	29.78	0.22
40	Kocaeli / Turkey	IZMIT (180)	1999	7.4	B	4.3	9.81	22.61	0.152
41	Kocaeli / Turkey	YARIMCA (330)	1999	7.4	D	3.3	50.98	62.16	0.349
42	Kocaeli / Turkey	YARIMCA (60)	1999	7.4	D	3.3	57.03	65.72	0.268
43	Chi-Chi	TCU065 (E)	1999	7.6	D	2.5	92.59	126.18	0.814
44	Chi-Chi	TCU065 (N)	1999	7.6	D	2.5	60.75	78.79	0.603
45	Chi-Chi	TCU067 (E)	1999	7.6	D	1.1	93.12	79.58	0.503
46	Chi-Chi	TCU067 (N)	1999	7.6	D	1.1	45.96	66.7	0.325
47	Chi-Chi	TCU084 (E)	1999	7.6	C	11.4	31.44	114.74	1.157

48	Chi-Chi	TCU084 (N)	1999	7.6	C	11.4	21.27	45.58	0.417
49	Chi-Chi	TCU102 (E)	1999	7.6	D	1.2	89.2	112.45	0.298
50	Chi-Chi	TCU102 (N)	1999	7.6	D	1.2	44.88	77.16	0.169
51	Duzce	DUZCE (180)	1999	7.4	D	11	42.11	59.97	0.348
52	Duzce	DUZCE (270)	1999	7.4	D	11	51.62	83.49	0.535
53	Denali Alaska	PS10 (47)	2002	7.9	D	5	102.73	134.73	0.319
54	Denali Alaska	PS10 (317)	2002	7.9	D	5	77.99	75.97	0.318

Furthermore, this study uses a wide range of nonlinear static and dynamic analysis to conduct the performance assessment of selected buildings. Besides, time history analysis used in NONLIN V8.0, a new and fast developing analysis method know as Incremental Dynamic Analysis (IDA) are performed for each of the templates in this study. Researchers have suggested that to achieve an acceptable performance assessment using IDA curves, a set of ten to twenty records must be provided with no directivity influence (Shome and Cornell, 2002). Therefore, for the purposes of performing Incremental Dynamic Analysis, a set of eighteen earthquakes showing no directivity influence is used. The set of earthquakes is presented in **Table 11**.

Table 11: The suite of eighteen ground motion records used for Incremental Dynamic Analysis

No	**Event**	**Year**	**Station**	**Ø°**	**Soil**	**M**	**R (km)**	**PGA (g)**
1	Erzincan	1992	Turkey, Erzincan	90	C	6.7	8.9	0.488
2	Imperial Valley	1979	Westmoreland Fire Station	90	C,D	6.5	15.1	0.074
3	Loma Prieta	1989	Agnews State Hospital	90	C,D	6.9	28.2	0.159
4	Loma Prieta	1989	Coyote Lake Dam Downstr.	285	B,D	6.9	22.3	0.179

5	Loma Prieta	1989	Hollister South & Pine	0	D	6.9	28.8	0.371
6	Loma Prieta	1989	Sunnyvale Colton Ave	270	C,D	6.9	28.8	0.207
7	Imperial Valley	1979	Chihuahua	282	C,D	6.5	28.7	0.254
8	Imperial Valley	1979	Plaster City	45	C,D	6.5	31.7	0.042
9	San Fernando	1971	LA, Hollywood Stor. Lot	180	C,D	6.6	21.2	0.174
10	Northridge	1994	LA, Hollywood Storage FF	360	C,D	6.7	25.5	0.358
11	San Fernando	1971	LA, Hollywood Stor. Lot	90	C,D	6.6	21.2	0.210
12	Spitak	1988	Armenia, Gukasian	90	C	6.8	36.1	0.207
13	Sup.erstition Hill	1987	Wildlife Liquefaction Array	360	C,D	6.7	24.4	0.200
14	Loma Prieta	1989	WAHO	0	D	6.9	16.9	0.370
15	Loma Prieta	1989	WAHO	90	D	6.9	16.9	0.638
16	Friuli	1976	Italy, Tolmezo	270	B	6.5	20.2	0.345
17	Corinth	1981	Greece, Corinth	0	C	6.6	19.9	0.264
18	Kocaeli	1999	Turkey, Duzce	180	C	7.1	1.6	0.427

The accelerograms for each of the earthquakes shown in **Table 11** are presented in Appendix D and plotted as acceleration versus time.

CHAPTER 6

ANALYTICAL MODELLING AND EVALUATION

6.1 Analysis methods

With the development of technology, improvements on the computer hardware and advancement of fast processing CPU, the computer methods used in civil engineering field have been expanding and developing over time too. There are several methods used to conduct the performance of structures using different analysis procedures. Depending on the analysis type, the execution time, accuracy of the results, and input parameters change from one to each other. Therefore, it is crucial that the scope of the study is well defined to select the suitable procedure. The analysis of structures may be conducted in two important categories known as Linear and Nonlinear analyses. Each of these categories is then subdivided into static and dynamic analyses. In addition, there are demonstrated both categories of the abovementioned analysis.

6.1.1 Linear analysis methods

Linear analysis is the first and the fundamental analysis procedure which is known and used massively by practicing engineers. This procedure assumes that all structural members behave elastically thus it does not take into account the plastic behavior. The time which is needed to execute this analysis is short compared to the non-linear analysis as the equations used to solve the structural unknowns are less complicated. However, the

accuracy of the results does not reach the level of the non-linear methods. Depending on the external loadings applied or studied, the linear analysis can be either static or dynamic.

6.1.1.1 Linear Static Analysis

Linear static analysis considers the applications of the loads gradually until their full magnitude. The effects of inertia and damping are neglected as the loads remain constant within time. The external loads are applied laterally in x- and y-directions. These loads are supposed to simulate maximum inertia forces induced by horizontal component of the seismic actions with the structure vibrating in the direction of its fundamental mode (Fardis, 2009). However, according to Eurocode 8 (Eurocode8, 2004) the application of linear static analysis is allowed only if two conditions are fulfilled. The first condition requires the building to be regular in elevation due to the fact that irregular building's shape in the first mode may be far from the simple approximations which are assumed in the linear static procedure. The second condition requires that the fundamental period of the building must be no more than 2 seconds or not bigger than $4T_c$ (corner period) among the constant-spectral-pseudo-velocity and pseudo-acceleration.

Additional regulations specified by Eurocode 8 are as below:

- **Regularity in plan:** the maximum story drift under the design seismic action should not exceed by 20% or more the mean drift of the story
- **Vertical regularity of mass:** story mass not exceeding by more than 50% that of an adjacent story
- **Vertical regularity of stiffness:** story stiffness not less than 70% of the story above or 80% of the average stiffness of the three stories above
- **Vertical regularity of geometry:** plan dimension of lateral-force-resisting system does not exceed by 30% or more the parallel dimension of an adjacent story

For linear static analysis, Eurocode 8 accounts especially for the effects of seismic actions on the story shears and structural period which are defined by the formulas shown below:

$$V_b = m_{eff,1} S_{a,d}(T_1) \quad \text{Equation 11}$$

where: $S_{a,d}(T_1)$ is the value taken from the design response spectrum of the first mode period $m_{eff,1}$ the estimation of the modal mass in that mode.

Furthermore, Eurocode 8 gives advice in the calculation of the first period of the structure (T_1) using the basis of mechanics centered on the Rayleigh quotient as shown below:

$$T_1 = 2\pi \sqrt{\frac{\sum_i m_i \delta_i^2}{\sum F_i \delta_i}} \quad \text{Equation 12}$$

where: $\boldsymbol{i}$ demonstrates the degrees of freedom (DOF) of the given system in vertical and horizontal directions when first period is calculated

$\boldsymbol{m_i}$ shows the mass concentrated in the degree of freedom *i*,

$\boldsymbol{F_i}$ stands for the later load applied to the degree of freedom *i*

$\boldsymbol{\delta_i}$ is the displacement of the degree of freedom *i* gained from the elastic analysis of the structure.

6.1.1.2 Linear Dynamic Analysis

Linear Dynamic Analysis is more complex than static one as it involves dynamic equations. It is also known as Modal Response Spectrum Analysis and accounts for the period of the structure. Its first step rests in the computing the modal shapes in 3D and the natural frequencies. Then, each of the modal shapes is expected to have rotations and displacement in x-, y-, and z-axis During this procedure, the eigenvector solution will be initialized which gives for each normal mode:

- The frequency of the structure, $\omega_n = 2\pi/T_n$ and its respective period T_n,

- Mode shape vector $\Phi_{n,}$
- Modal participation factors,
- Modal masses.

6.1.2 Non-linear analyses methods

In engineering design, when structures are usually designed for seismic safety using linear analysis, most will experience significant nonlinear deformations under severe earthquakes. Present and advanced design methods require to find the realistic behavior of the structure under deformations mentioned. The nonlinear analysis is a complex and more advanced procedures requiring more time to execute, therefore there are different advanced software or programs that make able this sort of analysis in easier and more precise way. Doing so, the nonlinear analysis provides the basic data for calculating structural behavior exceeding the limits that linear analysis sets up. For this section, the "Nonlinear structural analysis for seismic design," by NEHRP is used as the main source for review (NEHRP, 2010).

According to "Seismic Technical Brief No.4" by NEHRP, the main purposes where the non-linear analysis is applied are to: assess and design seismic retrofit solutions for existing buildings; design new buildings that employ new material, systems, or other features that do not conform to current building code requirements; asses the performance building for specific owner requirements. If there is the case that nonlinear analysis is used to validate the design that does not conform to the code requirements, it is very important to develop such conditions that would be justifiable to accept by the code authority.

6.1.2.1 Nonlinear Static Analysis

The Pushover analysis is a nonlinear static analysis in which the structure is subjected to gradually increasing loads. The distribution represents the inertia forces during shakings.

This analysis is carried out until the failure is reached, defining the collapse load and ductility capacity. Thus, the pushover analysis identifies any early failures or defines the weakness in the structure (FEMA-356, 2000; Eurocode8, 2004; Soni et. al., 2012; Fardis, 2009).

Considering the properties of this procedure, performing pushover static analysis is necessary especially for the existing structures. Existing structures may become deficient in the seismic aspect requirements since the codes are always advancing.

So, the main purpose of pushover analysis is to assess the performance of structures by observing its behavior, strength, and deformation requirements in earthquake design in the static inelastic analysis. The information obtained can be compared with the available capacities to reach the level desired. The most important parameters in pushover analysis are global drift, inter story drift, inelastic deformations, deformation between elements, and element connection forces, factors in which this evaluation is based on. Therefore, the nonlinear static pushover analysis is a method for predicting the seismic forces and demands and accounts the redistribution of forces that cannot be resisted in the capacity of elastic analysis.

As mentioned, an important factor in the Pushover analysis is the applied lateral load pattern which increases and makes able to follow the behavior of plastic hinges, with observing the deformations caused on the structure.

✎ Lateral Load Vector

The Pushover analysis is applied for both, 3D and 2D models, but the 2D model is mainly used because the lateral loading simulates the inertia due to horizontal seismic action. The fundamental version of the method is explained in the formula below:

$$F_i = \alpha m_i \Phi_i \qquad \text{Equation 13}$$

In which in the incrementally increased forces F_i applied on the mass of structure m_i, are proportional to the invariant pattern of displacement Φ_i.

The “Eurocode 8, Clause 4.3.3.4.2.2” states that pushover analysis should be performed by using both of the lateral load patterns stated below:

A "uniform" pattern, based on lateral forces that are proportional to mass regardless of elevation (uniform response acceleration);

A "modal" pattern, proportional to lateral forces consistent with the lateral force distribution in the direction under consideration determined in elastic analysis (Kalkan and Kunnath, 2004).

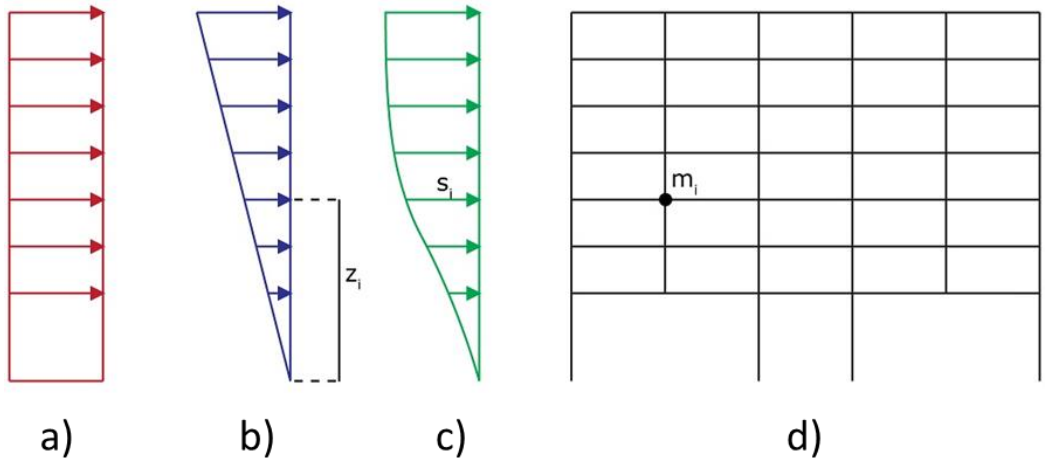

Figure 86: Load paterns in Pushover Analysis; a) uniform rectangular, b) uniform inverse triangular, c) modal, d) structural model

Obtaining the results from the two lateral force patterns, the most unfavorable result must be used.

✎ Capacity Curve

Eurocode 8 states that the capacity curve is determined by Pushover for values of the control displacement ranging between the initial value zero until the corresponding 150%

of the target displacement. This is done by determining the relation between base shear force and the control displacement. The figures below show the capacity curve of equivalent SDOF system in pushover analysis.

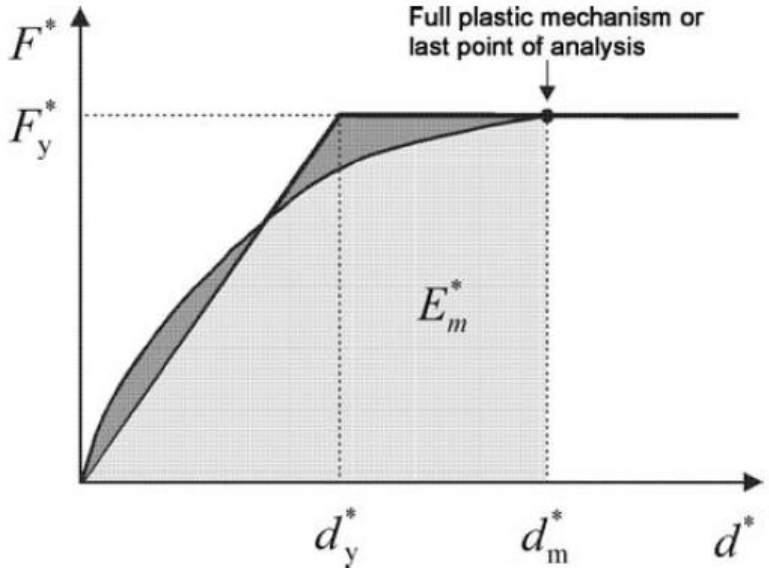

Figure 87: Elastic-perfectly plastic idealization of capacity curve of equivalent SDOF system in pushover analysis (Fajfar and Eeri, 2000).

✎ Target Displacement

The so called “Target Displacement” is another important parameter in “pushover” analysis. According to Eurocode 8, this factor is defined as the seismic demand derived from the elastic response spectrum in terms of displacement of an equivalent SDOF as shown in the **Figure 88**.

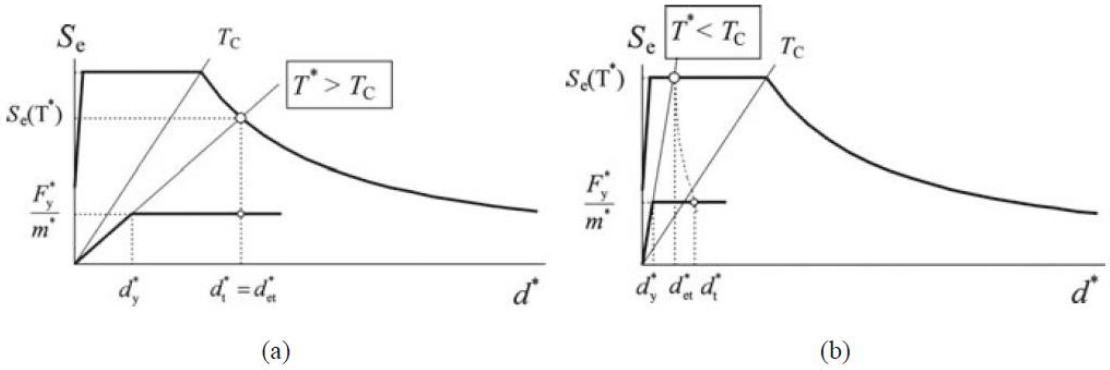

Figure 88: "Target displacement" of equivalent SDOF system in "pushover" analysis (Fajfar and Eeri, 2000): (a) long and intermediate period ranges; (b) short period range.

As can be seen in the previous figure, the "target displacement" is defined from the "equal displacement rule" modified for short period systems as the below equations state:

$$d_t = S_d(T^*) = \left[\frac{T^*}{2\pi}\right]^2 S_a T^* \qquad \text{if } T \geq Tc \qquad \text{Equation 14}$$

$$d_t = \left[\frac{S_d(T^*)}{q_u}\right]^2 (1 + (q_u - 1)\frac{Tc}{T^*} \geq S_d(T^*) \qquad \text{if } T \geq Tc \qquad \text{Equation 15}$$

6.1.2.2 Nonlinear Dynamic Analysis

The nonlinear dynamic analysis or time history analysis is a type of nonlinear analysis that provides accurate calculations for the response of the structure to strong ground shakings. It incorporates the inelastic member behavior under cyclic earthquake ground motions, and it stimulates energy dissipation in the nonlinear range (Fardis, 2009; Soni et. al., 2012).

The application of the time history analysis is mostly found in buildings with base isolation and so its behavior is run by isolation devices with strongly nonlinear force-deformation law. So, the isolation protects the building from seismic damages, but still there are some residual displacements of the isolation system. Therefore, the nonlinear dynamic analysis is of great importance. Those displacements can only be estimated

through this type of analysis. Nonlinear dynamic analysis is an advanced type of analysis that has some requirements for applying.

✎ Modeling of Inertial Mass and Gravity Load

As known, the inertial mass is the imposed mass and the self-weight of the building. It is usually required to lump the masses at each of the floor levels and include the inertial effects in two horizontal directions, including rotation about vertical axis. The vertical inertial effects should be modeled for buildings that have long span framing system, in which the vertical period may be excited by the vertical component of earthquake ground motion.

Defining the gravity loads is crucial in dynamic analysis, for considering their effects for force and deformation demands in members and large P- Δ effects.

✎ Damping

Damping is associated with the reduction of vibrations through energy dissipation. Usually in modeling and analysis, the 5% viscous damping ratio is considered to encompass all the sources of damping up to member yielding. Damping after member yielding should be reflected only by the nonlinear- force-deformation laws which describe the behavior of members in cyclic loading after member yield.

Recalling from the equation of motion, the damping is included in the equations as $C\dot{U}$. For convenience of the numerical integration of the nonlinear equation, the damping matrix is taken as Rayleigh type.

$$C = \alpha_0 M + \alpha_1 K \qquad \text{Equation 16}$$

And the damping ration as: ζ

$$\zeta = \frac{1}{2}\left(\frac{\alpha_0}{\omega} + \alpha_1\ \omega\right)$$ Equation 17

In order to achieve values for the damping ratio close to the target value $\zeta = \zeta_0 = 0.05$, a formula can be obtained:

$$\zeta = \frac{\zeta_0}{\omega_1 + \omega_2}\left(\frac{\omega_1\omega_2}{\omega} + \ \omega\right)$$ Equation 18

- **Numerical Integration**

The nonlinear time history involves the numerical integration of equation of motion which is as following:

$$M(\ddot{\mathrm{U}} + \sum_j \alpha_{gj}\ e_j) + C\dot{\mathrm{U}} + F_R$$ Equation 19

Where M is the mass matrix, U is the vector of nodal, α_{gj} are the acceleration time-histories, j denotes the translations, and F_R is the force vector.

- **Short Comparison of Nonlinear-Static and Nonlinear-Dynamic analysis**

Nonlinear dynamic analysis provides more realistic models of structures to strong ground shaking, as a result, provide more reliable assessment of earthquake performance than the static one. Also, the nonlinear dynamic analysis does not require approximate determination of global nonlinear seismic demand such as “target displacement”. The dynamic analysis does not only provide the peak deformations, but also the residual ones which are highly important for the safety and integrity of the structures. The nonlinear

static has some limitations such as capturing the transient dynamic behavior with cyclic loading and degradation. However, in general, nonlinear static analysis works well for low-rise buildings. Also, the nonlinear static analysis is effective to investigate models which may be difficult to do by nonlinear dynamic analysis.

There are also some limitations for nonlinear dynamic as shown below:

- Its complexity and lack of awareness to the practitioners,
- Lack of simple models for vertical members in 3D analysis,
- Certain sensitivity of the outcome to the choice of input ground motion.

6.1.3 Incremental Dynamic Analysis (IDA)

Incremental Dynamic Analysis (IDA) is e recently developed method by Bertero in 1977 and later adopted in the guideline of Federal Emergency Management Agency (FEMA-2000a, 2000). IDA, also called as Dynamic Pushover Analysis (DPO) (Vamvatsikos and Cornell, 2002; Mwafy and Elnashai, 2001) is a nonlinear dynamic method which is used to evaluate the performance of structures under seismic loadings. It takes into account a set of earthquake records to perform the analysis by continuously scaling each of them with a constant intensity measure (IM). Today, Incremental Dynamic Analysis is known as one of the accurate yet powerful methods in nonlinear dynamic analysis but at the same time it requires a huge computational storage and cost. Necessary steps to perform this analysis are as below:

1. Preparing an appropriate mathematical model in a computer program able to conduct IDA,
2. Preparing a set of earthquake records for the analysis,
3. Perform constant increment of intensity measure (IM) parameter until the solution does not converge during the analysis,

4. Defining appropriately the parameter of intensity measure, IM (for example: 5% damped first mode spectral acceleration $S_{a(T1,5\%)}$) and damage measure DM, (Θ_{max}, maximum interstory drift ratio),

   - Conduct an interpolation to IM and DM values to generate the dynamic pushover (IDA) curve,
   - Determination of the limit states in each of the IDA curves,
   - Summarization of the IDA curves and limit states into 16%, 50%, and 84% fractiles,

5. Interpretation of the results to estimate the performance of the selected structure.

Incremental dynamic analysis uses a set of ground motion records to perform time history analyses by scaling the intensity measure IM for each of the runs. As the IM values keep changing, the damage measure (DM) parameter will be monitored by the analysis. The critical value of the DM for each scale of IM will be gathered and plotted in a 2D graph. Therefore, structure will perform several time histories analyses until the convergence problems start occurring or global failure takes place. The end result will be a dynamic pushover curve plotted from the values gained from the analyses as shown **Figure 89**.

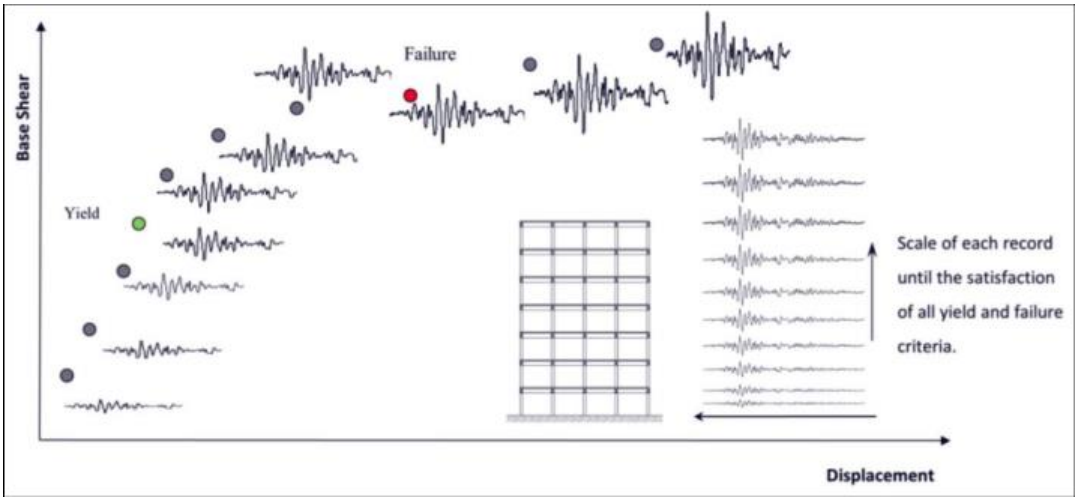

Figure 89: Performing Incremental Dynamic Analysis by scaling each of the records until global instability takes place (Constantinos, 2016)

6.1.3.1 Principles of Incremental Dynamic Analysis (IDA)

A summary of IDA fundamentals is provided in this section based on the work of previous studies (Fragiadakis and Vamvatsikos, 2011; Vamvatsikos, 2002) who developed more the existing algorithm of this method. In addition, he provided a good methodology for each of the steps required to accomplish the analysis procedure such as, the selection of the ground motions, determination of the intensity measure and damage measure, interpolation methods to generate the IDA curve, location of limit states and summarization of curves into 16%, 50% and 84% fractiles.

6.1.3.2 Important IDA parameters

The scale factor (SF): the scale factor λ is used as a step coefficient to scale the accelerogram applied to the to the time history analysis. Scale factor can be used to scale up the accelerogram when it is bigger than 1 and scale down when it is less than 1. Nonetheless, λ must be always positive value.

Intensity Measure (IM): once scale factor (λ) is defined, it will be used to scale the accelerogram to a certain intensity measure considering 5% damped first mode spectral acceleration $S_{a(T1,5\%)}$ for reinforced concrete buildings. IM must be a non-zero value which keeps increasing until the end of the analysis.

Damage Measure (DM): Damage measure (DM) is also a non-negative scalar parameter which is gained after the execution of the analysis. It refers to the maximum output damage of the structure during a certain time history analysis at a specific intensity measure. Depending on the interpretation of results or user preferences, the DM parameter can be obtained as: maximum base shear, node rotation, maximum story ductility, roof drift, global drift, interstory drift etc.

Single record IDA: After scale factor, intensity measure and damage measure parameters are determined, then the analysis can be performed. As the method of Incremental

Dynamic Analysis require a set of ground motion record, each of the records refers to one-single record IDA.

IDA Curve: The analysis for one record can be repeated multiple times for different scale factor – intensity measure, until the structural instability occurs, or convergence problem takes place. The IM and DM values are then plotted in a 2D graph as IDA curve. However, the procedure of curve drawing requires further explanations which are given in addition.

Multi Record IDA: multi record IDAs refer to the bunch of curves generated from the analysis using the set of ground motion records. Hence, for each of the records, one IDA curve is generated. The presentation of all curves in a graph for a certain structure is necessary for determining the limit states and fractiles. **Figure 90** demonstrates an example of multi record IDA curves.

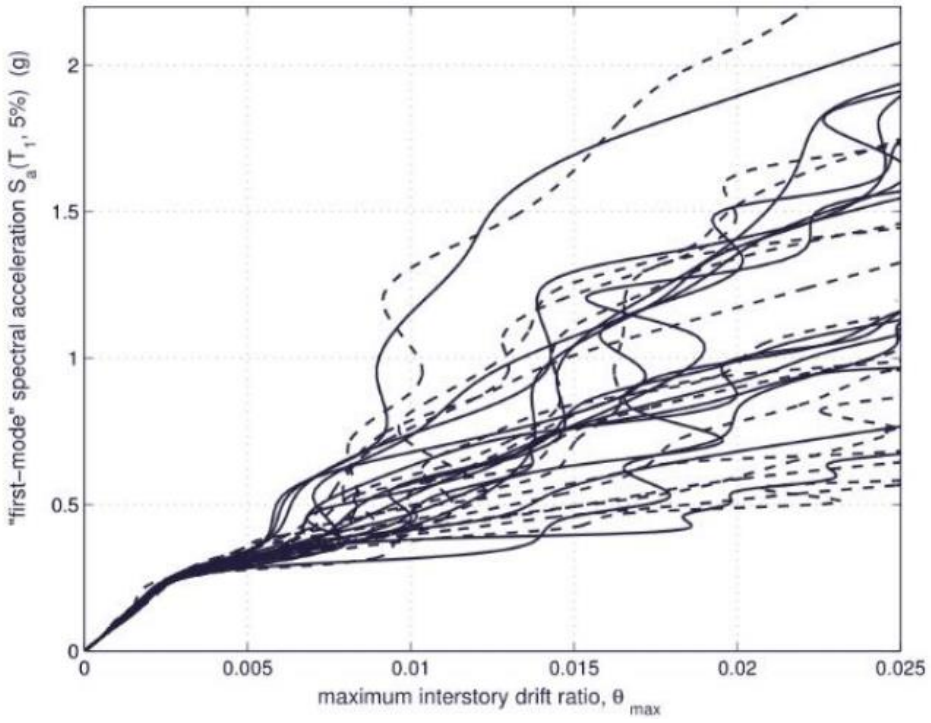

Figure 90: A set of 30 IDA curves plotted in a 2D graph as 5% damped first mode spectral acceleration $S_{a(T1,5\%)}$ vs maximum interstory drift ratio, Θ_{max}

IDA Curve Set: Once the IDA curves are generated and plotted, using the right procedure, the limit states must be determined in each of the curve. The limit states selected for IDA are immediate occupancy IO, collapse prevention CP and global instability GI. Furthermore, the IDA curves are required to be summarized into fractiles for performance assessment of the structure. Hence, the fractiles include 16%, 50%, also referred as IDA median, and 84% fractile. Presentation of these parameters in graphical manner, compose the set of IDA curves. An example of IDA limit states and IDA fractiles is given in **Figure 91**.

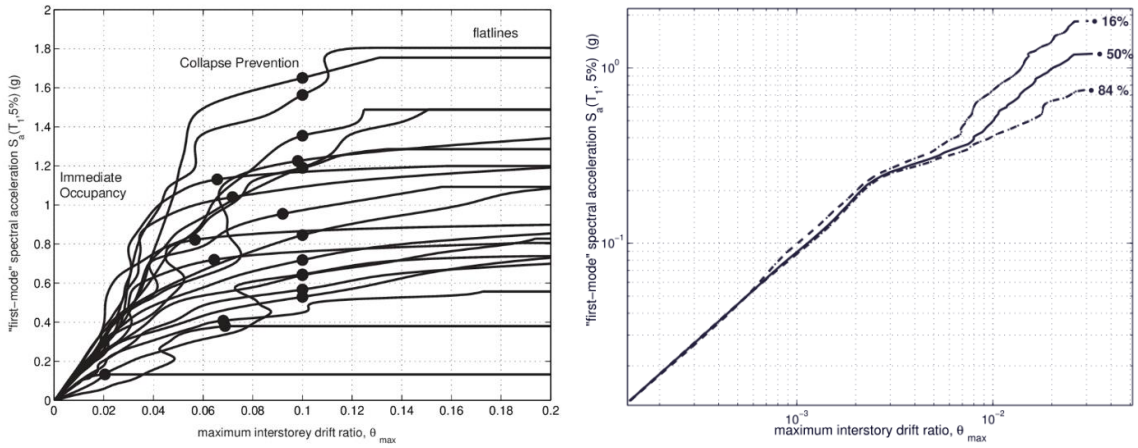

Figure 91: Example of IDA limit states (left) and IDA 16%, 50% and 84% fractiles (right)

6.1.3.3 General properties of IDA curve

As mentioned previously, while performing Incremental Dynamic Analysis, a set of earthquake records is necessary. According to previous researchers, for a reinforced concrete building, to get reliable results a set of ten to twenty ground motions is required (Shome and Cornell, 2002). Considering the nature of the earthquake and inherent characteristics of the accelerogram, predicting the IDA curve is almost impossible (Vamvatsikos, 2002). Therefore, the shape of the curve is dynamic and can be of any form as shown in **Figure 92**:

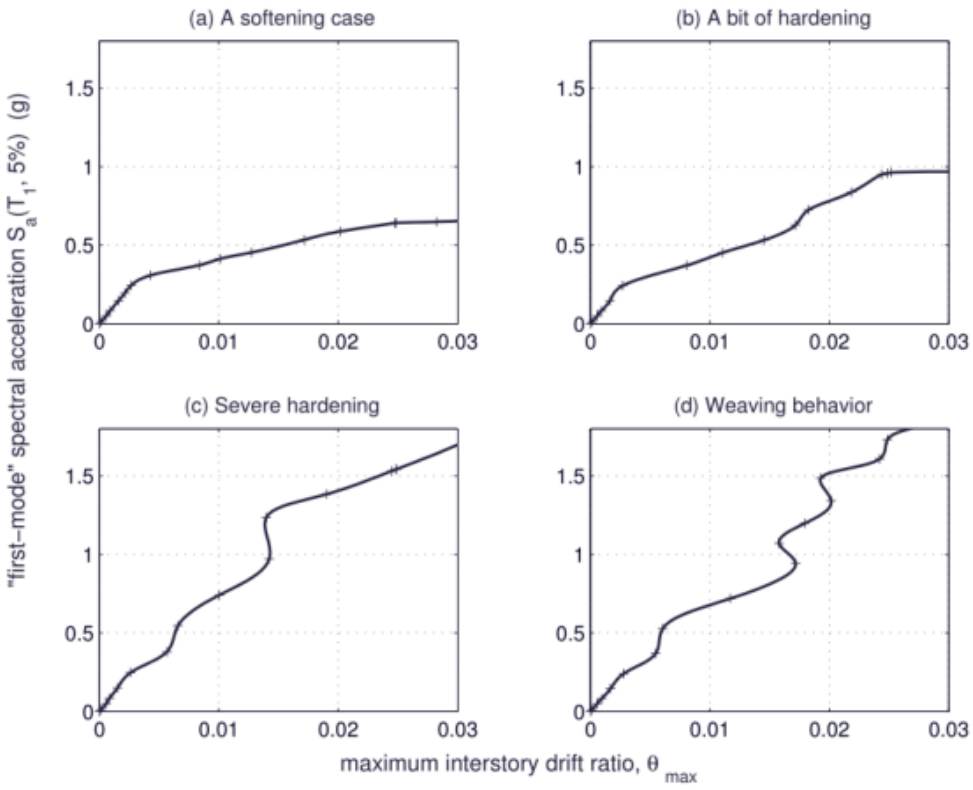

Figure 92: An example of IDA curves for a 5-story steel braced frame subjected to 4 different records (Vamvatsikos, 2002)

6.1.3.4 Determination of IDA limit states

Three main levels will be definitive for the determination of the limit states of the Incremental Dynamic Analyze curves. In compliance with previous studies (Vamvatsikos, 2002), the limit states required to conduct a structural assessment are immediate occupancy IO, collapse prevention CP and global instability GI. The methodology provided by previous researchers can be done manually (hand calculation) or using automation tools (mathematical software or programming).

Immediate Occupancy (IO): Usually belongs to the 1% of the damage measure value for a maximum global drift ratio (for example: $\theta_{max} = 1\%$). The respective IM value shall be calculated using interpolation or directly read from the curve.

Collapse Prevention (CP): for the collapse prevention limit state it must be considered a slope calculation of 20% of elastic region in the IDA curve as shown in **Figure 93**. Additional rule can be also 10% of damage measure (θ_{max} = 10%) if it happens before the 20% slope. Due to the complexity of an IDA curve, there may be more than one 20% slope appearing in the same curve. In such circumstances, the last slope occurring before reaching the 10% DM values will be taken into account as a safe limit state.

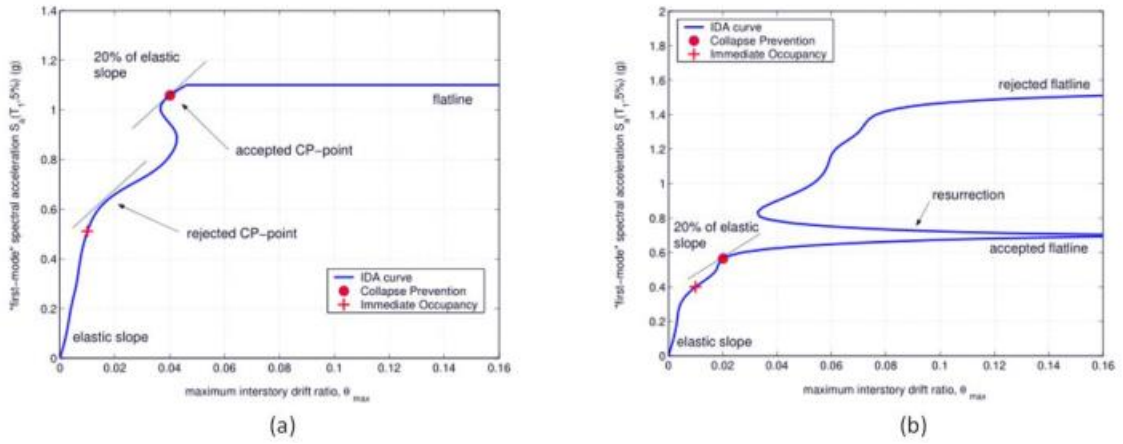

Figure 93: IDA curve with respective limit states. Multiple collapse prevention points are shown in the left figure (a), therefore the last one is considered

Global Instability (GI): Finally, the global instability limit state is required to be specified. For this limit state, the flatline of the IDA curve is considered after the softening of the curve. The beginning of the flatline is referred for the DM values. Additional occurrences to the global instability take place when there are more one flatlines in the curve. Basically, the curve after large DM values returns back and continuous hardening again as shown in **Figure 93-b**. This phenomenon is known as resurrection and must be considered as fake result not to compromise the safety of the structure.

6.1.3.5 Incremental Dynamic Analysis vs Nonlinear Static Pushover

Nonlinear static analysis, also known as Pushover, and nonlinear dynamic pushover, known as (IDA) have different properties, in their application and execution to a structure. As they both plot the performance of the structure from the elastic region to the collapse, there seems to have a correlation between them. This topic is studied further by previous researchers on the comparison and finding possible relationships among them (Vamvatsikos, 2002). It is with a great interest to study the common points between these analysis's curves as the pushover analysis is computationally costless but may underestimate or overestimate the performance of the structure compared with dynamic pushover curve (Vamvatsikos, 2002). However, the IDA procedure is considered recently as one of the accurate methods for nonlinear analysis under seismic loadings, but it requires huge computational cost and storage. Therefore, to accomplish this step, the parameters require to plot static and dynamic pushover curves must be examined carefully.

Incremental Dynamic Analysis uses different intensity and damage measure parameters from Pushover Analysis to plot the 2D curve. Therefore, the proper calibration of these procedures, targeting the same plot of two different curves is essential. Vamvatsikos (Vamvatsikos, 2002) suggests in his study to unify the damage measure parameter of the static and dynamic analysis to the same property, for example maximum roof drift θ_{max}. On the other hand, the intensity measure would be different from each other, for example, base shear ratio of the pushover and 5% damped first mode spectral acceleration $Sa_{(T1,5\%)}$ of IDA. Consequently, a calibration procedure is needed for this reason, to accomplish the step of plotting both curves in one graph. Hence, the equal displacement tangent is used to normalize the pushover IM values to the IDA's one. Equal displacement rule requires to meet the elastic region of pushover curve and IDA curve by using a coefficient which requires a trial-and-error procedure. One this process is finalized, then both curves can be compared with each other. It is worth mentioning that this comparison works the best from the 50% IDA fractile, known as IDA median.

In addition, Vamvatsikos correlates the elastic regions to be the same based on the previous procedure using equal displacement rule. Furthermore, it is seen that the collapse prevention limit state in the IDA curve corresponds with the non-negative segment of the Pushover curve. Finally, once IDA curve becomes flat, which indicates the global stability of the structure, the pushover curve starts dropping with a negative slope as shown in **Figure 94**.

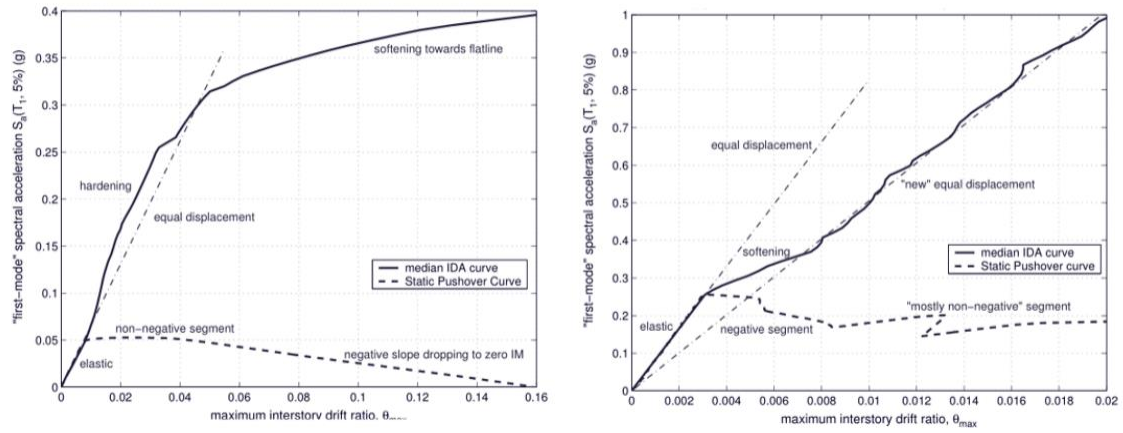

Figure 94: Comparison of Static Pushover Curve and IDA median in the same graph for a steel structure (Vamvatsikos, 2002).

6.1.3.6 IDA Algorithms

The algorithm of the analysis needs to perform multiple steps using one record to complete the IDA curve results. As the step of scaling will be defined by the user and having in mind that due to the nature of the earthquake accelerogram the output result can be unknown, the number of repetitions of the algorithm can not be predicted. For this reason, this section shows the IDA algorithm history and its evolution step by step presented before by (Yun et. al., 2002). Obviously, the algorithm needs a first value to initialize the execution. Furthermore, it will continuously repeat the logic until the structural instability or collapse. For each increment of IM value, a DM result is expected after conduction one

run. In this way, whole point values of the analysis will be gathered and plotted. A simple algorithmic schema is presented in **Figure 95**:

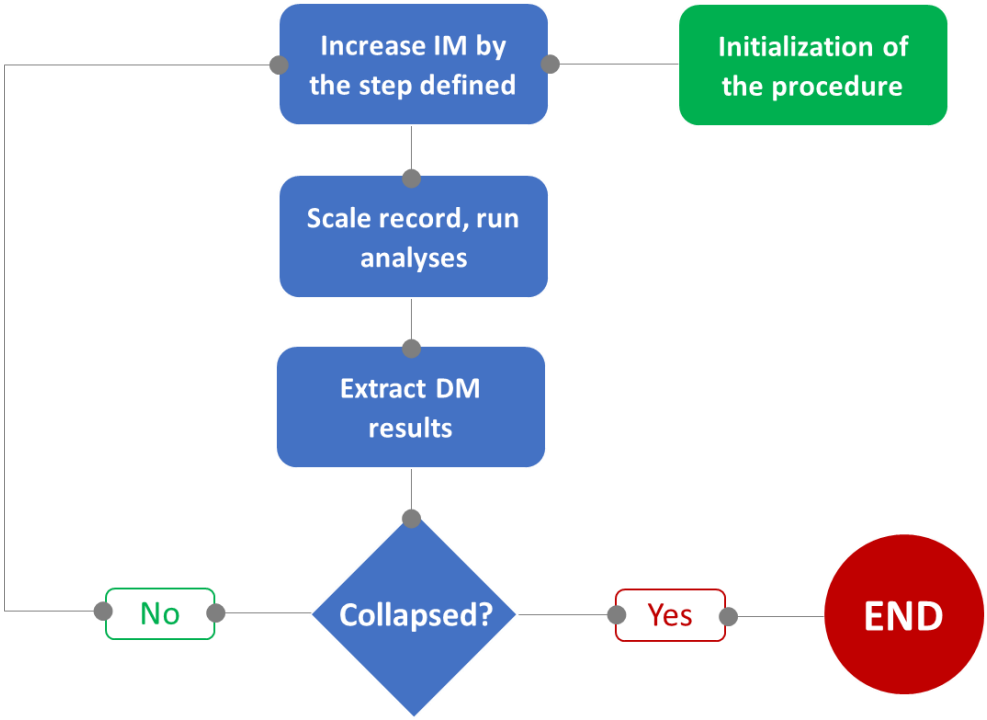

Figure 95: The flow chart algorithm used for the Incremental Dynamic Analysis (Yun et. al., 2002)

6.2 Non-linear modelling

The interpretation of global performance of the structure takes place after carefully analyzing the local-element behavior of the given model. The element capacities to maintain the structural sustainability are important to be studied in detail. To take into account the element capacity in nonlinear analysis methods, it is crucial to define the strength versus deformation relationships. To have a fulltime control of such relationships, plastic hinges are defined for each of the structural elements based on respective criteria and rules.

6.2.1 Plastic hinge concept

Plastic hinge refers to the zone of yielding in the structural element. This zone usually develops at the point of maximum bending moment reached in that member. An example for this could be the near end of the fixed support in a column, whereas for a simply supported beam, the plastic hinge will occur at the position where the concentrated load is applied as the maximum moment develops in that region. The concept of a plastic hinge is related with the well-known stress strain relationship of a ductile material such as steel. Recalling from this background, the steel material shows elastic behavior initially when the load is applied. As the load rate keeps increasing the stress and strain changes proportionally until the end of elastic region as shown in the **Figure 96**. Afterwards, material undergoes plastic behavior. In this stage the rate of strain is much larger compared with stress rate. This is justified by the reason that for any small increment in load, the deformation is large therefore produces large amount of stress respectively. At a specific point, steel material shows continuous increment of strain even though the stress does not increase. This point is known as Yield Stress. After this point, material undergoes plastic behavior as shown in the **Figure 96**.

It is exactly this zone when plastic hinge formation takes place in the structural element. When the material becomes fully plastic is defined as infinite strain value. At this point, this strain is resisted only from constant moment which develops at the region of plastic hinges and is known as *Plastic Moment*.

When the development of first plastic hinge takes place in the structure, it is expected to perform large deformations which leads the structure to turn in a Mechanism. The load at which strain gets great under the same constant moment values, is referred as Collapse load.

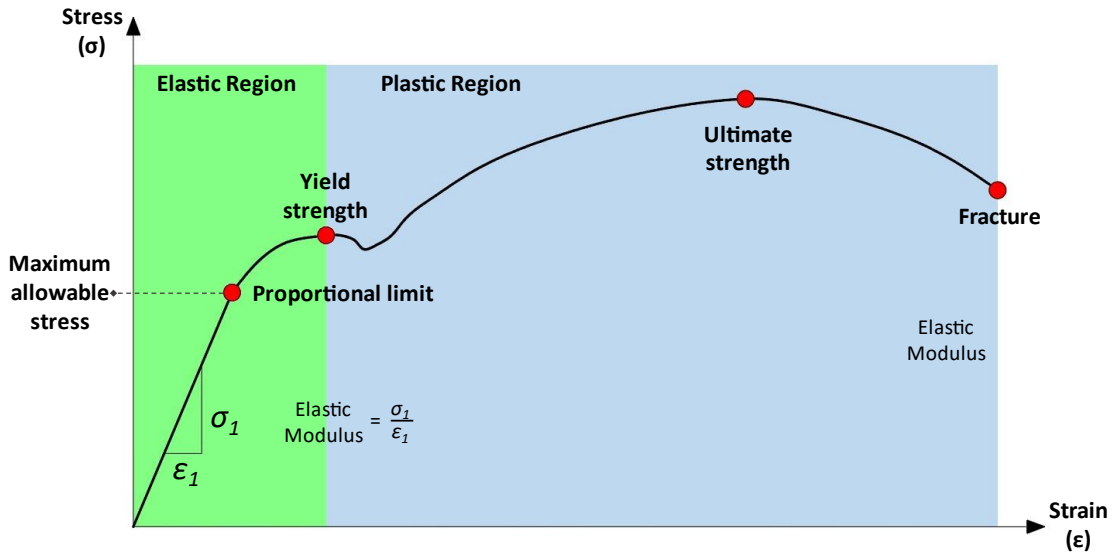

Figure 96: Stress-Strain relationship of a ductile material such as steel.

Furthermore, the rotation demand values which take place in the plastic hinge can be determined using the moment area theorems from the concepts of structural mechanics. Under increasing loads, the plastic hinges formed in the structure undergo several stages indicating the element behavior.

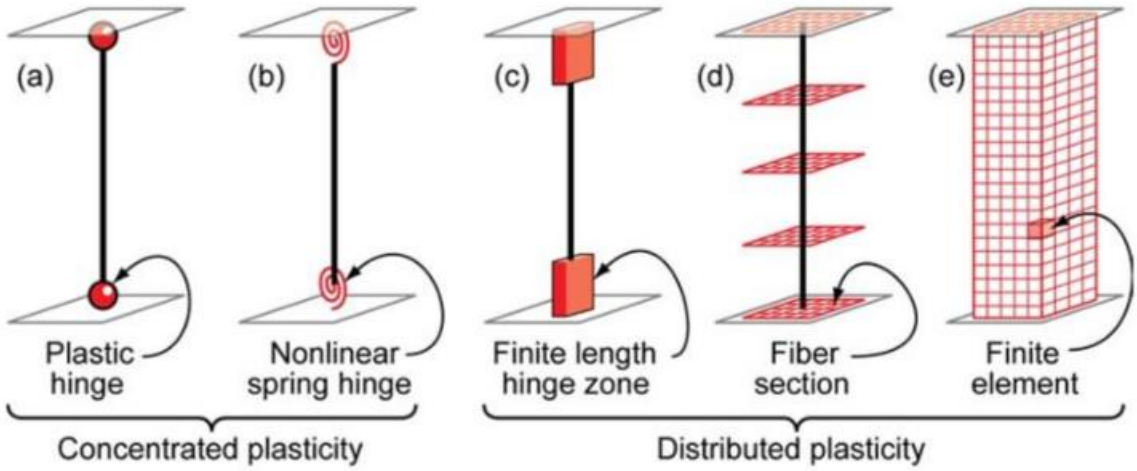

Figure 97: Idealized models of beam-column elements. ("Seismic Technical Brief No.4" by NEHRP)

The principles of the analysis require to conduct the necessary calculations for all stages of the plastic hinges excluding the last one. The last plastic hinge stage is avoided as it triggers the collapse of that element. After the rotation demand for all stages of the plastic hinge is determined, then these values must be compared with the capacity of the rotation existing in the cross section of that given element.

Figure 97 illustrates the example of the plastic hinge mechanisms. As shown in the figure, there are two main types of plastic hinges which may be defined in the analysis performed in a given structure. The first plastic hinge method refers to the Concentrated or Lumped plastic hinges. The second method refers to the Distributed plastic hinges. Both methods are described in the sections below.

6.2.1.1 Lumped plasticity approach

The concentrated or lumped plasticity hinges refer to the simplification of the process that involves inelastic deformations in a structural member in terms of load changes. The advantageous of the lumped plasticity approach relies on the simplicity of this models which reduces the computational cost and data storage. However, most of the lumped models underestimate the effects of hysteretic behaviors especially in reinforced concrete elements, hence their application is limited. In RC buildings, the plastic hinges are assigned into the ends of each of the members. In this way, the nonlinear behavior of the element is controlled by the backbone curve defined in each of the hinges. The element behavior is then plotted as a displacement versus force graph while different guidelines (FEMA-356, 2000; Eurocode8, 2004) give instructions on the determination of the performance levels such as A, B, Immediate Occupancy (IO), Life Safety (LS), Collapse Prevention (CP), C, D, and E as shown in .This method is integrated in many well-known software such as SAP2000, Etabs and more.

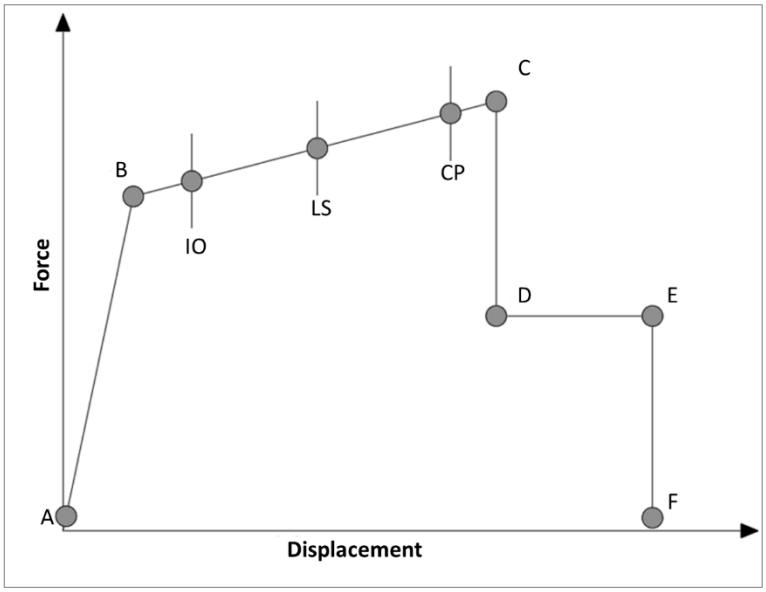

Figure 98: Lumped Hinge Behavior (FEMA-356, 2000)

6.2.1.2 Distributed (fiber) plasticity approach

Distributed or Fiber plasticity approach gives a more accurate inelastic behavior of the reinforced concrete members (Taucer et. al., 1991). Unlike plastic hinge models, these models comprise on the subdivision of the longitudinal fibers. In reinforced concrete elements there should be defined three fibers to cover all possible material behaviors. Therefore, one fiber must be defined for the confined concrete, another fiber for the longitudinal steel rebars and the last one for the unconfined concrete cover in RC members as shown in **Figure 99**.

Each of the element is composed of distributed control sections as shown in **Figure 99**-a and in different fiber cross-sections as given in **Figure 99**-b. By increasing the number of fibers distributed in a structural member will affect directly in the accuracy increase but will delay the computational execution thus leading to time cost.

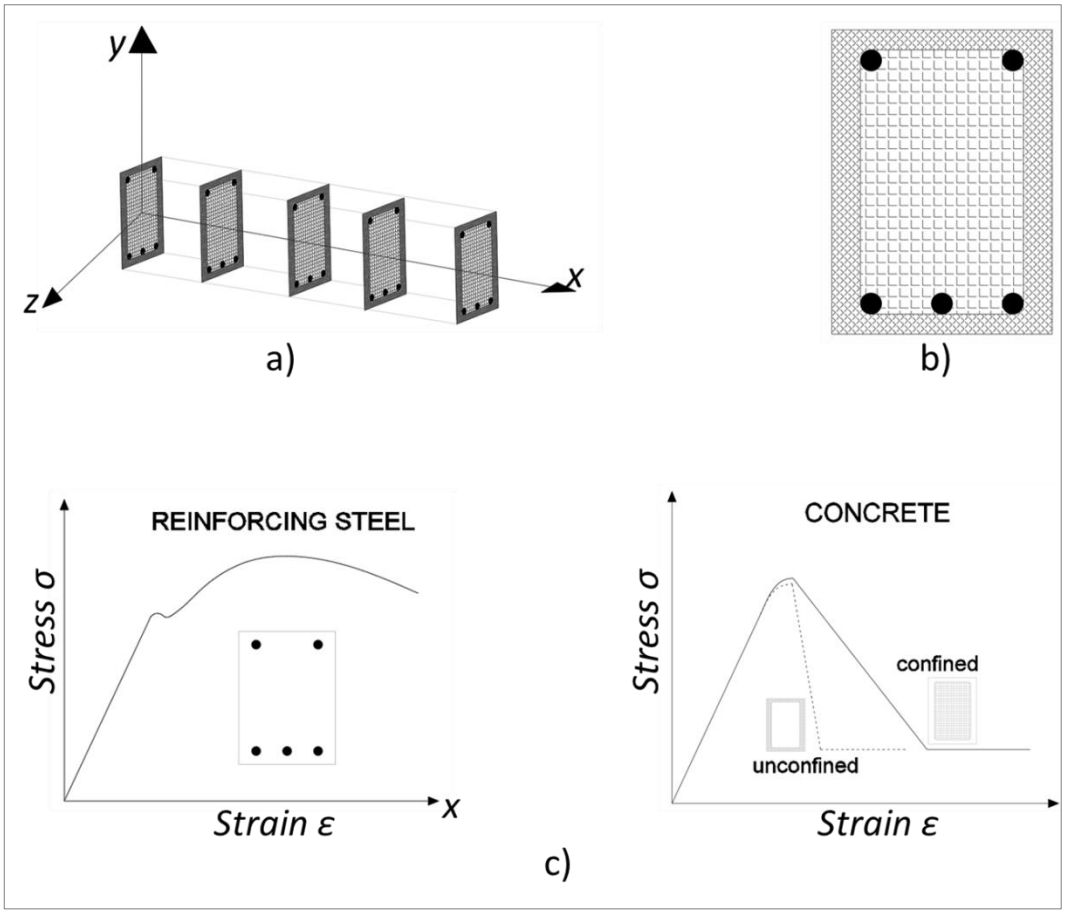

Figure 99: Distributed (Fiber) Approach model subdivided into Fibers: a) Distribution of control sections; b)Fiber subdivisions; c) Fibers for steel, unconfined and confined concrete

Furthermore, each of the fibers will be defined separately and plot the inelastic behavior graph of that specific material of the structural member. For reinforced concrete structures, fiber approach models include one fiber cross-section for steel material, one for concrete confined region and one for unconfined, concrete cover, region as illustrated in **Figure 99**-c. In this study, all models are prepared in the environment of Zeus-NL computer software which utilizes the Fiber plastic hinge method for the nonlinear analysis.

6.2.2 Plastic hinge zones for lumped plasticity

The nonlinear behavior and large damages for reinforced concrete members develop usually in the end of the structural elements, for beams and columns too. The middle part of the member is considered in the elastic region zone. The end of these members shows inefficient transverse reinforcement therefore the plastic hinges must be located in this zone. As the middle part is considered elastic, there will be no need to control the inelastic behavior hence no plastic hinges are defined. However, if the damages are expected in the middle part of the element, then plastic hinges can be defined to monitor the moment in this zone too. The plastic hinge zone for reinforced concrete beams and columns is demonstrated in **Figure 100.**

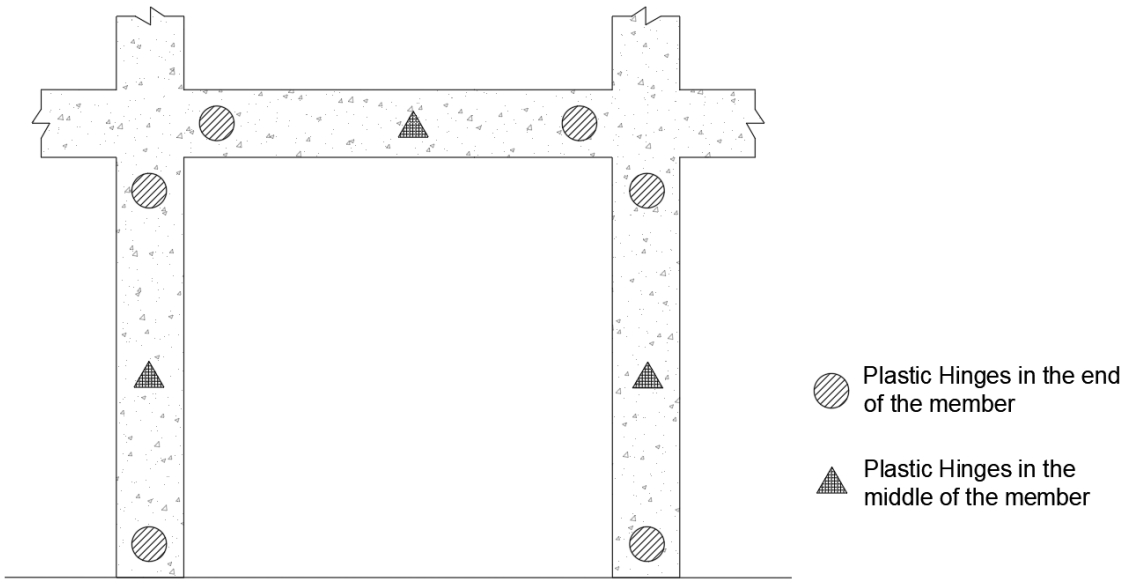

Figure 100: Plastic Hinge Zones assignment for RC beams and columns

6.3 Description of the material characteristics used in the analysis

As mentioned in the previous chapter, there are selected five reinforced concrete buildings to accomplish the scope of this study. First four buildings were designed during the communism period, 1982, and still in use nowadays. The fifth building falls in the

category of recent construction, 2005, but was heavily damaged during the November 26, 2019 Durrës earthquake. Each of the buildings serves as a residential midrise apartment. Their design was prepared to be implemented multiple times to reduce architectural cost and time during the urban development in the communism period. The recent constructed building also uses the same concept as there is one plan for two identical-twin structures. Therefore, each of the selected cases can be specified as a template building whereas their locations are in different cities of Albania.

To achieve the analytical modelling of the selected template residential buildings for this study, the material properties have to be specified. The blueprint of each of the templates includes sufficient information for the concrete and steel materials. However, after November 26, 2019 earthquake, an investigation has been conducted from the authors of this study in the damaged zones. From the site observations it has been concluded that most of the design specifications given in the blueprint on the concrete quality and stirrups spacings, were not in line with inspections done. Therefore, this study covers the experimental tests done to the concrete and steel materials in one of the template buildings selected in this study which has been damaged during the Durrës earthquake. In addition, there is provided sufficient information on the laboratory experiments as well as general material properties.

6.3.1 Determination of the concrete strength

The concrete class given in the blueprint of selected template buildings, belongs to M200 for the 1982, and M250 for the 2005 designed templates, based on the old Albanian concrete class labeling. As explained in previous chapter, M200 corresponds to C16/20 and M250 to C20/25 concrete classes. As the priority of this study is to consider old reinforced concrete buildings dating back to communism period, the laboratory experiments are conducted for one of the 1982 template building which was damaged during the Durrës earthquake on November 26, 2019. Based on the blueprint details for the concrete class, C16/20, the detailed material properties are given in **Table 12**.

Table 12: The properties for C16/20 (M200) concrete material

Properties of Concrete	**C16/20**
Cubic strength	f_{ck} = 16 MPa (fc,cube)
Compressive cylinder strength	f_{ck} = 20 MPa
Mean value of cylinder compressive strength (28 days)	f_{cm} = 28 MPa
Characteristic axial tensile strength	$f_{ctk(95\%)}$ = 2.9 MPa
Characteristic axial tensile strength	$f_{ctk(5\%)}$ = 1.5 MPa
Mean value of axial tensile strength	f_{ctm} = 2.2 MPa
Young's Modulus	E_{cm} = 30 GPa
Design value of modulus of elasticity	E_{cd} = 25 GPa
Design value of compressive strength	$f_{cd} = \alpha * fck/\gamma c$ = 11.3 MPa
Partial factor	γ_c = 1.5 and α = 0.85
Poisson's ratio	ν = 0.20

The laboratory results are done for the concrete in compression using a standard cylindrical sample as shown in **Figure 101**.

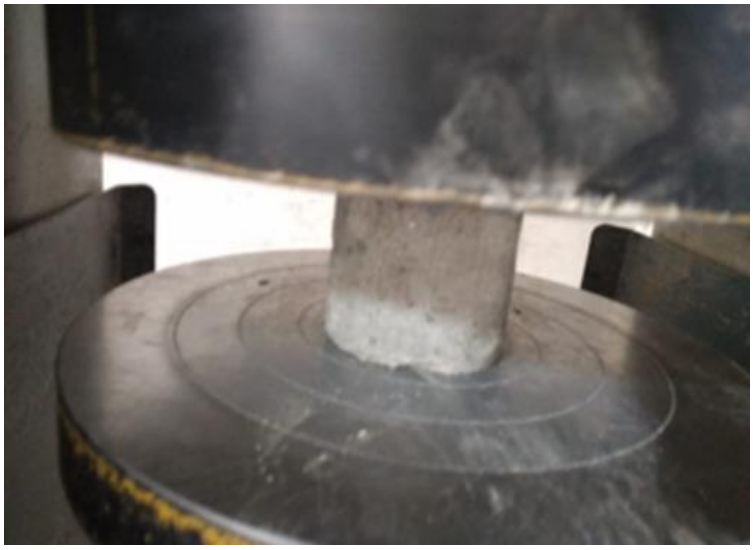

Figure 101: Laboratory test for the concrete sample of 1982 template building

Based on the findings of laboratory experiment results, compressive strength of the concrete samples was found to be about half of the design requirements of the Albanian design code (KTP-2-78, 1978) as shown in **Table 13**.

Table 13: Laboratory results on the concrete material of 1982 template design

Sample (Nr.)	**K1**	**K2**
Sample height (H)	77.0	77.5
Sample diameter (D)	75.0	75.0
H/D ratio	1.03	1.03
Weight (g)	778	797
Density (g/cm^3)	2.287	2.328
Load (kN)	27.9	35.6
Compression Strength (MPa)	6.32	8.06

The performance of these template buildings is expected to be low as a fact that they were designed prior to the last version of Albanian designed code KTP-N2-89.

6.3.2 Determination of the steel grade

For the steel reinforcement used in these buildings, the blueprint specified it as "Ç-3" with a strength capacity of 2100 Kg/cm^2. The properties for steel "Ç-3" based on the Albanian design code are shown in **Table 14**.

Table 14: Properties for steel material "Ç-3", 2100 Kg/cm^2

Properties of Steel Material	**"Ç-3"**
Tensile strength	f_{ck} = 250 MPa
Yield strength	f_{yk} = 320 MPa
Young's Modulus	E_s = 210 GPa
Partial factor	γ_s = 1.15

Design yield (shear)	f_{ywd} = 180 MPa
Design yield (strength)	f_{yd} = 215 MPa
Poisson's ratio	ν = 0.30

In addition to the material properties of steel, there are done laboratory test for three steel specimens taken from the damaged building during the November 26, 2019 earthquake. The experiment is conducted in tension for 14-, 16-, and 22-mm diameter steel bars. The results from each of the specimens are demonstrated in **Table 15**.

Table 15: Laboratory results on the steel material of 1982 template design

Sample (Nr.)	**1**	**2**	**3**
Nominal Diameter (mm)	14	16	22
Measured Diameter (mm)	14.96	15.87	21.91
Linear weight (kg/m)	1.377	1552	2.958
Cross-sectional area (mm^2)	175.4	197.66	376.75
Tensile strength (N/mm^2)σ_y	267.6	269.4	331.8
Ultimate strength (N/mm^2)σ_u	402.1	400.2	469.4
σ_u/σ_y Ratio	1.502	1.486	1.415
Relative Deformation (%)	32.14	35.00	30.00

Unlike concrete, the values gained from the laboratory tests on the concrete samples are acceptable according to the design definitions in compliance with the values given in **Table 14**.

Nevertheless, is worth mentioning and highlighting the observations from the site inspections done after the November 26, 2019 earthquake. Main problem from the reinforcement was especially focused on the stirrups spacing. Almost all examples exceed

the design parameters on this issue. From the investigations, stirrups vary from 20 cm to 25 cm leading to many possible failures in beams and columns.

6.4 ZEUS NL modelling

Majority of the analyses considered to estimate the seismic behavior of selected buildings in this thesis are performed using Zeus-NL software (Elnashai et. al., 2002). Zeus-NL is a computer program developed by Elnashai at the Mid-America Earthquake Center, University of Illinois at Urbana-Champaign. Zeus-NL is selected for its powerful computational background on running linear and nonlinear, static and dynamic analysis, considering geometrical nonlinearity and P-delta effects.

Zeus-NL performs a wide list of analysis such as Eigenvalue Analysis, Static Constant Load Analysis, Static Pushover Analysis, Static Adaptive Pushover Analysis, Static Time-History Analysis, Dynamic Time-History Analysis, and Incremental Dynamic Analysis. Its material types are predefined in the package library hence user can choose among different options such as concrete, steel, composite, and uniaxial constant fiber-reinforced plastic confined concrete materials. Zeus-NL software provides the option to apply in mathematical model loadings as forces, displacements, and accelerations. It also takes into account the prediction of large displacement of frames by considering both geometrical nonlinearity and P-delta effects. The advantageous of this software is that it provides an easy and well-organized method to run the predefined analyses.

Zeus-NL is a platform which has a two- and three-dimensional finite element analyses facility developed especially for earthquake engineering applications. It is accurate, efficient and fast processing software capable of undertaking inelastic displacement analyses of various complex frames by using the fiber approach with a group of material models and elements offered by software library. As mentioned before, the software can model steel, reinforced concrete and composite structures under static and dynamic forces considering the effects of geometric nonlinearities and inelasticity of the material (Elnashai et. al., 2002). As shown in the Figure 102, the software uses a fiber approach

for the nonlinear analyses of the reinforced concrete structures by dividing and monitoring the cross section into several fibers such as confined concrete fibers, unconfined concrete cover and finally the reinforcement fiber. Zeus-NL software has been used effectively to investigate the seismic vulnerability of reinforced concrete structures (Erberik and Elnashai, 2004; Jeong and Elnashai, 2005; Hueste and Bai, 2007)

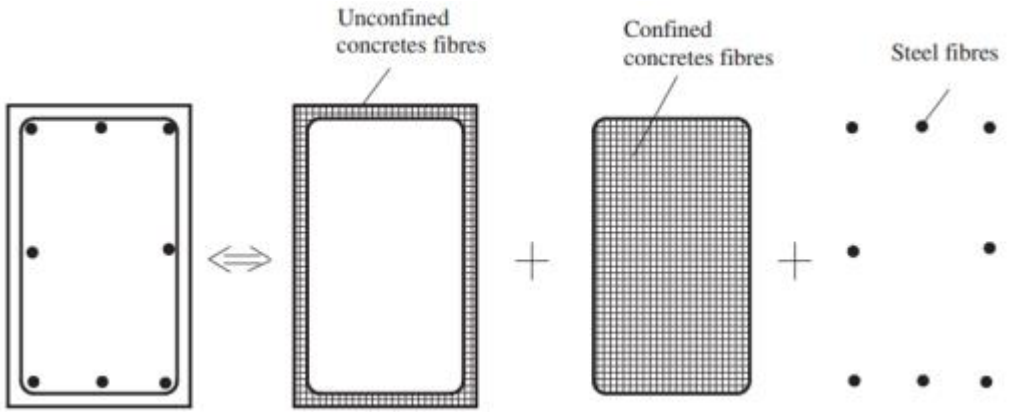

Figure 102: Fiber approach used in Zeus-NL for a RC rectangular section (Elnashai et. al., 2002).

6.5 Analyses

In the Zeus-NL software library there a provided a list of analysis considering from the conventional ones to the recent and modern analysis used in research and engineering practice. The program is capable of performing the static and dynamic of linear and nonlinear analysis of any mathematical model build in its environments. User can select among different analysis such as:

- Eigenvalue Analysis
- Static Constant Load Analysis
- Static Pushover Analysis
- Static Adaptive Pushover Analysis

- Static Time-History Analysis
- Dynamic Time-History Analysis
- Incremental Dynamic Analysis.

Figure 103 illustrates the main window which appears while starting a new project in Zeus-NL. The analysis can be switched at the loading category at the end of the **Figure 103**.

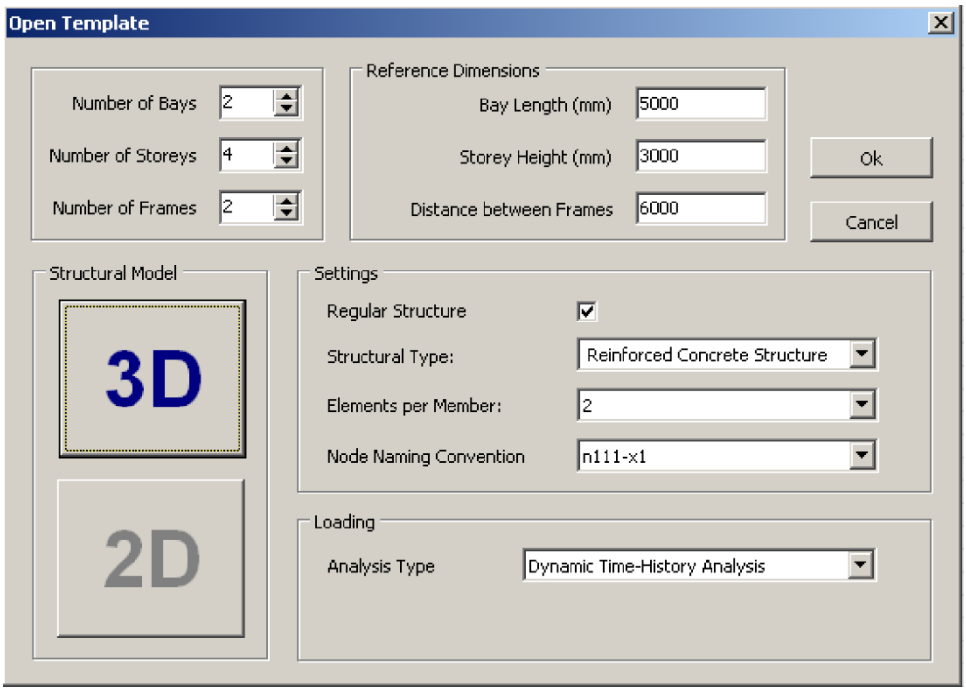

Figure 103: A graphical user interface (GUI) of the Zeus-NL window while starting a new project

6.5.1 Materials

Zeus-NL software provides a library with several materials which can be used during the modelling phase. The main material categories are steel, concrete, and other special materials which are defines accordingly. Using this of materials, user can have endless combinations due to the fact that they can be manually customized for any property

determined in the package library settings. The library includes a list of steel materials defined as stl0, stl1, stl2, for concrete defined as con1, con2, con3, con4 and frp1.

After defining the desired material, user is supposed to link these materials in the respective element section. Section properties may vary depending on their type therefore may cause an error if the wrong material is linked to them, for example linking concrete for the reinforcement of the element. Seems like software is not able to perform all possible checks hence user must be careful while preparing the material model. Some of the problems which may affect seriously the analysis could be the improper material association with the respective element section or usage of any special characters, including here the space as well, while renaming the material. Zeus-NL will end up showing an error prompt and the analysis will not be executed. Nevertheless, Zeus-NL offers a full user-control to material properties so it can be customized according to the exact project details. In case of deleting a material, section or other inputs, Zeus software provides an undo/redo function. By selecting different materials available from the library, the user can modify the properties of the materials due to the purpose of the project.

6.5.1.1 Steel material types:

There are four steel types predefined in the Zeus-NL material library which differs from each other in the parameters. Below it is provided a short description for each of the materials used in the package library:

- **stl0:** The first steel material from the Zeus-NL library is designed for linear elastic models and applied for uniaxial modeling of mild steel. stl0 requires only one parameter, the elastic modulus. **Figure 104** demonstrates an example of stl0 material and its parameters.

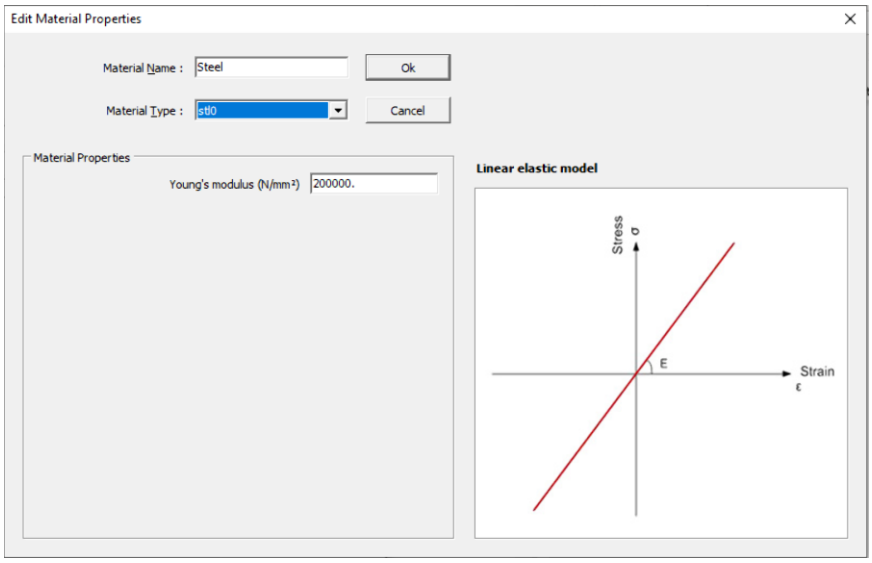

Figure 104: Steel "stl0" material properties dialog box

- **stl1:** The second steel material from the Zeus-NL library is designed for bilinear elasto plastic model with kinematic strain hardening and applied for uniaxial modeling of mild steel. stl1 requires three parameters, the elastic modulus, strain hardening and yield strength. **Figure 105** demonstrates an example of stl1 material and its parameters.

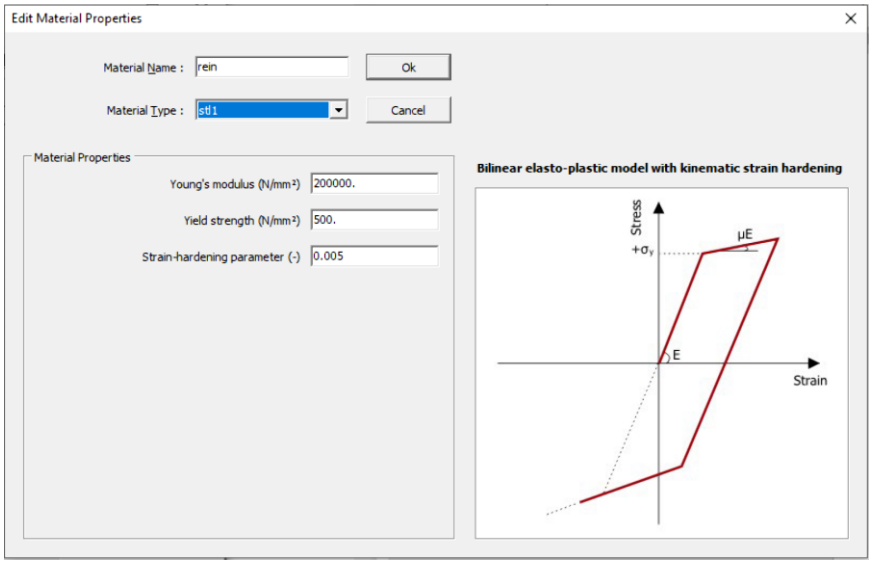

Figure 105: Steel "stl1" material properties dialog box

- **stl2:** This material type belongs to Ramberg-Osgood model (Power-Law) with Masing type hysteresis curve which is designed for bilinear elasto plastic model with kinematic strain hardening and applied for uniaxial modeling of mild steel. stl2 requires four parameters, the elastic modulus and three coefficients derived from the best fitting procedure of experimental data. **Figure 106** demonstrates an example of stl2 material and its parameters.

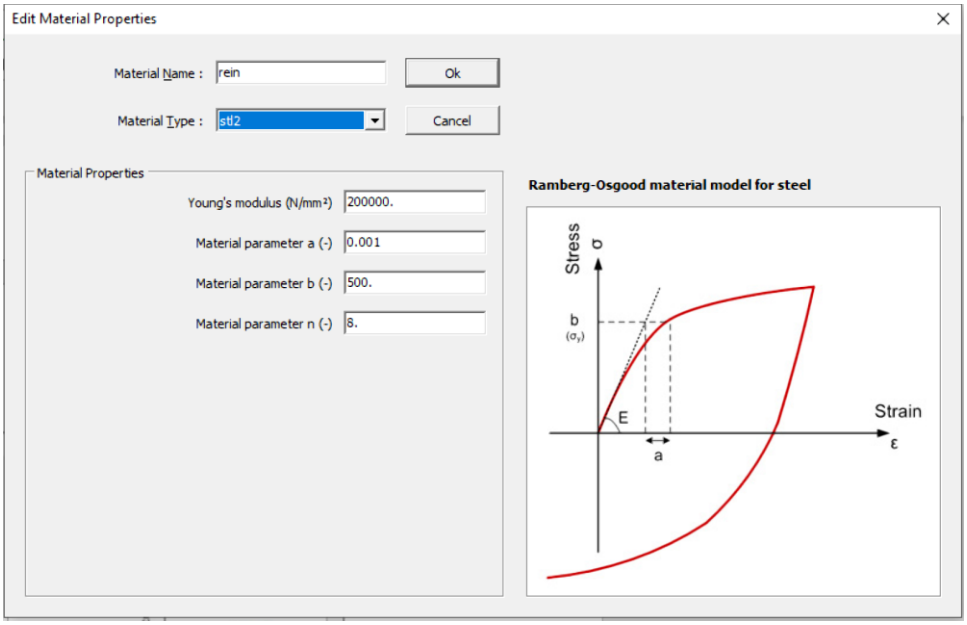

Figure 106: Steel "stl2" material properties dialog box

- **stl3:** The last steel material belongs to Menegotto-Pinto material model applied for uniaxial modeling of mild steel. stl5 requires eight parameters, the elastic modulus, initial secant modulus, strain hardening, initial curvature parameters and four constants derived from the best fitting procedure of experimental data. **Figure 107** demonstrates an example of stl3 material and its parameters.

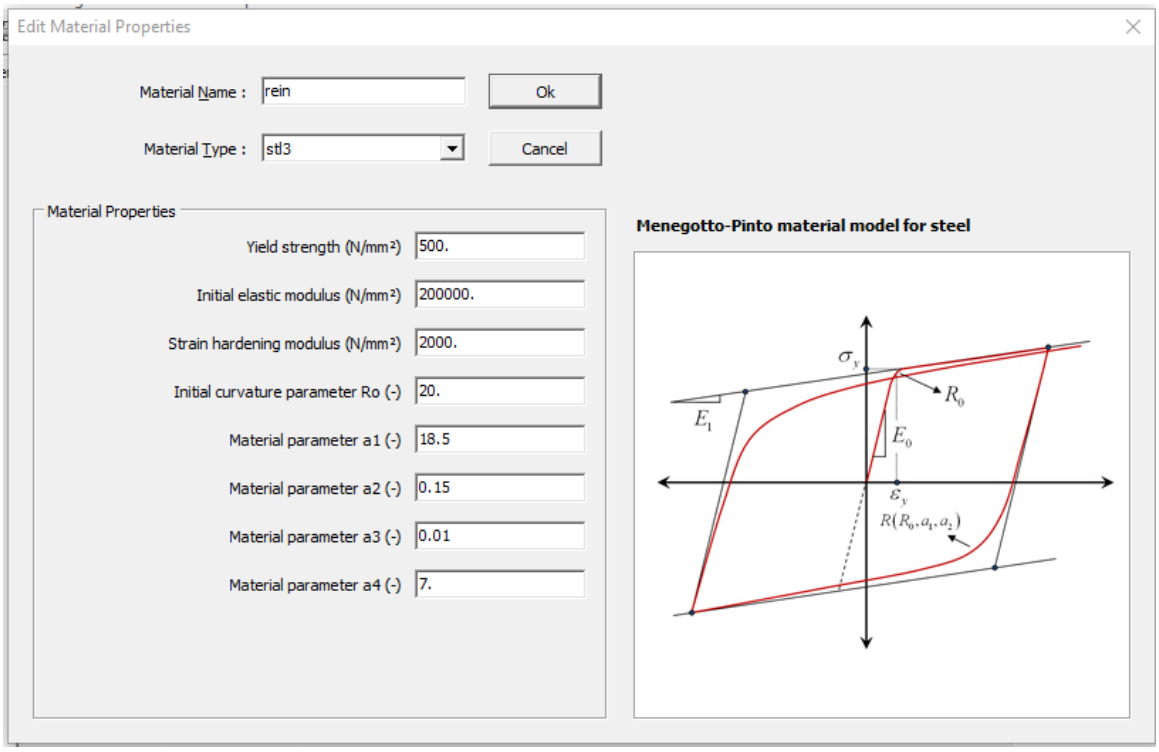

Figure 107: Steel "stl3" material properties dialog box

6.5.1.2 Concrete material types:

Zeus-NL library provides four concrete types to be used for the mathematical model. Each of concrete materials offered differ in the parameters user has to input. Below it is provided a short description for each of the materials used in the package library:

- **con1:** This concrete material refers to the trilinear concrete type and is the simplified uniaxial concrete model in the package library. The tension resistance and effects of confinement stirrups are not included as parameters therefore will not taken into account. Parameters involved in this concrete type are: Initial stiffness, compressive strength, degradation stiffness, and residual strength as shown in **Figure 108**.

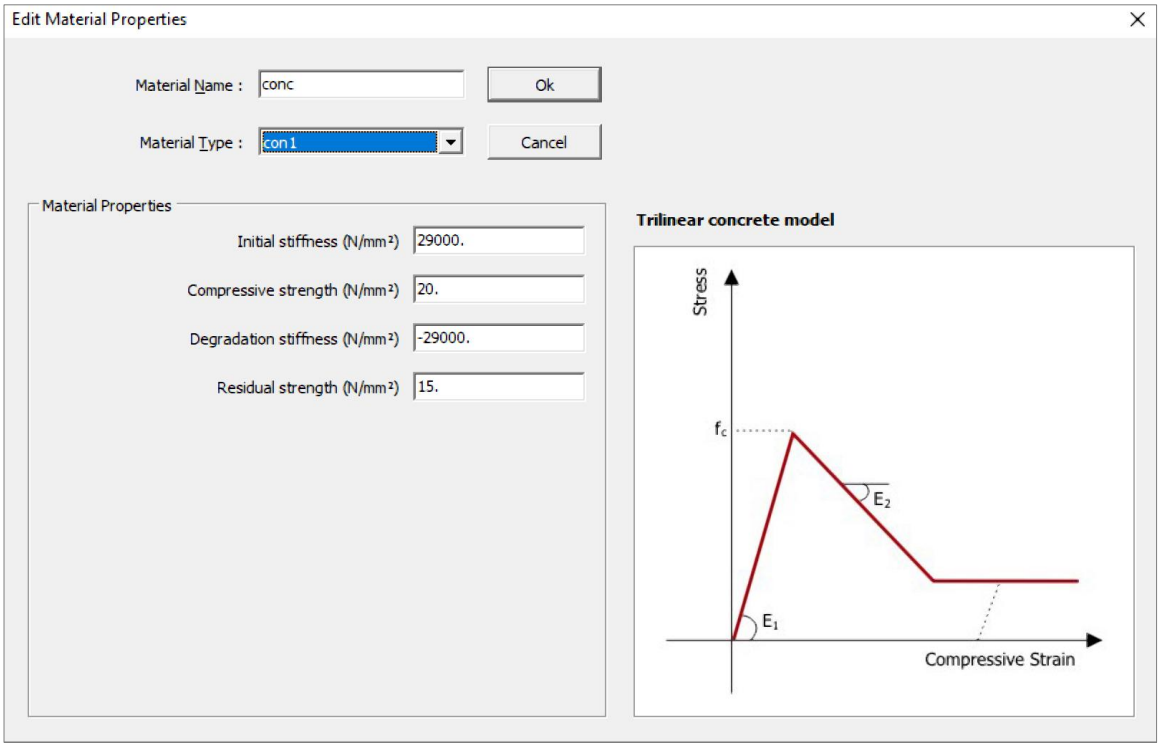

Figure 108: Concrete "con1" material properties dialog box

- **con2:** This concrete material refers to the Nonlinear concrete model with constant confinement modeling based on the work of Mander (Mander et. al., 1988). The confining pressure coefficient is assumed by taking into account the maximum pressure from the steel hooks and reflected in the material property as constant confinement factor. This factor then is used to scale the stress strain relationships. Moreover, the cyclic rules were modified by Martinez-Rueda and Elnashai (Martinez-Rueda and Elnashai, 1997) to make possible the insurance of cyclic degradation of stiffness and strength. The appropriate modelling would require four inputs for this material, considering the compressive strength, tensile strength, crushing strain and confinement factor.

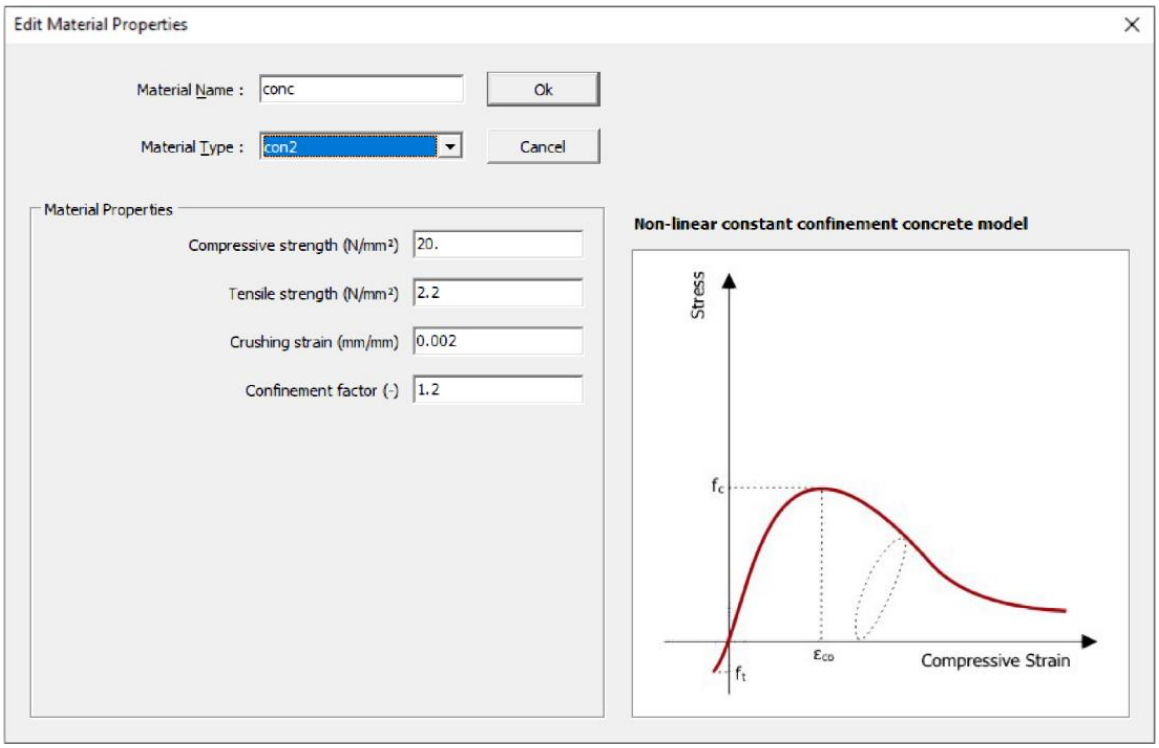

Figure 109: Concrete "con2" material properties dialog box

- **con3:** Concrete material type 3 is used for nonlinear concrete models with passive confinement modelling and uniaxial concrete model including more advanced variables as regards to the transverse confinement. This method was developed by Madas and Elnashai (Madas and Elnashai, 1992) and constantly updates the stress of the transverse confinement for a reinforced concrete element under cyclic or transient loading. Considering the wide list of parameters included in this material type, it can be emphasized that it completely defines the material model. The parameters included in this material are the concrete compressive strength, concrete tensile strength, concrete crushing strain, Poisson's ratio of concrete, yield stress of transverse steel, Modulus of elasticity of transverse steel, strain hardening parameter of transverse steel, diameter of stirrups, spacing of stirrups and diameter of concrete core as shown in **Figure 110**.

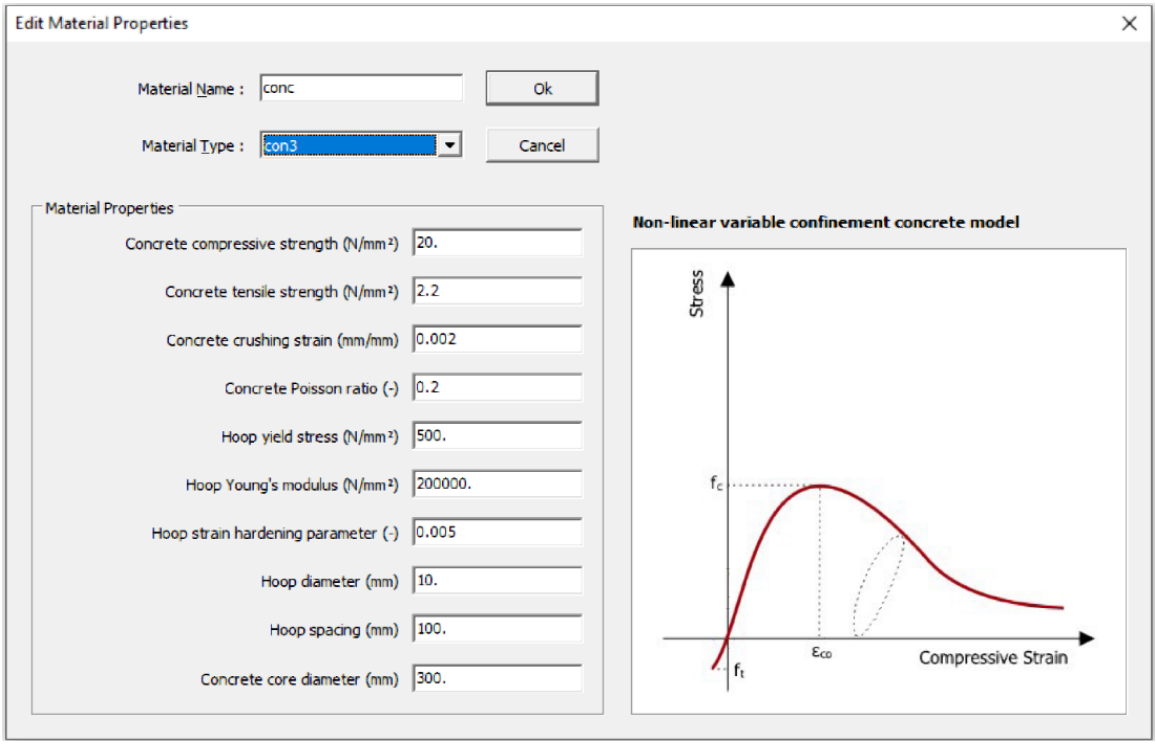

Figure 110: Concrete "con3" material properties dialog box

- **con4:** Concrete type 4 belongs to Sheikh-Uzumeri nonlinear concrete model which takes into account the effect of confinement concrete core as well as the effect of tie spacing. It is usually used for the simplified uniaxial concrete model for regular-square cross-sections with uniform distributed longitudinal steel bars. The parameters characterizing this material type are the concrete compressive strength, steel compressive strength, strain corresponding to maximum stress in plain concrete, ratio of the volume of total lateral reinforcement to the volume of core, center-to center distance of outer tie, tie spacing, number of longitudinal bars and area of one longitudinal bar.

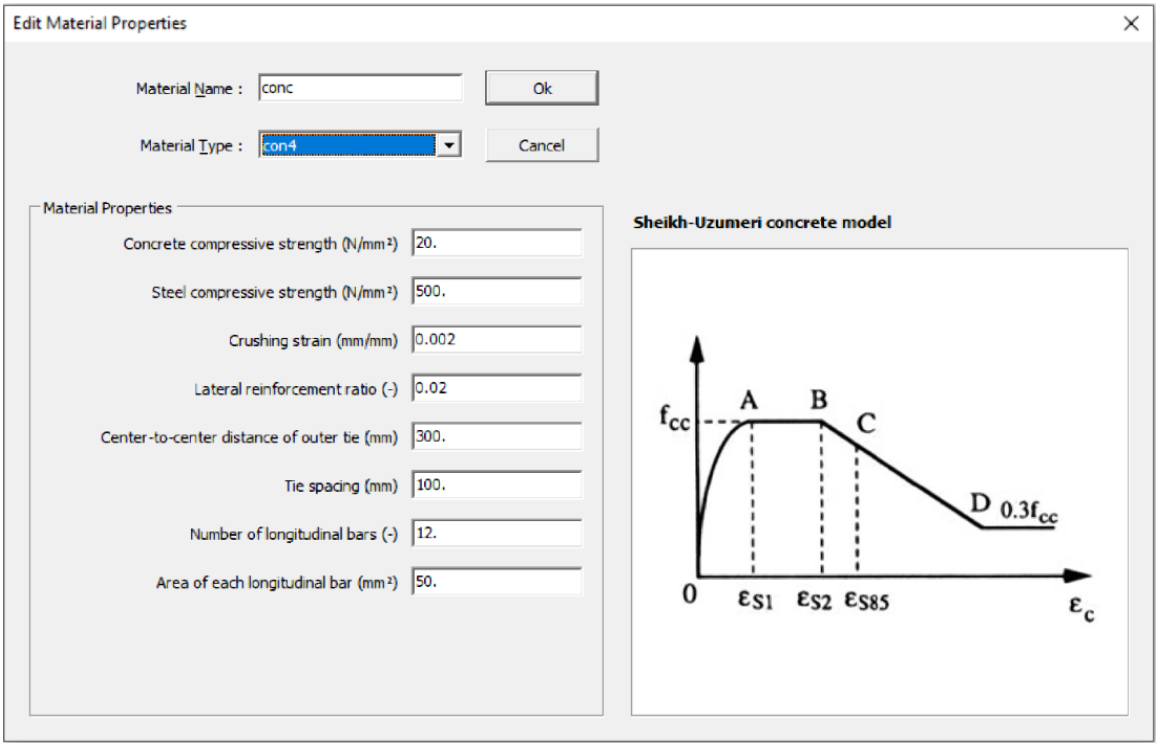

Figure 111: Concrete "con4" material properties dialog box

6.5.1.3 Special types of materials:

There are two special types of materials predefined in the Zeus-NL library, the ecc and frp1 as described below:

- **ecc:** This material belongs to the uniaxial constant fiber-reinforced plastic confined concrete model and has nine parameters to be specified as shown in the **Figure 112**.

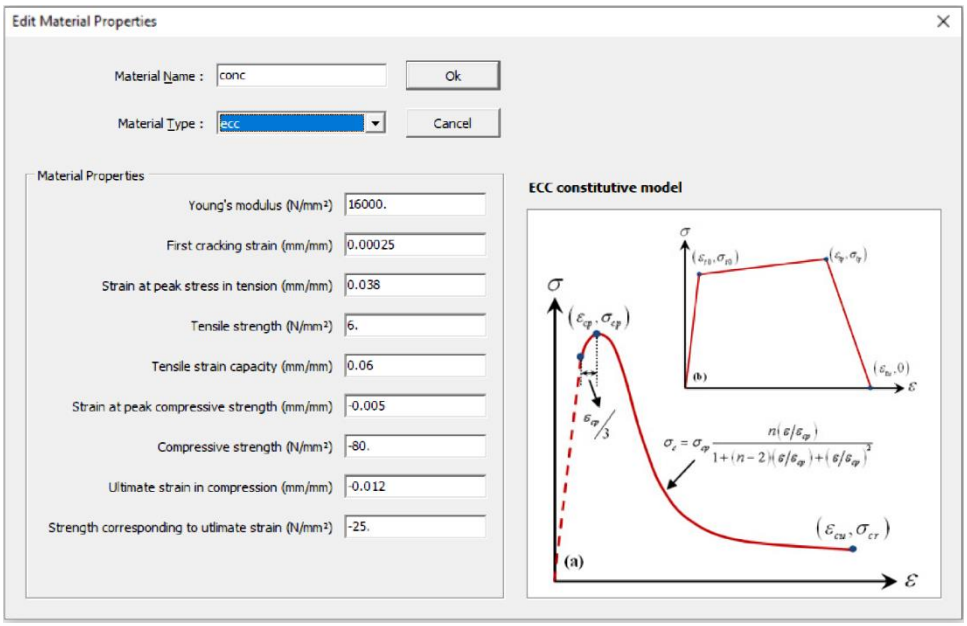

Figure 112: Concrete "ecc" material properties dialog box

- **frp1:** The last material in the package library is frp1, trilinear FRP model, which has four parameters to be specified as shown in the **Figure 113**.

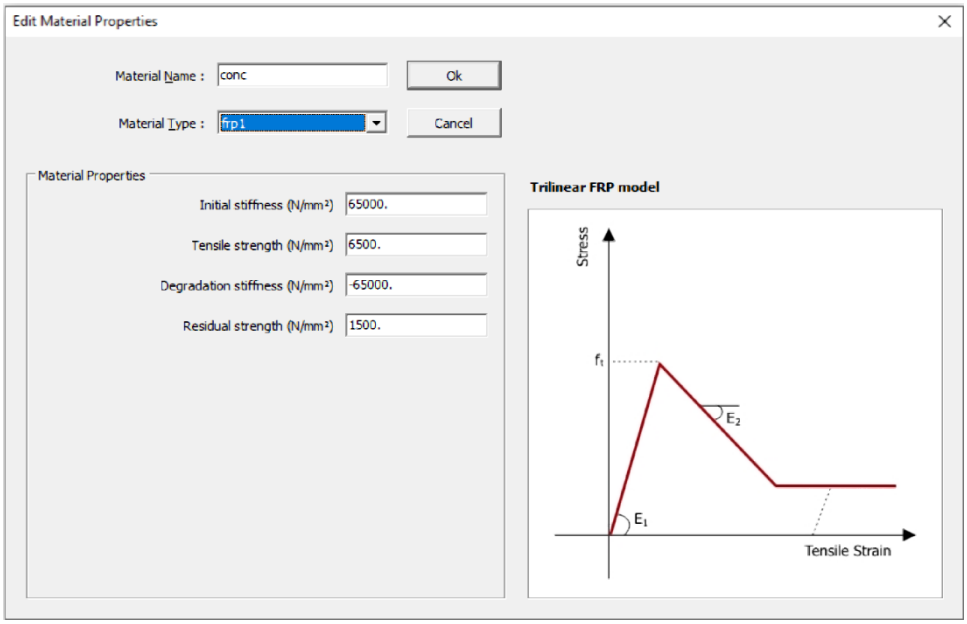

Figure 113: Concrete "frp1" material properties dialog box

6.5.2 Sections

The section module of Zeus-NL program provides different available cross-section types, including steel, reinforced concrete, and composite to model any structure considering these combinations. Section types are predefined in the package library and can be modified according to users' preferences considering their respective parameters. Special attention must be paid to the renaming process. Similar to materials definition, section's rename must not include special characters nor space and not more than eight characters are allowed. This seems something ignorable, but when dealing with multiple elements in a structure with different locations and/or orientations (therefore different labels) this may need to be well specified in the section name and give some limitations to the labeling phase.

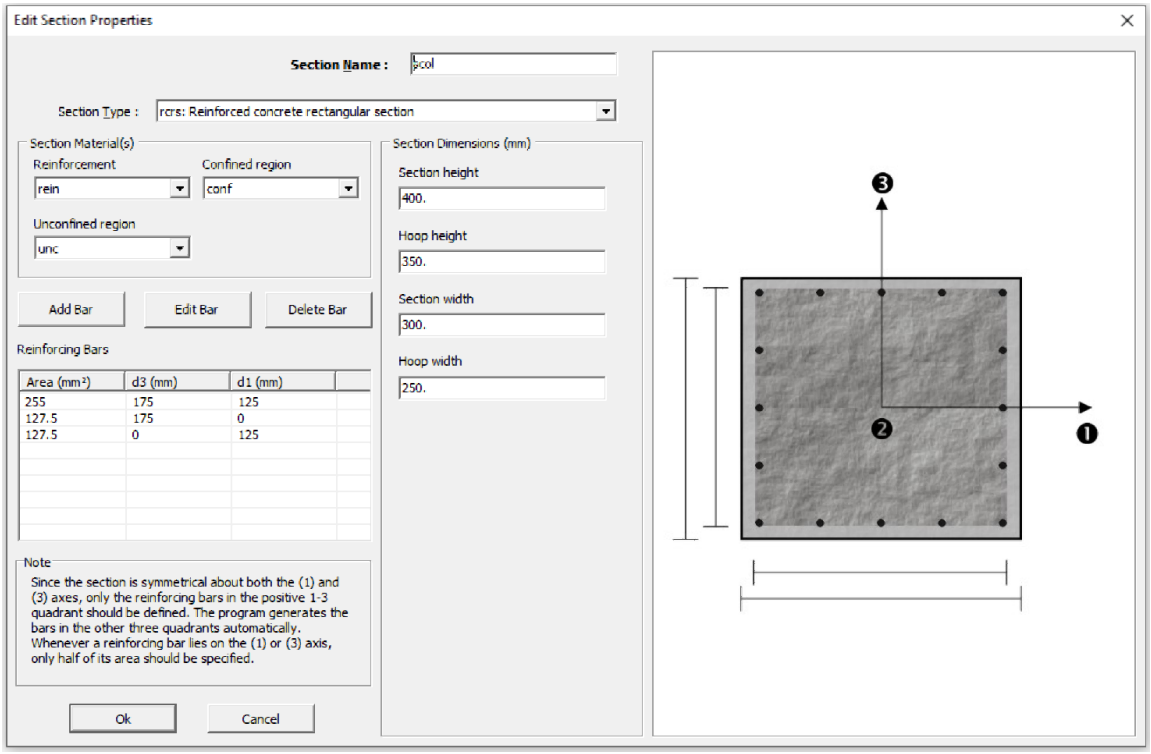

Figure 114: The Section Properties dialog box for a typical rectangular RC section in Zeus-NL.

Furthermore, the reinforcement of the RC members can be defined from the parameters of the section window as shown in **Figure 114**. The assigning method for the reinforcement differs from other well-known software such SAP2000, Etabs and more. Zeus-NL has a predefined way of locating the longitudinal bars into parallel axes. These axes, for example 1 and 3 from **Figure 114** are used to distribute the steel bars into different parts of the cross-section. However, user must specify the longitudinal reinforcement between axes mentioned above and the other part is generated automatically by the software.

Zeus-NL section library provides 14 different section to conduct the mathematical model in its environment. The sections can be used for steel, concrete, or composite structures. The list of sections is provided in **Figure 115**.

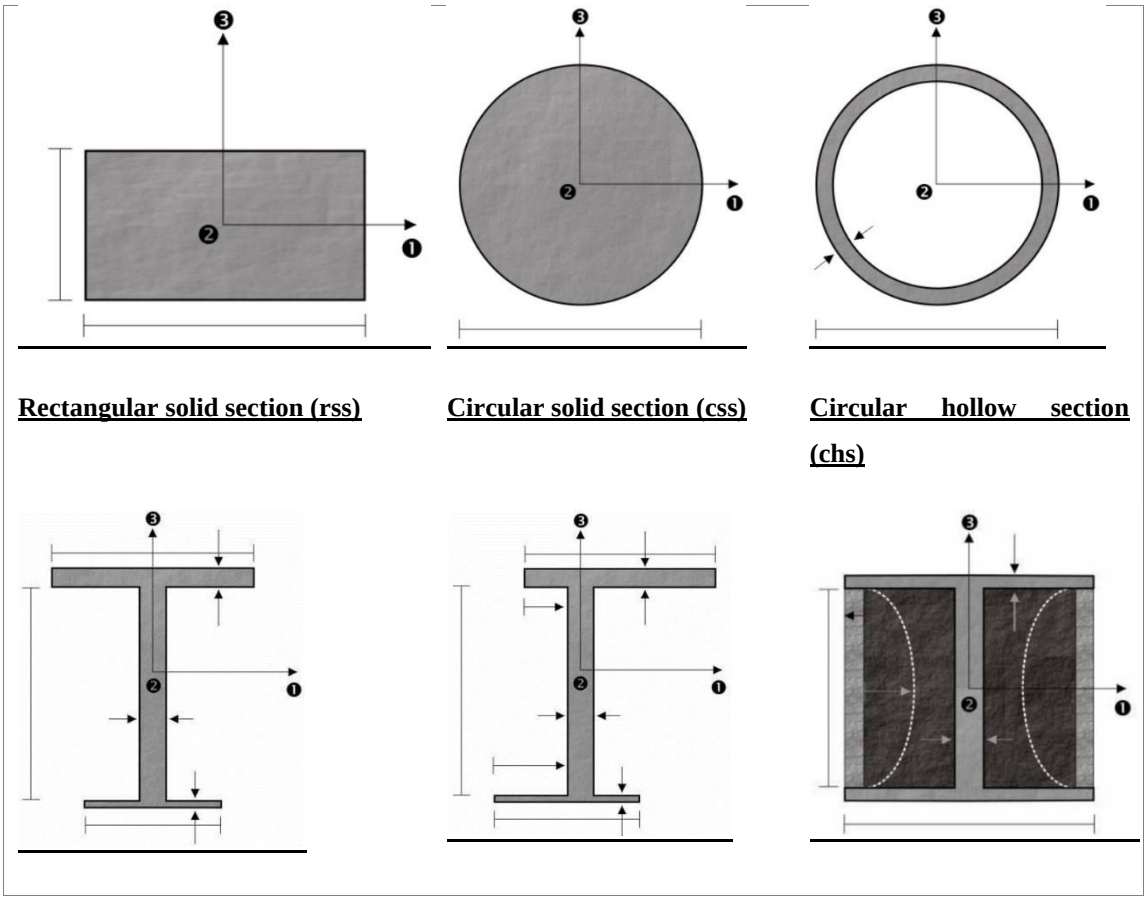

Rectangular solid section (rss)

Circular solid section (css)

Circular hollow section (chs)

Symmetric I- or T-section (sits)

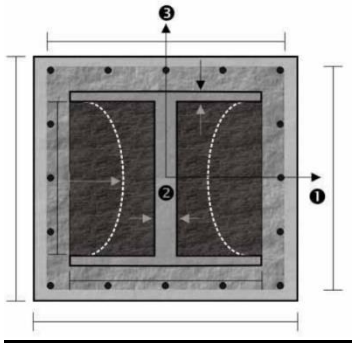

Asymmetric L- or C-section (alcs)

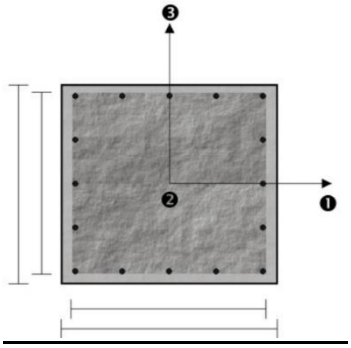

Partially encased composite I-section (pecs)

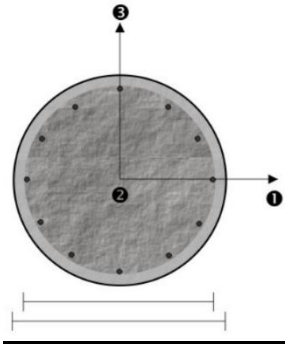

Fully encased composite I-section (fecs)

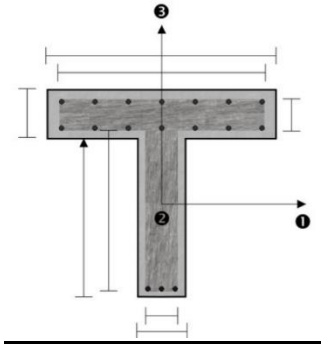

RC rectangular section (rcrs)

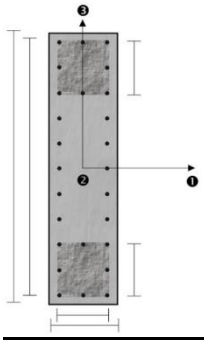

RC circular section (rccs)

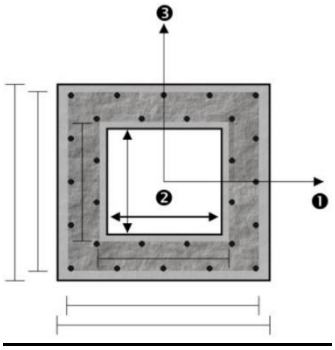

RC T-section (rcts)

RC flexural wall section (rcfws)

RC hollow rectangular section (rchrs)

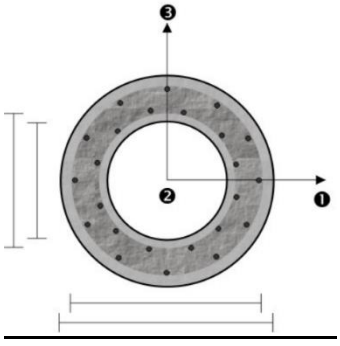

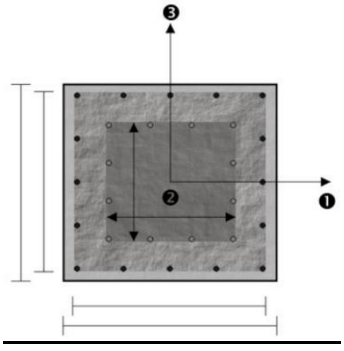

Reinforced concrete hollow circular section (rchcs)

Reinforce concrete jacket rectangular section (rcjrs)

Figure 115: Sections available in the Zeus-NL library

6.5.3 Element Classes

The element library of Zeus-NL consists of a group of element types used to model:

- Structural elements (columns and beams)
- Nonstructural elements (damping and mass)
- Restrains (joints and supports)

The software offers in the element classes library possibility of usage of different options such as:

Cubic. A Cubic elasto-plastic element used for 3D beam-column especially detailed for inelastic modelling. This element class considers the spread of inelasticity throughout the cross-section of the element as well as the member itself.

Joint. This element belongs to 3-dimensional join with uncoupled axial, shear, and moment actions which is used especially for supports and soil structure interaction, structural gaps etc.

$L_{mass.}$ Concentrated mass element (lumped) used to perform dynamic and eigenvalue analyses.

$D_{mass.}$ Cubic distributed mass element used to model uniform distributed forces in beams for dynamic and eigenvalue analyses.

$D_{damp.}$ Dashpot viscous damping element used in dynamic analyses.

$R_{damp.}$ Element that models Rayleigh damping for dynamic analyses.

The elements presented above are used to define the element classes. Later the element classes are used to determine the element connectivity which achieves the competition of the modelling part of a structural member such as beam, column, etc. The most used elements in the current study are Cubic elasto-plastic 3D beam-column element since the structure is modelled in 3-dimensional way and do not need the joint element. Besides that, the Lmass which represents the lumped mass, is another element used in order to simulate the self-weight of the elements modelled and the mass from the members which cannot be modelled by the Zeus NL such as slabs and walls. Lumped mass will play a vital role in the eigenvalue analyses to determine the period of the structure.

6.5.4 Nodes

The modelling process in Zeus-NL requires the definition and assignment of nodes with respective coordinates used as intermediaries. Nodes will be used to properly allocate the element in the respective place in the mathematical model. There are two types of nodes programmed in the software, the structural node, and the non-structural nodes.

Two structural nodes will be used for each element, mainly beams and columns, to define their boundaries. After defining these nodes, then user must connect one element with their respective nodes. The third node involved in the process belongs to non-structural node category. This node is used in Zeus-NL as additional element to define the orientation of the member, for example a rotation due to the longitudinal axis. As shown in **Figure 116**, the coordinate of each of the structural nodes is given in X-, Y-, and Z-axis. Moreover, the type of the node is given in the rightmost column as structural or non-structural node. In addition, one structural node is used to give a uniform orientation for

each of the members in this model. User is free to modify the coordinate of the nodes at any time.

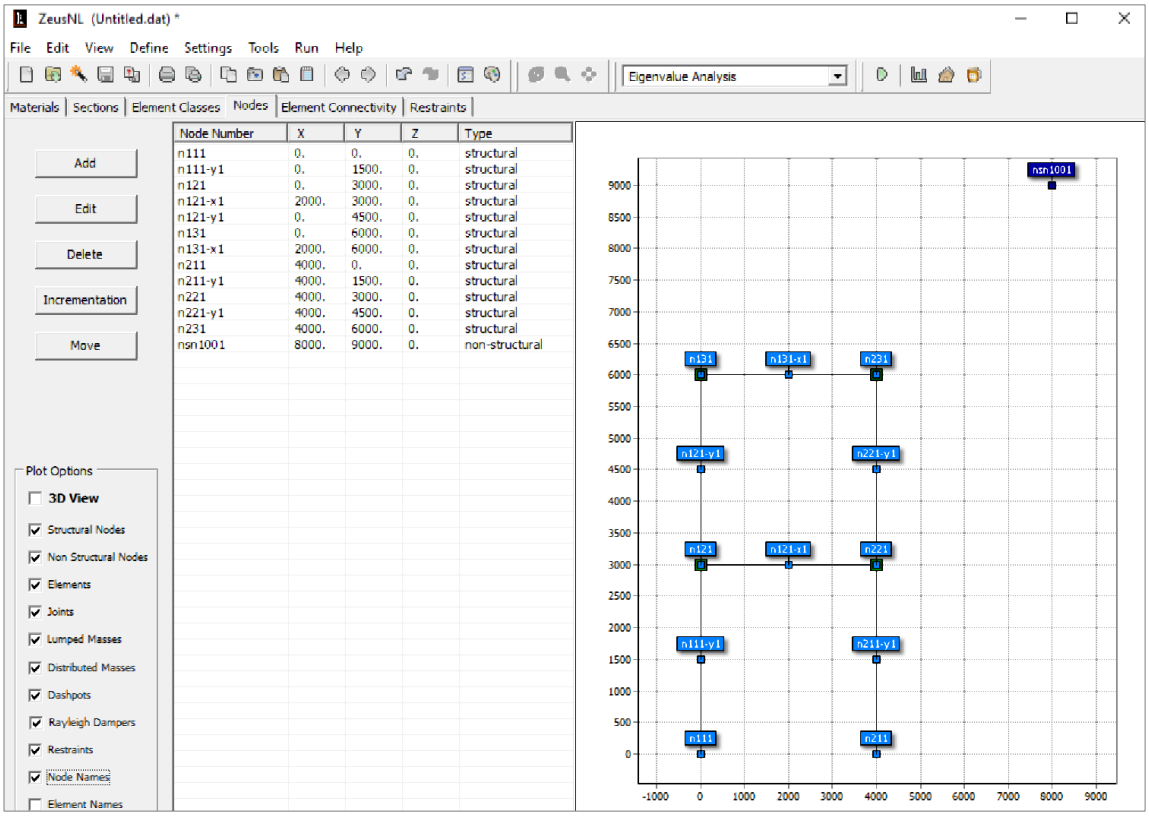

Figure 116: Zeus-NL window showing structural and non-structural nodes in a model.

6.5.5 Element Connectivity

After all nodes are defined, renamed, and assigned in the Zeus-NL database, then user can start assigning structural elements for the given model. To each of the elements used, there must be linked two structural elements to determine the boundary and one son-structural element for the orientation of the member. Furthermore, elements must be linked with element class, defined previously, such as beams or columns. By default, the labeling of one element start with a string prefix which is followed by a number. As shown in **Figure 117**, the element “bmx121” is a representation of beam element.

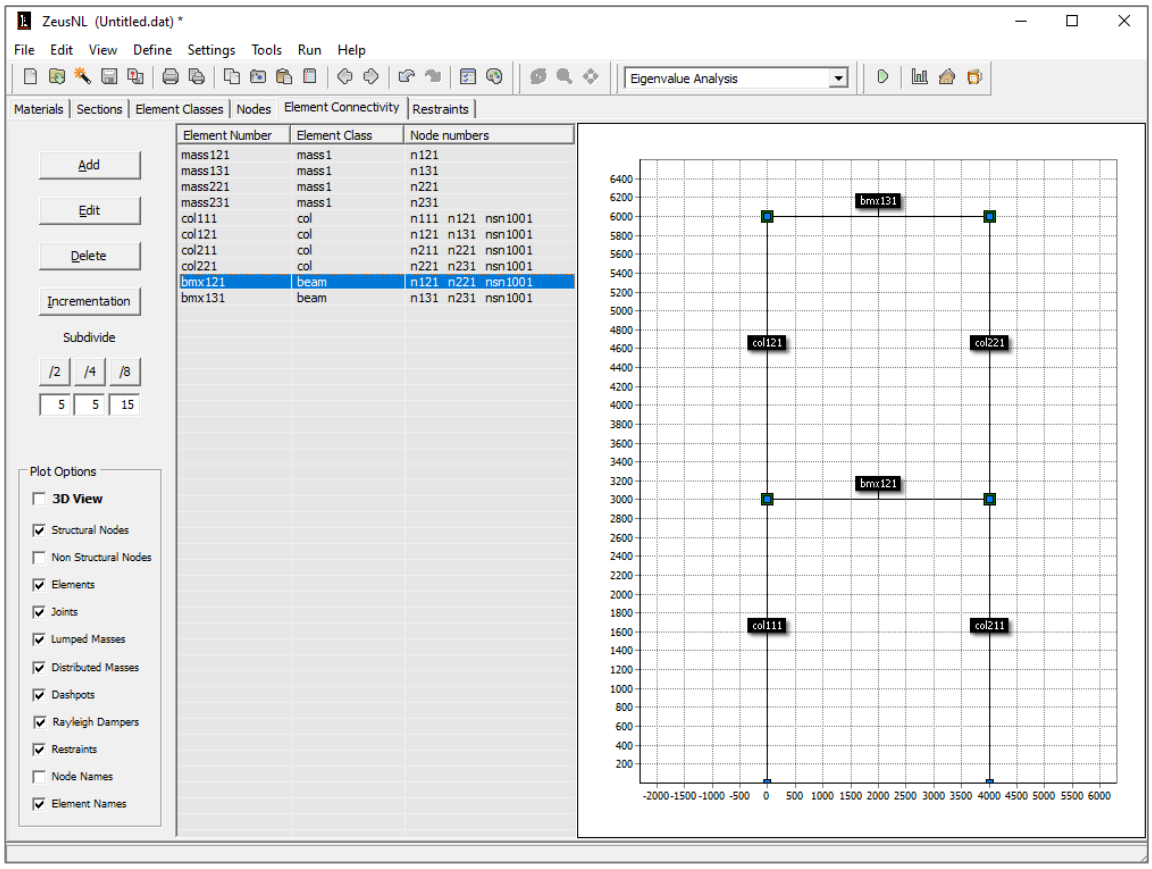

Figure 117: Element connectivity example from the Zeus-NL software

The “bmx” prefix indicates that beam is lying in x-axis whereas the “121” suffix shows the location in the model. The location refers to the x-, y-, z-coordinates respectively. In Zeus-NL, y- symbolizes the elevation axis. Therefore, “bmx121” corresponds to the beam in the first frame (“bmx***1***21”) of the first story (“bmx1***2***1”) in the first bay (“bmx12***1***”).

In addition to members such as beams and columns, the mass elements have to be associated with one single node as well. These masses are typically lumped mass, whereas the distributed masses are associated with two nodes similar to structural members.

6.5.6 Restraints

User can specify the restrain conditions for each of the nodes according to project details. Restrain criteria remain the same as in other well-known software such as SAP2000, Etabs etc., three axes for transition and rotation. Special attention must be given to the way Zeus-NL considers the restraining logic. Especially for dynamic analysis, the restrained degree of freedom (DOF) at the supports, in the direction of the earthquake, must be released (Elnashai et. al., 2002). This is the reason why the default configuration of the model in the Zeus-NL for dynamic analysis is y+z+rx+ry+rz, skipping the x direction since the earthquake is loading in that orientation. The software provides a very easy way of assigning the supports by selecting multiple nodes and apply changes simultaneously.

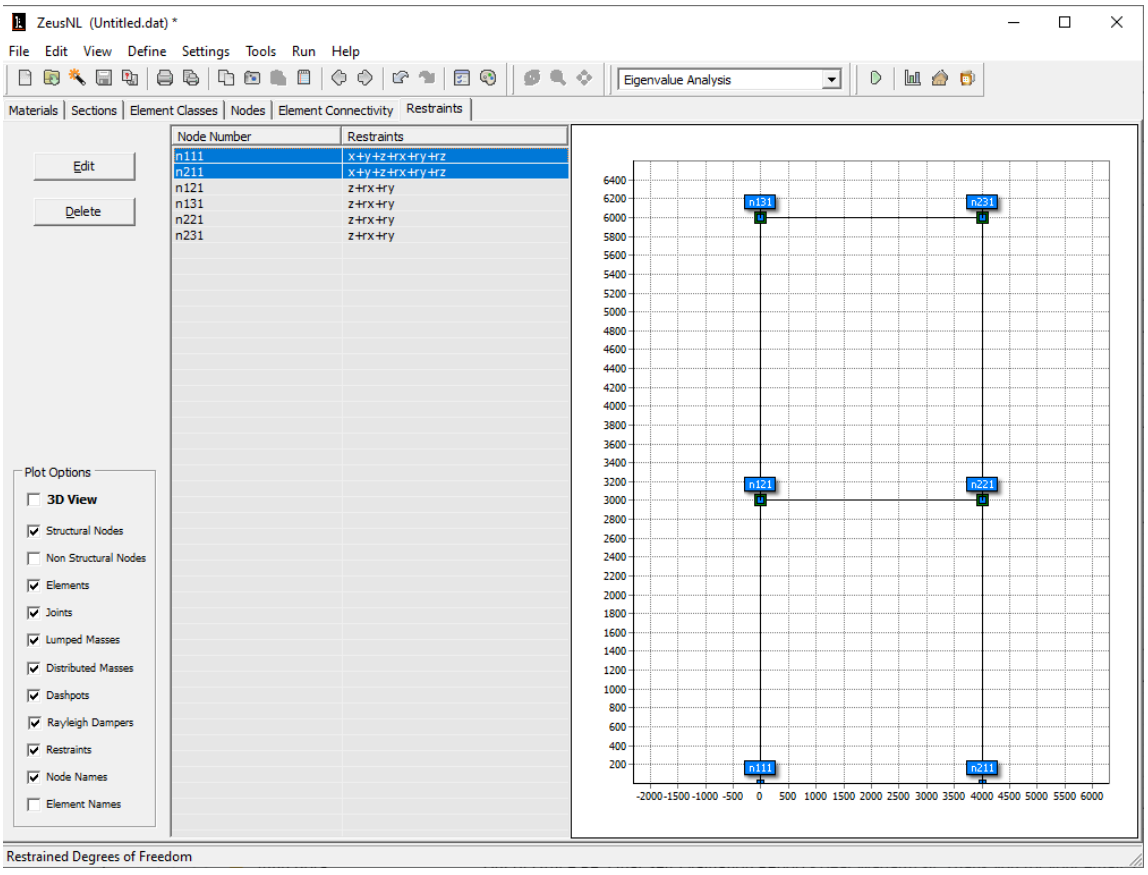

Figure 118: The frame model with 2 bays, restrained

6.5.7 Load Types

As mentioned before in the "Element Classes" section, Zeus-NL provides two types of load applications, the lumped mass (L_{mass}) and distributed mass (D_{mass}). Lumped mass requires one node to be assigned. This load type is used in dynamic and eigenvalue analysis. The unit of the lumped mass must be in N/(mm/sec^2). A schematic example of lumped mass is given in **Figure 119**. On the other hand, d_{mass} option is used for uniform distributed load in structural elements such as beams and columns.

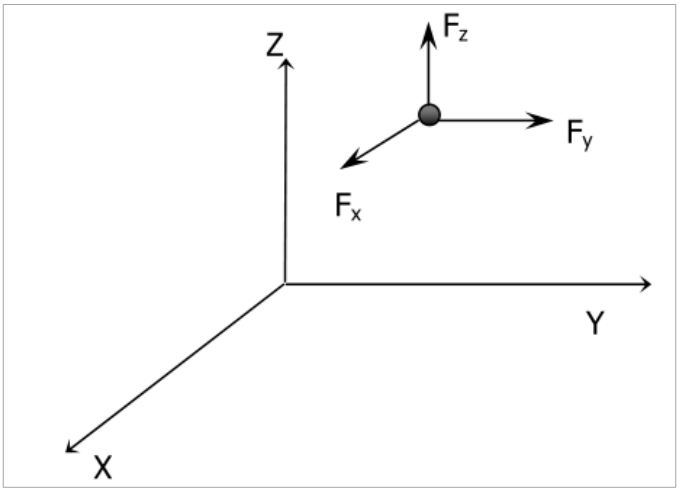

Figure 119: Schematic example of a lumped mass (L_{mass}) in Zeus-NL

The load (mass) is distributed throughout the beam, and it must be calculated in terms of element cross section per millimeter. The unit for the d_{mass} is N/(mm/sec^2)/m. An example of d_{mass} is given in **Figure 120**.

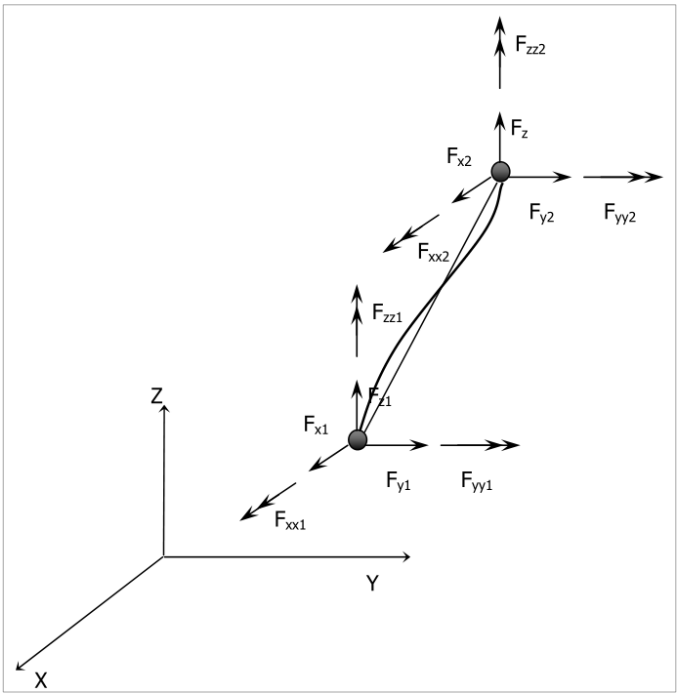

Figure 120: Schematic example of a uniform distributed mass (D_{mass}) in Zeus-NL

6.5.8 Definition of Local and Global Axes

Definition of local axis and global axis is essentially done in the element connectivity. The logic requires that each of the element must have two nodes to be bounded with following structural elements. However, the proper way of defining the element involve specifying the orientation of the element cross-section. For that reason, a plane must be introduced to complete this process. The determination of the plane is done using a third node in the global matrix. First two nodes are known in the software as structural nodes and will be used for the local definition (boundary condition) whereas the third node with define the global axes of the plane as regards to the orientation of the model element. The third node represents a non-structural node in the Zeus-NL language. **Figure 121** demonstrates the example for a T shape beam.

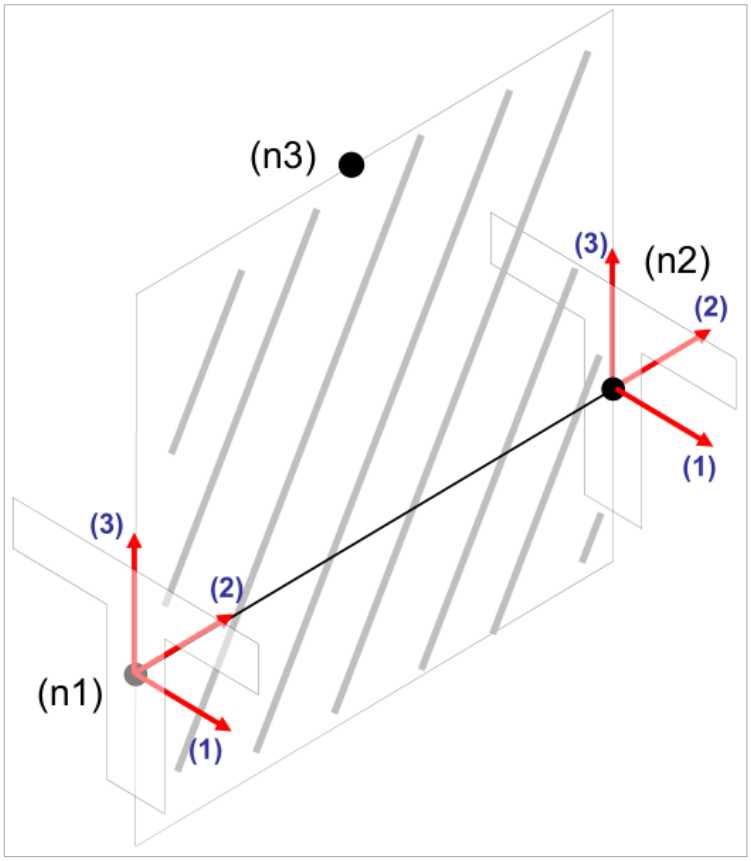

Figure 121: Defining local and global axes in Zeus-NL. An example for a T-shape beam.

6.5.9 Development of analytical models in ZEUS NL

Zeus-NL is a powerful, finite element analysis software developed especially for seismic engineering applications. It has a fast-processing algorithm and is capable of running most of the well-known analysis. Even though it seems very advanced and demanding computer program for civil engineering applications, it does not have the best user-friendly interaction when compared with other frequently used software such as SAP2000, Etabs etc. From the previous sections, it is explained the procedure of the modelling stage and parameters required to conduct a full 2D or 3D model of any possible material available in the package. As a matter of fact, it is easily recognized that there exists simple interaction between user and the software. The graphical user interface (GUI) provides a

sufficient way to input parameters, but it does not support a 3D, extruded view of the elements and the worst fact is that everything has to be input in coordinates, strings, and numbers with no possibility of selecting one element. Unlike SAP2000 or other developed software which allow user to interact with the model, for example selecting one element in 3D view and applying loads, changing supports, change cross-section properties etc., in Zeus-NL user must be extremely careful while inputting the parameters of one out of hundreds of elements available as may be easily confused. This would cause the least possible problem such as convergence error which is easily differentiated, up to a blunder and consequently producing wrong results with no error indication.

Therefore, in this thesis, there will be given instructions as regards to the modelling stage using Zeus-NL as well as other tools to facilitate, accelerate and improve this process further.

6.5.9.1 Preparing a Zeus-NL case model

To benefit as much as possible from the Zeus-NL facility and automation, each of the templates considered in this study is studied for the easiest way to be modeled in the software. Each of the buildings are prepared using 2D reinforced concrete moment-resisting frames in longitudinal and transverse direction. Thus, a 2D model is initiated in the Zeus-NL template with default parameters. Afterward, the parameters for concrete and reinforcement materials are inputted according to the project details. For the concrete it is used non-linear constant confinement concrete model (con3) from the material library as it accounts for the stirrups spacing which is in compliance with the scope of the study. Whereas for the steel reinforcement, it is used bilinear elasto-plastic model with kinematic strain hardening (stl1). Furthermore, from the section panel of the software, beam and columns cross-sections are defined based on the blueprint properties. As some of the buildings selected for this study use more than one type of the same element category, (for example three different types of columns) then there should be a reconfiguration in the element connectivity with its respective material. Moreover, E Template considered in

this study, uses different cross-section of the same column type for different elevation heights. Hence, new cross-sections must be developed, and properly assigned in the model. As the orientation of vertical elements cannot be defined easily using non-structural nodes, then this shall be considered in a separate section as well. In overall, there will be many combinations of elements with materials which must be allocated appropriately in the model manually. Also considering the fact that each of the elements is divided in four sections, then this leads to a large number of members and inputs which is confusing, tedious and time consuming to be managed manually.

To achieve this step, the utilization of Microsoft Excel (MS. Excel, 2018) has been taken into account. All elements of the model generated by Zeus-NL are copy pasted in a spreadsheet. Later, the suffix (for example "bmx***131***") of the element is filtered into x-, y- and z-axis. Using the suitable formulas and drop options to replicate the same logic in Microsoft excel, each of these elements is linked to their respective cross-section, material, mass, structural and non-structural node. As shown from **Table 16**, using x-, y-, z-axis is easily to filter the group of elements in a specific location in the model. Then to each of them is associated a respective load according to hand calculations.

Table 16: An example of Microsoft Excel utilization on filtering specific nodes/elements and assigning masses. Masses such as "m1" ,"m1_t", "m3" ,"m3_t" ,"m7" ,"m7_t" are calculated and assigned in the Zeus-NL load library.

Template_3 Y-Direction					
Mass Element	**Mass assigned**	**Node label**	**X**	**Y**	**Z**
mass221	m3	n221	2	1	2
mass271	m3_t	n271	2	1	7
mass121	m1	n121	1	1	2
mass171	m1_t	n171	1	1	7
mass521	m7	n521	5	1	2

mass571	m7_t	n571	5	1	7
…	…	…	…	…	…

The same procedure is followed for other properties, such as node connection to respective element, material assignment, cross-section etc. In this way the whole process can be managed easier.

Nonetheless, preparing a model for one building may be a matter of time, precision, patient, dedication, and carefulness, but this study considers five buildings modeled in x- and y-directions. Moreover, for each of the building there will be considered a certain amount of analysis, material and stirrups spacing combinations which in overall results in more than 520 models. Considering the limitations provided by the software, the need to establish a new and automated procedure has emerged.

6.5.9.2 Automation of Zeus-NL case models

Another advantageous of Zeus-NL software is that is saves the project file unencrypted which gives to user the possibility of modifying any of the variables using a third-party app or programming. Consequently, this study also presents a methodology in automatic preparation of structural models using python programming language (Van Rossum and Drake, 1995). The target is to automatically generate Zeus-NL project files of different combinations of materials, stirrups spacing, pushover loads, accelerograms and more. For this reason, Python version 3.0 is selected as an easy and efficient programming language for civil engineers. The algorithms prepared consist of different Python libraries used to read Zeus-NL files and consequently generate new ones. For this scope, it is requested to prepare one default model for each of the buildings in x- and y-directions and modify necessary variables into the file. This step is done manually, and it requires a repetitive of ten time considering two directions for each of the five buildings selected. Furthermore, these files

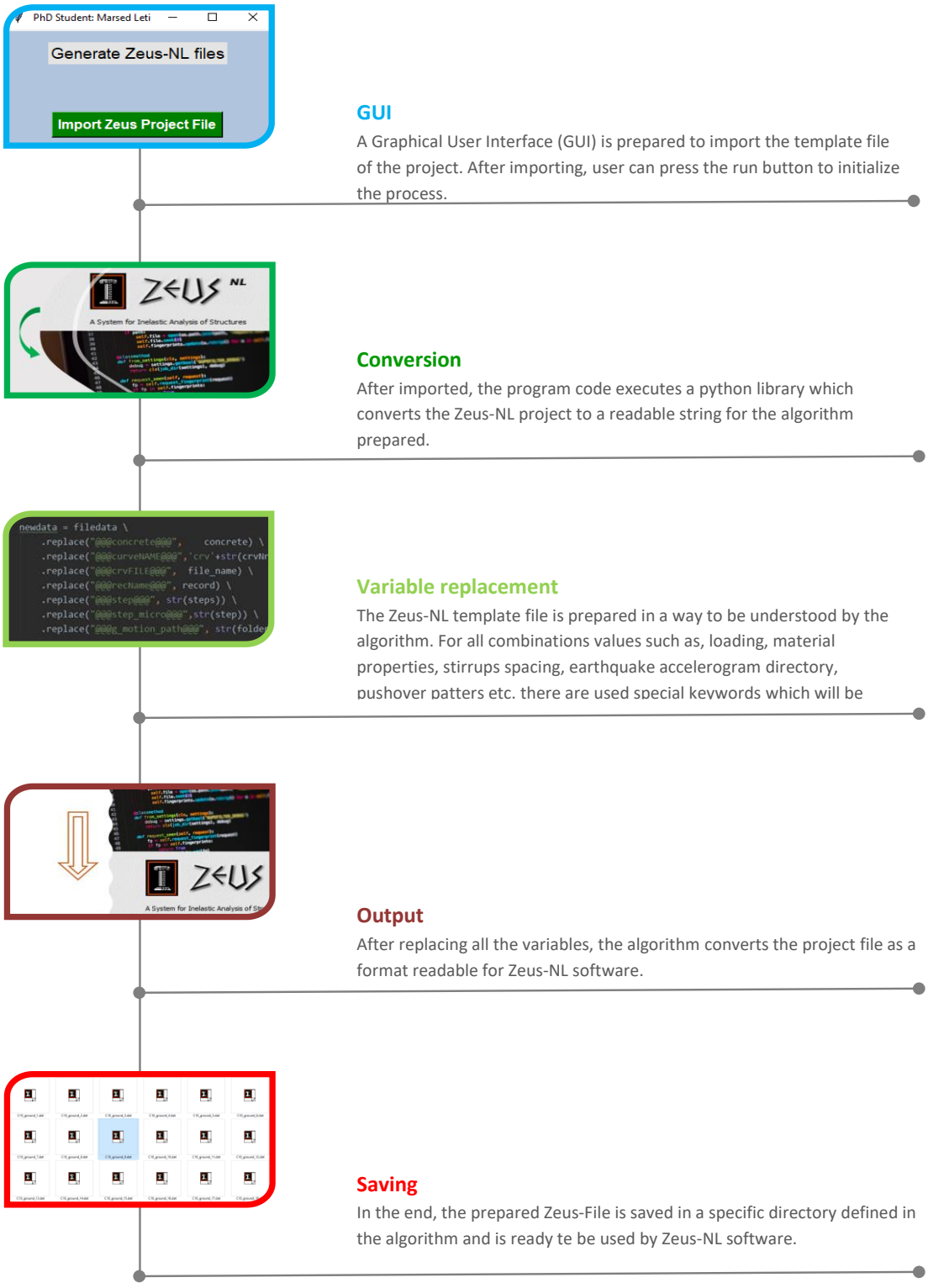

Figure 122: Automation of project files using Python V3.0, tkinter and libraries

are processed and modified by python accordingly to generate new ones ready for the analysis. In addition, a graphical user interface (GUI) is built to import the template files using Python Tkinter library (Lundh, 1999). The total running process takes less than 1 second to automatically generate over 500 Zeus-NL project files. The process of automation is shown in **Figure 122**.

CHAPTER 7

ANALYSES RESULS AND PERFORMANCE EVALUATION

7.1 Pushover analyses results

Pushover results are gathered from the nonlinear static analyses performed in Zeus-NL software. For the pushover analysis, Zeus-NL requires to apply gravitational loads together with lateral loads. Gravitational loads are assigned as lumped masses based on hand calculations. The lateral load for the pushover analysis is assigned as inverted triangular pattern in the environment of Zeus-NL software. This is configured using a multiplier coefficient at different story level of the building. In addition, the software increases the lateral loads according to the coefficients inputted before. While increasing the lateral load, the displacement is controlled in the roof top level of the building. In Zeus-NL this is done by controlling the displacement of a single node at that story level. Since 2D nonlinear models represent reasonably well their 3D nonlinear ones, 2D modelling using the middle frame can be preferred for buildings with no irregularity due to extensive labor and time required for 3D nonlinear models (Özer et. al., 2017). Hence, for this study the middle frames in orthogonal directions are considered. Pushover analyses are conducted for each of the template buildings in x- and y-direction. Furthermore, to represent the effect of the material quality and transverse reinforcement, there are considered four different concrete strengths and four types of stirrups spacing as explained in Section 5. In overall, this thesis presents 160 SPO curves which are interpreted based on different concrete strength, stirrups spacings and plan arrangements.

7.1.1 A Template capacity curves

A Template is composed of five stories and reaches a total building height of 14.42 m. It has five bays in longitudinal direction and three frames in transverse one. Middle frames are modelled in the environment of Zeus-NL for the pushover analysis as shown in **Figure 123**. The loading pattern is applied as demonstrated in the figure, in the shape of inverted triangular.

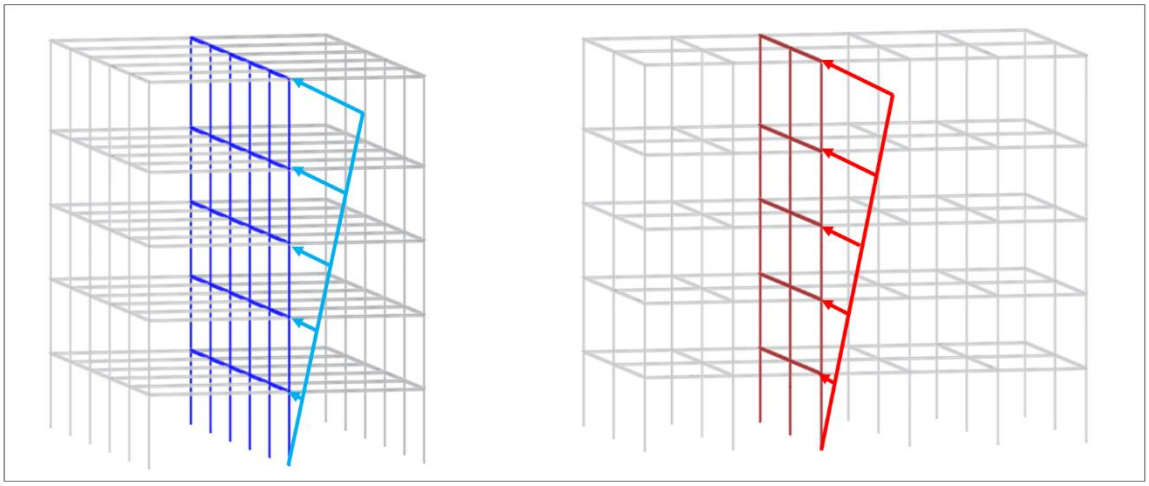

Figure 123: Inverted triangular load pattern applied to A Template building in x-direction (left) and y-direction (right)

The capacity curves are plotted in a 2D graph using global displacement values from the roof level of the building in x-direction and base shear forces in y-axis. Furthermore, base shear values are normalized by building weight and roof displacement values by building height. Capacity curves for 100 mm and 250 mm stirrups spacings are plotted together with concrete class C10 and C16 to interpret their influence in the global performance of the building. **Figure 124** and **Figure 125** demonstrate the capacity curves of A template building for x- and y- directions, respectively. As shown from the figures, the x-direction of the building obtains slightly higher lateral load bearing capacity ratios whereas the y direction in terms of ductility performs better than x-direction.

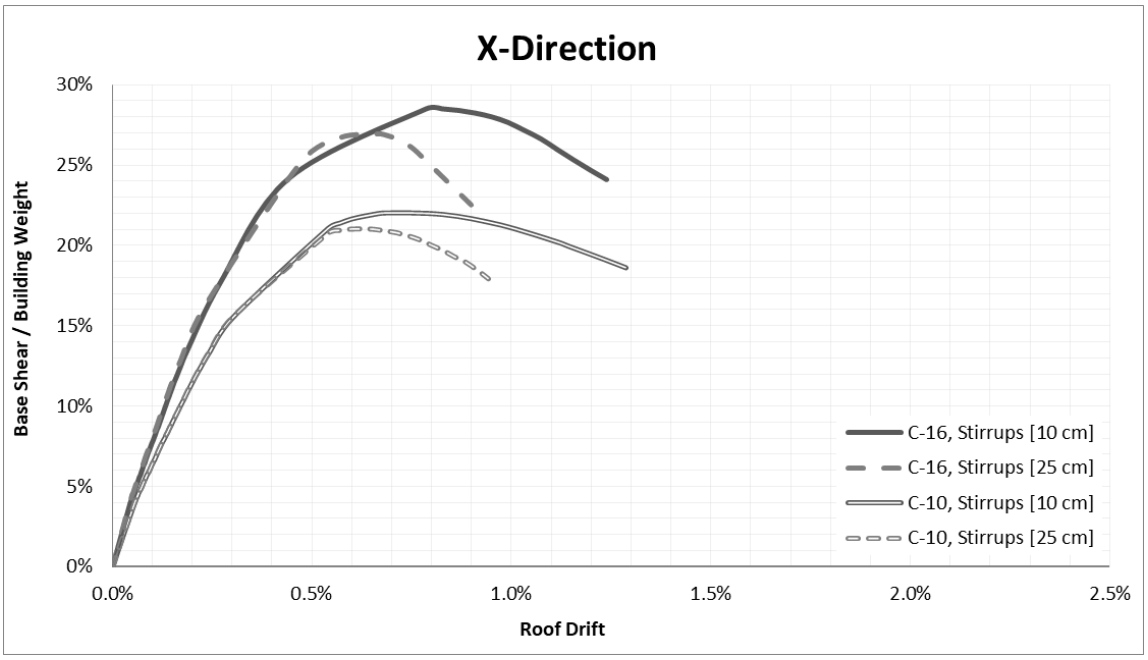

Figure 124: Capacity curves for A Template Design building in x-direction considering C10 and C16 concrete classes with S10 and S25 stirrups spacings

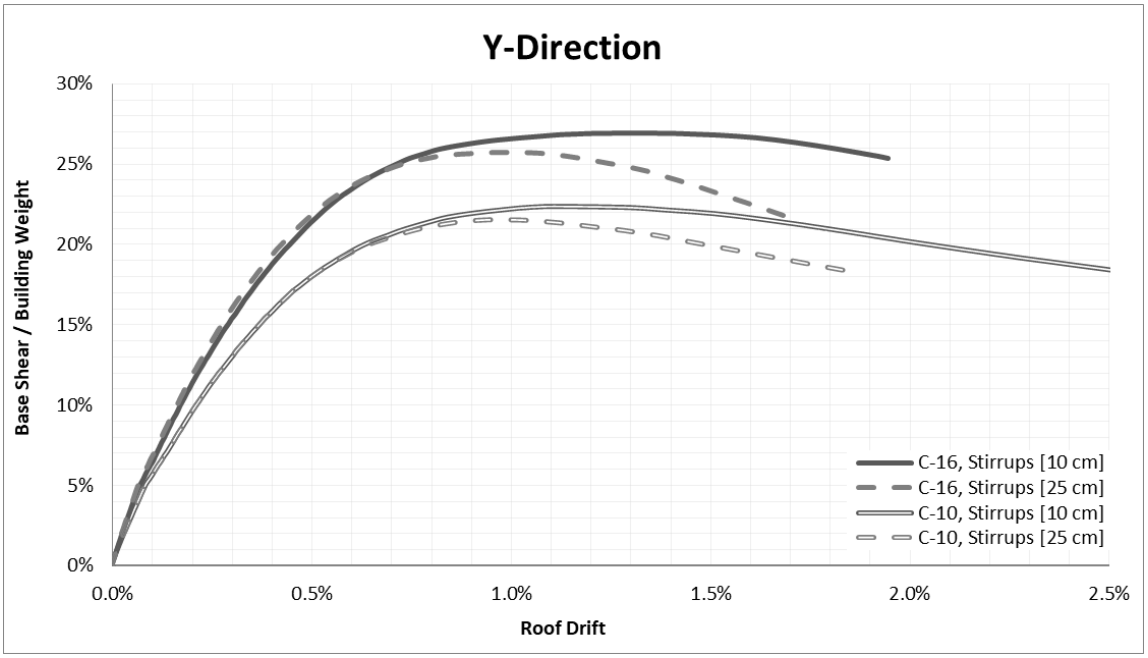

Figure 125: Capacity curves for A Template Design building in y-direction considering C10 and C16 concrete classes with S10 and S25 stirrups spacings

7.1.2 B Template capacity curves

B Template is composed of five stories and reaches a total building height of 14.42 m. In longitudinal direction it has six bays while in the transverse one three frames. It has a regular plan which is symmetrical in longitudinal direction. The pushover analysis is applied to middle frames of the building as shown in **Figure 126**. Loading pattern is configured in Zeus-NL using the inverted triangular shapes. The monitored displacement is defined in the roof level of each frame.

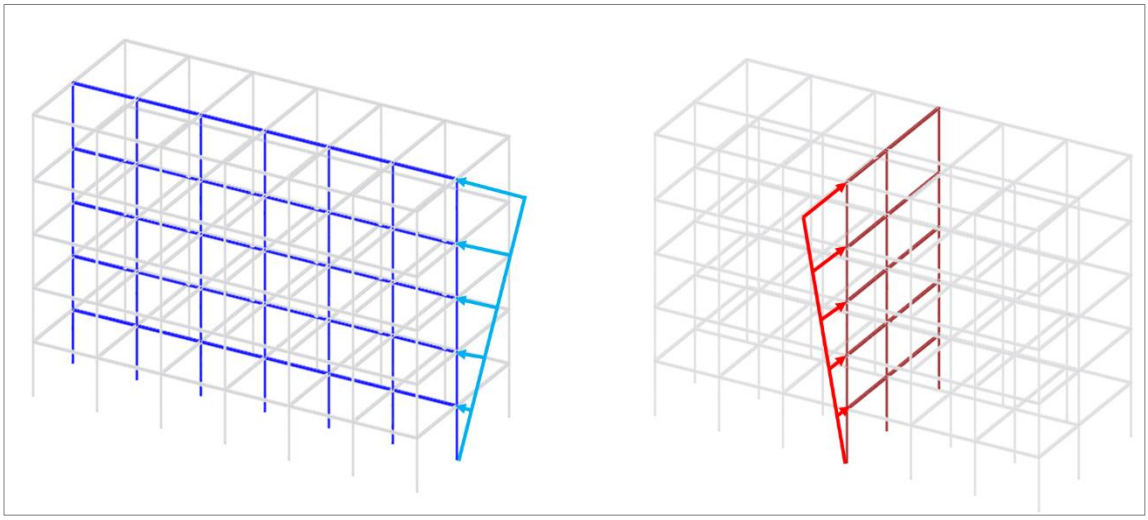

Figure 126: Inverted triangular load pattern applied to B Template building in x-direction (left) and y-direction (right)

After the analyses are performed, the results for each of the pushovers are plotted as roof displacement vs base shear in x- and y- direction respectively. The capacity curves for B Template building are shown in **Figure 127** and **Figure 128** for x- and y- direction respectively using the combinations between stirrups spacings 100 mm and 250 mm with concrete class C10 and C16. Similar to A Template, the x direction is prone to the higher lateral load bearing capacity but less ductile compared to y-direction.

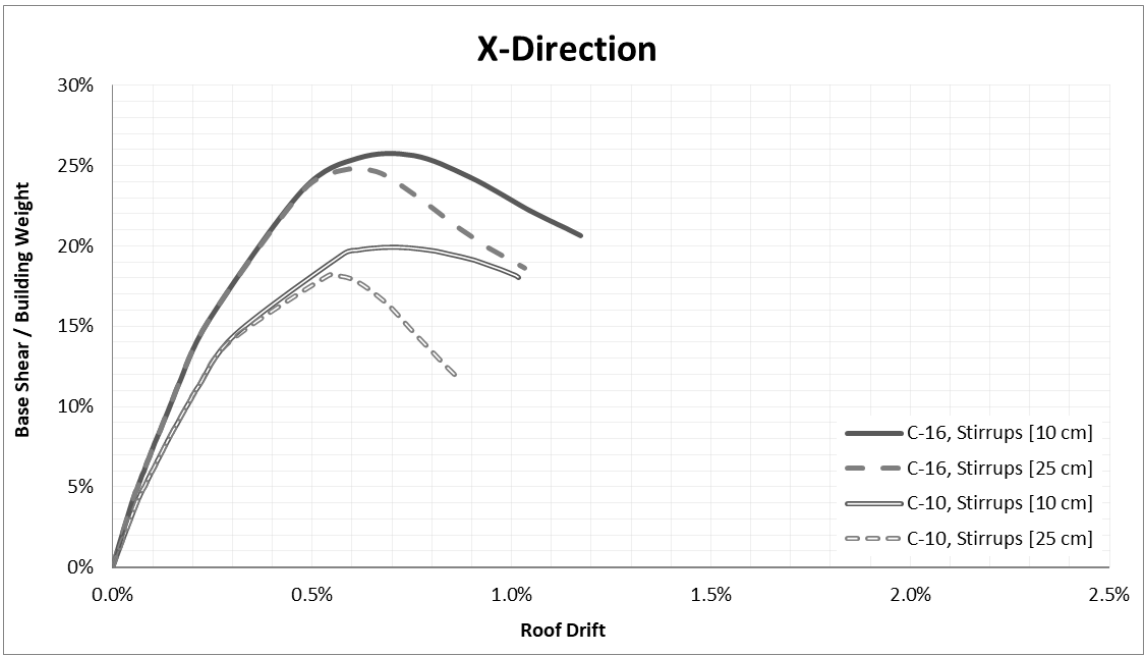

Figure 127: Capacity curves for B Template Design building in x-direction considering C10 and C16 concrete classes with S10 and S25 stirrups spacings

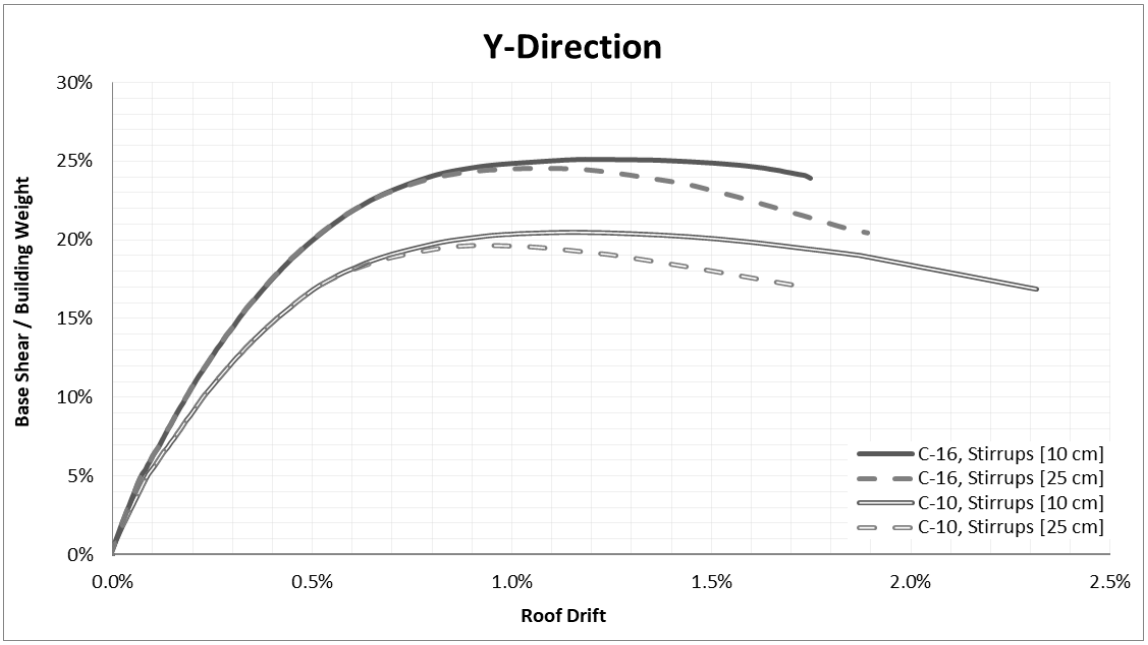

Figure 128: Capacity curves for B Template Design building in y-direction considering C10 and C16 concrete classes with S10 and S25 stirrups spacings

7.1.3 C Template capacity curves

C Template building shares the similar planimetry as B template, being symmetrical in longer direction and showing no plan irregularities. Having one more story, compared to the previous templates, it reaches an overall building height of 17.22 m. Similar to previous two templates, the middle frames are used for the modelling stage of the pushover analysis. The pattern used in the analysis belongs to the inverted triangular as shown in **Figure 129**.

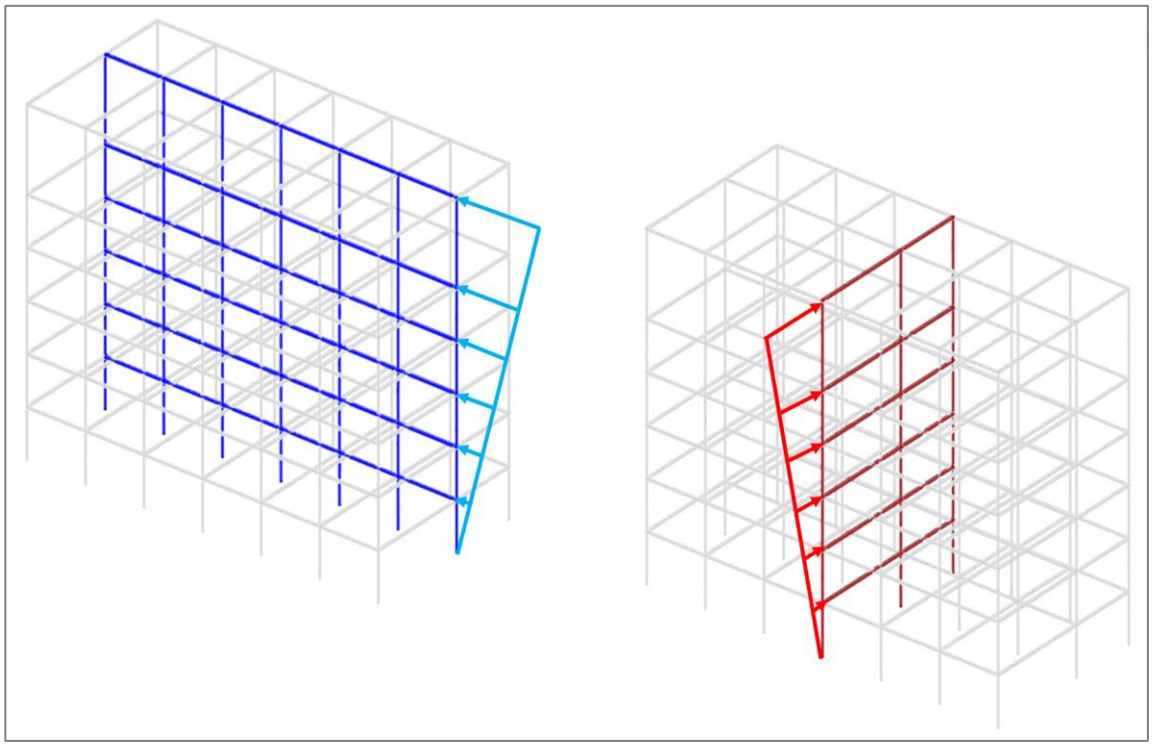

Figure 129: Inverted triangular load pattern applied to C Template building in x-direction (left) and y-direction (right)

Capacity curves are plotted as roof displacement normalized by building height in x-axis and base shear normalized by total weight of the building in y-axis as illustrated in **Figure 130** and **Figure 131**. As shown from the capacity values, the C Template building is more ductile in y direction whereas the values of lateral load bearing capacities are slightly higher in y-direction.

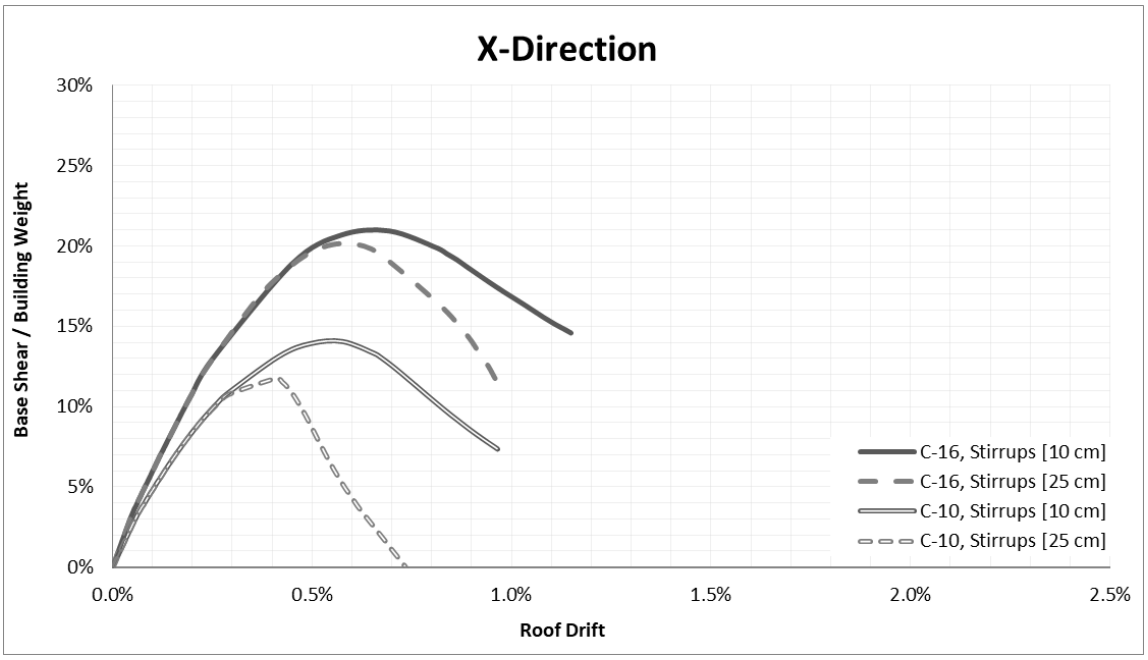

Figure 130: Capacity curves for C Template Design building in x-direction considering C10 and C16 concrete classes with S10 and S25 stirrups spacings

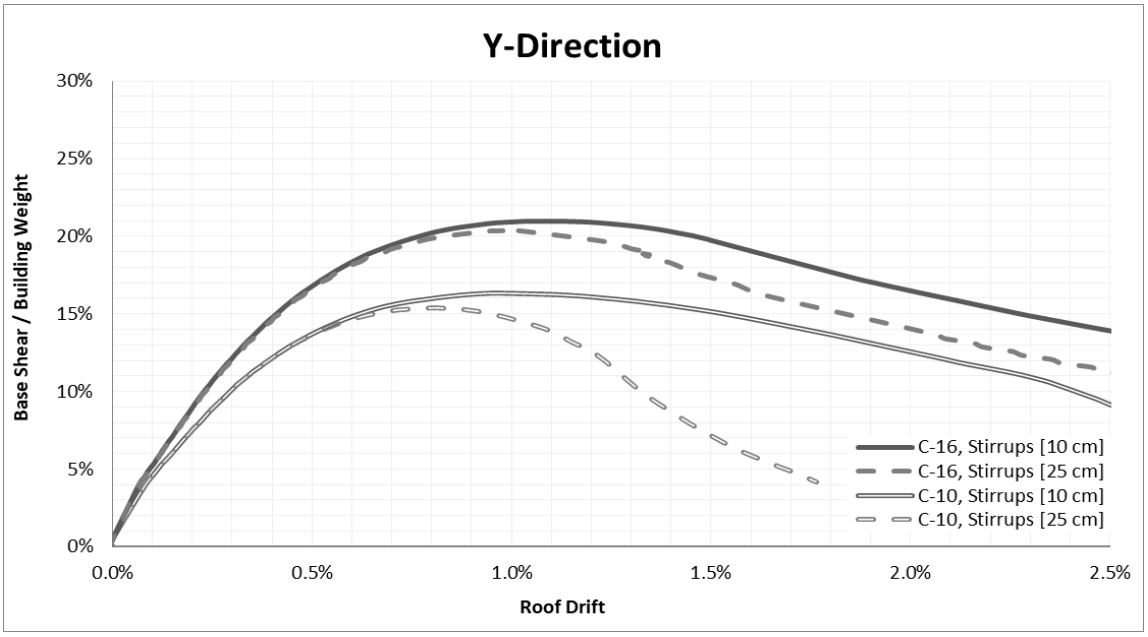

Figure 131: Capacity curves for C Template Design building in y-direction considering C10 and C16 concrete classes with S10 and S25 stirrups spacings

7.1.4 D Template capacity curves

D Template is composed of six stories, and the maximum building height is 17.67 m. The planimetry of the D Template is composed of five bays and five frames as shown in **Figure 132**. The modelling of the D Template is done similar to the previous buildings, using the middle frames. A good representation would be to model this template in 3D, however, due to the limitations in user interface of Zeus-NL, the modelling could be a challenge and the analysis would continue for a long duration of time (days).

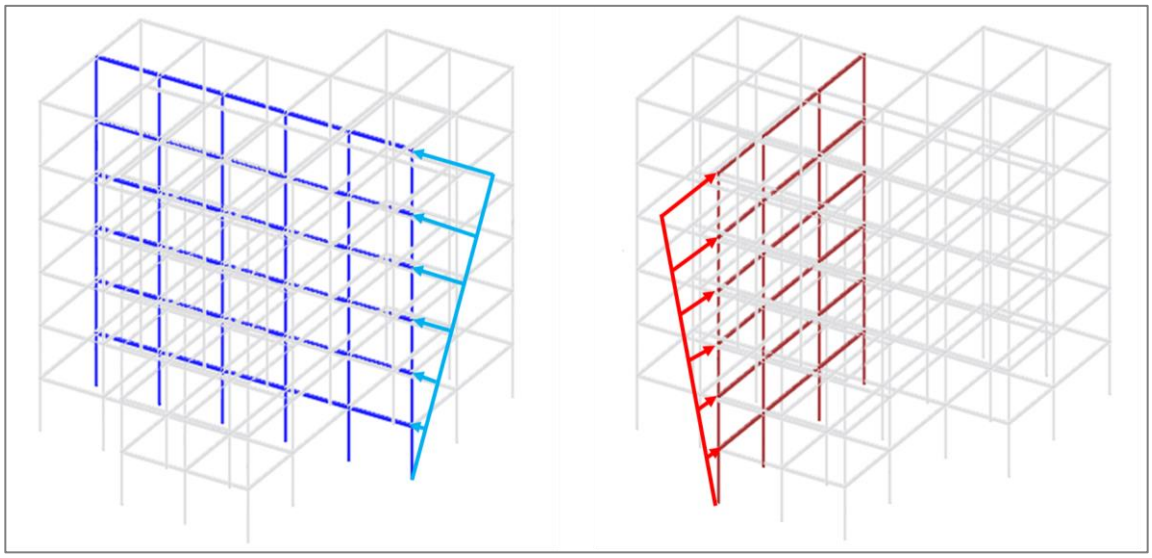

Figure 132: Inverted triangular load pattern applied to D Template building in x-direction (left) and y-direction (right)

Unlike the previous templates, the y-direction of the D type has a longer distance compared to the other one. Capacity curves are illustrated for x- and y- direction in **Figure 133** and **Figure 134** respectively. As shown from the results, the same trend of the capacity curves is followed by D Template. The lateral load bearing capacity is slightly higher in x-direction compared to the y-direction. Whereas in terms of ductility, y-direction show better values compared to the other one. In addition, the overall load bearing capacity of this template design is remarkably lower compared to the previous templates.

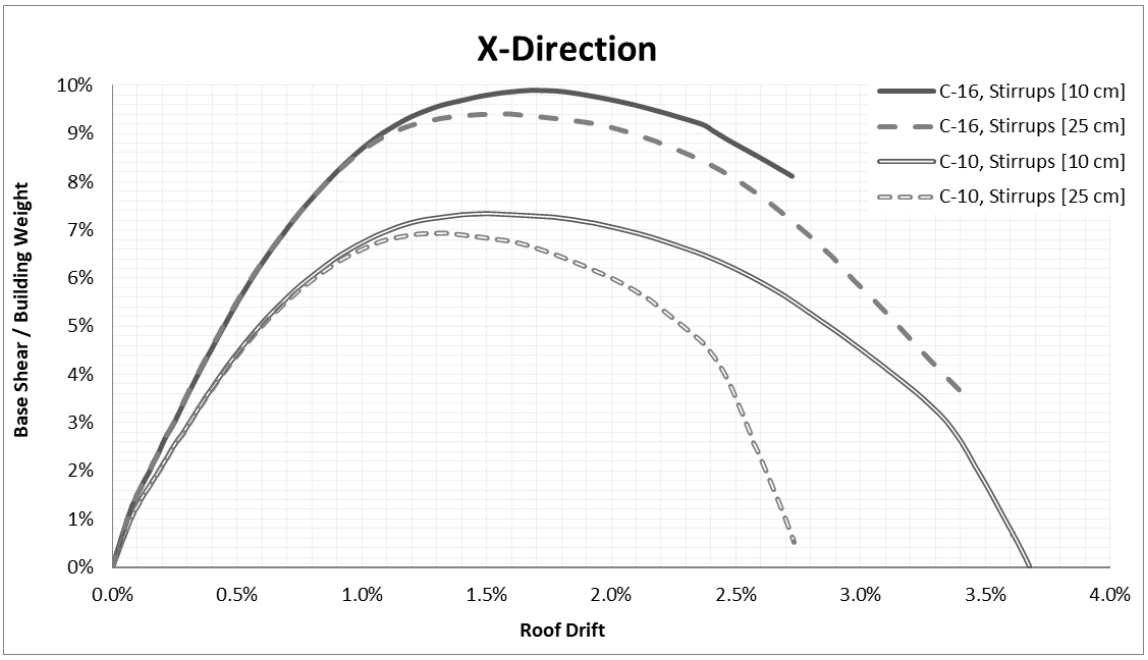

Figure 133: Capacity curves for D Template Design building in x-direction considering C10 and C16 concrete classes with S10 and S25 stirrups spacings

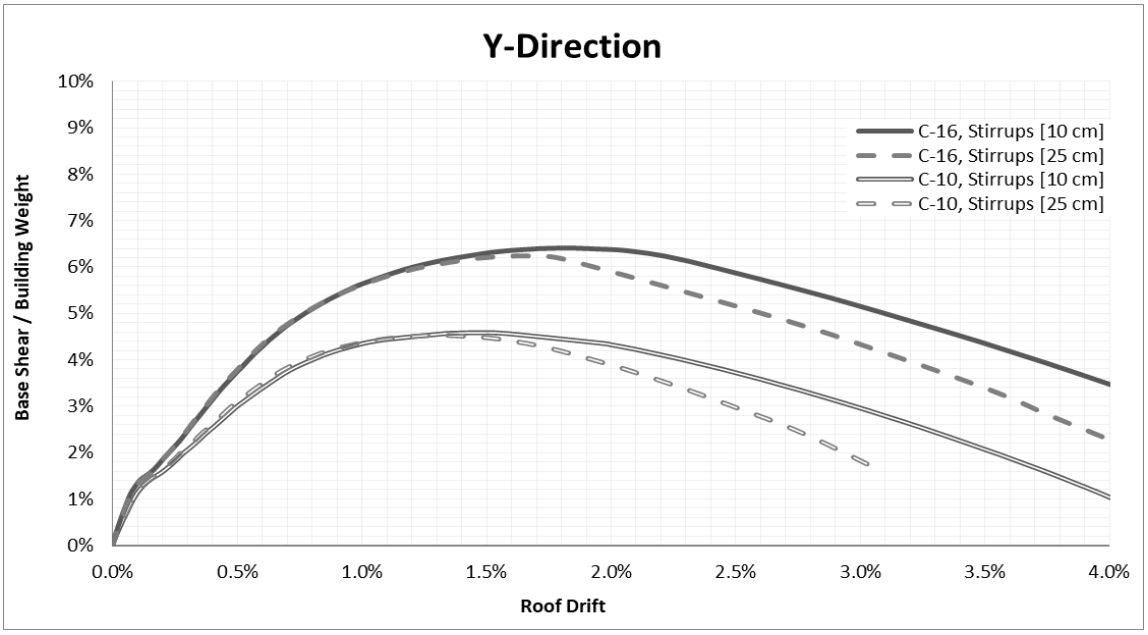

Figure 134: Capacity curves for D Template Design building in y-direction considering C10 and C16 concrete classes with S10 and S25 stirrups spacings

7.1.5 E Template capacity curves

The last building selected in this study is E Template. It is the tallest building among the others. Composed of seven stories, riches an overall height of 22.32 m.

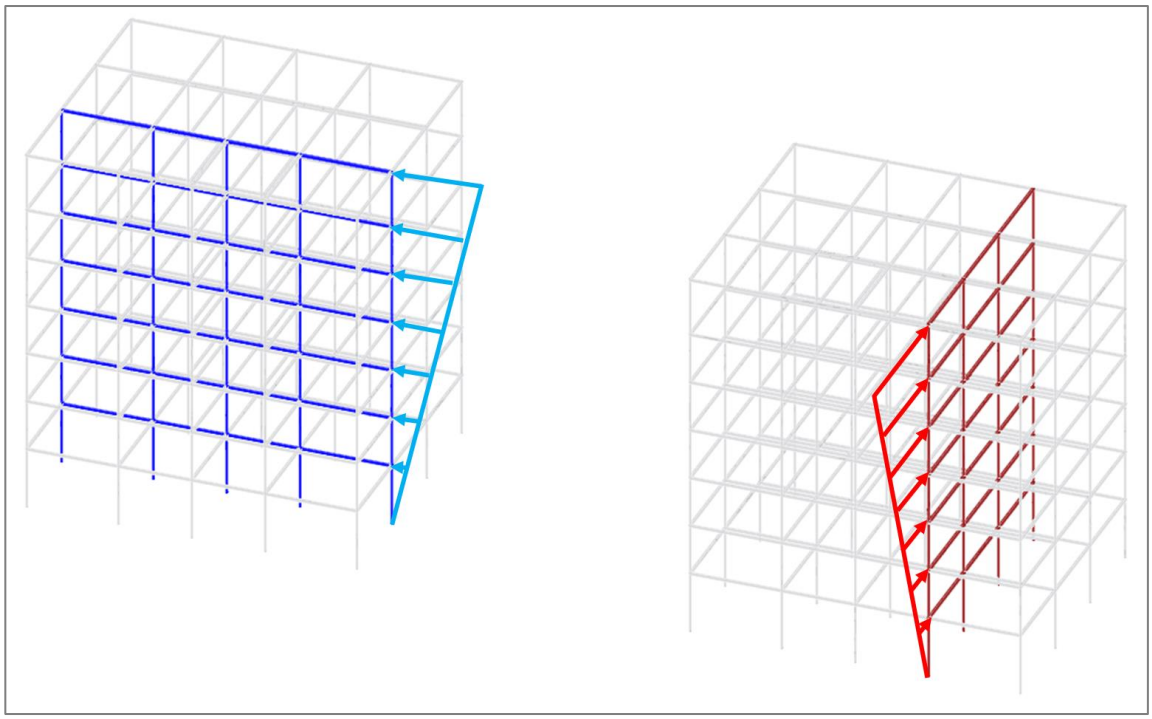

Figure 135: Inverted triangular load pattern applied to E Template building in x-direction (left) and y-direction (right)

E Template remains symmetrical in its plan view in both orthogonal directions and shows no irregularities in the elevation as shown in **Figure 135**. To check the effectiveness of stirrups spacings and concrete strength, the pushover curves for C10-S10, C10-S25, C16-S10 and C16-S25 are shown in **Figure 136** and **Figure 137** for x- and y- direction of D Template Building respectively. As shown from the graphs, the y-direction shows better ductility then the other one. Similar to other template, the lateral load bearing capacity of x direction compared to y, is slightly higher.

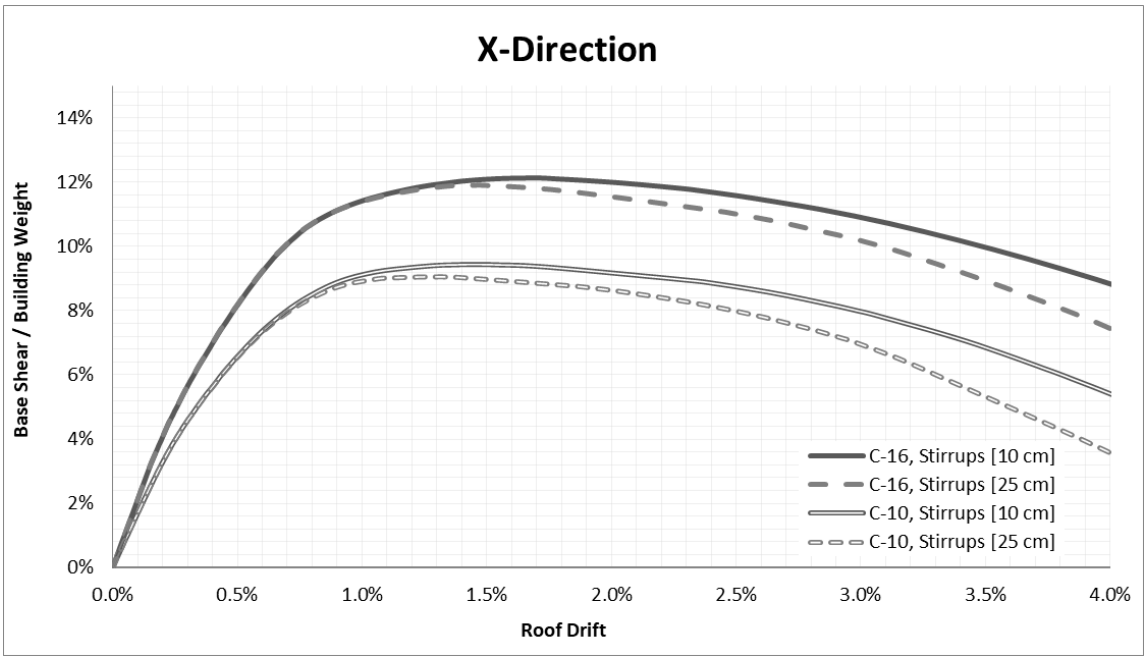

Figure 136: Capacity curves for E Template Design building in x-direction considering C10 and C16 concrete classes with S10 and S25 stirrups spacings

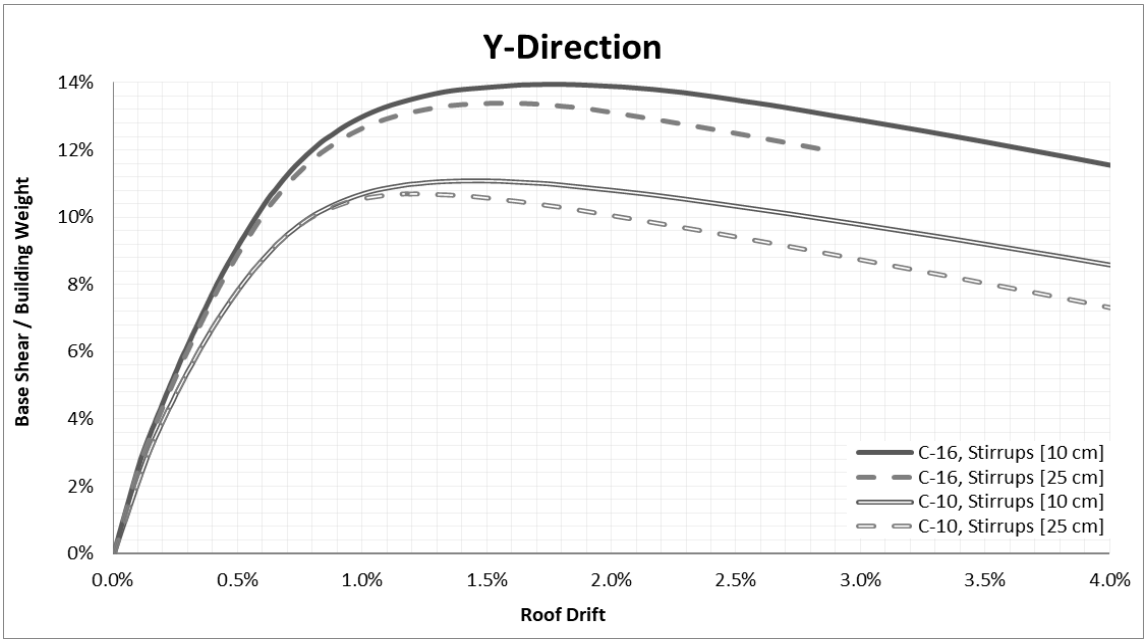

Figure 137: Capacity curves for E Template Design building in y-direction considering C10 and C16 concrete classes with S10 and S25 stirrups spacings

7.2 Interpretation of capacity curves

Pushover analysis for five template buildings considered in this study are performed using four different concrete classes and stirrups spacings in both orthogonal directions. All buildings are modelled using representative frames resulting in 160 different combinations. Pushover analysis is performed applying the inverted triangular lateral load pattern in the environments of Zeus-NL software. P-delta effects are considered while conducting the nonlinear static analysis, too. The capacity curves are plotted from the analysis outcomes as base shear normalized by seismic weight in vertical (y) axis and roof displacement divided by building height (Global Drift Ratio) in horizontal (x) axis. To check the influence of stirrups spacings the capacity curves for S10, S15, S20 and S25 (cm) are plotted in the same graph for each of concrete classes. On the other hand, to check the influence of concrete strength the capacity curves for C10, C12, C14 and C16 are plotted in the same graph for each stirrup spacings. Due to massive data and large number of graphs (40), they are presented in Appendix B. Furthermore, the IO, LS and CP performance levels are defined for each of the capacity curves. The detailed list is also presented in Appendix B.

Alternatively, a very practical combination of pushover curves to interpret the effect of stirrups and concrete on structural behavior, can be by grouping them according to average and lowest concrete class and stirrups spacing considered in this study. This is done in the previous section (7) where each of the graphs shows the capacity curves for the C10-S10, C10-S25, C16-S10 and C16-S25.

As shown from the figures, the influence of the concrete strength and stirrups spacings in global performance of the buildings is remarkable. By comparing stirrups spacings for the same concrete class, it is possible to observe the influence of transverse reinforcement in the ductility of the building. On the other hand, the concrete class ranges from a very poor concrete strength (C10) to an average one (C16). Based on observations from the site inspections as well as the laboratory tests, the results show that concrete quality is very

low for these template buildings. However, the blueprint shows in general an average concrete class of C16. Assessment of the pushover curves for the investigated buildings show that concrete quality and detailing have remarkable effects in both displacement and lateral load bearing capacity of the buildings.

Furthermore, the reduced percentage of lateral load bearing capacity as well as drift ratios from one combination to another one can be beneficial to better understand the impact of transverse reinforcement or concrete quality. However, comparing different curves by directly reading the results in graphs may be a tedious process. On the other hand, following massive values from the tables can be confusing at the same time. Therefore, a graphical presentation is demonstrated in **Figure 138** - **Figure 141**. The graphs present the difference of lateral load bearing capacity and global drift ratio values in percentage for both orthogonal directions. The comparison is done using three types of bars. The first two bars represent the reduced values (%) between C16-S100 and C10-S100. Using this combination, it can be very easy to observe the influence of concrete as the stirrups spacing remains the same. Moreover, second and third bar can be used to check the impact of stirrups spacings for the same concrete class. The combination is used as C10-S100 and C10-S250. Furthermore, any possible arrangement of available combinations in the chart can be easily interpreted. The comparison can be extended additionally among the results from other template buildings. The graphs given below are prepared for the A, B, C and D Template buildings as their design belong to the same year (1982).

As shown from **Figure 138**, the amount of the lateral load bearing capacity reduction, ranges from 22% - 32% when concrete strength lowers from C16-S100 to C10-S100 for the same stirrups spacings. Furthermore, the lateral load bearing capacity decrease is observed from A template to D template building. D template building has the highest building height compared to other previous designs. As seen from the figure, it can be concluded that concrete strength has a great impact on the load bearing capacity of the structure in X-direction. However, when comparing the reduced values when stirrups spacing changes from C10-S100 to C10-S250 small differences are observed. As shown

in the figure, these values are around 5-6% in A and D Template buildings and 9-17% in B and C Template.

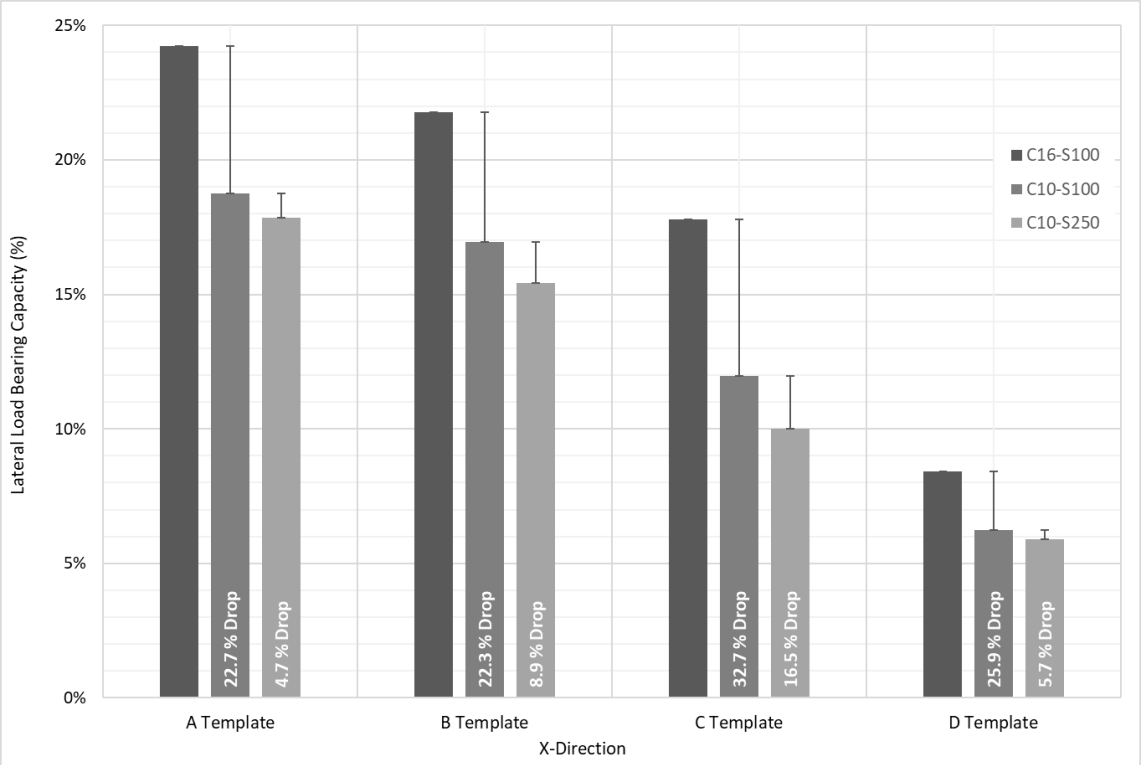

Figure 138: Lateral load bearing capacity reduction for different material quality and stirrups spacings of 1982 design Template Buildings in X-Direction

Similar trends are observed when comparing different stirrups spacings for Y-direction as shown in **Figure 139** when the decrease of the lateral load bearing capacity ranges from 2-6%. However, when observing the influence of concrete strength, it is seen that the values drop from C16-S100 to C10-S100 from 17-28% similar as in X-direction.

Therefore, it can be concluded that concrete strength has a great impact in lateral load bearing capacity of these structures whereas the stirrups spacings a relatively lower impact. This trend was observed in the previous studied by other researchers (Inel et. al., 2008).

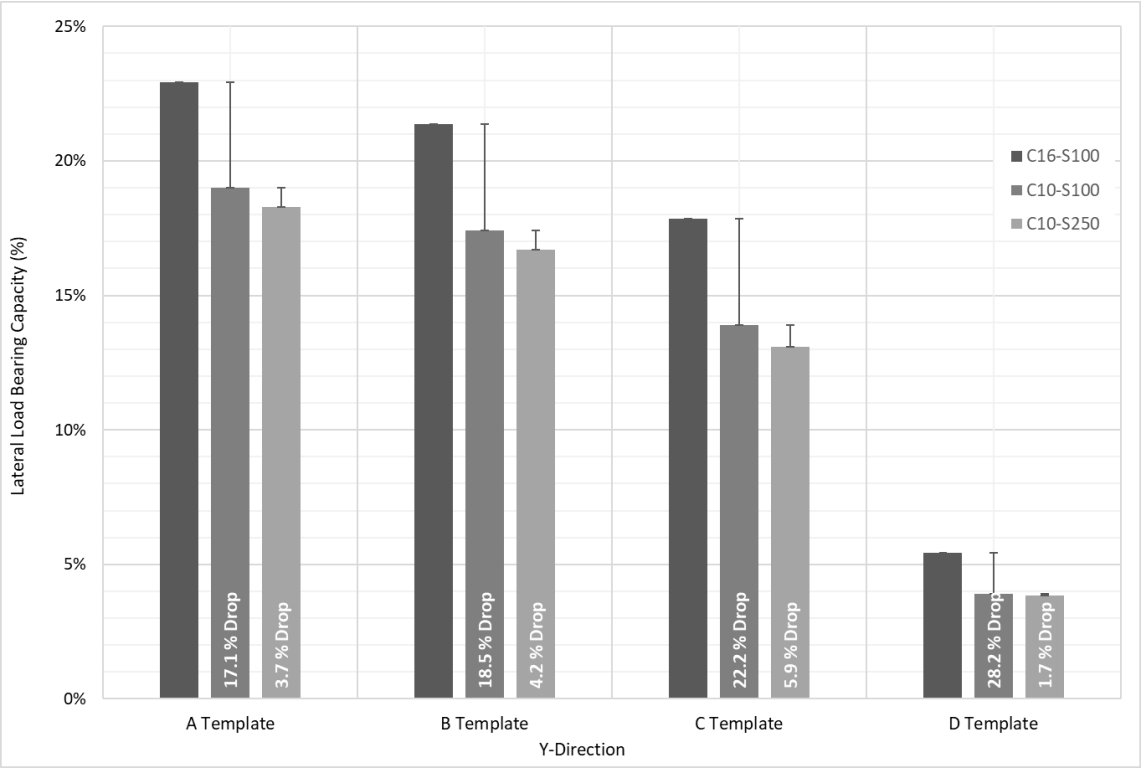

Figure 139: Lateral load bearing capacity reduction for different material quality and stirrups spacings of 1982 design Template Buildings in Y-Direction

Nonetheless, while observing the graphs for x- and y- directions of global drift ratio, the amount of drop reveals another phenomenon. Both **Figure 140** (x-direction) and **Figure 141** (y-direction), show a superior influence of transverse reinforcement on the ductility of the structures. For instance, the amount of the dropped values from C10-S100 to C10-S250 ranges 18-35% for x-direction and 15-34% for y-direction. Compared with reduced amount of lateral load bearing capacities, the difference is quite noticeable.

On the other hand, the effect of concrete strength seems to be not very dominant in the global drift ratios. The amount of decrease drift ratios for x-direction of C16-S100 and C10-S100 usually is under 5.5%. The only exception is seen in C template which experiences 22.4% drop of drift values.

Similarly, the results are influenced massively from the transverse reinforcement of the y-direction of all template buildings. Similar results, about the vital role of transverse reinforcement in the global performance of the buildings regardless of concrete class has been reported previously by other researchers (Bilgin, 2007).

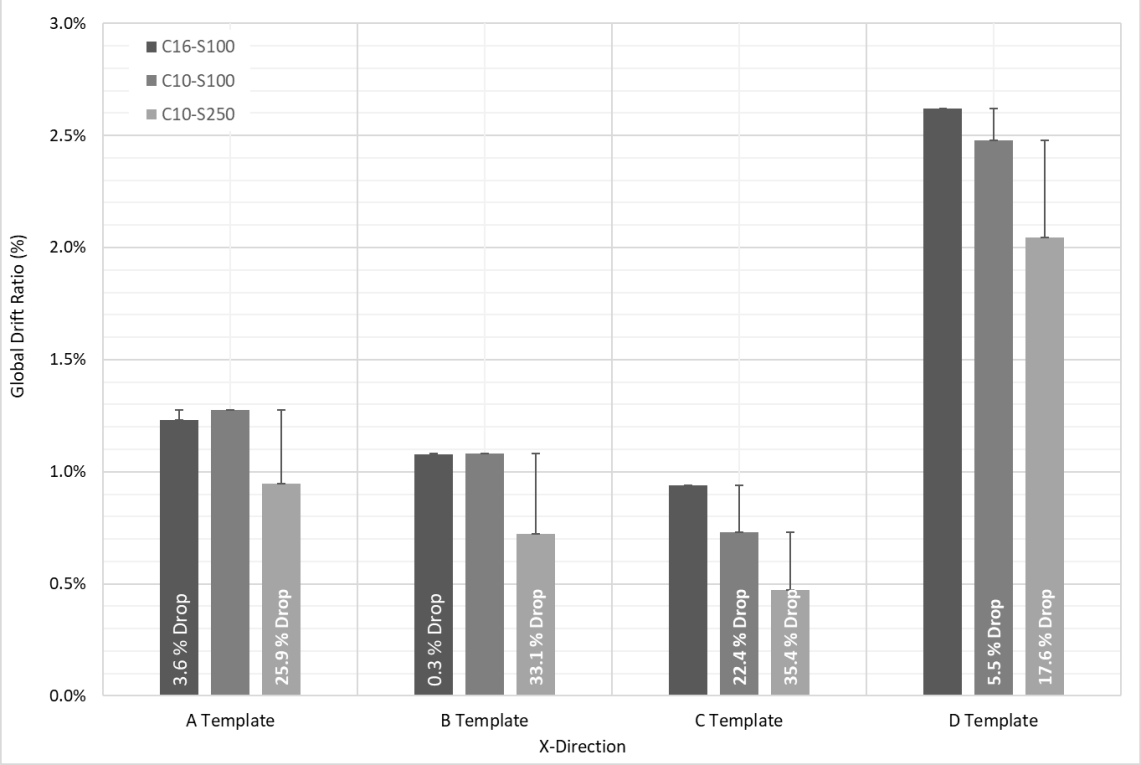

Figure 140: Global drift reduction for different material quality and stirrups spacings of 1982 design Template Buildings in X-Direction

As shown in **Figure 141**, the range of the reduced values of global drift are from 0.3% to 6% when for different concrete quality. However, considerably huge difference of values is seen from C template building while comparing the poor concrete quality with average one. As shown in the figure, the global drift drops with 22.4%. These exceptions can be justified by the fact that each of the first three template buildings share almost the same plan configurations. However, the height of the first two buildings remains the same but

the C Template has one more story which increases the overall height almost 3 meters (20%).

As the average lateral load bearing capacity for different material quality and stirrups spacings remains lower in the D Template building, compared with other three buildings, the global drift ratios seem to be higher for this template.

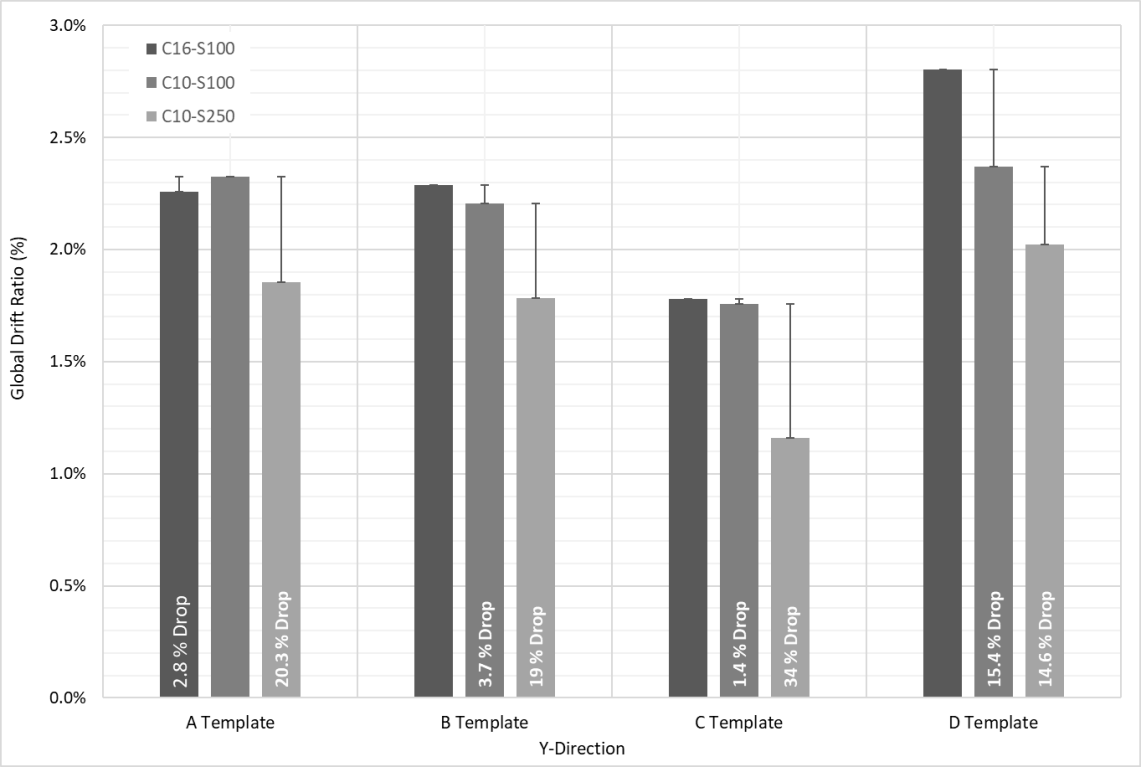

Figure 141: Global drift reduction for different material quality and stirrups spacings of 1982 design Template Buildings in Y-Direction

This is typically observed in x-direction (**Figure 140**) where the global drift ratio of D template building is over 2.6% whereas the average amount of other three template buildings is around 1%.

A careful consideration of **Figure 138** - **Figure 141** reveals that the yield base shear ratio and global drift capacity, especially at the CP performance level, appear to differ

significantly from those found in the relevant literature (JICA, 2000; HAZUS, 1999). This difference might be due to the code enforcements, construction practice and possibly the influence of modelling strategy. Another important observation for the low displacement capacities is related with the failure mechanisms of the buildings since the pre-modern code (KTP-78) requirements did not consider the weak-beam strong-column formation which has been a common problem for building construction practice of Albania or similar countries (Leti and Bilgin, 2022).

7.3 Evaluation of performance of template designs

The method of Capacity Spectrum (CSM) (ATC-40, 1996), the method of Displacement Coefficients (DCM) (FEMA-273, 1997) and N2 Method (Fajfar and Gašperšič, 1996) are considered the main nonlinear static analysis procedures to define the performance point of buildings. The evaluation of performance of template buildings selected in this study are done based on the Capacity Spectrum Method. As explained in Section 4.6.5, this method evaluates the maximum displacement by considering an intersection point between capacity curve of the building with a reduced response spectrum. However, the CSM method requires to convert the capacity curve and demand response spectra in Acceleration Displacement Response Spectra (ADRS) format. The method of conversion is based on the guidance of ATC-40 according to Procedure A.

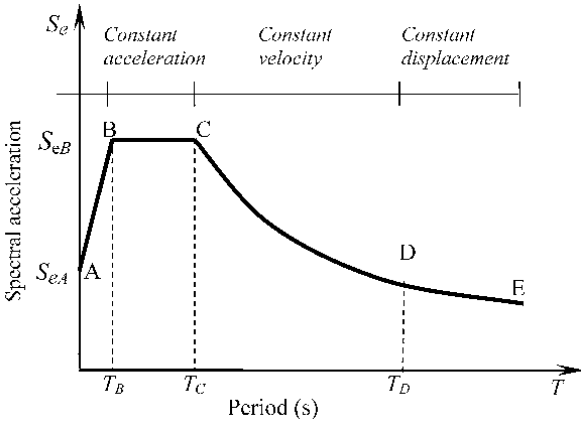

Figure 142: Response Spectra shown with corner periods (EC-8)

The response spectra used in this study is based on EC-8 as well as KTP-N2-89. This is done also to check the comparison among the regularly updated seismic code (EC-8) and the old seismic design code of Albania which was updated for the last time in 1989. Each of the codes define an equation for the development of response spectra.

According to Eurocode-8, the response spectra is calculated for five main corner periods as shown in **Figure 142**.

For each of the corner period, there is deployed one equation to plot the graph. The equations are given as below:

for $0 \le T \le T_B$	**$S_{e(T)} = a_g * S * (1+T/T_B*(\eta * 2.5 -1))$**	Equation 20
for $T_B \le T \le T_C$	**$S_{e(T)} = a_g * S * \eta * 2.5$**	Equation 21
for $T_C \le T \le T_D$	**$S_{e(T)} = a_g * S * \eta * 2.5 * (T_C / T)$**	Equation 22
for $T_D \le T \le 4s$	**$S_{e(T)} = a_g * S * \eta * 2.5 * (T_C * T_D / T^2)$**	Equation 23

Where: $S_{e(T)}$ is the elastic response spectrum; **a_g** is the design ground acceleration on type A ground; **T_B T_C T_D** are the corner periods in spectrum (NDPs); ***S*** is the soil factor (NDP); **η** is the damping correction factor (η = 1 for 5% damping).

On the other hand, KTP-N2-89 requires to use one formula as shown below for the response spectra calculations. Detailed description on the implementation of this method is explained in section 4.5.

$$S_a = k_E * k_r * \psi * \beta * g \qquad \text{Equation 24}$$

Where: S_a is the spectral acceleration of the horizontal seismic component, **k_E** is the seismic coefficient, **k_r** is the importance coefficient of the building type, **ψ** is the structural behavior coefficient under seismic loading, **β** is the dynamic coefficient, **g** is the acceleration of earth gravity.

The parameters used for the template buildings selected in this study are given in **Table 17**:

Table 17: Parameters of EC-8 and KTP-N2-89 used to define response spectra

Parameters	**EC-8**	**KTP-N2-89**
Structure Type factor	$\gamma_I = 1.0$	$k_r = 1.0$
Structure Importance factor	$q = 4$	$\psi = 0.3$
Type of the Soil	C	II
Acceleration	$a_g = 0.22$	$k_E = 0.22$

Furthermore, pushover results are converted together with demand response spectra in the ADRS format so both can be plotted in the same graph. After the conversion, the performance point is checked according to ATC-40. Detailed information about this implementation is given in section 4.6.5. However, it is important to emphasize that properly allocating the performance point (PP) in the capacity graph is an iterative and tedious process to be done manually. Therefore, a script has been prepared to achieve this task in the environments of python programming language. An example of the output from the script is shown in **Figure 143**:

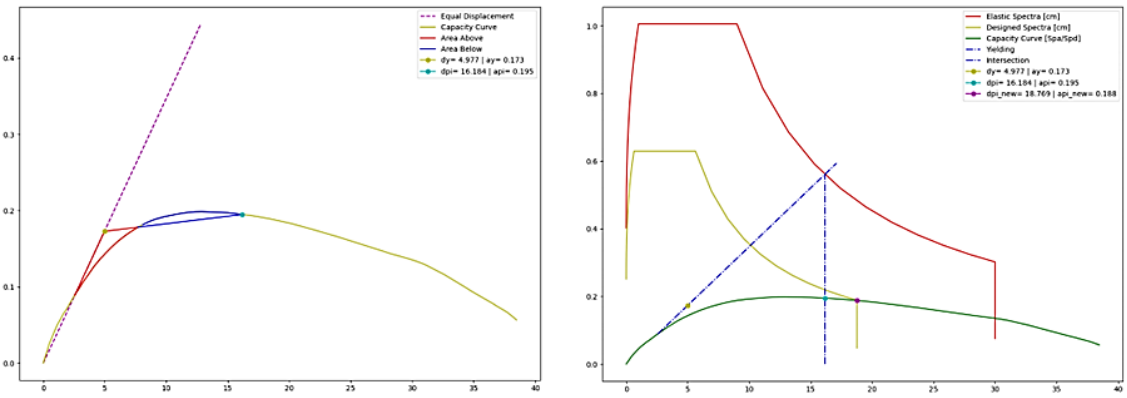

Figure 143: 1st output from the automation procedure, bilinearization (left) and performance point of trial calculations (right).

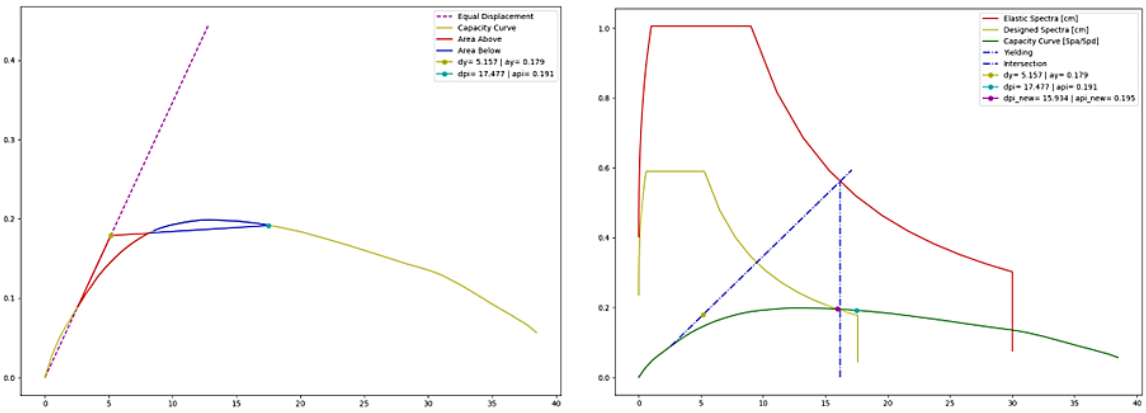

Figure 144: 2nd output from the automation procedure, bilinearization (left) and performance point of trial calculations (right).

Note that in **Figure 143 and Figure 144** the performance point is rejected as it does not satisfy the criteria determined in ATC-40 for difference between dpi points as given by the equation:

$$\mathbf{0.95\ d_{pi} \leq d_{pi\_new} \leq 1.05\ d_{pi}} \qquad \text{Equation 25}$$

After multiple trial and errors, the location of the performance point is accepted as soon as the difference between d_{pi} points satisfies the abovementioned equation. **Figure 145** shows the case of accepted performance point.

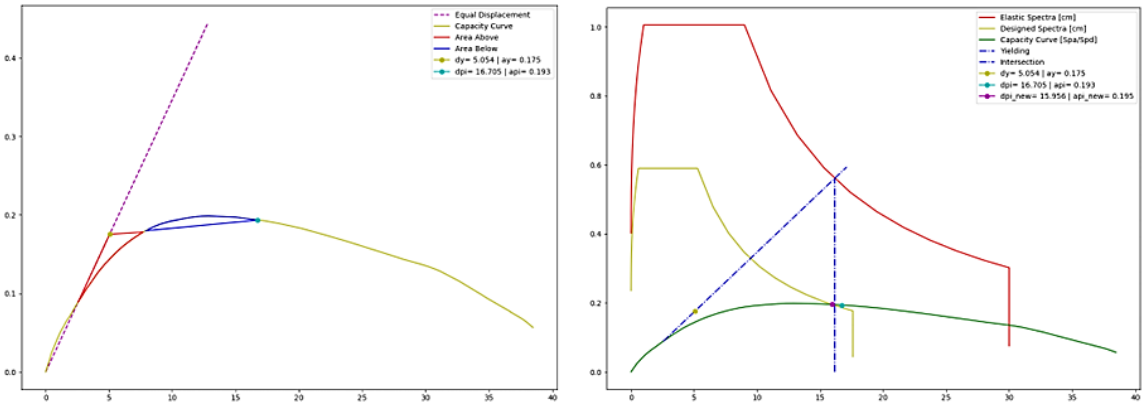

Figure 145: nth output from the automation procedure, bilinearization (left) and performance point trial calculations (right).

7.3.1 Evaluation of capacities

The evaluation of capacity curves is done through capacity spectrum method. The performance point is calculated using Procedure A defined in ATC-40. In addition, modern codes request that reinforced concrete residential buildings must ensure the safety of the structures for LS limit state. To check if the buildings satisfy this requirement, the performance point is compared with LS limit state. **Figure 146** shows an example of comparison between the capacity of the building (SPO curve) and the demand calculated based on capacity spectrum method (Performance Point – P.P.).

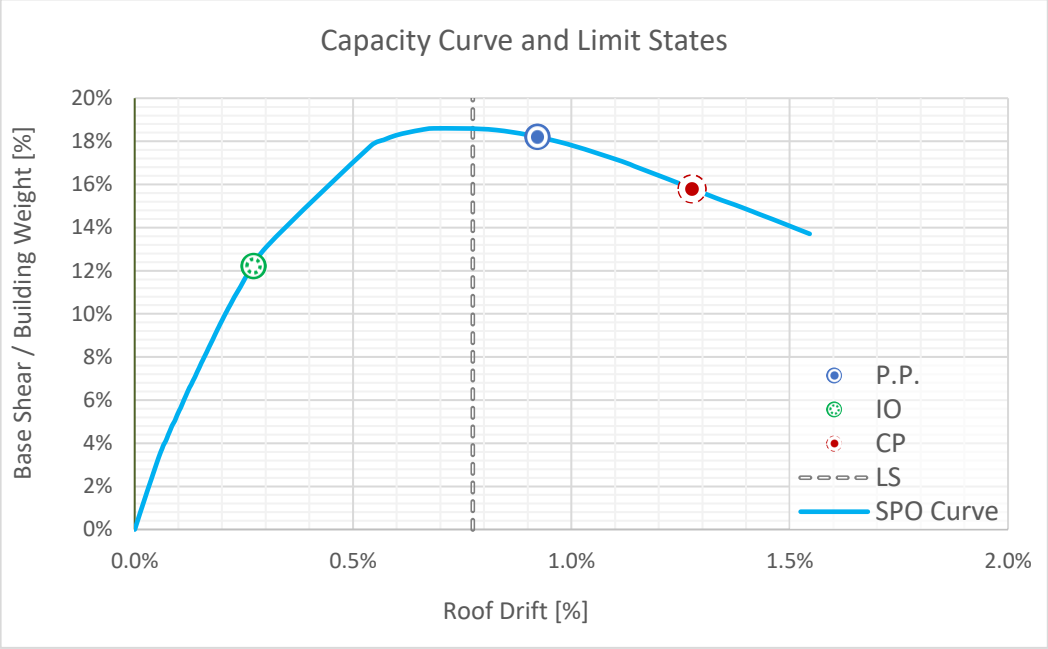

Figure 146: A sample capacity curve together with IO, LS, CP limit states and Performance Point

Performance point (PP) is calculated by comparing the capacity and demand and from the graph given in **Figure 146**, PP falls between LS and CP performance level which means building performance level is in LS.

Furthermore, the influence of concrete quality and transverse reinforcement is reflected using the comparison between capacity and demand values. Additionally, a comparison between the modern code (EC-8) and old code (KTP-N2-89) is conducted. The results from demand calculations, are presented together with immediate occupancy, life safety and collapse prevention of capacity curves, in the same graph. The IO and CP limit states are not target of this study but can be good points to evaluate the global performance of the selected buildings. Graphs are presented with bars for each concrete type, stirrup spacings and seismic codes. To show how close is the demand from exceeding the upcoming limit state, each bar is labeled with respective value calculated in percentage as shown in **Figure 147**. In this way, the comparison between material types, stirrups spacings and seismic codes can be done easily. For example, **Figure 147** demonstrates the exceedance of the limit states for A Template building in both directions. As shown in the figure, all building models composed with stirrups spacing 250mm do not satisfy the LS performance level according to EC-8 in x-direction. However, the KTP-N2-89 provides less demand in comparison to EC-8 for all the combinations given in the figure.

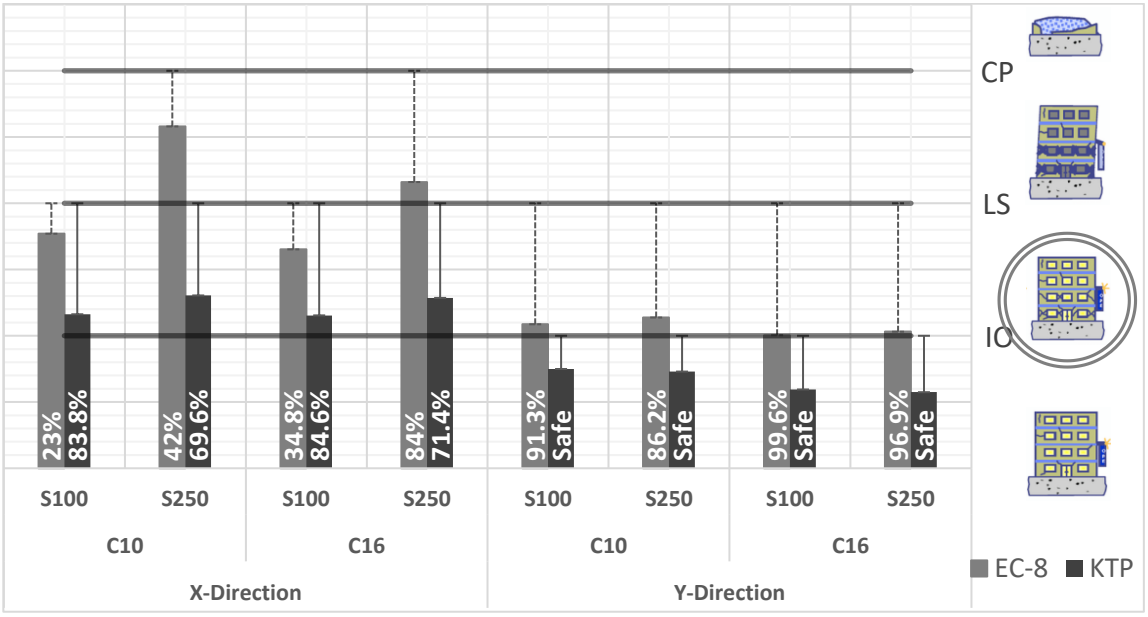

Figure 147: Performance of A Template in x- and y-direction for different concrete classes and stirrups spacings according to EC-8 and KTP-N2-89

Moreover, it can be concluded that the demand values of KTP-N2-89 are about the half from those calculated with EC-8.

The percentage values shown in the end of each bar increase slightly from C10 to C16 concrete for the same stirrups spacings. This indicates the impact of material quality on the global performance of this building. On the other hand, the influence of shear reinforcement is remarkable especially when calculated with EC-8. Finally, it can be concluded that all cases with stirrups spacings 250 mm do not the target performance level (LS) in x-direction. Alternatively, the demand values from KTP are considerably lower than those from EC-8. Similar effects are reported before by other researchers (Frangu, 2013)

Nevertheless, in y-direction none of the models exceed the LS limit state. From this point of view, the performance of the building is better compared to other direction. The weakest case is depicted from the poorest quality and widest stirrups spacing (C10-S250) from EC-8 demand values. The influence of stirrups spacings seems considerably higher than the impact of concrete quality. Whereas from the comparison between demand values calculated with EC-8 and KTP-N2-89, there exists clearly a significant difference. Finally, it is concluded that A Template building performs weak especially in its longitudinal direction, due to insufficient lateral load bearing capacity and stiffness. This phenomenon seems to be followed by the x-direction of B Template building. **Figure 148** shows the performance of B Template building according to Eurocode and KTP standards. As shown from the figure, demand values seem higher with respect to capacity of the structure. The most critical cases are once again illustrated from the S250 mm stirrups spacings. At least three building models exceeded LS performance level, one of which seems to attract enough displacement demands to lead the structure in global failure.

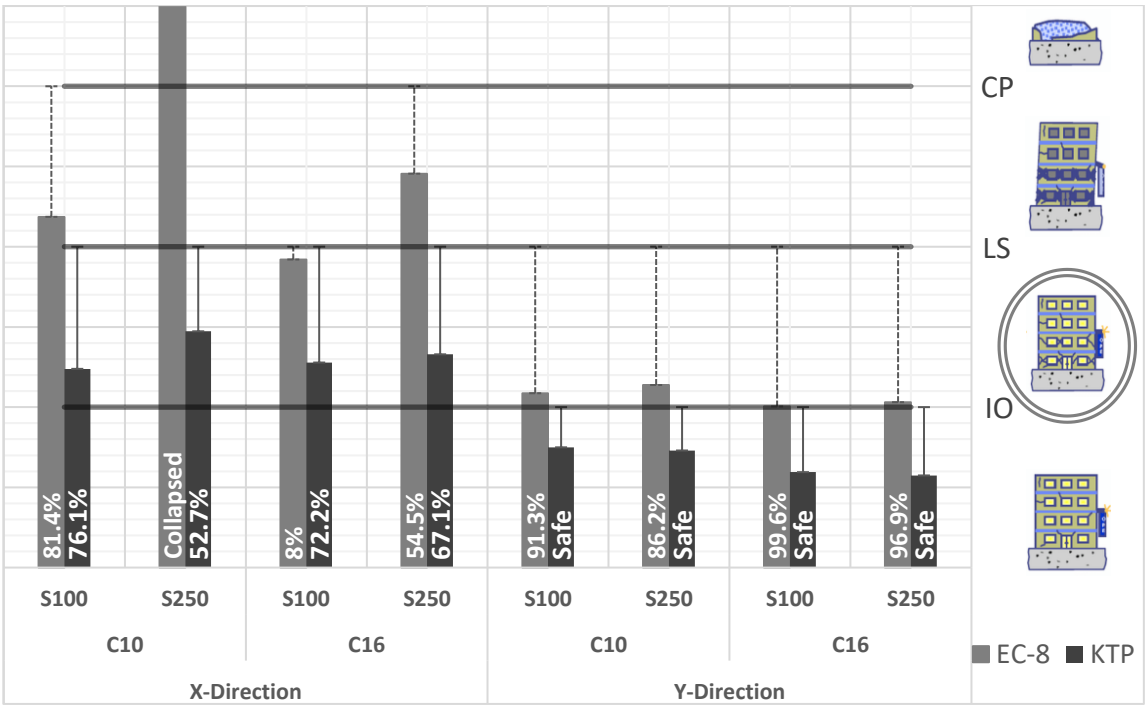

Figure 148: Performance of B Template in x- and y-direction for different concrete classes and stirrups spacings according to EC-8 and KTP-N2-89

Very similar observations from A Template building are conducted once more. The influence of shear reinforcement seems significant for all concrete types. The lower demand values of KTP-N2-89 compared to EC-8 are easily distinguishable.

On the other hand, the results from y-direction of A and B Template building are the same because they share the same plan configuration in this direction.

Therefore, it is concluded that in addition to previous building, B Template has one more frame in its longer (x) direction. The structure is less stiff therefore it performs considerable displacements to exceed the target limit state for this study (LS).

Further to the building typologies designed in 1982, C Template shares the same planimetry with B type and is comprised of one more story.

The demand values calculated according to EC-8 and KTP-N2-89 are presented graphically together with limit states in **Figure 149**.

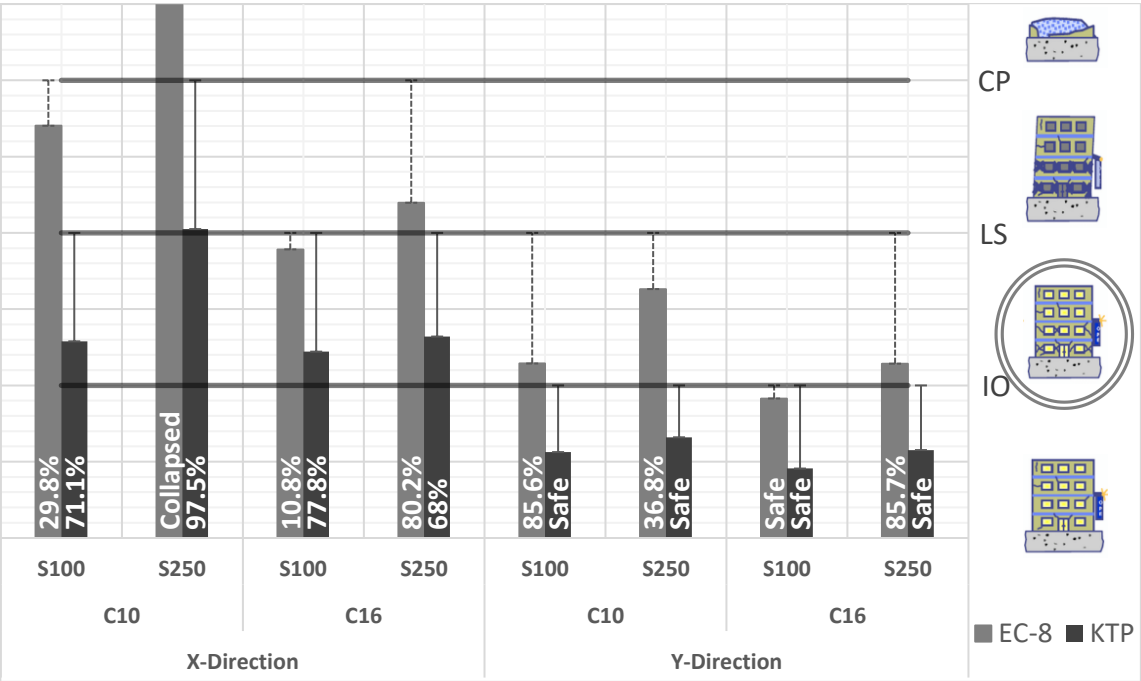

Figure 149: Performance of C Template in x- and y-direction for different concrete classes and stirrups spacings according to EC-8 and KTP-N2-89

As shown, almost all buildings modeled with stirrups spacings S250 in x-direction, exceed the LS performance level according to the modern code (EC-8). Additionally, the building modelled with C10-S250 goes beyond the collapse prevention. The impact of concrete quality can be easily observed for the same stirrups spacings based on both seismic standards. Furthermore, the influence of the transverse reinforcement reflects major differences in the structural performance. With great importance is comparing the poorest concrete/stirrups combination (C10-S250) versus the highest one in this study (C16-S100). The difference in terms stirrups spacings and concrete classes is massive for both directions. Compared with A Template building, where the influence of material quality is less than stirrup spacing, C Type building shows a great influence of both shear reinforcement and concrete quality. On the other hand, C Template shows a better

performance in y-direction. The demand values are about half of those in x-direction. To conclude, as structure gets higher in elevation, it loses stiffness thus the material quality plays a vital role in the overall performance. Whereas the impact of transverse reinforcement is noted to be dominating in all models of C Template building.

The demand values calculated for D Template building together with limit states are shown in **Figure 150.** The performance of the structure in x-direction is at the region between immediate occupancy and life safety. The only model which exceeds LS level in this direction is C10-S250. Unlike previous three template buildings, D type indicates better performance in x-direction compared to the other one. As shown in the figure, buildings modelled with C10 concrete exceeded the life safety performance level, whereas the models with C16 are very close to it. Recalling from the plan details, the distance of the building in longitudinal side compared with transverse one, is longer.

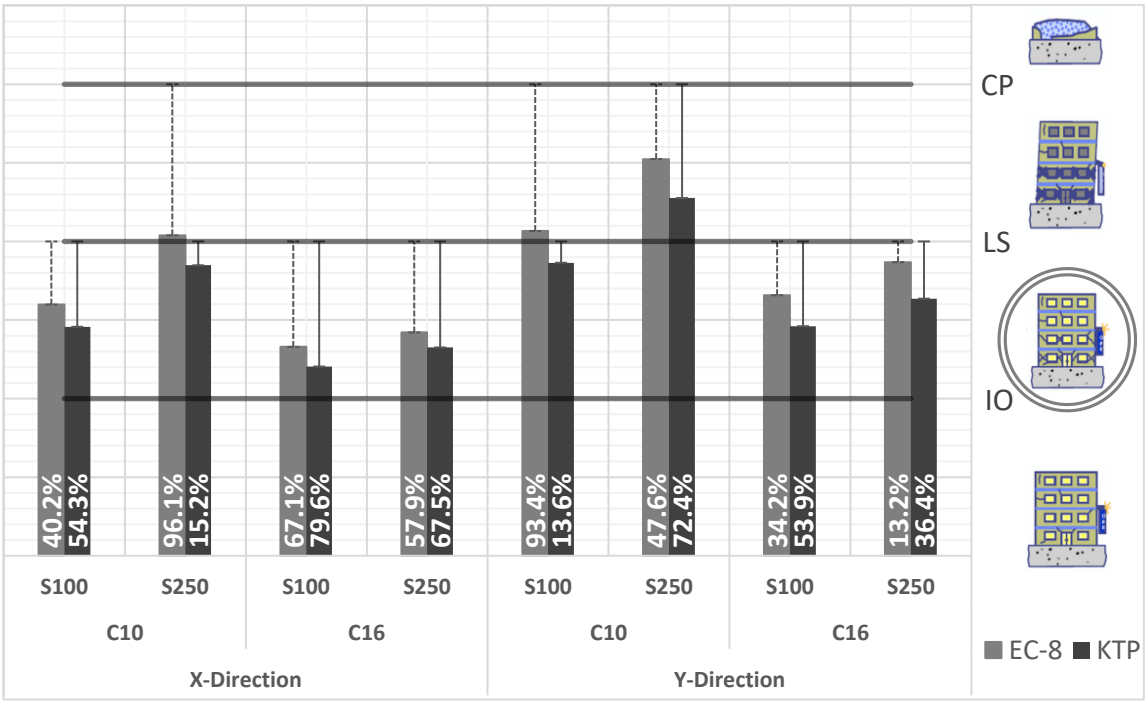

Figure 150: Performance of D Template in x- and y-direction for different concrete classes and stirrups spacings according to EC-8 and KTP-N2-89

Further to the previous observations, it is concluded that lateral load bearing capacity and stiffness ore some of the main causes of poor performance. This phenomenon is potentially supported by the capacity curves shown in section 0 in **Figure 133** and **Figure 134**. As shown, the roof drifts are remarkably higher than in previous template building. Whereas the lateral load bearing capacities are considerably less.

Finally, the performance of the E Template building designed later in 2005 is presented in **Figure 151**. From the overall perception, it seems that the increase of the size of structural elements, has played a great role. There are not drastic changes from one direction of the building to another. Nevertheless, the capacity spectrum is an approximation method. For this reason, the performance of the E Template will be analyzed also by using one of the most promising methods recently known as Incremental Dynamic Analysis.

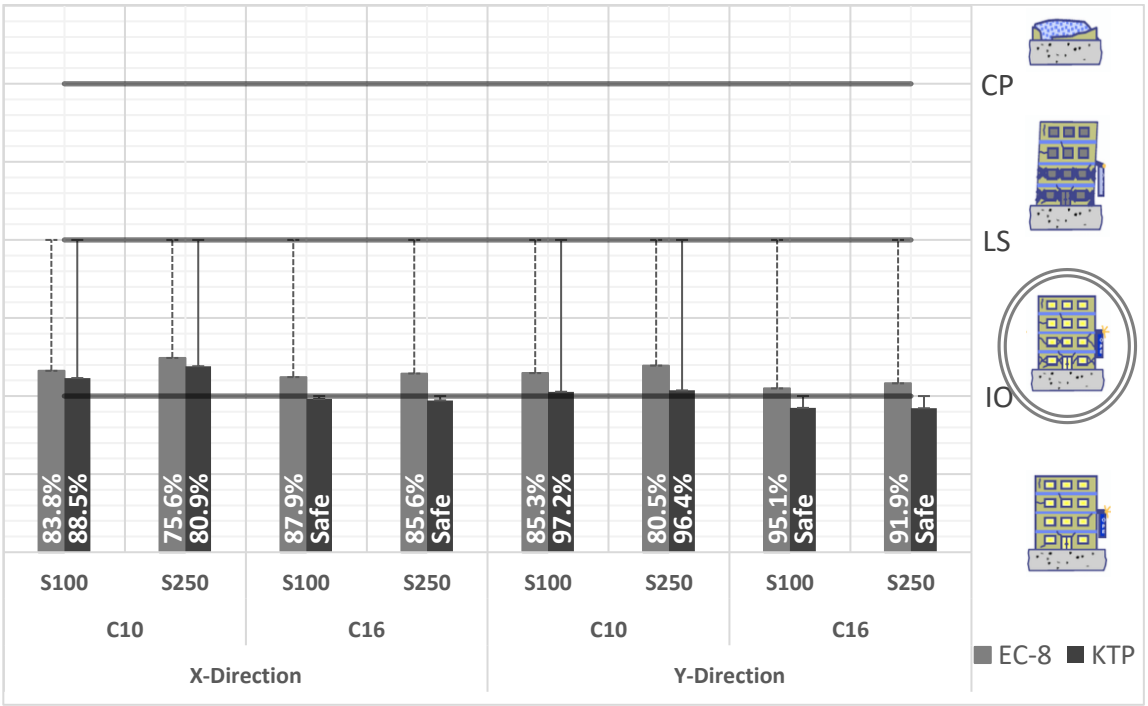

Figure 151: Performance of E Template in x- and y-direction for different concrete classes and stirrups spacings according to EC-8 and KTP-N2-89

7.4 Nonlinear time history analyses and performance evaluation

In this part of the study, to investigate the influence of near- and far-field ground motions records on the seismic performance of residential buildings selected, nonlinear time history analysis is used. Nonlinear time history analysis is performed using version 8.0 of the Computer Program for Nonlinear Dynamic Time History Analysis of Single and Multi-Degree-of-Freedom Systems, (NONLIN V8) software (Charney et. al., 2010). For the modelling case in NONLIN it is applied the equivalent single degree of freedom system (SDOF). Each of the pushover curve is used for the conversion from multi-degree of freedom (MDOF) to SDOF by using bilinearization as explained in section 4.6.5. For the conversion method and formulas, it is benefited from ATC-40 guidelines. An example of conversion from MDOF to SDOF is given in **Figure 152**.

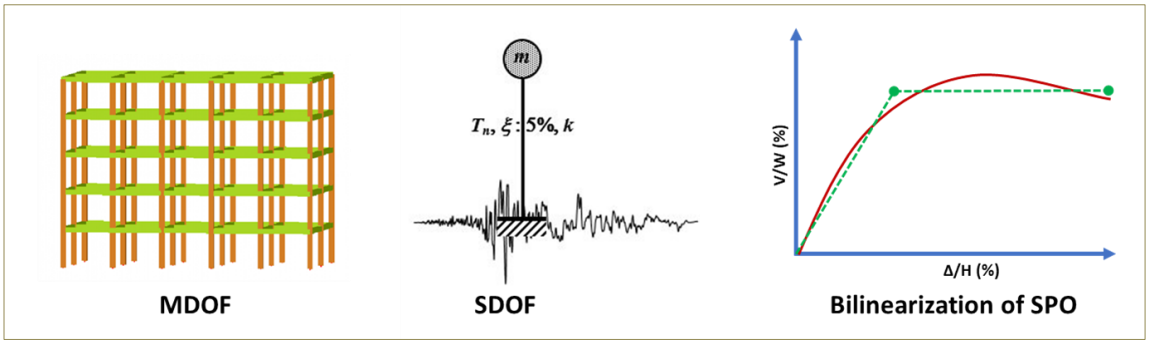

Figure 152: Idealization of conversion from MDOF to SDOF

The formulas used correspond to those in section 4.6.5. After each the conversion is done properly, then values must be prepared for the inputs of NONLIN V8 software.

7.4.1 Equal single degree of freedom system approach (ESDOF)

To perform the nonlinear dynamic (Time History) analysis in NONLIN, the following data are important to match with software input variables as shown in **Figure 153**:

- **Weight:** the weight of x- and y-frame is used
- **Damping ratio:** 5% damping ratio is used for RC residential buildings
- **Stiffness (K1):** the values obtained from bilinearization
- **Strength position:** determined by the ratio of yield and modal mass coefficient
- **Ground Motion:** determined among the group of earthquakes in NONLIN library

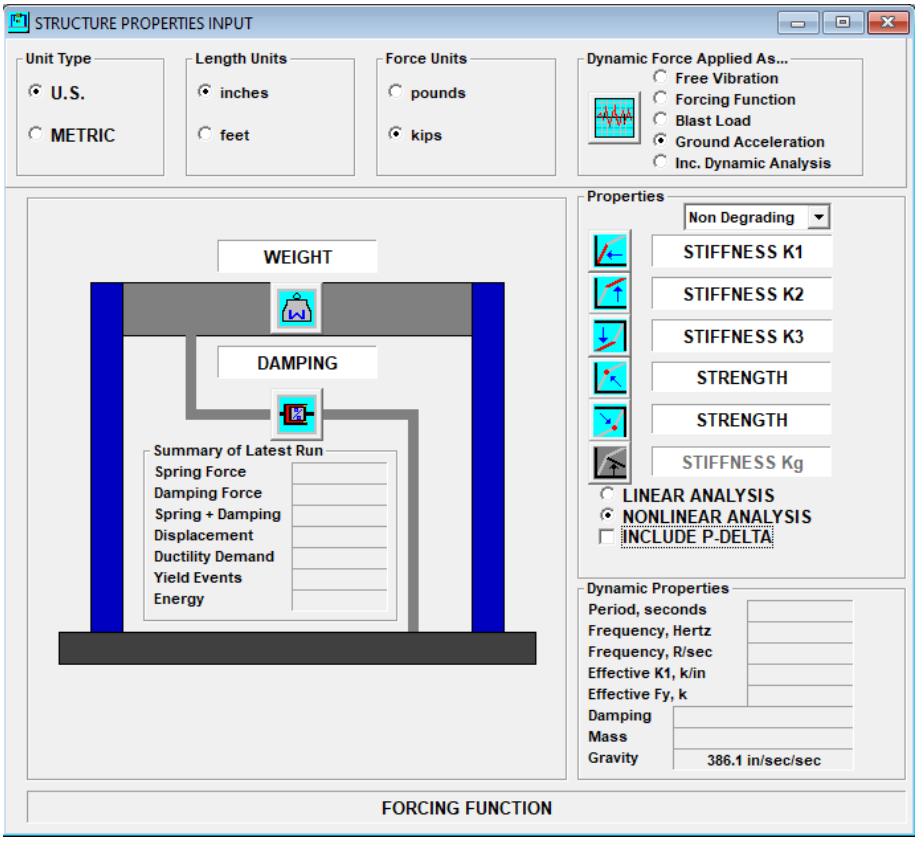

Figure 153: NONLIN V8 window of inputs

The set of earthquakes is grouped into two categories, the far field and near field records. The far field is composed of 68 records whereas the near field of 78 records. The detailed list for far and near field is given in **Table 9** and **Table 10** of section 5.2.

Once the inputs are ready and the earthquake records is selected, the analysis can be initiated. Due to the large number of analyses (18,688), they are automated through python programming language and a couple of libraries.

7.4.2 Near fault versus far fault results

The earthquake demands are evaluated comparatively under a set of far-fault and near-fault ground motions and the nonlinear dynamic characteristics were calculated using equally single degree of freedom (ESDOF) system approach. To check the influence of far versus near fault ground motions, a set of 68 and 78 records is used respectively while performing Time History analyses. For each of the buildings, a table with 4 672 values is filled. In this section, the graphical interpretation is prepared for each of the 1982 design templates considering far and near fault for different stirrups spacings and concrete classes. The graphs prepared, represent the percentage of each earthquake set (Far of Near fault) that exceeds the LS or CP performance level in x- and y-direction.

Figure 154 shows the percentage of earthquakes violating the life safety limit state for A Template building. As shown in the figure, x-direction is prone to more damages compared with the y-direction. This is in compliance with the results shown from capacity spectrum. Moreover, the remarkable influence of stirrups is clear from this graph. There are about 15% earthquakes more which violate the LS performance level while comparing stirrups spacing 100 mm and 250 mm of x-direction. On the other hand, the effect of concrete class from C16 to C10 influence less than 10% of the earthquakes to exceed LS level. In addition, the comparison between far fault and near fault records can be done using the graphical representation of **Figure 154**. As shown, the effect of near fault records is way more dominant than far fault records. A general observation would show that influence of near fault records almost doubles the damage impact of the A Template building.

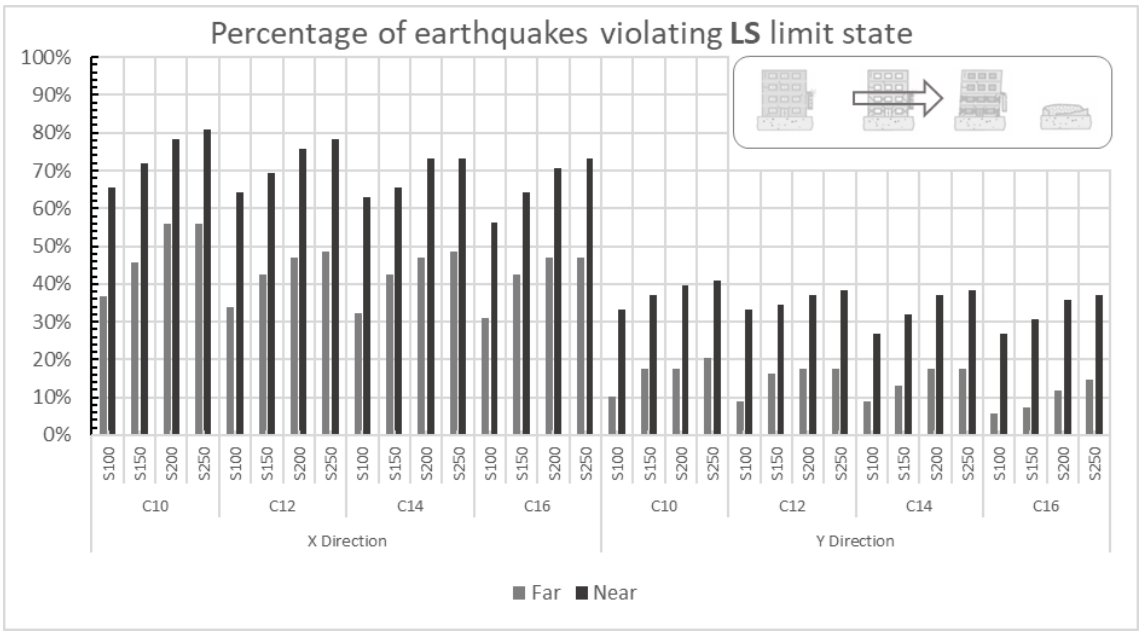

Figure 154: Percentage of earthquakes violating LS limit state for A Template Building

Figure 155 represents the percentage of the earthquakes violating CP performance level for A Template building.

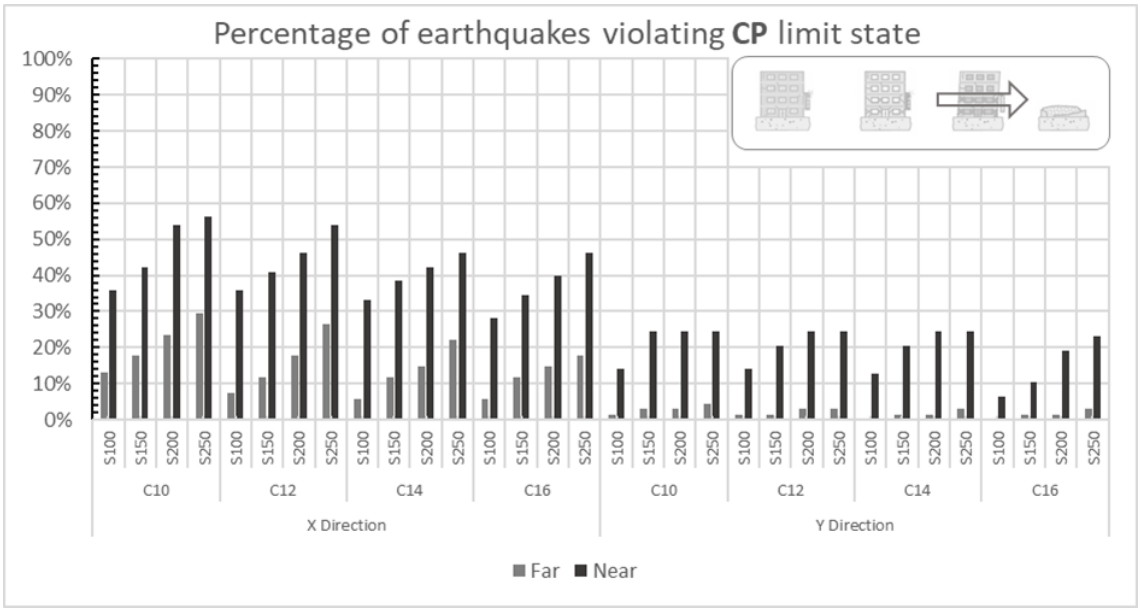

Figure 155: Percentage of earthquakes violating CP limit state for A Template Building

Similar effects as previously can be seen from the comparison of near fault and far fault records. On the other hand, the difference between x- and y-direction is obvious.

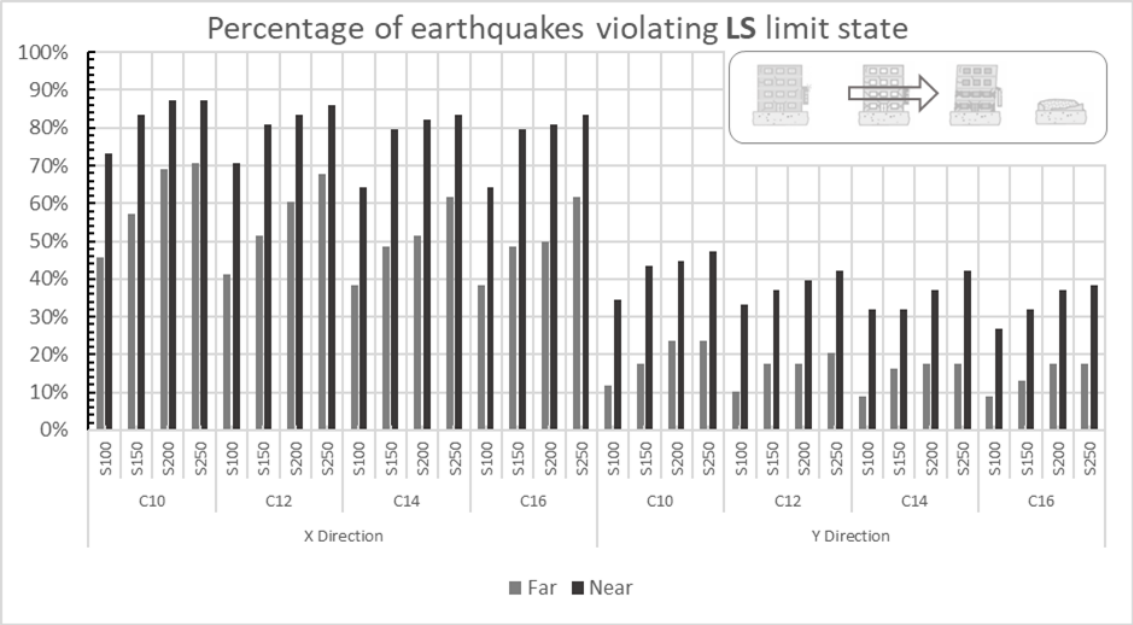

Figure 156: Percentage of earthquakes violating LS limit state for B Template Building

Figure 156 and **Figure 157** show the percentage of earthquakes exceeding LS and CP limit states respectively for B Template building.

As shown in **Figure 156**, there are about 70% to 90% of records exceeding the LS in x-direction and about 30% to 50% in y-direction. Whereas the effect of far fault earthquakes is less dominant. Another important observation is the influence of S100mm stirrups. As shown, it decreases the number of earthquakes by 10% compared with the S150, S200 and S250mm spacings which differ about 3% from each other. Once again, the importance of proper detailing of transverse reinforcement is highlighted especially for these old residential buildings.

Figure 157 shows the exceedance of CP limit state. Similar trends as previously can be recognized. The drastic change of earthquake percentage violating this limit state in y-

direction when comparing near and far fault records are again obvious. Similar results are also reported from researchers (Leti and Bilgin, 2022).

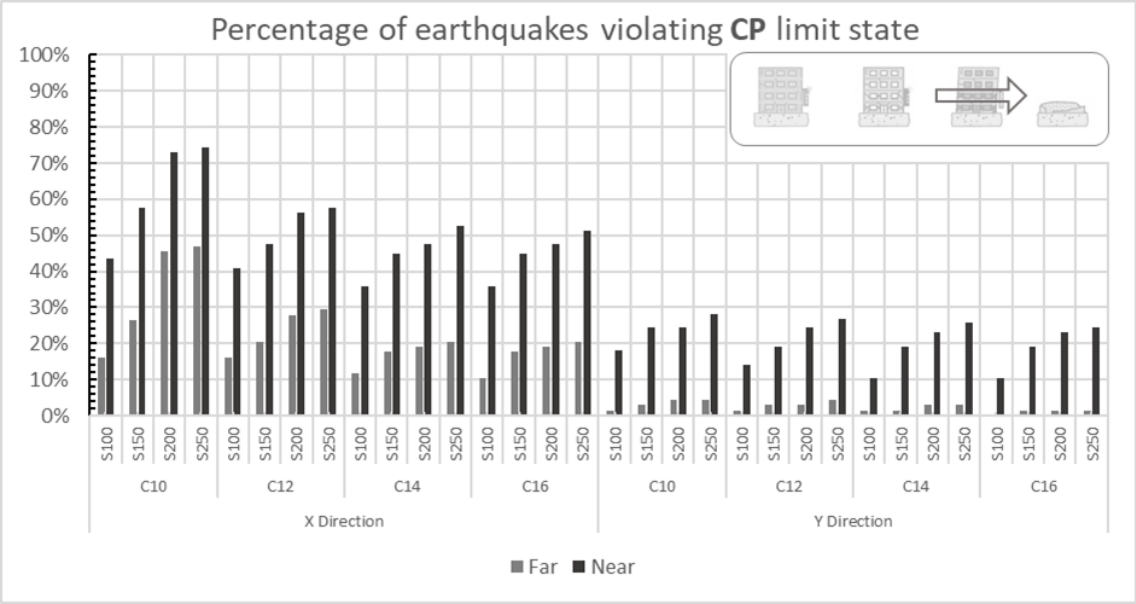

Figure 157: Percentage of earthquakes violating CP limit state for B Template Building

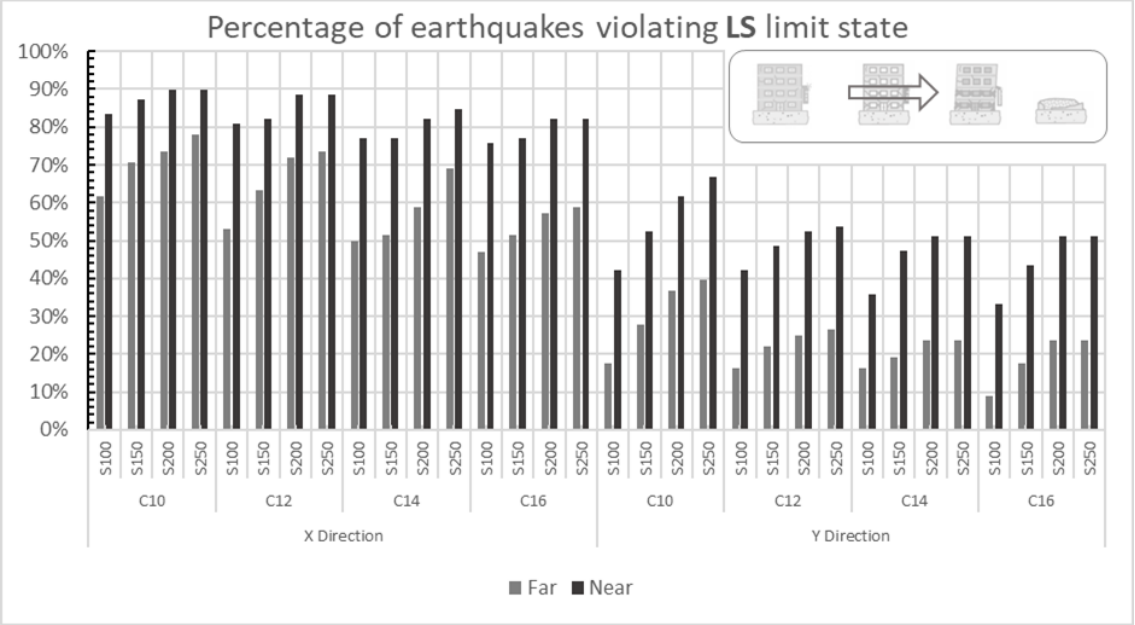

Figure 158: Percentage of earthquakes violating LS limit state for C Template Building

Even worse is the performance of C Template building which suffers the LS limit state by up to 90% of earthquakes in x-direction for wide stirrups spacing.

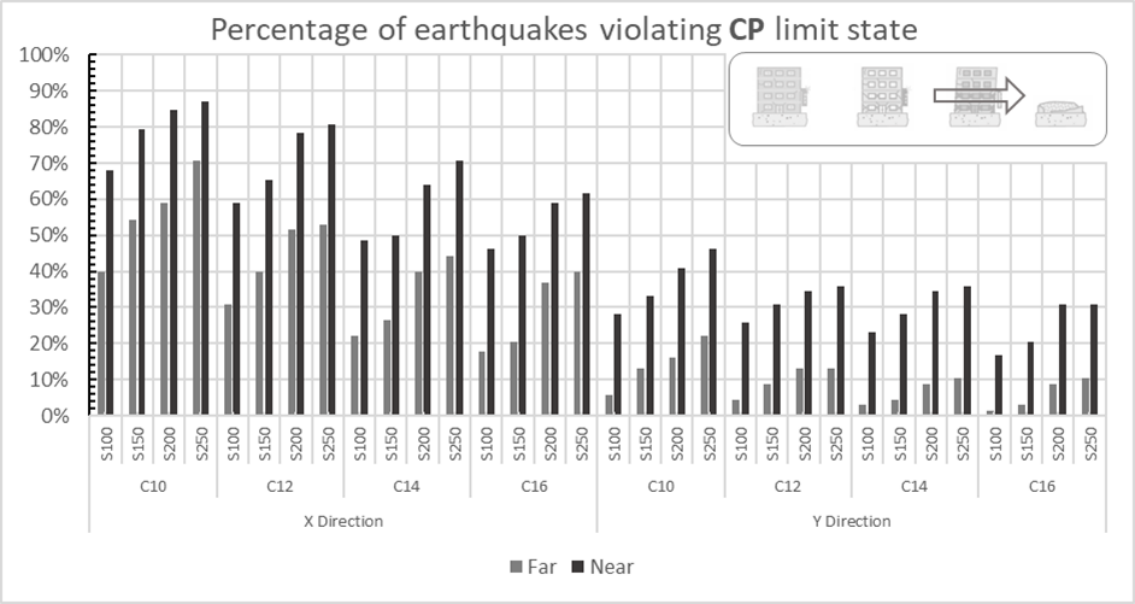

Figure 159: Percentage of earthquakes violating CP limit state for C Template Building

The influence of near fault earthquakes drops about 20% from the near fault, less than previous buildings which was about 50%.

The y-direction also experiences a larger number of earthquakes exceeding LS compared with the A and B Templates.

On the other hand, the number of earthquakes violating CP limit state in both orthogonal directions confirm again the poor performance of C Template building.

D Template building has an irregular plan configuration. The torsional effects are impossible to be captured as the building is modelled as frame system in x- and y-direction. This should be the reason that the performance is slightly better compared with previous template designs. Nonetheless, the percentage of earthquakes exceeding LS and CP limit states does not reflect a good performance of the structure in none of its

directions. The dominance of near fault records from the far ones, is pretty obvious from **Figure 160** and **Figure 161**.

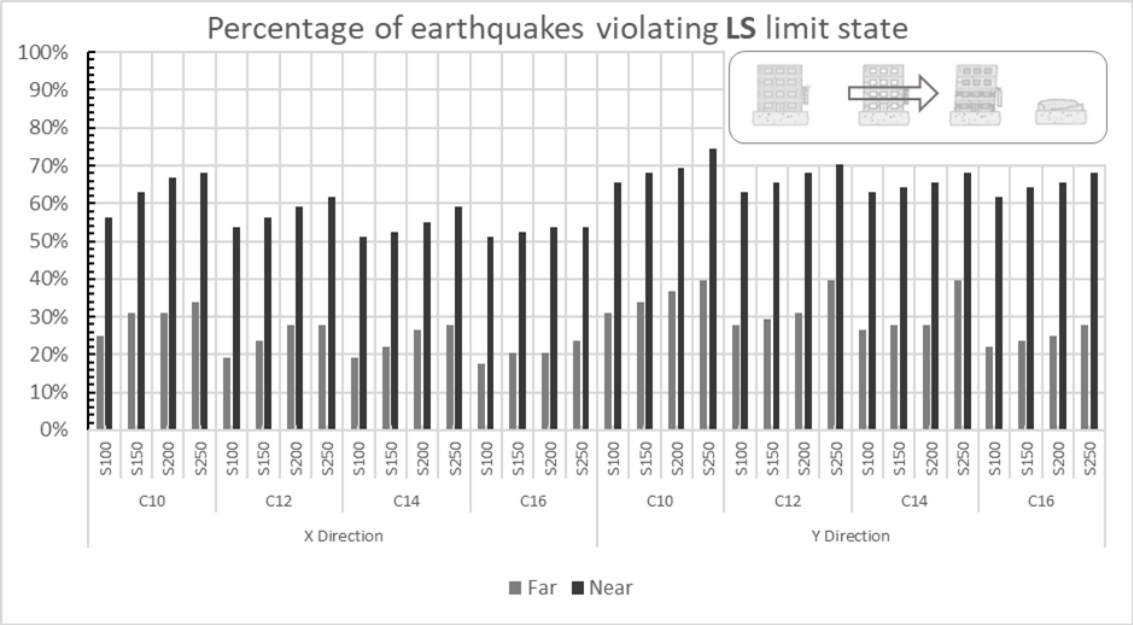

Figure 160: Percentage of earthquakes violating LS limit state for D Template Building

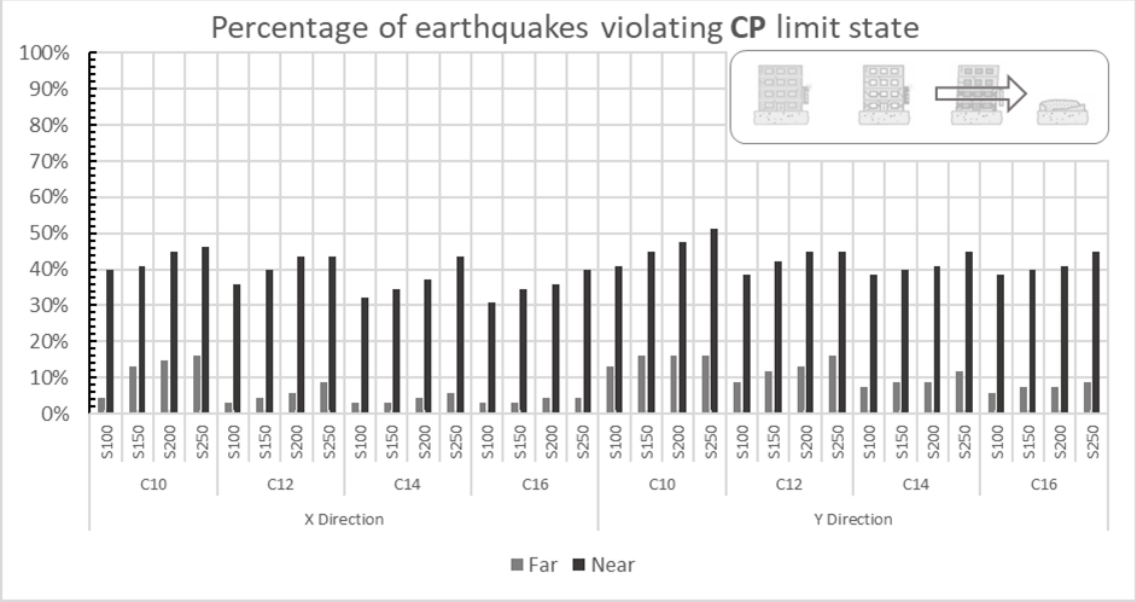

Figure 161: Percentage of earthquakes violating CP limit state for D Template Building

As conclusion, a general presentation of all performances for different limit states, using near fiend and far fault records for A, B, C and D Template designs are prepared as shown in **Figure 162**. Each of the buildings are grouped together for IO, LS and CP performance levels. As shown in the figure, the immediate occupancy is heavily exceeded by both far and near fault earthquake records for all 1982 building designs. The target performance level in this study (LS) is risked by 28%-42% from far fault records. Whereas the percentage values from near fault earthquakes are alarming. For both faults, the most fragile building is C Template. This is clearly seen in the CP performance level exceedance by far fault earthquakes which has a great jump compared to other templates. Exceeding CP point means that structure is towards the global failure. The percentage of near fault earthquakes ranges from 30% to almost 50%. This means that around 40 earthquakes (from the list of 78 records of near fault) can be destructive for these template buildings.

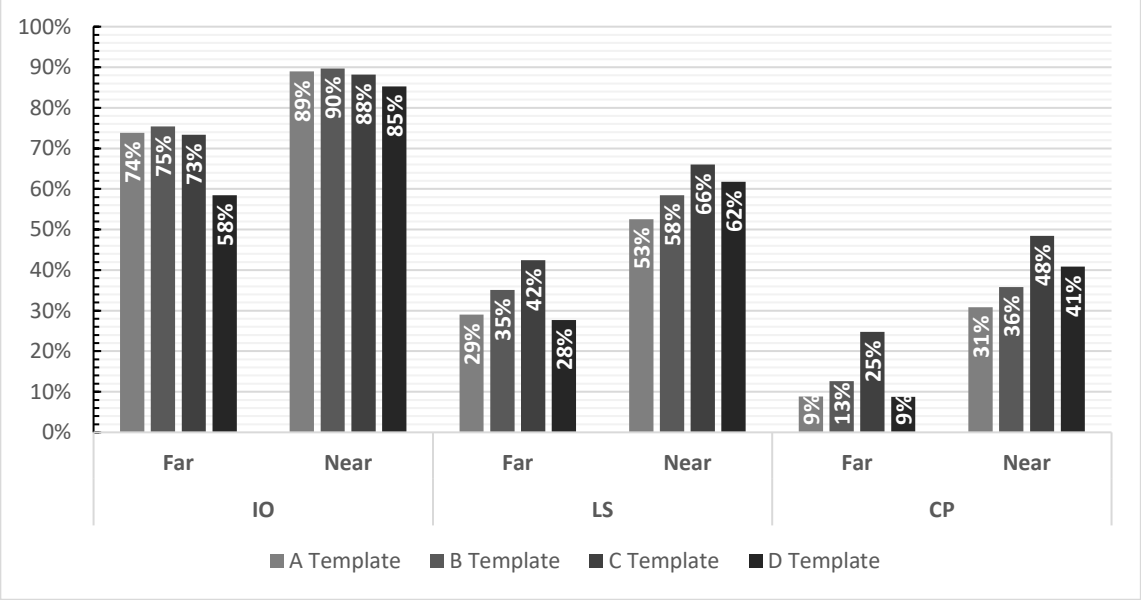

Figure 162: Percentage of earthquakes violating each of the limit states for A, B, C and D buildings

Finally, 18 688 analyses are performed in the environments of NONLIN V8 software using the SDOF models for concrete classes C10, C12, C14 and C16, stirrups spacings S100, S150, S200 and S250 mm and a set of 68 far-fault and 78 near-fault records for A, B, C and D Template designs. All analyses are aggregated and provided in different forms to better understand the global performance of the residential buildings constructed during communism period and still being used nowadays. Ultimately, results from 18 688 analyses are elaborated and presented in one single graph as shown in **Figure 162**. The poor performance of each of the templates is confirmed again by nonlinear dynamic time history analyses.

7.5 Evaluation of template designs by means of Incremental Dynamic Analyses

Incremental Dynamic Analysis (IDA) is an evolving analysis method that offers comprehensive seismic demand and capacity prediction capability by using a series of nonlinear dynamic analyses. The procedure can be executed by using a set of records and an appropriate tool capable of running this analysis. To achieve this scope, the mathematical model for all template designs is prepared in ZeusNL platform, under a set of 18 ground motion records as given in **Table 11** of section 5.2. The procedure of analysis is explained in detail in section 6.1.3.

The IDA analysis is very time-consuming procedure which takes several hours to execute even for a simple moment frame, midrise building. Therefore, the combinations considered are done for concrete type C16 and C10 using the average stirrups spacing of 100mm.

In the end, thousands of analysis results are gathered and aggregated for the interpretation of results based on previous researchers (Vamvatsikos, 2002; Vamvatsikos and Cornell, 2002; Vamvatsikos, 2002; Fragiadakis and Vamvatsikos, 2011).

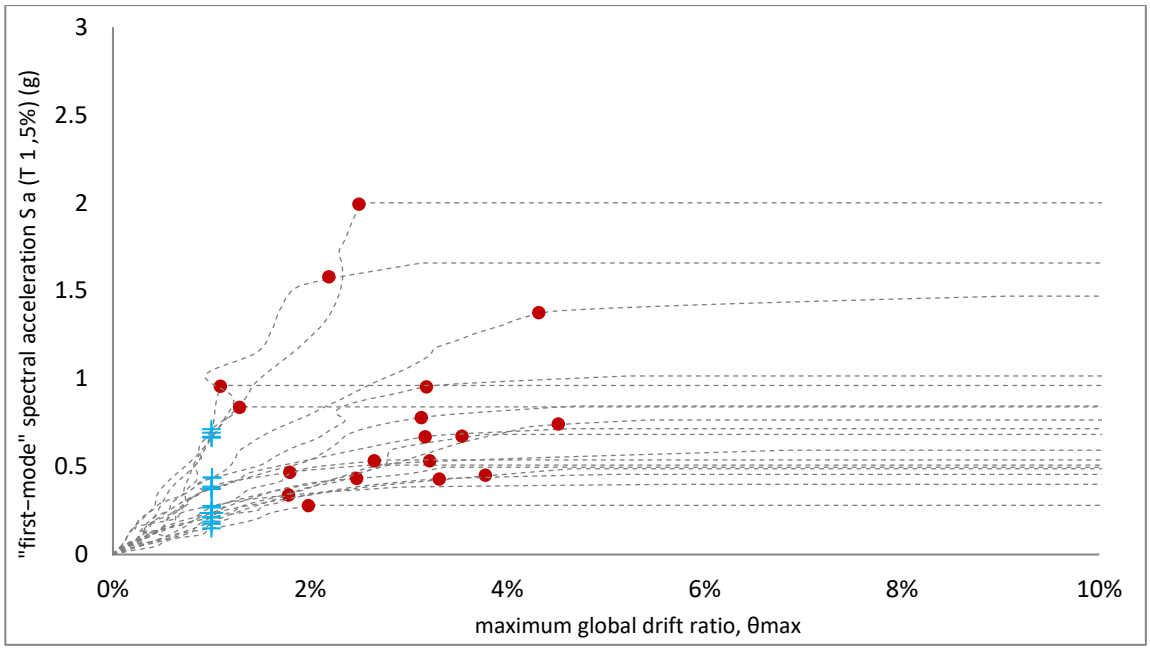

Figure 163: An example of 18 IDA curves together with IO and CP limit states

As suggested by different researchers, IDA outcomes can be demonstrated in different ways. The first presentation will be using simple IDA curves in the same graph with immediate occupancy (IO), collapse prevention (CP) and global instability (GI) limit states. An example is shown in **Figure 163**. The IDA curves are plotted as "first−mode spectral acceleration $Sa_{(T1,5\%)}$ (g)" in y-axis and "maximum global drift ratio, θ_{max}" in x-axis. The immediate occupancy is shown with "+" sign and collapse prevention with "●" sign for each of the IDA curves. The global instability or global failure is shown by the constant line in the end of IDA curve, also known as "IDA flatline". Based on this graph, the demand from each of the earthquake records can be seen clearly. Furthermore, the IM or DM values of collapse prevention and global instability can be easily read from the y- and x-axis respectively. Nevertheless, the interpretation of IDAs in this way is not with great efficiency due to several different curves. For this reason, 18 IDA curves are summarized into 16%, 50% and 84% fractiles as shown in **Figure 164** based on the work of previous researchers (Vamvatsikos and Cornell, 2002; Vamvatsikos, 2002).

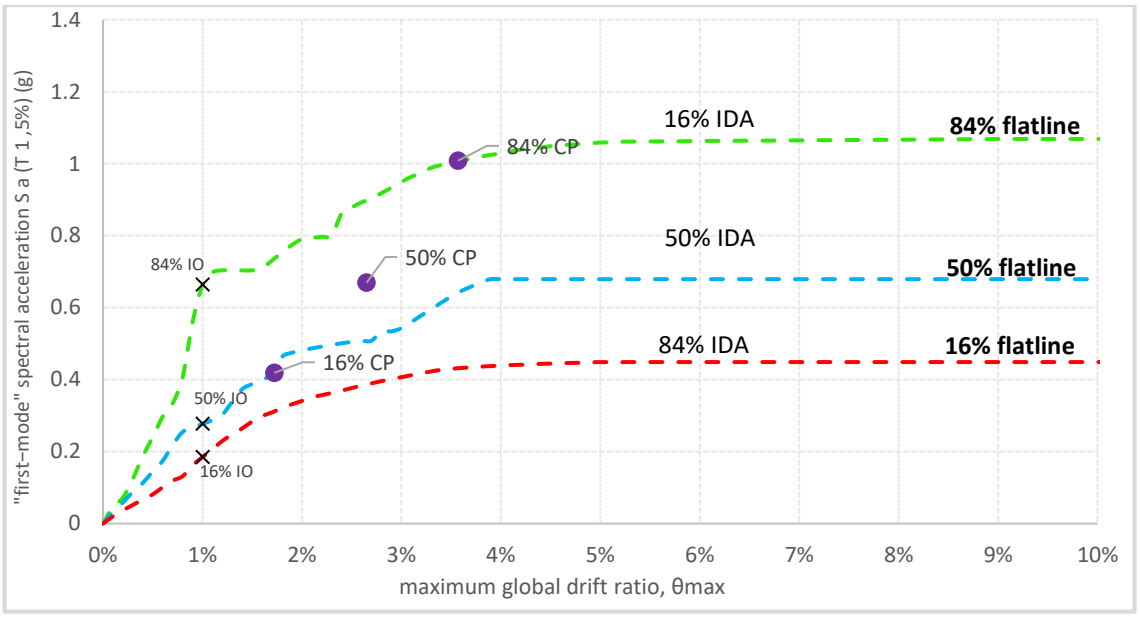

Figure 164: An example of 16%, 50% and 84% IDA fractiles together with IO and CP limit states

Together with IDA fractiles, the 16%, 50% and 84% limit states are plotted in the same graph for IO, CP and GI. Furthermore, IO and GI plotted as 16%, 50% and 84% match with 84%, 50% and 16% of IDA fractiles. However, the collapse presentation usually is located near the fractiles but there is no exact definition of it exactly in curve as reported by previous researchers (Vamvatsikos and Cornell, 2002).

Benefiting from IDA percentiles (fractiles), it can be interpreted that for a given $Sa_{(T1,5\%)}$ = 0.2g, 16% of the records produce $\theta_{max} \leq 0.4\%$, 50% of records $\theta_{max} \leq 0.6\%$ and 84% $\theta_{max} \leq 1\%$. On the other hand, the fractiles can be interpreted inversely such that for example, in order to generate θ_{max} = 2%, 84% of the records need to be scaled to $Sa_{(T1,5\%)} \geq 0.35$g, 50% of the records to $Sa_{(T1,5\%)} \geq 0.48$g and 16% of the records to $Sa_{(T1,5\%)} \geq 0.8$g.

In terms of limit states, the global performance of buildings can be easily taken into account. As shown in **Table 18**, each of the performance values are provided for 16%, 50% and 84% IDA fractiles.

Table 18: An example of IM and DM values for each of the fractiles of IO, CP and GI

	$Sa_{(T1,5\%)}$ (g)			Θ_{max} (%)		
	IM 16%	**IM 50%**	**IM 84%**	**DM 16%**	**DM 50%**	**DM 84%**
IO	0.19	0.28	0.66	1.0%	1.0%	1.0%
CP	0.42	0.67	1.01	1.7%	2.7%	3.6%
GI	0.45	0.68	1.06	$+\infty$	$+\infty$	$+\infty$

For instance, readding of table above, at $Sa_{(T1,5\%)}$ = 0.67g or alternatively θ_{max} = 2.7%, 50% of the earthquake records have force the building to exceed Collapse Prevention. Moreover, the interpretation can be extended for the global instability such as 16% of the records cause global failure of the structure when $Sa_{(T1,5\%)}$ = 0.45g, 50% of the records at $Sa_{(T1,5\%)}$ = 0.68g and 84% at $Sa_{(T1,5\%)}$ = 1.06g.

The same interpretation can be repeated for each of the structures, based on research interest. The complete list of graphs and tables prepared from Incremental Dynamic Analysis, are provided in **Appendix C**. The data for each of the models performed with incremental dynamic analysis is summarized in one graph for CP limit state as given in **Figure 165**. This graph demonstrates the exceedance of collapse prevention for different buildings modelled with concrete C16 and C10 according to 16%, 50% and 84% limit states. As shown, graph is prepared in a way to conduct a comparison between buildings and concrete strength effect for different percentiles. On the y-axis it is plotted the spectral acceleration (g) for each of the cases. The bars corresponding to C10 concrete are labeled with the value of spectral acceleration (g) dropped compared to C16 concrete. As shown from the graph, 16% of the records exceed collapse prevention when $Sa_{(T1,5\%)}$ = 0.42g, 0.41g, 0.35g, 0.05g and 0.36g for A, B, C, D and E Templates respectively when modelled with C16 concrete. Similarly, there are 50% of the records exceeding collapse prevention at $Sa_{(T1,5\%)}$ = 0.68g, 0.61g, 0.55g, 0.18g and 0.65g for A to E templates respectively of C16 concrete.

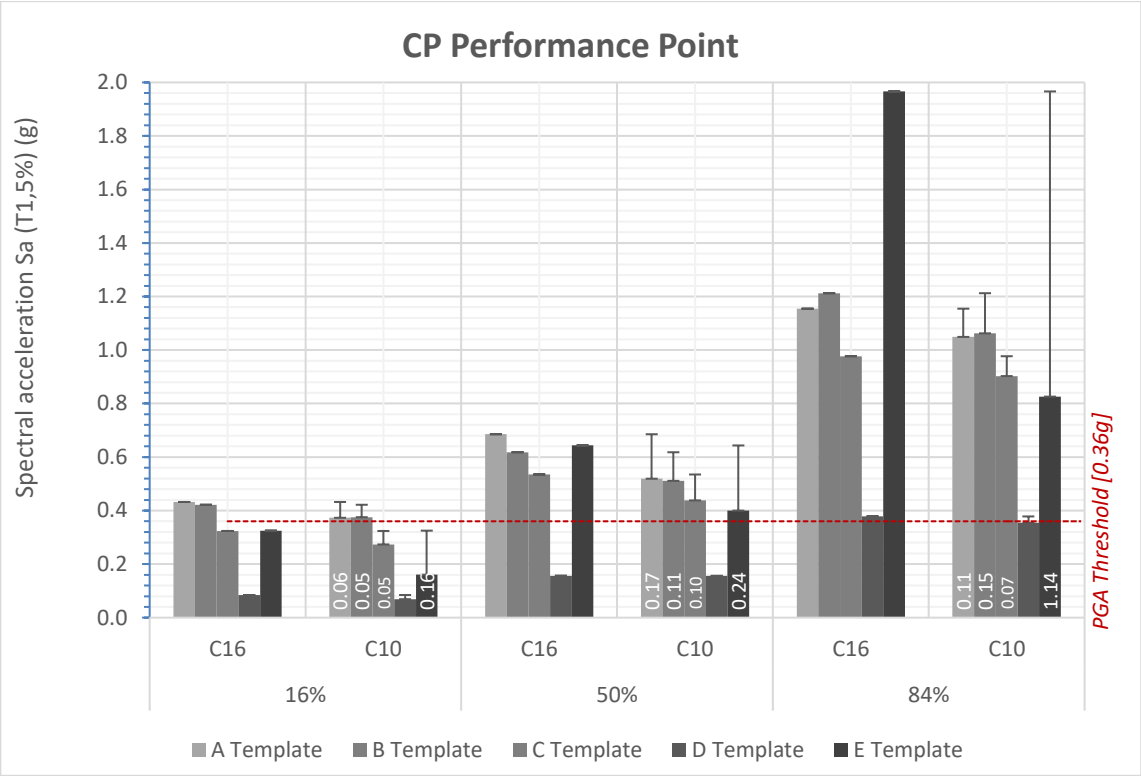

Figure 165: Percentage of records exceeding ***CP*** for different concrete classes of A, B, C, D and E Template buildings

Furthermore, from the graph can be indicated an increase in spectral acceleration from 16% to 50% and from 50% to 84% percentiles. In percentage, these values increase about 60% and 100% respectively.

Additionally, the effect of the concrete class can be observed directly from the error bars given in the chart among C16 and C10 concrete. For instance, in the 16% percentile category, the decreased values of spectral acceleration range about 0.05g to 0.16g. For 50% percentiles the difference is more remarkable. The decreased values from C16 to C10 range between 0.10-0.24g, about 20% drop. This means that building modelled with C10 concrete will exceed collapse prevention when records are scaled 20% less than in C16 concrete. The influence of concrete strength is surprising especially for the E Template building (designed in 2005). As seen from the graph, the values drop drastically from one

concrete to another one. Consequently, the earthquakes force E Template building modelled with C10 to exceed collapse prevention earlier than when modelled with C16. In terms of spectral acceleration, the drop from C16 to C10 for 16% of records is 0.16g, for 50% is 0.24g, and for 84% is 1.14g.

On the other hand, the large values of Sa shown in graph for E Template building compared with others may be due to the bigger cross-section of column and beams.

Reinforced concrete residential buildings shall be designed to satisfy the collapse prevention limit state for a return period of 475 years. According to the probabilistic seismic hazard map for our country (**Figure 10** in section 2.3.2) the horizontal PGA values for Albanian territory usually are in the boundaries of 0.3-0.4g (Bilgin et. al., 2022). To compare the number of buildings failing to provide the CP performance level, the PGA value is considered as a threshold of 0.36g based on the regions where most of considered buildings are found.

As shown in **Figure 165**, 16% of the earthquakes prevent C, D and E Template buildings from satisfying the collapse prevention performance level whereas the A and B Template buildings are on the verge of exceeding this level too. Additionally, 50% of the records force D Template and is very near to fail E Template modelled with C10. The poor performance of D Template building remains constant even for 84% of the records. This means that out of 18 earthquakes considered for IDA, more than 15 of them exceed collapse prevention.

7.5.1 Comparing SPO curves with IDA median

Similar to static pushover analysis (SPO), IDA is designed as a procedure to force the structure all the way from elastic region to global collapse. Researchers have reported a good correlation between SPO and IDA curves (Vamvatsikos, 2002). For comparison reasons, the SPO curve is plotted together with 50% fractile, also known as IDA median. Since nonlinear static analysis results are gathered as base shear and roof displacements,

they need to be transformed in IM ($Sa_{(T1,5\%)}$) and DM (θ_{max}) to match the axis of IDA graph. The θ_{max} can be easily calculated by dividing the roof displacement values by the height of the building. Whereas base shear can be converted to acceleration by dividing with the building mass and some other coefficients defined to match the elastic region of both SPO and IDA curves. After the calculations are performed, the IDA median is plotted together with four SPO curves generated previously for each stirrup spacings. As shown in **Figure 166**, the elastic region of IDA median and SPO curves is calibrated with the help of equally displacement line. A strong relationship is observed between the static and dynamic pushover curves. The negative slope of pushover curves is translated by the softening region of IDA median towards the flatline. Essentially, the end of SPO curve indicates the end of IDA softening region to become flatline.

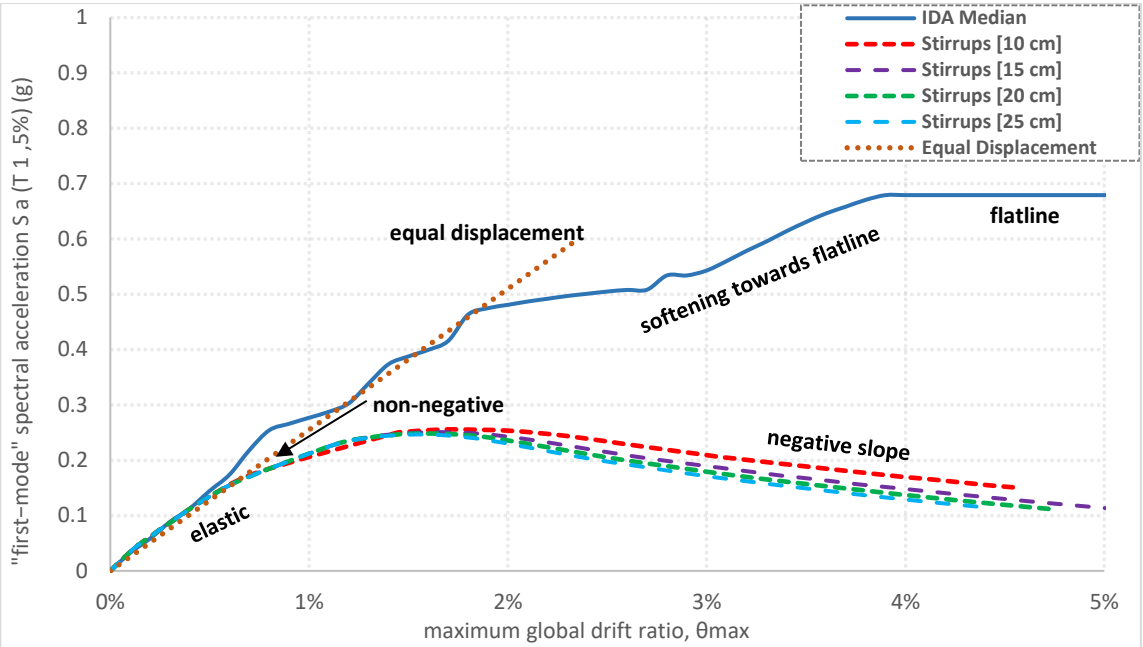

Figure 166: IDA median versus SPO curves for different concrete spacings of A Template building with concrete C16 in X-direction

Very good correlations are observed in all other SPO curves and IDA medians representing different concrete classes of five template buildings in x- and y-direction. The complete list of graphs is given in Appendix C.

CHAPTER 8

RESULTS, CONCLUSION AND RECCOMENDATIONS FOR FURTHER STUDIES

8.1 General

This study covers the performance assessment of five residential reinforced concrete (RC) buildings in Albania. Each of the buildings is intended as a template design. In Albania, template designs developed by the governmental authorities are used for many of the buildings planned both for residential and public services as a common practice to save architectural fees and ensure quality control during communist era, till 1990s (Leti and Bilgin, 2022). For easier interpretations, each of the templates is labeled as given in section 5.1 (A, B, C, D and E Template). Template buildings A-D fall in the category of old constructions, designed in 1982 during the communism period in our country. E Template is selected among the recent designs (2005) which was built in Durrës.

The timeline of Albanian design code starts with KTP-63 developed in 1963, continues with KTP-78 in 1978 and ends with KTP-N2-89 in 1989. The last version of seismic guideline (KTP-N2-89) is still in force nowadays. As can be understand, A-D Templates were prepared based on KTP-78 standard which was mostly founded on KTP-63 and lacks the consideration of seismic design calculations (Baballëku and Myftaraga, 2020). Therefore, the performance assessment of the selected buildings is with great importance and gives a valuable contribution on old RC constructions in Albania.

The selection of building typologies was determined based on the site investigations done after November 26, 2019 earthquake (Mw = 6.4 – Righter). From the site inspections in

the affected cities such as Durrës, Vorë, Tiranë, Thumanë etc., it was reported by the reconnaissance team that 1982 template designs were the most risked among other reinforced constructions categories in our region (Leti and Bilgin, 2022). Furthermore, the main problem of these building typologies were the poor material quality and inadequate detailing of transverse reinforcement. Among many structures destroyed after the main shock of earthquake, also one case of B Template collapsed. Furthermore, heavily damages were observed and reported from the E Template in the main structural elements.

From the ruins of the destroyed building (B Template), there were taken samples of concrete and steel to check the material quality. The laboratory tests show a very poor performance of concrete. Results of low quality of concrete were also observed from the visual inspection in other old and damaged buildings during November 26, 2019 Earthquake. Further deficiencies were noted from the detailing of shear reinforcement of the many damaged buildings. Hence the performance assessment of typically old, reinforced concrete template buildings in our country has a great importance.

The target of this study aims to assess the seismic performance of the reinforced concrete residential buildings built per premodern seismic code requirements in Albania considering the inelastic response of RC components. The performance of the selected buildings is conducted based on nonlinear procedures. In the first one, static pushover analysis is utilized to get the capacity curve of each of the models, using the inverted triangular load pattern. The seismic evaluation is done using capacity spectrum method based on EuroCode8 and KTP-N2-89 guidelines. Furthermore, nonlinear dynamic analysis (Time History) is performed using a set of 68 far-field and 78 near-field ground motion records. The performance evaluation based on Time History analysis is done for Template buildings designed in 1982. Furthermore, the influence of far- and near-field records is investigated. Lastly, Incremental Dynamic Analysis (IDA), also known as nonlinear dynamic pushover (DPO) analysis, is executed for each building template considered in this study. IDA interpretations are done considering the PGA value of most affected regions in Albania. The results from the analyses are presented in several ways

to better understand and interpret the structural performance according to the target of this study. The final conclusions are given in addition.

8.2 Conclusions

This section summarizes the final comments reached in the end of a long study process, site investigations, laboratory tests, computer simulations and analysis, interpretations of results etc. The conclusions are structured into four main categories based on:

- The damages of November 26, 2019 earthquake
- Performance assessment using Capacity Spectrum
- Performance assessment using Time History analysis
- Performance assessment using IDA

8.2.1 Conclusions based on the damages of November 26, 2019 earthquake

The scope and motivation of this study is highly influenced from the occurrences of November 26, 2019 earthquake with epicenter in Durrës. The selection of the case study buildings is done based on the observations of the heavy consequences of reinforced concrete building stock in our country. Therefore, during the site investigations with our reconnaissance team, the following conclusions are outlined:

1. The proximity of the major fault to the city of Tirana and Durrës triggered serious damage or partial collapse of some buildings, resulting in massive damage to both old and newly designed RC buildings and in loss of lives.

2. Most of the investigated buildings suffered from weak concrete strength, material aging, inappropriate reinforced detailing, poor workmanship, corrosion of steel bars, in-plane and out-plane failures.

3. Building stiffness and strength were found to be insufficient generally during the examination. This has caused excessive displacement demands and heavy infill wall damage in RC buildings.

4. In most of the cases it is reported that the stirrups spacings are spread every 250 mm or even more.

5. One template design building (B Template) was collapsed. From the laboratory results the compressive strength of concrete confirmed to be very low, less than 8 MPa.

6. Due to the lack of enough expansion joint and stiffness weaknesses hammering effect mechanisms were observed in the damaged buildings.

7. In addition, poor quality of the concrete used in construction, resulted in buckling of longitudinal reinforcements in columns and expansion of shear links due to extensive pressure applied as concrete was unable to be confined during the earthquake.

8. Aging of concrete and corrosion of steel bars besides the poor workmanship, has been constantly a factor of failure, observed in the damaged buildings.

9. Openings between columns above the walls caused formation of short columns which caused heavy shear damage in the RC vertical members.

10. Serious element failures were observed also from the in-plane and out-plane walls of the investigated buildings.

11. It is easily witnessed the rapid growing urbanization after 1990s. As a consequence of this, a rapid population growth and the acceleration of the migration from the rural areas to city triggered a rise in the need for housing in urban areas. Unfortunately, many RC buildings designed and constructed to meet this need during this period did not satisfy the requirements of modern seismic codes.

12. These observations have revealed that the main reasons causing heavy damage and collapse of the RC and masonry buildings are the lack of implementation of seismic code requirements and supervision of construction stages of these buildings.

Summary: *the most affected RC buildings during November 26, 2019 earthquake were the old template designs constructed during the communism period whereas the main failure reasons observed were the poor concrete quality and inadequate detailing of transverse reinforcement. According to the blueprint of template buildings, the concrete quality corresponds to C16/20 (M200) whereas the tests confirm a much lower compression strength of 6.32 and 8.06 MPa respectively for two samples taken. On the other hand, the average stirrups spacings determined in the blueprint is 100mm whereas from site investigations resulted to be more than 250mm.*

Therefore: *the influence of material quality and transverse reinforcement is conducted in this study by considering various types of concrete (C16, C14, C12 and C10) and stirrups spacings (S100, S150, S200 and S250 mm).*

8.2.2 Conclusions based on the performance assessment using Capacity Spectrum

The first method to assess the performance of the selected buildings is done through capacity spectrum. The calculation of the demand values is conducted using guidelines of ATC-40 and response spectra based on EC8 and KTP-N2-89. Moreover, the capacity curves are performed using nonlinear static analysis (Pushover-SPO) in the environment of Zeus-NL software. The application of lateral force is done using the inverted triangular load pattern. In addition, the following conclusions are outlined:

1. A large number of capacity curves (320) are generated for five template buildings modelled with different material quality and stirrups spacings in both orthogonal directions.

2. The determination of performance levels (IO, LS and CP) is done following the modern guidelines, regulations and research studies (FEMA-356, 2000; Eurocode8, 2004; Fajfar and Gašperšič, 1996).

3. From the capacity curves is clearly seen that the y-direction is more ductile than the x- whereas the lateral load bearing capacity in x-direction is slightly higher than in other direction.

4. Considering the characteristics of the structures examined, it is noteworthy that the long dimensions of all or most of the columns are in the short direction of the building. This situation was encountered not only in the template projects in this study, but also in many other residential structures examined by Epoka University civil engineering team (Bilgin et. al., 2021). As a result of the analysis, it was determined that this application was quite wrong. The short side of the columns works under the horizontal loads on the long sides of the buildings constructed in this way. Columns with low moment capacity in one direction are hinged before the beams, resulting in a weak column-strong beam mechanism. For this reason, the ductility values of the structures in the long direction are low. In addition, in most of the projects carried out at that time, these directions were not screened, with the misconception that the longer direction would have better capacity.

5. When the analysis results of the residential buildings modelled according to different material properties are examined; It has been observed that the difference in displacement capacities between 10 and 14 MPa concrete class decreases further compared to the ones between 14 and 16 MPa. This means that the transverse reinforcement spacing becomes more important, especially in residential buildings with concrete strength below 14 MPa.

6. The lateral load bearing capacity of D Template building is remarkably lower (around 50%) when compared with other designs.

7. Evaluation of the capacity curves for the examined buildings shows that the adequate shear detailing and concrete quality have significant effects on the deformation and lateral load carrying capacities of the buildings in both orthogonal directions.

8. There is observed a drop of lateral load bearing capacity values by more than 30% from the most favorable combination (C16-S100) to the lowest one (C10-S250).

9. According to demand calculations, A, B and C Templates failed to satisfy the LS performance level in their x-direction whereas D Template in y-direction.

10. The demand values calculated from EC-8 in comparison with KTP-N2-89 are higher in each of the buildings.

11. The influence of stirrups spacings seems considerably higher than the impact of concrete quality for most of the buildings.

12. Concrete class and stirrup spacing have remarkable effects on the displacement capacity in cases where the columns bear most of the seismic loads. The decrease in the concrete compressive strength or the decrease in the amount of stirrups can reduce the displacement capacity by up to half. In structures with low concrete strength and wide stirrup spacing, shear fractures may occur as a result of the brittle behavior of the columns. When the damage caused by the earthquakes in the last 20 years in public buildings is examined, it can be said that this problem is quite common.

13. With the increase in material quality, the performance of the structures increases. When the displacement capacities for different performance levels are compared, concrete class and stirrup spacing do not have a significant effect on IO, while this effect becomes evident at LS and CP levels. It has been observed that although the amount of lateral reinforcement does not have a decisive effect on the strength of the building, it significantly affects the displacement capacity if there are not

enough brittle elements to collapse before the yield strength is reached in the structure.

Summary: *Template designed buildings generally have uniform distribution of stiffness and mass in both vertical and horizontal planes due to similar architectural properties and purpose of use in all floors. One of the potential major shortcomings of these typologies per pre-modern Albanian Code is the strong beam-weak column response due to the lack of attention.*

Therefore: *Since there are no shear walls in their lateral load bearing systems, formation of plastic hinges in columns may remarkably affect overall response, causing loss of lateral stiffness in a single floor. This deficiency seems to be a critical weakness among these typologies.*

8.2.3 Conclusions based on the performance assessment using Time History analysis

The seismic performance assessment of 1982 design template buildings are done using Time History analyses. The nonlinear dynamic characteristics were represented by ESDOF systems in NONLIN V.8 software, and their seismic demands were calculated under selected ground motions. A total of 48 far-fault and 78 near-fault ground motions are used to comparatively investigate the effect of distant and near-fault earthquakes on the seismic behavior of the selected template designs. In addition, the following conclusions are outlined:

1. About 20,000 Time History analysis are generated using NONLIN software whereas the results are compared with capacity curves to check the exceedance ratio of old template buildings.

2. The percentage of exceeding IO is about 73% and 90% for far- and near-field respectively, whereas for LS the percentages are about 35% for far field and 60% for near field records.

3. The exceedance ratio in CP performance level is not required for the residential buildings but it give good indications for preventing the casualties and loos of lives. The exceedance percentage in this category ranges about 10-25% and 30-50% for far and near field records respectively.

4. The near-fault ground motions produce higher displacement demands compared to far-fault ones for all buildings. This explains the damage potential of near-fault records due to the various relative or absolute energy potential.

5. The highest exceedance ratios for LS performance level, are seen for the C Template design.

6. The influence of transverse reinforcement is playing an important role in the global performance of all limit states according to this procedure. The amount of demand when comparing C16-S100 with C10-S250 is dropped about 25%, whereas for the concrete quality, is about 10%.

Summary: *Such template designs reflecting the current building stock of Albania and many other developing countries have low lateral strength for an earthquake-prone area. This is due to poor quality materials, poor construction practices, and the low requirements of premodern seismic codes that were used when most buildings were built. Due to this low strength and rigidity, high displacement demands are required for buildings to dissipate seismic energy. Moreover, the reasons that cause low strength of buildings also cause them not to be ductile.*

Therefore: *it is unreasonable to expect acceptable earthquake performance from such building stocks.*

8.2.4 Conclusions based on the performance assessment using IDA

Incremental Dynamic Analysis (IDA) used as a new and promising analysis to evaluate the performance of five residential template buildings constructed with old seismic codes

using a set of 18 ground motion records. IDA is performed in Zeus-NL platform, developed especially for earthquake engineering applications. The results are presented in simple IDA curves, summarized into fractiles (percentiles), and lastly compared with Static Pushover Analysis (SPO). In addition, the following conclusions are outlined:

1. The graphical presentation of IDA curves gives certainly compelling information on the global performance of the buildings based on any intensity scale of the earthquake records from the linear region till the global instability.

2. Global performance is interpreted according to the limit states defined based on various studies and guidelines as IO, CP and GI.

3. It is indicated an average increase of the spectral acceleration values of 60% from 16% to 50% percentiles and 100% from 50% to 84% percentiles for all buildings.

4. The influence of concrete quality investigated with IDA is notable. From 16% of the records, the S_a values drop about 0.06g and from 50% of the records ~0.15g when considering C16-C10. The influence of the concrete for 84% of records faces similar trends as 50% percentiles except the E Template building which shows remarkable effect of concrete quality and about 1.14g drop of S_a value.

5. Reinforced concrete residential buildings shall be designed to satisfy the collapse prevention limit state for a return period of 475 years. According to the probabilistic seismic hazard map of Albania for this return period, it is observed that the PGA value in the most affected regions is about 0.36g. To compare the number of buildings failing to provide the CP performance level, this PGA is considered as a threshold value. In addition, all percentiles show that D Template Building does not satisfy the threshold value.

6. The threshold of PGA = 0.36g shows that 16% of the records force almost all buildings to exceed the collapse prevention performance level for both C16 and C10 models.

7. Lastly, 50% IDA fractile (IDA median) is compared with capacity curves for each of the template buildings. A strong relationship is investigated between IDA median and static pushover curves. The elastic region matches from both analyses based on the equally displacement segment. Furthermore, the negative slope of the static pushover curve corresponds to the softening region of the IDA median. Finally, as the SPO curve diminishes, the IDA median ends with a horizontal, constant fractiles, both indicating the total collapse of the building.

Summary: *Low performance of all template buildings are confirmed from Incremental Dynamic Analysis too. Each of the buildings failed to satisfy the collapse prevention limit state for an IM value of 0.36g. Considering that our country is part of an active earthquake zone, the heavy damages, especially from the buildings not fully designed in compliance with actual/modern seismic codes which encountered during the November 26, 2019 earthquake, but also in the past, are not to be surprised.*

Therefore: *According to analyses results, it can be noted that decision makers should be aware of the catastrophic nature of such brittle systems when weighing options for earthquake mitigation since such template designs of the current building stock were built before the legislation of new guidelines.*

8.3 Recommendations for future research

Some recommendations for future research further to this study which may contribute to the structural engineering field of Albania as listed as follows:

- As highlighted from the conclusions of this study, the main deficiencies with old residential RC buildings designed with premodern codes are the lateral load bearing capacity and stiffness. Thus, a retrofitting methodology using shear walls can be presented as an acceptable solution for the current condition of this building stock in Albania. Shear walls increase the lateral load strength of buildings and reduce earthquake demands. These defects can be avoided to some extent by the use of shear

walls in residential buildings whose load-bearing system consists of frames. The use of shear walls in residential buildings built in our country and similar countries, where poor quality workmanship is a common problem, could be an insurance against earthquakes.

- The conclusions of this study were limited to a small number of building configurations (five) and specific typologies. Further important factors should also be studied to enrich the findings.
- The performance assessment of masonry building stock in comparison with reinforced concrete buildings can generate interesting yet beneficial results for decision makers and other interested parties.

REFERENCES

Aliaj Sh., "Harta e carjeve sizmo-tektonike të Shqipërisë në shkallë 1:200.000" IGJEUM, Tirana (2000)

Aliaj Sh., "Seismic source zones in Albania", Paper presented in Albanian Seminar, Paris June 26-28, 2003 and published in Final Report, NATO Science for Peace Programme, Project "Seismotectonics and Seismic Hazard Assessment in Albania (2003)

Aliaj Sh., "Tipare to struktures neotektonike to Shqiperise: Studime Gjeografike", v. 3, p. 37-53 (1988)

Aliaj Sh., Koçiu S., Muco B., Sulstarova E., "SEISMICITY, SEISMOTECTONICS AND SEISMIC HAZARD ASSESSMENT IN ALBANIA", Akademia e shkencave e Shqiperise, Tiranë, 2010

"ATC-40, “Seismic Evaluation and Retrofit of Concrete Buildings”, Vol. 1 & 2, Applied Technology Council, CA 94065, (1996)"

Baballëku M., Myftaraga E., "A short history of seismic design codes in Albania," in INTERNATIONAL CONFERENCE GEOSCIENCES AND EARTHQUAKE ENGINEERING, CHALLENGES FOR BALKAN REGION ICGEE – 2020, Tirana, 2020.

Bilgin H, Shkodrani N, Hysenlliu M, Ozmen H.B, Işık E and Harirchain E., "Damage and performance evaluation of masonry buildings constructed in 1970s during the 2019 Albania earthquakes," Engineering Failure Analysis, vol. 131, Jannuary (2022).

Bilgin H, Shkodrani N, Hysenlliu M, Ozmen HB, Işık E, Harirchain E., "Damage and performance evaluation of masonry buildings constructed in 1970s during the 2019 Albania earthquakes. Engineering Failure Analysis, 2022; 131: 105824. https://doi.org/10.1016/j.engfailanal.2021.105824".

Bilgin H., Leti M., Hysenlliu M., Bidaj A., "The adriatic, albania earthquake of november 26, 2019 technical report", Tirana, (2021)

Bilgin H., Hysenlliu M., "Comparison of near and far-fault ground motion effects on low," Journal of Building Engineering, no. 30: 101248, 2020.

Bilgin H., Kamu yapilarinin deprem performanslarinin doğrusal ötesi analiz yöntemleriyle değerlendirilmesi ve çözüm önerileri, Denizli: Pamukale University (2007)

Bilgin H., Shkodrani N., Hysenlliu M., Baytan O H., Isik E., Harirchian E., "Damage and performance evaluation of masonry buildings constructed in 1970s during the 2019 Albania earthquakes," Engineering Failure Analysis, vol. 131 (2022).

"C.E.N. Eurocode 8: Design of structures for earthquake resistance – Part 1: General Rules, seismic actions and rules for buildings" Brussels, Belgium (2004)"

C.E.N. Eurocode 8: Design of structures for earthquake resistance – Part 1: General Rules, seismic actions and rules for buildings" Brussels, Belgium, (2004)

Charney F., Barngrover B., NONLIN: Software for earthquake engineering education. 1-12. 10.1061/40700(2004)177 (2004)

Charney F., Talwalkar R., Bowland A., Barngrover B., "Nonlin-eqt: A computer program for earthquake engineering education", Toronto, Ontario, Canada (2010)

Constantinos C.R., 'Seismic Performance Evaluation of Existing RC Buildings Without Seismic Details. Comparison of Nonlinear Static Methods and IDA', The Open Construction and Building Technology Journal, 158-179 (2016).

Cornell C. A., "Engineering seismic risk analysis", Bulletin of the Seismological Society of America 58 (5): 1583–1606, (1968)

Costa G., Panza G. F., Suhadolc P., Vaccari F., Zonning of Italian territory in terms of expected peak ground acceleration derived from complete synthetic seismograms: J. Appl.

Geophysics, v. In: R.Cassinis, K.Helbig and G.F. Panza (eds.), Geophysical Explotarion in Areas of Complex Geology, p. 149-160 (1993)

Dibra, Z., "Disa dukuri tè lèngézimit tè truallit nga termeti i 15 prillit 1979", Termeti i 15 prillit 1979, p. 404-414 (1983)

Elnashai A.S., Papanikolaou V., Lee D.H., 'ZEUS-NL User Manual, Mid-Amerika Earthquake Center, University of Illinois at Urbana-Champaign (2002).

Erberik M.A., Elnashai AS. 'Fragility analysis of flat-slab structures', Eng Struct, 26(7), 937–48 (2004)

Fajfar P., Eeri M., "A nonlinear analysis method for performance based design", Earthquake Spectra, Vol. 16, No.3, August (2000)

Fajfar, P., & Gašperšič, P., The N2 method for the seismic damage analysis of RC buildings. Earthquake Engineering & Structural Dynamics,25(1), 31-46 (1996)

Fardis M. N., "Seismic Design, Assesment and Retrofitting of Concrete Buildings", London, U.K: Springer, 2009.

FEMA (2000a), 'Recommended seismic design criteria for new steel moment-frame buildings', Washington, DC.: Federal Emergency Management Agency, (2000)

FEMA-273, NEHRP., Guidelines for the Seismic Rehabilitation of Buildings, Building Seismic Safety Council (Guidelines) and Report 274 (Commentary), Washington, D.C. (1997)

FEMA-356, "Prestandard and commentary for the seismic rehabilitation of buildings," Washington, 2000.

FEMA-750, NEHRP Recommended seismic provisions for new buildings and other structures, Washington, DC: Federal Emergency Management Agency, 2009.

Florsch, N., Fah D., Suhadolc P., G.F., "Complete synthetic seismograms for high-frequency multimode Love waves", Pageoph, v. 136, p. 529-560 (1991)

Fragiadakis M., Vamvatsikos D., 'Qualitative Comparison of Static Pushover Versus Incremental Dynamic Analysis Capacity Curves', Proceedings of the 7th Hellenic National Conference on Steel Structures. Volos, Greece (2011).

Frangu I., Seismic Performance Evaluation of a RC Public Building: A Case Study From Albanian Practice, Tirana: Epoka University (2013).

Freddi F., Novelli V. R., Gentile R., Veliu E., Andreev S., Andonov A., Greco F., Zhuleku E., "Observations from the 26th November 2019 Albania earthquake: the earthquake.," Bulletin of Earthquake, no. 19, pp. 2013-2044, 2021.

HAZUS, "Earthquake loss estimation methodology technical manual," National Institute of Building Sciences for FEMA (1999).

Hueste M.D., Bai J.W., 'Seismic retrofit of reinforced concrete flat-slab structures', Eng Struct., 29(6):1165–77 (2007).

Inel M. Bretz E., Black E., Aschheim M., Abrams D., "USEE 2001 : Utility Software for Earthquake Engineering Report and User's Manual" , University of Illinois (2001)

Inel M., Bilgin H., Baytan O. H., "Orta Yükseklikli Betonarme Binaların Türkiye'de Yaşanan Son Depremlerdeki Performansı," İMO Teknik Dergi, pp. 4319-4331 (2008)

"INGV, "Characteristics of Adriatic sea earthquake 26.11.2019", National Intitute of Geo-physics and Vulcanology, Italy (2019)"

Italian Seismic Code, "Norme tecniche di edilizia asismica per i paesi colpiti da terremoti," Italy, 1937.

Jeong S.H., Elnashai A.S., 'Analytical assessment of an irregular RC frame', ASCE J Struct Eng., 9(1):95–128 (2005).

JICA, "The study on a disaster prevention/mitigation basic plan in Istanbul including seismic microzonation in the Republic of Turkey," Turkey (2000).

Kalkan E., Kunnath K. S., "Method of modal combinations for pushover analysis of buildings", 13th World Conference on Earthquake Engineering, p. Paper No. 2713, 1-6 August 2004.

Kalkan E., Kunnath S.K., "Effective cyclic energy as a measure of seismic demand" Journal of Earthquake Engineering, Vol.11 No.5, 2007

Karnik V., Seismicity of European Area, Part I: Prague (1969)

Kociaj S. Pitarka A., "Check up ofseismic hazard assessment: Tirana case study". Natural Hazard, Kluwer Acad. Publ. The Netherlands, 293-303 (1990)

Koçiu S. Kapllani L., "Methods for seismic hazard assessment of sites of archaeological ruins" Durres case study. Proceedings of 3-d workshop "Statistical methods in Seismology. Applications on protection and Forecasting of earthquakes" Thera, Greece, 18-20 September 1995

Koçiu S. Kapllani L., Methods for seismic hazard assessment of sites of archaeological ruins: Durres case study. Proceedings of 3-d workshop "Statistical methods in Seismology. Applications on protection and Forecasting of earthquakes" Thera, Greece, 18-20 September 1995 (1995)

Kociu S., Si të mbrohemi nga termetet. Akademia e Shkencave, Tirane (2000)

KTP-2-78, "Kushte Teknike të Projektimit," Ministria e Ndërtimit, Tirana, 1978.

KTP-52, "Kondita Tektonike për Llogaritjen e Strukturave të Ndërtesave," Ministria e Ndërtimit, Tirana, 1952.

KTP-63, "Konditat teknike te projektimit te ndertimeve ne beton-arme. Teorija e thyerjes.," Ministria e Ndërtimit, Tirana, 1963.

KTP-N.2-89, "Kusht Tektonik Projektimi per Ndertimet Antisizmike KTP-N.2-89," Akademia e Shkencave, Qendra Sizmologjike, Tirana, 1989.

Kuka N., "Seismic hazard assessment and site-dependent response spectra parameters of the current seismic design code in Albania," Research Gate, Tirana, 2004.

Lapajne J., Sket-Motnikar B., Zabukovec B., Zupancic P., "Spatially - smoothed seismicity modelling of seismic hazard in Slovenia", Journal of Seismology, v. Vol.l, P. 13 - 85 (1997)

Leti M, Bilgin H., "Damage potential of near and far-fault ground motions on seismic response of RC buildings designed according to old practices," Res. Eng. Struct. Mater., vol. 8, no. 2, pp. 337-357 (2022).

Leti M., Bilgin H., "Performance of RC and Masonry Structures During 2019 Durrës Earthquake," Civil Engineering Beyond Limits, vol. 2, no. 4 (2022).

Lundh F., "An introduction to tkinter," Www. Pythonware. Com/Library/Tkinter/Introduction/Index. (1999)

Madas P., Elnashai A. S., “A new passive confinement model for transient analysis of reinforced concrete structures.” Earthquake Engineering and Structural Dynamics21: 409-431 (1992)

Makropoulos, K.C., Burton, P.W., "Seismic Hazard in Greece: I Magnitude recurrence.," Tectonophysics, vol. 17, pp. 205-257, 1985.

Mander J. B., Priestley M. J. N., Park R., "Theoretical Stress-Strain Model for Confined Concrete," vol. 114, no. 8 (1988)

Martinez-Rueda J.E., Elnashai A. S., “Confined concrete model under cyclic load.” Materials and Structures30(197): 139-147 (1997)

McGUIRE M.A., JANSE M.J., Ross L. D., “AV Nodal” Reentry:. Journal of Cardiovascular Electrophysiology, 4: 573-586. https://doi.org/10.1111/j.1540-8167.1993.tb01245.x, (1993)

Microsoft Corporation, Microsoft Excel. Retrieved from https://office.microsoft.com/excel (2018)

Mihajlovic D., Catalogue des tremblements de terre Epiro-Albanais, Travaux de I' Academie de Spiences Serbe, 1951

Mihajlovic D., Mouvements seismiques Epiro-Albanais. Beograd Academie de Sciences, 1927

Moreli C., Carta del seismica dell Albania, Firenze, 1942

Muço B., "The collision between Adria and Albanian orogen on the light of focal mechanism solutions", 10th European Conference on Earthquake Engineering, Duma (Ed.), p. 37-41 (1995)

Muço B., Catalogue of ML>3.0 earthquakes in Albania from 1976 to 1995 and distribution of seismic energy released: Tectonophysics, v. 292, p. 311-319 (1998)

Muço B., Vaccari F., Panza G., Kuka N., Seismic zonation in Albania using a deterministic approach: lectonophysics, p. 277-288 (2002a)

Mwafy A.M., Elnashai A.S., ‘Static pushover versus dynamic collapse analysis of RC buildings’, Eng. Struct., vol. 23, 407-424 (2001).

NATO SfP – 983054 "Harmonization of seismic hazard maps for the Western Balkan countries", BSHAP, (2007-2010).

NEHRP S.D., ‘A Guide for Practicing Engineers’, U.S: National Institute of Standards and Technology (2010).

NISEE, "The Earthquake Engineering Online Archive NISEE e-Library," 2022.

Özer, E. , Kamal, M. & İnel, M., "Comparison of Linear and Nonlinear Seismic Behavior of 2D and 3D RC Buildings," International Journal of Engineering and Applied Sciences, pp. 17-27 (2017)

Panza C. F., Vaccari F., Costa G., Suhadolc P., Fah D., "Seismic input modelling for zoning and microzoning", Earthquake Spectra, v. 12, p. 529-566 (1996)

Panza G. F., Suhadolc P., "Complete strong motion synthetic", v. In: B.A. Bolt (ed.) Seismic Strong Motion Synthetics, Computational Techniques 4 (1987)

Panza G. F., Vaccari F., Cazzaro R., Deterministic Seismic Hazard Assessment, v. In: Vrancea Earthquakes: lectonics, Hazard and Risk Mitigation. Eds. Wenzel, F., Lungu, D., Co-ed.: Novak, O., p. 269-286 (1999)

Papazachos B., Papazachos C., On Greek Earthquakes: Thessaloniki, Greece (1989)

Peci V., Scordilis E., Kiratzi A., Muco B., Kuka N., Shubleka Sh., "A new Catalogue of earthquakes in Albania and surrounding area for the period 1964-2000", Book of Abstracts, University of Genoa, Italy, 28th Gen. Ass. of ESC (2002)

Poljak M., Zupancie P., Lapajne J., Sket-Motnikar B., Seismotectonic input for spatially-smoothed seismicity approach.: Proceedings of Workshop: Seismicity modelling in seismic hazard mapping (2000)

Reicherter K., Fernandez-Steeger T., Hoffman N., Neotectonics and tectonic geomorphology of the Lake Ohrid Basin: Ohrid ICDP Workshop "Scientific Collaboration On Past Specification Conditions in Lake Ohrid (2008)

Rejec K., Fajfar P., "On the relation between the near collapse limit states at the element and structure level" Second European Conference on Earthquake Engineering and Seismology, pp. 1-12, 25-29 August 2014.

Shebalin N. V., Leydecker G., Mokrushina N. G., Tatevossian R. E., Erteleva O. O., Vassiliev V. J., "Earthquake Catalogue for Central and Southwestern Europe" (342 B.C -

1990 A.D.): European Commission, Rep.No.ETNU CT 93-0087, v. available also at web page: http://www.bgr.de/quakecat/eng/catalogs.htm,maintained by Günter Leydecker, Bundesanstalt für Geowissenschaften und Rohstoffe, Hannover, Germany) (1998)

Shebalin N.V., Karnik V., Hadzievski D. (eds), "Catalogue of earthquakes of the Balkan region," UNDP-UNESCO Survey of the seismicity of the Balkan region, p. 600, 1974.

Shehu V., Dhima N., Ndikimi i kushteve inxhiniero-geologjike nè perhapjen e intensitetit te termetit tè 15 prillit 1979 nè rajonin Shkodèr-Lezhe: Ne: Tèrmeti i 15 prillit 1979, p. 387-404 (1983)

Shome N., Cornell C.A., 'Probabilistic seismic demand analysis of nonlinear structures', Stanford: Stanford University (2002).

Soloviev S., Solovieva O., Go C. N., Kim K. S., Shcetnikov N. A., "Tsunamis in Mediterranean Sea, 2000 BC-2000AD", Kluwer Academic Publishers (2001)

Soni P. K., Durgabhavani T., Mounika K., Nageswari M., Poluraju P., "Non-Linear Pushover Analysis of Flat slab Building by using Sap2000," ANALELE UNIVERSITATII "EFTIMIE MURGU" RESITA, pp. 254-264, 2012.

Sulstarova E., Kociaj S., Aliaj Sh., "Harta e rajonizimit sizmik te Shqiperise ne shkallen 1:2 500.000" (shqip-anglisht) Bul.UT.ser.Shk.Natyres, Nr.4, Tirane pp. 110-196 (1971)

Sulstarova E., Koçiaj S., The Dibra (Albania) earthquake of November 30, 1967: Tectonophysics, v. 67, p. 333-343 (1980)

Sulstarova E., Muço B., Peçi V., Pitarka B., January 9, 1988 earthquake, Tirana, Albania. Proceedings of XXI General Assambly of ESC, 23-27 August 1988, Sofies, pp 119-127 (1989)

Sulstarova, E., Pegi P., Shuteriqi P., "Vlora-Ebasani-Dibra (Albania) transversal fault zone and its seismic activity", Journal of Seismology, v. 4. pp. 117-131 (2000)

Sulstrarova E., Koçiaj S., Some aspects from the catalogue of Albania earthquakes. Proceedings of XIV Genral Assembly of ESC, Trieste, Berlin, pp 73-76, 1975

Taucer F.F, Spacone E, Filippou F.C, "A fiber beam-column element for seismic analysis of reinforced concrete structures," Earthquake Engineering Research Center, 1991.

Tsompanakis Y., Earthquake Return Period and Its Incorporation into Seismic Actions, Crete, Greece: Encyclopedia of Earthquake Engineering, 2014.

USGS, Largest and Deadliest Earthquakes by Year. Retrieved: 15 May 2018, website: http://earthquake.usgs.gov/earthquakes/eqarchives/year/byyear.php

Vamvatsikos D., 'Seismic Performance Capacity and Reliability of Structures as seen through Incremental Dynamic Analysis', Stanford: Stanford University (2002).

Vamvatsikos D., Cornell C.A., 'The Incremental Dynamic Analysis And Its Application To Performance-Based Earthquake Engineering', European Conference on Earthquake Engineering. London: Elsevier Science Ltd (2002)

Vamvatsikos D., Jalayer F., Cornell C.A., 'Application of Incremental Dynamic Analysis to an RC- Structure', Proceedings of the FIB Symposium on Concrete Structures in Seismic Regions Athens (2003).

Van Rossum G, Drake Jr FL., "Python reference manual," Centrum voor Wiskunde en Informatica Amsterdam, 1995.

Yun S.Y., Hamburger R.O., Cornell C.A., Foutch D.A., 'Seismic performance evaluation for steel moment frames', ASCE Journal of Structural Engineering for steel moment frames, 534–545 (2002).

APPENDIX A

Geometrical properties of the template buildings selected for this study are shown in this section:

A Template Building

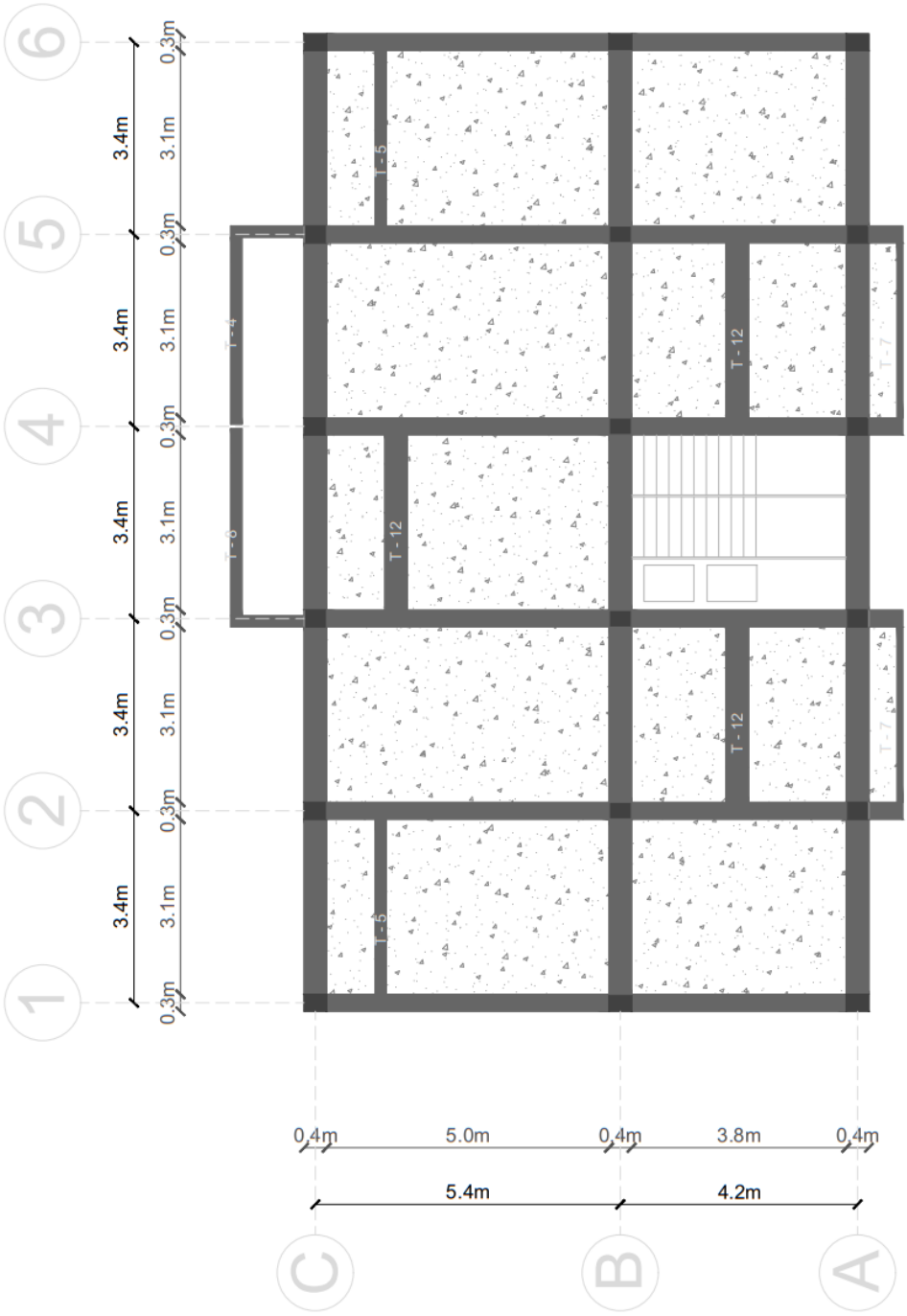

Figure 167: Plan layout of A Template Building

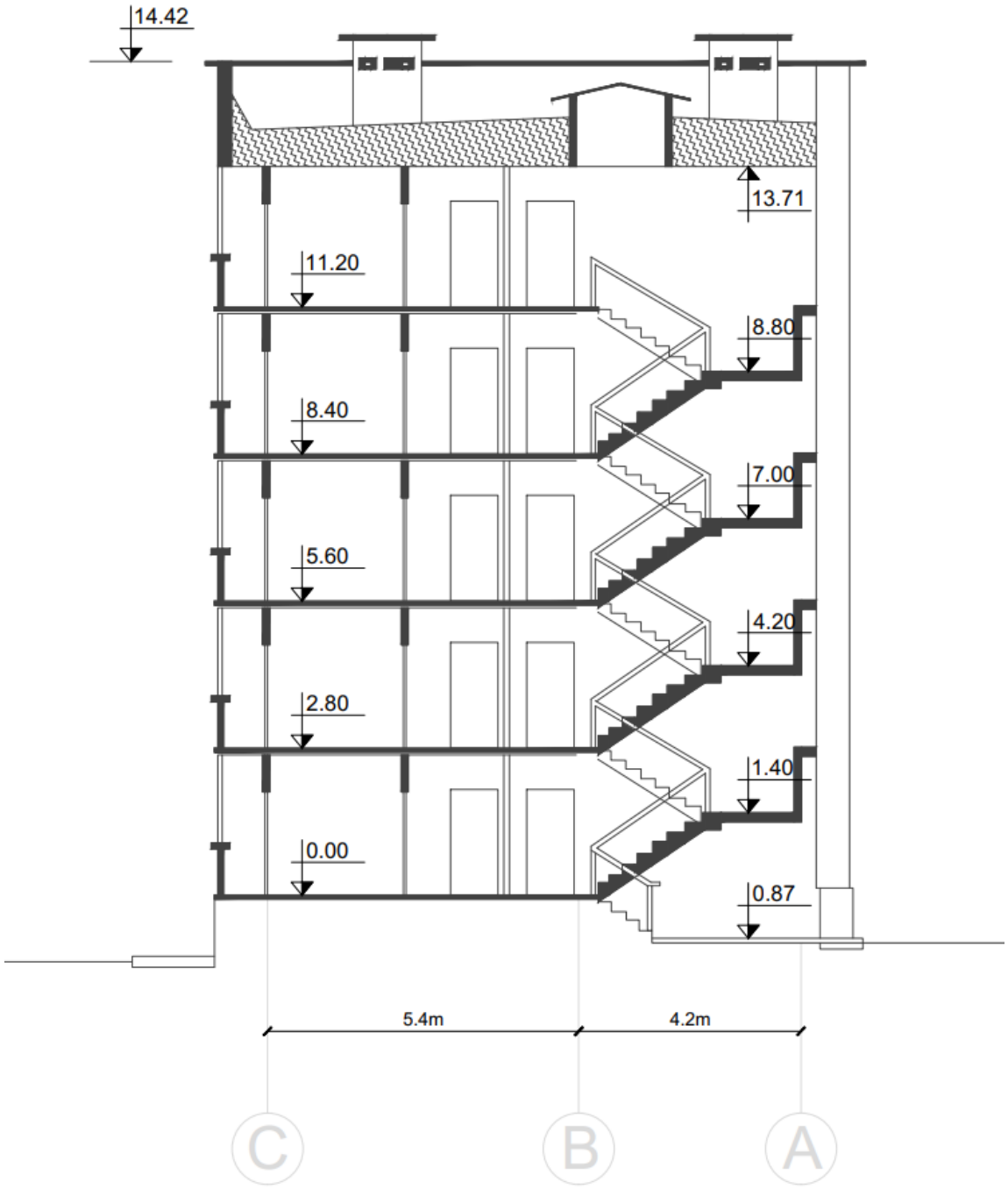

Figure 168: Elevation view of A Template building

B Template Building

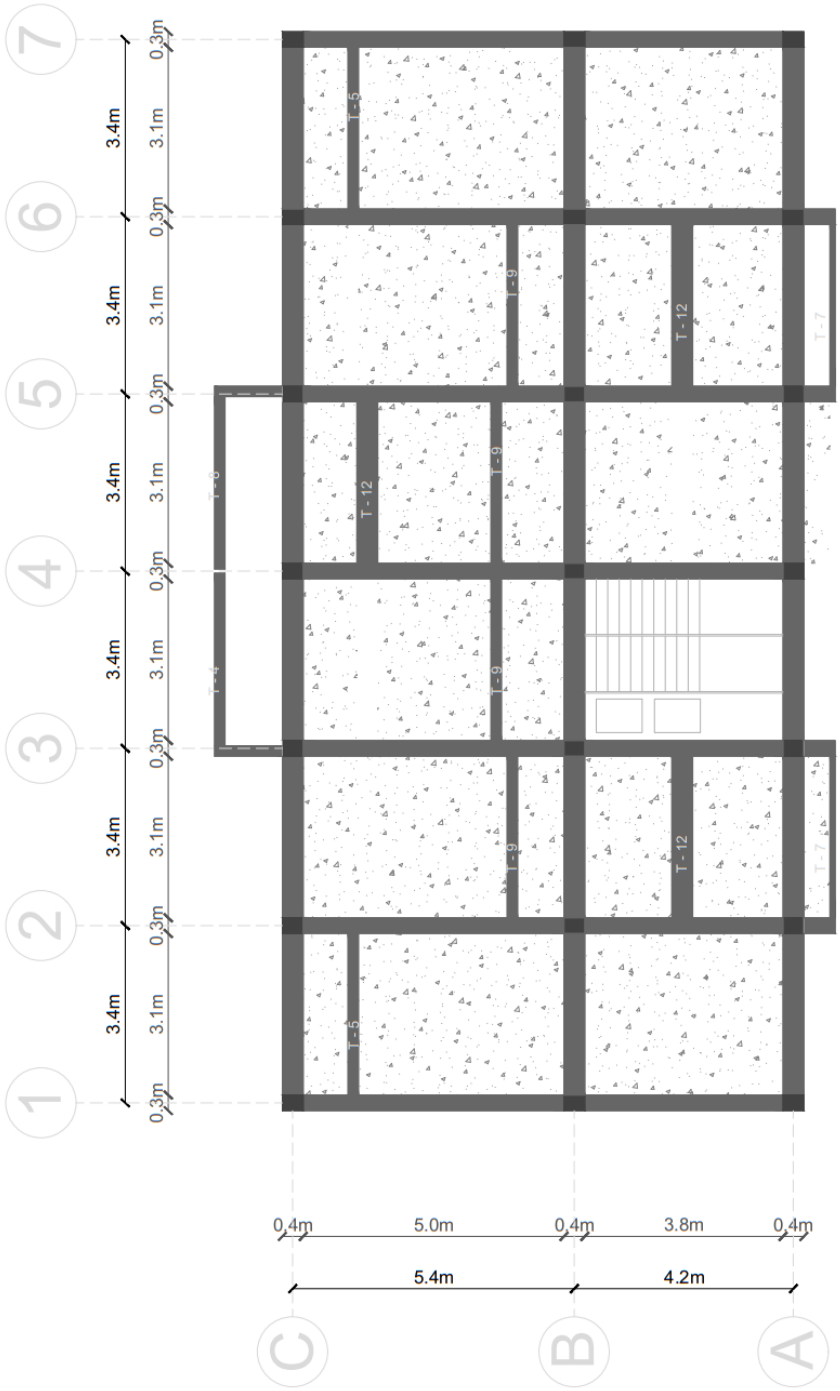

Figure 169: : Plan layout of B Template Building

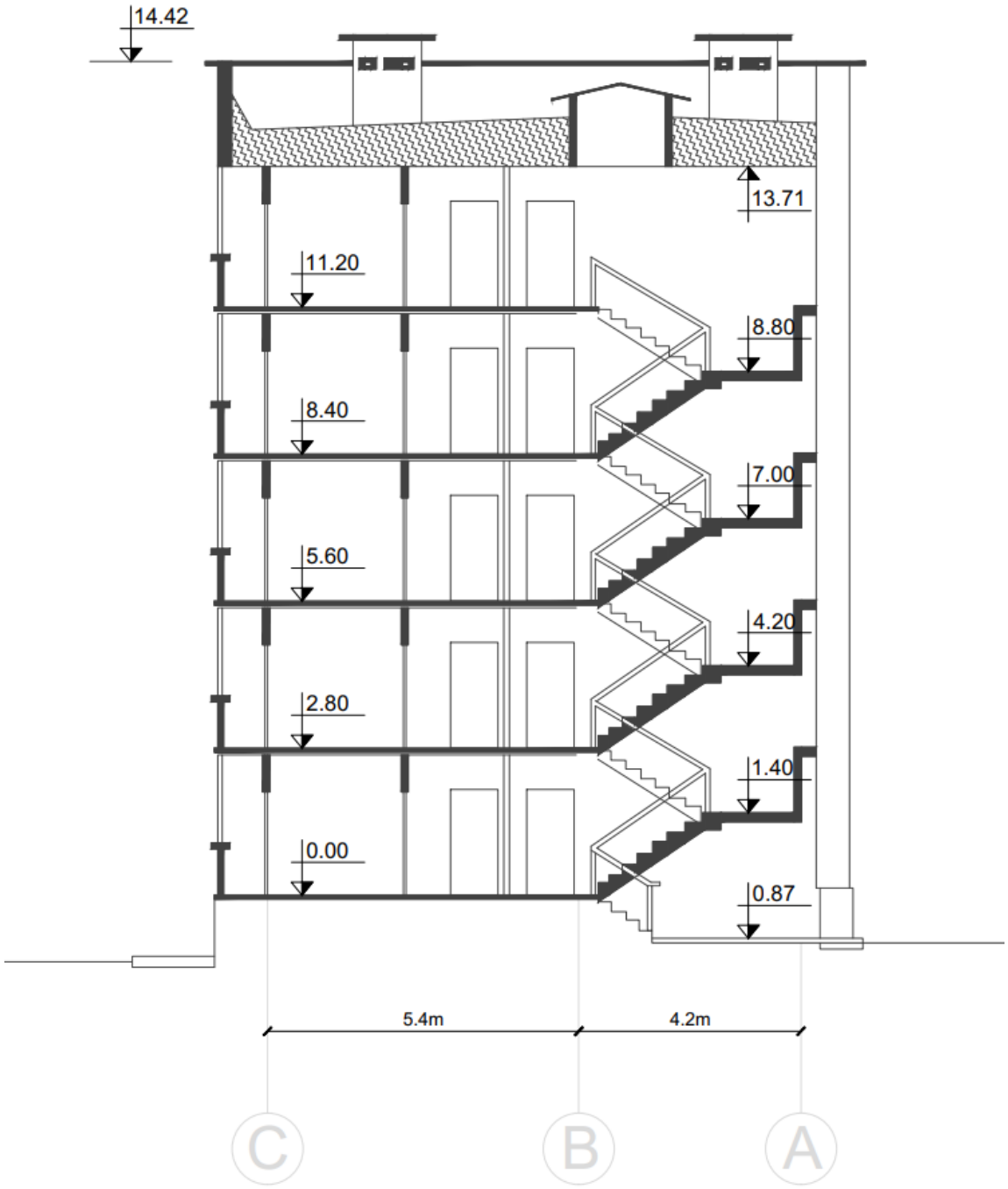

Figure 170: Elevation view of B Template building

C Template Building

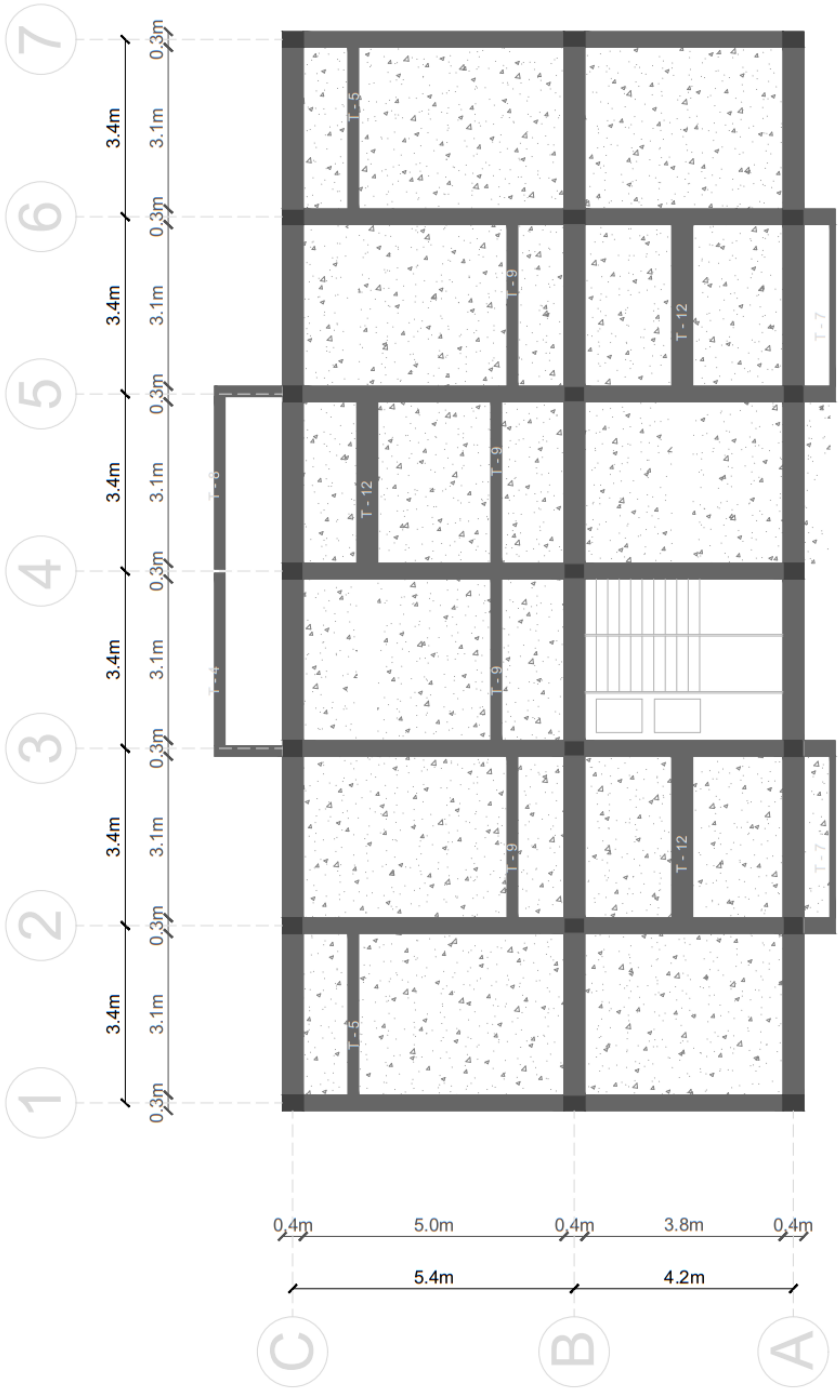

Figure 171: Plan layout of C Template Building

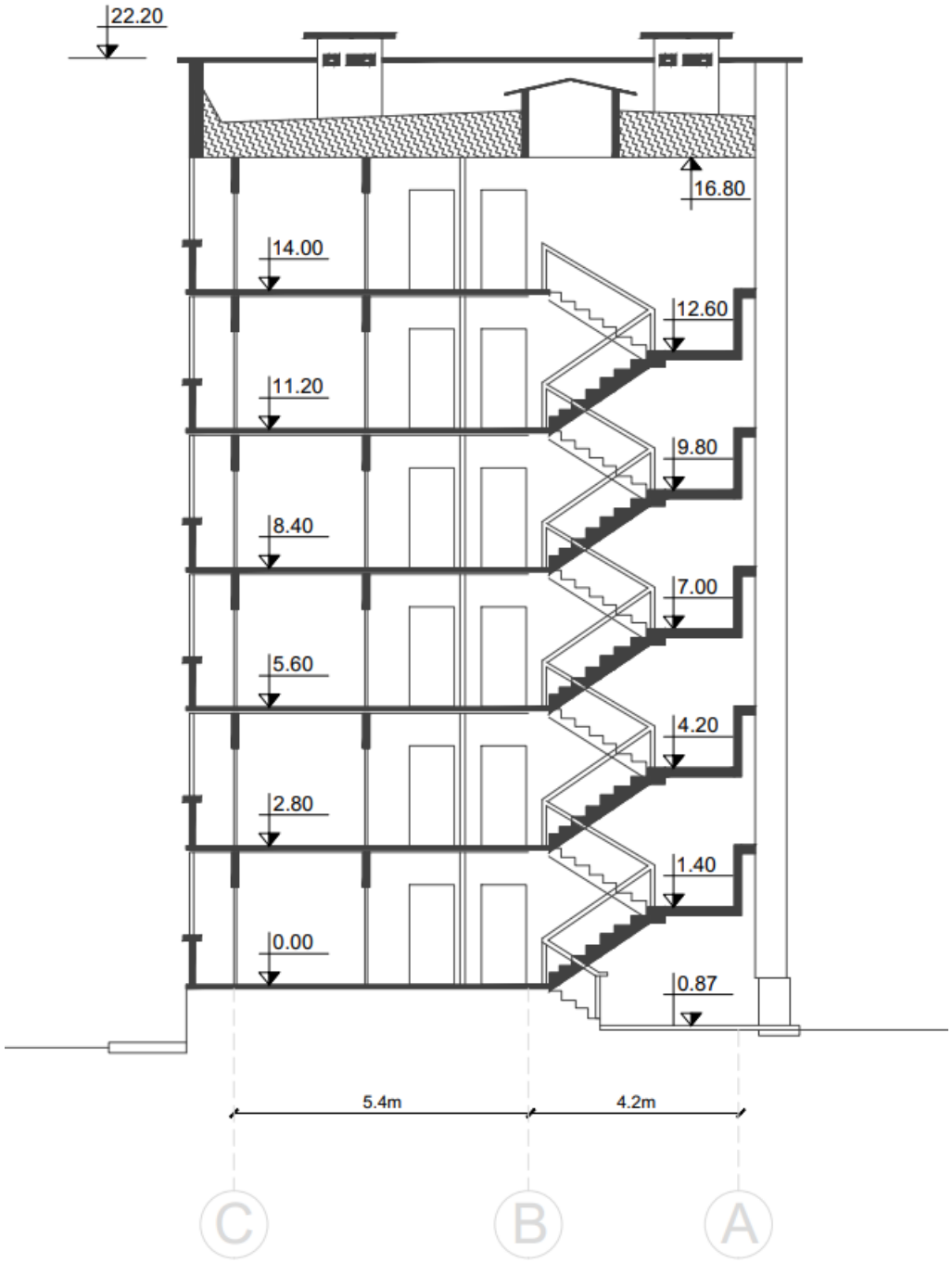

Figure 172: Elevation view of C Template building

D Template Building

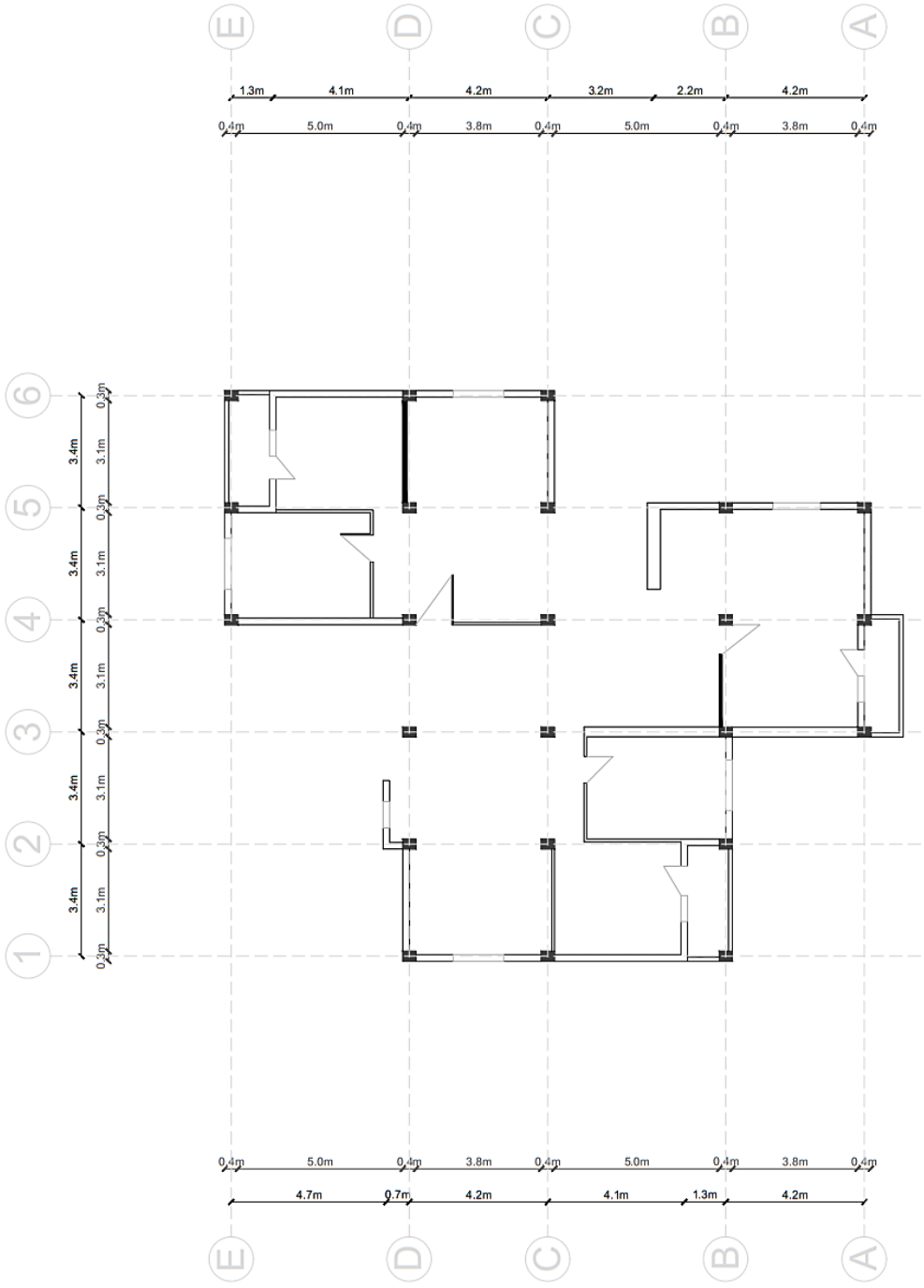

Figure 173: Architectural plan of the D Template Building

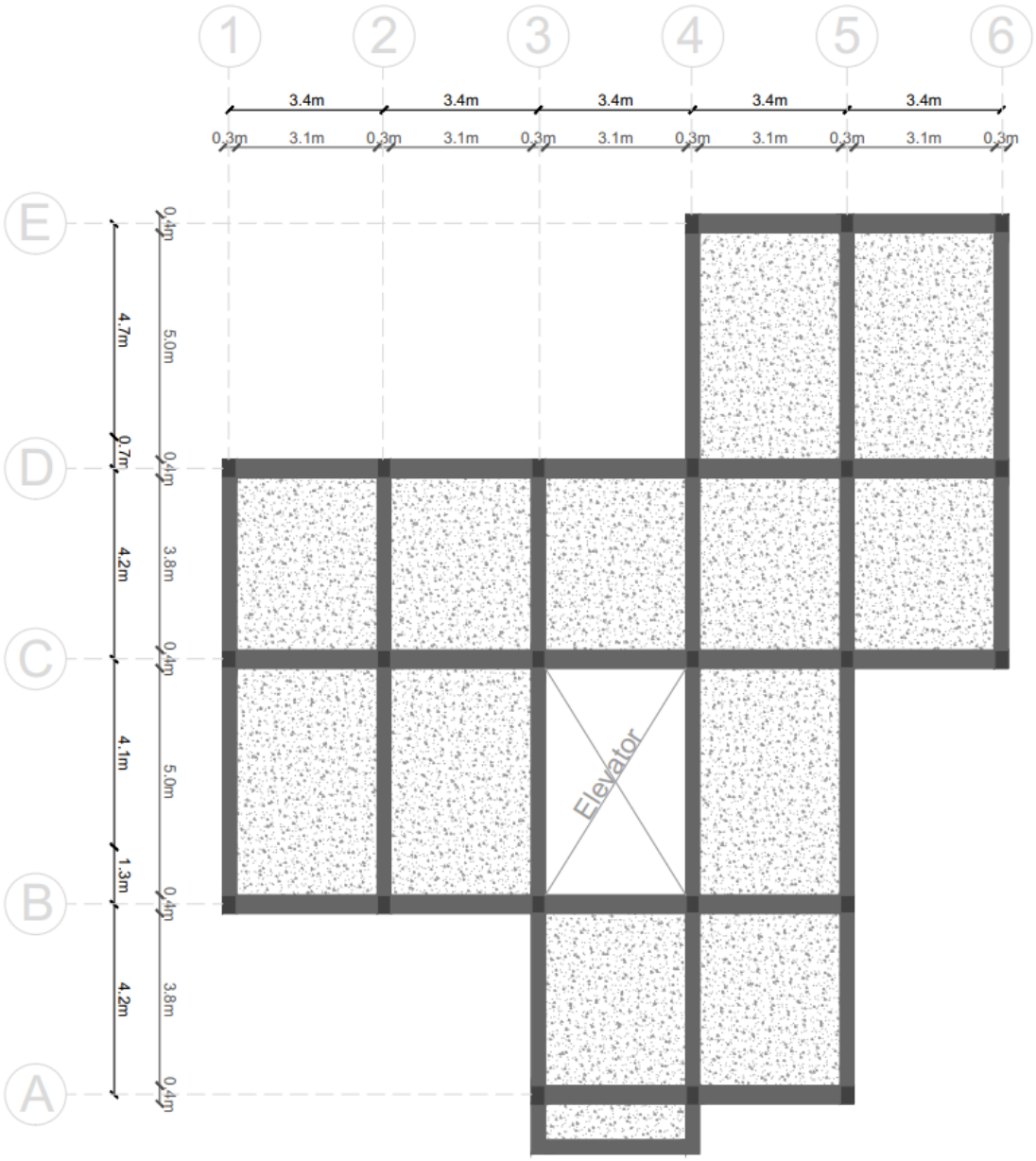

Figure 174: Plan layout of D Template Building

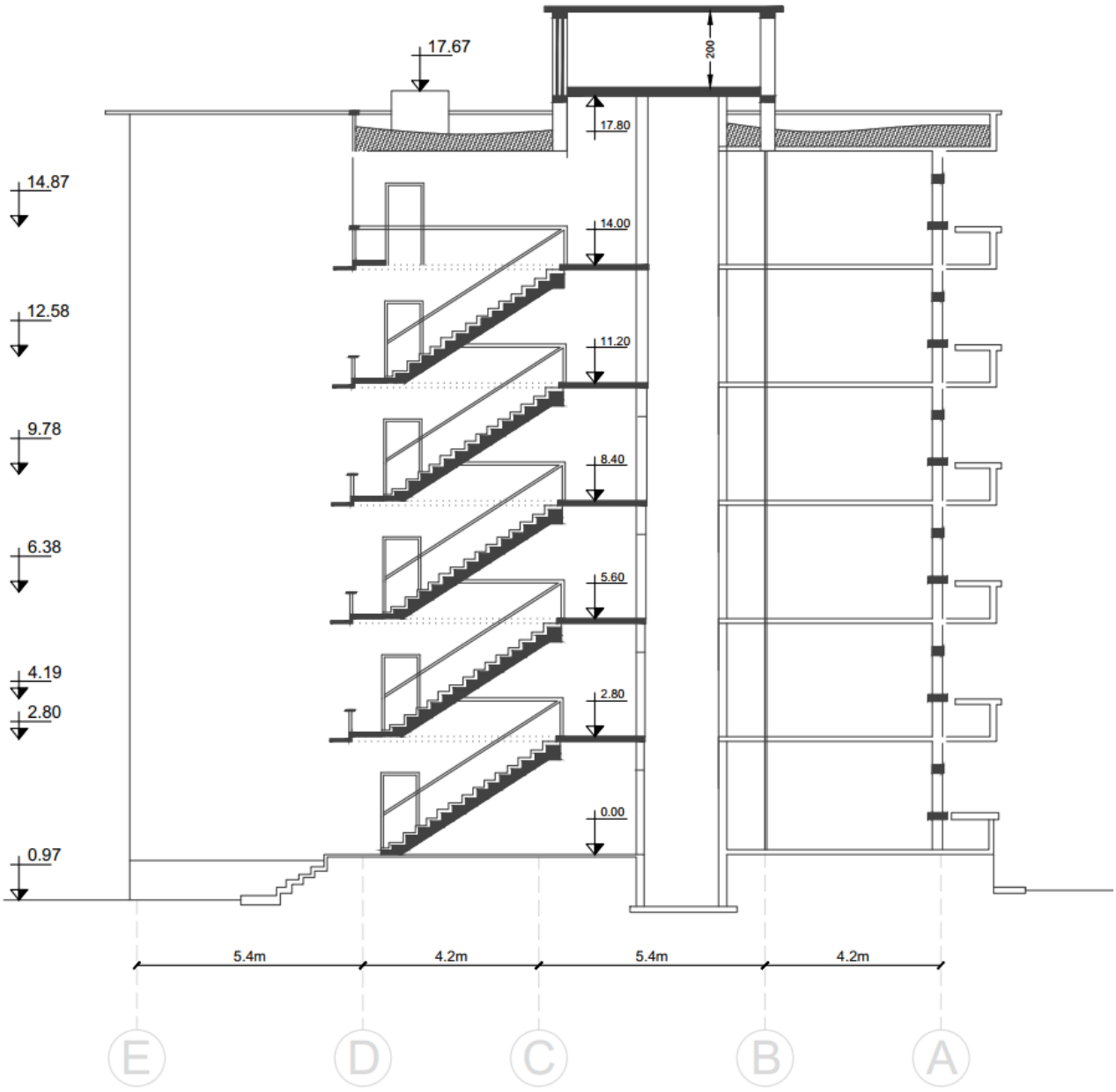

Figure 175: Elevation view of D Template building

E Template Building

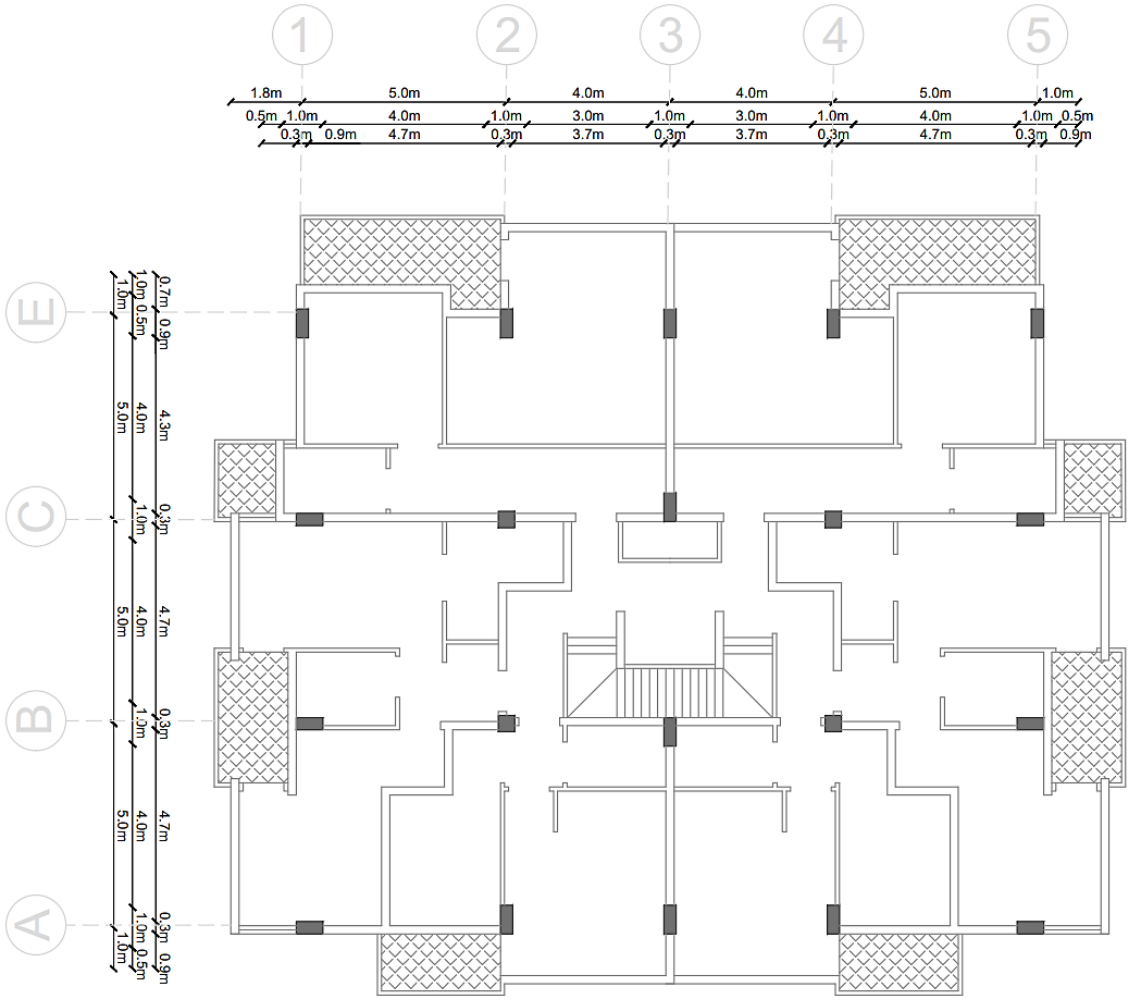

Figure 176: : Architectural plan of the E Template Building

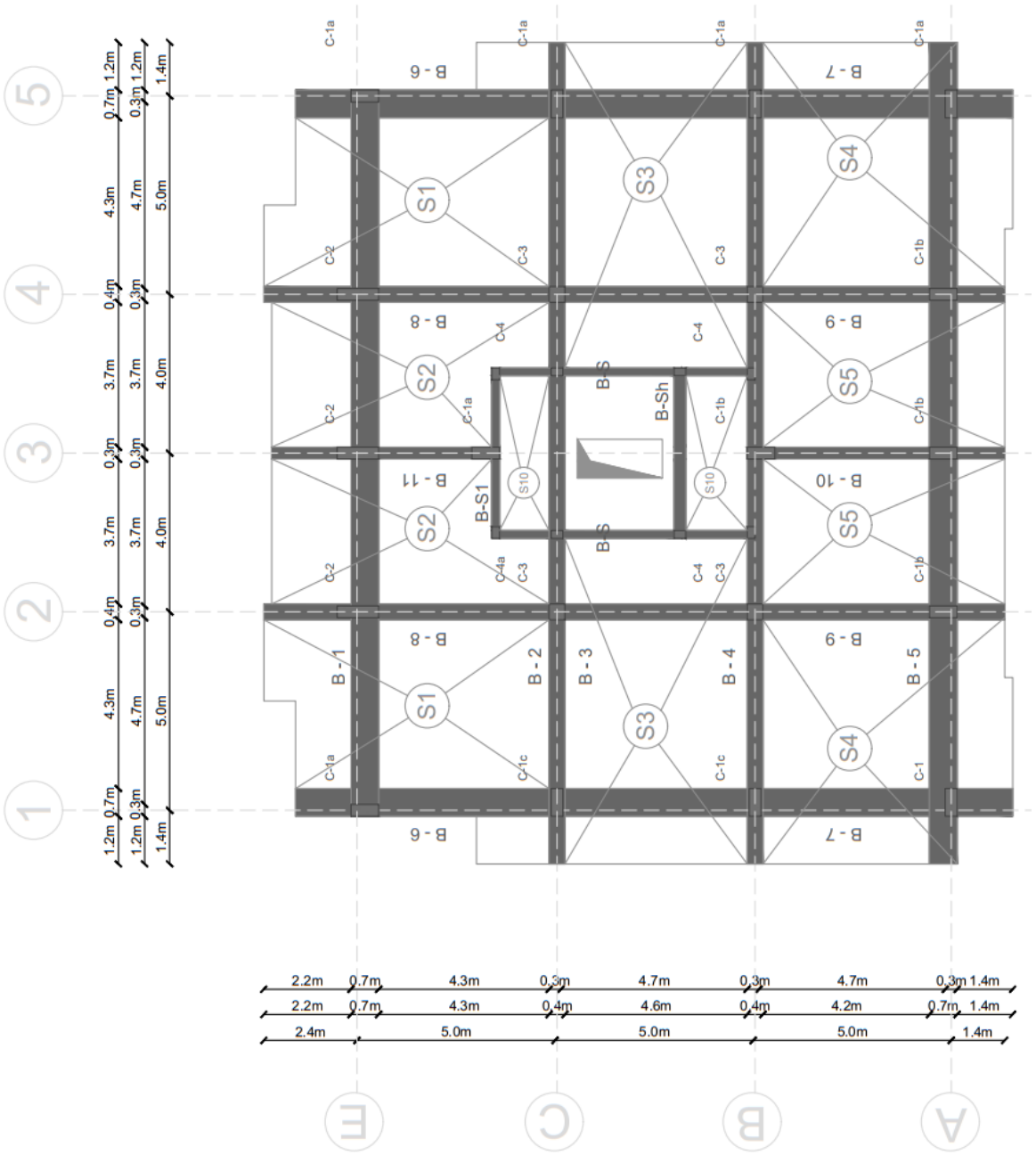

Figure 177: Plan layout of E Template Building

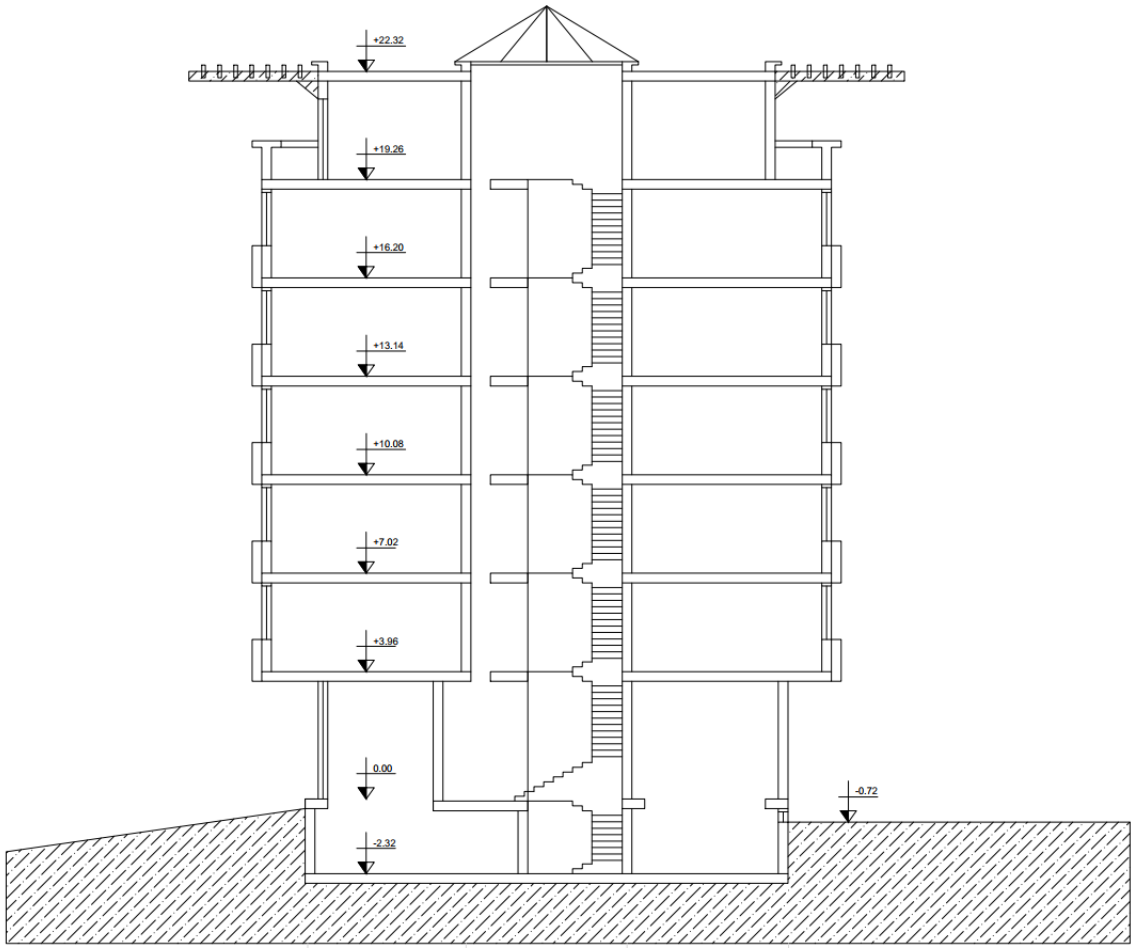

Figure 178: Elevation view of E Template building

APPENDIX B

Appendix B provides the outcomes generated from the static pushover analysis (SPO). Initially the results are presented for the immediate occupancy (IO), life safety (LS) and collapse prevention (CP) limit states. Base shear and roof displacement values are normalized by seismic weight and building height, respectively. Limit states are prepared in tabular form for each of the combinations included in this procedure. Among the combinations there are different concrete types such as, C16, C14, C12 and C10 and stirrups spacings S100, S150, S200 and S250mm. Furthermore, the results are shown for both orthogonal directions of the buildings (x- ad y-). In addition, the capacity curves are grouped for different stirrups spacings of each concrete type in one graph for comparative reasons.

A Template

Table 19: SPO Limit States for A Template Building

Direction	Concrete Class	Stirrups Spacing	IO		LS		CP	
			Δ/H	V/W	Δ/H	V/W	Δ/H	V/W
X_Frame	C10	10 cm	0.27%	14.4%	0.77%	21.9%	1.28%	18.7%
		15 cm	0.27%	14.4%	0.69%	21.4%	0.98%	18.3%
		20 cm	0.27%	14.5%	0.62%	21.1%	0.97%	18.0%
		25 cm	0.27%	14.5%	0.61%	20.9%	0.95%	17.9%
	C12	10 cm	0.24%	14.0%	0.73%	23.9%	1.22%	20.3%
		15 cm	0.24%	14.0%	0.67%	23.3%	1.10%	19.9%
		20 cm	0.24%	14.0%	0.64%	23.1%	1.03%	19.6%
		25 cm	0.24%	14.0%	0.61%	22.8%	0.99%	19.5%
	C14	10 cm	0.26%	15.5%	0.72%	25.4%	1.18%	21.7%
		15 cm	0.24%	14.9%	0.65%	25.0%	1.05%	21.3%
		20 cm	0.24%	14.9%	0.62%	24.8%	1.00%	21.1%
		25 cm	0.24%	14.9%	0.60%	24.4%	0.96%	20.9%
	C16	10 cm	0.23%	15.6%	0.73%	27.8%	1.23%	24.2%
		15 cm	0.21%	14.9%	0.63%	27.6%	1.06%	23.8%
		20 cm	0.21%	14.9%	0.59%	27.3%	0.97%	23.6%
		25 cm	0.20%	14.6%	0.54%	26.4%	0.88%	22.9%
Y_Frame	C10	10 cm	0.58%	19.2%	1.45%	22.1%	2.32%	19.0%
		15 cm	0.56%	19.0%	1.30%	21.5%	2.04%	18.6%
		20 cm	0.56%	19.0%	1.26%	21.2%	1.95%	18.4%
		25 cm	0.56%	19.0%	1.21%	21.0%	1.85%	18.3%
	C12	10 cm	0.57%	20.4%	1.41%	23.4%	2.26%	20.3%
		15 cm	0.58%	20.4%	1.30%	23.2%	2.02%	20.0%
		20 cm	0.58%	20.4%	1.25%	22.8%	1.93%	19.8%
		25 cm	0.58%	20.4%	1.20%	22.6%	1.83%	19.7%
	C14	10 cm	0.60%	21.8%	1.44%	25.0%	2.29%	21.4%
		15 cm	0.60%	21.8%	1.31%	24.6%	2.03%	21.1%
		20 cm	0.60%	21.8%	1.24%	24.4%	1.88%	20.9%
		25 cm	0.56%	21.4%	1.13%	23.9%	1.69%	20.4%
	C16	10 cm	0.57%	23.0%	1.41%	27.1%	2.26%	22.9%
		15 cm	0.57%	23.0%	1.35%	26.6%	2.12%	22.7%
		20 cm	0.59%	23.3%	1.21%	26.0%	1.84%	22.4%
		25 cm	0.55%	22.9%	1.11%	25.7%	1.68%	21.9%

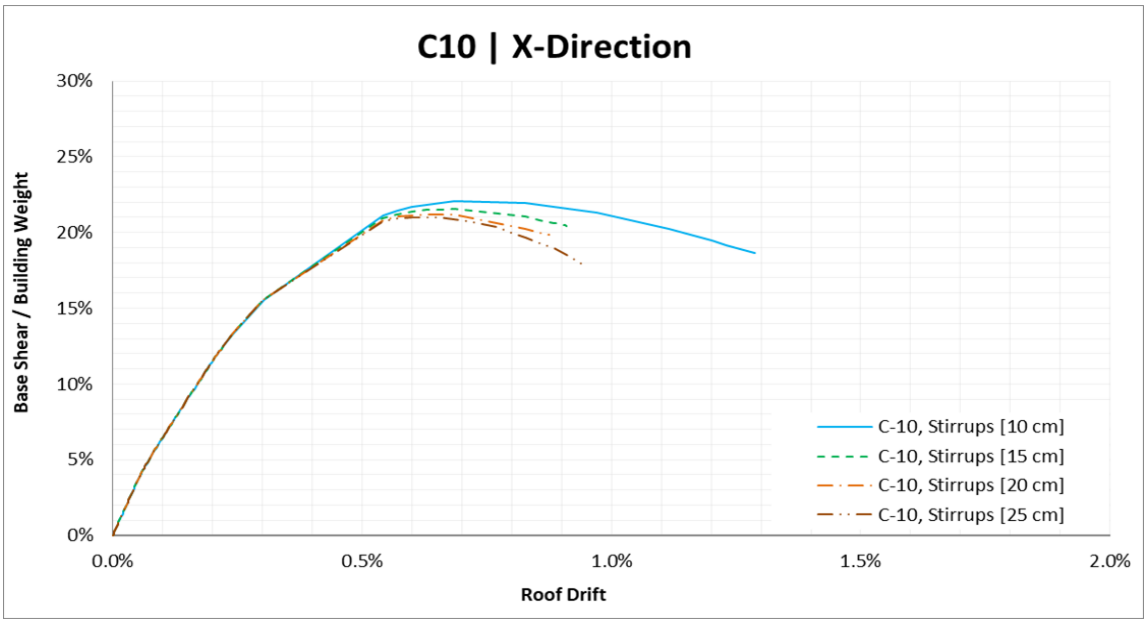

Figure 179: Capacity curves for A Template Design building, for C10 concrete with different stirrups spacings in X direction

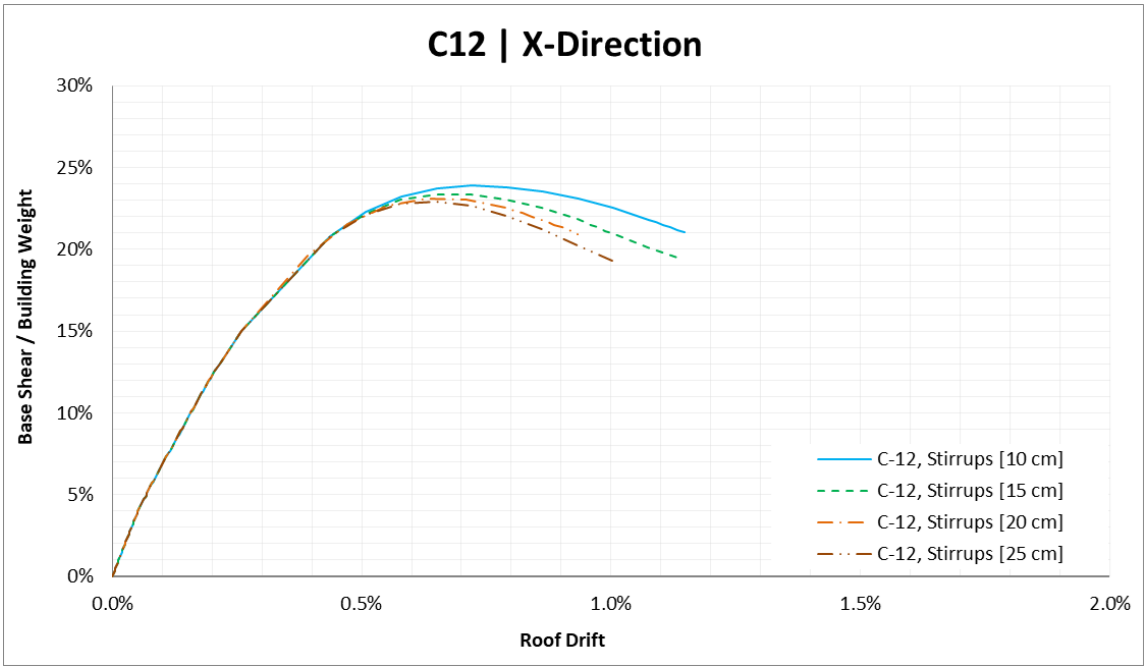

Figure 180: Capacity curves for A Template Design building, for C12 concrete with different stirrups spacings in X direction

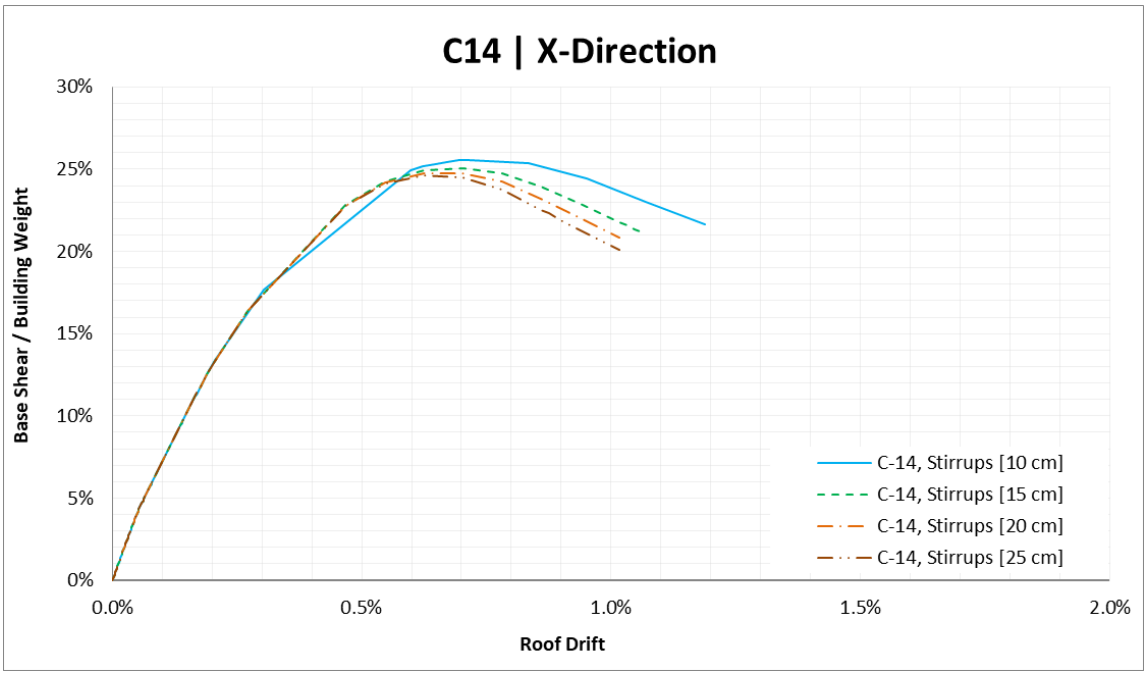

Figure 181: Capacity curves for A Template Design building, for C14 concrete with different stirrups spacings in X direction

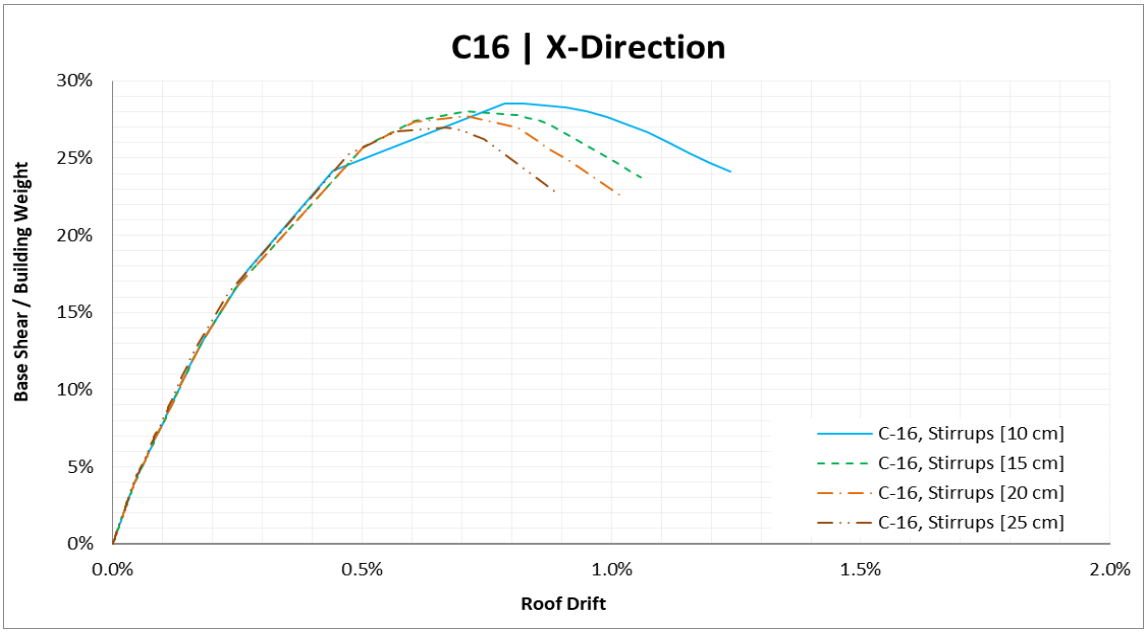

Figure 182: Capacity curves for A Template Design building, for C16 concrete with different stirrups spacings in X direction

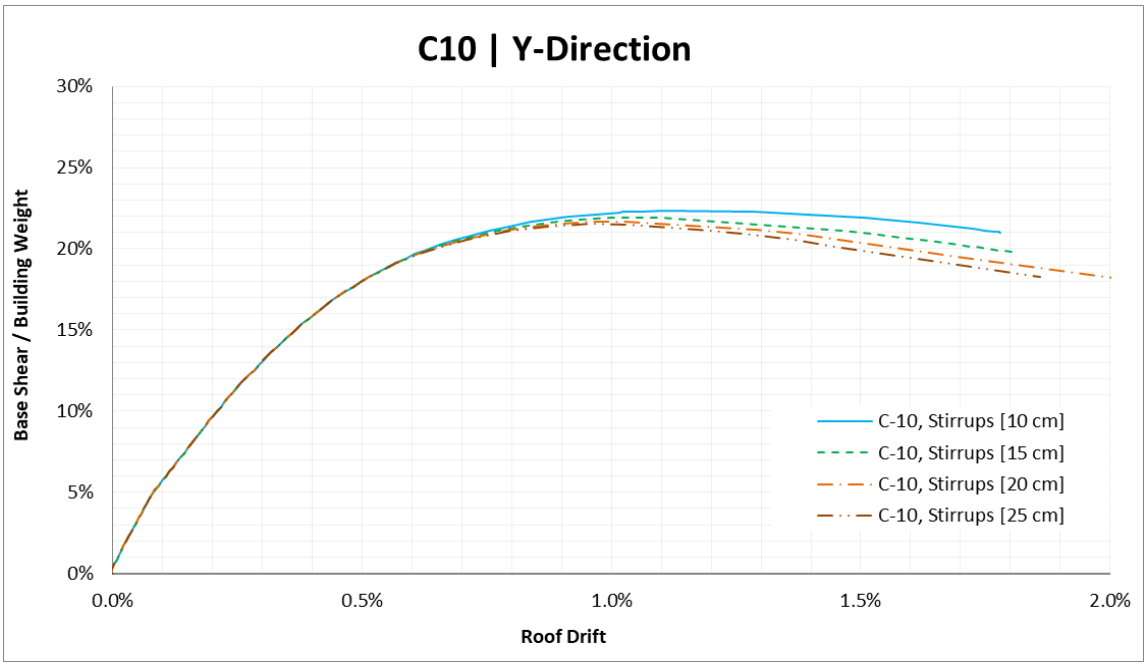

Figure 183: Capacity curves for A Template Design building, for C10 concrete with different stirrups spacings in Y direction

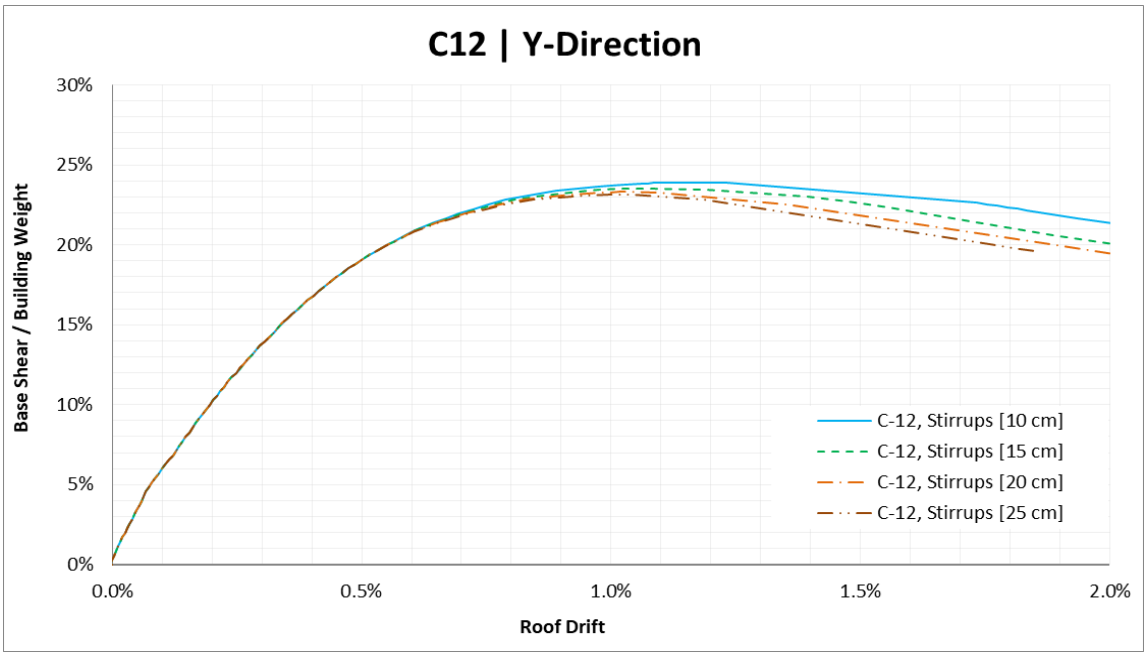

Figure 184: Capacity curves for A Template Design building, for C12 concrete with different stirrups spacings in Y direction

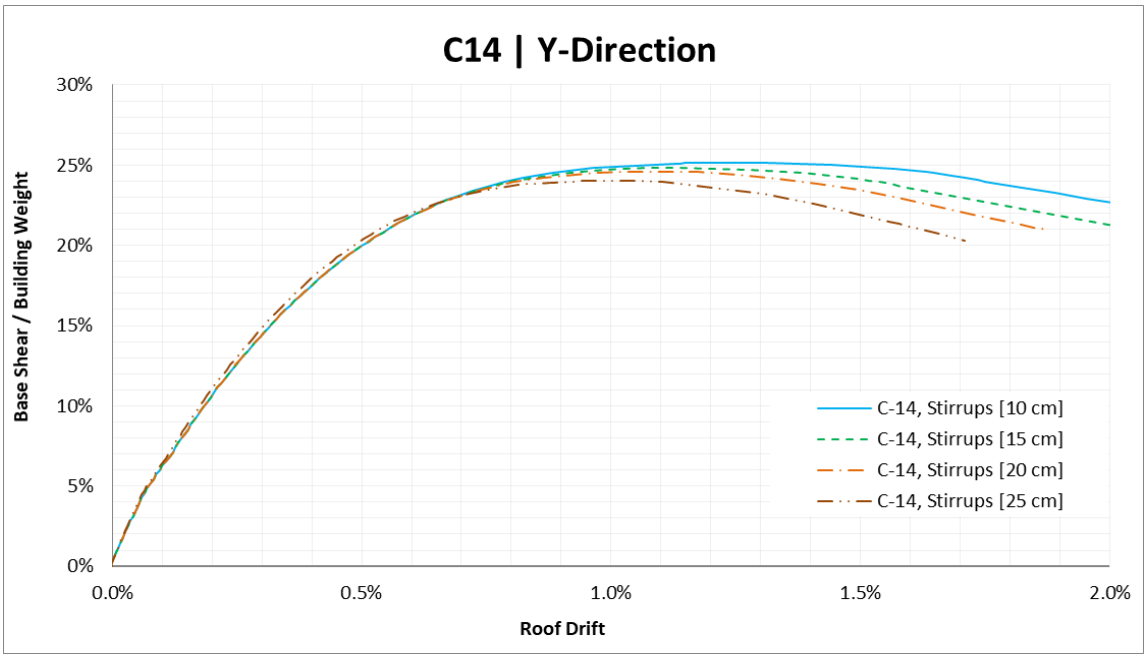

Figure 185: Capacity curves for A Template Design building, for C14 concrete with different stirrups spacings in Y direction

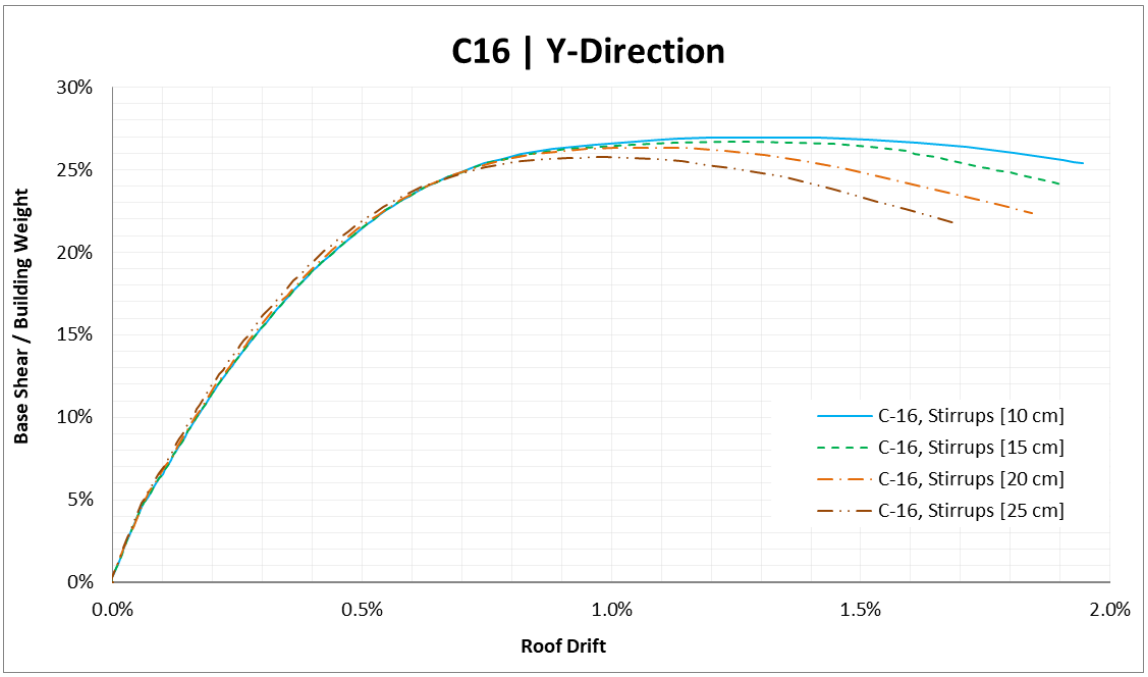

Figure 186: Capacity curves for A Template Design building, for C16 concrete with different stirrups spacings in Y direction

B Template

Table 20: SPO Limit States for B Template Building

Direction	Concrete Class	Stirrups Spacing	IO		LS		CP	
			Δ/H	V/W	Δ/H	V/W	Δ/H	V/W
X_Frame	C10	10 cm	0.26%	12.9%	0.67%	19.8%	1.08%	16.9%
		15 cm	0.26%	12.9%	0.57%	18.9%	0.89%	16.1%
		20 cm	0.25%	12.6%	0.50%	17.8%	0.74%	15.5%
		25 cm	0.25%	12.6%	0.49%	17.3%	0.72%	15.4%
	C12	10 cm	0.24%	13.3%	0.69%	22.0%	1.13%	18.7%
		15 cm	0.24%	13.3%	0.60%	21.6%	0.97%	18.3%
		20 cm	0.24%	13.3%	0.56%	21.1%	0.89%	18.0%
		25 cm	0.24%	13.3%	0.55%	20.7%	0.85%	17.9%
	C14	10 cm	0.21%	13.1%	0.66%	23.7%	1.11%	20.4%
		15 cm	0.21%	13.1%	0.60%	23.4%	0.98%	19.8%
		20 cm	0.21%	13.1%	0.58%	23.0%	0.94%	19.7%
		25 cm	0.21%	13.1%	0.56%	22.7%	0.90%	19.6%
	C16	10 cm	0.20%	13.4%	0.64%	25.4%	1.08%	21.8%
		15 cm	0.20%	13.4%	0.58%	24.7%	0.96%	21.4%
		20 cm	0.20%	13.4%	0.56%	24.4%	0.91%	21.2%
		25 cm	0.20%	13.4%	0.54%	24.2%	0.88%	20.9%
Y_Frame	C10	10 cm	0.57%	17.8%	1.39%	20.2%	2.20%	17.4%
		15 cm	0.55%	17.5%	1.31%	19.6%	2.07%	17.0%
		20 cm	0.55%	17.5%	1.23%	19.3%	1.91%	16.8%
		25 cm	0.53%	17.3%	1.16%	19.1%	1.79%	16.7%
	C12	10 cm	0.58%	19.2%	1.45%	21.9%	2.32%	19.0%
		15 cm	0.56%	19.0%	1.30%	21.4%	2.04%	18.6%
		20 cm	0.56%	19.0%	1.26%	21.1%	1.95%	18.4%
		25 cm	0.56%	19.0%	1.21%	20.9%	1.85%	18.3%
	C14	10 cm	0.57%	20.4%	1.41%	23.5%	2.26%	20.3%
		15 cm	0.58%	20.4%	1.30%	23.3%	2.02%	20.0%
		20 cm	0.58%	20.4%	1.25%	22.8%	1.93%	19.8%
		25 cm	0.58%	20.4%	1.20%	22.6%	1.83%	19.7%
	C16	10 cm	0.60%	21.8%	1.44%	25.0%	2.29%	21.4%
		15 cm	0.60%	21.8%	1.31%	24.7%	2.03%	21.1%
		20 cm	0.60%	21.8%	1.24%	24.4%	1.88%	20.9%
		25 cm	0.60%	21.8%	1.21%	24.1%	1.82%	20.8%

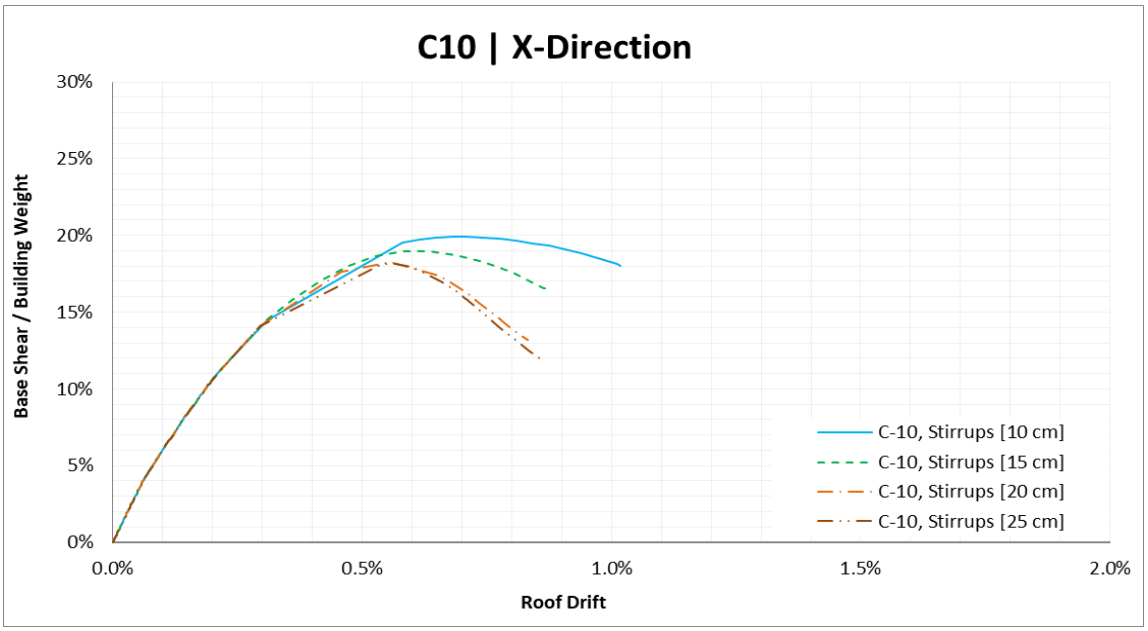

Figure 187: Capacity curves for B Template Design building, for C10 concrete with different stirrups spacings in X direction

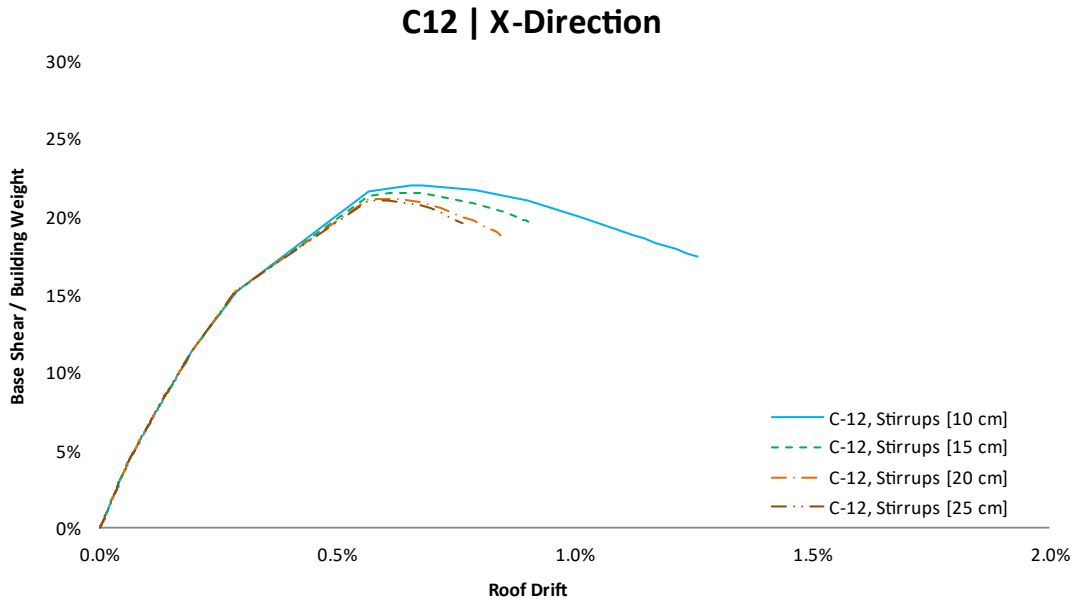

Figure 188: Capacity curves for B Template Design building, for C12 concrete with different stirrups spacings in X direction

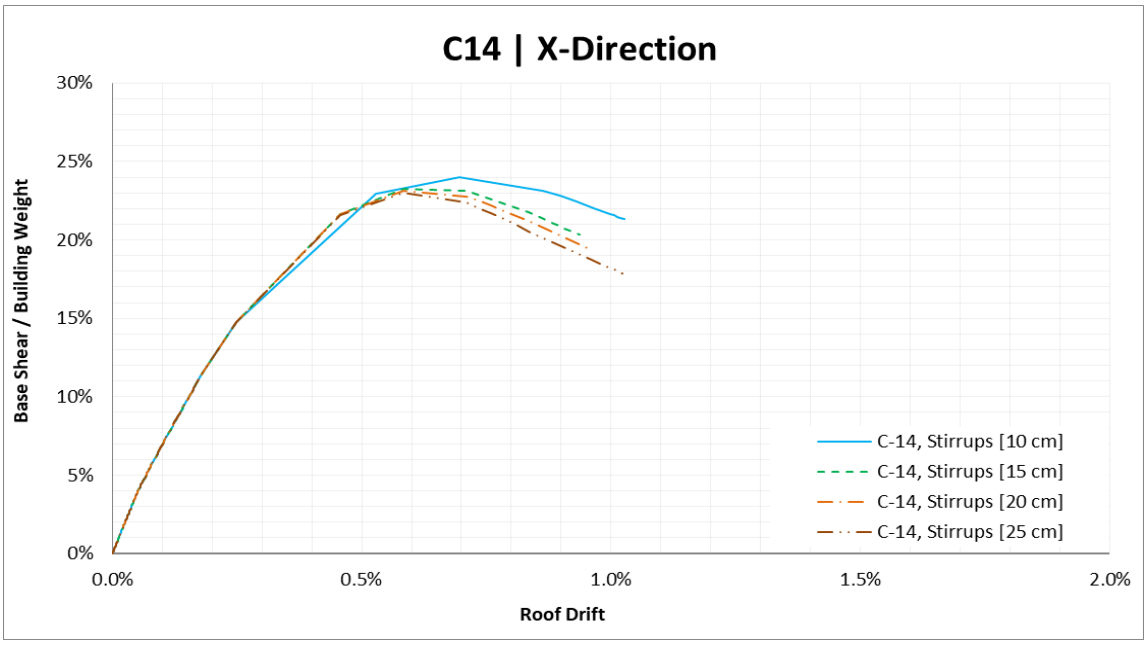

Figure 189: Capacity curves for B Template Design building, for C14 concrete with different stirrups spacings in X direction

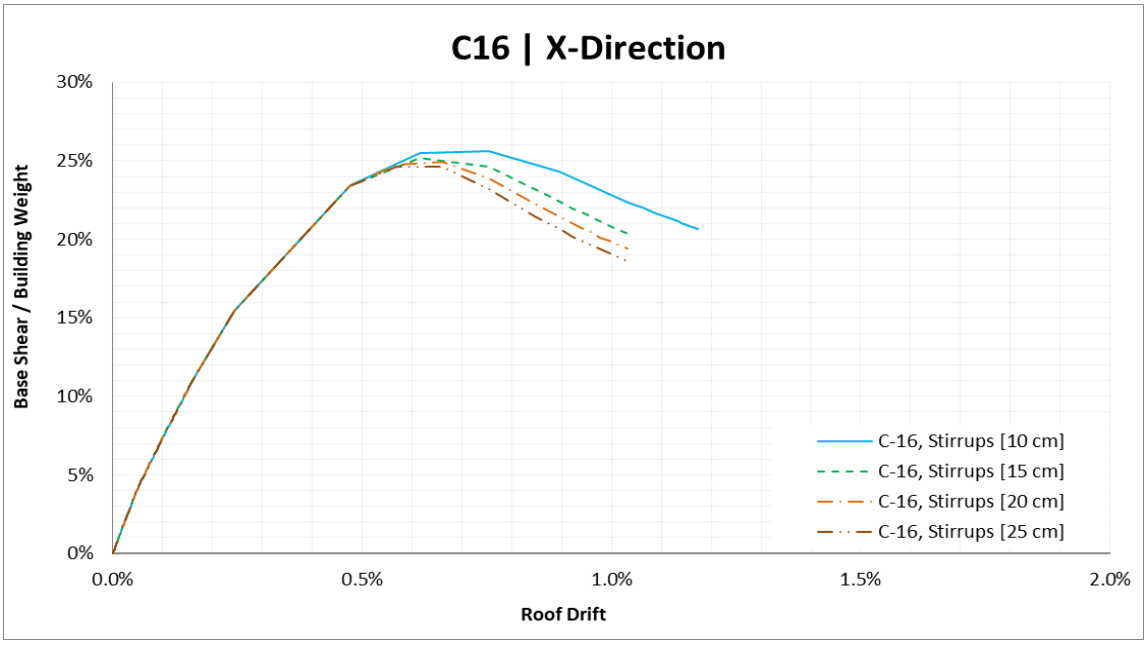

Figure 190: Capacity curves for B Template Design building, for C16 concrete with different stirrups spacings in X direction

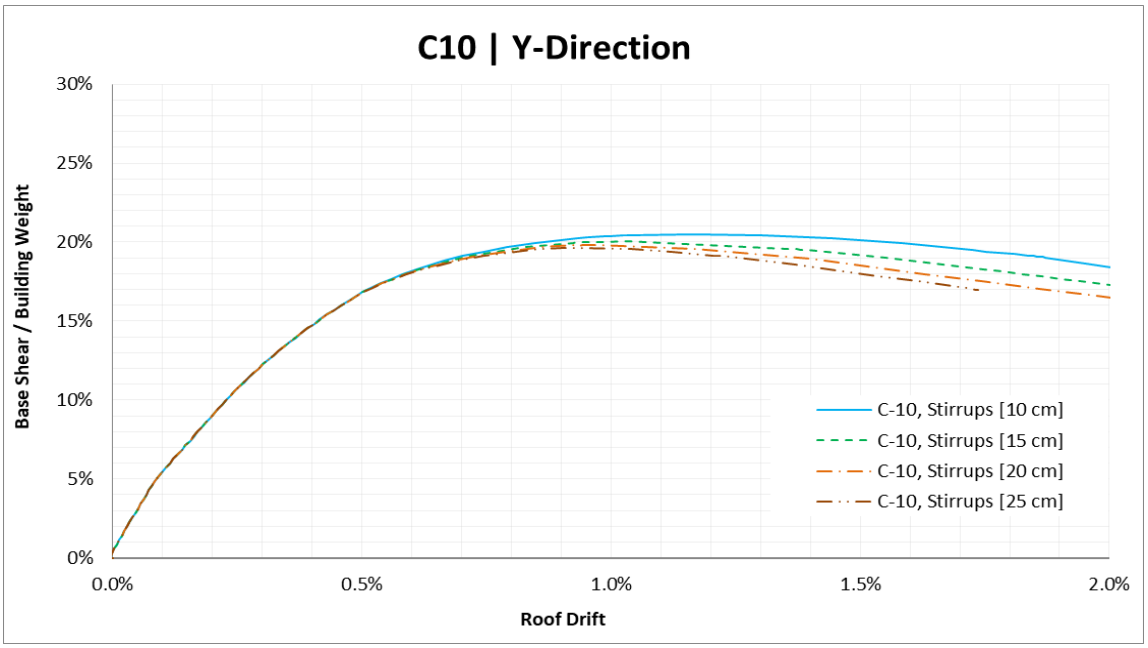

Figure 191: Capacity curves for B Template Design building, for C10 concrete with different stirrups spacings in Y direction

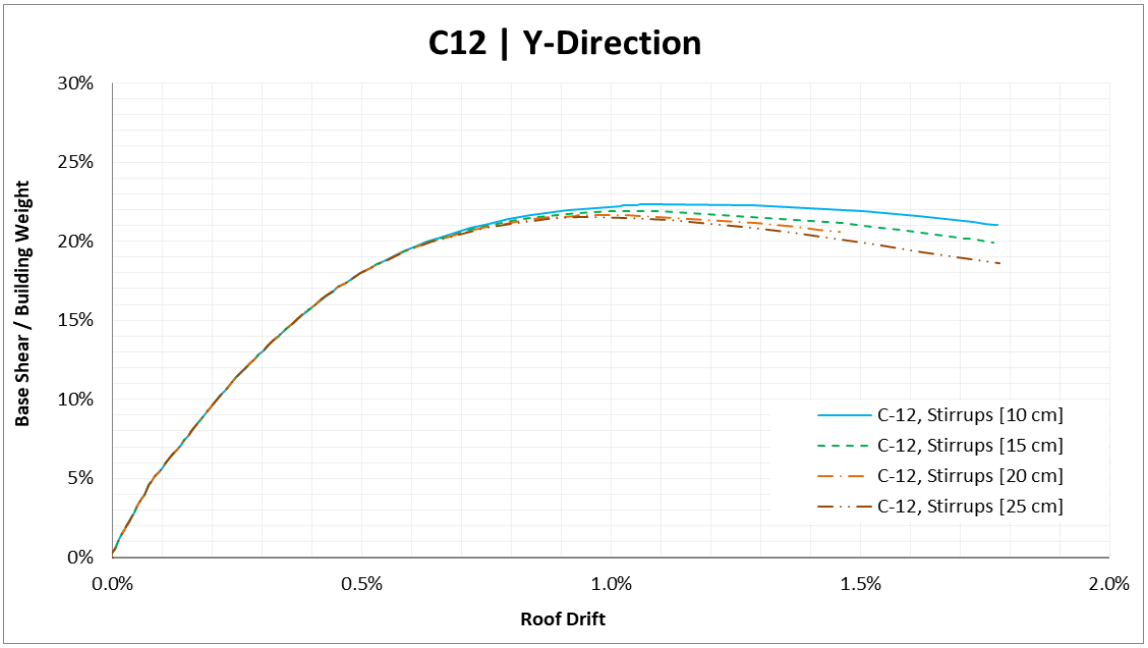

Figure 192: Capacity curves for B Template Design building, for C12 concrete with different stirrups spacings in Y direction

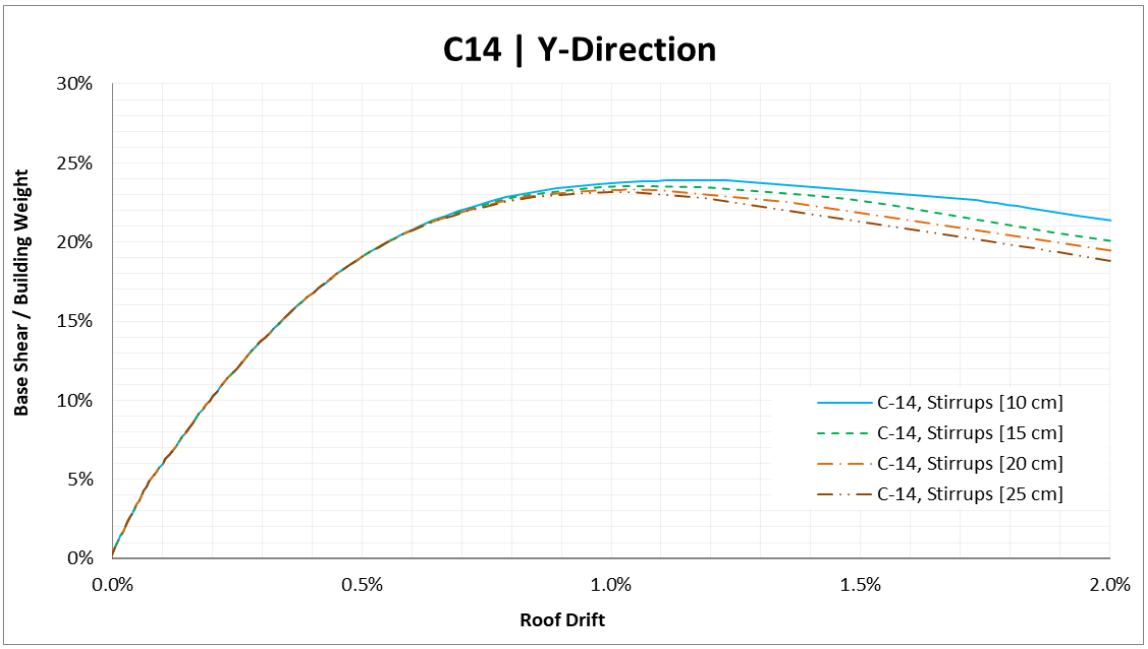

Figure 193: Capacity curves for B Template Design building, for C14 concrete with different stirrups spacings in Y direction

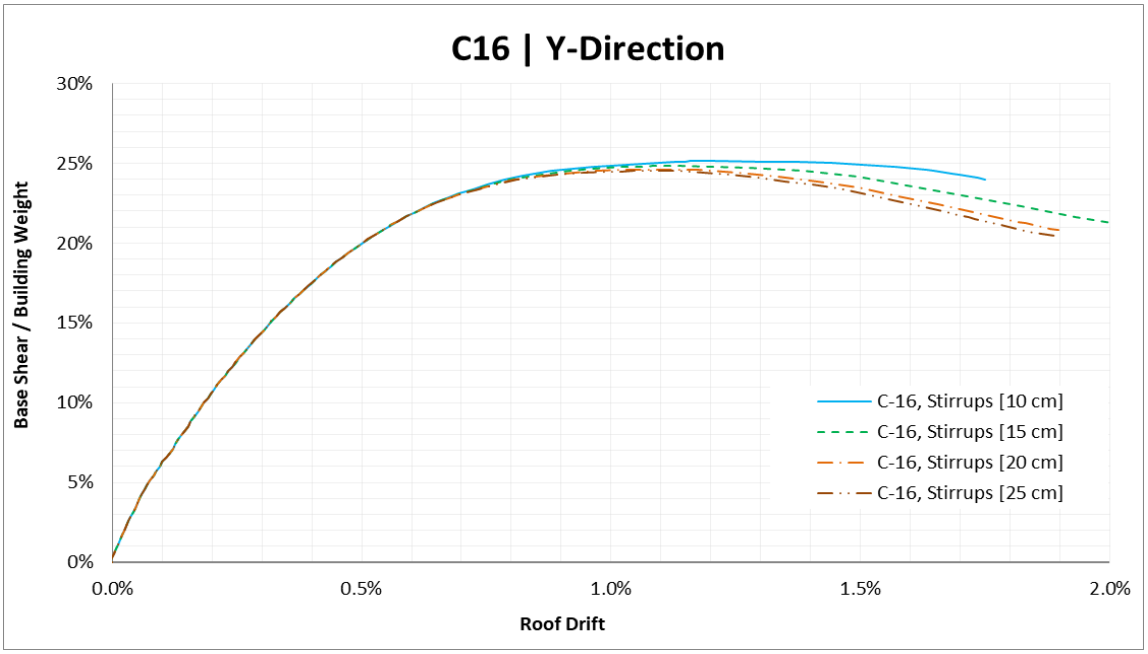

Figure 194: Capacity curves for B Template Design building, for C16 concrete with different stirrups spacings in Y direction

C Template

Table 21: SPO Limit States for C Template Building

Direction	Concrete Class	Stirrups Spacing	IO		LS		CP	
			Δ/H	V/W	Δ/H	V/W	Δ/H	V/W
X_Frame	C10	10 cm	0.27%	10.5%	0.50%	13.9%	0.73%	12.0%
		15 cm	0.28%	10.5%	0.44%	13.0%	0.60%	11.1%
		20 cm	0.28%	10.5%	0.42%	12.5%	0.56%	10.8%
		25 cm	0.28%	10.5%	0.38%	11.4%	0.47%	10.0%
	C12	10 cm	0.28%	11.9%	0.55%	17.1%	0.82%	14.5%
		15 cm	0.23%	10.6%	0.50%	15.9%	0.76%	13.6%
		20 cm	0.23%	10.6%	0.43%	15.2%	0.62%	13.4%
		25 cm	0.23%	10.5%	0.41%	14.9%	0.60%	13.4%
	C14	10 cm	0.26%	12.3%	0.59%	19.3%	0.92%	16.4%
		15 cm	0.25%	12.3%	0.58%	19.0%	0.90%	16.2%
		20 cm	0.25%	12.3%	0.51%	18.2%	0.76%	15.8%
		25 cm	0.25%	12.0%	0.48%	17.7%	0.71%	15.3%
	C16	10 cm	0.22%	11.8%	0.58%	20.7%	0.94%	17.8%
		15 cm	0.22%	11.8%	0.53%	20.0%	0.84%	17.3%
		20 cm	0.22%	11.8%	0.52%	19.7%	0.82%	17.3%
		25 cm	0.22%	11.6%	0.50%	19.4%	0.78%	17.2%
Y_Frame	C10	10 cm	0.60%	14.8%	1.18%	16.1%	1.76%	13.9%
		15 cm	0.57%	14.5%	1.01%	15.7%	1.45%	13.5%
		20 cm	0.55%	14.2%	0.92%	15.5%	1.29%	13.3%
		25 cm	0.55%	14.2%	0.86%	15.3%	1.16%	13.1%
	C12	10 cm	0.60%	16.2%	1.20%	17.9%	1.80%	15.4%
		15 cm	0.57%	15.9%	1.11%	17.6%	1.64%	15.2%
		20 cm	0.58%	15.9%	1.03%	17.3%	1.49%	14.9%
		25 cm	0.58%	15.9%	1.02%	17.1%	1.46%	14.9%
	C14	10 cm	0.62%	17.6%	1.21%	19.5%	1.79%	16.8%
		15 cm	0.60%	17.3%	1.13%	19.2%	1.66%	16.5%
		20 cm	0.60%	17.3%	1.06%	18.9%	1.52%	16.3%
		25 cm	0.60%	17.3%	1.04%	18.7%	1.49%	16.3%
	C16	10 cm	0.63%	18.7%	1.21%	20.9%	1.78%	17.8%
		15 cm	0.61%	18.5%	1.11%	20.7%	1.62%	17.6%
		20 cm	0.61%	18.5%	1.08%	20.5%	1.56%	17.5%
		25 cm	0.50%	16.6%	0.95%	20.2%	1.40%	18.3%

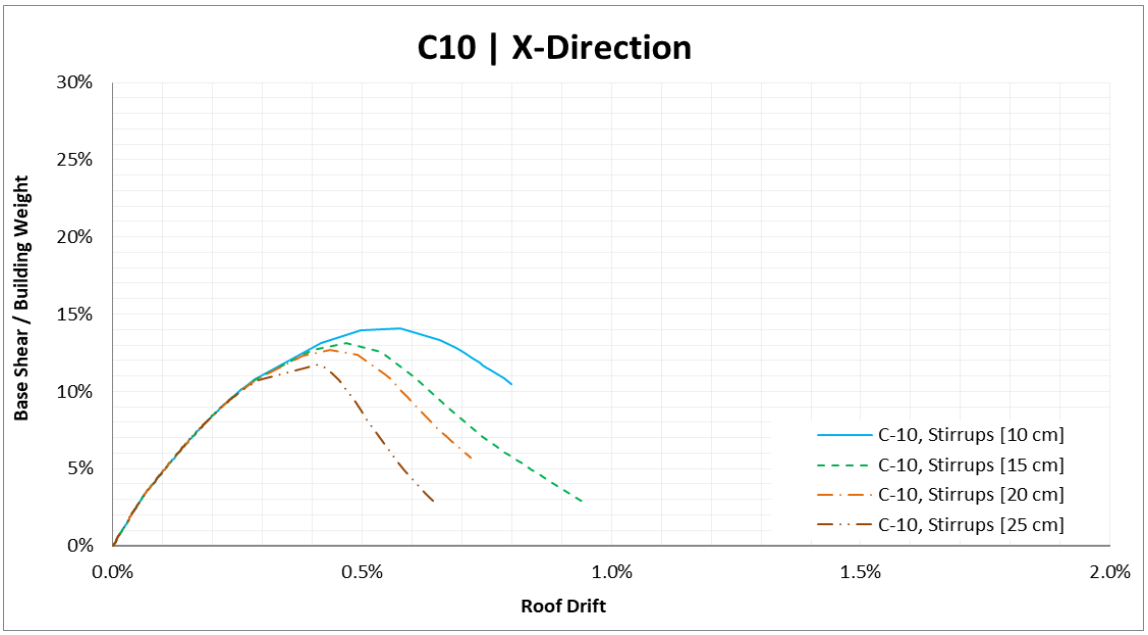

Figure 195: Capacity curves for C Template Design building, for C10 concrete with different stirrups spacings in X direction

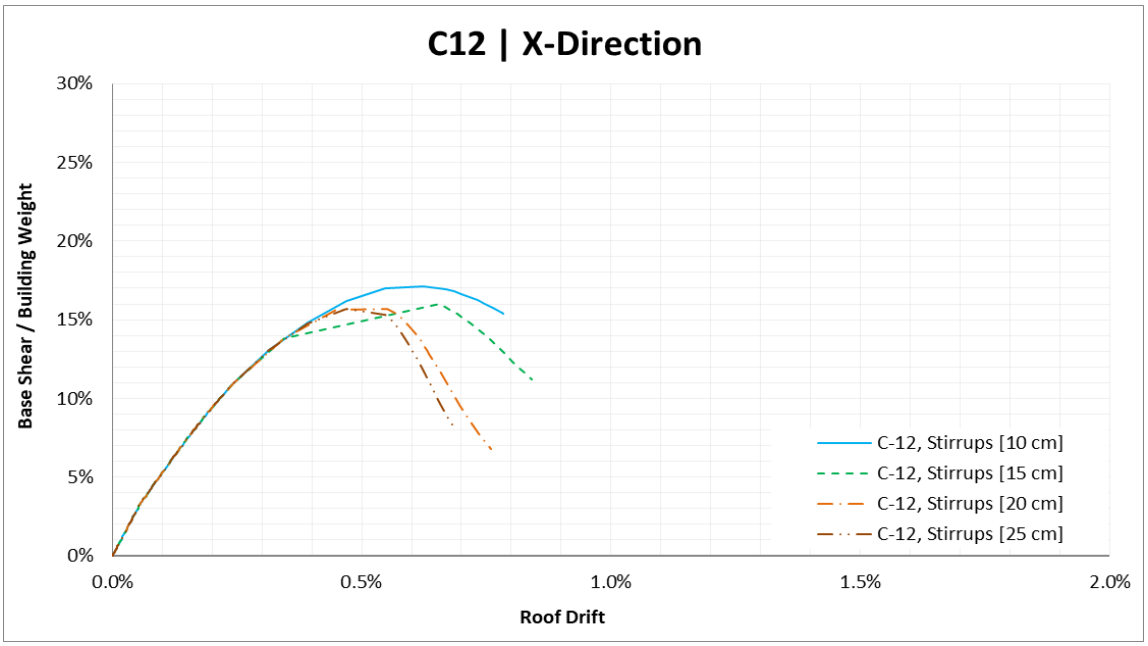

Figure 196: Capacity curves for C Template Design building, for C12 concrete with different stirrups spacings in X direction

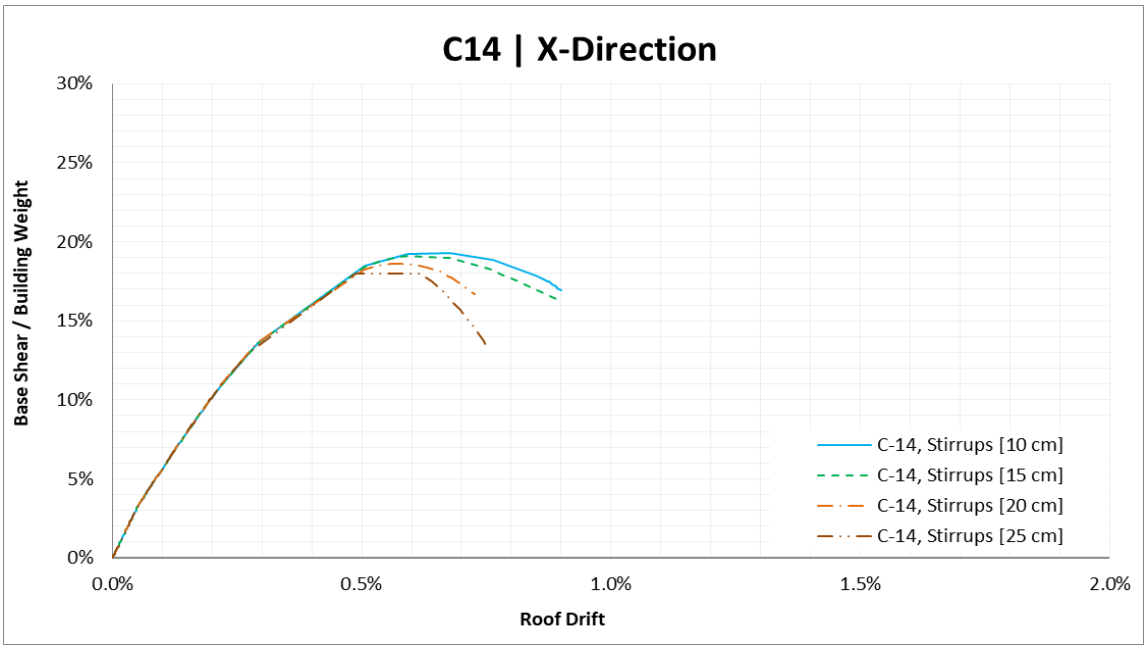

Figure 197: Capacity curves for C Template Design building, for C14 concrete with different stirrups spacings in X direction

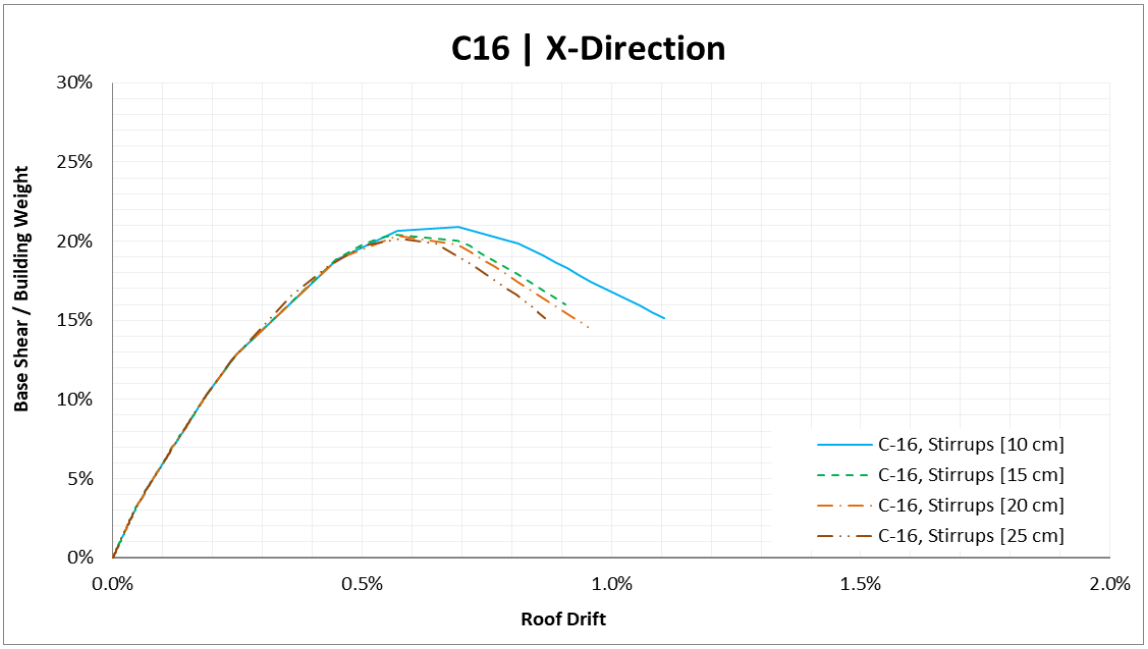

Figure 198: Capacity curves for C Template Design building, for C16 concrete with different stirrups spacings in X direction

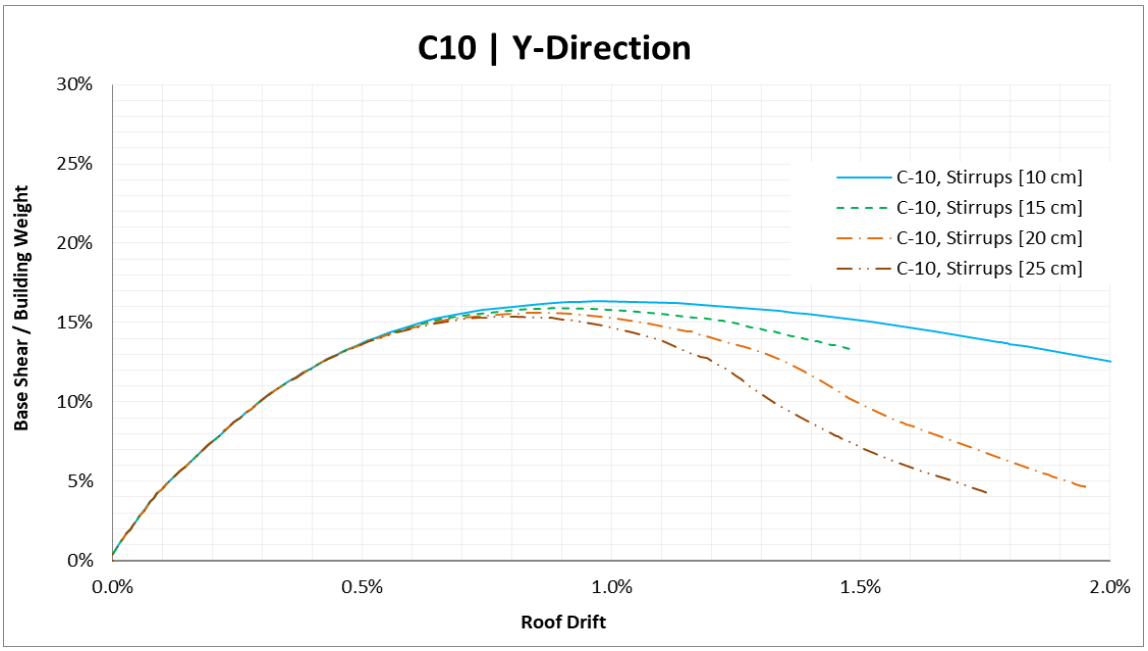

Figure 199: Capacity curves for C Template Design building, for C10 concrete with different stirrups spacings in Y direction

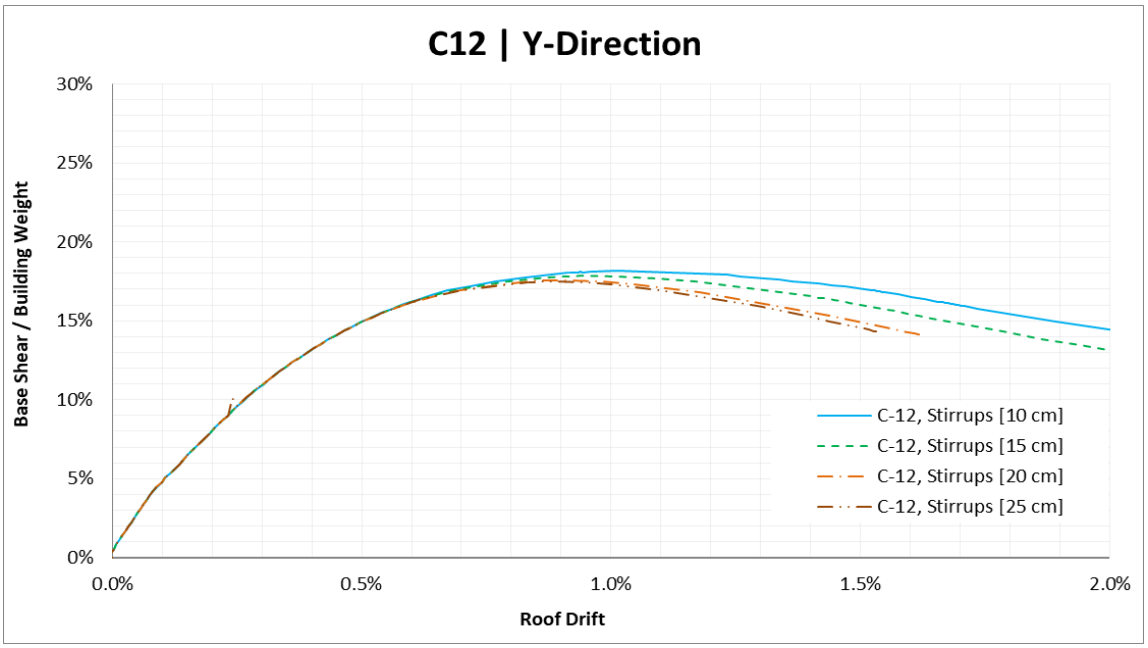

Figure 200: Capacity curves for C Template Design building, for C12 concrete with different stirrups spacings in Y direction

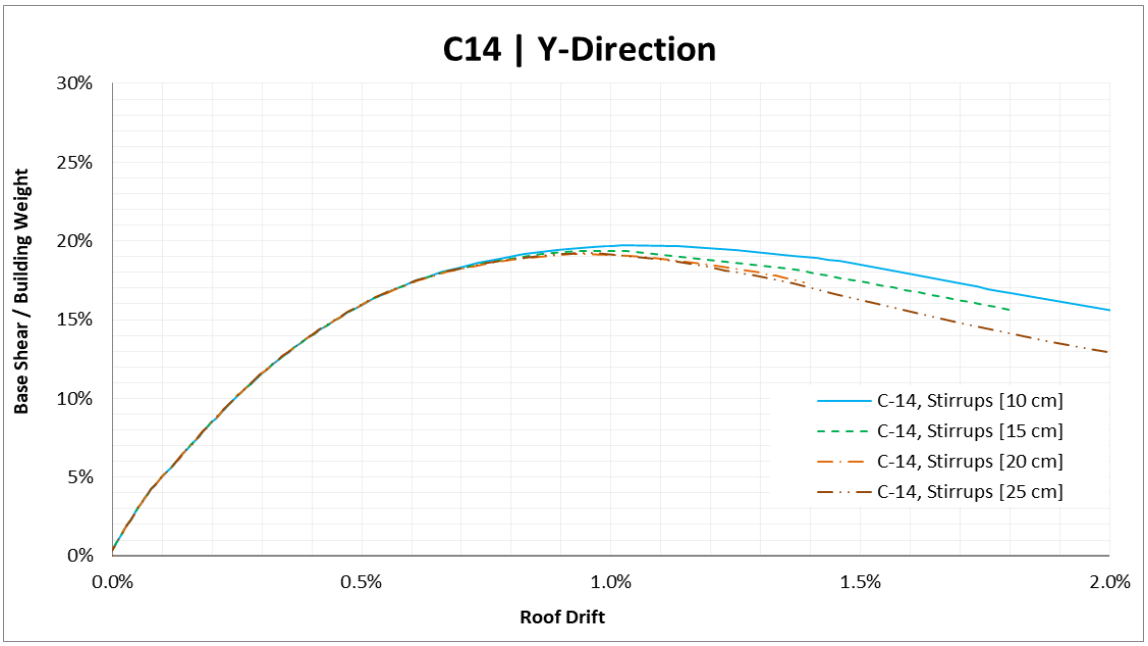

Figure 201: Capacity curves for C Template Design building, for C14 concrete with different stirrups spacings in Y direction

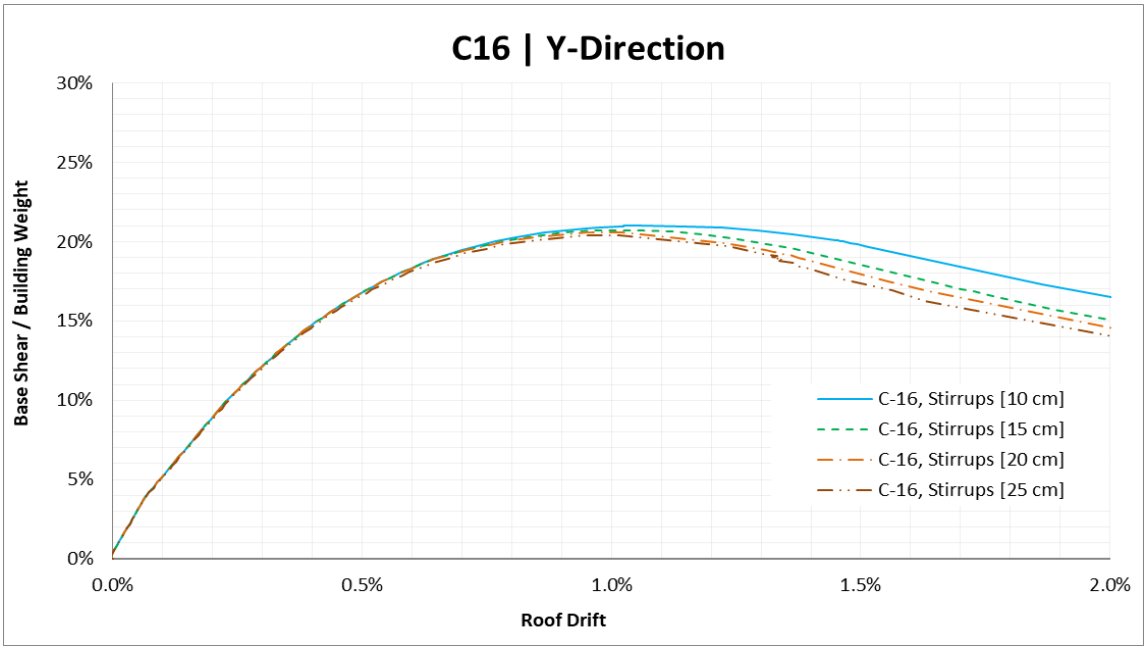

Figure 202: Capacity curves for C Template Design building, for C16 concrete with different stirrups spacings in Y direction

D Template

Table 22: SPO Limit States for D Template Building

Direction	Concrete Class	Stirrups Spacing	IO		LS		CP	
			Δ/H	V/W	Δ/H	V/W	Δ/H	V/W
X_Frame	C10	10 cm	0.88%	6.4%	1.68%	6.3%	2.48%	6.2%
		15 cm	0.87%	6.3%	1.58%	7.1%	2.28%	6.1%
		20 cm	0.85%	6.3%	1.46%	6.1%	2.07%	6.0%
		25 cm	0.85%	6.2%	1.45%	6.0%	2.04%	5.9%
	C12	10 cm	0.92%	7.2%	1.81%	7.1%	2.69%	7.0%
		15 cm	0.93%	7.2%	1.74%	8.0%	2.56%	7.0%
		20 cm	0.93%	7.2%	1.65%	7.0%	2.38%	6.8%
		25 cm	0.90%	7.1%	1.58%	7.9%	2.26%	6.7%
	C14	10 cm	0.96%	8.0%	1.92%	7.9%	2.88%	7.8%
		15 cm	0.96%	8.0%	1.70%	7.8%	2.45%	7.6%
		20 cm	0.96%	8.0%	1.77%	7.8%	2.59%	7.6%
		25 cm	0.96%	8.0%	1.72%	7.7%	2.48%	7.5%
	C16	10 cm	0.99%	8.7%	1.81%	9.9%	2.62%	8.4%
		15 cm	0.97%	8.6%	1.77%	8.4%	2.58%	8.2%
		20 cm	0.97%	8.6%	1.76%	8.4%	2.56%	8.1%
		25 cm	0.97%	8.5%	1.74%	8.3%	2.51%	8.0%
Y_Frame	C10	10 cm	0.69%	3.7%	1.53%	3.8%	2.37%	3.9%
		15 cm	0.69%	3.7%	1.47%	3.8%	2.25%	3.9%
		20 cm	0.69%	3.7%	1.41%	3.8%	2.13%	3.9%
		25 cm	0.65%	3.7%	1.34%	3.8%	2.02%	3.8%
	C12	10 cm	0.73%	4.1%	1.64%	4.2%	2.54%	4.3%
		15 cm	0.73%	4.1%	1.56%	4.2%	2.40%	4.3%
		20 cm	0.73%	4.1%	1.53%	4.2%	2.33%	4.3%
		25 cm	0.73%	4.1%	1.50%	4.2%	2.26%	4.3%
	C14	10 cm	0.69%	4.3%	1.63%	4.5%	2.57%	4.7%
		15 cm	0.69%	4.3%	1.61%	4.5%	2.52%	4.7%
		20 cm	0.67%	4.3%	1.57%	4.5%	2.46%	4.7%
		25 cm	0.64%	4.3%	1.49%	4.5%	2.34%	4.7%
	C16	10 cm	0.73%	4.9%	1.77%	5.2%	2.80%	5.4%
		15 cm	0.73%	4.9%	1.67%	5.1%	2.61%	5.4%
		20 cm	0.73%	4.9%	1.63%	5.1%	2.53%	5.4%
		25 cm	0.70%	4.8%	1.55%	5.0%	2.40%	5.3%

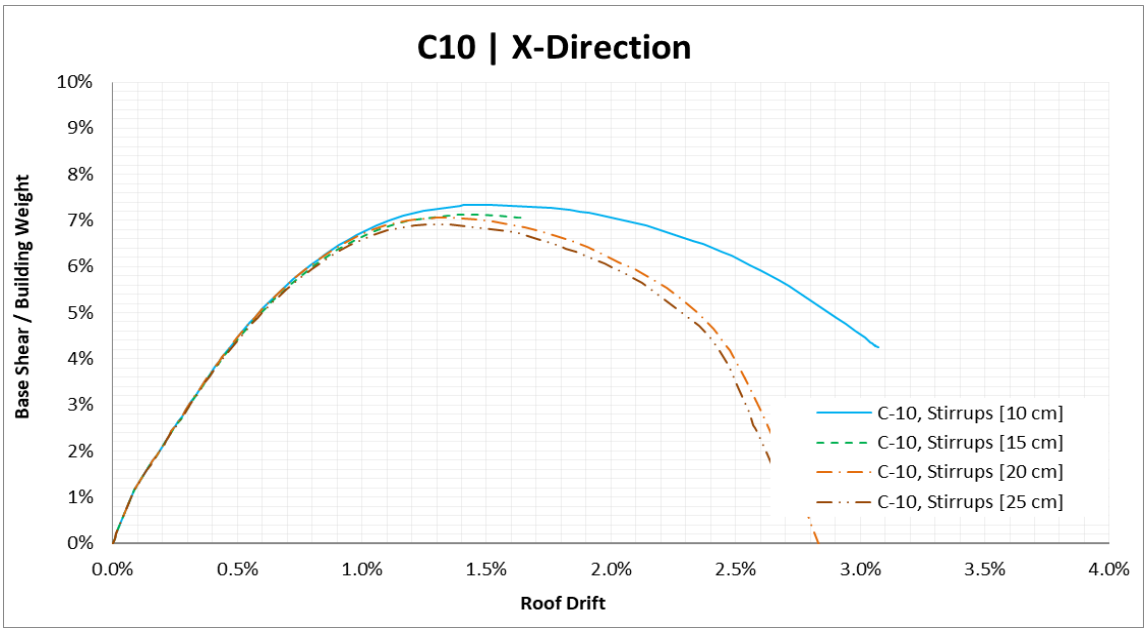

Figure 203: Capacity curves for D Template Design building, for C10 concrete with different stirrups spacings in X direction

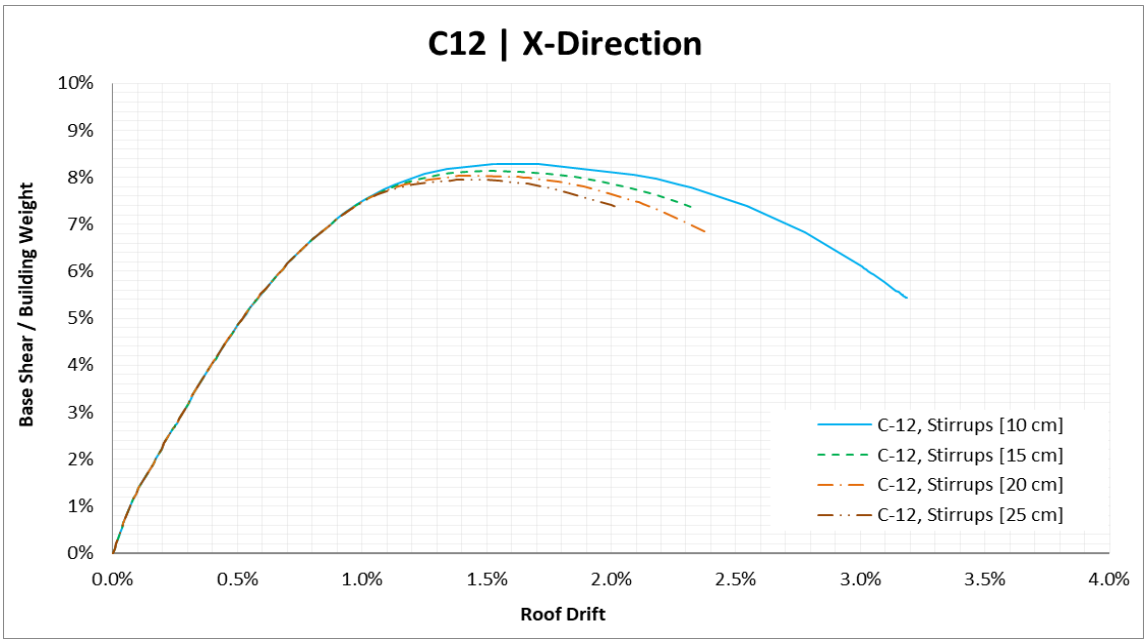

Figure 204: Capacity curves for D Template Design building, for C12 concrete with different stirrups spacings in X direction

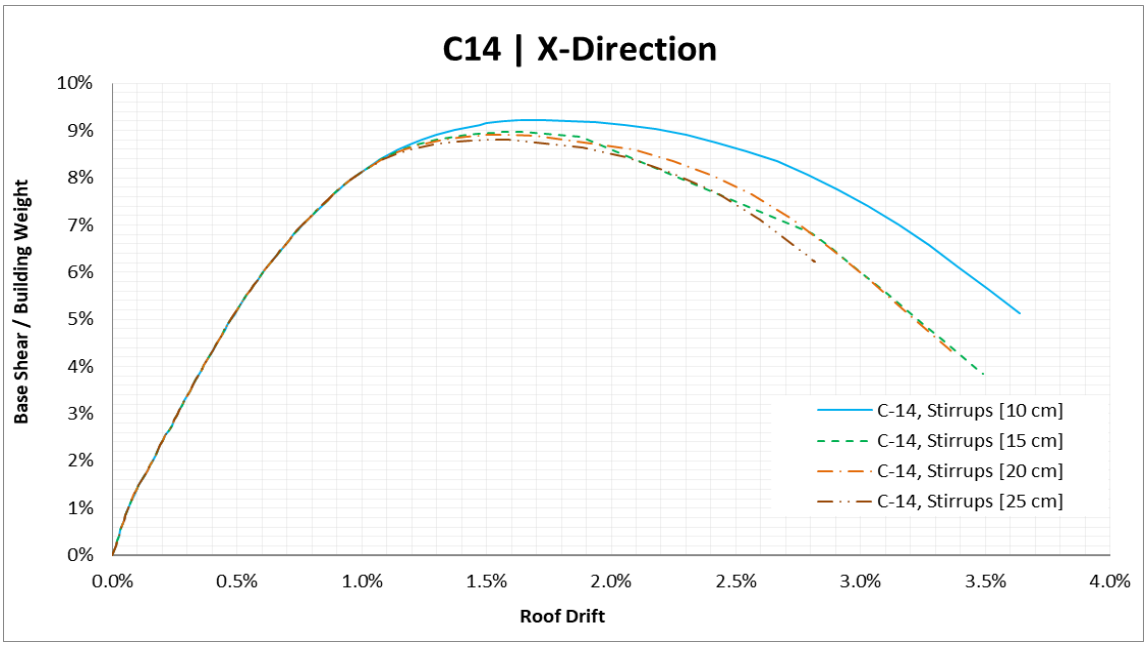

Figure 205: Capacity curves for D Template Design building, for C14 concrete with different stirrups spacings in X direction

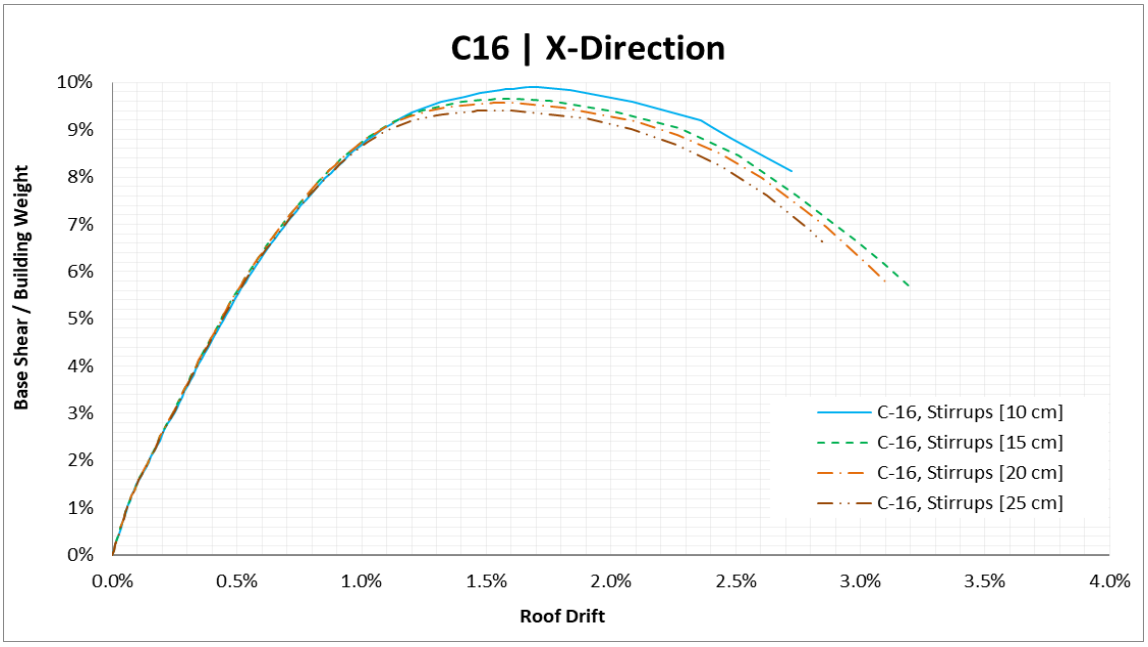

Figure 206: Capacity curves for D Template Design building, for C16 concrete with different stirrups spacings in X direction

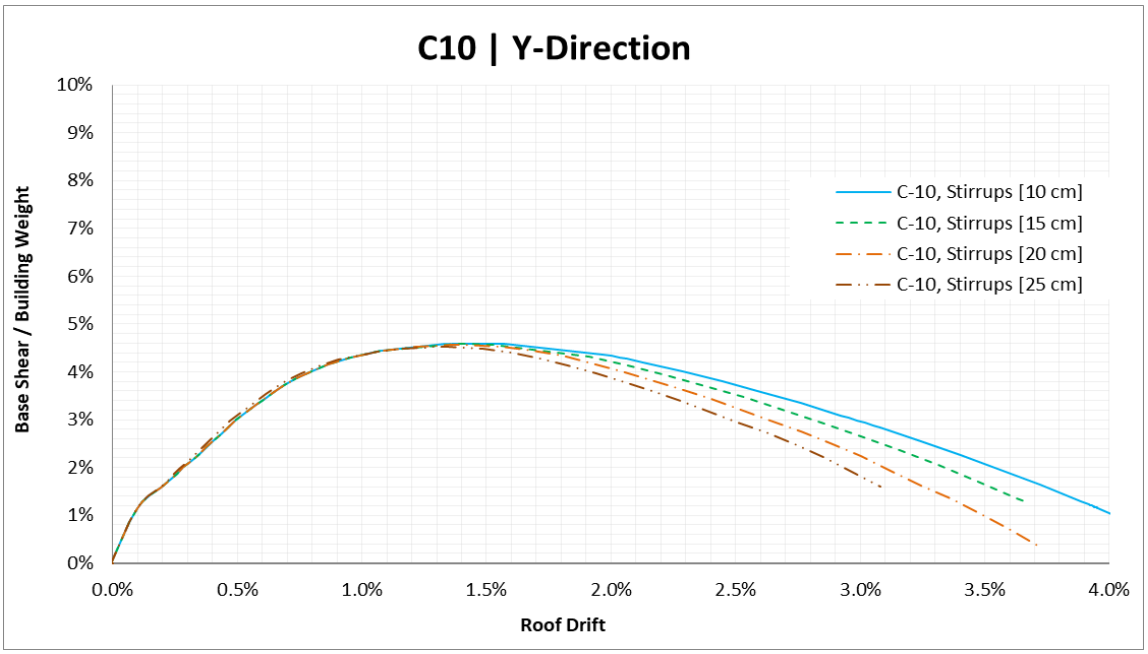

Figure 207: Capacity curves for D Template Design building, for C10 concrete with different stirrups spacings in Y direction

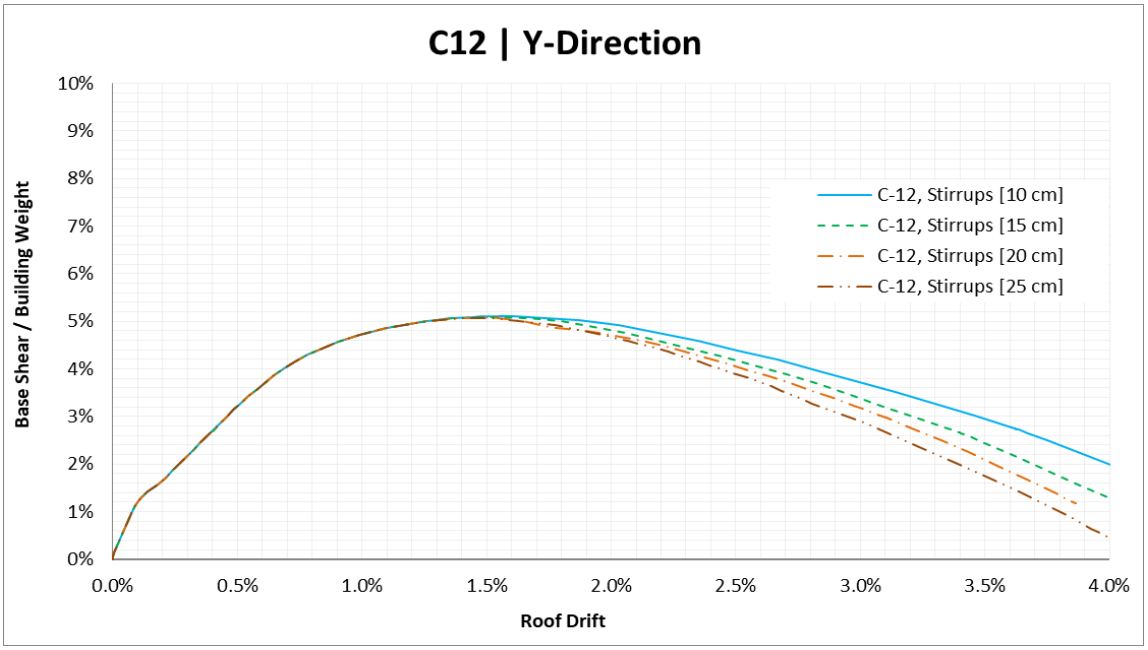

Figure 208: Capacity curves for D Template Design building, for C12 concrete with different stirrups spacings in Y direction

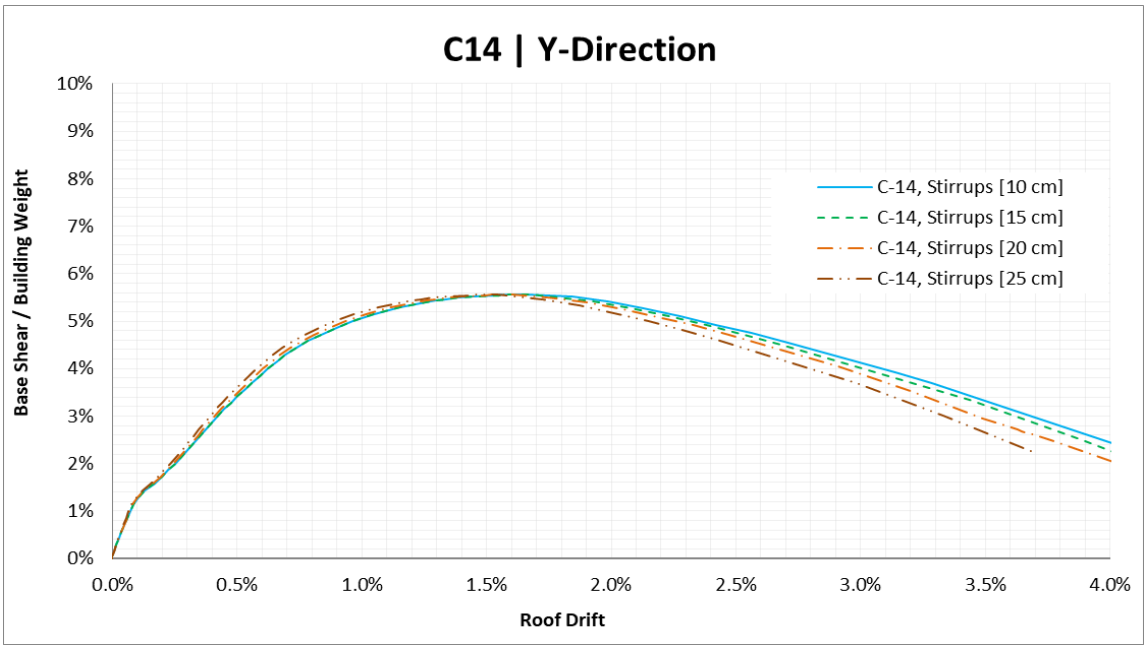

Figure 209: Capacity curves for D Template Design building, for C14 concrete with different stirrups spacings in Y direction

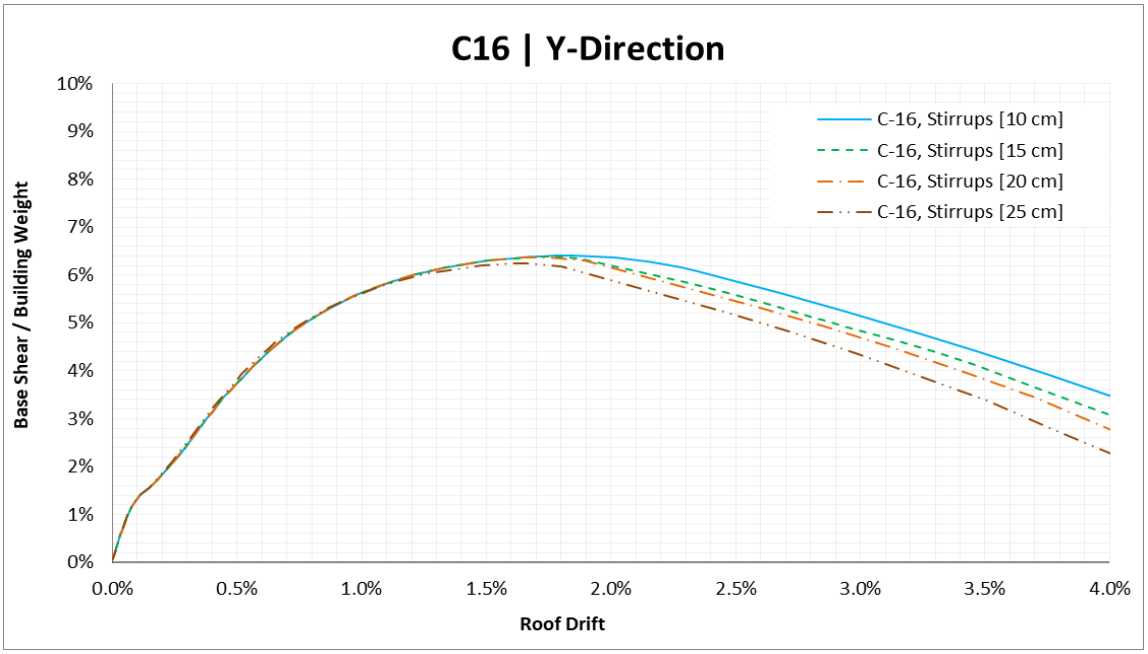

Figure 210: Capacity curves for D Template Design building, for C16 concrete with different stirrups spacings in Y direction

E Template

Table 23: SPO Limit States for E Template Building

Direction	Concrete Class	Stirrups Spacing	IO		LS		CP	
			Δ/H	V/W	Δ/H	V/W	Δ/H	V/W
X_Frame	C10	10 cm	0.50%	4.9%	44.76%	0.0%	0.96%	9.4%
		15 cm	0.50%	4.8%	44.76%	0.0%	0.93%	9.3%
		20 cm	0.50%	4.7%	44.76%	0.0%	0.90%	9.1%
		25 cm	0.50%	4.7%	44.76%	0.0%	0.89%	9.1%
	C12	10 cm	0.50%	5.3%	44.76%	0.0%	0.99%	10.2%
		15 cm	0.50%	5.2%	44.76%	0.0%	0.95%	10.1%
		20 cm	0.50%	5.1%	44.76%	0.0%	0.92%	10.0%
		25 cm	0.50%	5.1%	44.76%	0.0%	0.92%	9.9%
	C14	10 cm	0.50%	5.6%	44.76%	0.0%	1.03%	10.9%
		15 cm	0.50%	5.6%	44.76%	0.0%	0.97%	10.8%
		20 cm	0.50%	5.5%	44.76%	0.0%	0.94%	10.7%
		25 cm	0.50%	5.5%	44.76%	0.0%	0.92%	10.6%
	C16	10 cm	0.50%	6.2%	44.76%	0.0%	1.09%	12.1%
		15 cm	0.50%	6.2%	44.76%	0.0%	1.02%	12.0%
		20 cm	0.50%	6.1%	44.76%	0.0%	0.98%	11.9%
		25 cm	0.50%	6.1%	44.76%	0.0%	0.96%	11.9%
Y_Frame	C10	10 cm	0.50%	5.7%	44.76%	0.0%	0.99%	11.1%
		15 cm	0.50%	5.6%	44.76%	0.0%	0.92%	10.9%
		20 cm	0.50%	5.6%	44.76%	0.0%	0.88%	10.8%
		25 cm	0.50%	5.5%	44.76%	0.0%	0.84%	10.7%
	C12	10 cm	0.50%	6.2%	44.76%	0.0%	0.99%	12.0%
		15 cm	0.50%	6.1%	44.76%	0.0%	0.93%	11.8%
		20 cm	0.50%	6.0%	44.76%	0.0%	0.90%	11.7%
		25 cm	0.50%	6.0%	44.76%	0.0%	0.90%	11.7%
	C14	10 cm	0.50%	6.6%	44.76%	0.0%	1.01%	12.7%
		15 cm	0.50%	6.5%	44.76%	0.0%	0.95%	12.6%
		20 cm	0.50%	6.4%	44.76%	0.0%	0.94%	12.5%
		25 cm	0.50%	6.4%	44.76%	0.0%	0.93%	12.5%
	C16	10 cm	0.50%	7.2%	44.76%	0.0%	1.15%	13.9%
		15 cm	0.50%	7.1%	44.76%	0.0%	1.06%	13.8%
		20 cm	0.50%	7.1%	44.76%	0.0%	1.03%	13.7%
		25 cm	0.50%	6.9%	44.76%	0.0%	1.03%	13.4%

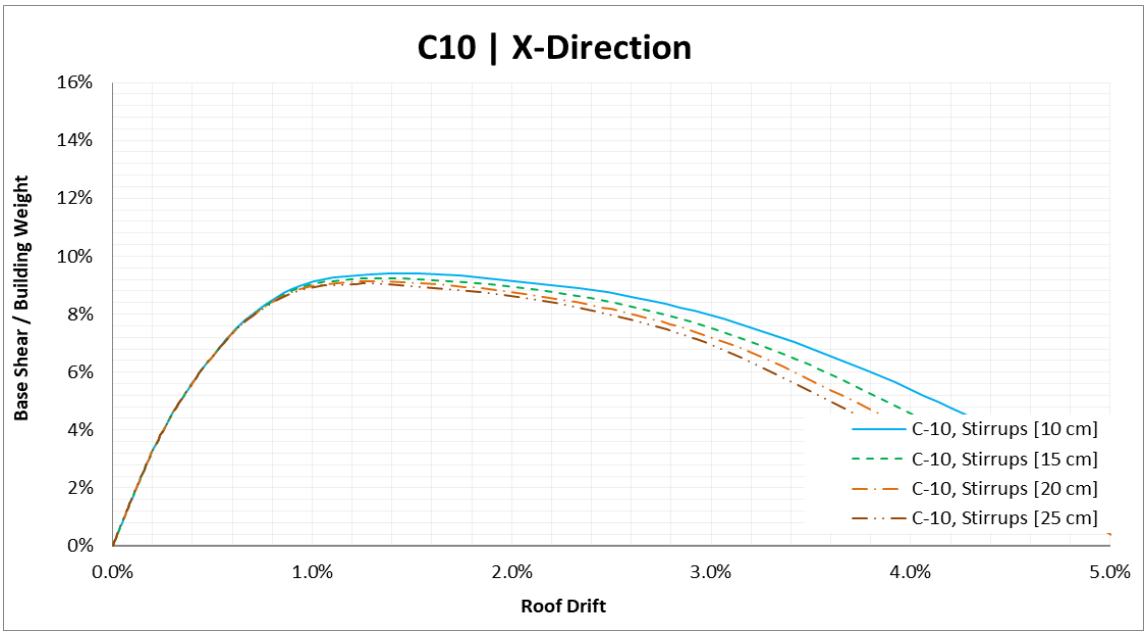

Figure 211: Capacity curves for E Template Design building, for C10 concrete with different stirrups spacings in X direction

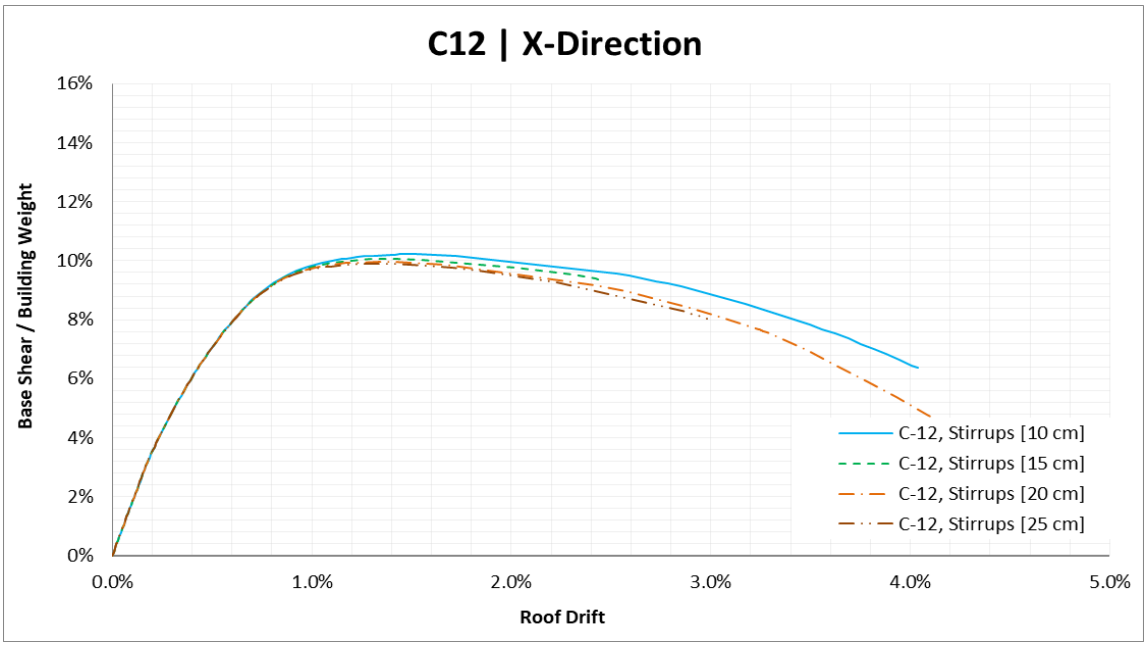

Figure 212: Capacity curves for E Template Design building, for C12 concrete with different stirrups spacings in X direction

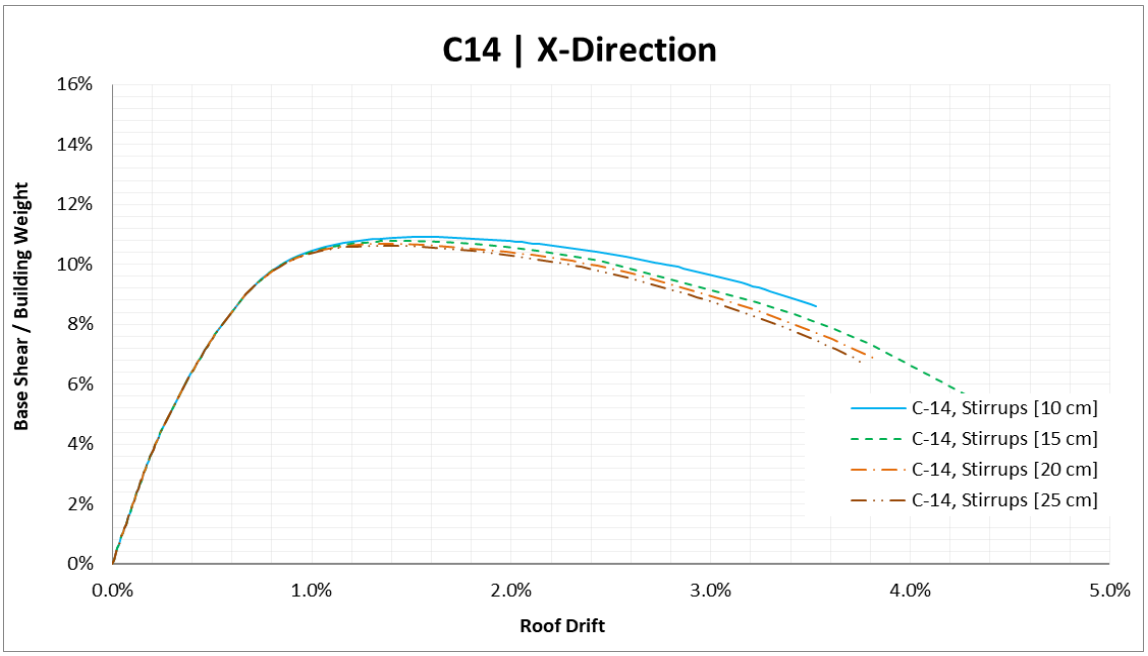

Figure 213: Capacity curves for E Template Design building, for C14 concrete with different stirrups spacings in X direction

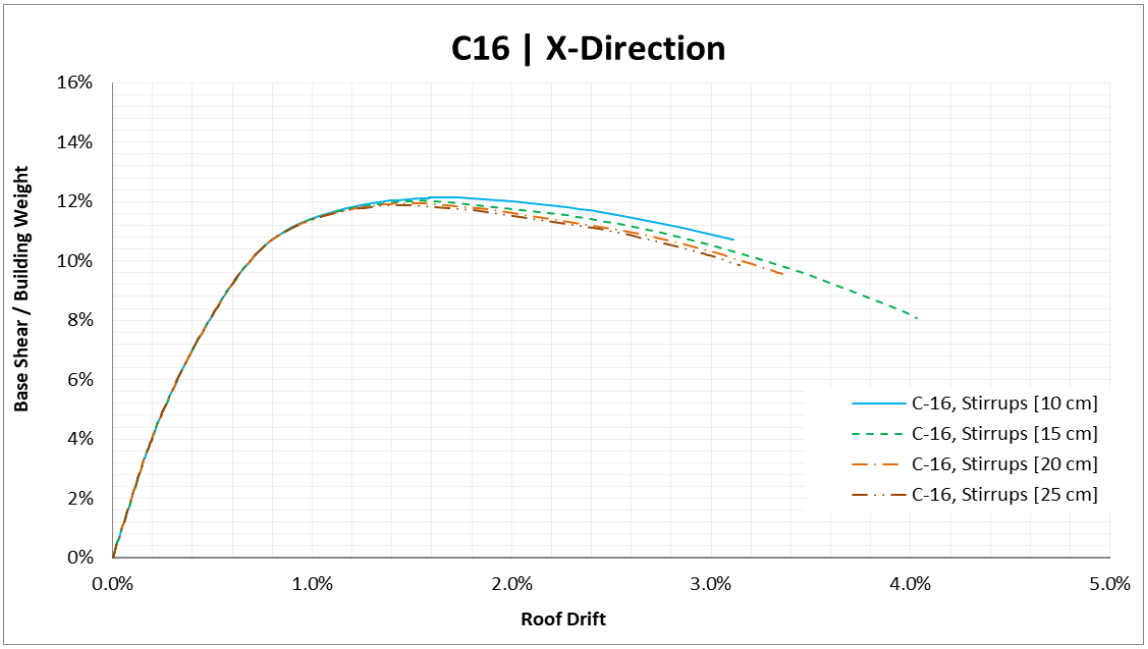

Figure 214: Capacity curves for E Template Design building, for C16 concrete with different stirrups spacings in X direction

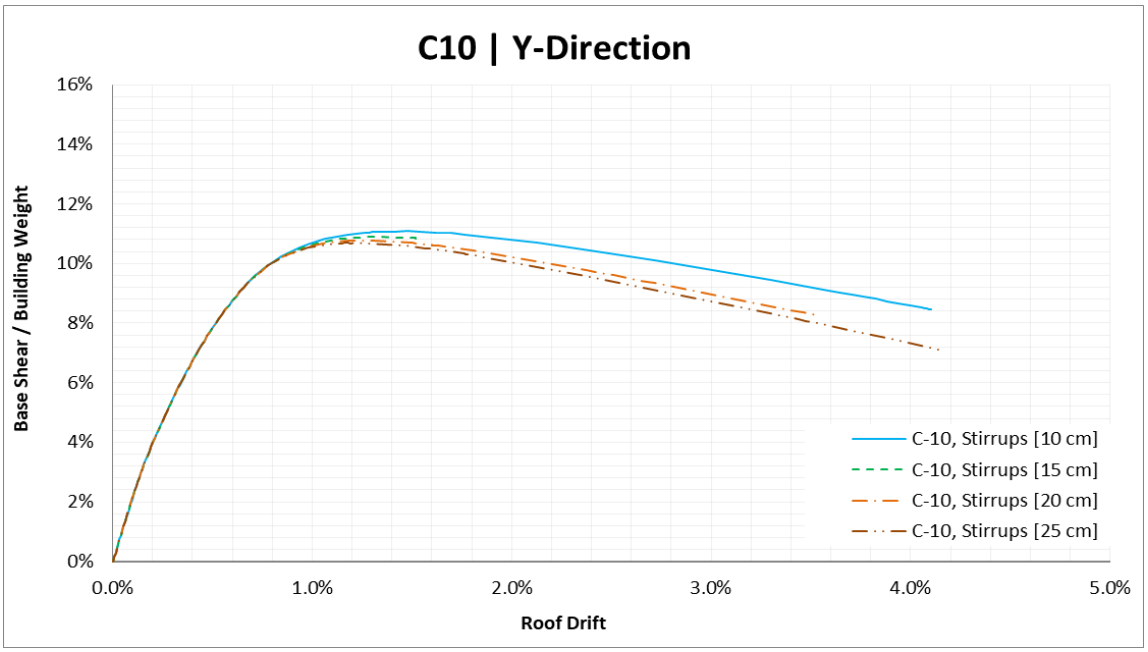

Figure 215: Capacity curves for E Template Design building, for C10 concrete with different stirrups spacings in Y direction

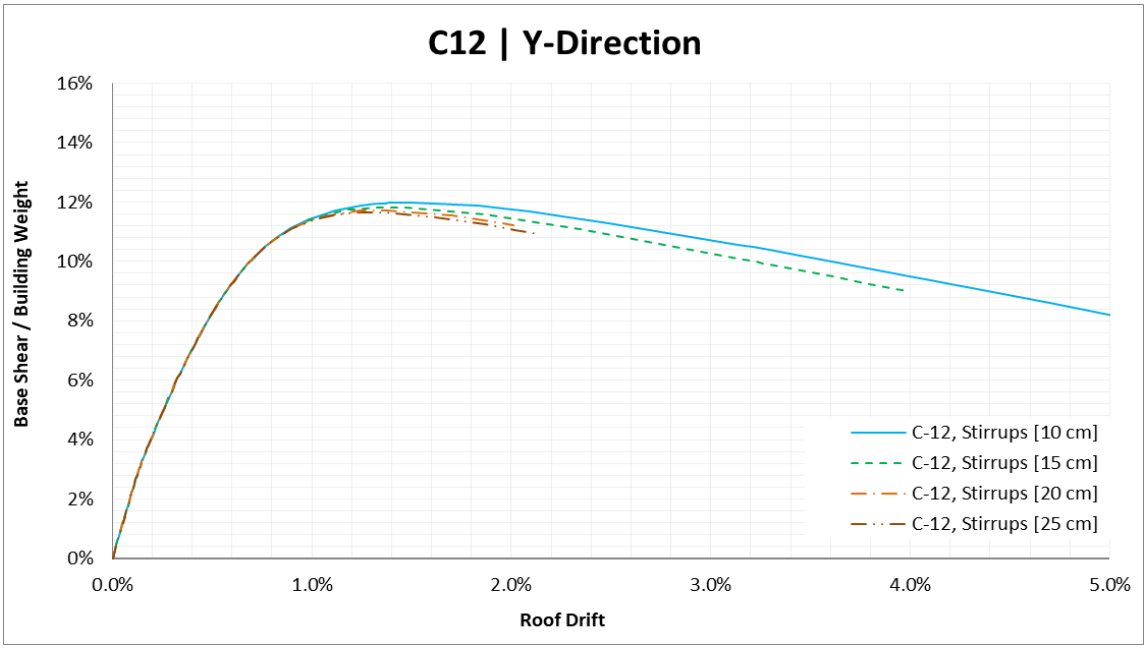

Figure 216: Capacity curves for E Template Design building, for C12 concrete with different stirrups spacings in Y direction

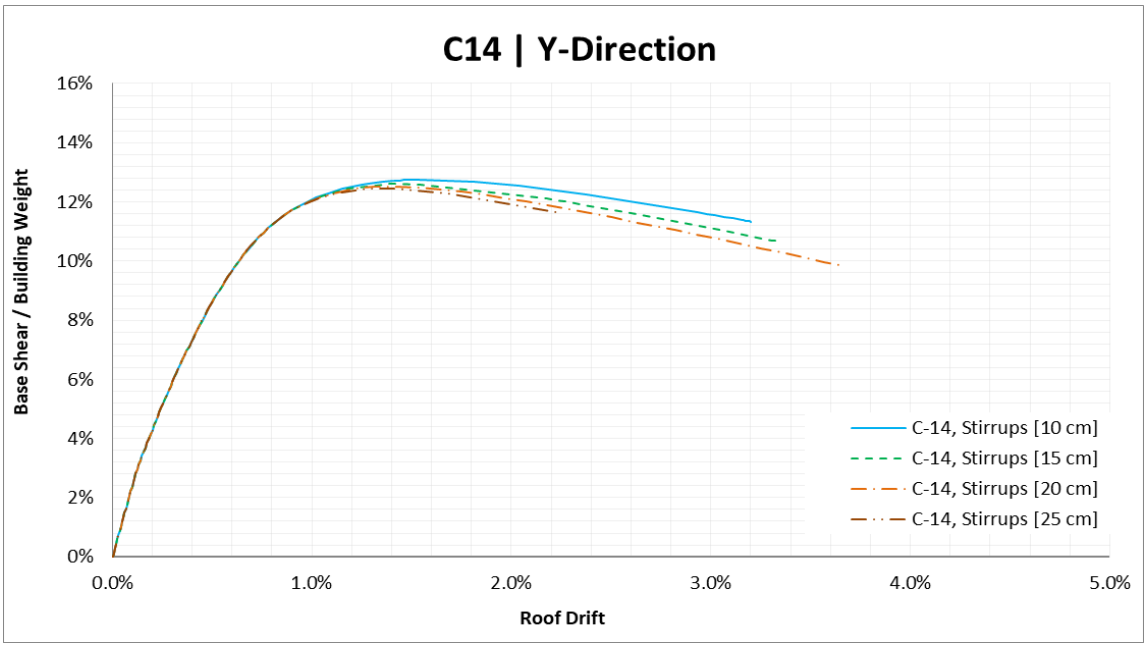

Figure 217: Capacity curves for E Template Design building, for C14 concrete with different stirrups spacings in Y direction

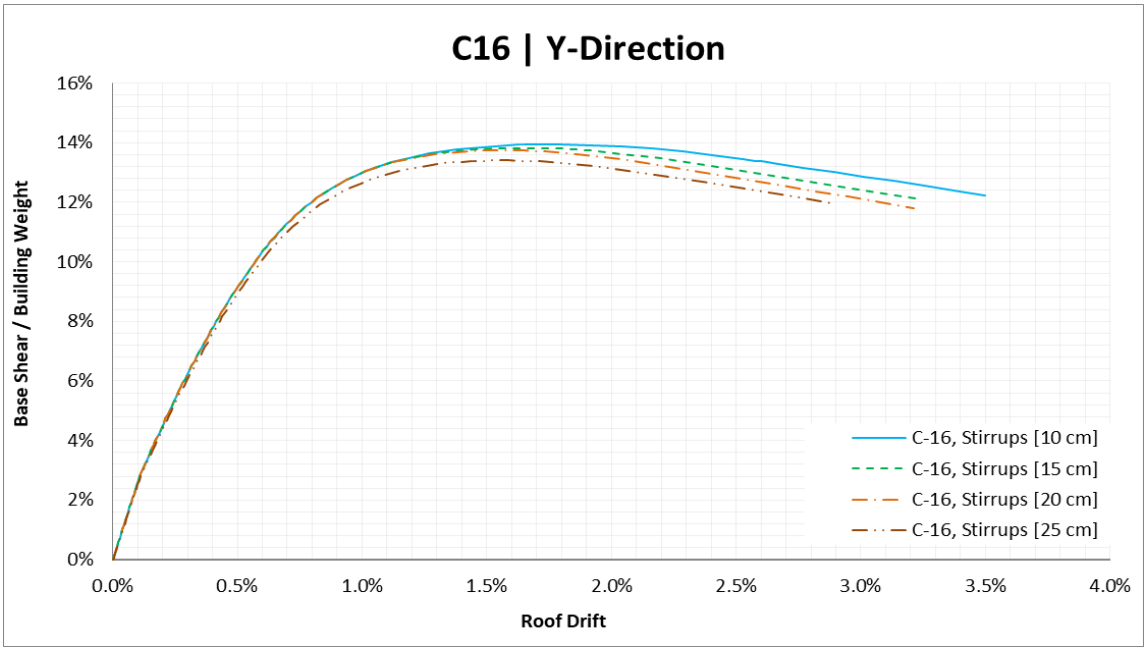

Figure 218: Capacity curves for E Template Design building, for C16 concrete with different stirrups spacings in Y direction

APPENDIX C

Appendix C provides the results of the Incremental Dynamic Analysis (IDA) considering the set of 18 ground motion records. For each of the buildings, the presentation of results is done using based on different ways. For instance, in the beginning the simple IDA curves together with immediate occupancy (IO), collapse prevention (CP) and global instability (GI) is presented. Furthermore, IDA fractiles summarized as 16%, 50% and 84% percentiles are provided together with IO, CP and GI limit states. Additionally, the values for each of the limit states is presented in a separate table. Finally, the comparison of IDA median and SPO curves are illustrated for each of the buildings of this study. In this analysis, the combinations used are C16 and C10 whereas the building is analyses in x- and y-direction.

A Template IDA curves

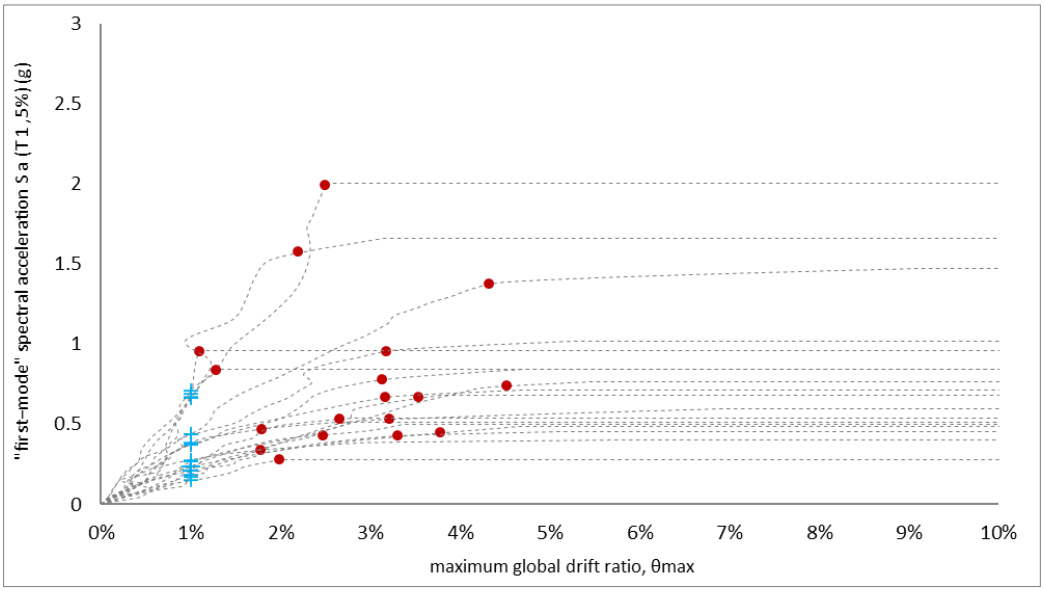

Figure 219: IDA curves for A Template, C16 concrete in x-direction together with IO and CP limit states

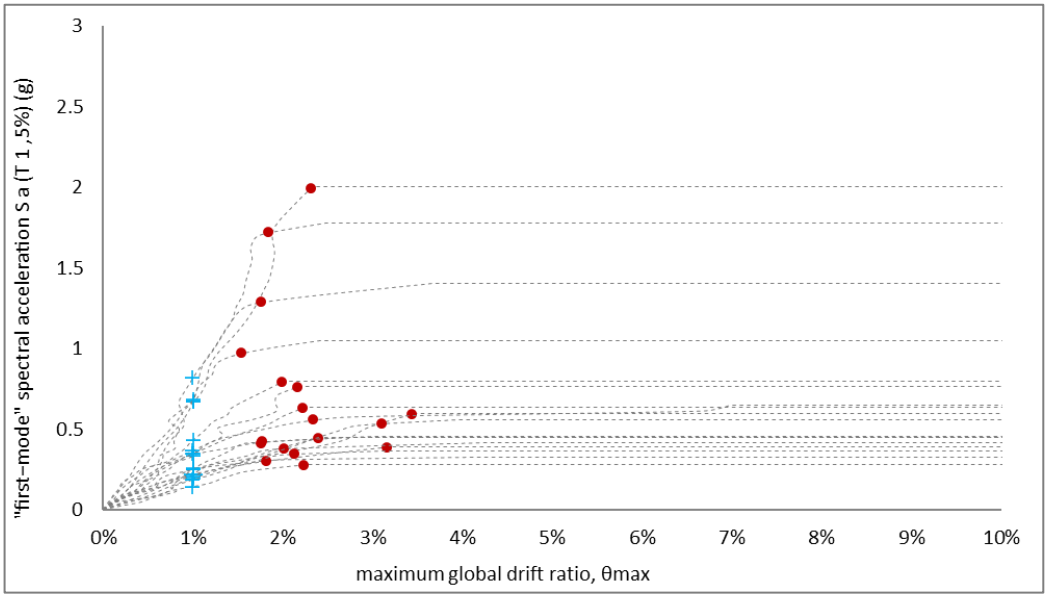

Figure 220: IDA curves for A Template, C10 concrete in x-direction together with IO and CP limit states

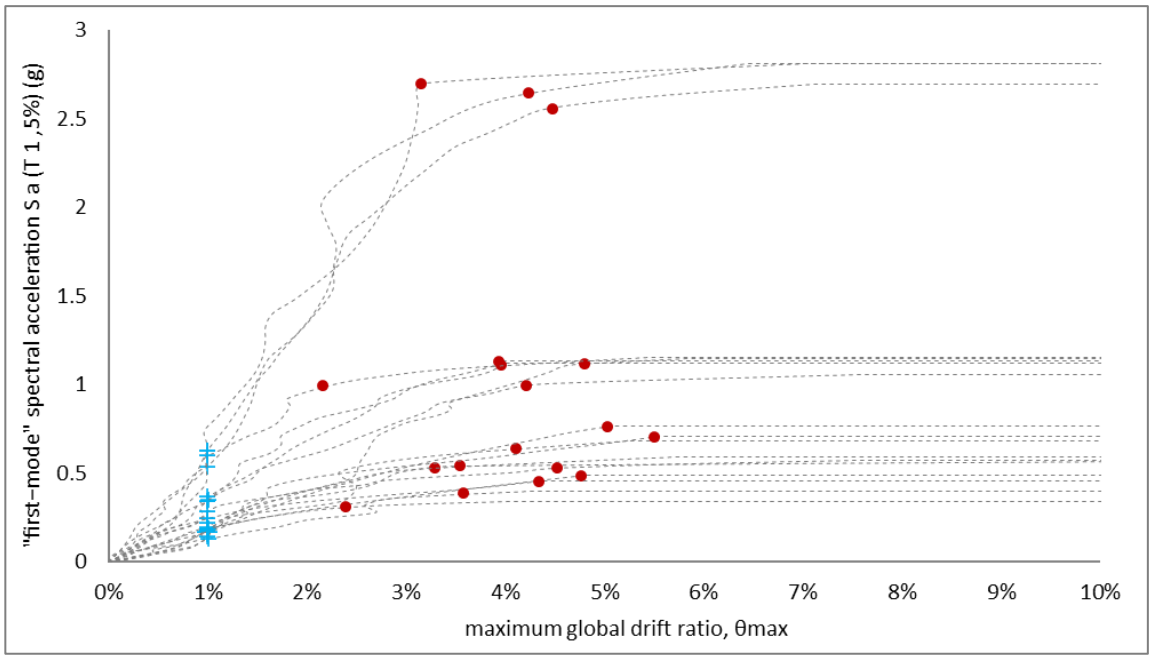

Figure 221: IDA curves for A Template, C16 concrete in y-direction together with IO and CP limit states

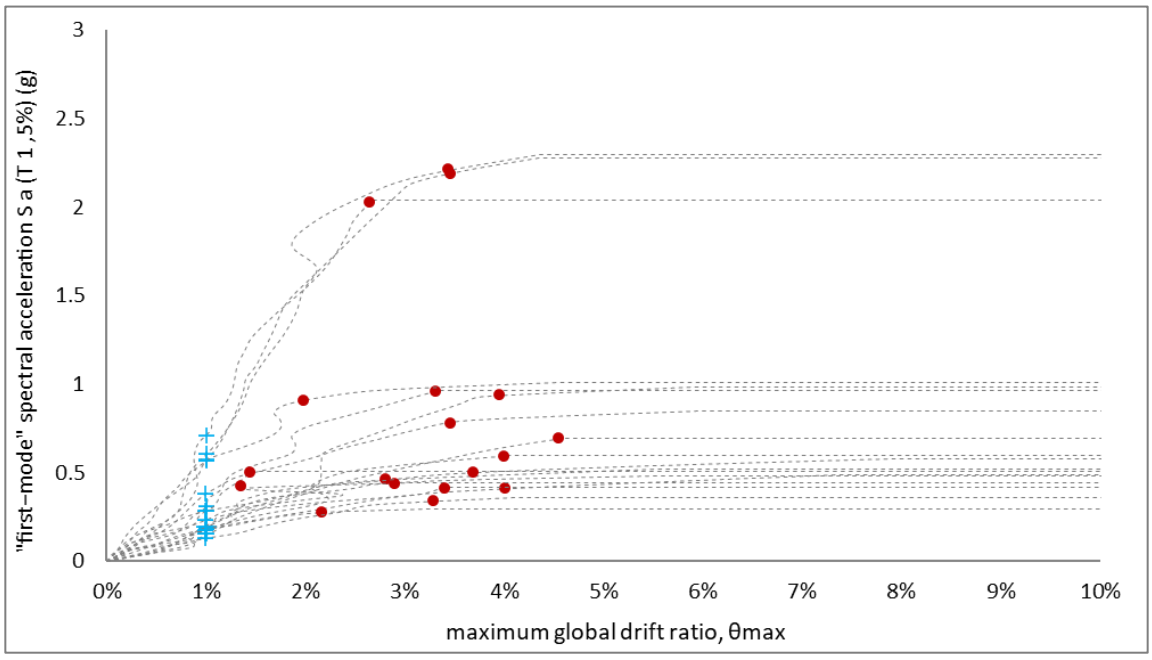

Figure 222: IDA curves for A Template, C10 concrete in y-direction together with IO and CP limit states

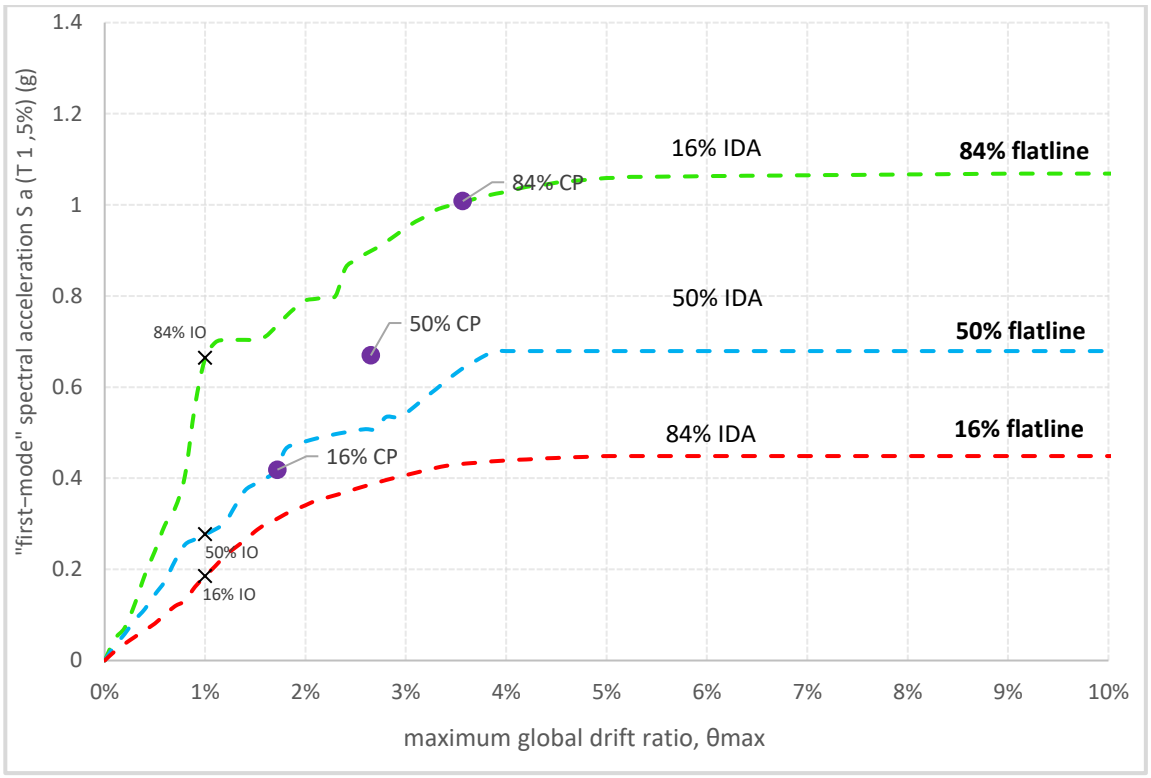

Figure 223: 16%, 50%, 84% IDA fractiles for A Template with concrete C16 in X-direction

Table 24: Intensity and damage measure values for each of the fractiles of corresponding limit states of A Template building with concrete C16 in X-direction

	$Sa_{(T1,5\%)}$ (g)			**Θ_{max} (%)**		
	IM 16%	**IM 50%**	**IM 84%**	**DM 16%**	**DM 50%**	**DM 84%**
IO	0.19	0.28	0.66	1.0%	1.0%	1.0%
CP	0.42	0.67	1.01	1.7%	2.7%	3.6%
GI	0.45	0.68	1.06	+∞	+∞	+∞

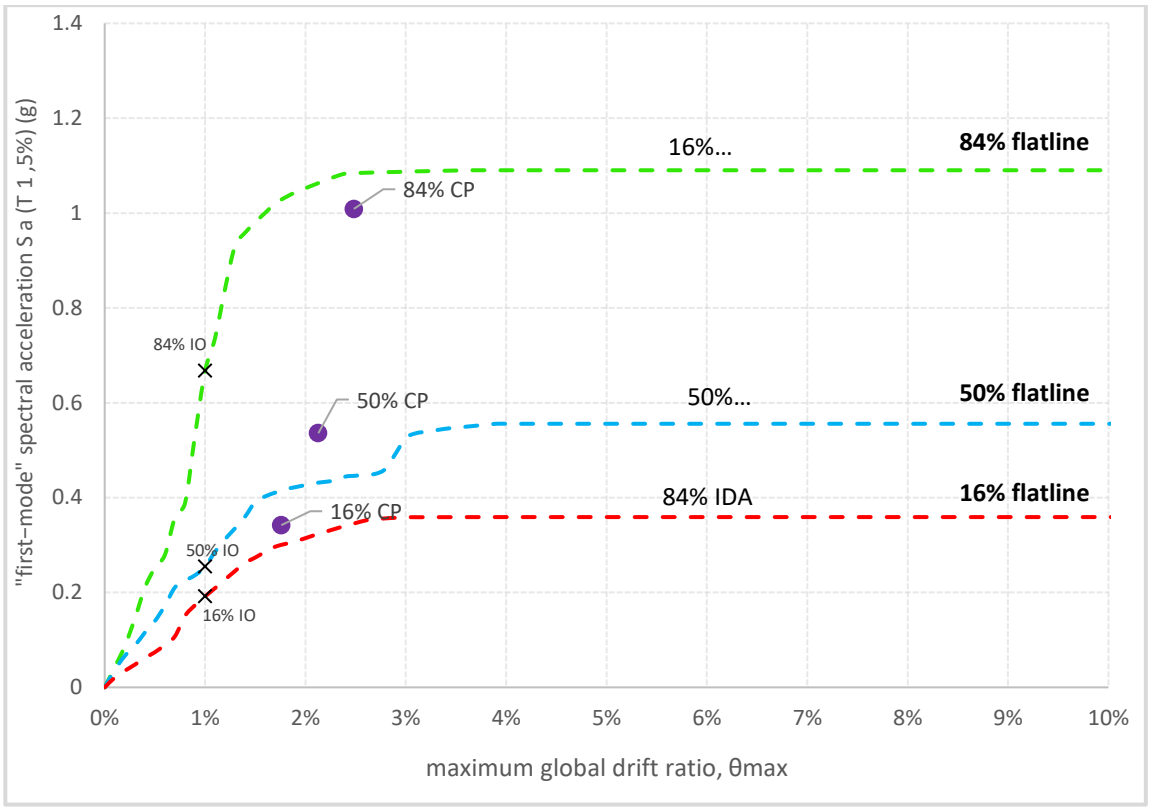

Figure 224: 16%, 50%, 84% IDA fractiles for A Template with concrete C10 in X-direction

Table 25: Intensity and damage measure values for each of the fractiles of corresponding limit states of A Template building with concrete C10 in X-direction

	$Sa_{(T1,5\%)}$ (g)			Θ_{max} (%)		
	IM 16%	**IM 50%**	**IM 84%**	**DM 16%**	**DM 50%**	**DM 84%**
IO	0.19	0.25	0.67	1.0%	1.0%	1.0%
CP	0.34	0.54	1.01	1.8%	2.1%	2.5%
GI	0.36	0.56	1.09	+∞	+∞	+∞

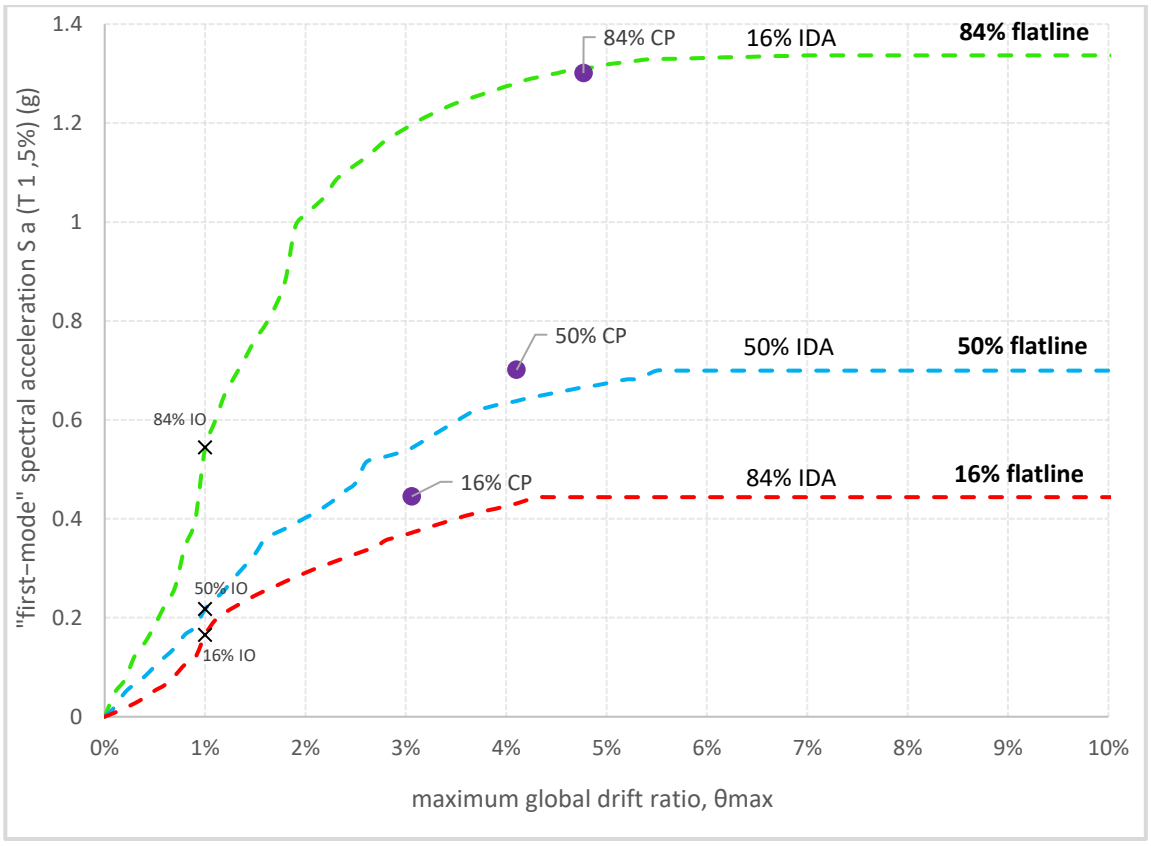

Figure 225: 16%, 50%, 84% IDA fractiles for A Template with concrete C16 in Y-direction

Table 26: Intensity and damage measure values for each of the fractiles of corresponding limit states of A Template building with concrete C16 in Y-direction

	$Sa_{(T1,5\%)}$ (g)			**Θ_{max} (%)**		
	IM 16%	**IM 50%**	**IM 84%**	**DM 16%**	**DM 50%**	**DM 84%**
IO	0.17	0.22	0.54	1.0%	1.0%	1.0%
CP	0.45	0.70	1.30	3.1%	4.1%	4.8%
GI	0.44	0.70	1.34	+∞	+∞	+∞

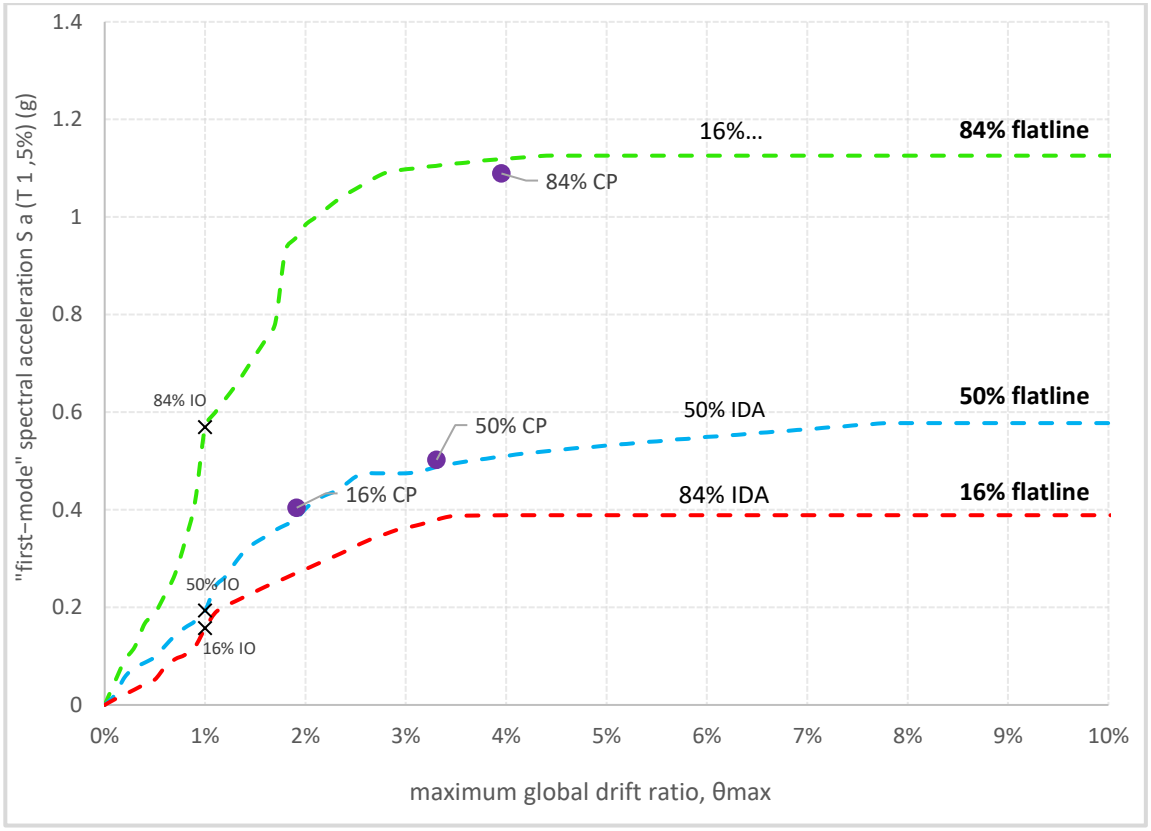

Figure 226: 16%, 50%, 84% IDA fractiles for A Template with concrete C10 in Y-direction

Table 27: Intensity and damage measure values for each of the fractiles of corresponding limit states of A Template building with concrete C10 in Y-direction

	$Sa_{(T1,5\%)}$ (g)			Θ_{max} (%)		
	IM 16%	**IM 50%**	**IM 84%**	**DM 16%**	**DM 50%**	**DM 84%**
IO	0.16	0.19	0.57	1.0%	1.0%	1.0%
CP	0.40	0.50	1.09	1.9%	3.3%	4.0%
GI	0.39	0.58	1.13	+∞	+∞	+∞

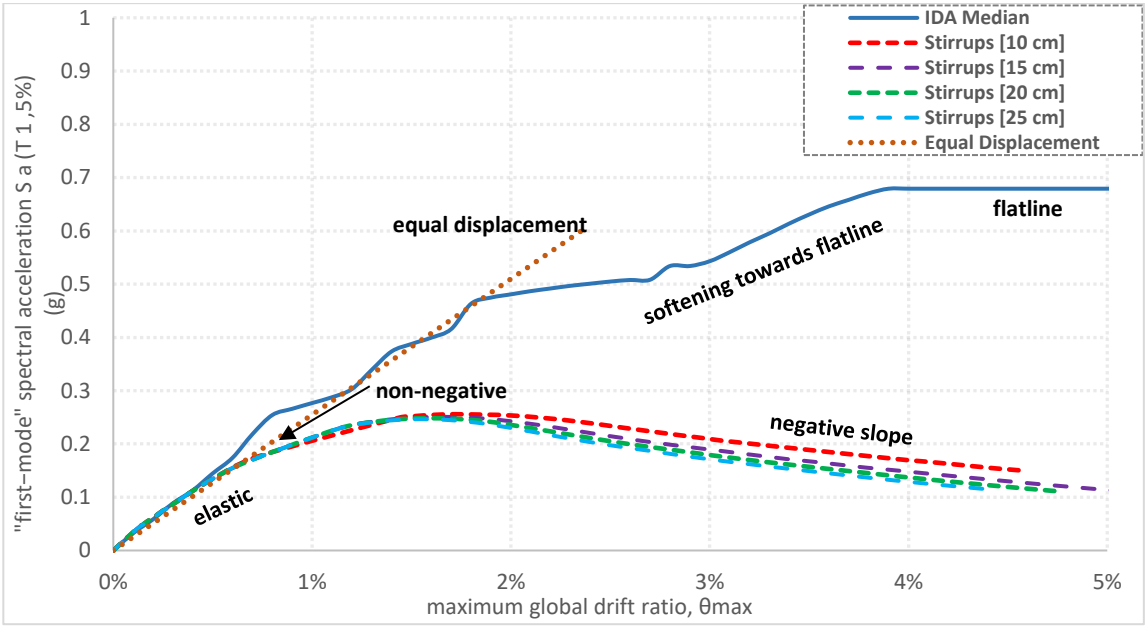

Figure 227: IDA median versus SPO curves for different concrete spacings of A Template building with concrete C16 in X-direction

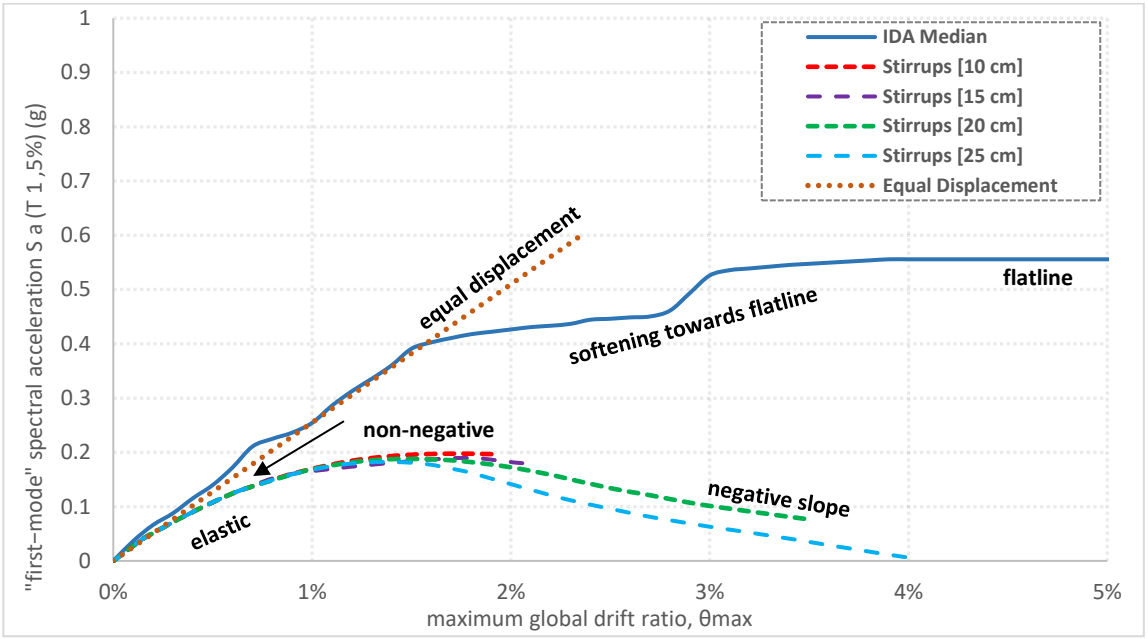

Figure 228: IDA median versus SPO curves for different concrete spacings of A Template building with concrete C10 in X-direction

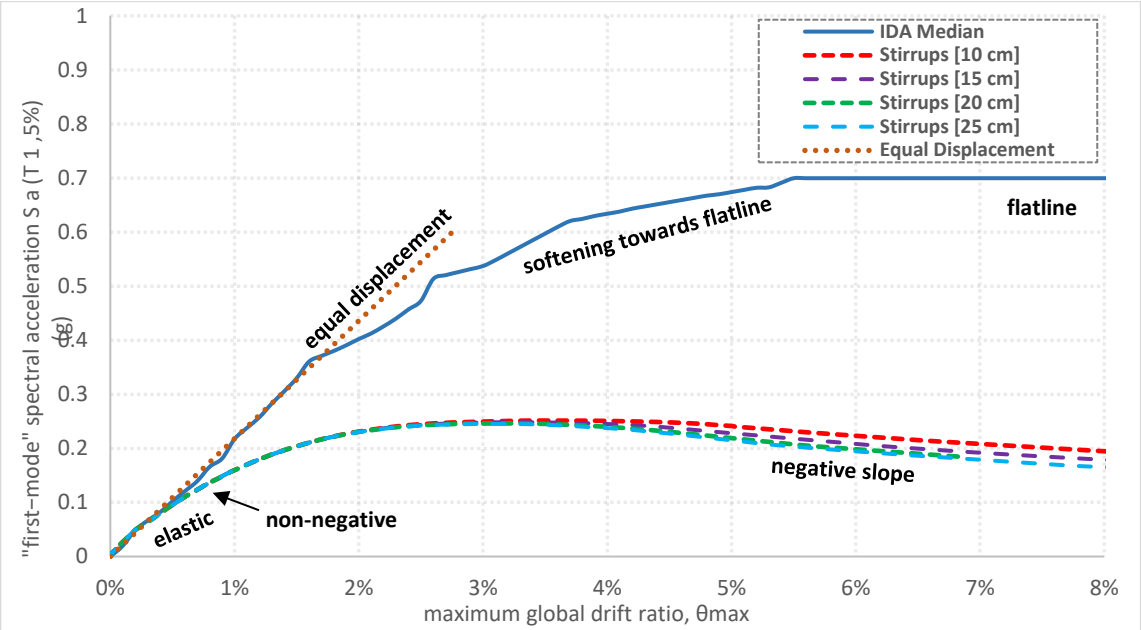

Figure 229: IDA median versus SPO curves for different concrete spacings of A Template building with concrete C16 in Y-direction

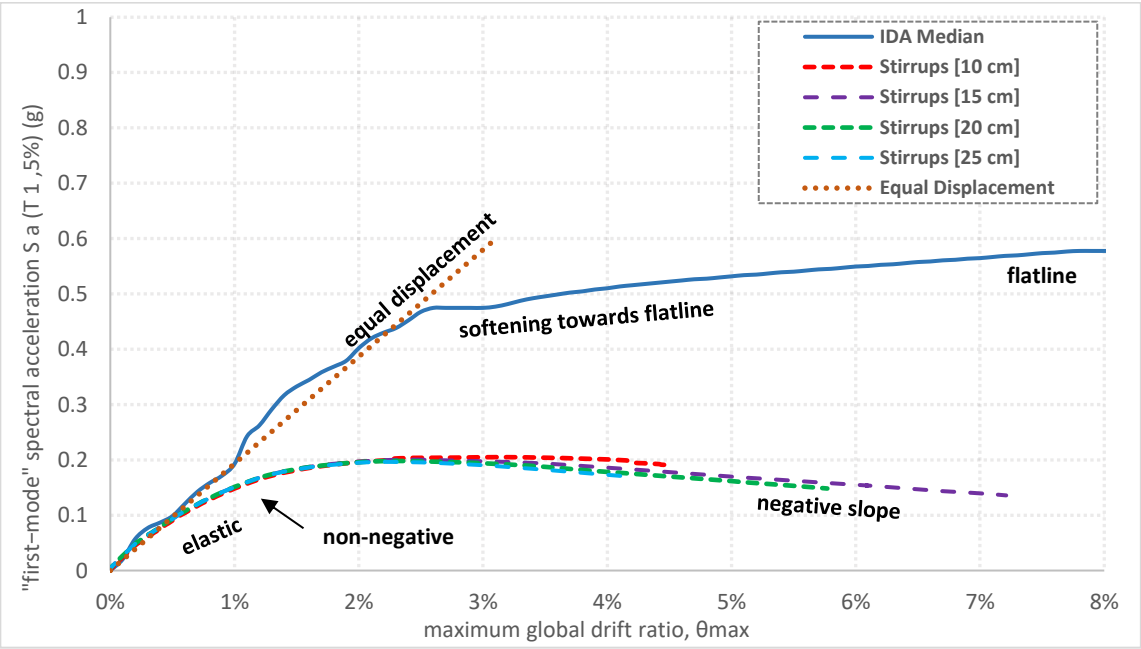

Figure 230: IDA median versus SPO curves for different concrete spacings of A Template building with concrete C10 in Y-direction

B Template IDA curves

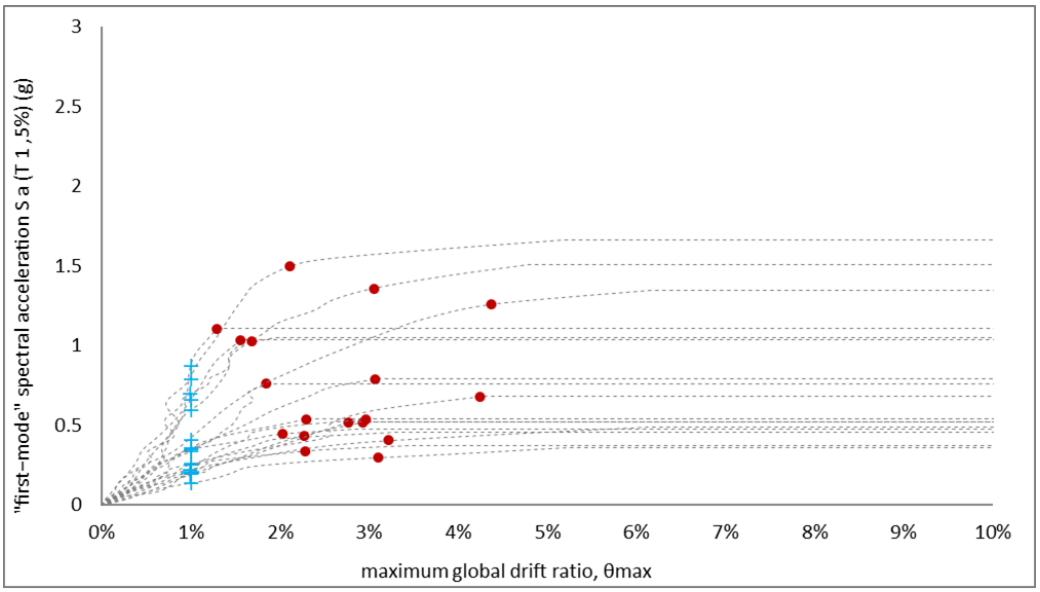

Figure 231: IDA curves for B Template, C16 concrete in x-direction together with IO and CP limit states

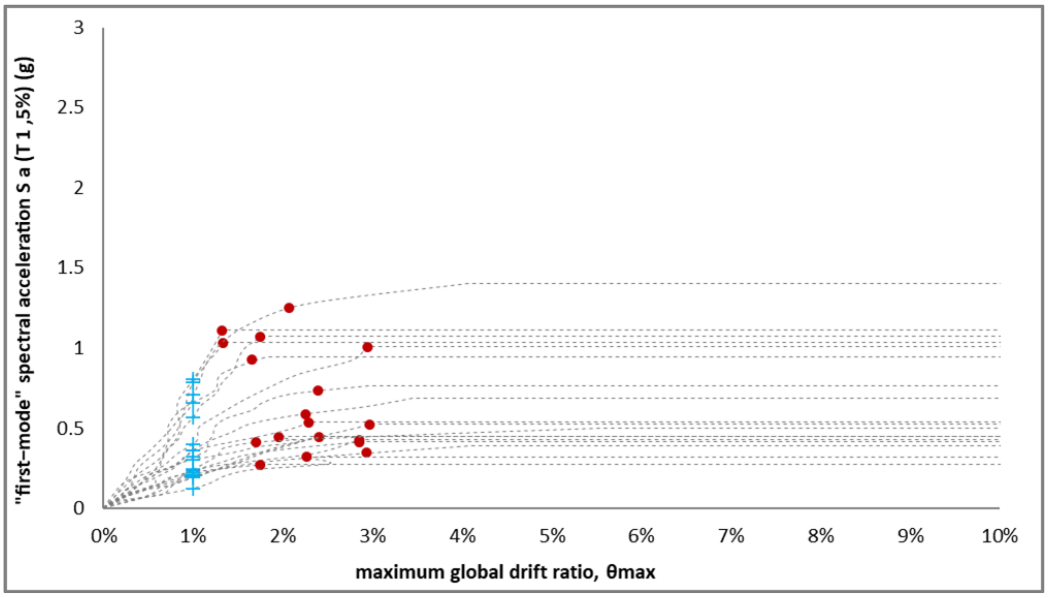

Figure 232: IDA curves for B Template, C10 concrete in x-direction together with IO and CP limit states

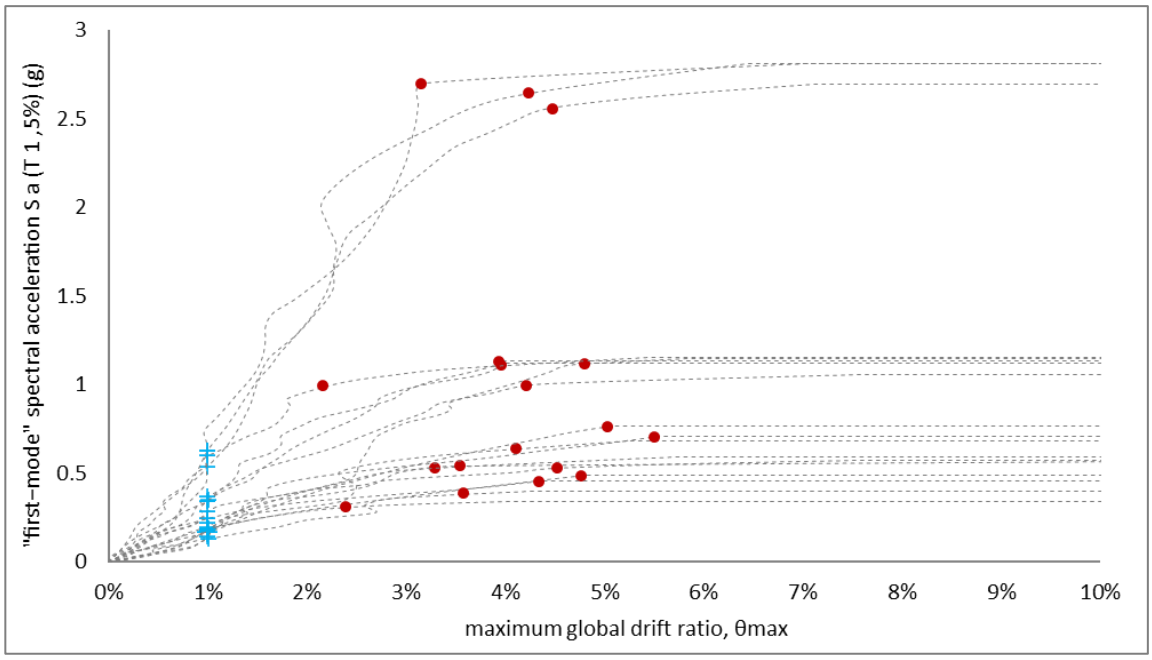

Figure 233: IDA curves for B Template, C16 concrete in y-direction together with IO and CP limit states

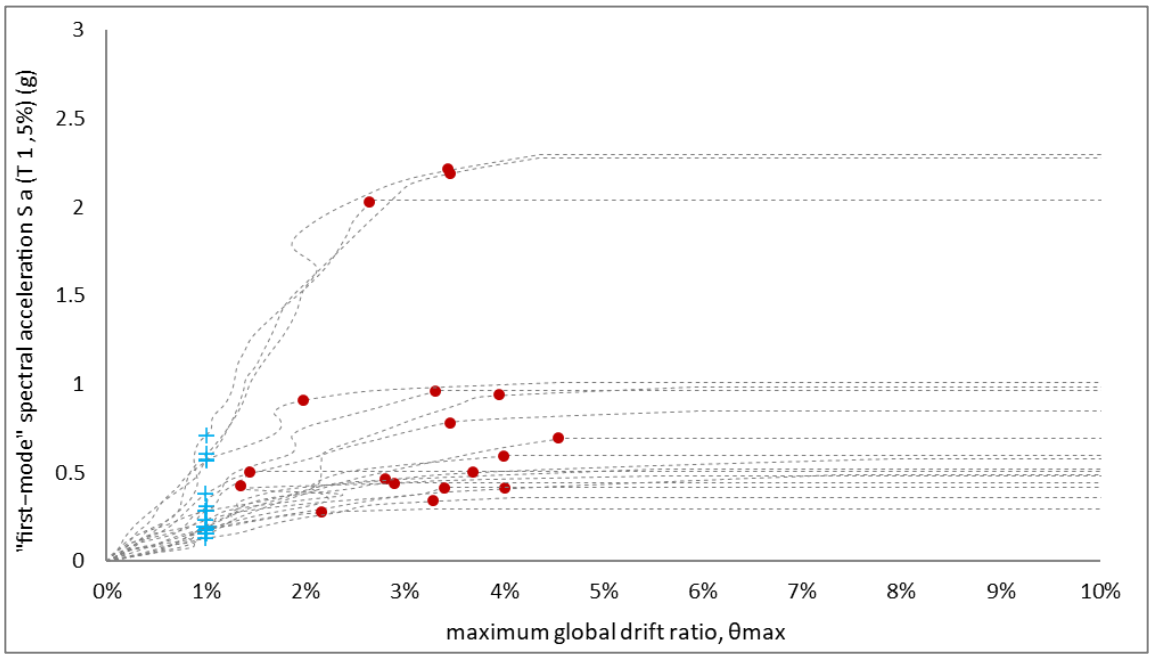

Figure 234: IDA curves for B Template, C10 concrete in y-direction together with IO and CP limit states

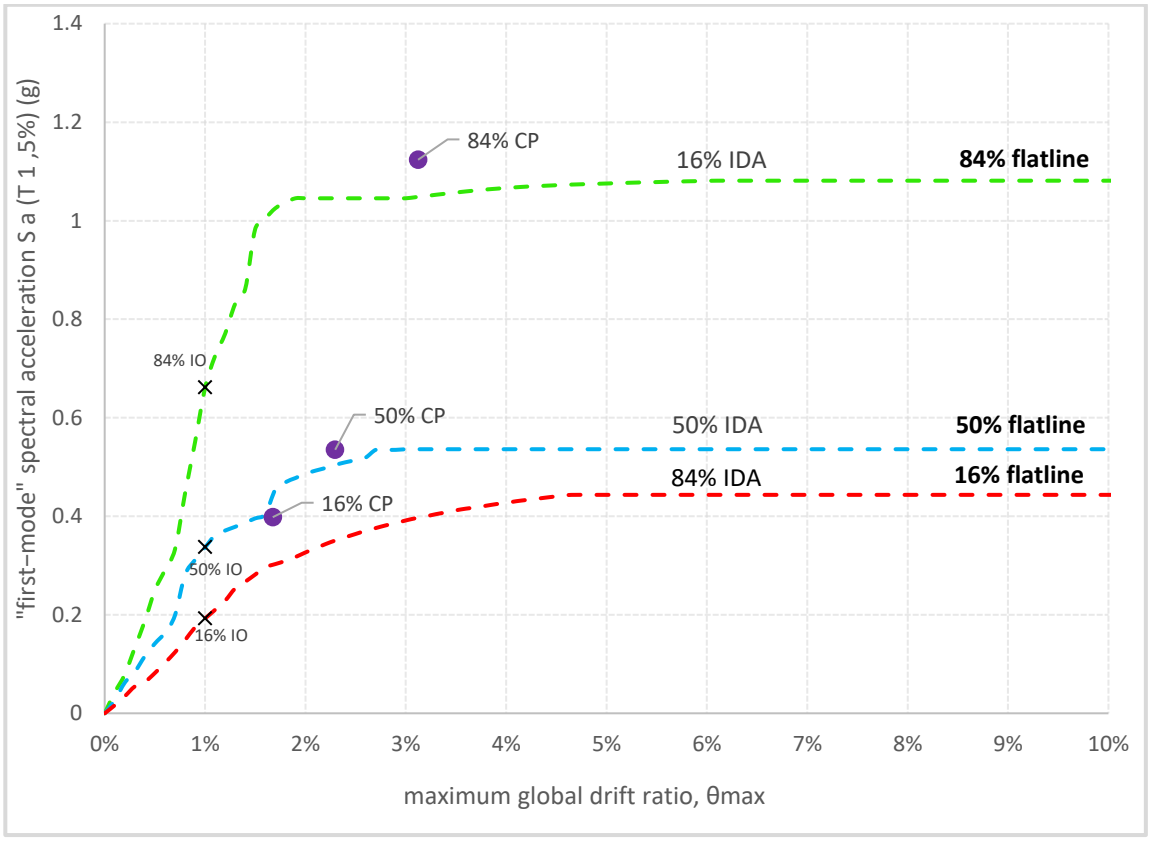

Figure 235: 16%, 50%, 84% IDA fractiles for B Template with concrete C16 in X-direction

Table 28: Intensity and damage measure values for each of the fractiles of corresponding limit states of B Template building with concrete C16 in X-direction

	$Sa_{(T1,5\%)}$ (g)			Θ_{max} (%)		
	IM 16%	**IM 50%**	**IM 84%**	**DM 16%**	**DM 50%**	**DM 84%**
IO	0.19	0.34	0.66	1.0%	1.0%	1.0%
CP	0.40	0.54	1.12	1.7%	2.3%	3.1%
GI	0.44	0.54	1.08	+∞	+∞	+∞

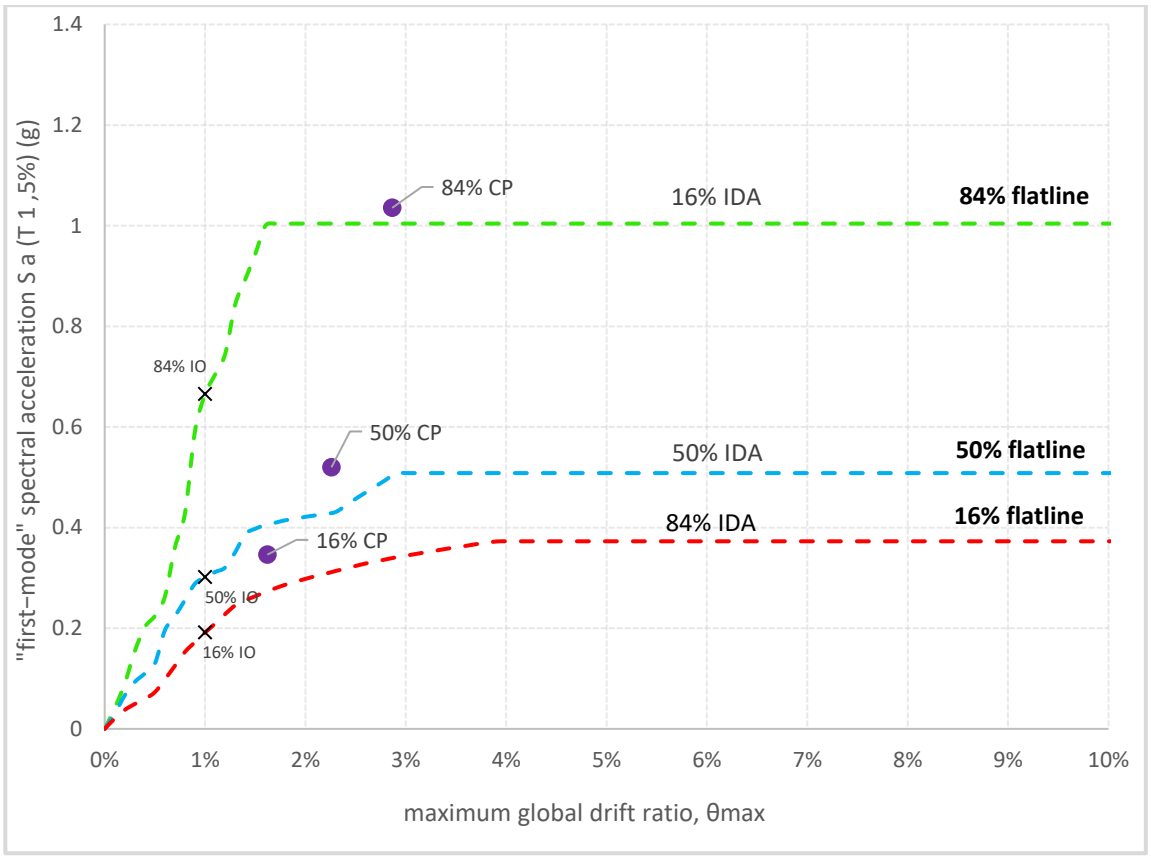

Figure 236: 16%, 50%, 84% IDA fractiles for B Template with concrete C10 in X-direction

Table 29: Intensity and damage measure values for each of the fractiles of corresponding limit states of B Template building with concrete C10 in X-direction

	$Sa_{(T1,5\%)}$ (g)			Θ_{max} (%)		
	IM 16%	**IM 50%**	**IM 84%**	**DM 16%**	**DM 50%**	**DM 84%**
IO	0.19	0.30	0.67	1.0%	1.0%	1.0%
CP	0.35	0.52	1.04	1.6%	2.3%	2.9%
GI	0.38	0.51	1	+∞	+∞	+∞

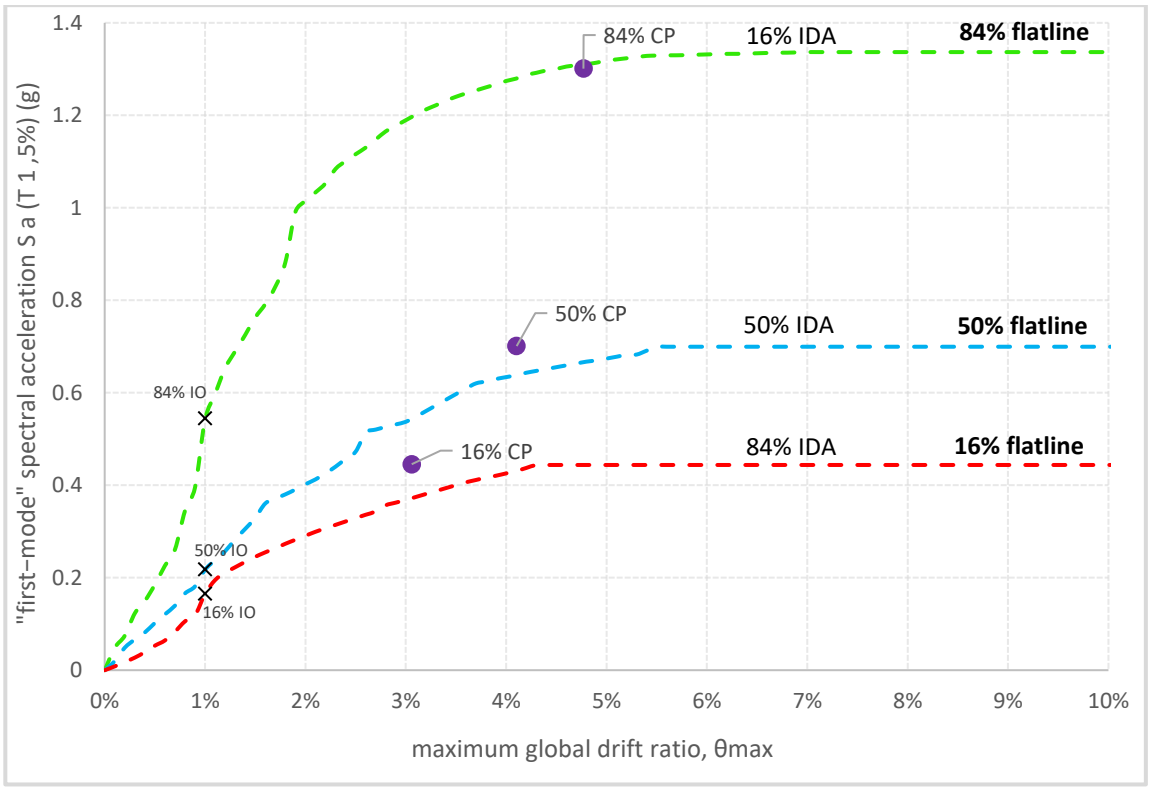

Figure 237: 16%, 50%, 84% IDA fractiles for B Template with concrete C16 in Y-direction

Table 30: Intensity and damage measure values for each of the fractiles of corresponding limit states of B Template building with concrete C16 in Y-direction

	$Sa_{(T1,5\%)}$ (g)			**Θ_{max} (%)**		
	IM 16%	**IM 50%**	**IM 84%**	**DM 16%**	**DM 50%**	**DM 84%**
IO	0.17	0.22	0.54	1.0%	1.0%	1.0%
CP	0.45	0.70	1.30	3.1%	4.1%	4.8%
GI	0.44	0.71	1.34	+∞	+∞	+∞

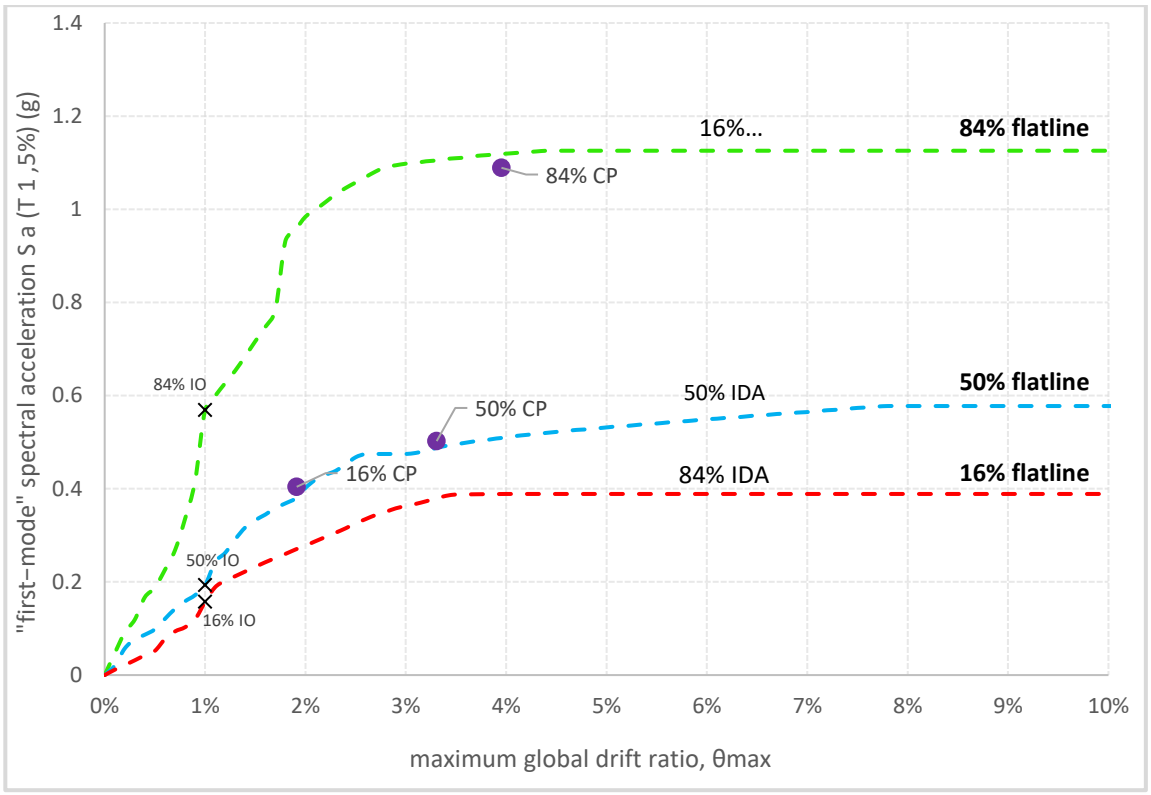

Figure 238: 16%, 50%, 84% IDA fractiles for B Template with concrete C10 in Y-direction

Table 31: Intensity and damage measure values for each of the fractiles of corresponding limit states of B Template building with concrete C16 in Y-direction

	$Sa_{(T1,5\%)}$ (g)			Θ_{max} (%)		
	IM 16%	**IM 50%**	**IM 84%**	**DM 16%**	**DM 50%**	**DM 84%**
IO	0.16	0.19	0.57	1.0%	1.0%	1.0%
CP	0.40	0.50	1.09	1.9%	3.3%	4.0%
GI	0.41	0.58	1.13	+∞	+∞	+∞

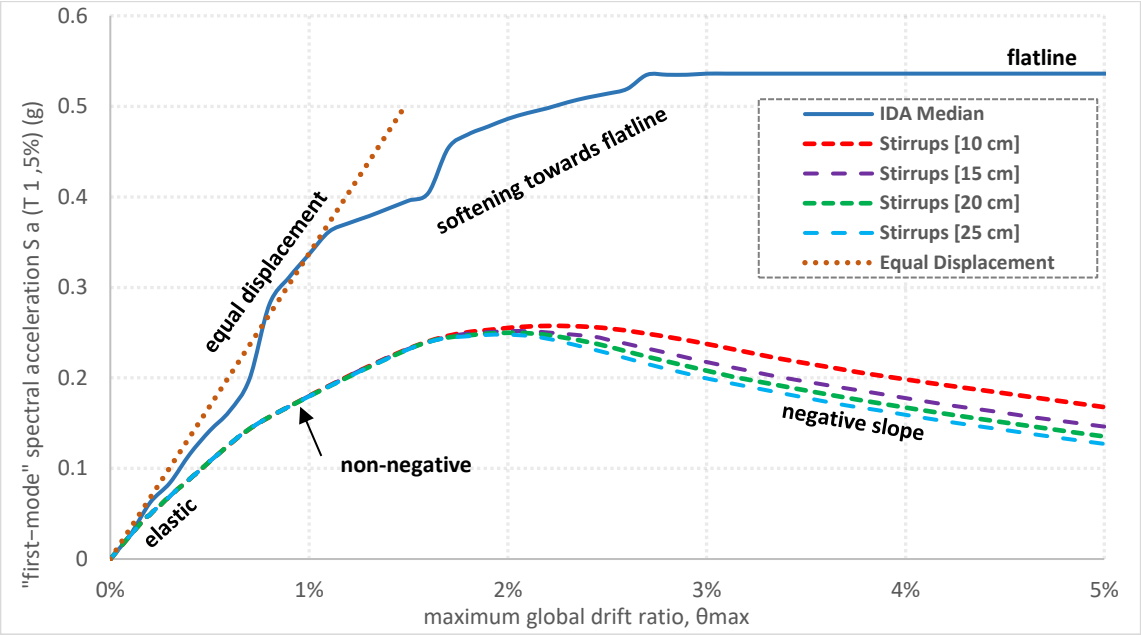

Figure 239: IDA median versus SPO curves for different concrete spacings of B Template building with concrete C16 in X-direction

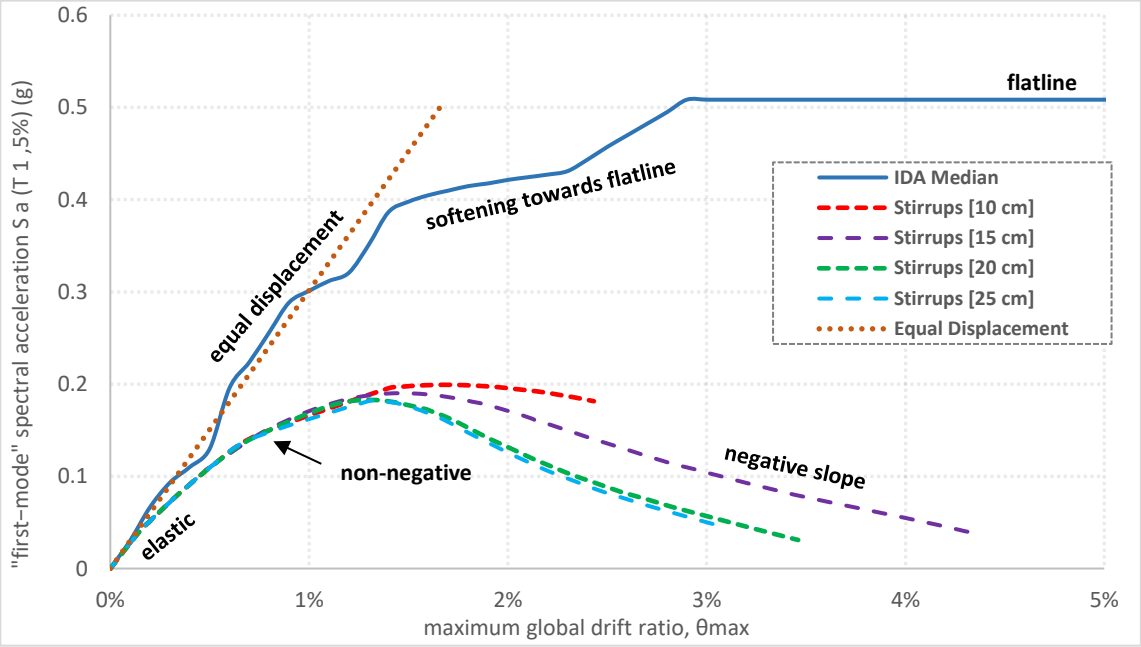

Figure 240: IDA median versus SPO curves for different concrete spacings of B Template building with concrete C10 in X-direction

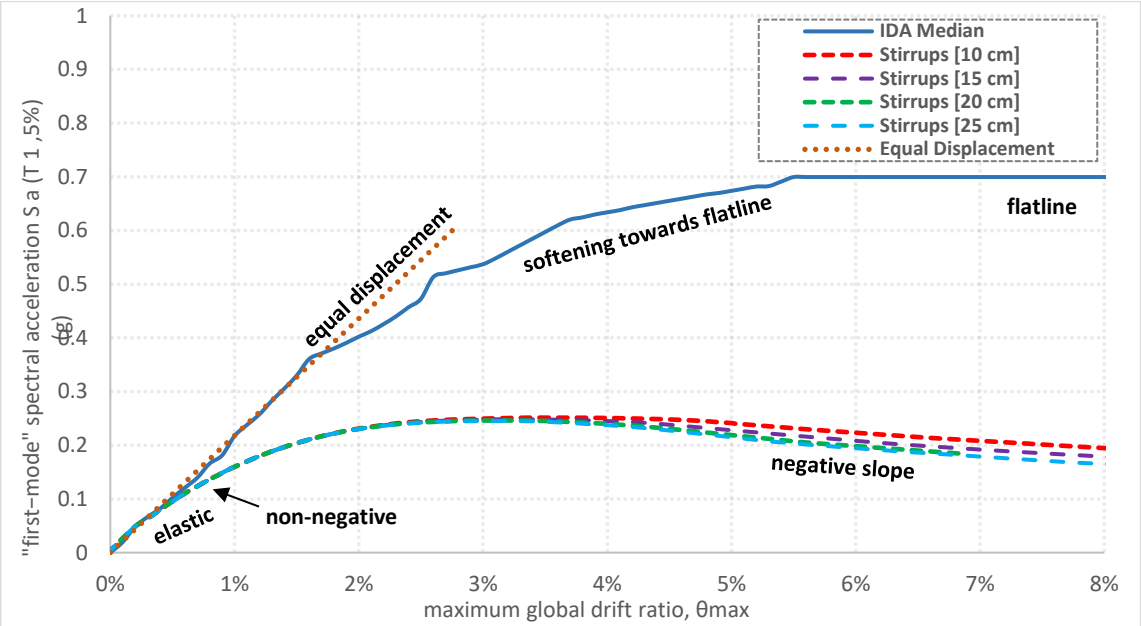

Figure 241: IDA median versus SPO curves for different concrete spacings of B Template building with concrete C16 in Y-direction

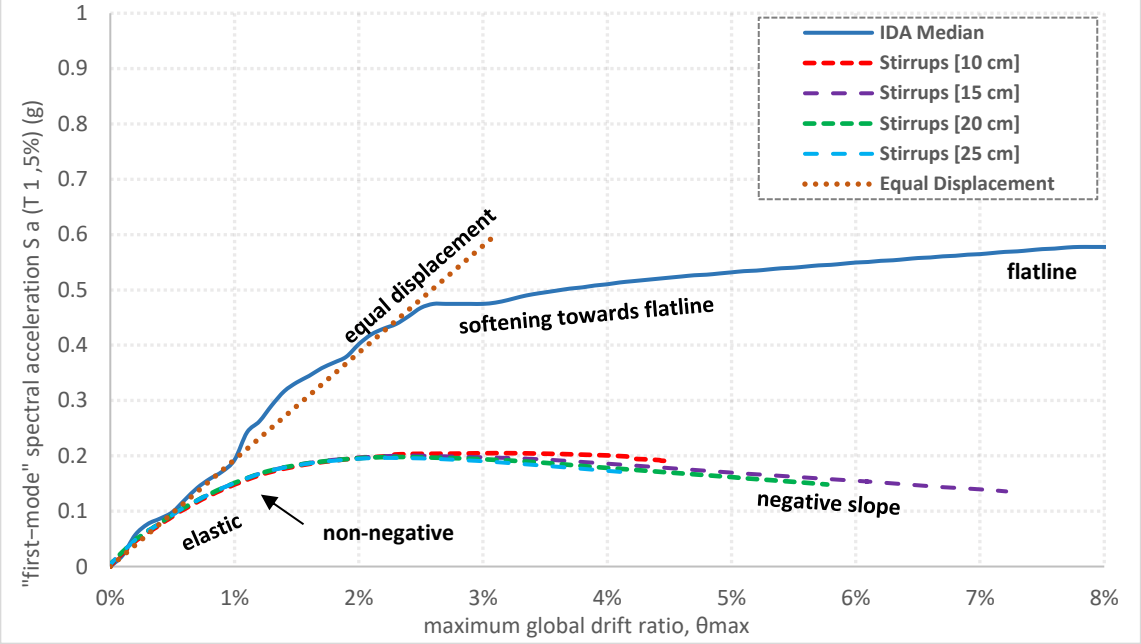

Figure 242: IDA median versus SPO curves for different concrete spacings of B Template building with concrete C10 in Y-direction

C Template IDA curves

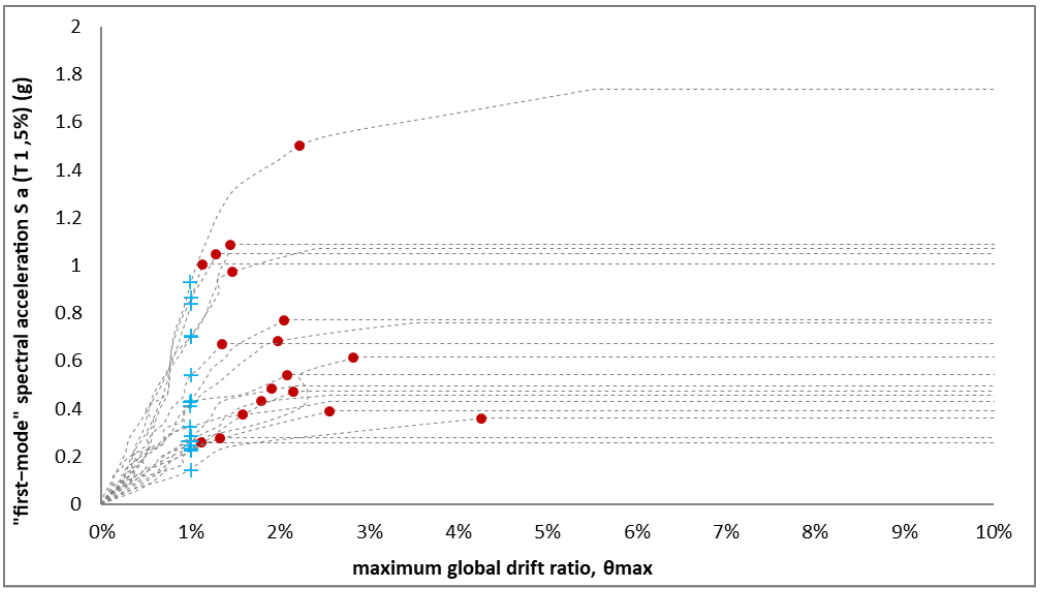

Figure 243: IDA curves for C Template, C16 concrete in x-direction together with IO and CP limit states

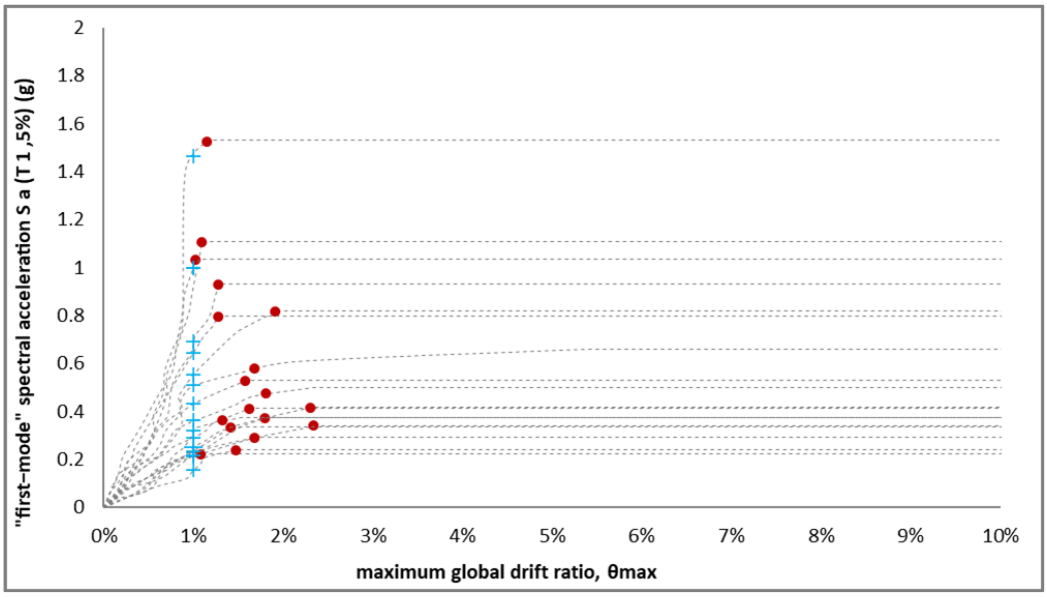

Figure 244: IDA curves for C Template, C10 concrete in x-direction together with IO and CP limit states

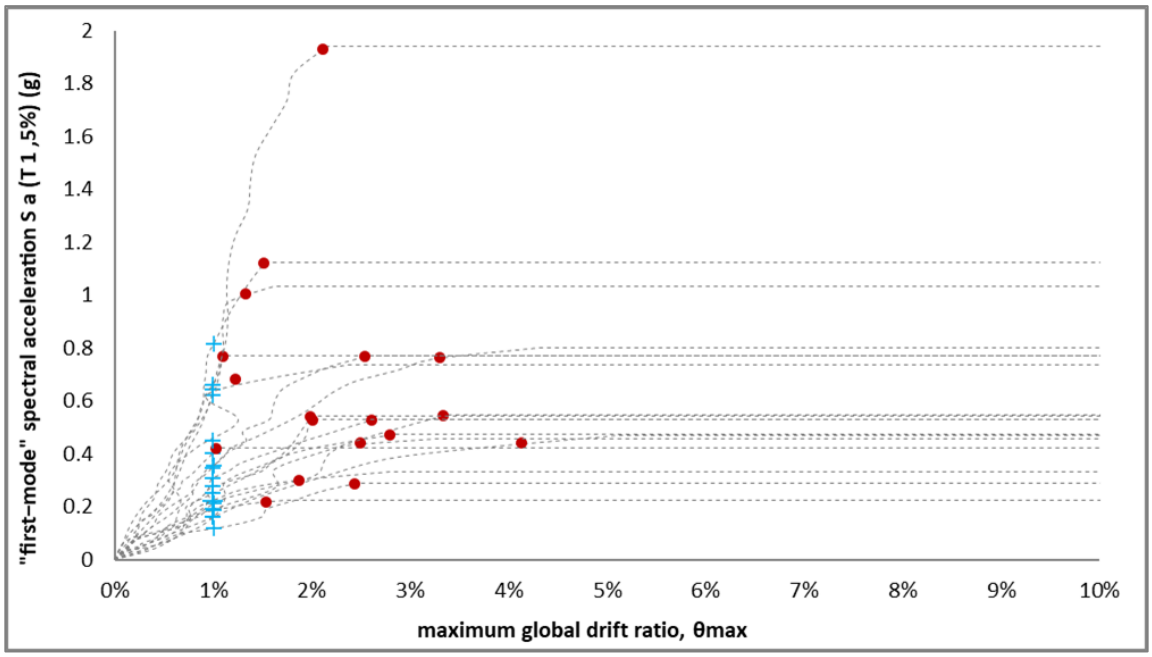

Figure 245: IDA curves for C Template, C16 concrete in y-direction together with IO and CP limit states

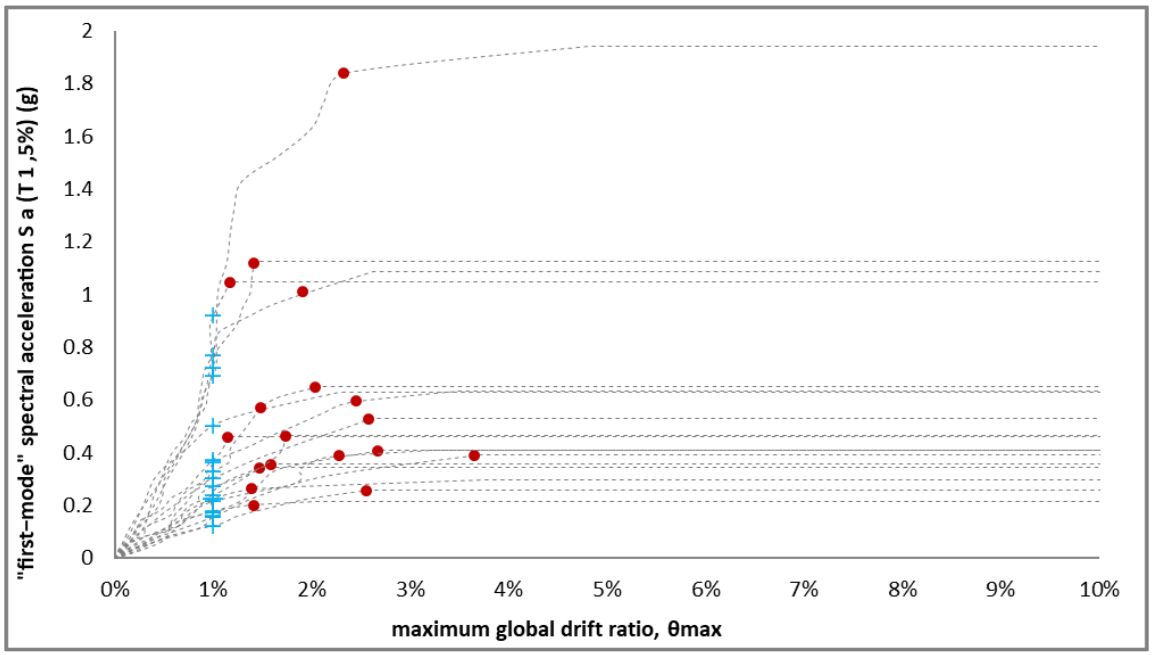

Figure 246: IDA curves for C Template, C10 concrete in y-direction together with IO and CP limit states

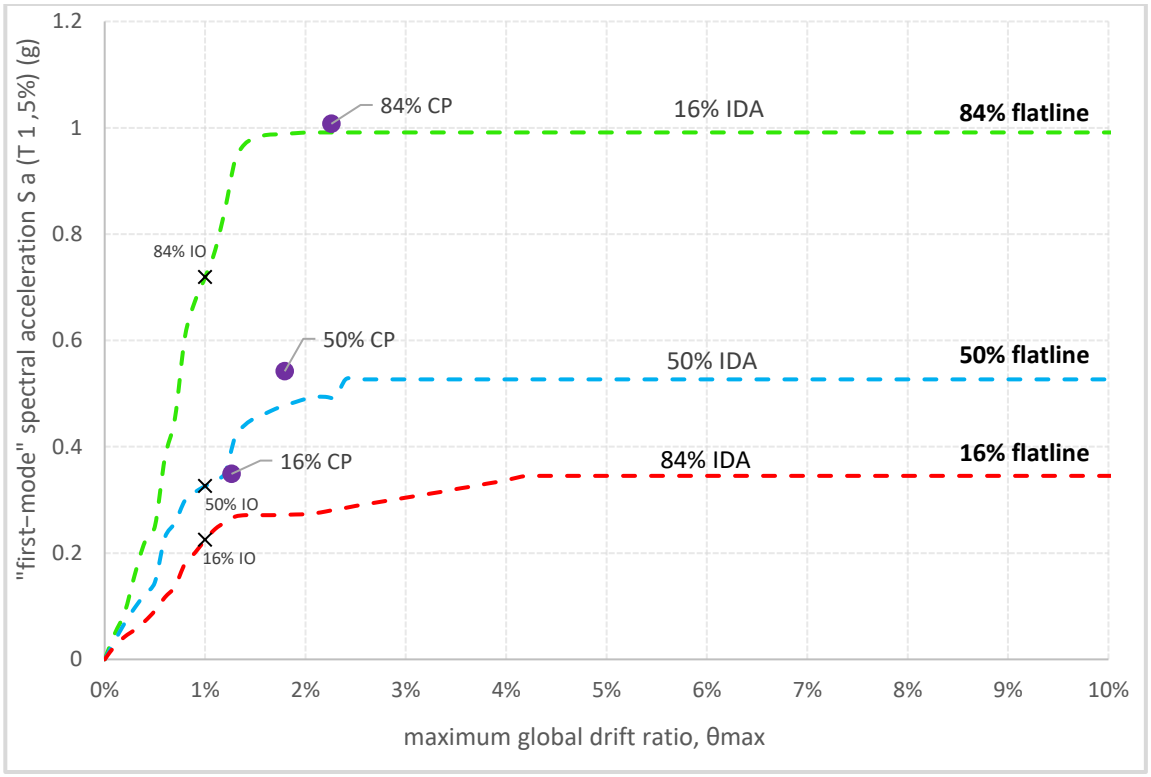

Figure 247: 16%, 50%, 84% IDA fractiles for C Template with concrete C16 in X-direction

Table 32: Intensity and damage measure values for each of the fractiles of corresponding limit states of C Template building with concrete C16 in X-direction

	$Sa_{(T1,5\%)}$ (g)			**Θ_{max} (%)**		
	IM 16%	**IM 50%**	**IM 84%**	**DM 16%**	**DM 50%**	**DM 84%**
IO	0.23	0.33	0.72	1.0%	1.0%	1.0%
CP	0.35	0.54	1.01	1.3%	1.8%	2.3%
GI	0.34	0.53	1.00	+∞	+∞	+∞

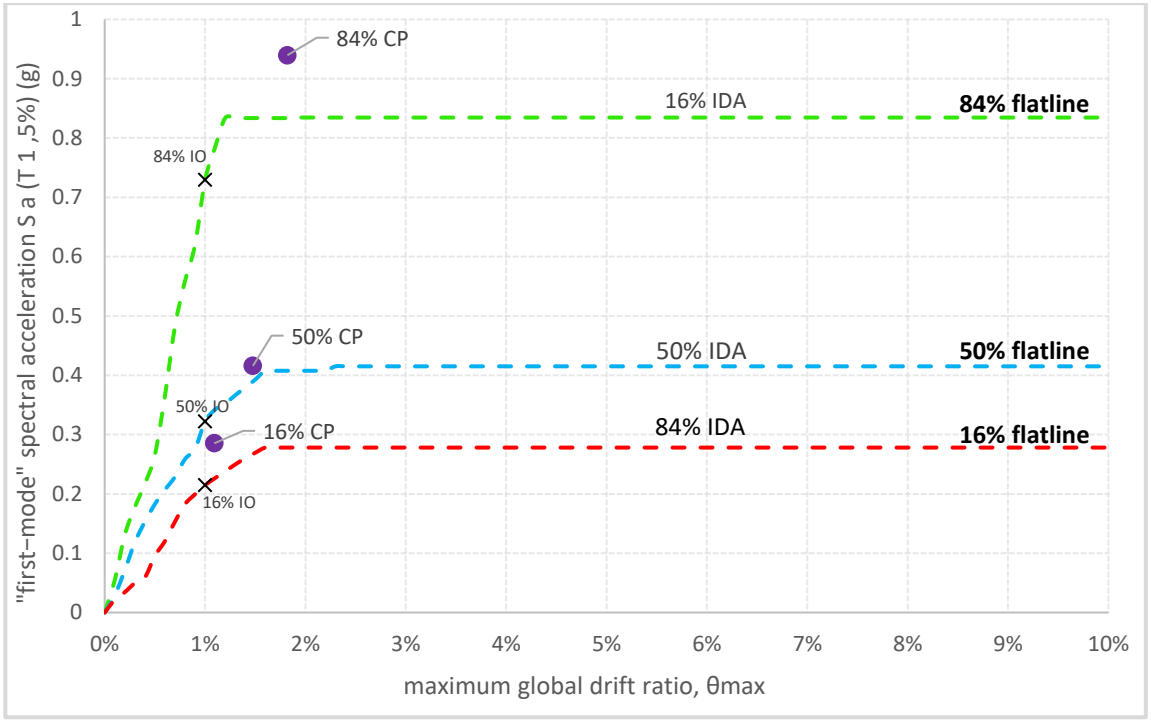

Figure 248: 16%, 50%, 84% IDA fractiles for C Template with concrete C10 in X-direction

Table 33: Intensity and damage measure values for each of the fractiles of corresponding limit states of C Template building with concrete C10 in X-direction

	$Sa_{(T1,5\%)}$ (g)			Θ_{max} (%)		
	IM 16%	**IM 50%**	**IM 84%**	**DM 16%**	**DM 50%**	**DM 84%**
IO	0.22	0.32	0.73	1.0%	1.0%	1.0%
CP	0.29	0.42	0.94	1.1%	1.5%	1.8%
GI	0.28	0.42	0.83	+∞	+∞	+∞

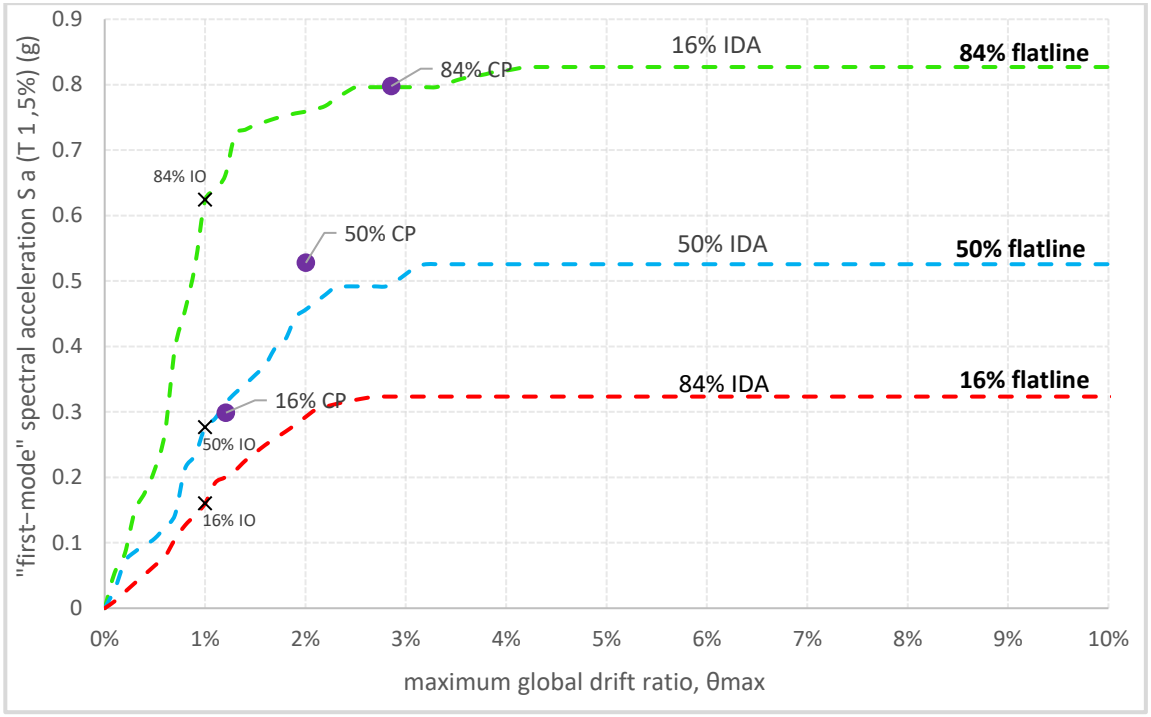

Figure 249: 16%, 50%, 84% IDA fractiles for C Template with concrete C16 in Y-direction

Table 34: Intensity and damage measure values for each of the fractiles of corresponding limit states of C Template building with concrete C16 in Y-direction

	$Sa_{(T1,5\%)}$ (g)			**Θ_{max} (%)**		
	IM 16%	**IM 50%**	**IM 84%**	**DM 16%**	**DM 50%**	**DM 84%**
IO	0.16	0.28	0.62	1.0%	1.0%	1.0%
CP	0.30	0.53	0.80	1.2%	2.0%	2.9%
GI	0.32	0.53	0.83	+∞	+∞	+∞

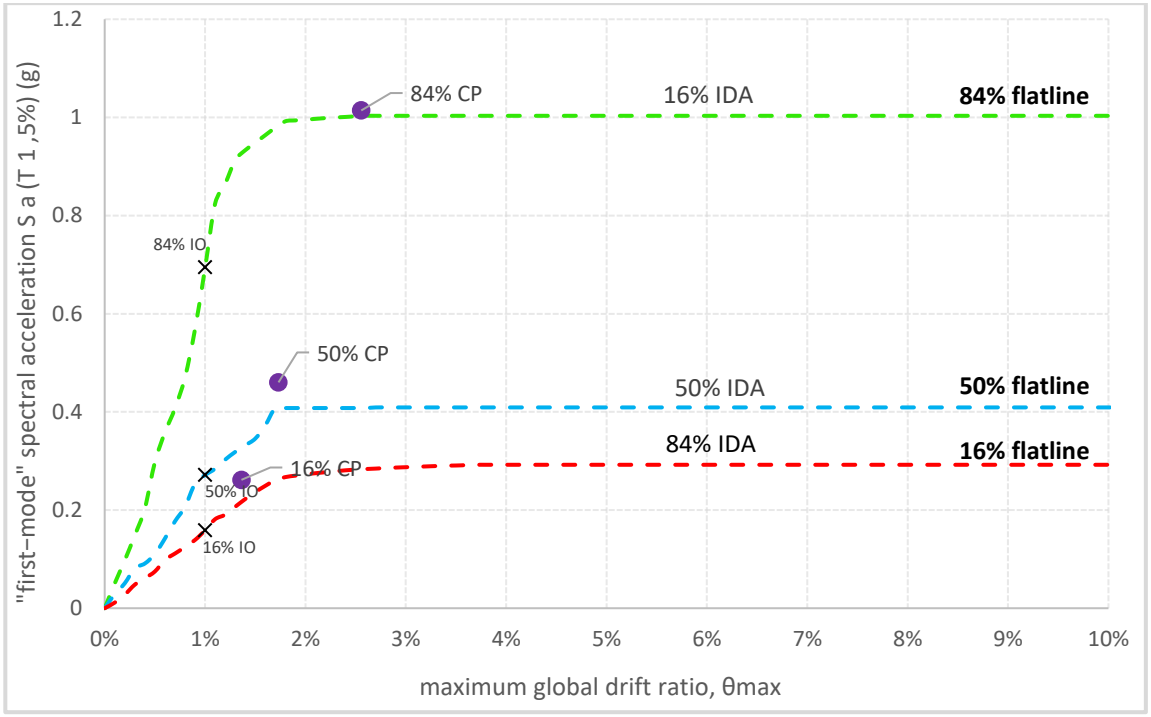

Figure 250: 16%, 50%, 84% IDA fractiles for C Template with concrete C10 in Y-direction

Table 35: Intensity and damage measure values for each of the fractiles of corresponding limit states of C Template building with concrete C10 in Y-direction

	$Sa_{(T1,5\%)}$ (g)			**Θ_{max} (%)**		
	IM 16%	**IM 50%**	**IM 84%**	**DM 16%**	**DM 50%**	**DM 84%**
IO	0.16	0.27	0.69	1.0%	1.0%	1.0%
CP	0.26	0.46	1.01	1.4%	1.7%	2.6%
GI	0.29	0.41	1.00	+∞	+∞	+∞

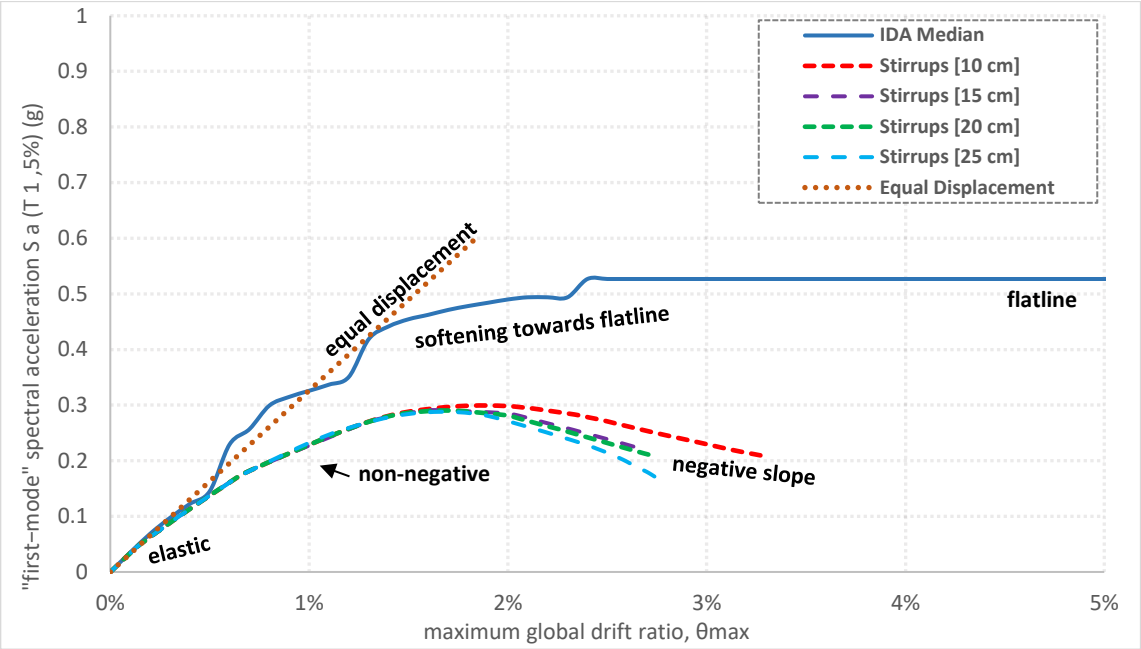

Figure 251: IDA median versus SPO curves for different concrete spacings of C Template building with concrete C16 in X-direction

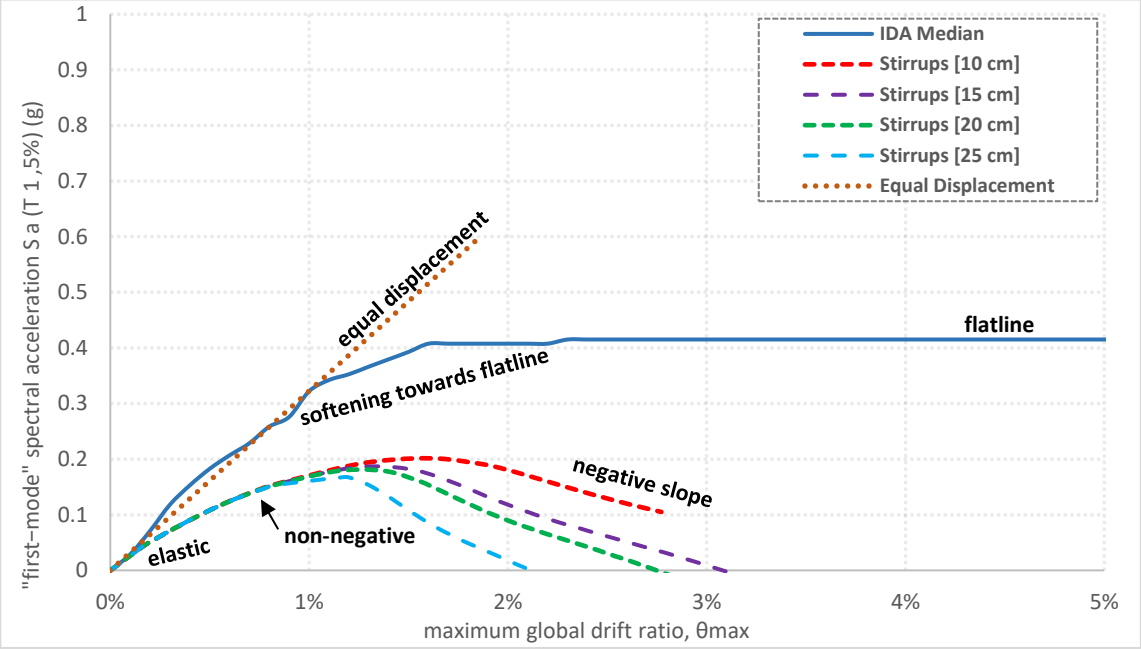

Figure 252: IDA median versus SPO curves for different concrete spacings of C Template building with concrete C10 in X-direction

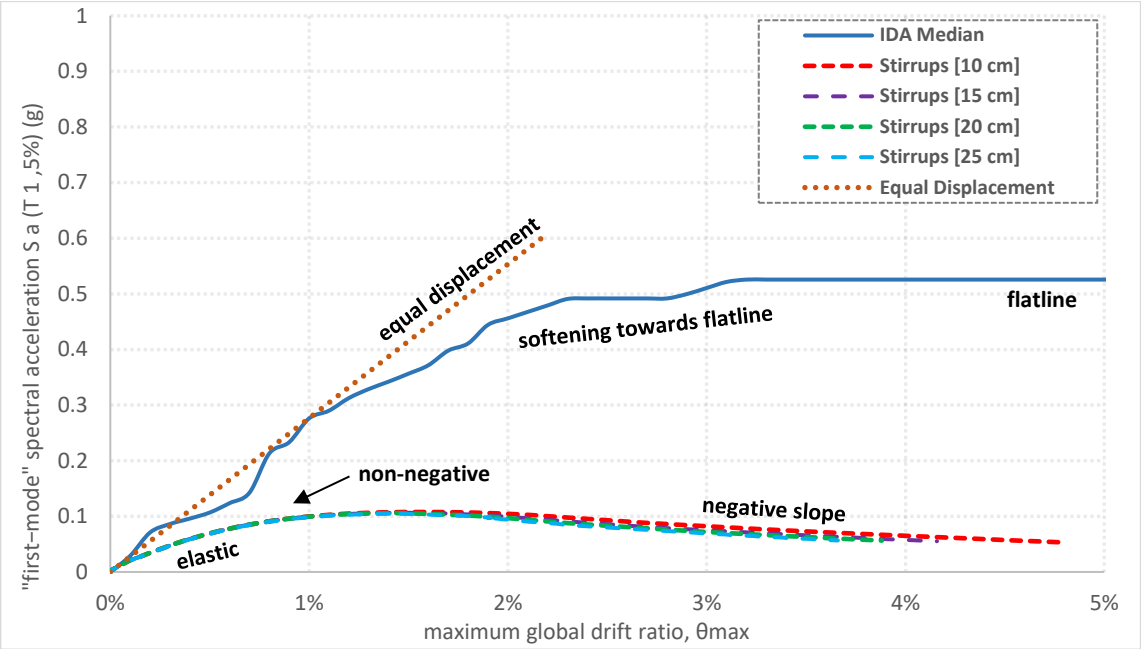

Figure 253: IDA median versus SPO curves for different concrete spacings of C Template building with concrete C16 in Y-direction

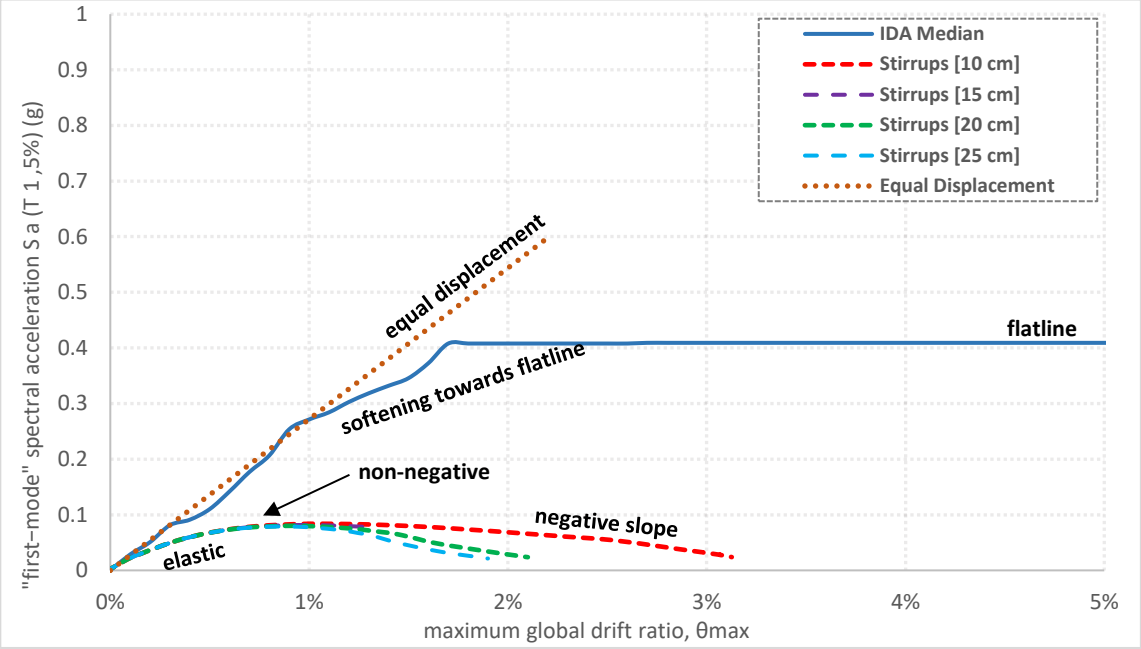

Figure 254: IDA median versus SPO curves for different concrete spacings of C Template building with concrete C10 in Y-direction

D Template IDA curves

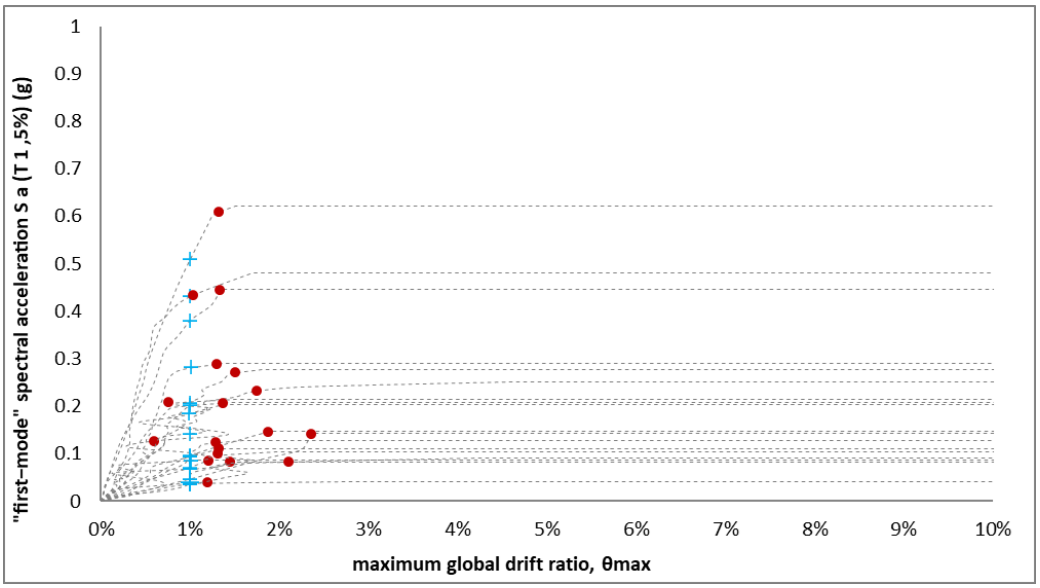

Figure 255: IDA curves for D Template, C16 concrete in x-direction together with IO and CP limit states

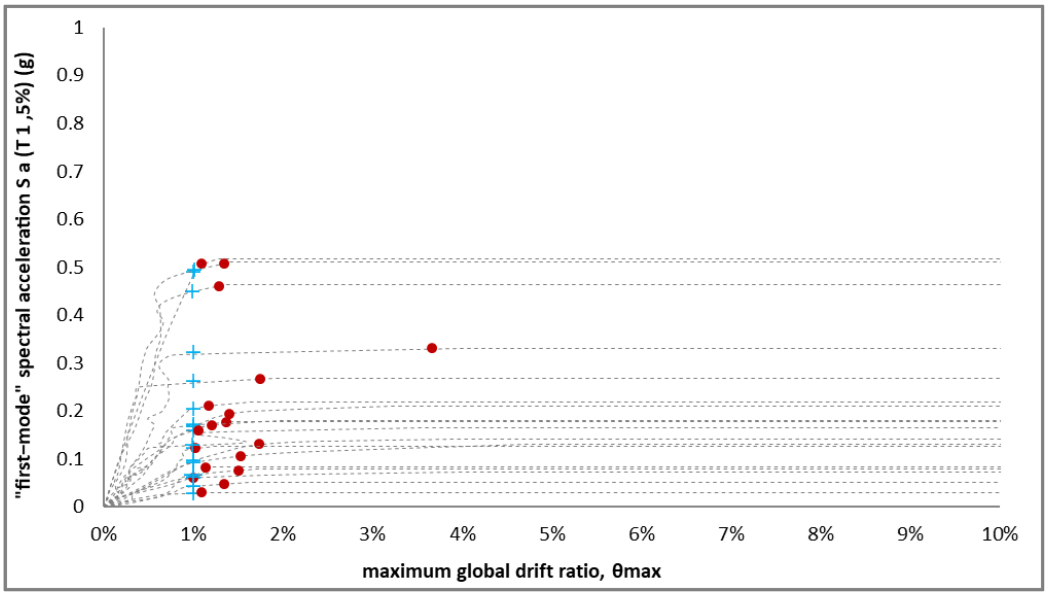

Figure 256: IDA curves for D Template, C10 concrete in x-direction together with IO and CP limit states

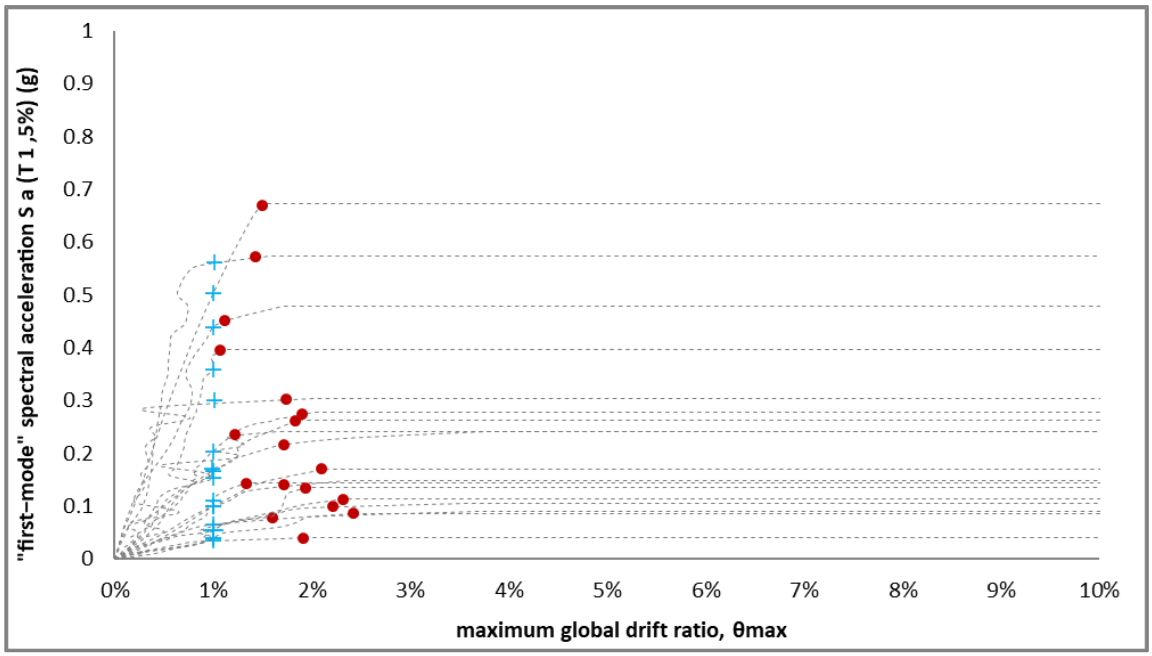

Figure 257: IDA curves for D Template, C16 concrete in y-direction together with IO and CP limit states

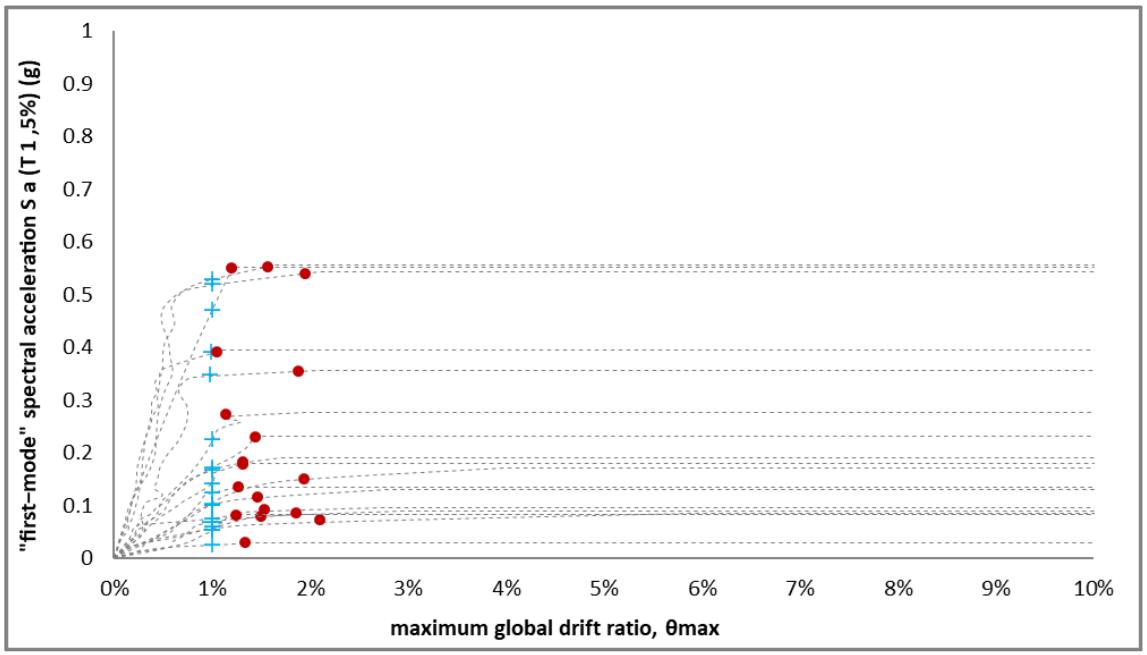

Figure 258: IDA curves for D Template, C10 concrete in y-direction together with IO and CP limit states

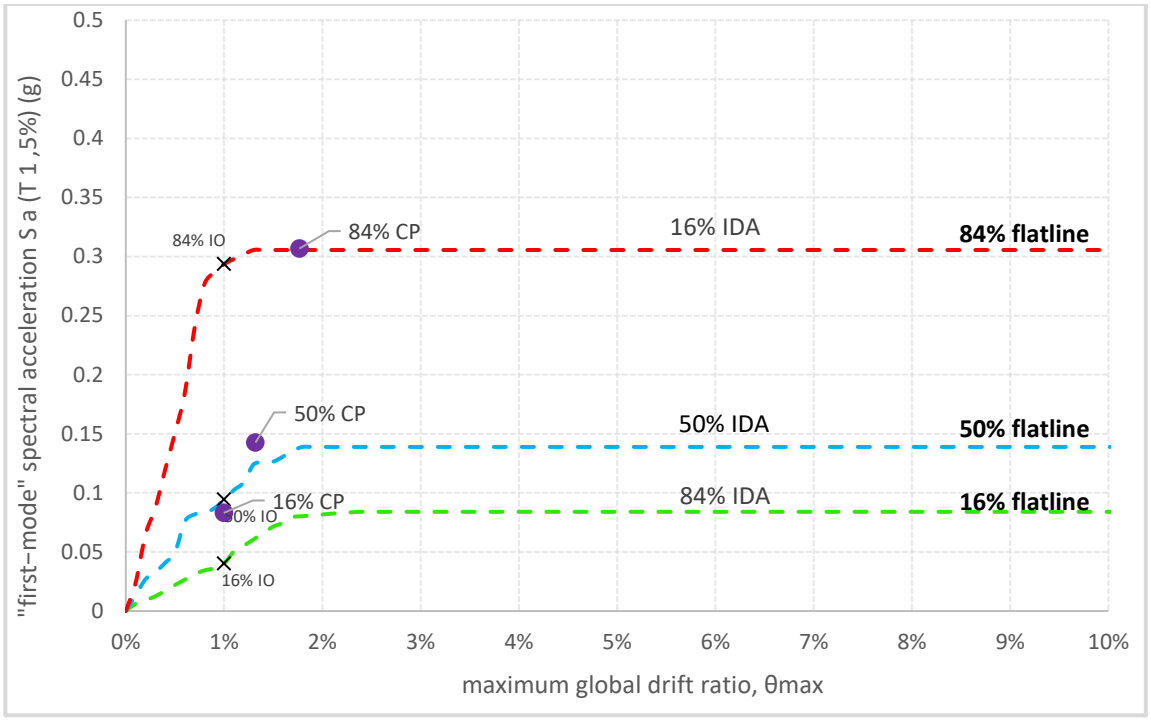

Figure 259: 16%, 50%, 84% IDA fractiles for D Template with concrete C16 in X-direction

Table 36: Intensity and damage measure values for each of the fractiles of corresponding limit states of D Template building with concrete C16 in X-direction

	$Sa_{(T1,5\%)}$ (g)			**Θ_{max} (%)**		
	IM 16%	**IM 50%**	**IM 84%**	**DM 16%**	**DM 50%**	**DM 84%**
IO	0.04	0.09	0.29	1.0%	1.0%	1.0%
CP	0.08	0.14	0.31	1.0%	1.3%	1.8%
GI	0.08	0.14	0.31	+∞	+∞	+∞

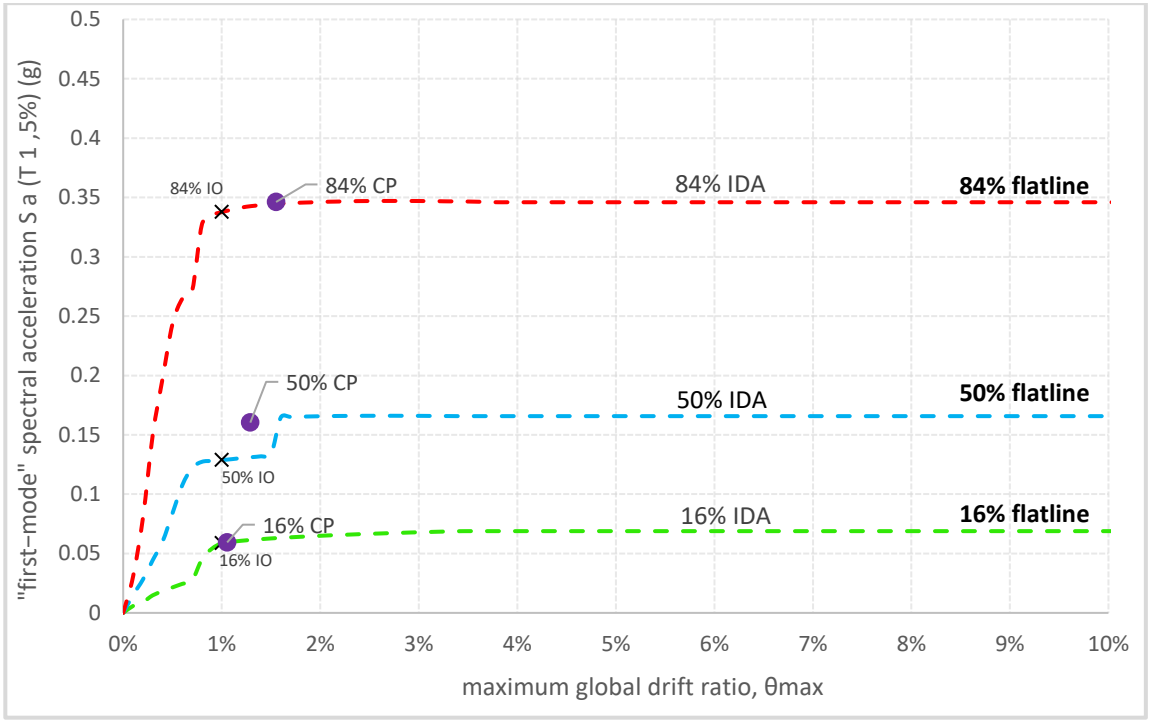

Figure 260: 16%, 50%, 84% IDA fractiles for D Template with concrete C10 in X-direction

Table 37: Intensity and damage measure values for each of the fractiles of corresponding limit states of D Template building with concrete C10 in X-direction

	$Sa_{(T1,5\%)}$ (g)			Θ_{max} (%)		
	IM 16%	**IM 50%**	**IM 84%**	**DM 16%**	**DM 50%**	**DM 84%**
IO	0.06	0.13	0.34	1.0%	1.0%	1.0%
CP	0.06	0.16	0.35	1.1%	1.3%	1.6%
GI	0.07	0.17	0.35	+∞	+∞	+∞

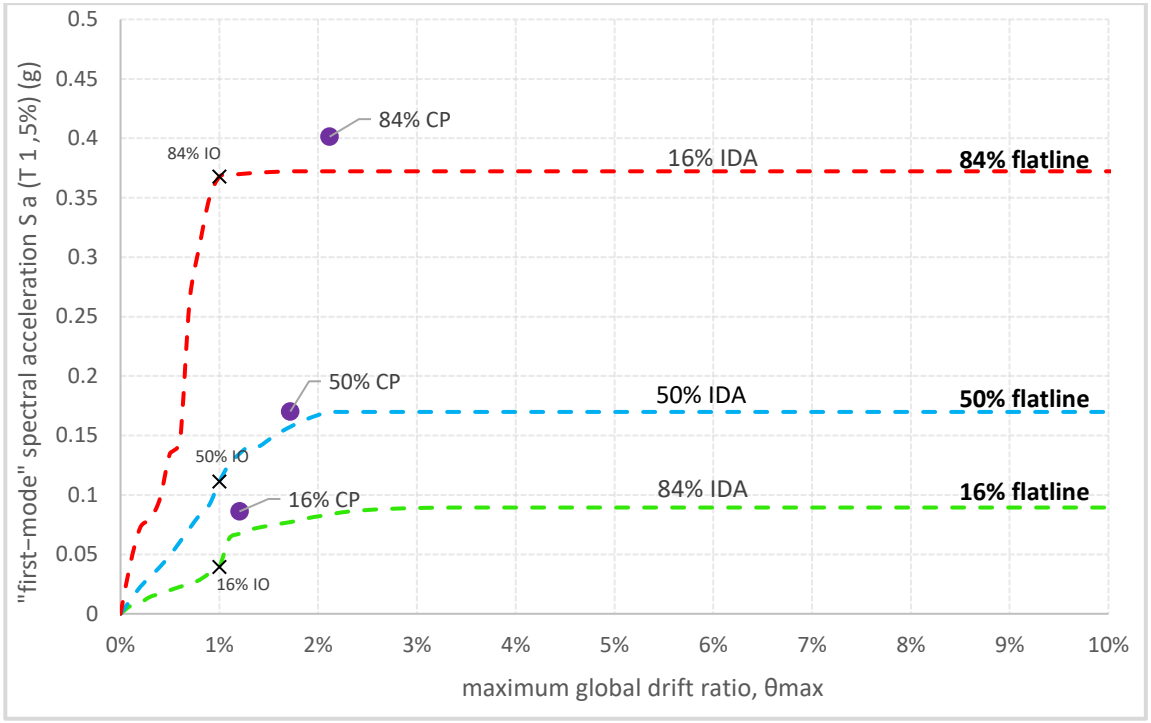

Figure 261: 16%, 50%, 84% IDA fractiles for D Template with concrete C16 in Y-direction

Table 38: Intensity and damage measure values for each of the fractiles of corresponding limit states of D Template building with concrete C16 in Y-direction

	$Sa_{(T1,5\%)}$ (g)			Θ_{max} (%)		
	IM 16%	**IM 50%**	**IM 84%**	**DM 16%**	**DM 50%**	**DM 84%**
IO	0.04	0.11	0.37	1.0%	1.0%	1.0%
CP	0.09	0.17	0.40	1.2%	1.7%	2.1%
GI	0.09	0.17	0.37	+∞	+∞	+∞

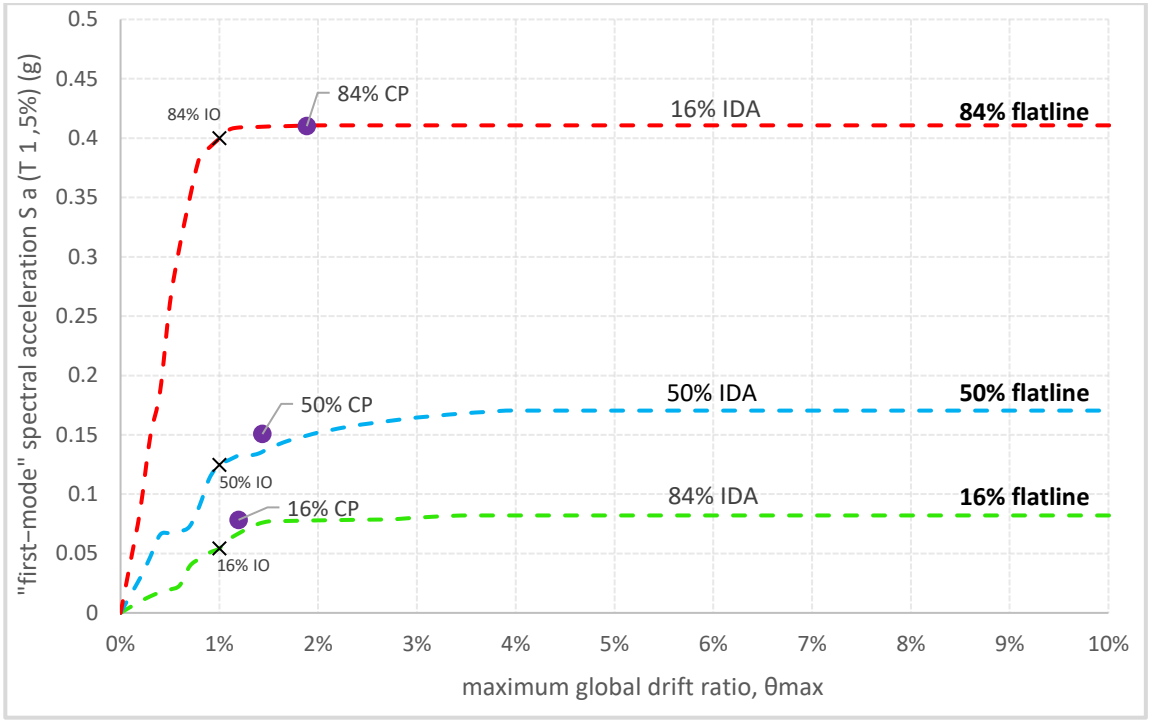

Figure 262: 16%, 50%, 84% IDA fractiles for D Template with concrete C10 in Y-direction

Table 39: Intensity and damage measure values for each of the fractiles of corresponding limit states of D Template building with concrete C10 in Y-direction

	$Sa_{(T1,5\%)}$ (g)			**Θ_{max} (%)**		
	IM 16%	**IM 50%**	**IM 84%**	**DM 16%**	**DM 50%**	**DM 84%**
IO	0.05	0.12	0.40	1.0%	1.0%	1.0%
CP	0.08	0.15	0.41	1.2%	1.4%	1.9%
GI	0.08	0.17	0.41	+∞	+∞	+∞

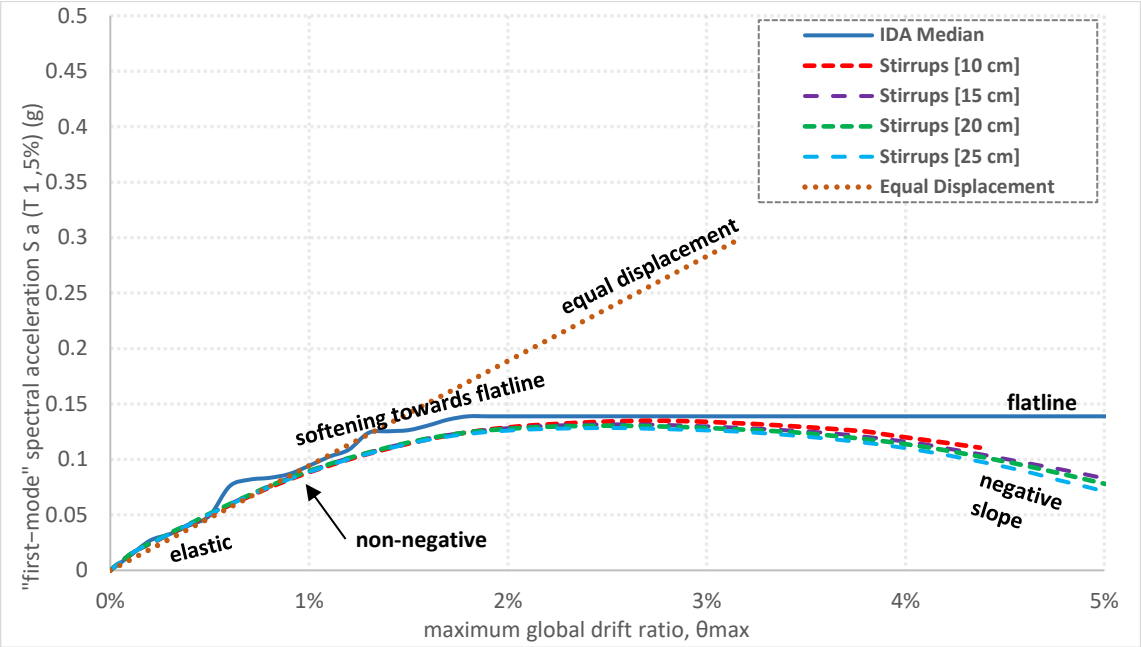

Figure 263: IDA median versus SPO curves for different concrete spacings of D Template building with concrete C16 in X-direction

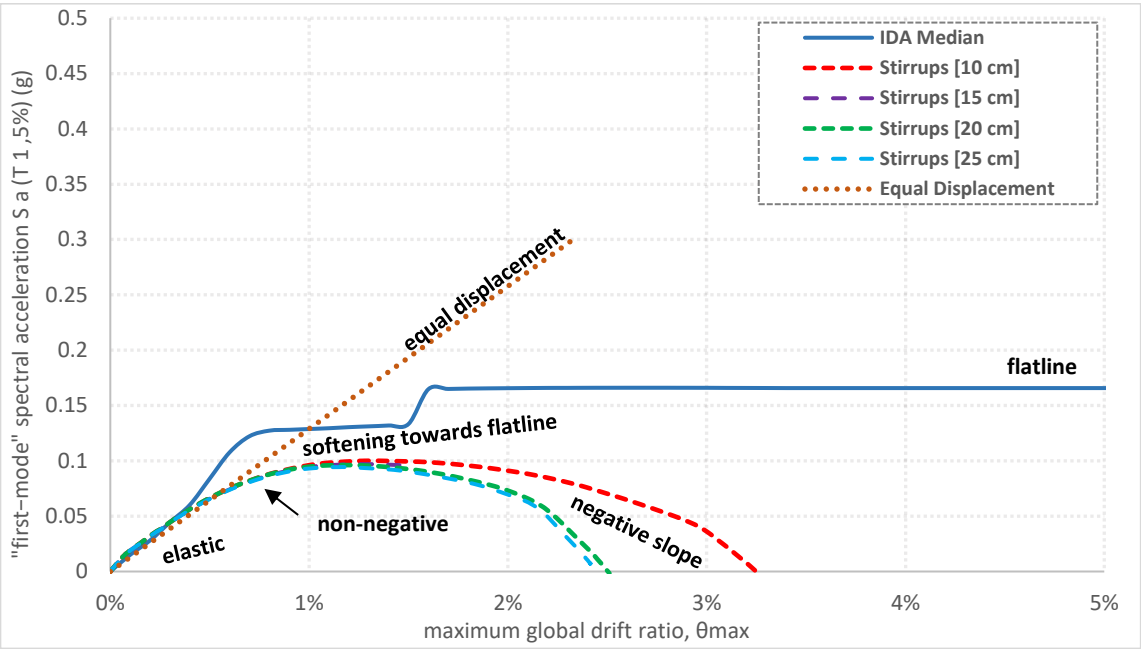

Figure 264: IDA median versus SPO curves for different concrete spacings of D Template building with concrete C10 in X-direction

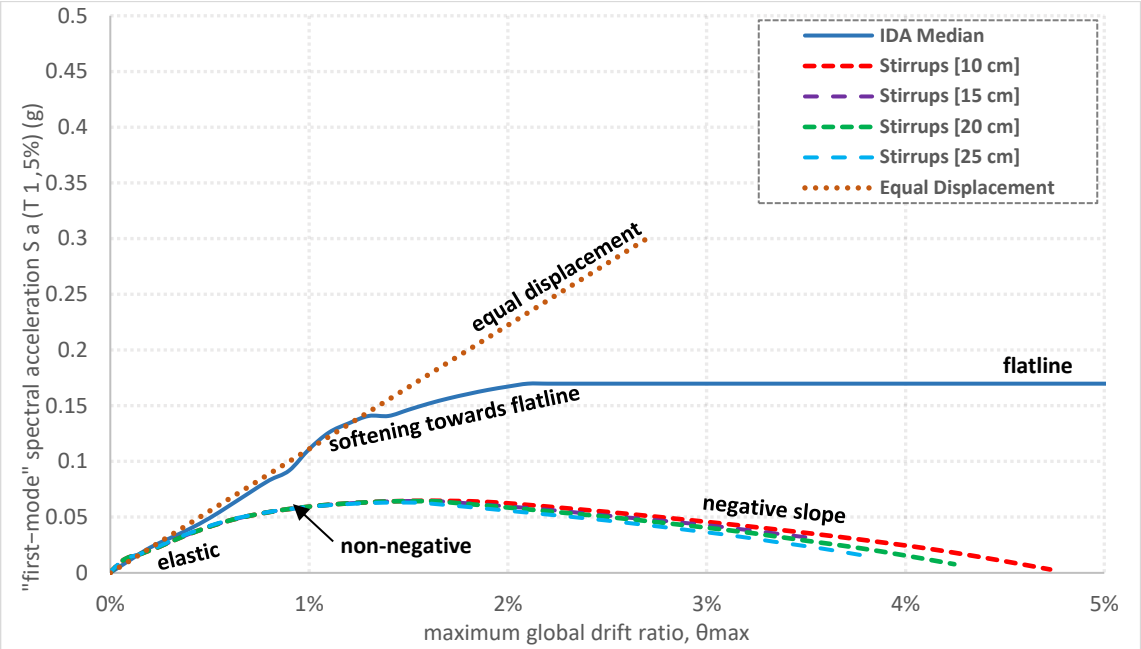

Figure 265: IDA median versus SPO curves for different concrete spacings of D Template building with concrete C16 in Y-direction

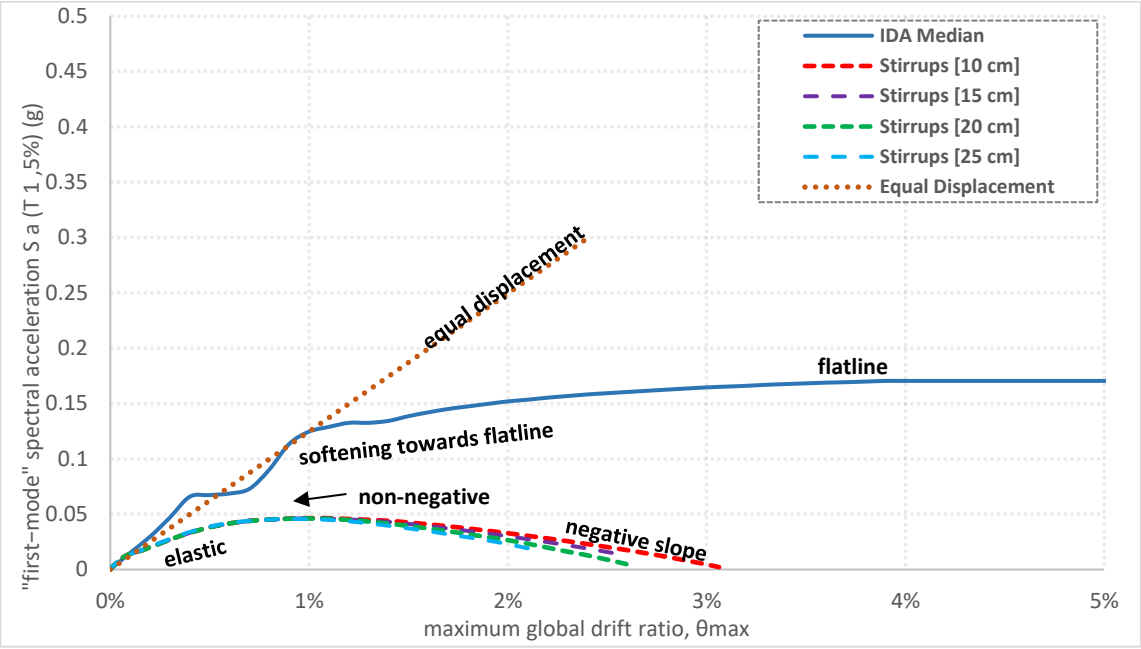

Figure 266: IDA median versus SPO curves for different concrete spacings of D Template building with concrete C10 in Y-direction

E Template IDA curves

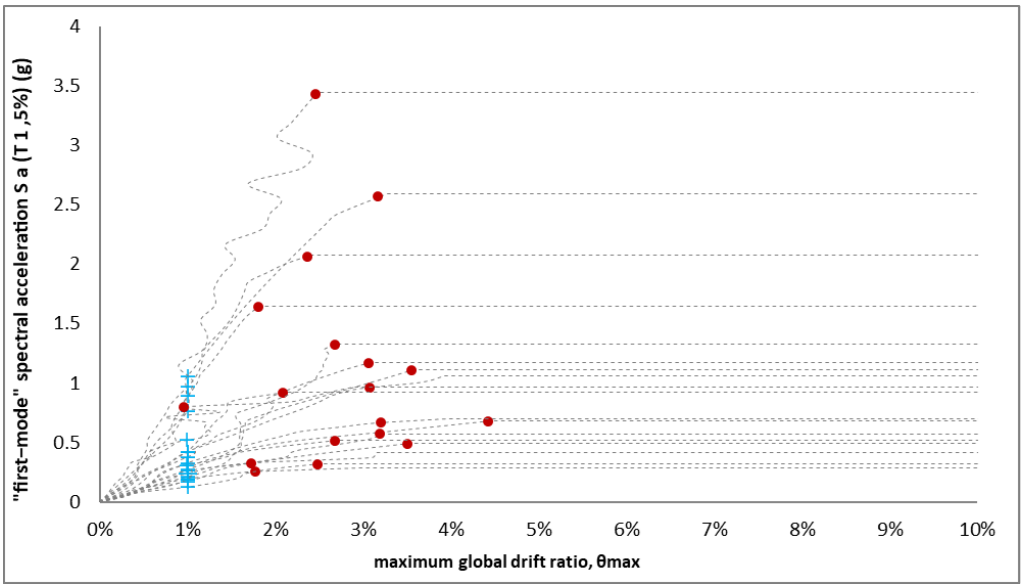

Figure 267: IDA curves for E Template, C16 concrete in x-direction together with IO and CP limit states

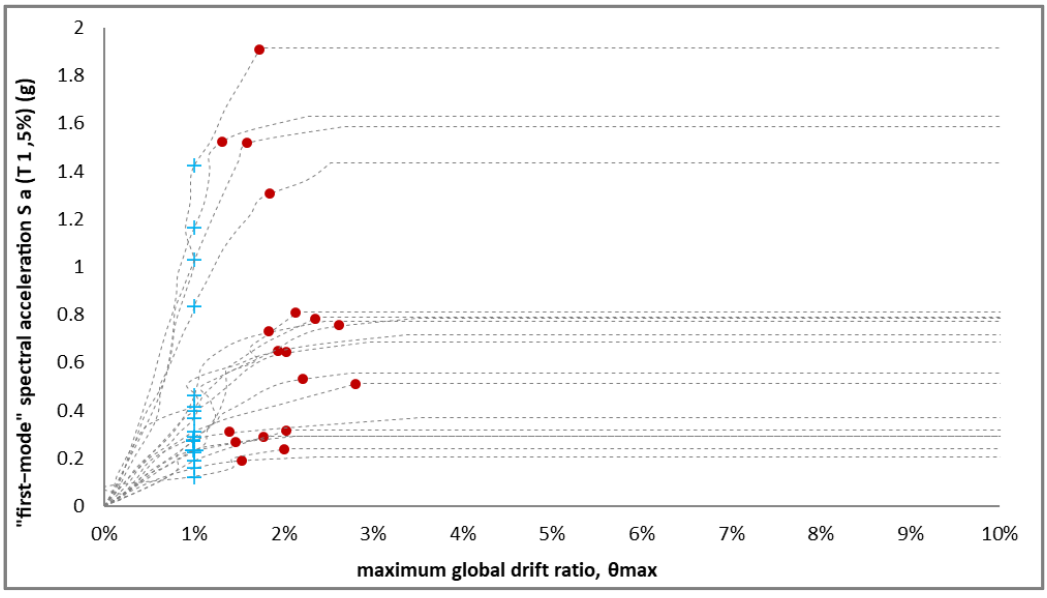

Figure 268: IDA curves for E Template, C10 concrete in x-direction together with IO and CP limit states

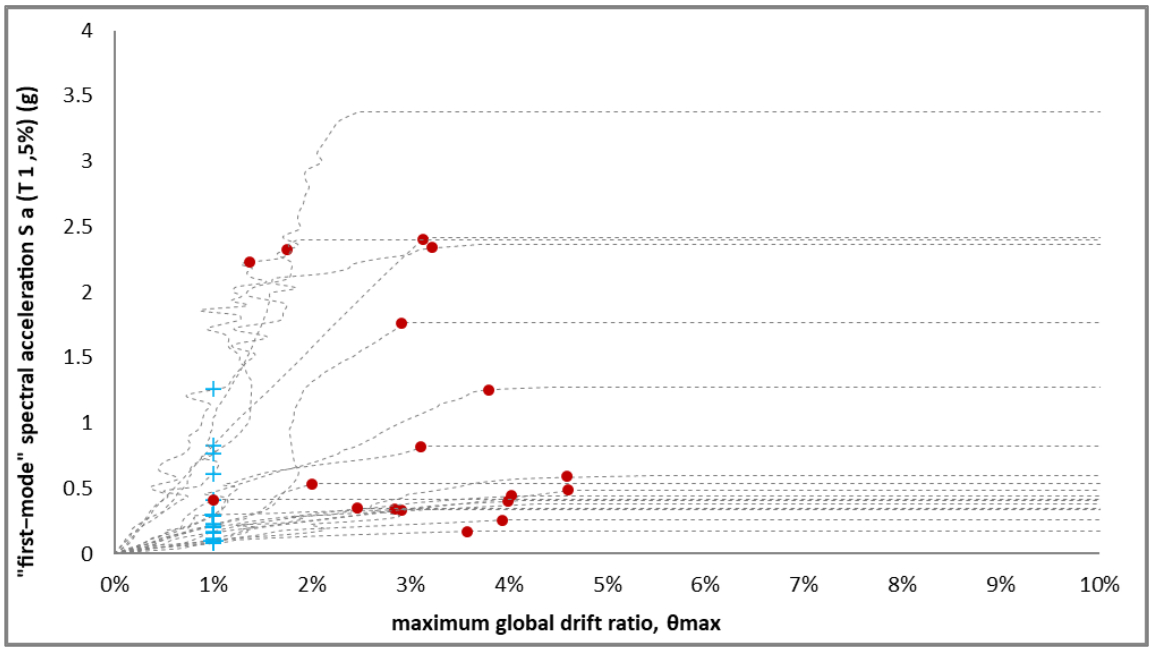

Figure 269: IDA curves for E Template, C16 concrete in y-direction together with IO and CP limit states

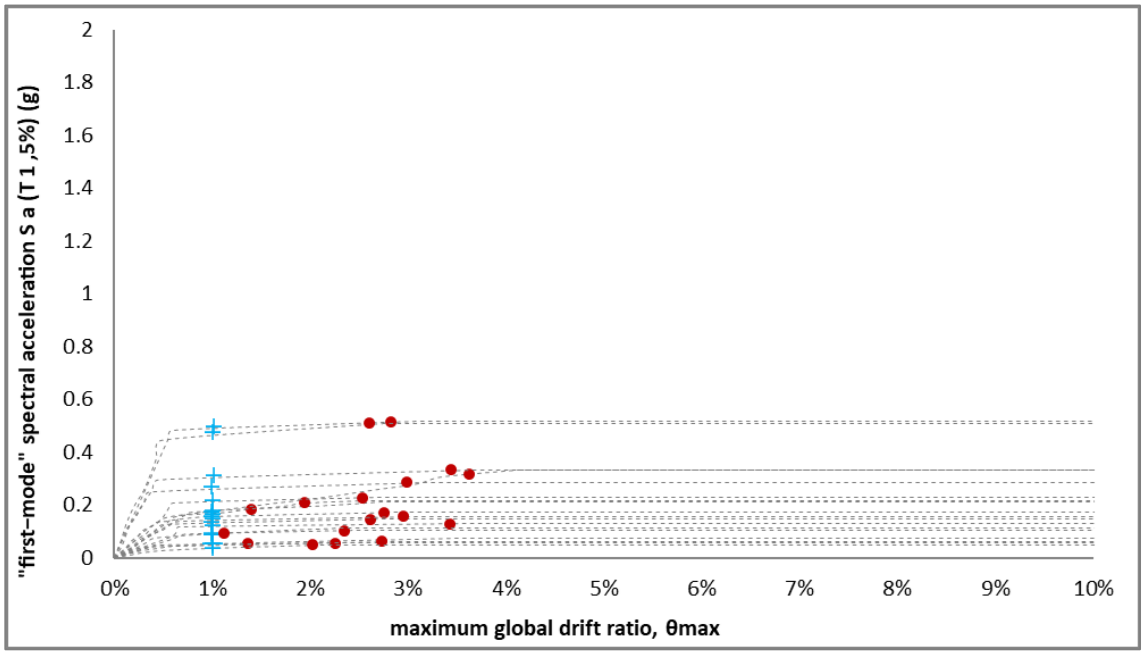

Figure 270: IDA curves for E Template, C10 concrete in y-direction together with IO and CP limit states

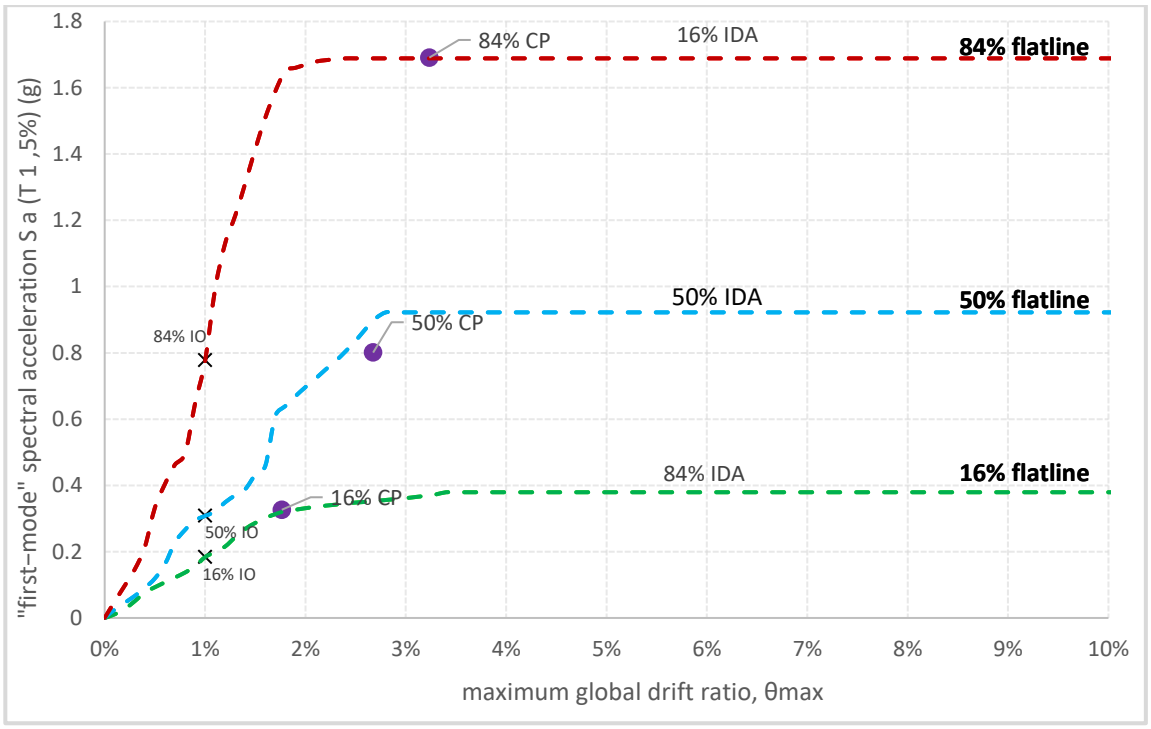

Figure 271: 16%, 50%, 84% IDA fractiles for E Template with concrete C16 in X-direction

Table 40: Intensity and damage measure values for each of the fractiles of corresponding limit states of E Template building with concrete C16 in X-direction

	$Sa_{(T1,5\%)}$ (g)			**Θ_{max} (%)**		
	IM 16%	**IM 50%**	**IM 84%**	**DM 16%**	**DM 50%**	**DM 84%**
IO	0.18	0.31	0.78	1.0%	1.0%	1.0%
CP	0.33	0.80	1.69	1.8%	2.7%	3.2%
GI	0.38	0.92	1.70	+∞	+∞	+∞

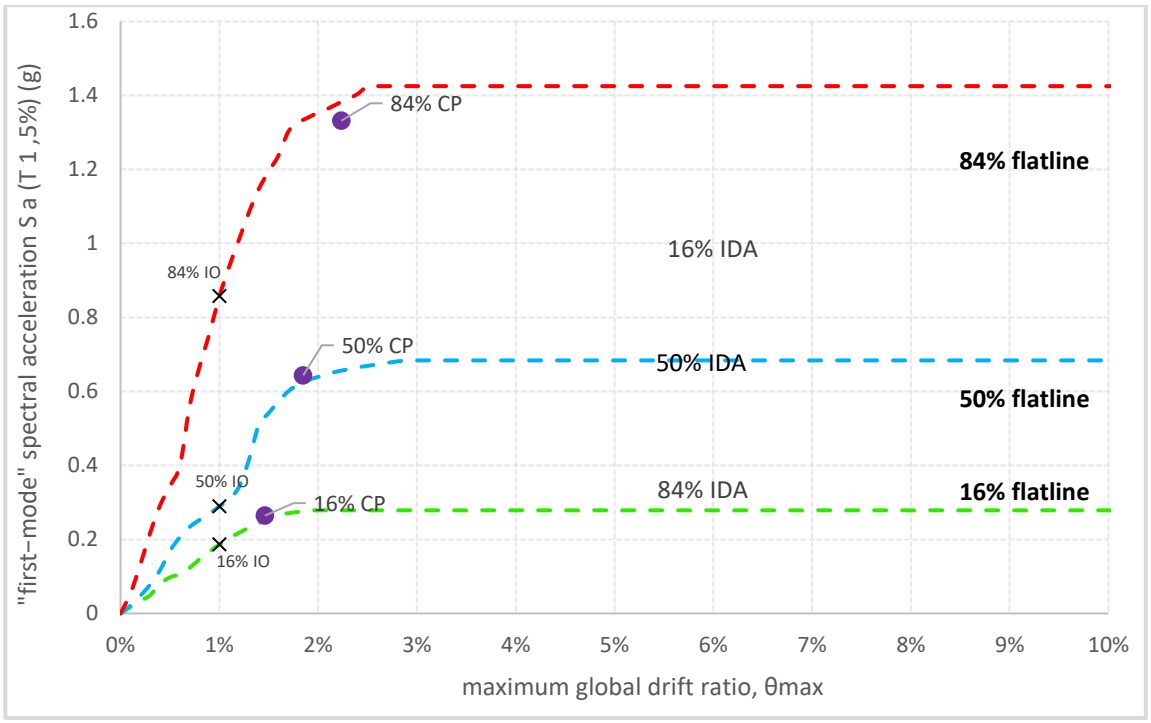

Figure 272: 16%, 50%, 84% IDA fractiles for E Template with concrete C10 in X-direction

Table 41: Intensity and damage measure values for each of the fractiles of corresponding limit states of E Template building with concrete C10 in X-direction

	$Sa_{(T1,5\%)}$ (g)			Θ_{max} (%)		
	IM 16%	**IM 50%**	**IM 84%**	**DM 16%**	**DM 50%**	**DM 84%**
IO	0.19	0.29	0.86	1.0%	1.0%	1.0%
CP	0.26	0.64	1.33	1.5%	1.8%	2.2%
GI	0.28	0.68	1.43	+∞	+∞	+∞

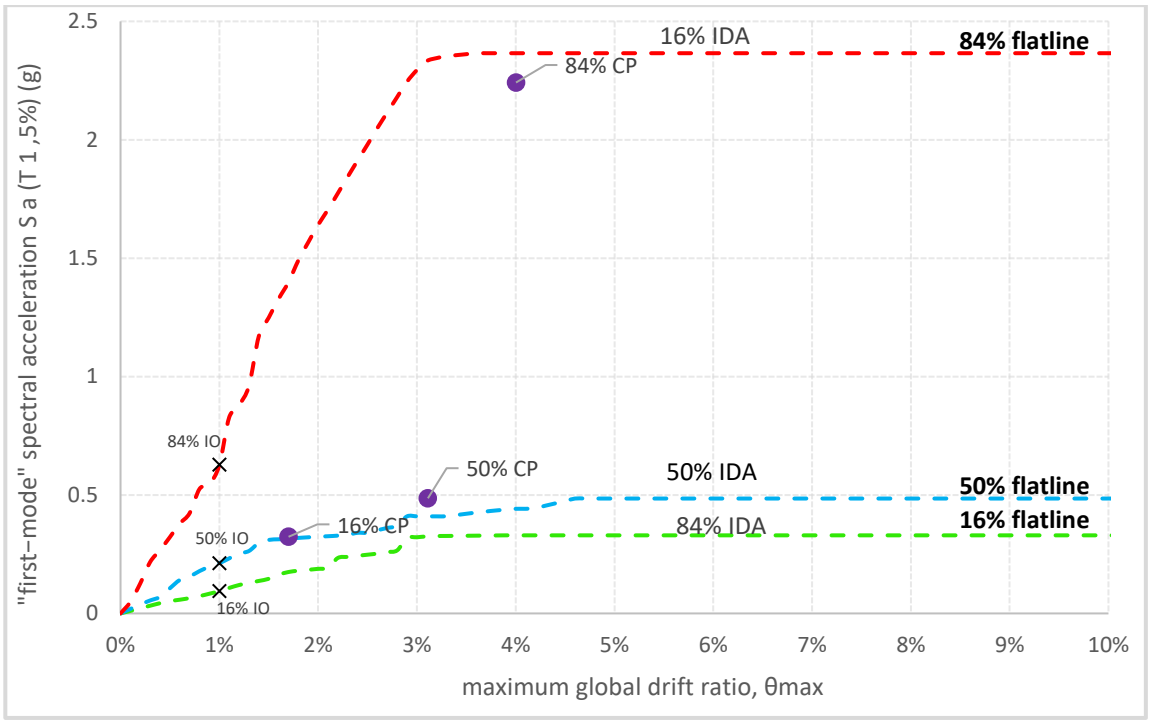

Figure 273: 16%, 50%, 84% IDA fractiles for E Template with concrete C10 in Y-direction

Table 42: Intensity and damage measure values for each of the fractiles of corresponding limit states of E Template building with concrete C16 in Y-direction

	$Sa_{(T1,5\%)}$ (g)			Θ_{max} (%)		
	IM 16%	**IM 50%**	**IM 84%**	**DM 16%**	**DM 50%**	**DM 84%**
IO	0.09	0.21	0.63	1.0%	1.0%	1.0%
CP	0.32	0.49	2.24	1.7%	3.1%	4.0%
GI	0.33	0.49	2.37	+∞	+∞	+∞

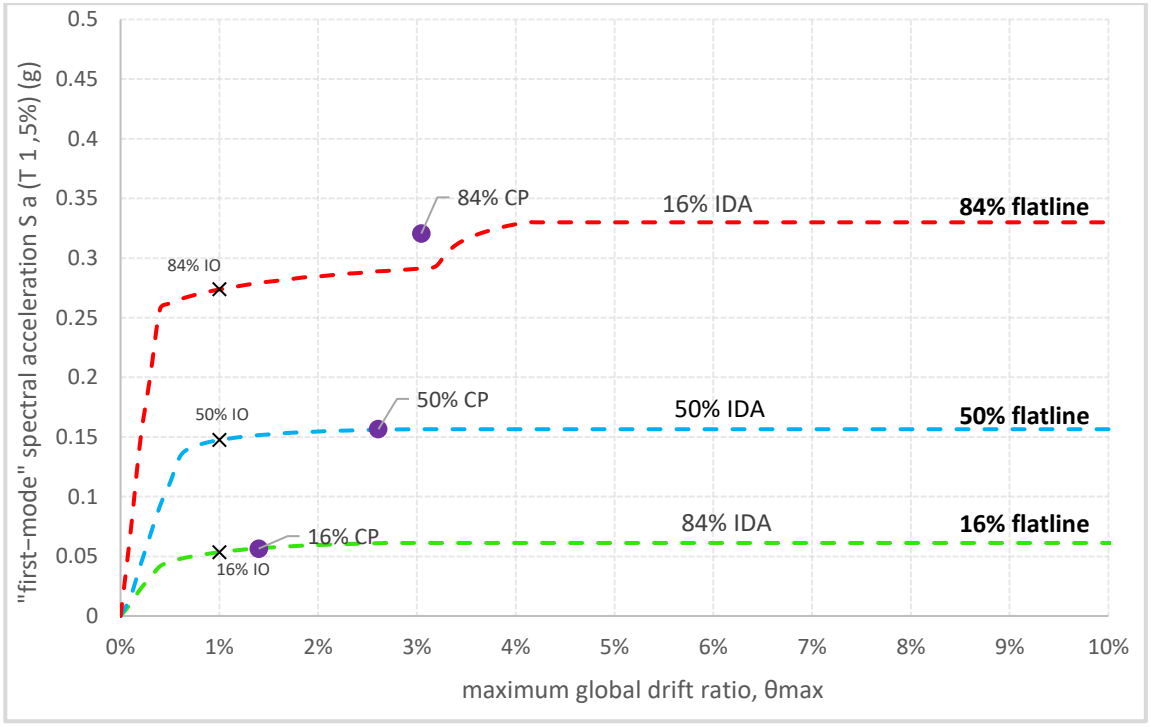

Figure 274: 16%, 50%, 84% IDA fractiles for E Template with concrete C10 in Y-direction

Table 43: Intensity and damage measure values for each of the fractiles of corresponding limit states of E Template building with concrete C10 in Y-direction

	$Sa_{(T1,5\%)}$ (g)			**Θ_{max} (%)**		
	IM 16%	**IM 50%**	**IM 84%**	**DM 16%**	**DM 50%**	**DM 84%**
IO	0.05	0.15	0.27	1.0%	1.0%	1.0%
CP	0.06	0.16	0.32	1.4%	2.6%	3.0%
GI	0.06	0.16	0.33	+∞	+∞	+∞

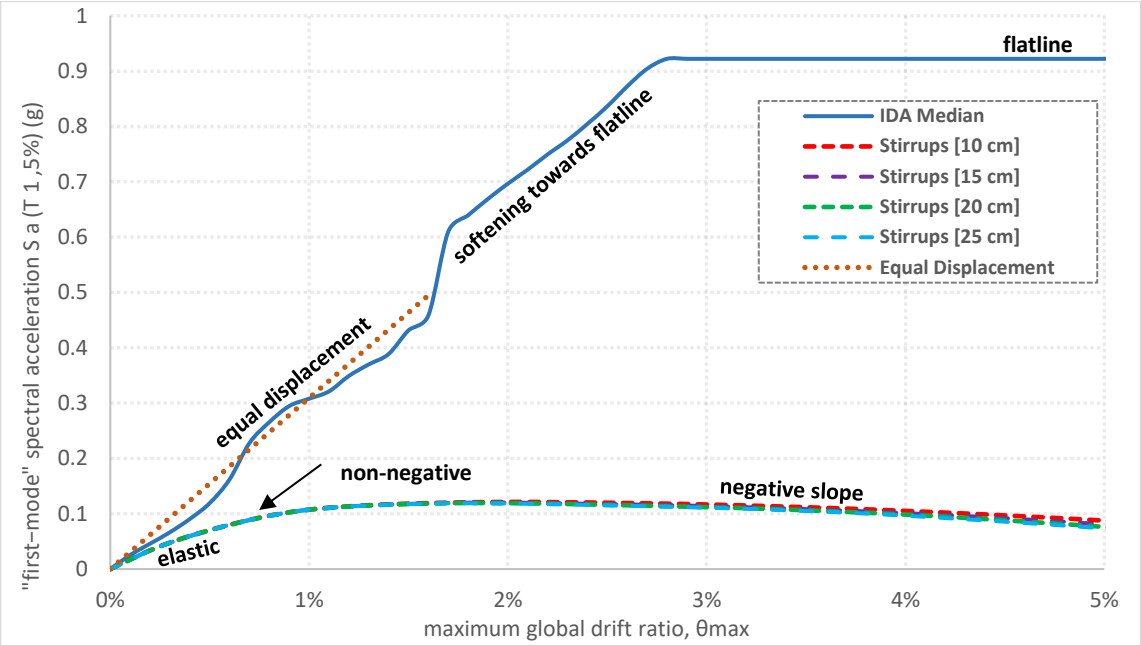

Figure 275: IDA median versus SPO curves for different concrete spacings of E Template building with concrete C16 in X-direction

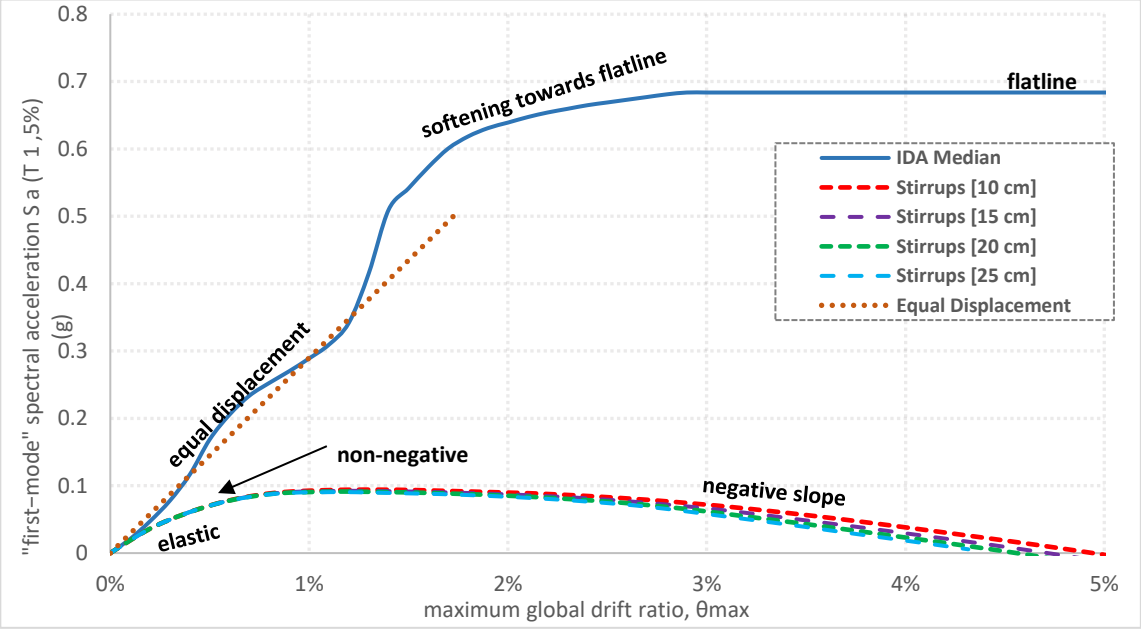

Figure 276: IDA median versus SPO curves for different concrete spacings of E Template building with concrete C10 in X-direction

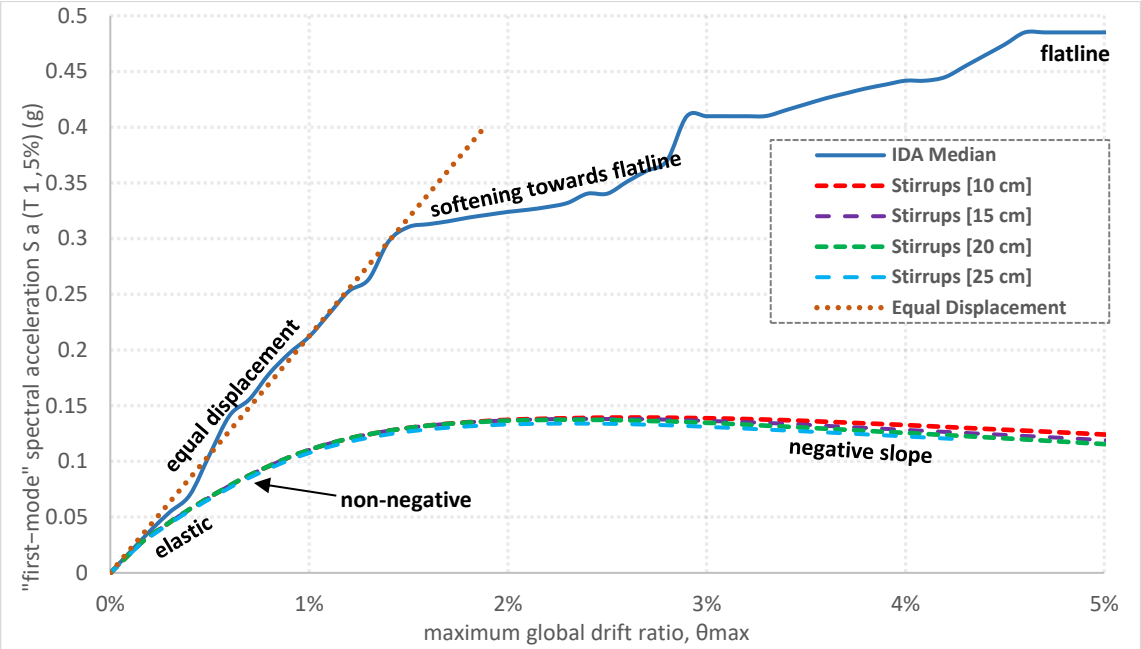

Figure 277: IDA median versus SPO curves for different concrete spacings of E Template building with concrete C16 in Y-direction

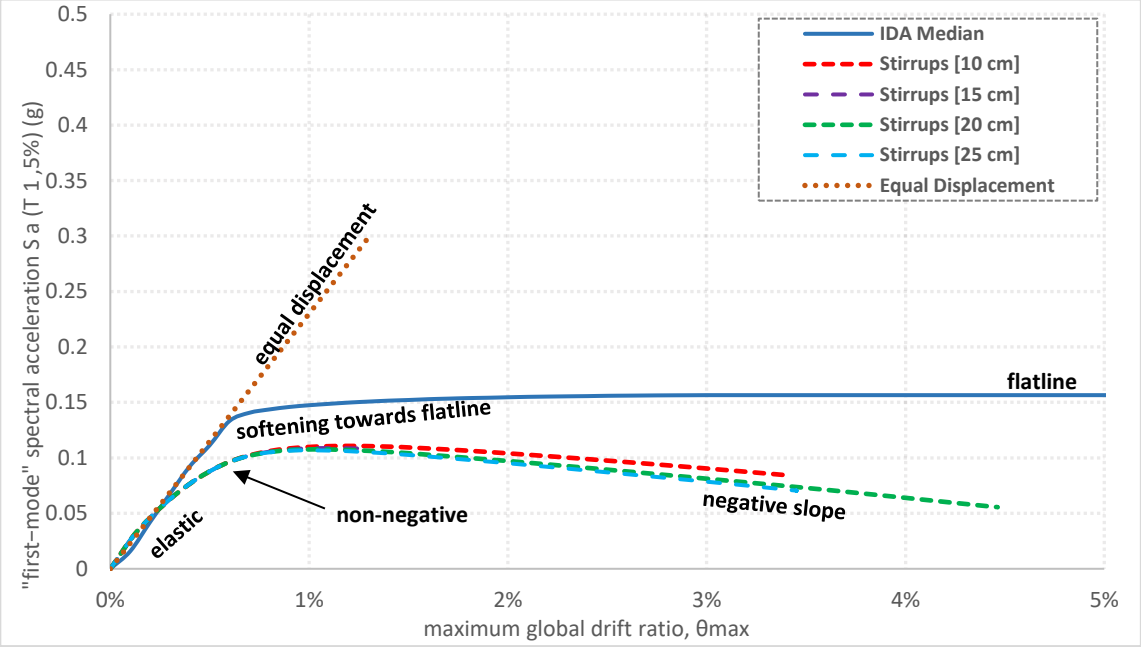

Figure 278: IDA median versus SPO curves for different concrete spacings of E Template building with concrete C10 in Y-direction

APPENDIX D

Accelerograms of the 18 records used for IDA

Accelerograms used for IDA analysis are presented below and plotted as “Acceleration (g)” versus “Time (sec)”

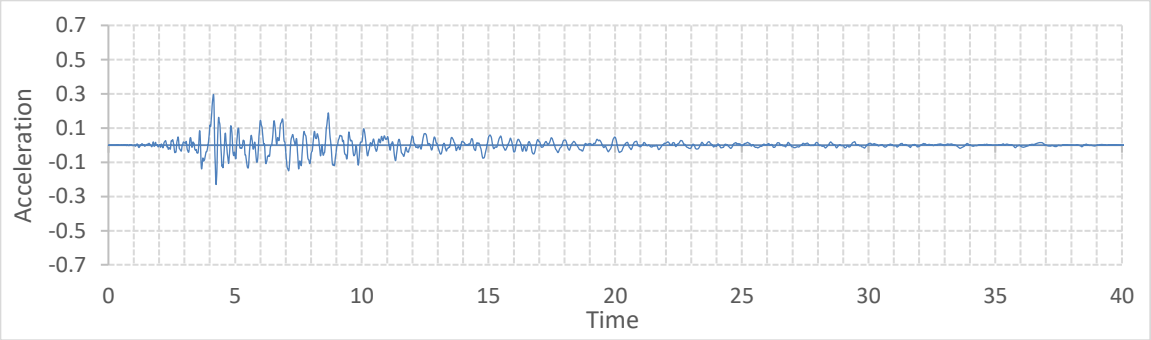

No: 1 Erzincan Turkey, Erzincan

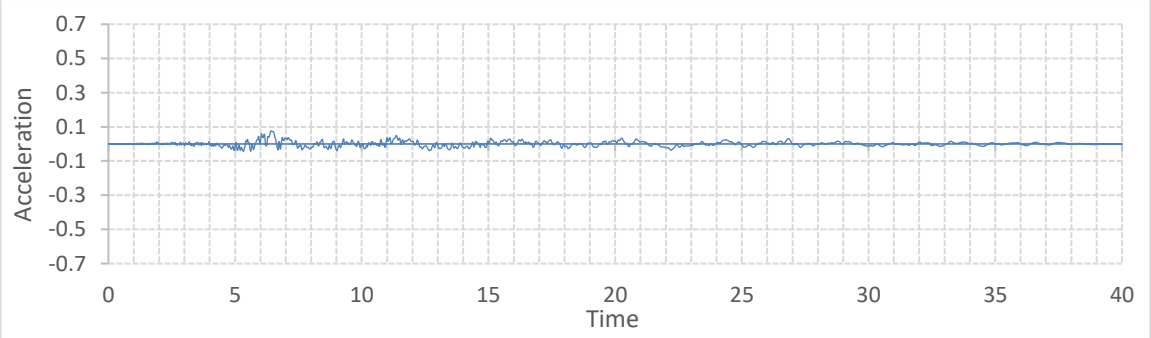

No: 2 Imperial Valley Westmoreland Fire Station

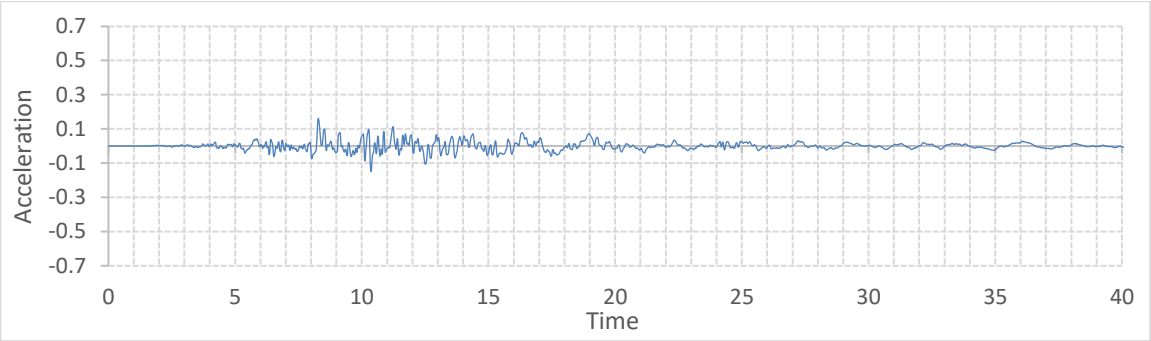

No: 3 Loma Prieta Agnews State Hospital

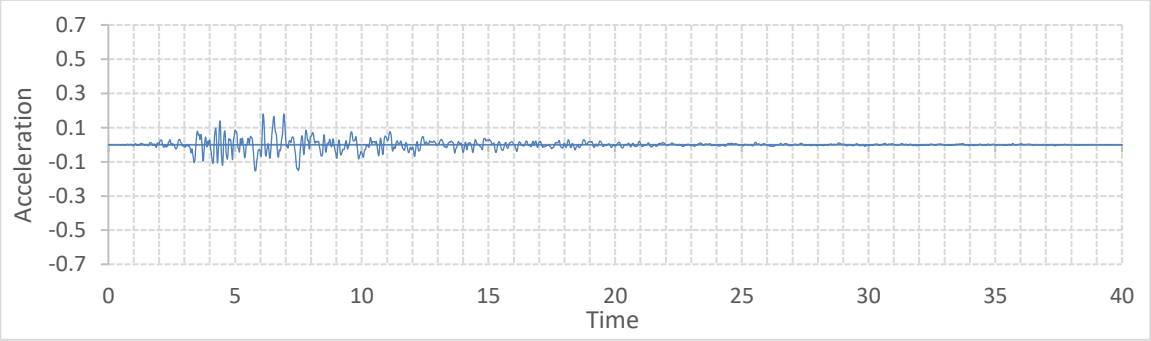

No: 4 Loma Prieta Coyote Lake Dam Downstream

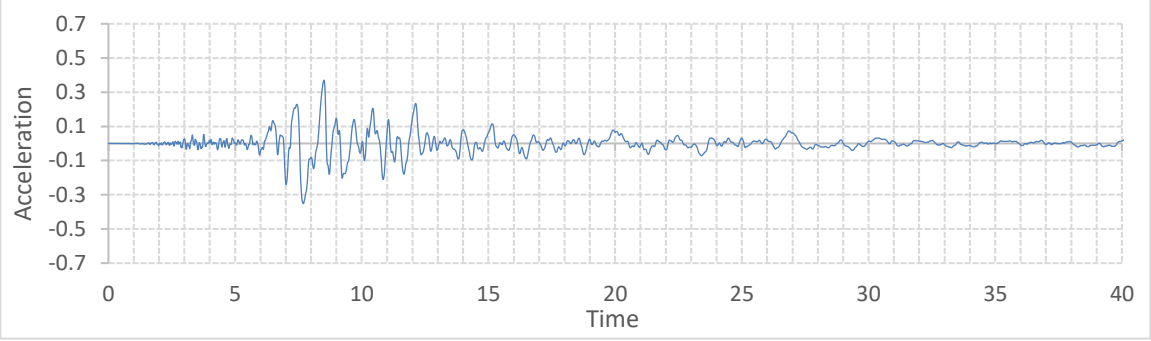

No: 5 Loma Prieta Hollister South & Pine

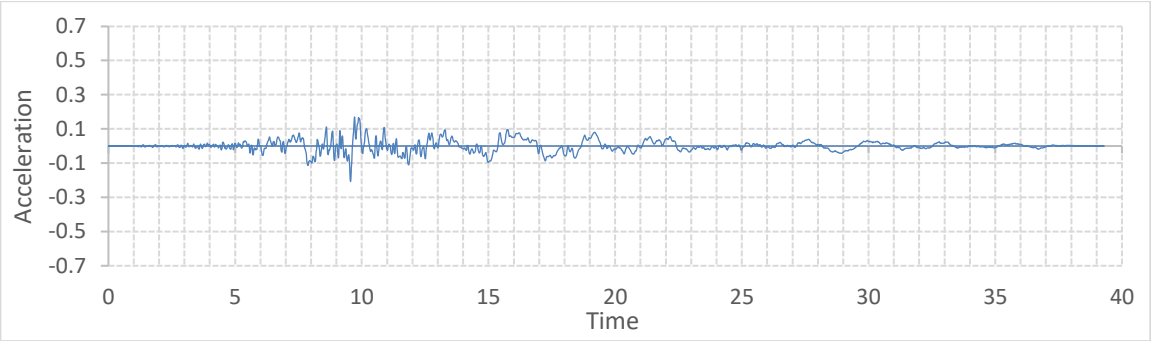

No: 6 Loma Prieta Sunnyvale Colton Ave

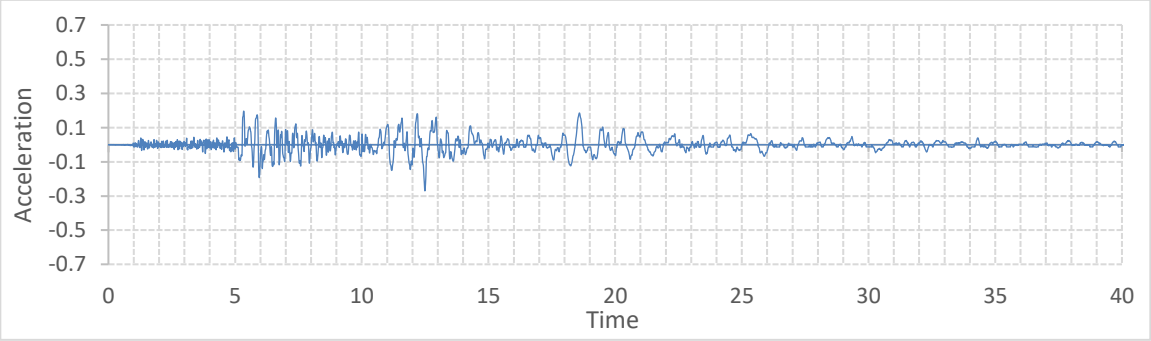

No: 7 Imperial Valley Chihuahua

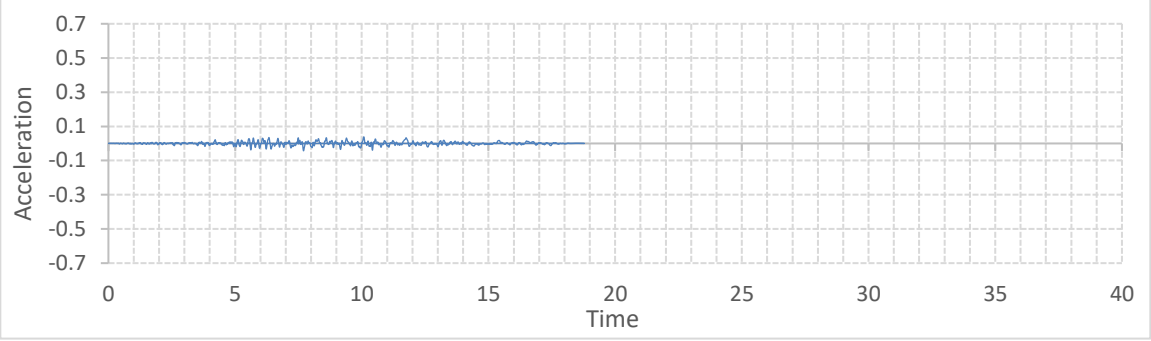

No: 8 Imperial Valley Plaster City

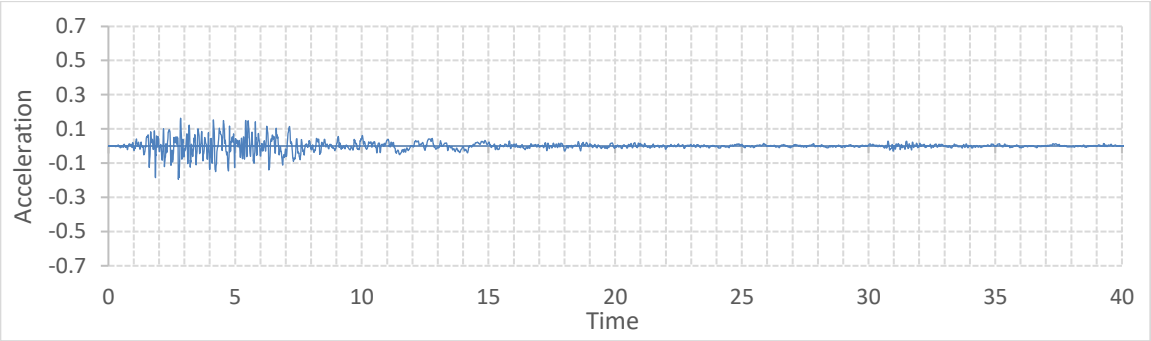

No: 9 San Fernando LA, Hollywood Stor. Lot

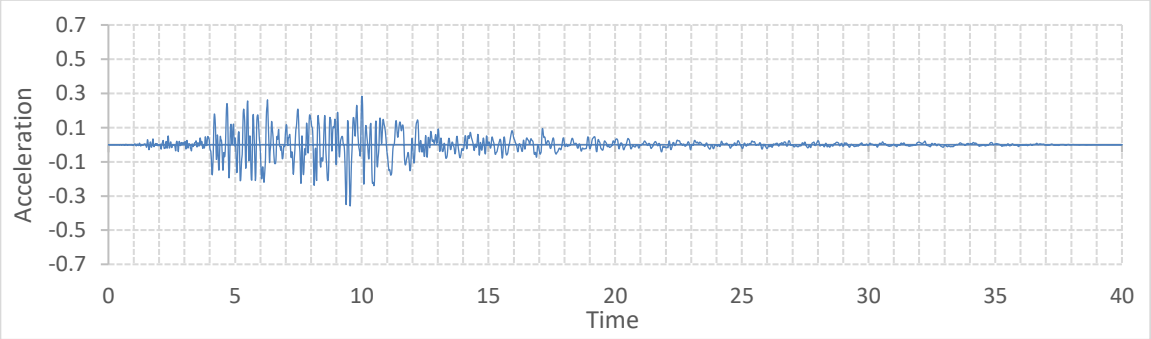

No: 10 Northridge LA, Hollywood Storage FF

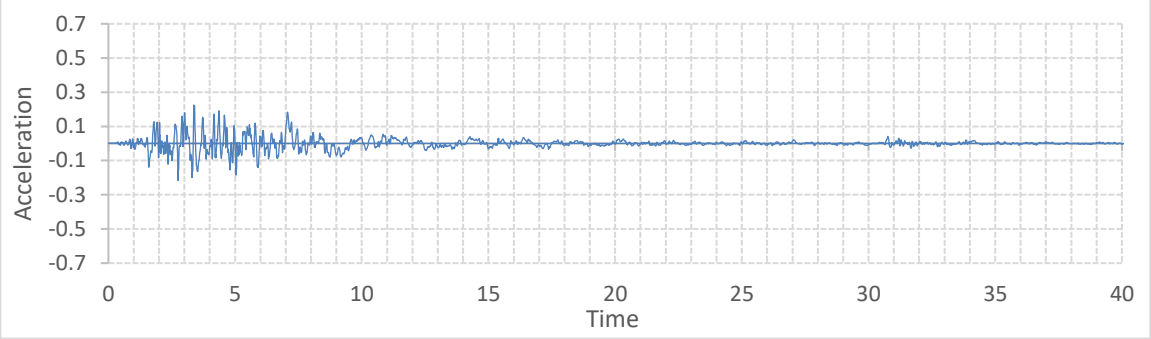

No: 11 San Fernando LA, Hollywood Stor. Lot

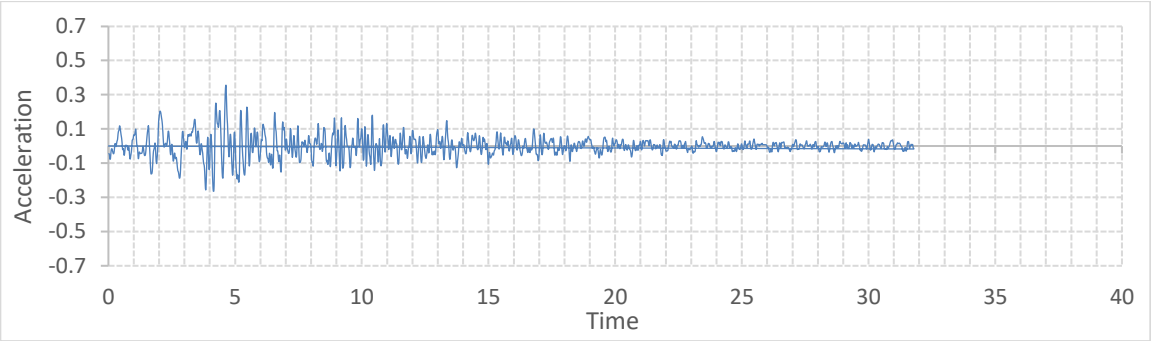

No: 12 Spitak Armenia, Gukasian

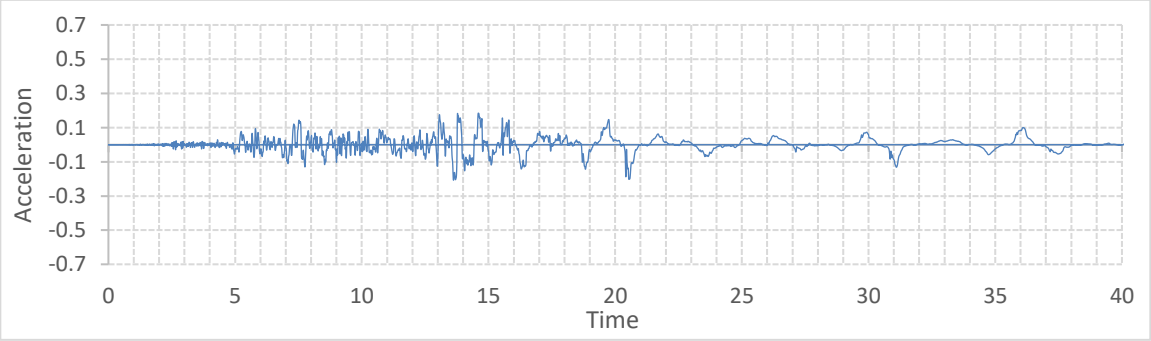

No: 13 Superstition Hills Wildlife Liquefaction Array

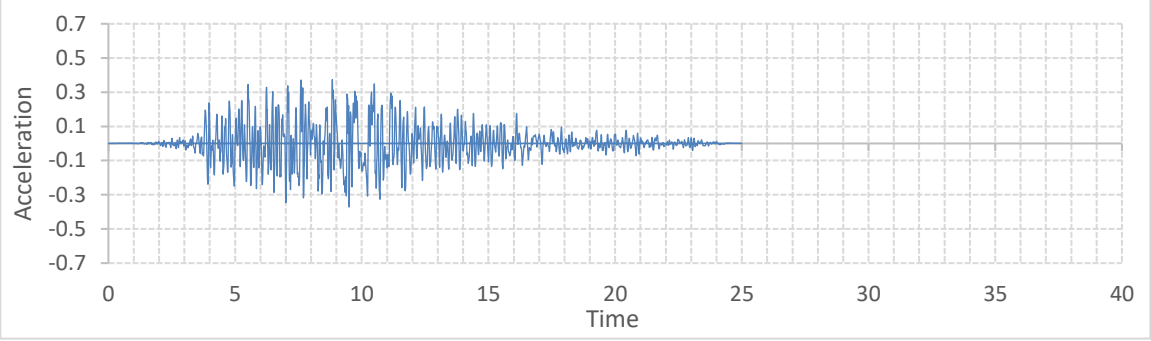

No: 14 Loma Prieta WAHO

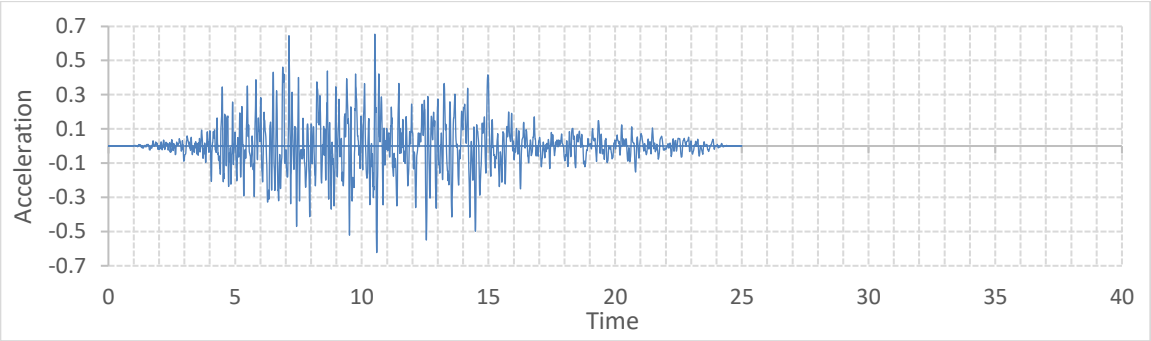

No: 15 Loma Prieta WAHO

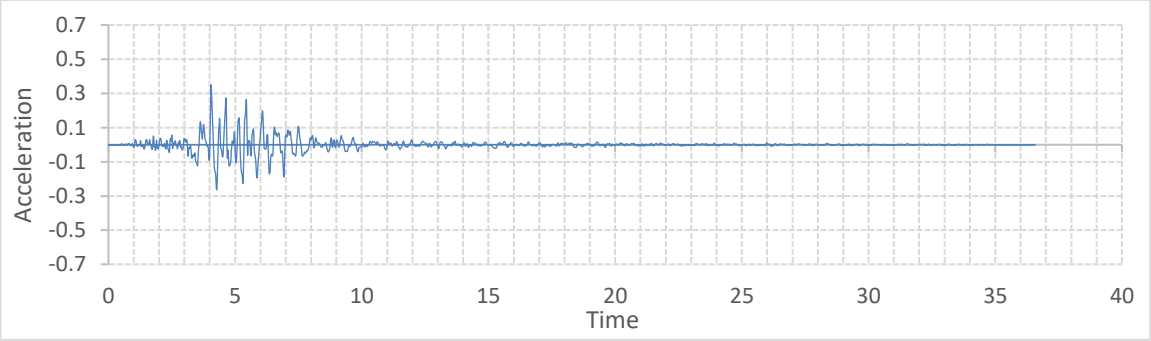

No: 16 Friuli Italy, Tolmezo

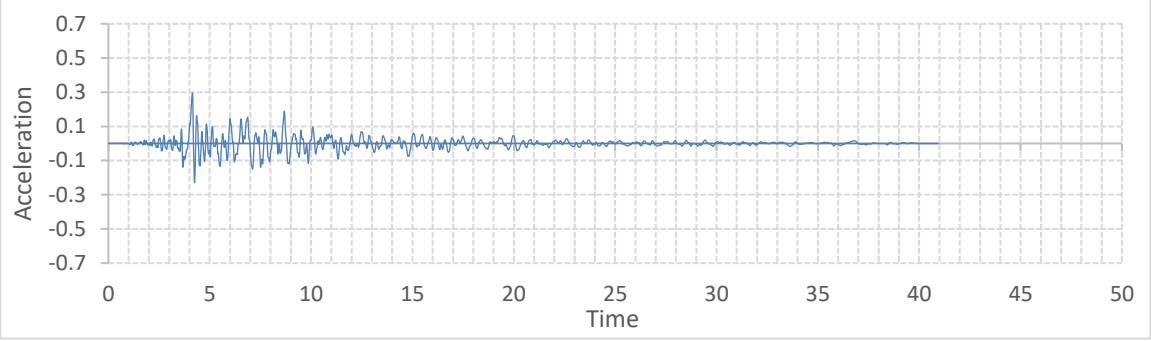

No: 17 Corinth Greece, Corinth

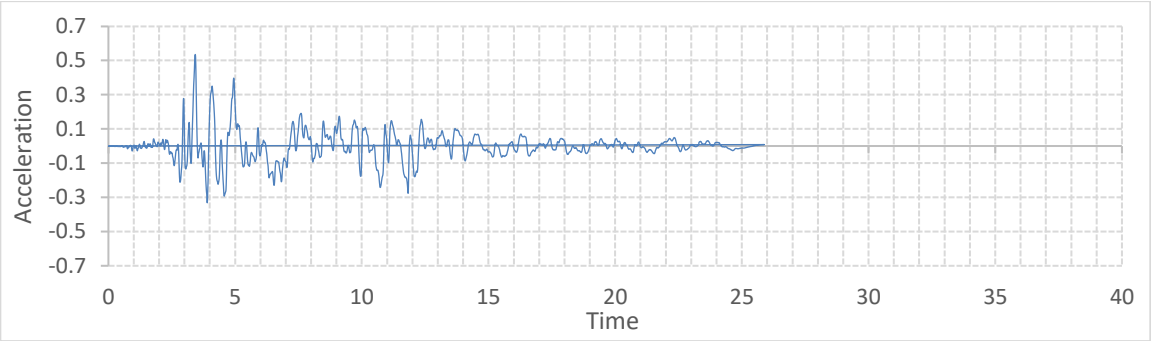

No: 18 Kocaeli Turkey, Duzce

CURRICULUM VITAE